

Structural, geochronological, and thermochronological constraints on the evolution of orogenic infrastructure in the Thor-Odin – Pinnacles area of southeastern British Columbia.

by

Deanne van Rooyen

A thesis submitted to the Faculty of Graduate and Postdoctoral Affairs in partial fulfillment of the requirements for the degree of

Doctor of Philosophy

in

Earth Sciences

Carleton University
Ottawa, Ontario

© 2013, Deanne van Rooyen

Abstract

The Thor-Odin dome is a basement-cored tectonothermal culmination in the southeastern Canadian Cordillera containing high grade metamorphic rocks, tectonically overlain by a heterogeneous tract of polydeformed medium to high grade metamorphic rocks exposed in the footwall of the Columbia River fault system. The Thor-Odin and Frenchman Cap domes comprise Paleoproterozoic “basement” gneiss infolded with Proterozoic to Paleozoic metasedimentary “cover” rocks. Detrital zircon geochronology from three samples of the inferred basal quartzite within the Thor-Odin dome contain two separate maximum depositional age populations at <1.65 Ga and <1.1 Ga, suggesting two temporally separate quartzite units, neither of which is correlative with the basal quartzite in the Frenchman Cap dome, c. 1.85 Ga. A Neoproterozoic to Cambrian panel structurally overlies the dome, as evidenced by a <600 Ma quartzite on Mount Symonds. Middle Jurassic, or younger, quartzites are present at Plant Creek, representing a transposed terrane boundary and the accretion of rocks on to the Laurentian margin. Four tectonothermal domains were defined based on timing of metamorphism, deformation and cooling, structural and petrographic data, and $^{40}\text{Ar}/^{39}\text{Ar}$ thermochronology. The structurally highest domain (Whatshan – Pinnacles) was polyfolded in the Late Cretaceous. The second highest domain (South Fosthall) was penetratively deformed in the mid-crust at c. 73 – 64 Ma. Deformation ended in the rocks of the South Fosthall area after c. 64 Ma, but continued in the structurally lower third domain (North Fosthall – Cariboo Alp). The North Fosthall– Cariboo Alp domain became suprastructure relative to the deforming rocks in the structurally lowest domain

(Thor-Odin dome) after c. 58 Ma. The Thor-Odin dome remained in the infrastructure until c. 52 Ma. Exhumation and cooling through 500 °C in the upper part of the structural section was ongoing during the last stages of transposition and folding in the dome in the Late Paleocene to Early Eocene. All the rocks cooled through 300 °C together between 52.5 – 51 Ma. Extensional structures were active at all structural levels by c. 51 Ma, reflecting a regional switch from transpression to transtension, expressed as crustal scale extension and exhumation via the east-dipping Columbia River and west-dipping Okanagan Valley extensional fault systems.

Acknowledgements

Thank you first and foremost to Dr. Sharon Carr for superb supervision and mentorship, scientific and otherwise. Thank you for introducing me to the wonderful Monashee Mountains through this project. I am truly grateful for the immense amount of time, training, support and advice you have provided over the years. This project was financially supported by NSERC grants to Dr. Sharon Carr and Dr. Jim Lee, and by additional funding from Dr. Don Murphy (Yukon Geological Survey). I am also grateful for student funding through NSERC PGS Scholarships, Ontario Graduate Scholarships, Mineralogical Association of Canada Travel and Research Grants, Geological Association of Canada Travel Grants, and scholarships through the Department of Earth Sciences and Graduate Studies at Carleton University.

I have benefited greatly from having the Cordilleran research community as a wonderfully encouraging venue for scientific discussion and learning. Thanks in particular to Phillip Simony, Don Murphy, Félix Gervais, Alana Hinchey, Stefan Kruse, and Paul Williams. To Susan Banman, Arlene Carr and Marianne Marot, thank you for being great company in the field and providing cheerful and efficient assistance in all weather conditions, even while surrounded by bears, snowstorms, forest fires, and countless mosquitos. Thank you to John Blenkinsop, Doug Archibald, Mike Tubrett, Ron Hartree, Peter Jones, Lizzy Ann Spencer, Brian Cousens, Mike Jackson and Mike Smith for training and support in analyses of all kinds. Thank you to Claudia Schröder-Adams and Bob Burk for getting me started on the road to a science degree and eventually a career.

Thanks to Nancy Dlouhy, Rhea Mitchell, Michéle Asgar-Deen, Kelly Batten-Hender and Haley Sapers for friendship, support, and encouragement through the years. Without you this process would have been a lot less enjoyable! The list is too long to itemize, it includes care packages with knitted socks and chocolate sent to a field site by helicopter, letting me use a living room as a staging ground for field seasons, places to stay, lots of running, and endless cups of coffee.

Thank you to Kevin Driscoll for years of love and support, accompanied by lots of patience. And to Erin for always giving me a reason to smile!

Original Contribution

My thesis research solves tectonic, geochronological and structural problems related to the evolution of a basement-cored structural culmination and structurally overlying panel of rocks in the southeastern Canadian Cordillera. This study involved an interdisciplinary approach which included field mapping, structural geology, $^{40}\text{Ar}/^{39}\text{Ar}$ thermochronology, LA-ICP-MS detrital zircon U-Pb geochronology and complementary techniques in analytical geochemistry and isotope geochemistry.

For this project I completed three seasons (5 months) of field work focused on structural and lithological mapping, and sampling. Mapping was done at 1:20000 and 1:5000 scale, using topographic base maps (contained within NTS 1:50000 sheets 82L/8 and 82L/9). I performed all stages of sample collecting, crushing, grinding, mineral separation, mineral picking, preparation for analysis, and data interpretation under the supervision of Sharon Carr at Carleton University, with occasional assistance with sample preparation.

For the detrital zircon geochronology study I prepared epoxy grain mounts and scanning electron microscope photographs under the supervision of Mike Smith. I performed laser ablation inductively coupled plasma mass spectrometry (LA-ICP-MS) on zircon grains from five quartzite samples, at Memorial University, NL, under the supervision of Mike Tubrett. I performed $^{40}\text{Ar}/^{39}\text{Ar}$ thermochronology analyses at Queen's University, ON, under the supervision of Doug Archibald. I analyzed 80 samples of hornblende,

biotite and muscovite from all structural levels of the study area, from a variety of lithologies. As part of the geochemical study I performed thermal ionization mass spectrometry (TIMS) for Sr and Nd isotopic analyses under the supervision of Lizzy Ann Spencer and Brian Cousens at Carleton University, and X-ray fluorescence analyses for acquiring major element data under the supervision of Ron Hartree at the University of Ottawa. Peter Jones supervised electron microprobe analysis of mineral compositions at Carleton University. Inductively coupled plasma mass spectrometry (ICP-MS) for trace element analyses were acquired commercially at GeoLabs in Sudbury, ON.

My thesis comprises the first comprehensive $^{40}\text{Ar}/^{39}\text{Ar}$ thermochronology study in the Thor-Odin area incorporating geochronology of structures (e.g. syn- and post-tectonic pegmatites) in conjunction with cooling and metamorphic histories. It is also the first LA-ICP-MS detrital zircon U-Pb geochronology study to include rocks of Thor-Odin dome as well as structurally overlying rocks and has refined the known stratigraphic relationships and improved the geochronological framework for the area. This project has produced an extensive internally consistent dataset that has made it possible to refine and significantly improve our understanding of the metamorphic and deformation history of the area of the structural and tectonic history of the Thor-Odin dome and surrounding rocks in southeastern British Columbia and the tectonic processes responsible for exhuming deep-seated basement rocks in extensional settings.

Table of Contents

Abstract	ii
Acknowledgements	iv
Original Contribution	vi
Table of Contents	viii
List of Tables	xiv
List of Illustrations	xv
1 Chapter: Introduction	1
1.1 Purpose of this study	1
1.2 Tectonic setting of the southeastern Canadian Cordillera	2
1.3 Tectonothermal culminations	4
1.4 Shuswap Complex terminology	6
1.5 Geological setting of the Thor-Odin – Pinnacles area in southeastern British Columbia 10	
1.6 Specific questions addressed in this study	13
2 Chapter: Geology of the Thor-Odin – Pinnacles area: A complex history of diachronous metamorphism and deformation defining suprastructure- infrastructure transitions during the Late Cretaceous to Eocene	28
2.1 Introduction	28
2.2 Map scale geology of the study area from the southern Thor-Odin dome and the Whatshan batholith	29
2.2.1 Jurassic intrusive rocks – Kuskanax batholith and Nelson intrusive suite	34
2.2.2 Cretaceous intrusive rocks – Whatshan batholith	35
2.2.3 Late Cretaceous to Eocene intrusive rocks – Ladybird granite suite	36

2.2.4	Eocene intrusive rocks – Three Valley lamprophyres	39
2.3	Normal faults in the Thor-Odin – Pinnacles area	40
2.4	Petrology, deformation and metamorphism of the Pinnacles-Thor-Odin area	43
2.4.1	Whatshan – Pinnacles	44
2.4.2	Plant Creek – South Fosthall	45
2.4.3	North Fosthall – Mount Symonds to Cariboo Alp	46
2.4.4	The Thor-Odin dome	55
2.5	Post-transposition deformation, brittle deformation and retrograde metamorphism 60	
2.6	Conclusions regarding diachronous metamorphism, deformation in the Thor-Odin – Pinnacles area.....	62

3 Chapter: Age and provenance of marker quartzites in Thor-Odin dome: Are apparent markers correlative and do Thor-Odin and Frenchman Cap domes of the Monashee complex represent a single basement domain?..... 132

3.1	Introduction.....	132
3.2	Tectonic setting of the southeastern Canadian Cordillera and a brief history of the evolution of the Laurentian margin in the Thor-Odin – Pinnacles area	134
3.3	Monashee Complex and Monashee décollement terminology and interpretations. 139	
3.3.1	Basement rocks: Thor-Odin and Frenchman Cap domes	142
3.3.2	Cover rocks: Thor-Odin and Frenchman Cap domes	145
3.3.3	Basal quartzite age in the Thor-Odin dome	150
3.3.4	Basal quartzite age in the Frenchman Cap dome	151
3.3.5	Metamorphism and deformation in the domes	153
3.3.6	Geology of specific study areas.....	154
3.3.6.1	Mount Thor	154

3.3.6.2	Icebound Lake.....	155
3.3.6.3	Cariboo Alp.....	156
3.4	Methods.....	158
3.4.1	Sample preparation.....	158
3.4.2	Analytical Methods.....	161
3.5	Results.....	165
3.5.1	DA224 – Mount Thor, Thor-Odin dome.....	165
3.5.2	DC422 – Icebound Lake, Thor-Odin dome.....	166
3.5.3	DC165 – Cariboo Alp, Thor-Odin dome south-western flank.....	167
3.6	Discussion.....	168
3.6.1	Thor-Odin quartzites, Mount Thor and Icebound Lake.....	168
3.6.2	Cariboo Alp.....	174
3.6.3	The Thor-Odin cover sequence and Monashee décollement.....	177
3.6.4	Implications of two quartzites in Thor-Odin dome.....	180
3.7	Conclusions and implications.....	180
4	Chapter: LA-ICP-MS detrital zircon results from two quartzites in the Thor-Odin – Pinnacles area: Constraints on age and provenance of the metasedimentary and metavolcanic rocks overlying the Thor-Odin dome; Implications for interpretations of accreted or autochthonous terranes.....	215
4.1	Introduction.....	215
4.2	Geological setting of the Thor-Odin – Pinnacles area in the southeastern Canadian Cordillera.....	218
4.2.1	Quesnellia terrane rocks in the Thor-Odin – Pinnacles area.....	220
4.2.2	Geology of specific study areas.....	221
4.2.2.1	Mount Symonds.....	221

4.2.2.2	Plant Creek	222
4.3	Methods	224
4.4	Results	224
4.4.1	DC395 – Mount Symonds.....	224
4.4.2	DC490 – Plant Creek.....	225
4.5	Discussion	226
4.6	Conclusions and implications	233
5	Chapter: $^{40}\text{Ar}/^{39}\text{Ar}$ thermochronology studies of the Thor-Odin – Pinnacles area, southeastern British Columbia: tests of structural models.....	252
5.1	Introduction.....	252
5.2	Tectonic and geological setting	254
5.2.1	Study locations and map area.....	257
5.2.2	Diachronous metamorphism, deformation and suprastructure-infrastructure transitions.	257
5.2.3	Recent work relating to the cooling history of the Thor-Odin – Pinnacles area....	259
5.2.4	Excess argon.....	260
5.3	Methods	263
5.3.1	Petrography and geochemistry studies	263
5.3.2	Sample picking and preparation	264
5.3.3	Irradiation and analysis	265
5.3.4	Step-heating and the definition of plateaus	267
5.3.5	Closure temperatures	269
5.3.6	Limitations of the closure temperature concept	270
5.4	Results	272

5.4.1	Hornblende plateau ages from a range of rock types and thermotectonic domains	273
5.4.1.1	Hornblende samples from the Thor-Odin dome	273
5.4.1.2	Cariboo Alp	274
5.4.1.3	Fawn Lakes and Mount Symonds	276
5.4.1.4	Twin Peaks and North Fosthall	277
5.4.1.5	Plant Creek and Cusson Creek	279
5.4.2	Biotite plateau ages from a range of rock types and structural levels	279
5.4.2.1	Thor-Odin dome	279
5.4.2.2	Cariboo Alp	280
5.4.2.3	Fawn Lakes	282
5.4.2.4	Mount Symonds	282
5.4.2.5	North Fosthall	283
5.4.2.6	Plant Creek	283
5.4.3	Muscovite plateau ages from a range of structural levels	284
5.4.3.1	Muscovite in leucosomes, Cariboo Alp	284
5.4.3.2	Muscovite in Ladybird granite pegmatites	284
5.5	Discussion	285
5.5.1	Hornblende	286
5.5.2	Biotite	291
5.5.3	Muscovite	296
5.5.4	Cooling ages versus reset ages	298
5.5.5	Cooling rates	300

5.5.6	The nature of the boundary between the Thor-Odin dome and overlying rocks at Cariboo Alp.....	303
5.5.7	Contribution of the Columbia River fault to cooling and exhumation of high grade rocks	305
5.6	Conclusions and implications	310
6	Chapter: Implications for the tectonic evolution of the Thor-Odin – Pinnacles area	382
6.1	Introduction.....	382
6.2	Detrital zircon U-Pb geochronology studies: new interpretations of protolith ages and provenance of the rocks in the Thor-Odin – Pinnacles area	382
6.3	Exhumation mechanisms.....	386
6.3.1	Suprastructure-infrastructure transitions in the Thor-Odin – Pinnacles area related to core complex models.....	387
6.3.2	Late Cretaceous to Eocene thermal history of the Thor-Odin – Plant Creek area related to exhumation and extension.....	391
6.3.3	Diapirism within the Thor-Odin dome related to core complex models.....	394
6.3.4	Crustal flow in the Thor-Odin and Frenchman Cap domes.....	396
6.4	A hybrid model for the evolution of the Thor-Odin dome in the Late Cretaceous to Eocene and implications for the tectonic history of the southeastern Canadian Cordillera ..	398
6.5	Future work	402
	References	412
	Appendices	453
	Appendix A Detrital zircon U-Pb data tables	453
A.1	LA-ICP-MS U-Pb isotopic analyses of detrital zircons, Mount Thor (DA224)	453

A.2	LA-ICP-MS U-Pb isotopic analyses of detrital zircons, Icebound Lake (DC422)	456
A.3	LA-ICP-MS U-Pb isotopic analyses of detrital zircons, Cariboo Alp (DC165)	459
A.4	LA-ICP-MS U-Pb isotopic analyses of detrital zircons, Mount Symonds (DC395) ..	462
A.5	LA-ICP-MS U-Pb isotopic analyses of detrital zircons, Plant Creek (DC490).	465
Appendix B Geochemical data.....		468
B.1	Major element data from XRF analysis	468
B.2	Trace element data from XRF analysis.....	469
B.3	Trace element data from IC-PMS for selected samples.....	470
B.4	Sr and Nd isotopic ratios from TIMS analysis.....	472
Appendix C Argon thermochronology data.....		473
C.1	Hornblende thermochronology data	473
C.2	Biotite thermochronology data.....	485
C.3	Muscovite thermochronology data	495
C.4	All thermochronology data arranged by sample number.....	501
Appendix D Map		529
D.1	Selected structural and lithological data used for the map.....	529

List of Tables

Table 5.1	Sample locations and rock types for thermochronology.	317
Table 5.2	$^{40}\text{Ar}/^{39}\text{Ar}$ data for samples from all study areas which include 80% or more ^{39}Ar in a robust plateau age.	317
Table 5.3	$^{40}\text{Ar}/^{39}\text{Ar}$ data for samples from all study areas which are not considered robust because they do not include 80% or more ^{39}Ar in a plateau age.	320

List of Illustrations

Figure 1.1 Tectonic map of the southeastern Canadian Cordillera.....	20
Figure 1.2 Geological map of the Thor-Odin – Pinnacles study area..	24
Figure 2.1 Major tectonic elements in the Thor-Odin – Pinnacles area.....	67
Figure 2.2 Lithology of major units in the Thor-Odin – Pinnacles area.....	69
Figure 2.3 Garnet–muscovite granitic pegmatite of the Ladybird granite in the South Fosthall area.....	70
Figure 2.4 Ladybird granite crosscutting calc-silicate amphibolite in the North Fosthall area.....	71
Figure 2.5 Undeformed pegmatite of the Ladybird granite at Plant Creek area.....	72
Figure 2.6 Deformed pegmatite and granite of the Ladybird suite in the Twin Peaks – Mount Baldur area.....	73
Figure 2.7 Pegmatites of the Ladybird granite suite at Mount Symonds.....	74
Figure 2.8 Undeformed pegmatites of the Ladybird granite crosscutting the grey migmatitic gneiss at Cariboo Alp.....	75
Figure 2.9 Steeply dipping north-south striking fractures that cross-cut all other structural features at Cariboo Alp.....	76
Figure 2.10 Large lamprophyre dyke ~8 m wide crosscutting garnet–sillimanite–biotite gneiss at Twin Peaks.....	77
Figure 2.11 Detail of the contact between a lamprophyre dyke (Figure 2.10) and the host gneiss at Twin Peaks.....	78

Figure 2.12 Lamprophyre dyke, 50 cm wide, at Twin Peaks.	79
Figure 2.13 Detail of the edge of the lamprophyre dyke in Figure 2.12, showing the lamprophyre crosscutting a pegmatite of the Ladybird granite.....	80
Figure 2.14 Tectonostratigraphic column of the study area summarizing timing of deformation and metamorphism at different structural levels.	86
Figure 2.15 Shallow south dipping metasedimentary and calc-silicate rocks in the Plant Creek – South Fosthall area.	87
Figure 2.16 Quartzite unit near Plant Creek dipping shallowly to the south.	88
Figure 2.17 Marble unit from Plant Creek showing outcrop-scale asymmetric folds.....	89
Figure 2.18a View looking north from the Twin Peaks.....	90
Figure 2.18b View to the north at Twin Peaks showing a strongly developed regional fabric.	91
Figure 2.19 Westward view of pegmatites of the Ladybird granite at Twin Peaks.....	92
Figure 2.20 Pegmatite of the Ladybird granite surrounding a raft of calc-silicate amphibolite in the Twin Peaks Area.	93
Figure 2.21 Pegmatite and folded amphibolite in the Twin Peaks area.....	94
Figure 2.22 Migmatitic garnet–biotite gneiss at Twin Peaks.....	95
Figure 2.23 Migmatitic calc-silicate amphibolite in the Twin Peaks area	96
Figure 2.24 Ultramafic pod (a) at Twin Peaks with bright green serpentine minerals in outcrop (b).	97
Figure 2.25 Sillimanite contained in a well-developed transposition foliation in migmatitic garnet–sillimanite–biotite gneiss at Twin Peaks.	98

Figure 2.26 Migmatitic amphibolite gneiss at Twin Peaks with a well-developed transposition foliation.....	99
Figure 2.27 Small scale folds in migmatitic garnet–biotite gneiss at Twin Peaks illustrative of the regional fold style.....	100
Figure 2.28 Boudinaged pegmatite layer in highly strained calc-silicate amphibolite in the North Fosthall area.....	101
Figure 2.29 Moderately southwest dipping calc-silicate amphibolite gneiss in the North Fosthall area.....	102
Figure 2.30 Moderately south dipping metasedimentary rocks in the Mount Symonds area.....	103
Figure 2.31 Garnet–biotite gneiss with a cm-scale asymmetric isoclinal S fold at Mount Symonds.....	104
Figure 2.32 Boudinaged pegmatitic leucosome in moderately south dipping garnet–biotite gneiss at Mount Symonds.....	105
Figure 2.33 Amphibolite and Ladybird pegmatite deformed together at Mount Symonds.....	106
Figure 2.34 Moderately southwest dipping semipelitic paragneiss at Fawn Lakes.....	107
Figure 2.35 Garnet–biotite paragneiss at Fawn Lakes.....	108
Figure 2.36 Southwest dipping transposition foliation in paragneiss at Cariboo Alp. ...	109
Figure 2.37 Ladybird pegmatites at Cariboo Alp.....	110
Figure 2.38 Migmatitic biotite gneiss at Cariboo Alp.....	111
Figure 2.39 Details of the grey quartzofeldspathic gneiss at Cariboo Alp.....	112

Figure 2.40 Garnet amphibolite boudin with foliation at an acute angle to the transposition foliation in the paragneiss (a) and a snowball garnet (from a different boudin) with internal foliations.	113
Figure 2.41 Northeast verging folds at Cariboo Alp.	114
Figure 2.42 Photomicrographs of garnet sillimanite biotite paragneiss (DC184) at Cariboo Alp in cross polarized light (a) and in plane polarized light (b).	116
Figure 2.43 Asymmetric pressure shadows on a large diopside crystal in grey calc-silicate gneiss at Cariboo Alp.....	117
Figure 2.44 Sillimanite lineation plunging shallowly to the southwest at Cariboo Alp..	118
Figure 2.45 Two generations of sillimanite lineations at Cariboo Alp.....	119
Figure 2.46 The Icebound Lake study area with a view facing west.	120
Figure 2.47 Garnet amphibolite rafts and lenses in migmatitic garnet–biotite gneiss at Icebound Lake.	121
Figure 2.48 Fold interference (Type 3) pattern in layering within the main migmatitic garnet–biotite quartzofeldspathic paragneiss unit at Icebound Lake outlined by garnet amphibolite.	122
Figure 2.49 Migmatitic garnet–biotite–quartzofeldspathic paragneiss unit at Icebound Lake.	123
Figure 2.50 Migmatitic garnet–biotite–quartzofeldspathic paragneiss with cm long sillimanite clumps, possibly as pseudomorphs after kyanite..	124
Figure 2.51 Garnet–biotite–plagioclase–gedrite amphibolite at Icebound Lake.	125

Figure 2.52 Close-up view of a garnet–biotite–plagioclase–gedrite amphibolite in the Icebound Lake area.	126
Figure 2.53 Gedrite–anthophyllite amphibolite with crystals up to 5 cm long in a matrix of quartz and plagioclase.	127
Figure 2.54 Lens of chloritized garnets in the layer of migmatitic garnet–gedrite anthophyllite illustrated in Figures 2.51 – 2.53.	128
Figure 2.55 Muscovite crystals in leucosomes at Cariboo Alp.	129
Figure 2.56 Proposed locations for suprastructure/infrastructure zones preserved within the study area and their associated ages.	131
Figure 3.1 The Monashee Complex made up of the Frenchman Cap dome and the Thor-Odin dome, outlined by the basal quartzites.	184
Figure 3.2 The Frenchman Cap (a) and Thor-Odin (b) domes, making up the Monashee Complex.	188
Figure 3.3 Southern flank of the Thor-Odin dome with the locations of the study areas at Mount Thor, Icebound Lake and Cariboo Alp marked.	189
Figure 3.4 Simplified stratigraphy in the Thor-Odin and Frenchman Cap domes.	193
Figure 3.5 Stratigraphy of the Thor-Odin and Frenchman Cap domes with known protolith ages.	196
Figure 3.6 Basal quartzite outlined in yellow at Mount Thor, looking north-northeast (from Hinchey 2005).	197
Figure 3.7 Basal quartzite at Icebound Lake.	198
Figure 3.8 View of the Cariboo Alp area looking at Mount Fosthall to the southwest. .	199

Figure 3.9 The basal quartzite at Cariboo Alp (DC165).....	200
Figure 3.10 Detrital zircons from the Mount Thor quartzite (DA224).....	202
Figure 3.11 Detrital zircon U-Pb ages for Mount Thor quartzite (DA224).....	204
Figure 3.12 Detrital zircons from the Icebound Lake quartzite (DC422).....	206
Figure 3.13 Detrital zircon U-Pb ages from the Icebound Lake quartzite (DC422).	208
Figure 3.14 Detrital zircons from the Cariboo Alp quartzite (DC165).	210
Figure 3.15 Detrital zircon U-Pb ages from the Cariboo Alp (DC165).	212
Figure 3.16 Comparison of the detrital zircon populations in samples from Mount Thor, Icebound Lake and Cariboo Alp.	214
Figure 4.1 Map of the Mount Symonds area.....	236
Figure 4.2 Steeply south to southwest dipping quartzite layers of sample DC395 in the Mount Symonds area.....	237
Figure 4.3 Map of the Plant Creek area.....	239
Figure 4.4 Moderately southwest dipping quartzite at of the Plant Creek area.....	240
Figure 4.5 Zircon morphology from the Mount Symonds quartzite.	241
Figure 4.6 Detrital zircon U-Pb data for sample DC395, Mount Symonds.	244
Figure 4.7 Typical zircons from the Plant Creek quartzite unit.	245
Figure 4.8 Detrital zircon U-Pb data for sample DC490, Plant Creek.	248
Figure 4.9 Interpreted protoliths for the rocks in the Thor-Odin – Pinnacles area, in the hanging walls and footwalls of the normal fault systems..	250
Figure 4.10 New interpretation of possible Middle Jurassic Quesnellia rocks as protoliths for the metamorphic rocks in the footwall of the Columbia River fault.	251

Figure 5.1 Structural styles and timing of deformation in the Thor-Odin – Pinnacles area.	322
Figure 5.2 Range of closure temperatures for argon in hornblende, biotite and muscovite in this study.	323
Figure 5.3 Garnet amphibolite DC446 boudin in migmatitic garnet–biotite– quartzofeldspathic gneiss at Icebound Lake.....	324
Figure 5.4 Garnet amphibolite layer DC423 in migmatitic garnet–biotite– quartzofeldspathic gneiss.	325
Figure 5.5 Details of garnet amphibolite DC423. Garnets range between 0.1 and 1 cm and some show reaction rims containing biotite, sillimanite and plagioclase.....	326
Figure 5.6 Photomicrograph of garnet amphibolite DC423 in plane polarized light (a) and in cross polarized light (b).....	328
Figure 5.7 Electron microprobe image of a hornblende grain from sample DC169.	329
Figure 5.8 Calc-silicate amphibolite layer DC176 in grey sillimanite–biotite– quartzofeldspathic paragneiss at Cariboo Alp.....	330
Figure 5.9 Photomicrograph of amphibolite DC186 in plane polarized light (a) and in cross polarized light (b).....	332
Figure 5.10 Garnet amphibolite boudin in rusty garnet–sillimanite–biotite paragneiss at Cariboo Alp.....	333
Figure 5.11 Electron microprobe image of a hornblende grain from sample DC188 showing minor chlorite alteration in some fracture planes.	334

Figure 5.12 Garnet amphibolite sample DC320 in the western Fawn Lakes Assemblage south of Cariboo Alp.	335
Figure 5.13 Garnet amphibolite DC342 in the Fawn Lakes Assemblage north of Mount Symonds.....	336
Figure 5.14 Amphibolite DC400 at Mount Symonds.	337
Figure 5.15 Plagioclase amphibolite sample DC414 infolded with south dipping in garnet–sillimanite–biotite paragneiss and pegmatite of the Ladybird granite.....	338
Figure 5.16 Amphibolite DC370 at Mount Symonds.	339
Figure 5.17 Pegmatite and amphibolite interleaved along the south-southwest dipping transposition foliation at Mount Symonds.....	340
Figure 5.18 Pegmatite of the Ladybird granite crosscutting amphibolite at Twin Peaks.	341
Figure 5.19 Calc-silicate amphibolite DC473 at Twin Peaks.	342
Figure 5.20 Amphibolites at Twin Peaks which did not produce plateau dates.	343
Figure 5.21 Calc-silicate amphibolite gneiss DC219 in North Fosthall.	344
Figure 5.22 Electron microprobe image of hornblende in calc-silicate amphibolite gneiss DC219 showing fractures with a small titanite grain.....	345
Figure 5.23 Exposure of a foliated plagioclase amphibolite gneiss DC209 in the North Fosthall area.....	346
Figure 5.24 Calc-silicate amphibolite gneiss in the North Fosthall area DC239 showing moderately south-southwest dipping foliation.	347
Figure 5.25 Electron microprobe photograph of hornblende grain from plagioclase amphibolite DC048 from Plant Creek	348

Figure 5.26 Photomicrograph of plagioclase amphibolite DC080 in plane polarized light (a) and in cross polarized light (b).....	350
Figure 5.27 : Exposure of a boudinaged layer of migmatitic garnet–gedrite–anthophyllite amphibolite containing sample DC536.....	351
Figure 5.28 Gedrite and anthophyllite crystals up to 5 cm long in a boudinaged layer of migmatitic garnet–gedrite–anthophyllite amphibolite containing samples DC536 and DC532.....	352
Figure 5.29 Example of a migmatitic garnet–biotite–quartzofeldspathic paragneiss that makes up the dominant basement rock in the Icebound Lake area..	353
Figure 5.30 Details of the southwest dipping grey calc-silicate gneiss at Cariboo Alp ..	354
Figure 5.31 Photomicrograph of garnet–biotite–quartzofeldspathic gneiss DC178 in plane polarized light (a) and in cross polarized light (b).....	356
Figure 5.32 Photomicrograph of garnet–biotite–quartzofeldspathic gneiss DC178 in plane polarized light (a) and in cross polarized light (b).....	358
Figure 5.33 Moderately southwest dipping rusty-weathering garnet–sillimanite–biotite paragneiss DC193 at Cariboo Alp.	359
Figure 5.34 Details of the rusty-weathering garnet–sillimanite–biotite paragneiss DC193 at Cariboo Alp.	360
Figure 5.35 Moderately foliated garnet–plagioclase–biotite amphibolite at Cariboo Alp.	361
Figure 5.36 Typical exposure of the moderately southwest dipping migmatitic semipelitic biotite paragneiss at Fawn Lakes.	362

Figure 5.37 Semipelitic garnet–biotite paragneiss of sample DC330 in the Fawn Lakes area.	363
Figure 5.38 Pegmatite of the Ladybird granite crosscutting garnet–biotite paragneiss at Mount Symonds.	364
Figure 5.39 Photomicrograph of garnet–muscovite–biotite schist DC028 in plane polarized light (a) and in cross polarized light (b).	366
Figure 5.40 Calc-silicate amphibolite DC299 showing a transposition foliation dipping steeply to the south.	367
Figure 5.41 Migmatitic grey biotite gneiss at Cariboo Alp.	368
Figure 5.42 Detail of migmatitic grey biotite gneiss with coarse-grained granitic leucosomes crosscutting the transposition foliation.	369
Figure 5.43 Detailed view of a boudinaged leucosome in migmatitic gneiss at Cariboo Alp.	370
Figure 5.44 Conjugate Ladybird pegmatites crosscutting the transposition foliation in the rusty garnet sillimanite paragneiss at Cariboo Alp.	371
Figure 5.45 Ladybird pegmatite sample DC543 at Icebound Lake.	372
Figure 5.46 Ladybird pegmatite DC418 at Icebound Lake.	373
Figure 5.47 Typical appearance of the undeformed Ladybird pegmatite.	374
Figure 5.48 Pegmatite crosscutting moderately dipping metasedimentary country rocks at sample DC295P.	375
Figure 5.49 ⁴⁰ Ar/ ³⁹ Ar thermochronology results with sample locations.	377

Figure 5.50 Summary of all $^{40}\text{Ar}/^{39}\text{Ar}$ hornblende, biotite and muscovite cooling ages organized by structural level and location throughout the study area..... 379

Figure 5.51 Summary of all $^{40}\text{Ar}/^{39}\text{Ar}$ hornblende, biotite and muscovite ages, presented as individual sample ages with error bars. 381

Figure 6.1 Summary of interpretations of the thermotectonic evolution of the Thor-Odin – Pinnacles area as presented in this study..... 409

Figure 6.2 Model for the Late Cretaceous to Eocene evolution of the Thor-Odin dome as proposed in this study.....411

1 Chapter: Introduction

1.1 Purpose of this study

The Monashee Mountains of British Columbia (Figure 1.1) are located in the core zone of the southeastern Canadian Cordillera which comprises polydeformed, generally high grade metamorphic rocks. The approximately 50 x 20 km study area, southwest of Revelstoke, exposes deep to mid-crustal rocks in a structural window in the footwall of the east dipping Columbia River normal fault (Figure 1.2). The study area is made up of a generally southwest to southerly dipping panel of rocks that has a roughly 12 km structural thickness and another 4 – 5 km panel of rocks with variable dips structurally overlying them (Figures 1.3, 1.4). The deepest structural levels are exposed in the northern part of the study area, in the core of the high grade metamorphic, migmatitic, Paleoproterozoic basement-cored Thor-Odin dome. They are structurally overlain by Laurentian-derived metasedimentary rocks which are in turn overlain by metamorphosed rocks of the pericratonic and the most inboard of the accreted terranes (Monger and Price 2000).

The rocks of the study area, located to the west of the eastern foreland thrust and fold belt, are of interest because they were being penetratively deformed in the mid-crust, and in part exhumed, during the Cretaceous to Eocene constructional phase of orogenesis. This study investigates the rocks of this structural window in order to clarify

the affinity and age of Cordilleran basement rocks, timing of Proterozoic to Mesozoic sedimentation on the Laurentian margin and the most inboard of the accreted terranes, as well as the history of progressive mid-crustal deformation and eventually cooling paths during orogenesis.

1.2 Tectonic setting of the southeastern Canadian Cordillera

The rocks of the southeastern Canadian Cordillera have a protracted history of deformation and metamorphism. At the present latitude of the southern Canadian Cordillera, the orogeny developed into a doubly-vergent, medium-sized, warm orogenic belt (Evenchick et al. 2007; Simony and Carr 2011) in a transpressional setting during the Cretaceous to Eocene (Monger and Price 2000). The main periods of crustal thickening and shortening of supracrustal rocks in the eastern retrowedge side of the orogeny occurred between c. 100 Ma and 52 Ma (Simony and Carr 2011 and references therein). Crustal shortening on the western edge of the Laurentian craton occurred in the Jurassic and continued until the Late Cretaceous to Paleocene and juxtaposed parautochthonous and oceanic terranes with the Laurentian miogeoclinal successions (Monger et al. 1982; Colpron et al. 1996). By the Middle Jurassic some of the accreted terranes (e.g. the Slide Mountain ocean basin and the juvenile oceanic arc rocks of the Quesnel terrane) had been obducted over the pericratonic Kootenay terrane (Brown et al. 1986; Ross et al. 2005). The collision of the Alexander and Wrangell terranes with the Cordilleran margin occurred during the mid-Cretaceous to Tertiary (Monger et al. 1982;

Monger and Journeay 1994). Contractional deformation ended during the Paleocene-Eocene when the southern Cordillera experienced a period of widespread crustal extension due to changes in the relative motion of the Kula plate (Lonsdale 1988; Andronicos et al. 2003). Eocene regional extension, accommodated by mainly north-south striking normal faults and synchronous east-west oriented strike-slip faults resulted in the exhumation of the high grade rocks exposed in the Monashee Complex (Monger et al. 1982; Parrish et al. 1988; Johnson and Brown 1996; Johnson 2006).

Following the terminology presented by Carr and Simony (2006), the southeastern retrowedge of the Canadian Cordillera, in southeastern British Columbia (Figure 1.2), can be discussed in terms of a belt which contains an internal and external zone, separated roughly along the southern Rocky Mountain Trench (Figure 1.3), with thrusts in the external zone linked to mid-crustal flow zones in the internal zone.

The foreland thrust and fold belt, containing the Foothills, Front and Main ranges of the Rocky Mountains make up the external zone of the orogen. It comprises Paleozoic and Mesozoic North American platformal and marginal strata and Mesozoic to Paleocene Alberta foreland basin deposits deformed in the Cretaceous to Paleocene crustal shortening during the Cordilleran orogeny (Gabrielse et al. 1991; Monger and Price 2000; Carr and Simony 2006 and references therein). The Western Rockies as well as the Purcell, Cariboo, Selkirk and Monashee Mountains make up the internal zone of the

orogen, composed of Proterozoic to Mesozoic North American rocks and the pericratonic Kootenay terrane rocks. The internal zone has different structural levels exposed in different areas: the eastern internal zone preserves the Middle Jurassic to Early Cretaceous tectonothermal history with younger overprints, while the western internal zone has the exhumed tracts of high grade metamorphic rocks with the mid-Cretaceous to Eocene deformation history. This study focuses on the history of the western internal zone, in the Thor-Odin – Pinnacles area (Figures 1.2, 1.3).

Shortening in the orogen (at least 200 km since the Jurassic) was accommodated by folding and crustal thickening of up to 50 – 60 km in the internal zone (Gabrielse et al. 1991; Monger and Price 2000). Structures in the internal zone of the orogen have been correlated with thrust faults in the foreland (Evenchick et al. 2007; Simony and Carr 2011 and references therein). The Paleocene to Eocene thrusts in the foreland include the McConnell, Lewis thrust, and the thrust faults of the foothills triangle zone (Stockmal et al. 1997; Farmor 1999; McMechan 1995, 2001; Sears 2001; Langenberg et al. 2002; Van der Pluijm et al. 2006; Price 2007; Lerbekmo et al. 2008). Based on geochronological and structural data from the papers cited above, Simony and Carr (2011) suggest that the last movement on these foreland faults occurred between c. 57 and 54 Ma, and possibly as late as c. 51 Ma.

1.3 Tectonothermal culminations

The internal zone of the orogen contains metamorphic and igneous rocks, and includes several tectonothermal culminations which expose high grade metamorphic and plutonic rocks (also known as “domes”). Some of these culminations contain exposures of Laurentian basement rocks, for example the Malton gneiss complex, Frenchman Cap dome and the Thor-Odin dome (Murphy 1987; Parkinson 1991; Armstrong and Parrish 1991). In others, for example, the Kettle-Grand Forks dome, the Okanagan dome, the Priest River complex, and the Valhalla dome, the basement rocks are not exposed (Carr 1987; Parrish et al. 1988; Doughty and Price 1999; Hallett and Spear 2011). These domes have all been described as metamorphic core complexes (Ewing 1980; Armstrong 1982; Coney and Harms 1984). Metamorphic core complexes are characterized by domal culminations of deeply exhumed, high grade metamorphic rocks bounded by shallowly outward dipping normal faults with low grade metamorphic rocks in the hanging walls (Whitney et al. 2013). The formal definition as stated by Whitney et al. (2013) is: *“A core complex is a domal or arched geologic structure composed of ductilely deformed rocks and associated intrusions underlying a ductile-to- brittle high-strain zone that experienced tens of kilometers of normal-sense displacement in response to lithospheric extension”*. As a descriptive term, this definition fits all the complexes mentioned above; however, the specific mechanisms proposed to explain the tectonic evolution of the domes of the southeastern Canadian and northwestern United States vary, as discussed in subsequent paragraphs. This study aims to clarify the Paleocene – Eocene evolution of the Thor-Odin dome with reference to some of the main

mechanisms that have been proposed to explain the evolution of other domes in the North American Cordillera.

Models that have been applied to explain the evolution of the Thor-Odin and Frenchman Cap domes include channel flow models (Glombick 2005; Teyssier et al. 2005; Brown and Gibson 2006; Lemieux 2006; Kuiper et al. 2006; Williams et al. 2006; Gervais and Brown 2011) and thrust sheet models (Brown et al. 1986; McNicoll and Brown 1995; Price 1994, 2001). Diapirism has been investigated as an important process in the Shuswap Complex and the Thor-Odin dome (Norlander et al. 2002; Vanderhaeghe et al. 1999, 2003; Teyssier et al. 2005; Gordon et al. 2008). Diapirism has also been proposed to be the driving force for exhumation in the Valhalla dome (Kruckenberg et al. 2009). In contrast, it has been proposed that transport of a ductile thrust sheet up a pre-existing basement ramp (Hallett and Spear 2011) and decompression melting in pelitic rocks (Carr and Simony 2006) is responsible for the structural culmination in the Valhalla dome. The relative importance of exhumation along Eocene extensional fault systems (Parrish et al. 1988; Thompson et al. 2004, 2006; Brown 2010) is also under debate.

1.4 Shuswap Complex terminology

The nomenclature used to refer to the tracts of high grade metamorphic rocks in the western internal zone has been problematic. The study area is part of what has been

considered a larger metamorphic domain, the Shuswap Complex. The term “Shuswap Complex” refers to the tract of high grade metamorphic rocks within the sillimanite isograd (the pink areas on Figure 1.1) (Okulitch 1984). Some of the rocks in the eastern internal zone preserve Early Cretaceous metamorphic ages, for example those in Cariboo – Monashee – Selkirk Mountains and the Purcell Mountains (Simony and Carr 2011). Other areas of the Shuswap Complex have rocks preserving Late Cretaceous to Eocene metamorphic ages, for example those exposed in the footwalls of the Okanagan Valley – Eagle River, Columbia River, and the Slocan Lake – Champion Lake fault systems; all Eocene, low to moderate angle, extensional faults that juxtapose Cretaceous to Paleocene high grade footwall metamorphic rocks with low to medium grade hanging wall rocks with Jurassic age metamorphism (Parrish et al. 1988; Johnson and Brown 1996; Johnson 2006 and references therein). At the latitude of the Thor-Odin dome, the eastern margin of the Shuswap Complex is the east dipping Columbia River normal fault (Read and Brown 1981; Parrish et al. 1988) and the western margin is the west dipping Okanagan Valley – Eagle River normal fault system (Tempelman-Kluit and Parkinson 1986).

The original definition of the Shuswap Complex (or “Shuswap Metamorphic Complex” as it is also called) was as an area roughly delineated by the sillimanite-in isograd in the south-eastern Cordillera (Reesor 1970; McMillan 1973; Okulitch 1984). This definition did not take into account the possibility that the timing of sillimanite grade

metamorphism is different throughout the “complex”, and that there are complicated overprinting relationships in both deformation and metamorphism documented within this area (Simony and Carr 2011 and references therein). The assignment of sillimanite grade rocks to the Shuswap Complex without recognition of different periods of metamorphism continued to be present in the literature in different forms with subsequent workers (e.g. the “Middle Unit” of Vanderhaeghe et al. 1999, 2003; the “mid-crustal zone” of Carr 1990; the Selkirk Allochthon of Brown et al 1986). The rocks in the Thor-Odin dome – Pinnacles area make up a complex structural section with diachronous metamorphism and deformation histories (this study) in the Late Cretaceous, Paleocene, and Eocene. Each of these phases of metamorphism and deformation may overprint older metamorphism, therefore, the description of this area as a part of the “Shuswap Complex” should be viewed more as a geographic term rather than a genetic one.

Based on the geology of the Thor-Odin – Pinnacles area, Carr (1991) proposed a three-fold tectonic division to represent the relative structural levels during the Eocene, of rocks now exposed. In this framework, the rocks in the hanging walls of the extensional faults represent an “Upper Crustal Zone”, the high grade metamorphic rocks in the footwalls of the extensional faults a “Mid-crustal Zone”, and the rocks in the Thor-Odin dome represent the “Basement Zone”. This Mid-crustal Zone has also been referred to as the “Middle Unit” by Vanderhaeghe et al. (1999, 2003) to discuss the footwall rocks.

In the Frenchman Cap dome, to the north of the Thor-Odin dome, the term “Selkirk Allochthon” was used by Brown et al. (1986) and other workers to refer to the rocks that were thrust over the Laurentian basement rocks. Another division refers to the rocks in the footwalls of the extensional faults in the Frenchman Cap area as the “Lower Selkirk Allochthon”, and the rocks in the hanging walls of the extensional faults as the “Upper Selkirk Allochthon” (Gervais 2009).

The Thor-Odin – Pinnacles study area is described here with reference to its current position in the footwall of the Columbia River fault. However, to better illustrate the evolution of these footwall rocks through time, the area is described in terms of orogenic infrastructure and suprastructure. The infrastructure-suprastructure framework used here reflect the use of the terms by Murphy (1987), Williams and Jiang (2005), Carr and Simony (2006) and Culshaw et al. (2006) in which the lower structural levels of the Cordillera (and other orogenic belts) are composed of high grade, penetratively deformed metamorphic rocks with transposed structures in isoclinal regional folds. The upper structural levels, or suprastructure, contain rocks of lower metamorphic grades, with variably oriented upright open folds, and thrust faults. An important contribution of this study is to extend the definition and description of infrastructure-suprastructure associations in the study area to include a temporal dimension, recognizing that these divisions are dynamic and the boundary between suprastructure and infrastructure migrates with time.

1.5 Geological setting of the Thor-Odin – Pinnacles area in southeastern British Columbia

This study is based in a roughly 50 x 20 km area in the Monashee Mountains of British Columbia, west of the town of Nakusp (Figure 1.2). It is bound to the north by the Thor-Odin dome and to the south by the Pinnacles culmination and the *c.* 77 – 75 Ma Whatshan batholith. The area is bound to the east by the Columbia River fault, a shallow to moderately east-dipping Eocene age ductile-brittle normal fault which juxtaposed Middle Jurassic igneous rocks and Paleozoic to Mesozoic rocks with predominantly greenschist facies assemblages in the hanging wall against predominantly high grade metamorphic rocks which have Cretaceous to Eocene thermal and deformation histories (Parrish et al. 1988; Carr 1991a; see Chapter 2 for discussion). The area is bound to the southwest by the steeply west dipping Beaven normal fault, an approximately 500 m wide predominantly brittle fault zone that juxtaposed Triassic to Jurassic rocks preserving greenschist facies metamorphism in the hanging wall against sillimanite-muscovite bearing metamorphic rocks that preserve a Cretaceous thermal history. The Beaven fault is interpreted to be a breakaway zone of the shallowly west dipping Okanagan Valley – Eagle River fault system (Carr 1990), another Eocene age normal fault system (Tempelman-Kluit 1989; Brown 2010; Brown et al. 2012).

The Thor-Odin dome comprises an approximately 4 – 5 km exposed structural thickness of polydeformed, migmatitic rocks which includes rocks of the Laurentian basement affinity and supracrustal cover rocks that have been complexly infolded with the basement rocks (Reesor and Moore 1971; Parkinson 1991; Spark 2001; Kuiper 2003; Hinchey et al. 2006). The main structural features of these rocks are well-developed transposition foliation and northeast verging isoclinal to tight folds. Figure 1.3a illustrates the southwest dipping rocks that overlie the Thor-Odin dome, and the complex fold interference patterns interpreted in the Thor-Odin dome cover and basement rocks (Williams and Jiang 2005).

The rocks that overlie, and in map view surround, the dome (extending to Cusson Creek) comprise a roughly 7 km thick south to southwest dipping panel of heterogeneous, polydeformed, medium- to high grade metasedimentary and metavolcanic rocks that include the South Fosthall pluton, a S-type granitic intrusion of the Ladybird granite suite (Carr 1991). The rocks in the structurally lower part of this section, structurally below the South Fosthall pluton, are migmatitic, while the rocks structurally above the pluton are generally high grade K-feldspar-sillimanite to sillimanite-muscovite bearing rocks. Transposition foliations are found throughout these rocks. Within the part of the study area between the South Fosthall pluton and Cusson Creek there are klippen of the hanging wall of the Columbia River fault (Read and Brown 1981), in which greenschist facies Jurassic rocks are in fault contact with high grade footwall rocks with Cretaceous

to Eocene thermal and deformation histories (see Chapter 3 of this study for discussion of these klippe). Figure 1.3b illustrates the south to southwest dipping geometry of the rocks exposed on the surface and shows the interpretation of the subsurface structure, based in part on Lithoprobe seismic reflection surveys (summary in Cook et al. 1995).

South of Cusson Creek, the Whatshan – Pinnacles area is a further 4 – 5 km structural thickness of rocks that have a distinct structural style and metamorphic and deformation histories different from the structurally deeper rocks. These rocks are polyfolded with Type 3 interference patterns, and lack the transposition foliations found in the deeper rocks. All together, the study area effectively represents a roughly 15 – 17 km thick tilted structure section with the deepest exposed rocks in the north.

There are a number of volumetrically significant igneous units of Mesozoic to Eocene age in the study area. Some of the important igneous rocks discussed in subsequent sections of Chapter 2 include the Jurassic Nelson suite (Armstrong and Parrish 1987), the Cretaceous Whatshan batholith (Carr 1992), the Paleocene to Eocene Ladybird granite (Carr 1990; Hinchey et al. 2006) and the Eocene Three Valley lamprophyre suite (Adams et al. 2005). The Jurassic to Eocene intrusive rocks in the study area are important as strain markers, and in providing geochronological constraints on timing of deformation used to make interpretations regarding the evolution of the rocks. They also mark major

periods of igneous activity found throughout the Canadian Cordillera (Parrish et al. 1988; Gabrielse and Yorath 1991; Parrish 1995).

1.6 Specific questions addressed in this study

Chapter 2 of this study addresses the geology of the study area with respect to structure and the timing of deformation and metamorphism of the medium to high grade metamorphic rocks. This is done by integrating petrology and structural mapping with published U-Pb zircon and monazite geochronology data relating to the timing of metamorphism, deformation, and igneous intrusive events. The deformation and thermal history before the onset of cooling (as discussed in Chapter 5) is relevant to reconstructing the tectonic evolution of penetratively deformed infrastructural flow zones.

Chapters 3 and 4 of this study address the provenance of the protoliths of the rocks, using U-Pb detrital zircon geochronology by laser ablation inductively-coupled mass spectrometry (LA-ICP-MS). Chapter 3 presents the first detrital zircon U-Pb data from quartzites in the Thor-Odin dome (Mount Thor, Icebound Lake, and Cariboo Alp) in order to demonstrate that only some of the quartzites in the Thor-Odin dome are correlative to each other, and to determine whether or not the basal quartzites in the Thor-Odin and Frenchman Cap domes have protoliths of the same age (Read 1980) and together make up one domain, the Monashee Complex. This may suggest that the

domes have a shared Proterozoic history and acquired their current geometry by the same processes, for example, exhumation of basement rocks via channel flow (Gervais and Brown 2011) or exhumation of basement rocks via diapirism (Teyssier et al. 2005). If the two domes do not share a Proterozoic depositional history, they may have been juxtaposed later in their evolution, implying that they may have different Cretaceous to Eocene exhumation histories and that the two domes in the “Monashee Complex” may be better described as two separate domains.

Chapter 4 presents U-Pb detrital zircon geochronology from quartzite marker units in the high grade metamorphic rocks overlying the Thor-Odin dome in order to test two main hypotheses relating to the age of the rocks in this panel. The first hypothesis is that they are Neo-Proterozoic to Early Cambrian at the base of the section (as represented by the Mount Symonds area), ranging up to Late Paleozoic (Mississippian) at the top of the section in the Plant Creek area (Fritz et al. 1991 and references therein). The quartzites and the sedimentary and volcanic rocks associated with them were deposited on pericratonic to allochthonous terranes and subsequently accreted to the Laurentian margin during Mesozoic orogenesis (Brown et al. 1986; Price 1994). This hypothesis is based mainly on stratigraphic correlations and palinspastic cross section reconstructions with strata in the Purcell, Selkirk, and Rocky Mountains. The second hypothesis is that the quartzites and associated rocks are Proterozoic to Devonian (Thompson et al. 2004, 2006) and were deposited unconformably in a basin that formed on attenuated

Laurentian crust and subsequently shortened during Mesozoic orogenesis. This hypothesis is based mainly on mapping (Thompson et al. 2004, 2006; Glombick 2005) that reevaluated the role of the Columbia River and Okanagan Valley – Eagle River fault systems and proposed correlations of strata across faults, and on studies that suggest that the Laurentian margin extended further outboard (Erdmer et al. 2001, 2002; Petersen et al. 2004) than some reconstructions show (Brown et al. 1986; Price 1994 and references therein).

Chapter 5 addresses the timing of exhumation and cooling of the mid-crustal rocks of the study area using $^{40}\text{Ar}/^{39}\text{Ar}$ thermochronology integrated with petrology and structural mapping. It specifically addresses the high-temperature cooling histories of the mid-crustal rocks in the southern Thor-Odin dome and the structurally overlying rocks in the footwall of the Columbia River fault in order to determine whether there are different thermal domains with sharp boundaries between them that could indicate fault contacts. It also addresses the relationship between cooling histories from $^{40}\text{Ar}/^{39}\text{Ar}$ thermochronology and the infrastructure-suprastructure transitions discussed in earlier chapters, as well as the significance of the Columbia River fault in the cooling and exhumation of these rocks.

Chapter 6 summarizes the conclusions from all chapters. It also discusses the tectonic evolution of the Thor-Odin – Pinnacles area with particular emphasis on the Late Cretaceous to Eocene with reference to tectonic models proposed in the area.

EXTERNAL ZONE
(THRUST BELT)

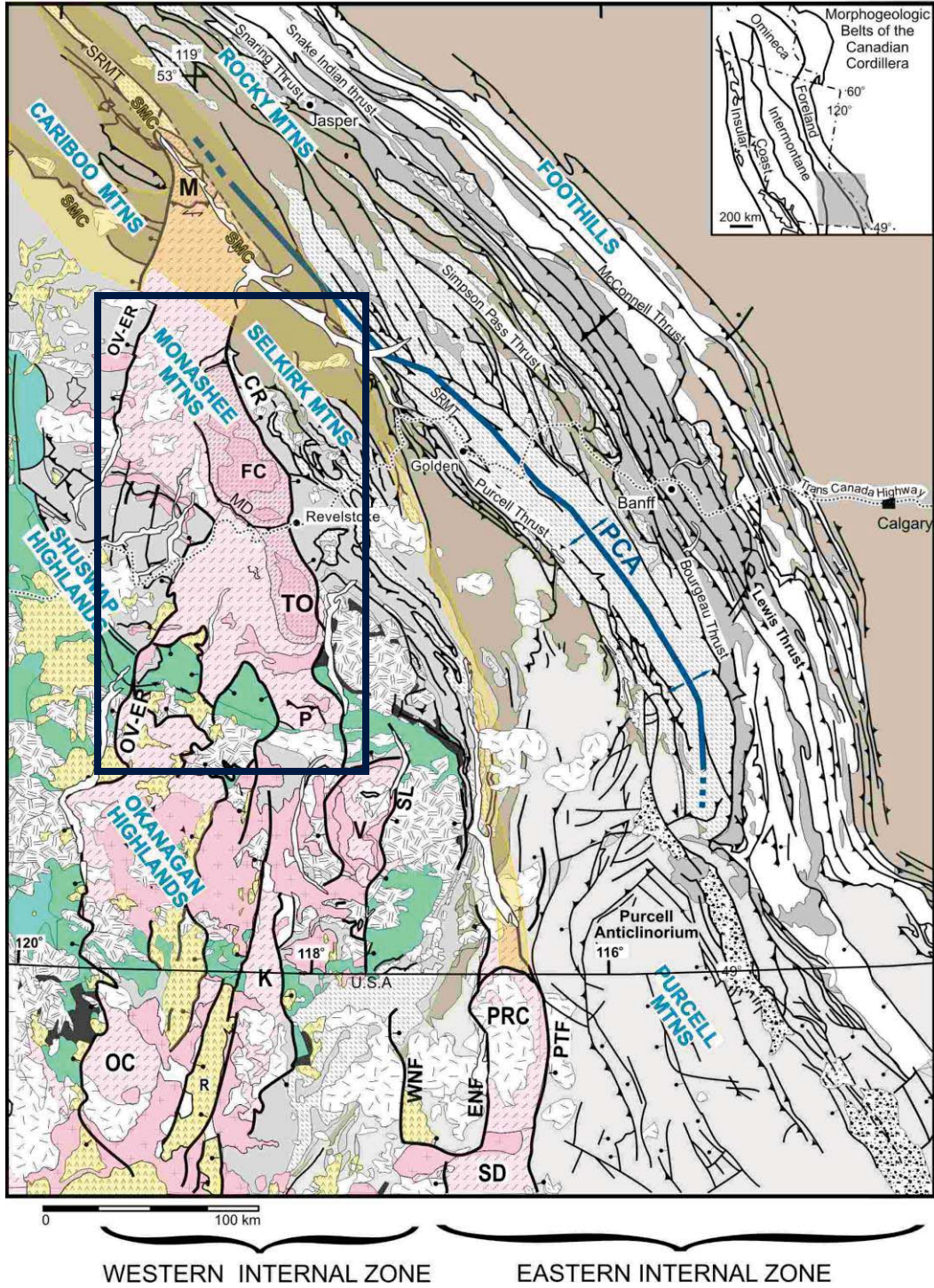


Figure 1.1a

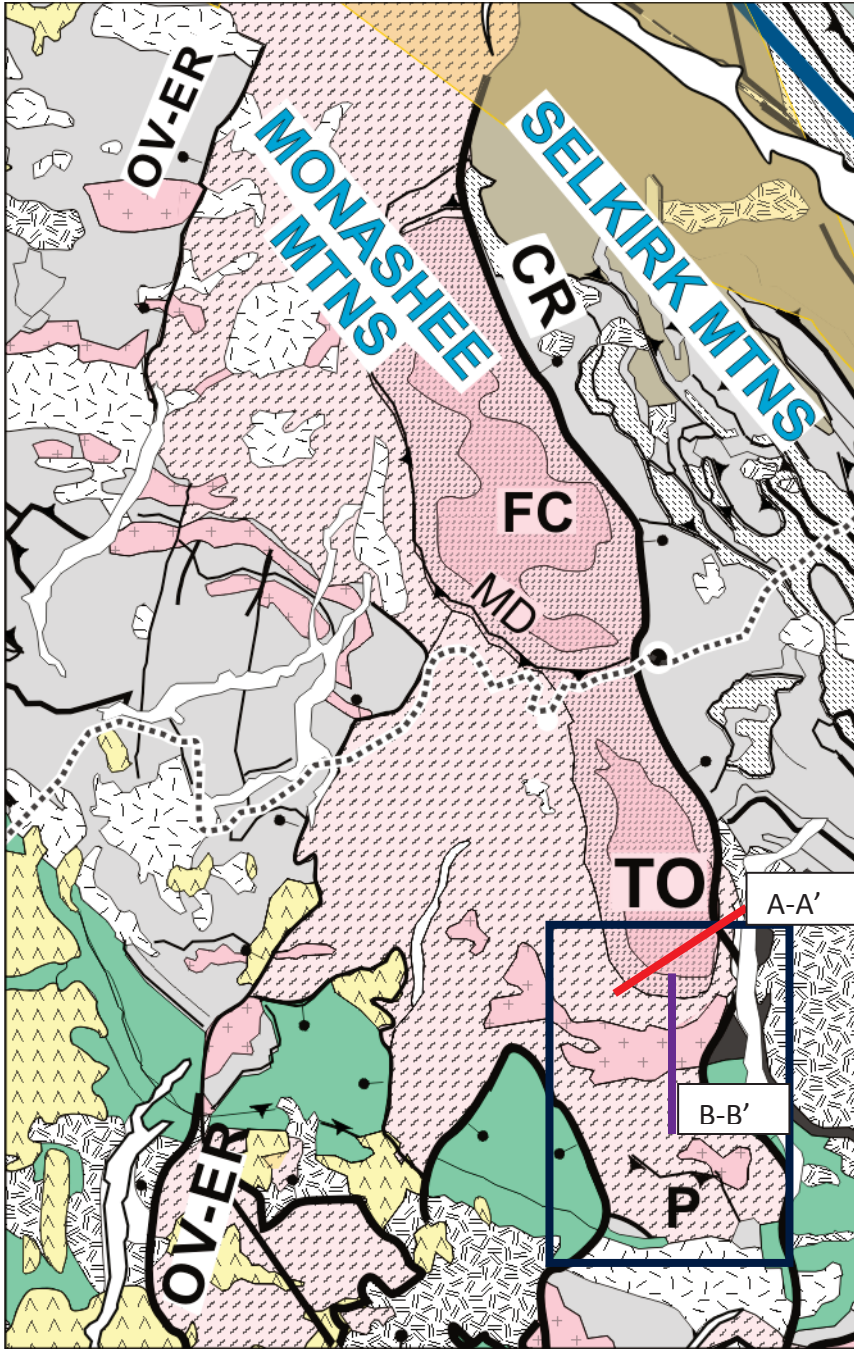


Figure 1.1b

Legend for Figure 1

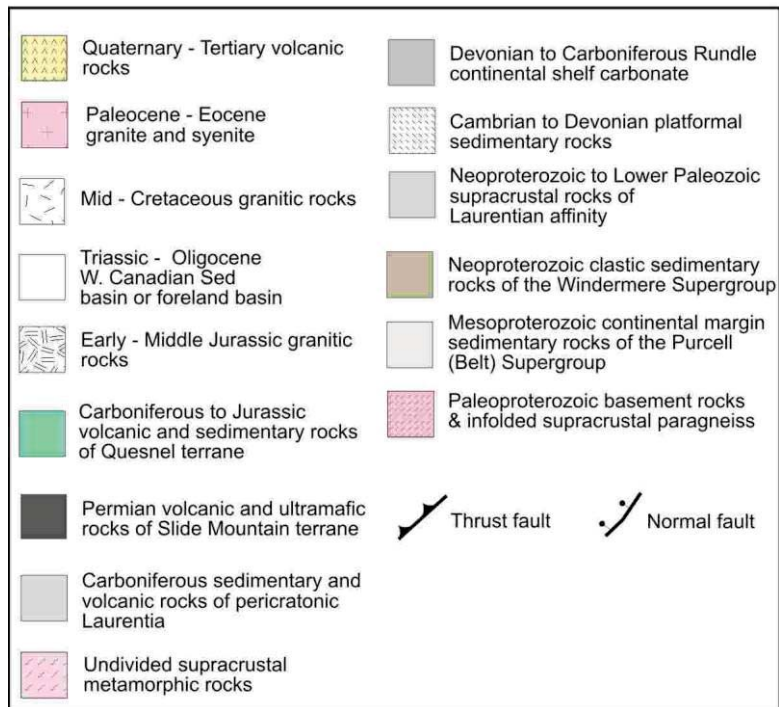
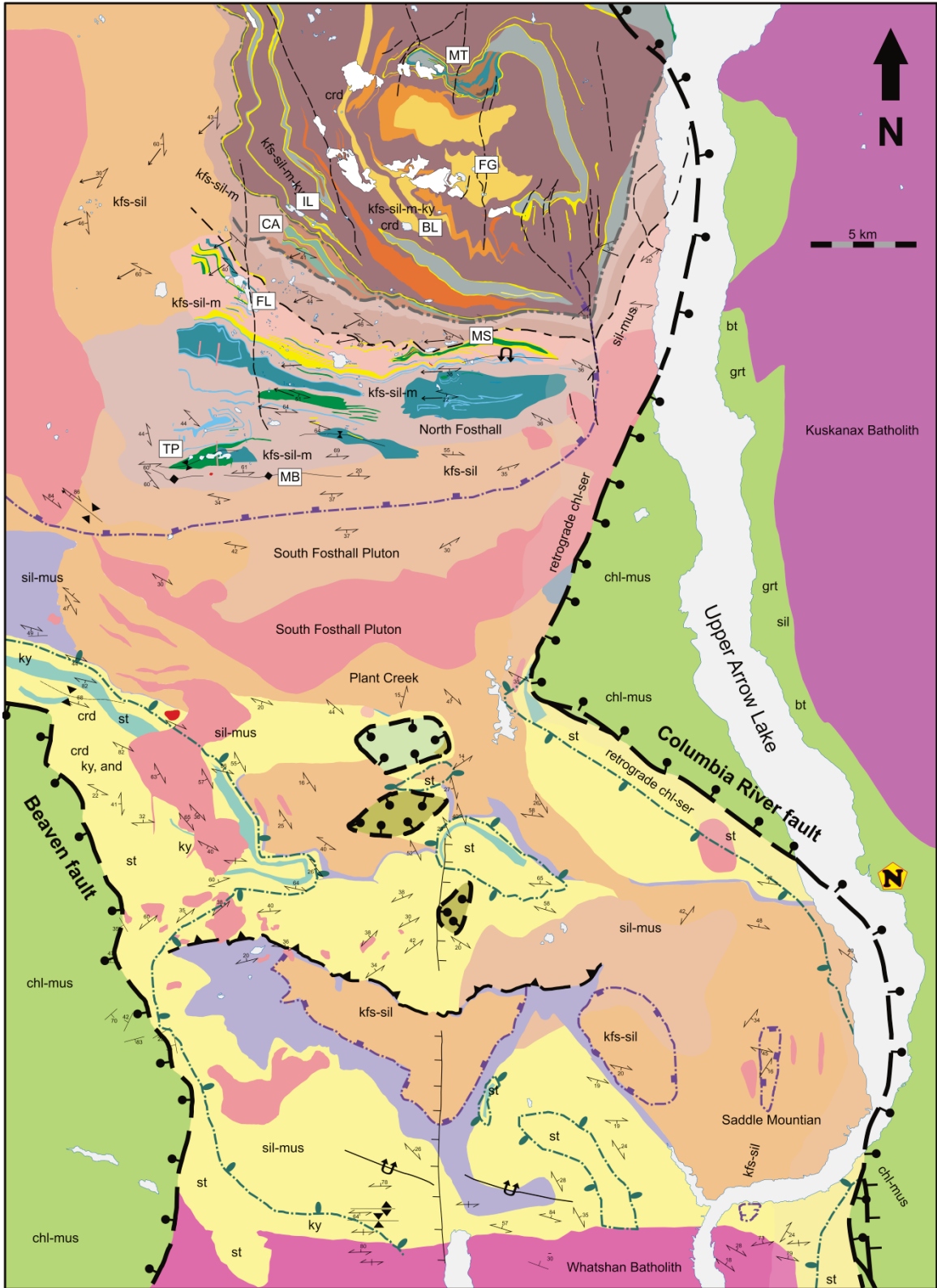


Figure 1.1 Tectonic map of the southeastern Canadian Cordillera. It shows the external, western internal and eastern internal zones, (from Simony and Carr, 2011) (Figure 1.1a). The shaded area of the inset locates the map within the morphogeological belts of the Canadian Cordillera. The rectangle indicates the location for cut-out Figure 1.1b. In Figure 1.1b the rectangle outlines the Thor-Odin – Pinnacles study area shown in Figure 1.2.

In the eastern internal zone, PRC = Priest River Complex and bounding Western (WNF) and Eastern Newport faults (ENF). PTF = Purcell Trench fault and SD = Spokane dome; in the western internal zone, K = Kettle – Grand Forks Complex, OC = Okanagan – Okanagan complex, R = Republic Graben, V = Valhalla complex; and complexes with basement rocks include the Frenchman Cap dome (FC); Malton complex (M); and Thor-Odin dome (TO). Eocene normal fault systems that bound high grade rocks in the Western Internal zone include the Okanagan Valley – Eagle River fault system (OV-ER); Columbia River fault (CR), and Slocan Lake-Champion Lake fault systems (SL). PCA = Porcupine Creek Anticlinorium; SMC = Selkirk-Monashee-Cariboo metamorphic complex; SRMT = southern Rocky Mountain Trench.

The two cross section lines on Figure 1.1b indicate the locations of cross sections A-A' (red) and B'B' (purple) in Figure 3.



LEGEND for Map

Rocks in the hanging wall of the Columbia River Fault

Intrusive rocks

-  **Kuskanax batholith** – Middle Jurassic ca. 170 Ma (Parrish and Wheeler 1983).
Part of the Nelson Intrusive Suite, which includes granite, syenite, diorite.

Metasedimentary and metavolcanic rocks

-  **Rossland Group** metavolcanic rocks including breccia, tuff, basalt, augite porphyry. (Lower Jurassic)
-  **Slocan Group** siliciclastic rocks including phyllite, argillite, quartzite and minor volcanoclastic tuffs. (Upper Triassic)
-  Generally greenschist to lower amphibolite grade metavolcanic rocks including breccia, tuff, basalt, augite porphyry, siliciclastic and carbonate rocks including phyllite, argillite, quartzite, marble, and minor volcanoclastic tuffs. The hanging wall rocks in the Columbia River Fault (E) and the Beavan Fault (W) include Paleozoic - Lower Jurassic stratified rocks from the Kaslo, Slocan and Rossland Groups as well as Hamill, Badshot, Lardeau and Milford Groups. Rocks in the footwall of these faults are interpreted as the deformed and metamorphosed equivalents of some of these rocks.

Rocks in the footwall of the Columbia River Fault

Intrusive rocks

-  **Ladybird Granite Suite** – Late Paleocene to Eocene ca. 62 – 55 Ma (Carr 1992)
Biotite granite to quartz monzonite +/- garnet, muscovite, tourmaline. occurs as dykes, stocks, sills, makes up the South Fosthall Pluton dated at 55 ± 1.5 Ma (Parrish et al. 1988). Occurs as pegmatite, aplite and granite.
-  **Whatshan batholith** – Late Cretaceous ca. 77 Ma (Carr 1990)
Hornblende - potassium feldspar quartz monzonite to diorite

Metasedimentary and metavolcanic rocks

Proterozoic to Jurassic metasedimentary and metavolcanic rocks of autochthonous and pericratonic affinity (Van Rooyen et al. 2010, Carr 1991, Fritz 1991). Protoliths correlated with the Proterozoic Horsethief Creek Group of the Windermere Supergroup Group (Fawn Lakes), Cambrian Hamill and Badshot Groups (Mount Symonds) and the Paleozoic Lardeau to Milford Groups (Arrow Lake schists and Gold Range Composite units) and are as young as Middle Jurassic in the Plant Creek area.

-  **Staurolite schist**
-  **Calcareous quartzite**
-  **Arrow Lake garnet sillimanite muscovite biotite schist**
Muscovite-biotite schist +/- garnet, sillimanite, local staurolite, kyanite. Includes micaceous quartzite, minor psammitic gneiss, marble and amphibolite layers. Local carbonaceous schist and staurolite schist.
- Composite units.**
Metasedimentary and metavolcanic including migmatitic paragneiss, semi-pelitic gneiss, pelitic and semipelitic schist, amphibolite, calc-silicate gneiss, quartzite and marble.
-  **Undivided semipelite - Pelite - Amphibolite:** South of South Fosthall Pluton, includes Saddle Mountain, Viddler Ridge, continuing to Pinnacles. Psammitic, semi-pelitic, pelitic schists and gneisses: contains sillimanite and garnet; contains lenses and layers of calc-silicate schist or gneiss, marble, amphibolite or quartzite. Extensively intruded by granite and pegmatite of the Ladybird Granite Suite.
-  Undivided semipelite - Pelite - Amphibolite (above) with >50% intrusive rocks intruded by granite and pegmatite of the Ladybird Granite Suite.
-  **Ultramafic rocks,** serpentinite occurring as pods or lenses. Interpreted as a marker unit to define the base of the Lardeau group, representing obducted ocean crust.
-  **Calc-silicate - Pelite - Amphibolite - Ultramafic:** Empress marble marker to South Fosthall Pluton. Pelitic and semi-pelitic schists and gneiss, migmatitic gt-sil-bt paragneiss, sillimanite and garnet common in schists. Includes diopside hornblende calc-silicate gneiss. Contains lenses and layers of pelitic schist, quartzite, amphibolite (including garnet, plagioclase and biotite amphibolite) and marble. Ultramafic marker occurs as pods and lenses. Extensively intruded by granite and pegmatite of the Ladybird Granite Suite.
-  **Amphibolite**
-  **Marble**
-  **Calc-silicate gneiss**
-  **Quartzite**
-  **Quartzite - Semipelite - Amphibolite - Marble:** Mount Symonds to Empress marble marker unit. Semipelitic to pelitic migmatitic gt-sil-bt paragneiss interlayered with continuous layers of quartzite, marble, amphibolite and psammitic. Contains stratiform Pb-Zn deposit associated with the Empress Marble marker layer. Extensively intruded by granite and pegmatite of the Ladybird Granite Suite.
-  **Fawn Lakes paragneiss**
Migmatitic biotite-quartz-feldspar paragneiss and semipelitic gneiss. Includes garnet amphibolite boudins and layers, extensively intruded by granitic pegmatite; distinct flaggy weathering appearance, predominantly aluminum-poor throughout section, sillimanite rare. Includes minor quartzite and psammitic layers.

LEGEND for Map

Cariboo Alp rocks

-  Grey migmatitic hornblende biotite gneiss (+/- sillimanite, garnet) with amphibolite lenses and layers, hornblende diopside calc-silicate gneiss layers.
-  Rusty migmatitic gt-sil-bt paragneiss with amphibolite boudins, includes quartzite, marble layers

Thor-Odin dome rocks

-  **Cover paragneiss**
Heterogeneous psammitic and calc-silicate gneiss, pelitic (Ky-Sil) gneiss, calc-silicate gneiss with interlayered marble, amphibolite boudins and layers.
-  Pelitic and semi-pelitic schists and gneisses: Generally rich in aluminosilicate minerals and garnet. May contain lenses of quartzite, calc-silicate and amphibolite.
-  Calc-silicate and amphibolite gneiss.
-  **Basal Quartzite**
-  **Basement orthogneiss**
Hornblende-biotite granodiorite orthogneiss: Includes augen orthogneiss, biotite orthogneiss, as well as biotite granite orthogneiss and hornblende leucogranite.
-  Leucoquartz monzonite, gneissic quartz monzonite and granitic biotite orthogneiss: May contain hornblende and range in composition from granite to granodiorite.
-  Granodiorite orthogneiss
-  **Basement Paragneiss**
Predominantly migmatitic paragneiss, includes psammitic biotite-feldspar-quartz paragneiss with lenses of pelitic schist, garnet-feldspar-quartz gneiss and amphibolite. Also includes biotite-quartz-feldspar paragneiss containing abundant garnet amphibolite boudins and granitic pegmatite. Cordierite gedrite amphibolite occurs as boudinaged layers within the basement paragneiss, may contain cordierite, kyanite, spinel, olivine, garnet.

Symbols

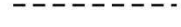
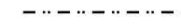
	Thrust fault		sil-kfs-melt isograd
	Normal Fault		sil-mus isograd
	Slate Mountain Shear Zone		retrograde chlorite-sericite
	Cariboo Alp Shear Zone	and	andalusite
	Normal fault, steep, < Eocene age	st	staurolite
	Normal fault, steep, unknown age	chl-mus	chlorite-muscovite
	Syncline, overturned	bt	biotite
	Syncline	grt	garnet
	Anticline	ky	kyanite
	Fold hinge, no generation assigned	crd	cordierite
	Bedding	sil-mus	sillimanite-muscovite
	Lineation, no generation assigned	sil	sillimanite
	Foliation, no generation assigned	kfs-sil	K-feldspar-sillimanite
	Contact defined (Kruse et al. 2004 compilation, this study)	kfs-sil-m	K-feldspar-sillimanite-melt
	Contact assumed (Kruse et al. 2004 compilation)	kfs-sil-m-ky	K-feldspar-sillimanite-melt-kyanite
	Contact approximate (Kruse et al. 2004 compilation)		
	Contact interpreted/compiled (Carr 1990, this study)		
	Contact interpreted/compiled (Thompson et al. 2004, this study)		

Figure 1.2 Geological map of the Thor-Odin – Pinnacles study area. This map shows metamorphic isograds, major study locations and lithology. (Modified after Reesor and Moore 1971; Carr 1990; Coleman 1990; Kruse et al. 2004; Thompson et al. 2004; Hinchey 2005.) Mineral abbreviations from Kretz (1983) except for m = melt.

Note: The legend for Figure 1.2 is applicable to figures in subsequent chapters, e.g. Figures 1.3, 2.1, 2.14.

This is a summary version of a larger map in Appendix D. Geological contacts are omitted in this figure because of the scale of the map and the page size.

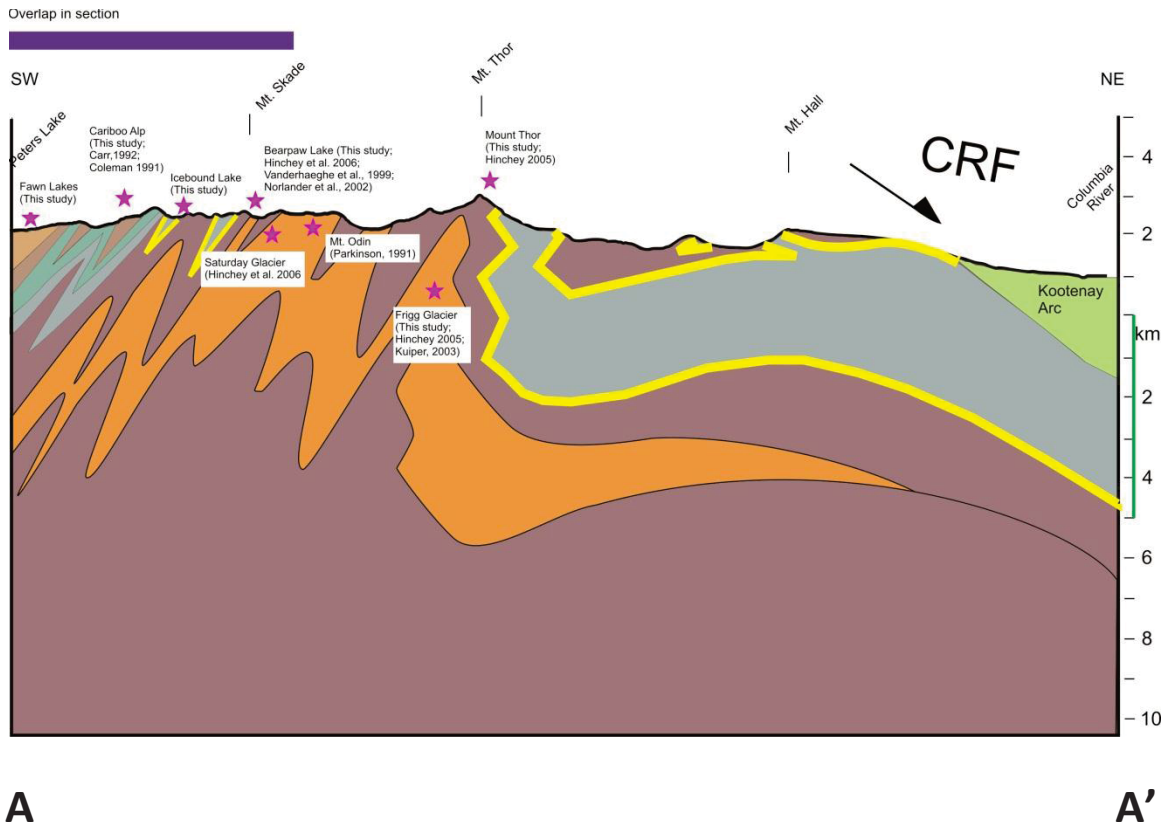


Figure 1.3a

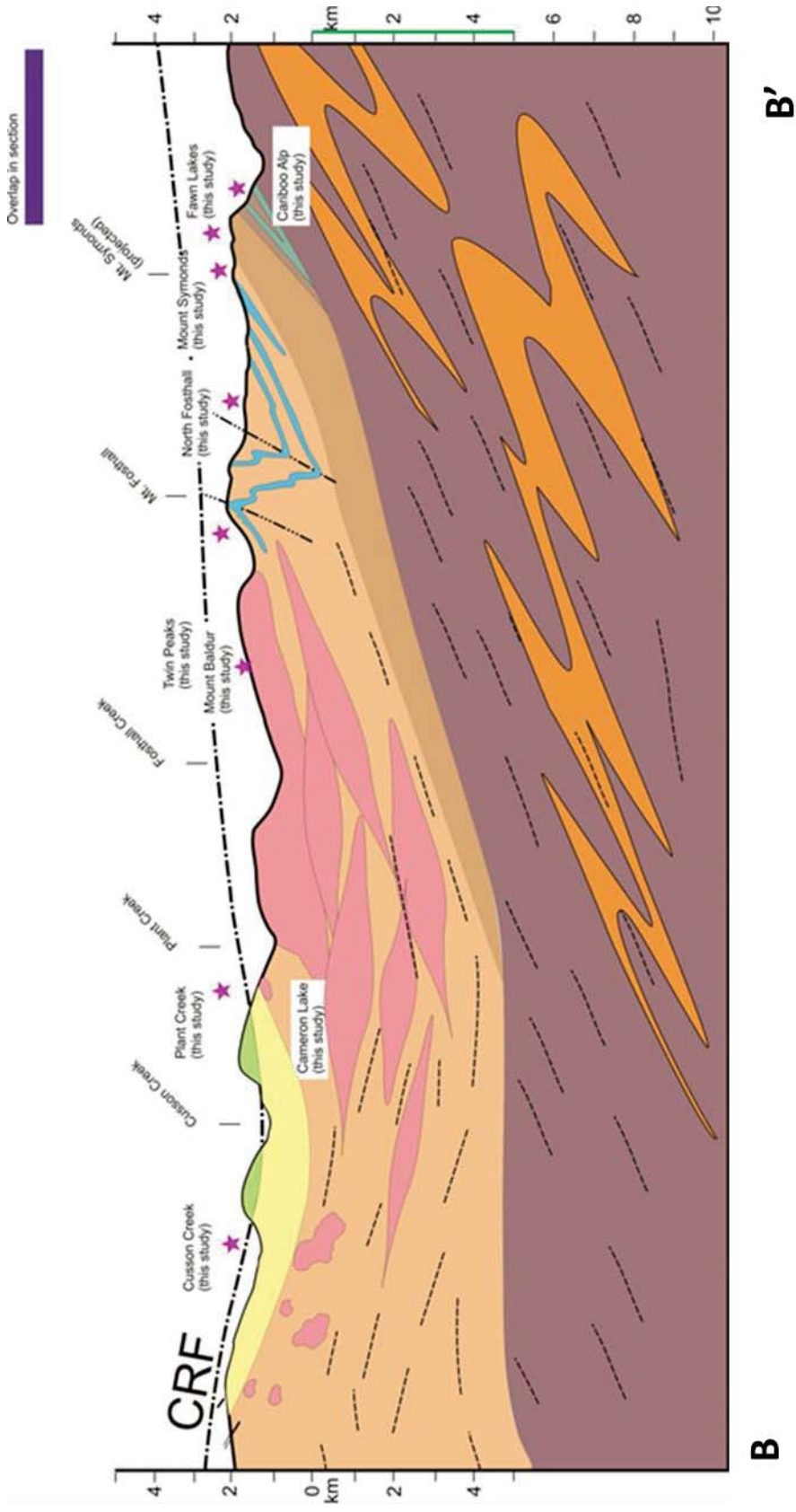


Figure 1.3: (a) Cross section A-A' through the Thor-Odin dome to the Cusson Creek area, and (b) B-B' through the south-western flank of the Thor-Odin dome in the Cariboo Alp area as illustrated in Figure 1.1b. The cross sections show that the southwest dip of the panel of rocks overlying the Thor-Odin dome is controlled by the orientation of the long limbs of the northeast verging folds. (Modified after Reesor and Moore 1971; Carr 1990; Coleman 1990; Hinchey 2005; Williams and Jiang 2005.) The stars indicate where the specific study areas project into the cross sections. Figures in Chapter 2 include more information on fold generations.

Notes: These two cross sections are summary sections intended to illustrate the structural styles seen in the study area. As such, some units have exaggerated width (e.g. the marble on Mount Symonds) and others are left out completely for clarity (e.g. the calc-silicates in North Fosthall). They are not intended as exact copies of the surface geology.

The dashed lines in the subsurface for (b) refer to interpretations of subsurface structure made from LITHOPROBE seismic reflection surveys along specific lines 6, 7, 8 and 9.

2 Chapter: Geology of the Thor-Odin – Pinnacles area: A complex history of diachronous metamorphism and deformation defining suprastructure-infrastructure transitions during the Late Cretaceous to Eocene

2.1 Introduction

This chapter introduces geology of the study locations in the Thor-Odin – Pinnacles area (Figures 1.2 and 2.1). It documents major lithological units, structural styles and map scale geometry, important intrusive igneous rocks, and integrates published data on the timing of metamorphism and deformation. This information is intended to serve as a backdrop for discussion in subsequent chapters, and as such, does not contain any conclusions or discussions regarding protolith origin of basement and overlying rocks (Chapters 3 and 4), cooling history of the rocks in the footwall of the Columbia River fault (Chapter 5) and major conclusions of this study (Chapter 6). The discussion of different areas is presented in order of structural level, with the highest levels discussed first. Figure 2.1 is a tectonostratigraphic column that summarizes locations mentioned in the text, as well as major lithological units and structural styles. Refer to Figure 1.2 for legend, the same legend which is followed throughout the text unless another legend is indicated.

The purpose of this chapter is to address the geological history of these high grade metamorphic rocks in the Thor-Odin dome – Pinnacles area (Figure 1.2), their evolution during the Cretaceous to Eocene, and their thermal history before the onset of Paleocene to Eocene exhumation and cooling. This chapter integrates a number of published geochronological, metamorphic and thermochronological datasets with new structural data, mapping, and thermochronology to construct a history of these mid-crustal rocks during the Cretaceous to Eocene. We present data supporting the interpretation that there are a number of tectonothermal belts in the Thor-Odin – Pinnacles area that each preserve different Cretaceous to Eocene deformation and metamorphic histories.

2.2 Map scale geology of the study area from the southern Thor-Odin dome and the Whatshan batholith

This section presents the map scale geometry and structure of the study area only; lithology, metamorphism, age and deformation history are explained in Section 2.4. The study area (Figure 1.2) effectively represents an approximately 15 – 17 km thick tilted structural section with the deepest exposed rocks to the north. Figure 2.1 illustrates the main structural styles of the rocks in the study area in a stylized tectonostratigraphic column. The study areas are discussed in order of increasing structural depth, starting at the top of the tectonostratigraphic column in Figure 2.1 as follows: i) Whatshan – Pinnacles, ii) Plant Creek – South Fosthall, iii) North Fosthall – Mount Symonds, iv) Fawn

Lakes – Cariboo Alp, and v) the Thor-Odin dome. Figure 2.2 shows the main lithologies and divisions of units used in this study. Note that the level of detail for different study areas varies, particularly in the coverage in Section 2.4. This is an artifact of the data available for different areas. The study areas at Bearpaw Lake, Mount Thor and Frigg Glacier were not included in field work for this study, relevant data is reported from Hinchey (2005) and others. For this reason no field photographs are included. Likewise, the Pinnacles – Whatshan areas were not included in field work and data is reported from Carr (1992, 1995) and others.

The Whatshan – Pinnacles area, in the southern part of the study area, makes up a roughly 4 – 5 km structural thickness of sillimanite–muscovite to K-feldspar–sillimanite bearing high grade metamorphic rocks. The map pattern in this area is formed by rocks which are polyfolded with Type 3 interference patterns (Carr 1991a, 1992; Glombick 2005). These rocks do not generally have transposition foliations. The rocks of the Saddle Mountain area extending across Arrow Lake in the southeast corner of the map are interpreted here as being the same structural level as Pinnacles, are correlated by use of marker units (e.g. calcareous quartzite) and are cut by the Whatshan batholith. Based on the c. 73 Ma age of deformed pegmatites at Joss Mountain and the c. 70 ma age of undeformed ones, and the structural styles along with lithological similarities, this structural level is considered to be equivalent to the Joss Mountain area on the western flank of the Thor-Odin (Carr 1992; Johnston et al. 2000).

The central part of the study area, the Plant Creek – South Fosthall area, comprises a structural thickness of approximately 2 – 3 km. Contained within this central area between the Pinnacles culmination and the South Fosthall pluton are study areas at Plant Creek, Cusson Creek, and Cameron Lake. In general, the map pattern is controlled by tight asymmetric F3 folds with moderate to steeply dipping axial planes that fold the dominant foliations and earlier F2 fold generations (Carr 1991a). The axial planes of folds north of Plant Creek dip to the south, and axial planes of folds south of Cusson Creek dip to the north, exposing metamorphic rocks, with the youngest protoliths of this study area, in the core of a syncline. This structural interpretation is supported by the geometry of crustal reflectors imaged by the Lithoprobe survey as shown on Figure 1.3 as dashed lines in the subsurface. The rocks in the Plant Creek, Cusson Creek and South Fosthall areas include sillimanite–muscovite bearing rocks, locally containing staurolite, and ranging to sillimanite–K-feldspar bearing high grade rocks closer to the South Fosthall pluton. Within this part of the study area there are klippen of the hanging wall of the Columbia River fault, where greenschist facies Jurassic rocks are in fault contact with the high grade footwall rocks with Cretaceous to Eocene thermal and deformation histories (See Chapter 4 for further discussion of these klippen).

The North Fosthall area, from the South Fosthall pluton to the southern margin of the Thor-Odin dome (including study areas at Twin Peaks, Mount Symonds, Fawn Lakes; and

Cariboo Alp) makes up a structural thickness of roughly 4 – 5 km (2 – 3 km of which are within the boundaries of the South Fosthall pluton). The rocks structurally above the pluton are sillimanite–K-feldspar to sillimanite–muscovite bearing while the rocks in the lower part of this section, structurally below the South Fosthall pluton, are migmatitic. The rocks between the South Fosthall pluton and the southern margin of the Thor-Odin dome (Figure 1.2) comprise a south-southwest dipping panel (Figure 1.3) of heterogeneous, polydeformed, medium to high grade metasedimentary and metavolcanic rocks (Carr 1991a). The map pattern is created by northeast verging km-scale tight asymmetric F2-F3 folds with moderate to steeply dipping axial planes (Reesor and Moore 1971; Carr 1991a) which fold a pervasive transposition foliation present in all the rocks. The southeastern dip of the panel is controlled by the long limbs of the F2 – F3 folds. Figure 1.3b illustrates the south-southwest dipping geometry of the rocks exposed on the surface and shows the interpretation of the subsurface structure, based, in part, on Lithoprobe seismic reflection surveys (summary in Cook 1995).

The southwestern margin of the Thor-Odin dome at Cariboo Alp area is an approximately 1 km thick structural package of highly strained rocks with a pervasive southwest dipping transposition foliation and northeast verging isoclinal folds (Reesor and Moore 1971; McNicoll and Brown 1995). The structural interpretation of the margin of the dome is controversial and has been interpreted as a ductile thrust fault, part of a shear zone termed the Monashee décollement (Brown et al. 1992; McNicoll and Brown

1995), the border of a diapir (Norlander et al. 2002; Fayon et al. 2004; Vanderhaeghe 1999; Vanderhaeghe et al. 2003), or as a high strain zone that formed as a result of ductile extension during normal faulting (Kruse and Williams 2007). It has also been proposed that there is no structural break at the Monashee décollement and that the highly strained rocks are part of a zone of crustal channel flow that includes both the dome and overlying rocks (Johnston et al. 2000; Kuiper et al. 2006; Williams and Jiang 2005; Williams et al. 2006).

The Thor-Odin dome comprises a roughly 4 – 5 km structural thickness of polydeformed, migmatitic rocks which includes rocks of the Laurentian basement affinity and supracrustal cover rocks complexly infolded with the basement rocks (Reesor and Moore 1970; Parkinson 1991; Hinchey et al. 2006 and references therein). Specific locations within the dome include Icebound Lake (IL), Bearpaw Lake (BL), Mount Thor (MT), and Frigg Glacier (FG). Northeast verging isoclinal F1 folds and tight asymmetric coaxial F2 and F3 folds occur generally dip to the southwest on the southwestern flank of the dome. All areas of the Thor-Odin dome and overlying rocks were affected by F4 folds; broad, upright folds which gently arch older structures. In the rocks overlying the Thor-Odin dome this folding did not significantly alter the map pattern created by F3 folds, but in the Thor-Odin dome itself F4 folding was in part responsible for the outward dipping domal geometry of the culmination (Williams and Jiang, 2005). In other words, the shape of the Thor-Odin dome is interpreted as a result of the interference

pattern between the late F4 and the dominant Eocene age F2 – F3 structures within the dome (Hinchey, 2005; Williams and Jiang, 2005).

The map in Figure 1.2 includes metamorphic mineral isograds (K-feldspar–sillimanite, K-feldspar–sillimanite–melt, sillimanite–muscovite, staurolite) that are drawn across the study area. It is important to note that the isograds in the rocks exposed in the footwall of the Columbia River fault do not represent metamorphic events that are all the same age. For example, the K-feldspar–sillimanite isograds include K-feldspar–sillimanite metamorphism that is Early Cretaceous (e.g. Whatshan – Pinnacles area; Carr 1992; Glombick 2005; Lemieux 2006) as well as Late Cretaceous to Paleocene (e.g. South Fosthall, Twin Peaks; Carr 1991b, 1992; Glombick 2005; Lemieux 2006). The isograds give a broad overview of the metamorphic rocks in the area, and although different grades for rocks may have been metamorphosed at different times, the isograds they do not bound metamorphic zones of different ages. The timing constraints on metamorphism and deformation will be discussed for each area in Section 2.4.

2.2.1 Jurassic intrusive rocks – Kuskanax batholith and Nelson intrusive suite

Note: in this chapter the ages quoted in the text without errors are averages or compilations from several published works. For this reason errors are not included in the text summary, the exact ages with errors from specific studies can be found in the

compilation figures using the tectonostratigraphic columns like Figure 2.1 at the end of the chapter.

The Kuskanax batholith, located in the hanging wall of the Columbia River fault in the eastern part of the study area (Figure 1.2) is a Jurassic hornblende–biotite monzonite to leucogranite and leucosyenite (Wheeler 1965; Parrish and Armstrong 1987) with igneous U-Pb zircon and titanite U-Pb crystallization ages of c. 175 to 170 Ma (Parrish and Armstrong 1987; Carr 1991b). It is part of the calc-alkalic granodioritic Nelson intrusive suite which is c. 160 Ma and older (Parrish and Armstrong 1987). The intrusions are syn- to post-tectonic, and crosscut Middle Jurassic (and older) folds and foliations. The surrounding country rock contains chlorite. The metamorphic minerals in the contact aureole include garnet and biotite with local sillimanite (Read and Wheeler 1976; Parrish and Armstrong 1987; Colpron et al. 1996).

2.2.2 Cretaceous intrusive rocks – Whatshan batholith

The Whatshan batholith marks the southern border of the study area. It is a Late Cretaceous hornblende–quartz monzonite to diorite intrusive suite that has igneous U-Pb zircon and titanite U-Pb crystallization ages of c. 80 – 75 Ma (Carr 1991b, 1992). Metamorphic minerals in the contact aureole include biotite, garnet, sillimanite, and local kyanite and staurolite (Carr 1992; Glombick 2005). The Whatshan batholith crosscuts penetrative structures in the country rocks (Carr 1992) and in turn is cut by

both the Beaven and the Columbia River faults (Figure 1.2). The Whatshan batholith and country rocks of the Pinnacles area are at the same structural level as the rocks in the Joss Mountain area west of the Thor-Odin dome, where temporally similar intrusive igneous rocks are present. Deformed granitic pegmatites at Joss Mountain are dated at c. 73 Ma, and undeformed ones at c. 70 Ma (Johnston et al. 2000; Kuiper 2003).

2.2.3 Late Cretaceous to Eocene intrusive rocks – Ladybird granite suite

The Ladybird granite suite is the dominant igneous suite in the Thor-Odin – Pinnacles area. The Ladybird granite is a peraluminous, anatectic leucogranite, generated from melting of the basement paragneiss of the Thor-Odin dome or similar Proterozoic protoliths (Hinchey and Carr 2006). It contains medium- to coarse-grained leucogranites (Figure 2.3) and volumetrically significant pegmatites (e.g. >50%) in some areas mapped by Reesor and Moore (1971), locally with muscovite, biotite, garnet or tourmaline (Hinchey and Carr 2006). The largest intrusion of Ladybird granite in the area is the South Fosthall pluton, a roughly 4 – 5 km thick composite laccolithic complex where sheets of granite or pegmatite are concordant with the metasedimentary layers comprising the country rock (Carr 1990). The U-Pb zircon crystallization ages for the Ladybird granite range between c. 64 and 52 Ma and are generally older towards the south in the Valhalla Complex (Parrish et al. 1988). The youngest pegmatites related to the Ladybird granite are tourmaline-bearing (Figure 2.4) and may locally be as young as c. 50 Ma on the western margin of the Thor-Odin dome (Johnston et al. 2000). The

Ladybird pegmatites at Cariboo Alp, Icebound Lake and South Fosthall to Plant Creek (Figure 2.5) areas contain muscovite as a primary igneous mineral which was sampled for thermochronology (See Chapter 5 of this study).

The area between Plant Creek and the southern Flank of the Thor-Odin dome was mapped by Reesor and Moore (1971) with respect to the volume of pegmatite or granite relative to country rock, with map units designated as having >50% granite and pegmatite or <50% granite and pegmatite. The contact of the South Fosthall pluton placed at the >50% cut-off. The Ladybird pegmatites and granites do not have chilled margins, suggesting the surrounding host rocks were still hot during their emplacement. Carr (1990) presented evidence of strain variations within the South Fosthall pluton and surrounding Ladybird granite, indicating that the Ladybird granite was intruded, in part, while penetrative deformation was ongoing. This is consistent with observations in this study of, some of the pegmatites in the Icebound Lake, Cariboo Alp, Fawn Lakes, and North Fosthall area, including and Twin Peaks (Figure 2.6) and Mount Symonds (Figure 2.7), were deformed concordantly with the host rock, indicating that they experienced at least the last increment of deformation together. Other pegmatites of the area crosscut the fabrics in the host rocks and appear undeformed (Figure 2.8). The pegmatites in the Plant Creek area, in the upper part of the structural section, crosscut all the fabrics in the host rocks, indicating that the host rocks were not actively deforming during pegmatite intrusion.

The South Fosthall pluton is located above an inferred southwest dipping ramp (see Lithoprobe reflectors in Figure 1.3 cross section) linked to the Monashee décollement at Cariboo Alp (Carr 1991a). The South Fosthall pluton is located between the shallowly east dipping Columbia River fault and the moderately west dipping Beaven fault, interpreted to be a splay of the Okanagan Valley fault system (Carr 1991b). The structures in the South Fosthall pluton occur primarily as shallowly east dipping mylonitic fabrics on the eastern side of the pluton, linked to the east dipping Columbia River fault; and west dipping directed mylonitic fabrics and shear zones, linked to the west dipping Beaven fault (Parrish et al. 1988; Carr 1991b; Vanderhaeghe et al. 2003). U-Pb zircon crystallization ages in the east-dipping mylonitic fabric indicate that the Columbia River fault was actively deforming the Ladybird granite at 55.1 ± 1.5 Ma (Parrish et al. 1988). This 55 Ma date is the earliest evidence of extensional activity on the Columbia River fault.

The South Fosthall pluton is one of several examples of laccolithic composite bodies of intrusive granite in the eastern internal zone. The Pukeashun granite (another anatectic leucogranite suite of Eocene age, c. 56 Ma, located to the north-west of the Thor-Odin dome in the Shuswap Lake transfer zone between the North Thompson – Adams and Okanagan Valley – Eagle River fault systems) occupies a similar structural setting as the Ladybird granite, and was also intruded during extensional deformation (Johnson 2006). Ladybird granite is also present as a laccolithic complex of sheet-like bodies in the

Valhalla Complex south of Thor-Odin – Pinnacles, intruded between c. 59 and 56 Ma (Carr et al. 1987) where the upper margin of the granites coincide, in part, with the Valkyr Shear Zone, a zone of ductile deformation linking the east dipping Columbia River and the Slocan Lake normal faults (Carr 1995). Johnson (2006) suggests that the South Fosthall pluton, the Pukeashun granite and the Ladybird granite, in the Valhalla Complex, all occupy step-over zones between sets of extensional normal faults, and that the distribution of these granites may be linked to the presence of releasing zones in basement ramps. The emplacement of granite was localized in low-angle extensional shear zones, providing a weak rheology in which deformation was concentrated during extension (Johnson 2006).

2.2.4 Eocene intrusive rocks – Three Valley lamprophyres

Throughout the Thor-Odin dome – Pinnacles area, brittle late-stage deformation is represented by steep north-south striking fractures that cross-cut all structural features and are filled with very fine-grained greenschist facies minerals, including chlorite (Figure 2.9). These fractures are interpreted as the latest Eocene deformation in the area. North-south striking normal faults, in the interior of the Thor-Odin dome, are larger in scale (>100's m displacement) and have a strike-slip component that offsets map units (Kruse and Williams 2007).

The pervasive north-south striking fractures described here are associated with a steeply dipping, north-south striking mafic lamprophyre mafic dyke suite (Figures 2.10 – 2.13) that occurs throughout the study area. At Twin Peaks these dykes vary in width from 8 – 10 m (Figure 2.10) to 50 cm (Figure 2.12). Related lamprophyres are also documented on Mount Fosthall (Carr 1990), Three Valley Gap (Adams et al. 2005), and in the core of the Thor-Odin dome (Spark 2001; Kruse et al. 2004). The lamprophyre dykes at Twin Peaks do not have chilled margins (Figure 2.13), in contrast to the distinct chilled margins on the mafic dykes described north of the Thor-Odin dome by Adams et al. (2005). These dykes intruded between c. 50 and 48 Ma (based on $^{40}\text{Ar}/^{39}\text{Ar}$ thermochronology of minerals in the lamprophyres and country rock) and are referred to as the Three Valley suite (Adams et al. 2005). They are classified as calc-alkaline lamprophyres and shoshonitic diorites and have been linked to the Kamloops Group volcanics to the west of the Monashee Complex, interpreted as a possible feeder system for an extensive Eocene volcanic event containing mantle derived mafic melts related to crustal scale regional extension (Adams et al. 2005).

2.3 Normal faults in the Thor-Odin – Pinnacles area

The eastern part of the study area contains the southern segment of the Columbia River fault zone (Figure 1.2). The Columbia River fault zone is a shallow to moderately (10 – 30 degrees) east dipping brittle-ductile extensional fault, which strikes generally north-

south along the eastern margin of the Thor-Odin – Pinnacles culminations, along the Arrow Lakes valley (Read and Brown 1981; Parrish et al. 1988; Carr 1991). The Columbia River fault zone cuts into Thor-Odin dome basement rocks on the eastern margin of the dome, and progressively cuts up-section towards the south, where it gradually dies out and terminates east of the Pinnacles culmination (Brown and Read 1983). The Columbia River fault zone was active between c. 58 – 50 Ma (Parrish et al. 1988; Carr 1991) and was reactivated periodically until c. 30 Ma (Lorencak et al. 2001). The Columbia River fault zone is a system of ductile-brittle extensional faults that together have significant displacements of 10 – 30 km and make up a crustal scale detachment that played a major role in the exhumation of lower crustal high grade rocks (Parrish et al. 1988). This interpretation is supported by data from seismic reflection profiles (Varsek and Cook 1994; Cook 1995; Cook et al. 1992), geological mapping (Brown and Read 1983; Johnson 2006; Johnson and Brown 1996; Read and Brown 1981) and thermochronology studies (Archibald et al. 1983; Vanderhaeghe et al. 2003). In one interpretation, the Columbia River fault zone is linked to a proposed extensional shear zone that wraps around the southern margin of the Thor-Odin dome; termed the Cariboo Alp High Strain Zone (Kruse and Williams 2007).

In the center of the map area, near Arrow Lakes (Figure 1.2), there are greenschist facies metamorphic rocks belonging to the Permian Slocan Group, the Triassic Nicola and the Jurassic Rossland groups of the Quesnel terrane (Brown and Read 1983; Parrish et al.

1988; Carr 1990, 1991a; Gabrielse et al. 1991; Lemieux et al. 2003, 2004). These low grade rocks have been interpreted as klippen of the hanging wall of the Columbia River fault zone (Read and Brown 1981; Parrish et al. 1988) sitting structurally on sillimanite–K-feldspar and sillimanite–muscovite bearing, Late Cretaceous to Paleocene metamorphic rocks (Carr 1992; Lemieux 2006). In contrast, another proposed model interprets the low grade rocks to be unconformably deposited on the sillimanite–muscovite and sillimanite–K-feldspar bearing rocks (Thompson et al. 2004, 2006). In this interpretation the Columbia River fault as well as the west-dipping Okanagan Valley – Eagle River fault are considered to be minor tectonic elements of the area, and are proposed to have displacements on the scale of < 1km in contrast to the 30 – 90 km of displacement primarily proposed in the literature (Brown and Read 1983; Parrish et al. 1988; Tempelman-Kluit 1989).

The controversy concerning the magnitude of displacement on the Okanagan Valley – Eagle River fault was addressed by Brown (2010). Based on mapping and structural analyses she concluded that the large displacement hypothesis is correct, and that the apparent continuity of Devonian and Jurassic rocks in the Vernon area is due to corrugations in the fault surface of the Okanagan Valley – Eagle River fault, and not a result of unconformable deposition. Chapter 3 discusses the Plant Creek klippen and investigates whether the juxtaposition of Jurassic and Triassic low grade rocks with Jurassic to Cretaceous high grade rocks requires a fault contact in the Plant Creek area.

The Beaven fault (Figure 1.2) is a moderately (average 45 degrees) west dipping, predominantly brittle (at the present exposure level), normal fault which is part of the west dipping Okanagan Valley – Eagle River fault system (Carr 1990), an Eocene extensional fault system on the western margin of the Shuswap complex. The Okanagan Valley – Eagle River fault system displays evidence for magnitudes of displacement between 30 – 90 km, ductile deformation between c. 56 – 49 Ma, and anatexis in the footwall as late as c. 49 Ma (Brown et al. 2012). The amount of displacement on the Beaven fault is not well constrained, but it has appressed isograds in the footwall and juxtaposes greenschist facies rocks with Jurassic cooling ages and Jurassic igneous rocks in the hanging wall with the sillimanite–muscovite bearing amphibolite facies rocks of the Pinnacles area in the footwall, and probably terminates south west of Pinnacles in the Whatshan batholith area (Carr 1991).

2.4 Petrology, deformation and metamorphism of the Pinnacles-Thor-Odin area

The following sections present a compilation and integration of different datasets and studies from the Thor-Odin – Pinnacles area. The data for all the sections are presented on Figure 2.1 and 2.2 (tectonic elements and lithology) and Figure 2.14 (age constraints for igneous and metamorphic events, and pressure-temperature conditions of metamorphism). Study areas are discussed in the same order as in Section 2.4 starting at the top of the tectonostratigraphic columns and working structurally downwards.

Figures 2.14a, b, and c present the data with reference to the stratigraphic column and Figure 2.14d provides an alternative presentation with metamorphic and igneous constraints.

2.4.1 Whatshan – Pinnacles

The age of metamorphism in the Whatshan – Pinnacles area (Figure 2.14) is constrained by U-Pb dating of monazite (Glombick 2005; Lemieux 2006) and spans the Early to Late Cretaceous, between c. 130 and 90 Ma, with some evidence for earlier metamorphism as old as c. 200 Ma. The metamorphic rocks range from sillimanite–muscovite to sillimanite–K-feldspar–melt bearing rocks with local staurolite and kyanite preserved in the footwall of the Beaven fault (Carr 1990; Thompson et al. 2004; Glombick 2005).

These assemblages are pervasive throughout the rocks in the Pinnacles area, and the foliation and associated metamorphic minerals are cut by the Late Cretaceous Whatshan batholith, suggesting an Early Cretaceous metamorphic history. In contrast, andalusite, garnet, and biotite are present in the contact aureole of the Whatshan batholith, overprinting the previously discussed metamorphic assemblages (Glombick 2005).

The upright, doubly vergent structures defining the Type 3 interference patterns are older than Late Cretaceous since they are cut by the c. 77 – 75 Ma Whatshan batholith (Carr 1991b). The Whatshan batholith has a U –Pb titanite crystallization age of $75.5 \pm$

1.5 Ma from a sample locale south of the Pinnacles area (Carr 1991b). This constrains the age of deformation in the host rocks to be older than c. 75 Ma. This structural level is considered to be equivalent to the Joss Mountain area on the western flank of the Thor-Odin dome where deformed granitic pegmatites have been dated at c. 73 Ma, and undeformed pegmatites at c. 70 Ma, indicating that the end of deformation is bracketed within that time period (Johnston et al. 2000). Metamorphic titanite in the contact aureole of the Whatshan batholith dated at c. 64 Ma is interpreted as a cooling age after the intrusion of the batholith (Carr 1992). The Whatshan – Pinnacles area represents rocks that are in the suprastructure of the orogen by c. 75 Ma because the regional penetrative foliation and associated metamorphic mineral assemblages predated the low pressure andalusite in the contact aureole of the Whatshan batholith (Carr 1992), and there is no evidence of overprinting of Paleocene or Eocene events on the regional metamorphism and deformation (Glombick 2005).

2.4.2 Plant Creek – South Fosthall

The Plant Creek – South Fosthall area contains a variety of metasedimentary and metavolcanic rocks, including garnet–sillimanite–biotite paragneiss, garnet–sillimanite–muscovite–biotite schist, amphibolite including plagioclase amphibolite and calc-silicate amphibolite gneiss (Figure 2.15), quartzite (Figure 2.16), psammite, marble (Figure 2.17) and minor staurolite muscovite schist. The metamorphic grades of the rocks in the Plant Creek – Cameron Lake areas are the lowest of the rocks that are exposed in the footwall

of the Columbia River fault in the study area, and include sillimanite–muscovite-bearing amphibolite facies rocks, locally containing staurolite, and range to sillimanite–K-feldspar amphibolite facies rocks to the north closer to the South Fosthall pluton. The protolith ages of these rocks range from Cambrian to Devonian, with some as young as Jurassic (See Chapter 4 of this study).

Metamorphic minerals occur within foliations that developed together with F2 folds, and are generally refolded by F3 folds. In some cases F3 folds contain axial planar foliations. The timing of the onset of prograde metamorphism is not well constrained, but it is likely that prograde metamorphism in the Plant Creek area was ongoing during the Late Cretaceous, spanning the time between c. 100 – 80 Ma, based on U-Pb monazite dating (Lemieux 2006), continuing to the Late Cretaceous during penetrative deformation. Folded rocks are cut by the c. 62 – 54 Ma Ladybird suite (Carr 1992). At c. 73 – 64 Ma the rocks of the Plant Creek-South Fosthall area, structurally above the South Fosthall pluton, were being penetratively deformed in the infrastructure.

2.4.3 North Fosthall – Mount Symonds to Cariboo Alp

The Twin Peaks area (Figure 2.18a) is located northwest of the South Fosthall pluton area and consists mostly of migmatitic–garnet–sillimanite–biotite paragneiss with a well-developed composite transposition foliation, primarily moderately south to southwest dipping. Ladybird granite intrusive rocks are abundant and are concordant

with the layering in the host rocks in some cases, and crosscut the layering in others (Figure 2.18b). There are two contrasting styles of pegmatite in the Twin Peaks area. In Figure 2.19 the pegmatites of the Ladybird granite are concordant with the regional south to southwest dipping transposition foliation in the country rock, which indicates pre- or syn-deformational intrusion of pegmatites. In Figure 2.20 the pegmatite completely surrounds a raft of calc-silicate amphibolite. The amphibolite contains the regional transposition foliation, and the pegmatite is undeformed, indicating a phase of post-deformational intrusion of pegmatite.

The area is located on a regional scale northeast verging F2 fold, similar in orientation and style to folds in other study areas (e.g. Mt. Symonds), but contains fold closure with hinge plunging to the west-southwest and axial plane dipping steeply to the south. In Figure 2.21 this fold style is seen in a folded amphibolite surrounded by pegmatite.

Lithologies in addition to the dominant migmatitic–garnet–sillimanite–biotite paragneiss (Figure 2.22) include; amphibolite layers, rafts (Figure 2.20) and boudins including calc-silicates (Figure 2.23) and several small (<10 m diameter) pods of ultramafic metamorphic rocks (Figure 2.24) containing serpentinized olivine and pyroxene, with brucite and talc. These rocks may represent ultramafic intrusions into the paragneiss, or be part of a regional layer of ultramafic rocks interpreted as a boudinaged remnant of

oceanic crust in an obduction surface within the pericratonic Kootenay Group rocks (Okulitch 1984, Carr 1991a).

Structures within the migmatitic–garnet–sillimanite–biotite paragneiss include a well-developed transposition foliation (Figure 2.25). All the paragneiss and most of the amphibolite outcrops are strongly foliated, only garnet amphibolites display poorly developed foliation. In the migmatitic–garnet–sillimanite–biotite gneiss units foliations are generally defined by sillimanite-rich layers and gneissic layering. Figure 2.25 shows oblate garnets which lie within the foliation plane and sillimanite–biotite foliations that bend around the garnets, indicating that garnet and sillimanite grew during development of the transposition foliation. It is also possible that the garnets are syn-tectonic and grew in oblate shapes, or they may have been resorbed to form oblate crystals. Figure 2.26 shows migmatitic amphibolite gneiss with a strong transposition foliation. In this example the foliation is crosscut by coarse-grained granitic leucosome, suggesting that these rocks underwent several episodes of deformation and melting. The structures and metamorphic assemblages are consistent with high temperature deformation, and syn-metamorphic transposition foliation development.

The regional transposition foliations in this area generally dip steeply (40-60 degrees) towards the south and southwest, with some on the northern side of the valley dipping towards the north and northeast. There are also numerous S and Z folds in the

paragneiss, with M folds (for example in Figure 2.21) concentrated in the western part of the area in the region of the fold closure. Figure 2.27 shows Z folds in migmatitic paragneiss that illustrate the regional fold style. These cm-scale folds have axial planes that dip steeply to the south and fold hinges that plunge shallowly to the west. These orientations mimic the limbs of the map-scale fold closure illustrated on Figure 1.2.

Mount Baldur is situated east of the Twin Peaks area, within the South Fosthall pluton (Carr 1990; Hinchey 2005) and is representative of the Ladybird granite in the area. The Mount Baldur area contains up to 30% screens of metasedimentary paragneiss, psammite, quartzite and amphibolite country rock within the granite (Hinchey and Carr 2006). Around the South Fosthall pluton the formation of the transposition foliation is Late Cretaceous to Paleocene, bracketed by U-Pb zircon ages from deformed and undeformed Ladybird granite which indicate that the deformation was ongoing at c. 62 Ma, and largely over by c. 55 Ma (Carr 1992). All the amphibolite facies metamorphic assemblages are folded by the transposition foliation and the granites cuts the foliation, proving that the age of the thermal peak metamorphism is older than the intrusion age of the Ladybird granite and coeval with the transposition foliation in the area.

The Mount Symonds and North Fosthall area contain a mixed assemblage of metasedimentary rocks interlayered with amphibolite layers. Calc-silicate amphibolites are common in the North Fosthall area, some of which contain boudinaged pegmatite

layers (Figure 2.28) and are highly strained. Other exposures lack the pegmatite intrusions (Figure 2.29).

The Mount Symonds area comprises migmatitic–garnet–sillimanite biotite–paragneiss, quartzite, amphibolite, marble and psammite. There is a pervasive, well-developed, moderately south-southwest dipping composite transposition foliation (Figure 2.30).

The area is located on the long limb of km-scale isoclinal folds, interpreted as F2, which formed during northeast directed transport and compression. Figure 2.31 illustrates a cm-scale asymmetric isoclinal S fold in garnet biotite gneiss at Mount Symonds. The axial plane of this fold dips steeply to the south, similar to the regional km-scale folds at Fawn Lakes and Mount Symonds. Figure 2.32 illustrates a boudinaged pegmatitic leucosome in moderately south dipping garnet–biotite gneiss. The orientation of the boudinaged leucosome suggests elongation in a northeast-southwest direction.

Pegmatites crosscut the transposition foliation in some instances, and are concordant with it in others (Figure 2.33) indicating a combination of syn- and post-deformational intrusion of pegmatites.

There are several marker units with Proterozoic (Fawn Lakes Assemblage) to Cambrian protolith ages (Empress Marble south of Mount Symonds) which can be traced along strike for up to 30 km. The apparent age of at least some stages of tight F2 and F3 folding and metamorphism is older than c. 58 Ma, and formed, in part, at c. 62 Ma (Carr

1992). The Ladybird granite west of Mount Symonds is concordant with folds in the host paragneiss and has a U-Pb zircon crystallization age (for magmatic zircons) of c. 60 Ma (Vanderhaeghe et al. 1999), indicating that folding was still ongoing after that date. Metamorphism was ongoing in the Mount Symonds and North Fosthall rocks at c. 61 – 60 Ma based on metamorphic ages in titanite and zircon (Carr 1995).

The Fawn Lakes area contains primarily garnet–biotite–migmatitic paragneiss (\pm minor sillimanite) with subordinate quartzite, amphibolite and psammite known as the Fawn Lakes Assemblage (Carr 1991a). It is situated on the long limb of a regional scale northeast verging F2 fold and has a well-developed south-southwest dipping composite transposition foliation in all units. The rocks have a distinct flaggy weathering style on foliation planes (Figure 2.34), and do not contain a large amount of granitic intrusive rocks (<20%). The geometry of the panel of rocks is controlled by the enveloping surface of two phases of coaxial northeast verging coaxial folds (Figure 2.35, cm-scale). Metamorphism was ongoing in the Fawn Lakes rocks at c. 61 – 60 Ma based on metamorphic ages in titanite and zircon (Carr 1995).

At Cariboo Alp (CA; Figure 1.2) there is a well exposed section of rocks on the southwestern flank of the Thor-Odin dome marked by the structurally highest level of apparent basement rocks that are highly strained. The structural significance of this domain is controversial and is addressed in this study. This southwest dipping panel of

rocks is characterized by 1 x 5 km lozenges of transposed migmatitic sillimanite–K-feldspar gneisses folded and refolded by northeast verging tight rootless antiforms (Figure 2.36). The Cariboo Alp area contains alternating lenses and layers of predominantly grey migmatitic–garnet–biotite–quartzofeldspathic paragneiss and rusty migmatitic–garnet–sillimanite–biotite paragneiss with southwest plunging sillimanite and hornblende mineral lineations and stretching lineations. There are minor layers of calc-silicate gneiss, quartzite, marble, anthophyllite-gedrite amphibolites and amphibolite. The lozenges thin and pinch into a high strain zone out on the western, southern and southeastern flanks of the dome (McNicoll and Brown 1995).

Variable deformation and cross-cutting relationships in the pegmatites at Cariboo Alp suggest that progressive emplacement of pegmatite dykes out-last ed deformation.

Figure 2.37 illustrates a pre- to syn-tectonic pegmatite intrusion style where pegmatites are concordant with the foliations in the host gneisses and have been deformed. Figure 2.38 shows the post-tectonic intrusion of pegmatites where undeformed pegmatites cut the host gneisses at high angles.

Figure 2.38 illustrates foliations at Cariboo Alp that are defined by layers of biotite, sillimanite and garnet with layers of quartzofeldspathic leucosome making up a coarse continuous gneissic foliation. Figure 2.39 shows details of the composite transposition

foliation such as rootless isoclinal fold hinges (a) and cm scale gneissic layering (b) in the grey migmatitic gneiss. Primary layering, as seen in the different lithologies contained in the main gneiss units, is concordant with the foliation (Figure 2.36). Amphibolite boudins in the rusty gneiss provide evidence for protracted metamorphism and deformation at Cariboo Alp. The boudins (Figure 2.40) are internally foliated (Figure 2.40a), and the predominant foliation in the gneiss wraps around the boudins. The internal foliation is at an angle to the surrounding foliation. Garnets within another boudin show snowball inclusion trails (Figure 2.40b) indicating garnet growth during deformation.

The most prominent folds at Cariboo Alp are isoclinal northeast verging F2 folds. Figure 2.41 illustrates this fold style in two different rock types: grey migmatitic gneiss (a), and marble (b). The axial planes and limbs of the F2 folds are approximately concordant with the predominant gneissic foliation. Figure 2.42 shows a thin section of a folded rusty sillimanite–biotite gneiss unit, with the same fold style and sense of movement. The folded sillimanite needles are interpreted as evidence for pre- or syn-deformational growth of the high temperature metamorphic assemblage. The calc-silicate unit of the grey gneiss contains pressure shadows which are good examples of kinematic indicators (Figure 2.43). The large (10 – 20 cm) diopside crystals in this unit have pressure shadows containing leucosome and hornblende. The asymmetries of the leucosomes indicate a

top-to-the-northeast sense of movement. Shear bands are found between boudinaged pegmatite lenses and also indicate top-to-the-northeast sense of movement.

Mineral lineations, stretching lineations and mineral aggregate lineations are present at Cariboo Alp. In the rusty gneiss, sillimanite forms northeast-southwest lineations concentrated along, and concordant with, southwest dipping foliation planes defined by biotite (Figure 2.44). At least two orientations for sillimanite lineations exist at Cariboo Alp (Figure 2.45). Both generations are present on foliation surfaces in the grey gneiss, suggesting that they may represent evidence for reactivation of foliation planes.

Generally the finer grained sillimanite forms lineations on the foliation planes of the grey gneiss (Figure 2.45) and coarse grained sillimanite is found on fracture surfaces (Figure 2.44) concordant with the foliation planes.

At Cariboo Alp the transposition fabric is older than 58 Ma. Deformation and high-strain shearing was ongoing at Cariboo Alp at c. 62 – 59 Ma, and stopped by c. 58 Ma (Carr 1992), based on the U-Pb zircon crystallization age of an undeformed pegmatite cross-cutting the dominant transposition foliation (Carr 1992). There is evidence for reactivation of the transposition foliation F2 structures during exhumation and cooling (Chapter 5, this study). The timing of the onset of metamorphism is not well constrained, but based on U-Pb ages in metamorphic titanite (58 ± 4 Ma) from paragneiss at Cariboo Alp (Carr 1992) and metamorphic zircon U-Pb dates (61 ± 0.5 Ma)

in the Fawn Lakes Assemblage (Carr 1992) indicates that prograde metamorphism forming K-feldspar–sillimanite-bearing migmatitic rocks was active in the Cariboo Alp area between c. 62 – 58 Ma. U-Pb monazite ages from a quartzite at Cariboo Alp yielded metamorphic ages of c. 56 – 54 Ma with errors ranging between 1 and 4 Ma (Coleman 1990) and overlaps with the 21 – 58 Ma dates from other minerals mentioned. This is consistent with the documented Paleocene-Eocene period of anatexis and metamorphism found throughout Thor-Odin dome (Hinchey et al. 2006). Cariboo Alp area represents infrastructure to the structurally higher and deactivated South Fosthall – Plant Creek suprastructure by c. 64 Ma. The Cariboo Alp area transitioned to being suprastructure to the deeper rocks within the Thor-Odin dome by c. 58 Ma.

2.4.4 The Thor-Odin dome

The Thor-Odin dome section includes specific discussions of study areas at Icebound Lake (this study), Bearpaw Lake, Mount Thor, and Frigg Glacier as mapped and described by Hinchey (2005). The southern part of the Thor-Odin dome consists of migmatitic gneiss with transposition foliation (Reesor and Moore 1971; Parkinson 1992; Spark 2001; Hinchey et al. 2006). The pervasive transposition foliation is folded and the structure is dominated by interference patterns between early isoclinal folds, with limb lengths of 60-80 km involving Proterozoic Laurentian basement rocks and a cover sequence of metamorphic supracrustal rocks of uncertain age (Reesor and Moore 1971; Parkinson 1991), and three subsequent generations of fold, designated F2, F3 and F4 by

Kruse et al. (2004) and Williams and Jiang (2005) (Figure 1.2 and 1.3). Basal quartzites of the cover sequence shown on maps and cross sections depict the structure (see Chapter 3, this study for further discussion of the basal quartzites in the Thor-Odin dome). The main metamorphic assemblages in the migmatitic gneiss are sillimanite–K-feldspar \pm kyanite \pm cordierite, formed during anatexis associated with decompression from 8 – 10 kbar to 4 – 5 kbar (Norlander et al. 2002, Hinchey et al. 2006).

Icebound Lake 1 km north of Cariboo Alp (Figure 2.46) is located on the southwestern flank of the Thor-Odin dome and represents the structurally highest rocks in the dome. The area consists primarily of diatexite migmatitic garnet–biotite–quartzofeldspathic paragneiss (Figure 2.47) with complex fold interference patterns (Figure 2.48). This unit is interpreted as a diatexite migmatite because no original layering is preserved (Figure 2.49). Some sections of the migmatite contain cm long sillimanite clumps, possibly as pseudomorphs after kyanite (Figure 2.50), indicating that high temperature decompression may have occurred in this area. There are amphibolite boudins and lenses throughout the paragneiss, ranging from < 1 m in diameter to > 10 m (Figure 2.47).

Structurally overlying the diatexite migmatite there is a 2 – 3 m thick layer of metamorphosed mafic rocks (Hinchey and Carr 2007), comprising gedrite–anthophyllite–tremolite amphibolite with lenses of garnet–biotite–plagioclase gedrite

(Figure 2.51 – 2.53). This gedrite–anthophyllite–tremolite amphibolite layer, with minor lenses of garnet, plagioclase, gedrite/anthophyllite and biotite rocks occur as boudinaged layers along strike of the predominant foliation surfaces.

The dominant garnet biotite paragneiss is unconformably overlain by a southwest dipping metasedimentary package dominated by garnet–sillimanite–biotite paragneiss, with a distinct layer of quartzite near the base of the package. There are well developed moderately southwest dipping composite transposition foliations in metasedimentary rocks. These rocks are interpreted to be part of a southwest dipping panel of transposed rocks on the lower limb of a regional southwest dipping overturned synform, following the interpretation of Reesor and Moore (1971) (Figure 1.2).

At Bearpaw Lake the dominant lithologies are migmatitic hornblende–biotite—orthogneiss and migmatitic garnet sillimanite biotite paragneiss (Hinchey and Carr 2007). Leucosome is abundant in all units, particularly in the paragneiss where it comprises up to 50% of the rock volume (Hinchey 2005). The paragneiss is interlayered with migmatitic muscovite–biotite paragneiss and contains boudinaged layers of cordierite–gedrite amphibolites, garnet amphibolite. The paragneiss is also infolded with minor quartzite and calc-silicate gneiss (Spark 2001; Hinchey 2005). The amphibolites and cordierite–gedrite amphibolites occur as boudinaged layers within this foliation (Hinchey and Carr 2007).

At Mount Thor, the dominant rock type is migmatitic hornblende biotite orthogneiss which is interpreted to be unconformably overlain by a heterogeneous package of moderately northeast dipping metasedimentary rocks with a quartzite layer at its base (Reesor and Moore 1971; Duncan 1984; Spark 2001; Hinchey 2005). The metasedimentary rocks comprise sillimanite garnet biotite pelitic schist with abundant leucosome and calc-silicate garnet biotite schist (Hinchey 2005, Spark 2001). The Mount Thor area is located on the lower limb of a regional scale F2 northwest verging fold (Reesor and Moore 1971; Spark 2001; Hinchey 2005) (Figure 1.2).

At Frigg Glacier, the structurally deepest rocks exposed in Thor-Odin dome (see Figures 1.2, 1.3); the dominant lithologies are migmatitic hornblende biotite orthogneiss and migmatitic K-feldspar augen hornblende biotite granodiorite, both containing abundant (30 – 40%) leucosome, with minor amphibolite boudins present throughout the area (Hinchey 2005).

While there is no firm date for the onset of prograde metamorphism, it is likely that metamorphism was ongoing by the Paleocene to Eocene, between c. 65 to 56 Ma (Norlander et al. 2002, Hinchey et al. 2006). Monazite growth over a period of 62.3 ± 3 Ma to 50.1 ± 2 Ma (Coleman, 1990; Hinchey et al., 2007) has been interpreted as evidence for a protracted period of metamorphism. Monazite growth and

recrystallization can occur over a wide range of temperatures in different lithologies and these ages do not necessarily represent peak metamorphic conditions (Parrish 1990; Spear 1993; Crowley and Parrish 1999; Rubatto et al. 2001; Gibson et al. 2004). Monazite growth could be linked to fluid circulation promoting recrystallization (Glombick 2005).

Deformation in the Thor-Odin dome interior was ongoing c. 56 – 54 Ma as determined by U-Pb igneous zircon crystallization ages in deformed leucosomes (Hinchey et al. 2006). The age of at least some stages of isoclinal folding and metamorphism is as young as c. 56 – 54 Ma (Hinchey et al. 2006; Norlander et al. 2002). Deformation ended between c. 54 and 52.5 Ma (Hinchey et al. 2006), based on zircon U-Pb crystallization ages in undeformed leucosomes. The rocks of the Thor-Odin dome are estimated to have been exhumed from a depth of 26 – 33 km within the crust based on estimates of peak pressures between 8 and 10 kbar (Norlander et al. 2002).

The Thor-Odin area represents the structurally deepest infrastructure level present in this study area (Reesor and Moore 1971; Parkinson 1991; Spark 2001; Kuiper 2003; Hinchey 2005). When the rocks in the overlying Cariboo Alp area were structurally deactivated c. 58 Ma, the rocks of the dome were still being penetratively deformed in the infrastructure. The Thor-Odin rocks were structurally deactivated during the c. 54 Ma – 52.5 Ma period when penetrative deformation ended. It is interesting to note that

penetrative deformation in the Frenchman Cap dome north of Thor-Odin continued after c. 52 Ma until c. 49 Ma (Crowley 1999). Therefore, it is permissible to suggest that the Thor-Odin dome represents a higher structural level that became suprastructure to the deeper rocks in the Frenchman Cap dome after c. 52.5 Ma.

2.5 Post-transposition deformation, brittle deformation and retrograde metamorphism

As discussed in section 2.2, the Columbia River fault was active as a brittle to ductile fault between c. 55 and 50 Ma (Parrish et al. 1988; Carr 1992; Johnson 2006), and was reactivated periodically until c. 30 Ma (Lorencak et al. 2001). It therefore overlaps the formation of F2 folding and transposition in the structurally deepest levels of the structural section, showing that exhumation along extensional faults was active during compressional deformation in the structurally deepest levels. Brittle deformation in the Thor-Odin dome – Pinnacles area is present in steeply dipping north-south striking fractures that cross-cut all structural features and are filled with very fine-grained greenschist minerals including chlorite. These fractures are interpreted to represent the latest Eocene deformation in the area. In the interior of the Thor-Odin dome the north-south striking fractures normal faults are larger in scale (>100's m displacement) and have a strike-slip component that offsets map units (Kruse and Williams, 2007).

The largest continuous zone of retrograde metamorphism is a greenschist facies overprint in the rocks adjacent (1 – 2 km zone) to the Columbia River fault (Reesor and Moore 1971; Read and Brown 1981; Lemieux 2006) characterized by syn-mylonitic chlorite and muscovite representing the last stages of ductile deformation in the CRF footwall, shown on Figure 1.2. Chlorite filled fractures are also found throughout the study area, specifically illustrated at Cariboo Alp in Figure 2.9.

Additionally, at Icebound Lake, the layer of migmatitic garnet–gedrite–anthophyllite illustrated in Figures 2.51 – 2.53 contains local lenses of chloritized garnets (Figure 2.54). In the migmatitic rocks of the Cariboo Alp area, muscovite is found as large (1cm) crystals in pressure shadows of peritectic K-feldspar or plagioclase crystals in leucosome pods within the host migmatitic gneiss, locally intergrown with chlorite (Figure 2.55). Both minerals are present as euhedral crystals, 0.1 –10 mm in diameter with sharp grain boundaries. The mineral textures, habits and grain boundaries suggest that the two minerals grew together and there is no evidence that one is replacing or overgrowing the other. The presence of chlorite in rocks with granitic composition indicates that the mineral growth occurred at temperatures in the range for greenschist facies metamorphism, between ~350 – 450 °C (Spear 1993). The muscovite in the leucosomes in Cariboo Alp is interpreted as representative of greenschist facies retrograde metamorphic mineral growth which occurs during the exhumation and cooling phase of the rock history.

2.6 Conclusions regarding diachronous metamorphism, deformation in the Thor-Odin – Pinnacles area.

The rocks of the Thor-Odin – Pinnacles area discussed in this study experienced protracted, but not necessarily continuous, deformation and metamorphism throughout the Cretaceous to Paleocene and into the Eocene, possibly overprinting Early Cretaceous or older events. The following presents a brief summary of conclusions regarding the timing of deformation and metamorphism as illustrated in Figure 2.56.

In this study, we identify the time at which belts of rocks were penetratively deforming in the infrastructure, and when the formation of transposition foliation ended, cooled (Chapter 5, this study), and translated in the suprastructure. In the area between the Thor-Odin dome and the Whatshan batholith, the timing of tectonothermal events young structurally downwards, reflecting the downward migration of the suprastructure-infrastructure boundary through time. Metamorphic grade generally increases downwards throughout the structural section into the dome. Based on a data compilation which includes timing of metamorphism, deformation, anatexis in basement rocks, and intrusion of leucogranites, there are at least four belts of rocks, or tectonothermal domains, that experienced regional metamorphism, deformation and high temperature cooling (below ~650 °C) at different times (Figure 2.56).

Metamorphism in each structural level was broadly coeval with the penetrative ductile deformation, with thermal peak metamorphism predating the end of deformation. However, the timing of the onset of prograde metamorphism is uncertain. Periods of prograde metamorphism are recorded from c. 130 – 90 Ma in rocks of the Whatshan area (Glombick 2005) continuing to sometime before c. 75 Ma (Carr 1992), c. 100 – 80 Ma in the Plant Creek/South Fosthall area (Lemieux 2006) and continuing to c. 64 Ma (Carr 1992), c. 73 – 62 in the North Fosthall – Mount Symonds area (Carr 1991b, 1992), c. 65 – 58 Ma at Cariboo Alp (Carr 1991b, 1992; Coleman 1990), and c. 65 – 56 Ma in the Thor-Odin dome (Norlander et al. 2002; Hinchey et al. 2006, 2007).

Penetrative deformation progressively youngs down section (from >75 Ma at the top in rocks of the Whatshan area, to c. 56 – 54 Ma within the Thor-Odin dome at the bottom) and represents progressive heating and deformation migrating downwards due to burial, incubation and structural weakening of structurally lower rocks. The end of penetrative ductile deformation (or deactivation of the transposition foliation) marks the transition of specific structural levels from infrastructure to suprastructure. This has been dated throughout the structural section. On the basis of cross cutting granitoids dated by U-Pb studies, transposition and folding had ceased by: (i) c. 73 Ma at the highest structural levels in the southern part of the study area near Whatshan Lake and west of the dome at Joss Mountain (Section 2.4.1); (ii) c. 64 – 62 Ma in the central Plant – Creek North Fosthall section west of Arrow Park lake (Section 2.4.2); (iii) c. 58 Ma on

the upper margin of the dome at Mount Symonds, Fawn Lakes, and Cariboo Alp (Section 2.4.3); and, (iv) c. 54 – 52 Ma within the dome (Section 2.4.4).

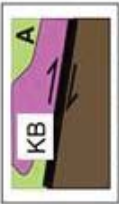
The top part of the section at Whatshan – Pinnacles preserves Cretaceous metamorphism and deformation and was not remobilized during Late Paleocene – Eocene northeast directed transport. As discussed above, this section underwent progressive heating and deformation due to burial and incubation. This hypothesis is consistent with the known preservation of an orogenic base in the Frenchman Cap dome, below which Proterozoic deformation is preserved, and the limit of Eocene strain and the Eocene thermal overprint can be documented (Crowley et al. 2008; Gervais et al. 2010).

In conclusion, the rocks exposed in the footwall of the Columbia River fault in the Thor-Odin – Pinnacles area record Cretaceous metamorphism and cooling in the upper structural levels and three stages of infrastructural flow at progressively deeper crustal levels in the Late Cretaceous, Paleocene and Eocene, respectively, in the deeper part of the structural section. The generally downward younging progression of metamorphism and deformation as well as the structural style and transposition foliation in the lower part of the section is consistent with a model in which rocks are progressively heated and deformed during compressional transport, possibly up a basement ramp facilitating doming and exhumation.

Tectonostratigraphic column summary of the tectonic elements and lithologic units

Rocks in the hanging wall of the Columbia River Fault

Generally greenschist to lower amphibolite grade metavolcanic rocks including breccia, tuff, basalt, augite porphyry, siliciclastic and carbonate rocks including phyllite, argillite, quartzite, marble, and minor volcanoclastic tuffs. The hanging wall rocks in the Columbia River Fault (E) and the Beavan Fault (W) include Paleozoic - Lower Jurassic stratified rocks from the Kaslo, Slocan and Rossland Groups as well as Hamill, Badshot, Lardeau and Milford Groups. Rocks in the footwall of these faults are interpreted as the deformed and metamorphosed equivalents of some of these rocks. Intruded at this latitude by Middle Jurassic plutons.



Columbia River Fault

Study area rocks are exposed in the footwall of the Columbia River Fault. The Columbia River Fault, active after ~55 Ma, is a shallow E dipping normal fault which cuts through all structural levels of the study area. Cut-outs A, B, C, D show relationships between the hanging wall and footwall rocks at different structural levels. A shows a generic hanging wall/footwall relationship, with the fault cutting through Jurassic intrusive rocks in the hanging wall. B shows the relationship south of the study area with the fault cutting Cretaceous intrusive rocks, C with Paleocene intrusive rocks, and D with Eocene age migmatitic rocks.



Fault activity crosscuts transposition foliation and folding in the upper structural levels of the study area, but is coeval with folding in the lower structural levels.

Rocks in the footwall of the Columbia River Fault

Metasedimentary and metavolcanic rocks

Locations: Pinnacles (P), Whatshan (W), Saddle Mountain (SM), Cusson Creek (CC), Plant Creek (PC), Cameron Lake (CL), South Fosthall (SF), South Fosthall Pluton (SFP), Mount Baldur (MB), Twin Peaks (TP), North Fosthall (NF), Mount Symonds (MS), Fawn Lakes (FL)



Proterozoic to Jurassic metasedimentary and metavolcanic rocks of autochthonous and pericratonic affinity (See Chapters 2 and 3, this study; Carr 1991, Fritz 1991). Protoliths correlated with the Proterozoic Horsechief Creek Group of the Windermere Supergroup (Fawn Lakes), Cambrian Hamill and Badshot Groups (Mount Symonds) and the Paleozoic Lardeau to Milford Groups (Arrow Lake schists and Gold Range Composite units) and are as young as Middle Jurassic in the Plant Creek area.

Cariboo Alp rocks

Locations: Cariboo Alp (CA)

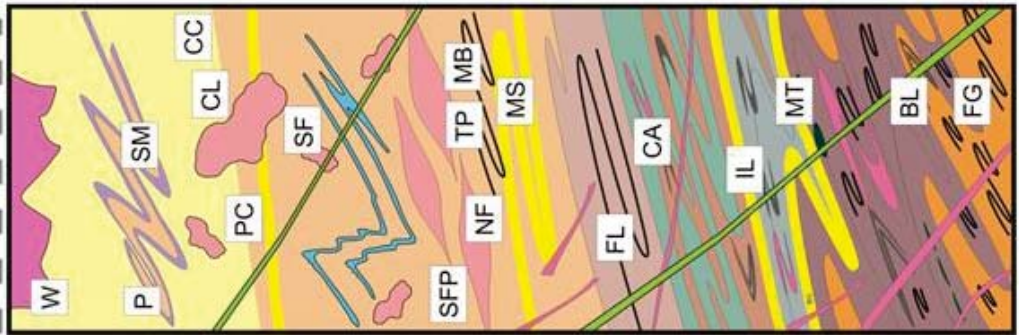
Transition zone between rocks of the Thor-Odin dome and overlying rocks in the Gold Range Assemblage. Highly strained migmatitic rock, infolded slices of different paragneiss also containing amphibolites, calc-silicates, quartzite and marble. Protolith ages are younger than ~1.1 Ga. (See Chapters 2 and 3, this study.)

Thor-Odin dome rocks

Locations: Icebound Lake (IL), Mount Thor (MT), Bearpaw Lake (BL), Frigg Glacier (FG)



Paragneiss and intrusive orthogneiss of Laurentian affinity, protoliths of which are broadly Paleoproterozoic in age, (all >1.8 Ga) with heterogeneous succession of supracrustal metasedimentary and minor metavolcanic rocks over a basal quartzite layer which is younger than ~1.7 Ga (see Chapters 2 and 3, this study). Complex infolding of cratonic and supracrustal rocks. Deepest crustal level exposed in the study area, rocks exhumed from ~2.5 - 3.0 km depth in the Eocene.



LEGEND for Lithotectonic column and cross sections

Rocks in the hanging wall of the Columbia River Fault

Intrusive rocks

-  **Kuskanax batholith** – Middle Jurassic ca. 170 Ma (Parrish and Wheeler 1983).
Part of the Nelson Intrusive Suite, which includes granite, syenite, diorite.

Metasedimentary and metavolcanic rocks

-  Generally greenschist to lower amphibolite grade metavolcanic rocks including breccia, tuff, basalt, augite porphyry, siliciclastic and carbonate rocks including phyllite, argillite, quartzite, marble, and minor volcaniclastic tuffs. The hanging wall rocks in the Columbia River Fault (E) and the Beavan Fault (W) include Paleozoic - Lower Jurassic stratified rocks from the Kaslo, Slocan and Rossland Groups as well as Hamill, Badshot, Lardeau and Milford Groups. Rocks in the footwall of these faults are interpreted as the deformed and metamorphosed equivalents of some of these rocks.

Rocks in the footwall of the Columbia River Fault

Intrusive rocks

-  **Ladybird Granite Suite** – Late Paleocene to Eocene ca. 62 – 55 Ma (Carr 1992)
Biotite granite to quartz monzonite +/- garnet, muscovite, tourmaline. occurs as dykes, stocks, sills, makes up the South Fosthall Pluton dated at 55 ± 1.5 Ma (Parrish et al. 1988). Occurs as pegmatite, aplite and granite.

-  **Whatshan batholith** – Late Cretaceous ca. 77 Ma (Carr 1990)
Hornblende - potassium feldspar quartz monzonite to diorite

SW dipping panel of metasedimentary and metavolcanic rocks

Proterozoic to Jurassic metasedimentary and metavolcanic rocks of autochthonous and pericratonic affinity (Van Rooyen et al. 2010, Carr 1991, Fritz 1991). Protoliths correlated with the Proterozoic Horsethief Creek Group of the Windermere Supergroup (Fawn Lakes), Cambrian Hamill and Badshot Groups (Mount Symonds) and the Paleozoic Lardeau to Milford Groups (Arrow Lake schists and Gold Range Composite units) and are as young as Middle Jurassic in the Plant Creek area.

-  **Arrow Lake garnet sillimanite muscovite biotite schist**
Muscovite-biotite schist +/- garnet, sillimanite, local staurolite, kyanite. Includes micaceous quartzite, minor psammitic gneiss, marble and amphibolite layers. Local carbonaceous schist and staurolite schist.
-  **Gold Range Composite units.**
Metasedimentary and metavolcanic including migmatitic paragneiss, semi-pelitic gneiss, pelitic and semipelitic schist, amphibolite, calc-silicate gneiss, quartzite and marble. Extensively intruded by Ladybird Granite Suite.
-  Marble
-  Quartzite
-  **Fawn Lakes paragneiss**
Migmatitic biotite-quartz-feldspar paragneiss and semipelitic gneiss. Includes garnet amphibolite boudins and layers, extensively intruded by granitic pegmatite; distinct flaggy weathering appearance, predominantly aluminum-poor throughout section, sillimanite rare. Includes minor quartzite and psammitic layers.

Cariboo Alp rocks

-  Grey migmatitic hornblende biotite gneiss (+/- sillimanite, garnet) with amphibolite lenses and layers, hornblende diopside calc-silicate gneiss layers.
-  Rusty migmatitic gt-sil-bt paragneiss with amphibolite boudins, includes quartzite, marble layers

Thor-Odin dome rocks

-  **Cover paragneiss**
Heterogeneous psammitic and calc-silicate gneiss, pelitic (Ky-Sil) gneiss, calc-silicate gneiss with interlayered marble, amphibolite boudins and layers.
-  **BQ** Basal Quartzite
-  **Basement orthogneiss**
Leucoquartz monzonite and gneissic quartz monzonite; hornblende-biotite granodiorite orthogneiss, granitic biotite orthogneiss. May contain hornblende and range in composition from granite to granodiorite. Includes augen orthogneiss, biotite orthogneiss, as well as biotite granite orthogneiss.
-  **Basement Paragneiss**
Predominantly migmatitic paragneiss, includes psammitic biotite-feldspar-quartz paragneiss with lenses of pelitic schist, garnet-feldspar-quartz gneiss and amphibolite. Also includes biotite-quartz-feldspar paragneiss containing abundant garnet amphibolite boudins and granitic pegmatite. Cordierite gedrite amphibolite occurs as boudinaged layers within the basement paragneiss, may contain cordierite, kyanite, spinel, olivine, garnet.

Figure 2.1 Major tectonic elements in the Thor-Odin – Pinnacles area.

This column shows the relative positions, structural styles and protolith ages of the different study areas. Total structural thickness is 15 – 17 km. Repetitions of particular units are not illustrated here. The small boxes show where the Columbia River fault cut through the study area at different structural levels. Specific areas discussed in the text are Bearpaw Lake (BL), Cameron Lake (CL), Cariboo Alp (CA), Cusson Creek (CC), Fawn Lakes (FL), and Frigg Glacier (FG). Icebound Lake (IL), Mount Baldur (MB), Mount Symonds (MS), Mount Thor (MT), North Fosthall (NF), Plant Creek (PC), Pinnacles (P), Saddle Mountain (SM), South Fosthall (SF), South Fosthall pluton (SFP), Twin Peaks (TP), and Whatshan batholith (W). Data from Read and Wheeler 1976; Archibald et al. 1983; Parrish and Wheeler 1983; Parrish and Armstrong 1987; Parrish et al. 1988; Coleman 1990; Fritz et al. 1991; Parkinson 1991; Carr 1990, 1991, 1992, 1995; Colpron et al. 1996; Vanderhaeghe et al. 1999; Johnston et al. 2000; Norlander et al. 2002; Gibson et al. 2003; Kuiper 2003; Thompson et al. 2004; Kruse et al. 2004; Adams et al. 2005; Glombick 2005; Hinchey et al. 2006, 2007; Lemieux 2006; this study.

Note: This legend is used for all column figures Figures 2.1, 2.2, and 2.14.

Tectonostratigraphic column summary of the tectonic elements and lithologic units present in the study area.

Simplified lithostratigraphic column summarizing the tectonic elements, structural styles and major lithologic units, and projected locations of study areas. The rocks exposed in the footwall of the normal fault are a package of polydeformed amphibolite grade (or higher) metamorphic rocks. The east dipping Columbia River fault cuts through the rocks of the study area at different structural levels, juxtaposing rocks with Jurassic or older cooling and deformation histories with rocks exhumed and cooled in the Late Cretaceous to Eocene.

Rocks in the hanging wall of the Columbia River Fault

Intrusive rocks

Kukuanax batholith (KB) - Middle Jurassic ca. 170 Ma (Parrish and Wheeler 1983). Part of the Nelson Intrusive Suite, which includes granodiorite, granite, syenite, diorite.

Metasedimentary and metavolcanic rocks

Generally greenschist to lower amphibolite grade metavolcanic rocks including breccia, tuff, basalt, augite porphyry, siliciclastic and carbonate rocks including phyllite, argillite, quartzite, marble, and minor volcanoclastic tuffs. The hanging wall rocks in the Columbia River Fault (E) and the Beavan Fault (W) include Paleozoic - Lower Jurassic stratified rocks from the Kasko, Staccan and Rossland Groups as well as Hamill, Badshot, Lardcan and Milford Groups. Rocks in the footwall of these faults are interpreted as the deformed and metamorphosed equivalents of some of these rocks.

Rocks in the footwall of the Columbia River Fault

Locations: Pinnacles (P), Whatshan (W), Saddle Mountain (SM), Cusson Creek (CC), Plant Creek (PC), Cameron Lake (CL), South Foothill (SF), South Foothill Pluton (SFP), Mount Baldur (MB), Twin Peaks (TP), North Foothill (NF), Mount Symonds (MS), Fawn Lakes (FL)

Intrusive rocks

Three Valley Lamprophyres - ~48 Ma (Adams et al. 2005)

Ladybird Granite Suite - Late Paleocene to Eocene ca. 62 - 55 Ma (Carr 1992)

Biotite granite to quartz monzonite +/- garnet, muscovite, tourmaline. occurs as dykes, stocks, sills, makes up the South Foothill Pluton dated at 55 ± 1.5 and 55 ± 0.1 Ma (Parrish et al. 1988). Occurs as pegmatite, aplite and granite.

Whatshan batholith - Late Cretaceous ca. 77 Ma (Carr 1990). Hornblende - potassium feldspar quartz monzonite to diorite

Metasedimentary and metavolcanic rocks

Proterozoic to Jurassic metasedimentary and metavolcanic rocks of autochthonous and peritrochian affinity (Van Rooyen et al. 2010, Carr 1991, Fritz 1991). Protoliths correlated with the Proterozoic Horseshief Creek Group of the Windermere Supergroup (Fawn Lakes), Cambrian Hamill and Badshot Groups (Mount Symonds) and the Paleozoic Lardcan to Milford Groups (Arrow Lake schists and Gold Range Composite units) and are as young as Middle Jurassic in the Plant Creek area.

Calcareous quartzite marker unit

Arrow Lake garnet sillimanite muscovite biotite schist

Muscovite-biotite schist +/- garnet, sillimanite, local staurolite, kyanite. Includes micaceous quartzite, minor psammite gneiss, marble and amphibolite layers. Local carbonaceous schist and staurolite schist.

Composite units

Metasedimentary and metavolcanic including migmatitic paragneiss, semi-pelite gneiss, pelitic and semipelite schist, amphibolite, calc-silicate gneiss, quartzite and marble. Extensively intruded by Ladybird Granite Suite.

Marble

Quartzite

Fawn Lakes paragneiss

Migmatitic biotite-quartz-feldspar paragneiss and semipelite gneiss. Includes garnet amphibolite boudins and layers, extensively intruded by granitic pegmatite, distinct flaggy weathering appearance, predominantly aluminum-poor throughout section, sillimanite rare. Includes minor quartzite and psammite layers.

Cariboo Alp rocks

Locations: Cariboo Alp (CA)

Grey migmatitic hornblende biotite gneiss (+/- sillimanite, garnet) with amphibolite lenses and layers, hornblende diopside calc-silicate gneiss layers.

Rusty migmatitic gtl-sil-bt paragneiss with amphibolite boudins, includes quartzite, marble layers

Thor-Odin dome rocks

Locations: Icebound Lake (IL), Mount Thor (MT), Bearpaw Lake (BL), Frigg Glacier (FG)

Cover paragneiss

Heterogeneous psammite and calc-silicate gneiss, pelitic (Ky-Sil) gneiss, calc-silicate gneiss with interlayered marble, amphibolite boudins and layers.

Basal Quartzite

Basement orthogneiss

Leucocratic monzonite and gneissic quartz monzonite; hornblende-biotite granodiorite orthogneiss, granitic biotite orthogneiss. May contain hornblende and range in composition from granite to granodiorite. Includes augen orthogneiss, biotite orthogneiss, as well as biotite granite.

Basement Paragneiss

Predominantly migmatitic paragneiss, includes psammite biotite-feldspar-quartz paragneiss with lenses of pelitic schist, garnet-feldspar-quartz gneiss and amphibolite. Also includes biotite-quartz-feldspar paragneiss containing abundant garnet amphibolite boudins and granitic pegmatite. Cordierite gneiss amphibolite occurs as boudinaged layers within the basement paragneiss, may contain cordierite, kyanite, spinel, olivine, garnet.

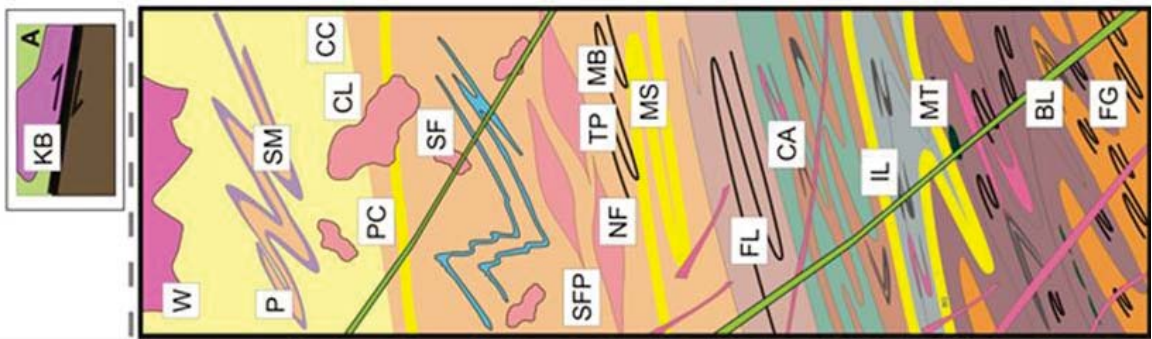


Figure 2.2 Lithology of major units in the Thor-Odin – Pinnacles area.

This column shows the main rock types and divisions used in this study. Specific areas discussed in the text are Bearpaw Lake (BL), Cameron Lake (CL), Cariboo Alp (CA), Cusson Creek (CC), Fawn Lakes (FL), and Frigg Glacier (FG). Icebound Lake (IL), Mount Baldur (MB), Mount Symonds (MS), Mount Thor (MT), North Fosthall (NF), Plant Creek (PC), Pinnacles (P), Saddle Mountain (SM), South Fosthall (SF), South Fosthall pluton (SFP), Twin Peaks (TP), and Whatshan batholith (W). Data from Read and Wheeler 1976; Archibald et al. 1983; Parrish and Wheeler 1983; Parrish and Armstrong 1987; Parrish et al. 1988; Coleman 1990; Fritz et al. 1991; Parkinson 1991; Carr 1990, 1991a, 1992, 1995; Colpron et al. 1996; Vanderhaeghe et al. 1999; Johnston et al. 2000; Norlander et al. 2002; Gibson et al. 2003; Kuiper 2003; Thompson et al. 2004; Kruse et al. 2004; Adams et al. 2005; Glombick 2005; Hinchey et al. 2006, 2007; Lemieux 2006; this study.



5 cm

Figure 2.3 Garnet–muscovite granitic pegmatite of the Ladybird granite in the South Fosthall area. The Ladybird granite is variably deformed throughout the study area; this is an example of the undeformed, post-tectonic Ladybird granite.



5 cm

Figure 2.4 Ladybird granite crosscutting calc-silicate amphibolite in the North Fosthall area. The pegmatite is interpreted as part of the youngest Ladybird intrusions in this area, based on the presence of tourmaline (Carr 1992) and the crosscutting nature of this granite.



1 m

Figure 2.5 Undeformed pegmatite of the Ladybird granite at Plant Creek area. This pegmatite crosscuts the steeply south dipping metasedimentary country rocks on the left of the photograph and is an example of a post-tectonic pegmatite of the Ladybird granite.



1 m

Figure 2.6 Deformed pegmatite and granite of the Ladybird suite in the Twin Peaks – Mount Baldur area. Mount Baldur is within the boundaries of the South Fosthall pluton, a granite batholith composed of variably deformed Paleocene to Eocene Ladybird granite (Carr 1990; Hinchey et al. 2006). These pegmatites are an example of a pre- or syn-tectonic pegmatite intrusion common in the study area.



50 cm

Figure 2.7 Pegmatites of the Ladybird granite suite at Mount Symonds.

These pegmatites are concordant with the south dipping foliation of the paragneiss units into which they intrude, indicating pre- or syn-deformational intrusion.



1 m

Figure 2.8 Undeformed pegmatites of the Ladybird granite crosscutting the grey migmatitic gneiss at Cariboo Alp. The steeply dipping pegmatites are a conjugate set; the plane bisecting the acute angle between them striking to the south, dipping steeply to the west.



20 cm

Figure 2.9 Steeply dipping north-south striking fractures that cross-cut all other structural features at Cariboo Alp. These fractures are filled with very fine-grained greenschist facies minerals, including chlorite. These fractures are interpreted as the latest Eocene deformation in the area. They are parallel to the lamprophyre intrusions in Figures 2.10 – 2.13.



2 m

Figure 2.10 Large lamprophyre dyke ~8 m wide crosscutting garnet–sillimanite–biotite gneiss at Twin Peaks. This lamprophyre dyke does not have chilled margins. The dyke strikes to the north and dips 80° to the east. It is interpreted as part of the Three Valley suite of lamprophyre dykes which intruded the Thor-Odin – Pinnacles area at c. 48 Ma (Adams et al. 2005).



5 cm

Figure 2.11 Detail of the contact between a lamprophyre dyke (Figure 2.10) and the host gneiss at Twin Peaks. This lamprophyre dyke does not have chilled margins and crosscuts the regional transposition foliation in garnet–sillimanite–biotite gneiss.



50 cm

Figure 2.12 Lamprophyre dyke, 50 cm wide, at Twin Peaks. This dyke strikes north-south and is vertical. It crosscuts Ladybird granite at Twin Peaks and has no chilled margins.

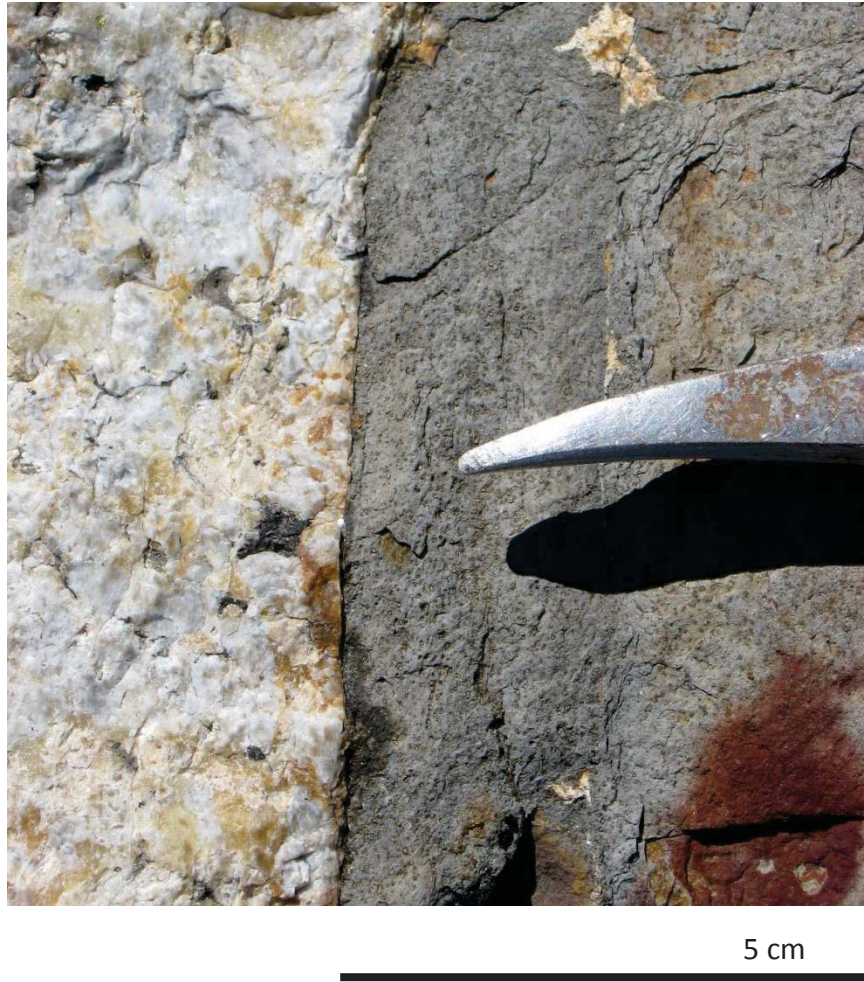


Figure 2.13 Detail of the edge of the lamprophyre dyke in Figure 2.12, showing the lamprophyre crosscutting a pegmatite of the Ladybird granite. The lamprophyre dyke is part of the Kamloops suite that intruded the Thor-Odin – Pinnacles area and the adjacent areas of southeastern British Columbia at c. 48 Ma (Adams et al. 2005).

Igneous U-Pb geochronology show downward younging progression of pegmatite intrusion, leucosome crystallization and downward younging of deformation

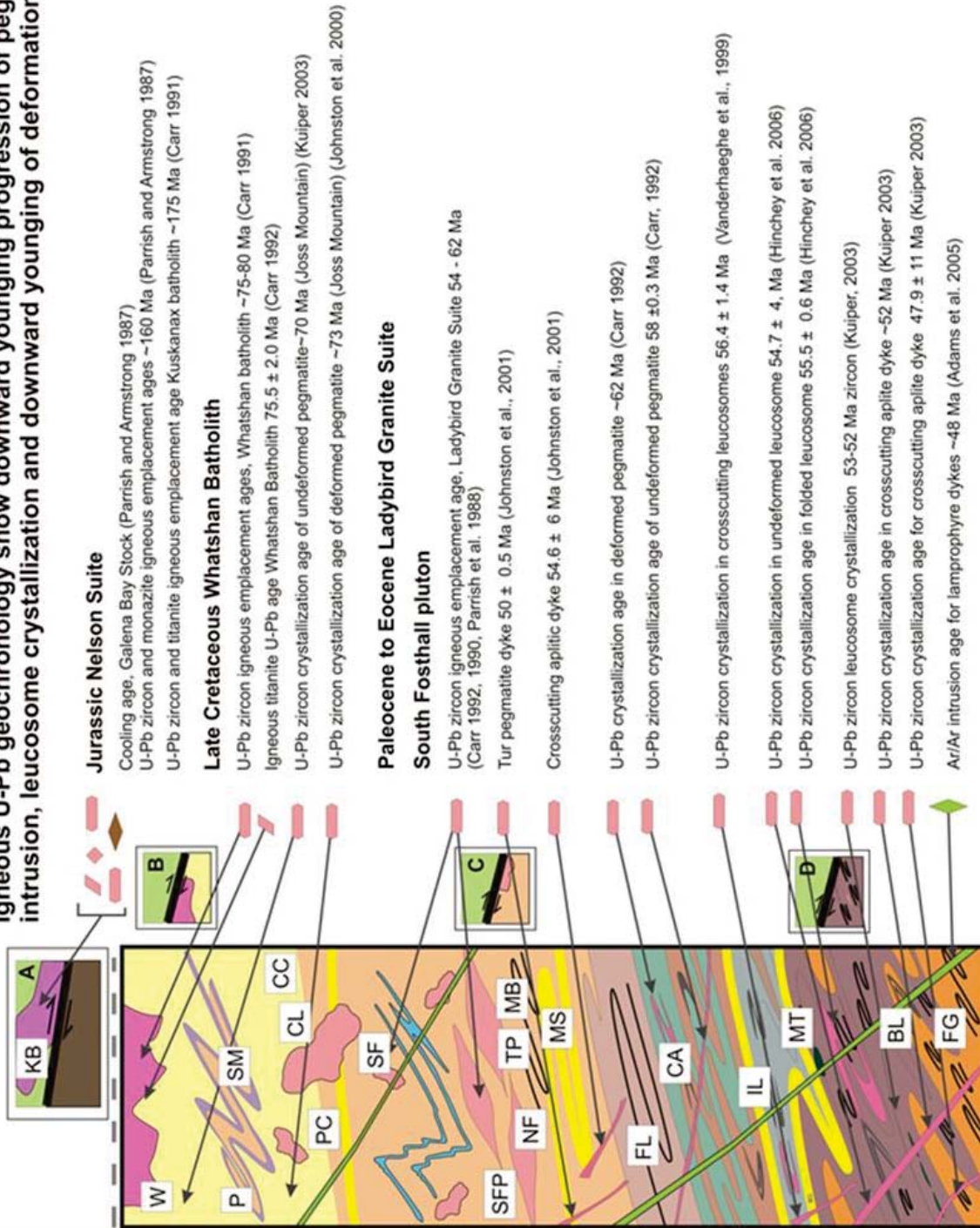


Figure 2.14a



Figure 2.14b

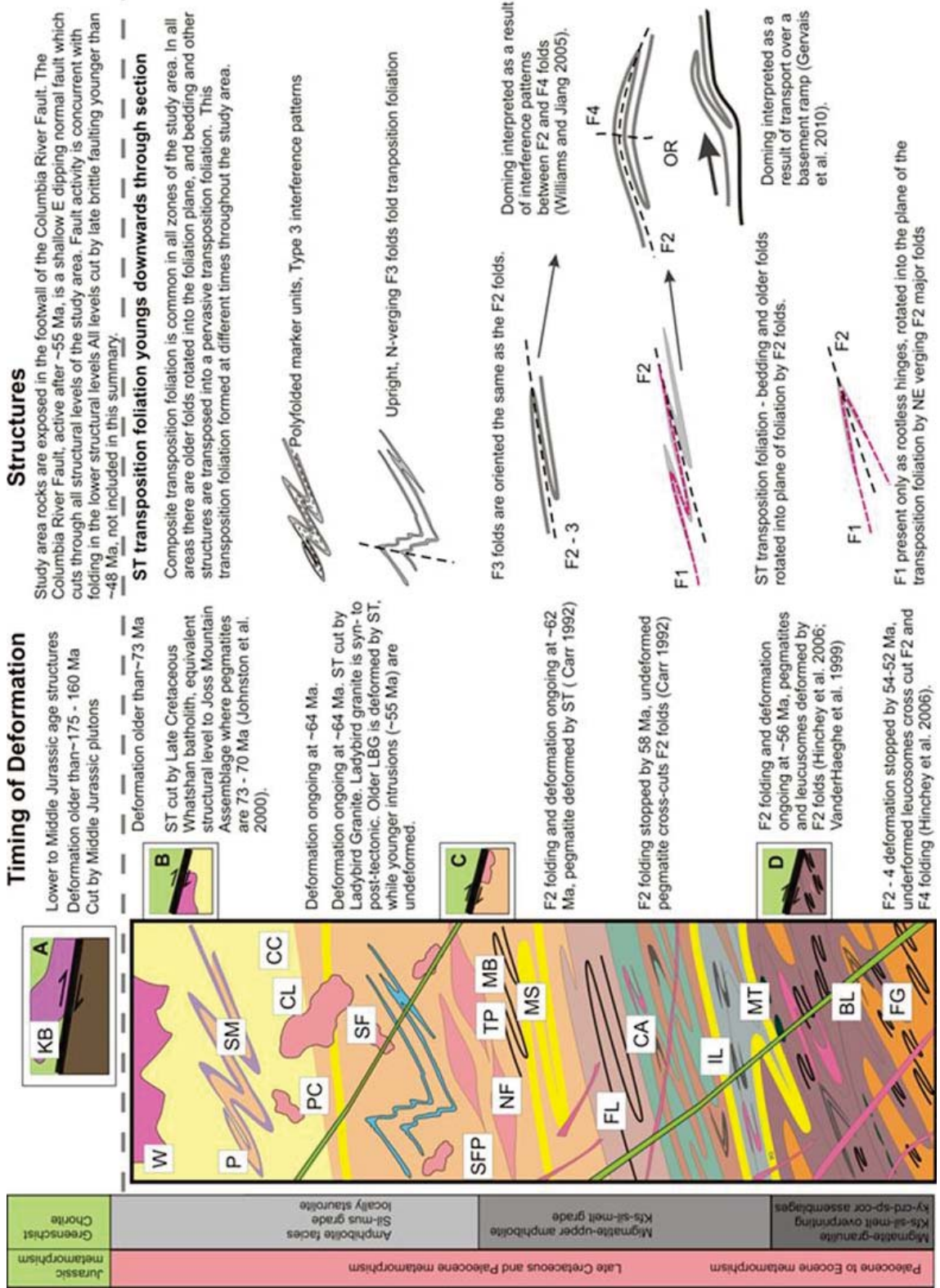


Figure 2.14c

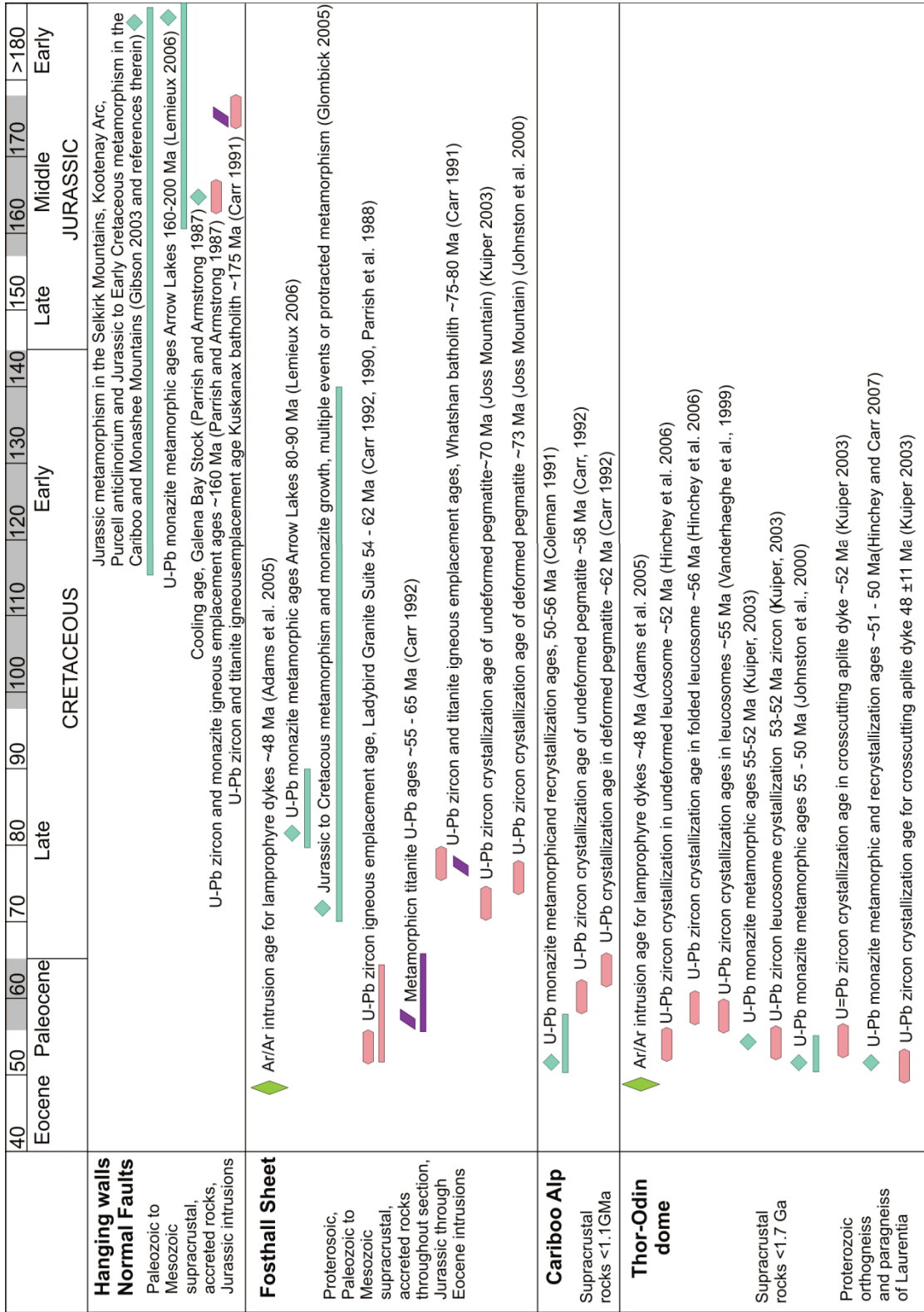


Figure 2.14d

Symbols



Normal fault - Columbia River Fault projected into section; active < 55 Ma



Igneous zircon age



Igneous titanite age



Igneous monazite age



Biotite cooling age, plutonic granodiorite



Biotite cooling age, intrusive lamprophyre



Metamorphic monazite age



Metamorphic titanite age



Metamorphic zircon age

Figure 2.14 Tectonostratigraphic column of the study area summarizing timing of deformation and metamorphism at different structural levels.

The column representing the study area summarized U-Pb zircon ages of deformed and undeformed igneous rocks (2.2a) and metamorphic data including timing of

metamorphism, pressure and temperature conditions, and metamorphic grade (2.2b).

Figure 2.2c contains a summary of information on metamorphic age, grade, timing of deformation and structural styles. Specific areas discussed in the text are Bearpaw Lake (BL), Cameron Lake (CL), Cariboo Alp (CA), Cusson Creek (CC), Fawn Lakes (FL), and Frigg Glacier (FG). Icebound Lake (IL), Mount Baldur (MB), Mount Symonds (MS), Mount Thor (MT), North Fosthall (NF), Plant Creek (PC), Pinnacles (P), Saddle Mountain (SM), South Fosthall (SF), South Fosthall pluton (SFP), Twin Peaks (TP), and Whatshan batholith (W).

(Data from Read and Wheeler 1976; Archibald et al. 1983; Parrish and Wheeler 1983;

Parrish and Armstrong 1987; Parrish et al. 1988; Coleman 1990; Carr 1990, 1991, 1992,

1995; Smith and Gehrels 1992; Colpron et al. 1996; Vanderhaeghe et al. 1999; Johnston

et al. 2000; Norlander et al. 2002; Gibson et al. 2003; Kuiper 2003; Adams et al. 2005;

Glombick 2005; Hinchey et al. 2006, 2007; Lemieux 2006; this study.)

Figure 2.14a: Timing of deformation and intrusion of igneous rocks in the Thor-Odin – Pinnacles area.

Figure 2.14b: Timing and grade of metamorphism in the Thor-Odin – Pinnacles area.

Figure 2.14c: Summary of timing and style of deformation in the Thor-Odin – Pinnacles area.

Figure 2.14d: Geochronology summary to complement Figures 2.14a-c.



1 m

Figure 2.15 Shallow south dipping metasedimentary and calc-silicate rocks in the Plant Creek – South Fosthall area. These metamorphic rocks are typical of the mixed assemblage of upper amphibolite facies metasedimentary and metavolcanic rocks found in the center of the study area (Figure 1.2).



50 cm

Figure 2.16 Quartzite unit near Plant Creek dipping shallowly to the south. This photograph illustrates the closely spaced steeply dipping north-south striking fractures found throughout the study area.



10 cm

Figure 2.17 Marble unit from Plant Creek showing outcrop-scale asymmetric folds.

This pattern is repeated in the km-scale F3 folds that create the map pattern illustrated in cross section 1.3b. This sample is not in-situ but is included because it illustrates the style of folding so well.



Figure 2.18a View looking north from the Twin Peaks. The first ridge is the northern edge of Twin peaks, the range in the middle distance are the rocks of the southern flank of the Thor-Odin dome and the rocks in the far distance are rocks of the core of the dome.

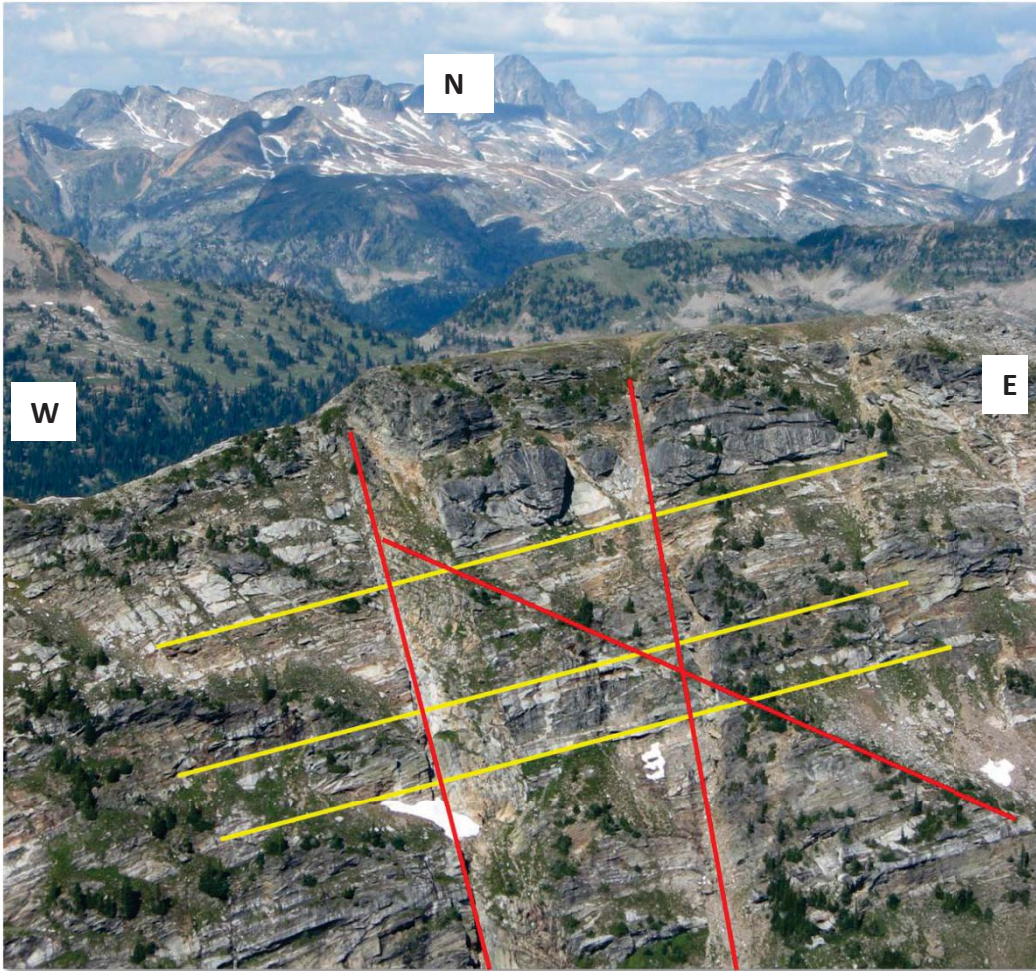


Figure 2.19b View to the north at Twin Peaks showing a strongly developed regional fabric. The structures shown in (a) are annotated in (b). The yellow lines (b) highlight the trace of the regional south-southwest dipping transposition foliation and the red lines highlight granitic dykes (Reesor and Moore 1971) interpreted as part of the Ladybird granite suite that crosscut the regional foliation.

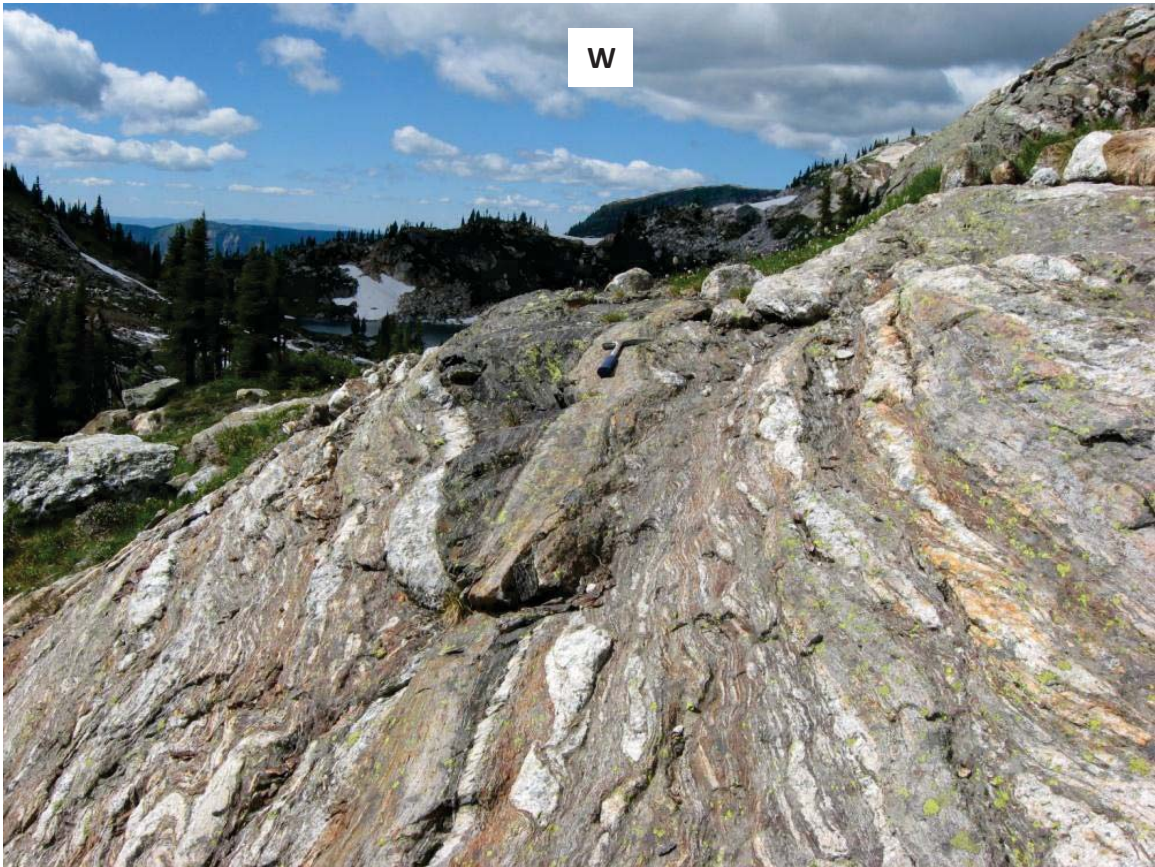


Figure 2.20 Westward view of pegmatites of the Ladybird granite at Twin Peaks.

Pegmatites are concordant with the regional south-southwest dipping transposition foliation in the country rock indicating pre- or syn-deformational intrusion of pegmatites. The foliation dips shallowly to the north on the short limb of a regional F3 fold that has an axial plane dipping steeply to the south as illustrated in Figure 1.3.



20 cm

Figure 2.21 Pegmatite of the Ladybird granite surrounding a raft of calc-silicate amphibolite in the Twin Peaks Area. The amphibolite contains the regional transposition foliation as do the pegmatites, indicating pre or syn-deformational intrusion of the pegmatite.



Figure 2.22 Pegmatite and folded amphibolite in the Twin Peaks area. The amphibolite outlines the regional fold closure at Twin Peaks illustrated on Figure 1.2; this regional fold hinge plunges shallowly to the west, and the axial plane dips steeply to the south.



5 cm

Figure 2.23 Migmatitic garnet–biotite gneiss at Twin Peaks. This view illustrates the abundant leucosome present in this rock.



50 cm

Figure 2.24 Migmatitic calc-silicate amphibolite in the Twin Peaks area. Although this rock is not in situ illustrates the regional folding style of minor folds near the core of a F3 fold hinge.



Figure 2.24a

2 m



Figure 2.24b

5 cm

Figure 2.25 Ultramafic pod (a) at Twin Peaks with bright green serpentine minerals in outcrop (b). The rock contains serpentized olivine with pyroxene, brucite, and talc. These ultramafic rocks can be traced throughout the study area and may represent a remnant of the Slide Mountain ocean basin (Carr 1991).



5 cm

Figure 2.26 Sillimanite contained in a well-developed transposition foliation in migmatitic garnet–sillimanite–biotite gneiss at Twin Peaks. Prolate garnets also lie within the south-southwest dipping foliation plane. Sillimanite needles are bent around the garnets, interpreted as evidence that the garnet and sillimanite both grew during development of the transposition foliation.



20 cm

Figure 2.27 Migmatitic amphibolite gneiss at Twin Peaks with a well-developed transposition foliation. Below the hammer there is a crosscutting vein of coarse-grained granitic leucosome. The leucosomes in the foliation are crosscut by this coarse grained pegmatite vein which in turn has been deformed, illustrating the progressive nature of leucosome generation, pegmatite intrusion and deformation.



5 cm

Figure 2.28 Small scale folds in migmatitic garnet–biotite gneiss at Twin Peaks illustrative of the regional fold style. These cm-scale folds have axial planes that dip steeply to the south and fold hinges that plunge shallowly to the west, similar to the regional fold closure mapped at Twin Peaks (Figure 1.2).



5 cm

Figure 2.29 Boudinaged pegmatite layer in highly strained calc-silicate amphibolite in the North Fosthall area. The orientation of the boudinaged leucosome within the south dipping foliation plane suggests elongation in an east-west direction.



50 cm

Figure 2.30 Moderately southwest dipping calc-silicate amphibolite gneiss in the North Fosthall area. This example illustrates a medium grade amphibolite that is not crosscut by pegmatites or granite.



2 m

Figure 2.31 Moderately south dipping metasedimentary rocks in the Mount Symonds area. The Mount Symonds and Fawn Lakes study areas are both located on the long limbs of km-scale folds with axial planes dipping to the south to south-southwest.



5 cm

Figure 2.32 Garnet–biotite gneiss with a cm-scale asymmetric isoclinal S fold at Mount Symonds. The axial plane of this fold dips steeply to the south, similar to the regional km-scale folds at Fawn Lakes and Mount Symonds.



5 cm

Figure 2.33 Boudinaged pegmatitic leucosome in moderately south dipping garnet–biotite gneiss at Mount Symonds. The orientation of the boudinaged leucosome within the south dipping gneiss suggests elongation in a northeast-southwest direction, similar to those documented at Plant Creek in Figure 2.28.



50 cm

Figure 2.34 Amphibolite and Ladybird pegmatite deformed together at Mount Symonds. The concordant natures of the pegmatites indicate pre- or syn-deformational intrusion of the pegmatite in this area.



50 cm

Figure 2.35 Moderately southwest dipping semipelitic paragneiss at Fawn Lakes. This semipelitic gneiss illustrating the distinctive flaggy weathering style characteristic of the Fawn Lakes Assemblage.



5cm

Figure 2.36 Garnet–biotite paragneiss at Fawn Lakes. The cm-scale folds show sheared out fold limbs and some coarse grained leucosomes that are late in the transposition history.



2 m

Figure 2.37 Southwest dipping transposition foliation in paragneiss at Cariboo Alp. This transposition foliation is present in all gneiss units on Cariboo Alp. This photograph shows rusty weathering garnet–sillimanite–biotite gneiss with a layer of quartzite dipping moderately to the southwest.



1 m

Figure 2.38 Ladybird pegmatites at Cariboo Alp. These pegmatites are concordant with the regional southwest dipping transposition foliation in the country rock, indicating pre- or syn-deformational intrusion of pegmatites.



50 cm

Figure 2.39 Migmatitic biotite gneiss at Cariboo Alp. There are coarse-grained granitic leucosomes that crosscut the transposition foliation as well as boudinaged pegmatites elongated in a northeast-southwest direction along the southwest dipping foliation planes.



Figure 2.39a

2 cm



Figure 2.39 b

2 cm

Figure 2.40 Details of the grey quartzofeldspathic gneiss at Cariboo Alp. These photos show the composite transposition foliation, rootless isoclinal fold hinges (a), cm-scale gneissic layering (b) defined by biotite, diopside and hornblende alternating with quartz and plagioclase.



Figure 2.40a

20 cm



Figure 2.40b

2 cm

Figure 2.41 Garnet amphibolite boudin with foliation at an acute angle to the transposition foliation in the paragneiss (a) and a snowball garnet (from a different boudin) with internal foliations. These structures are interpreted as evidence for a long-lived transposition foliation with syn-tectonic garnet growth as well as the existence of older deformation events.



Figure 2.41a

50 cm



Figure 2.41b

50 cm

Figure 2.42 Northeast verging folds at Cariboo Alp. This photograph shows a marble-quartzite package (a) with heterogeneous deformation visible in the marble, and a grey quartzofeldspathic gneiss (b). The fold vergence indicates a top-to-the-northeast directed sense of movement as the dominant structural orientation at Cariboo Alp.

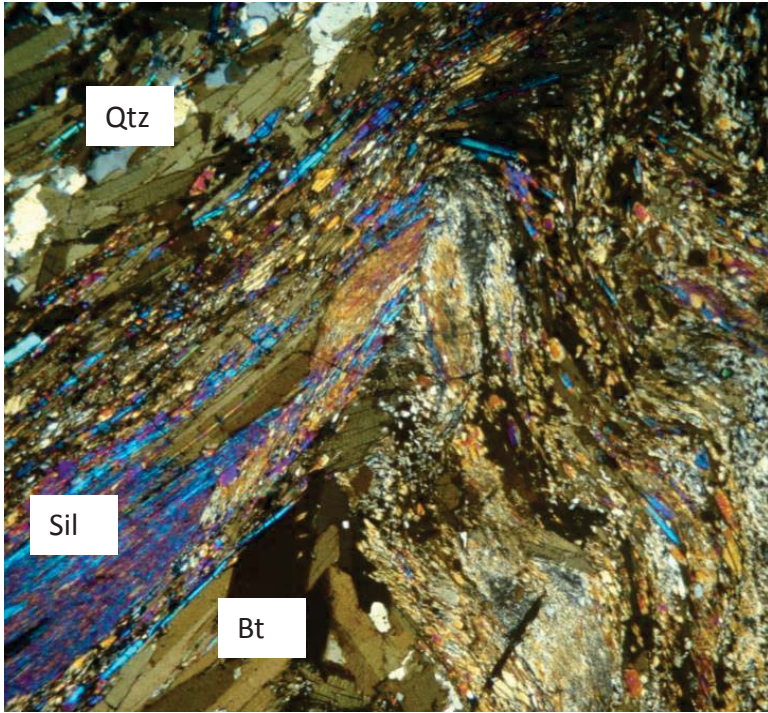


Figure 2.42a

0.5 mm

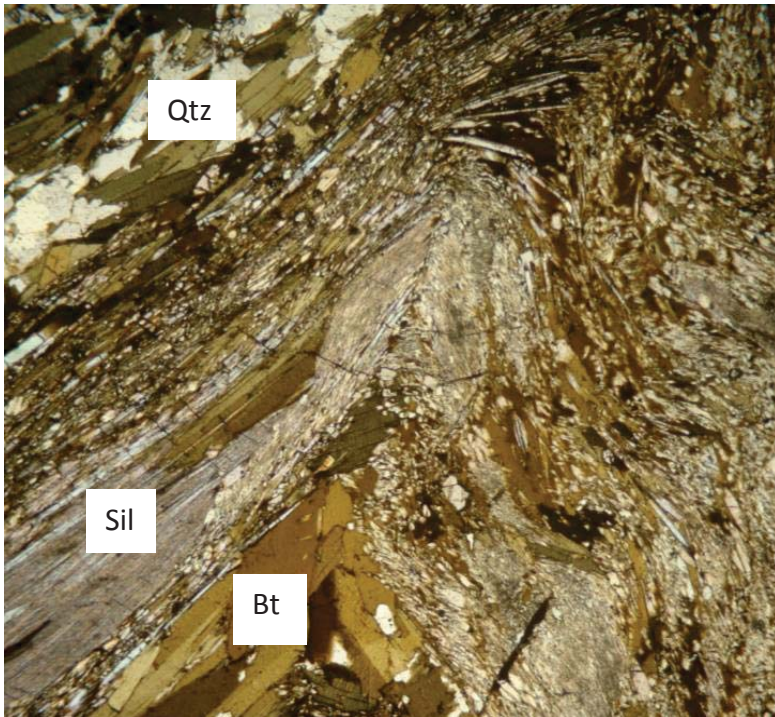


Figure 2.42b

Figure 2.43 Photomicrographs of garnet sillimanite biotite paragneiss (DC184) at Cariboo Alp in cross polarized light (a) and in plane polarized light (b).

The folded sillimanite needles are interpreted as evidence for pre- or syn-deformational growth of the high temperature metamorphic assemblage. The fold in this section shows a northeast verging sense of motion, similar to the direction of motion determined from outcrop scale folds (Figure 2.41). The section is oriented perpendicular to the northeast-southwest “motion plane”.



Figure 2.44 Asymmetric pressure shadows on a large diopside crystal in grey calc-silicate gneiss at Cariboo Alp. The shear sense is top-to-the-northeast, consistent with the northeast verging folds observed at Cariboo Alp (Figure 2.41, 2.42).

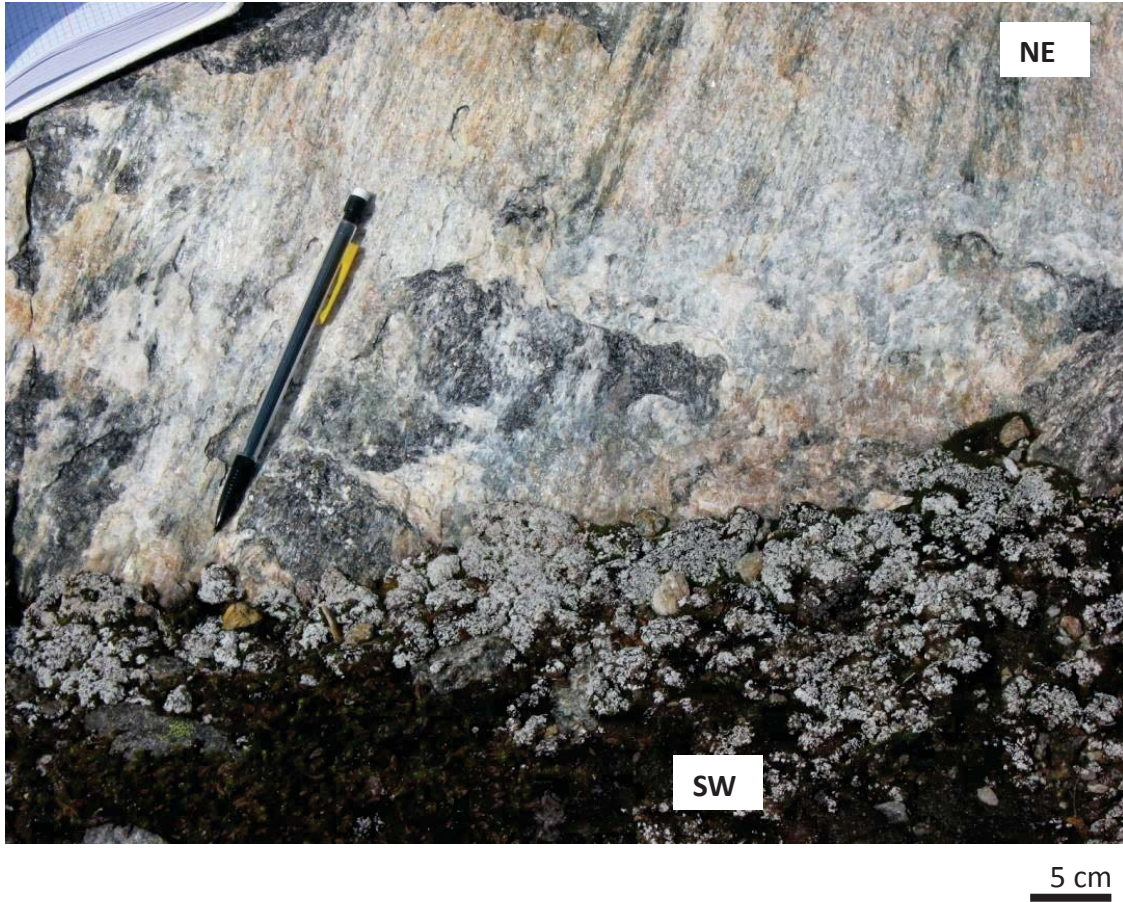


Figure 2.45 Sillimanite lineation plunging shallowly to the southwest at Cariboo Alp. Coarse sillimanite lineations are limited to foliation surfaces and could represent high-temperature syn-tectonic growth of sillimanite during reactivation.



5 cm

Figure 2.46 Two generations of sillimanite lineations at Cariboo Alp. The one shown with the blue pencil plunges shallowly to the southwest while the one shown with the red pencil plunges shallowly to the west. Both generations are present on fracture planes that are concordant with foliation surfaces in the grey gneiss, suggesting that they may represent evidence for reactivation of foliation planes.



Figure 2.47 The Icebound Lake study area with a view facing west. Southwest dipping layers form the cliff at the top left of the photograph. Cariboo Alp is located on top of the cliff. The yellow dots in the cliff shadow are tents for scale. These are migmatitic basement rocks of the Thor-Odin dome in the bottom right of the photograph, overlain by migmatitic cover rocks in the cliff face on the top left. This represents the area between Cariboo Alp and Icebound Lake as shown in the tectonostratigraphic columns in Figures 2.1, 2.2 and 2.14.



50 cm

Figure 2.48 Garnet amphibolite rafts and lenses in migmatitic garnet–biotite gneiss at Icebound Lake.



10 cm

Figure 2.49 Fold interference (Type 3) pattern in layering within the main migmatitic garnet–biotite quartzofeldspathic paragneiss unit at Icebound Lake outlined by garnet amphibolite.



10 cm

Figure 2.50 Migmatitic garnet–biotite–quartzofeldspathic paragneiss unit at Icebound Lake. Due to a lack of preserved original layering this migmatite is classified as a diatexite migmatite.

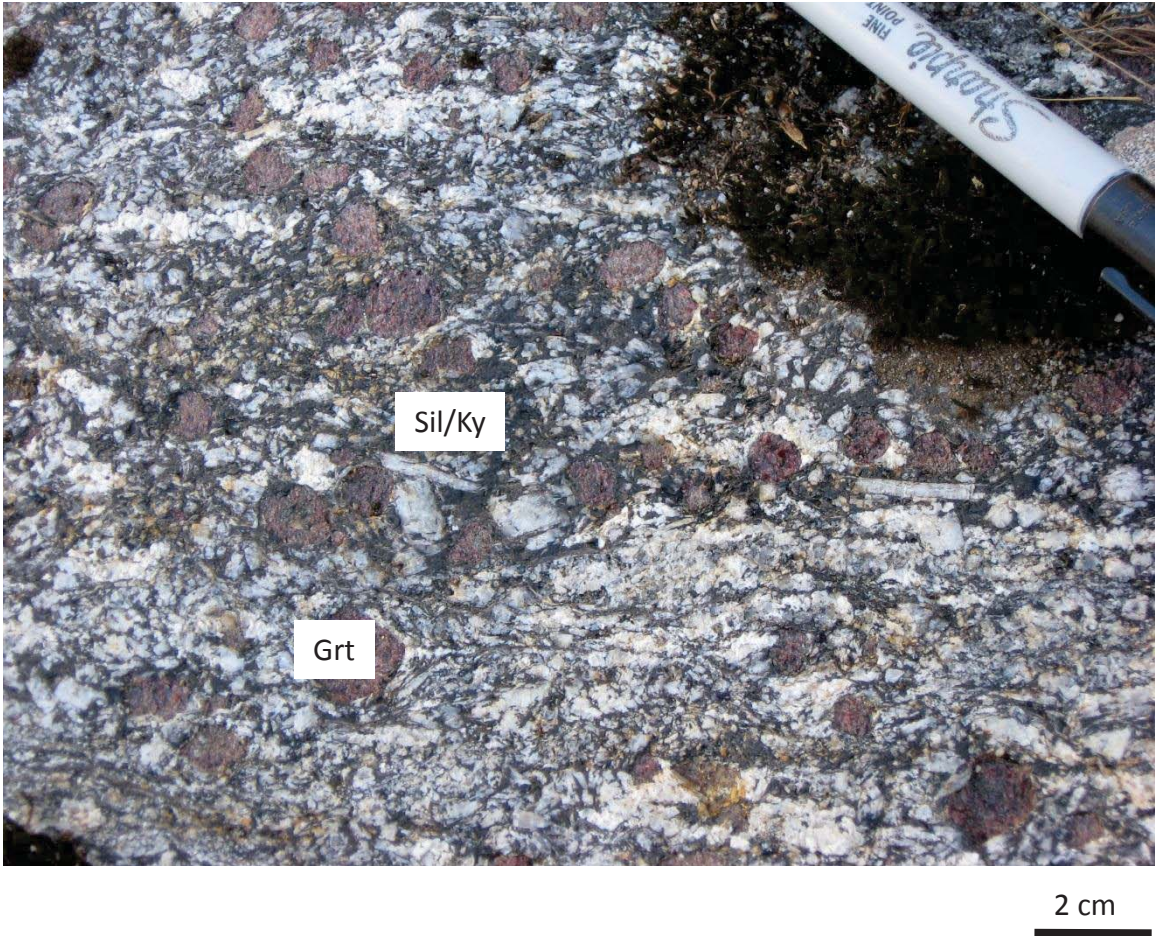


Figure 2.51 Migmatitic garnet–biotite–quartzofeldspathic paragneiss with cm long sillimanite clumps, possibly as pseudomorphs after kyanite. The presence of pseudomorphed kyanite suggests high temperature decompression may have occurred here. This is consistent with instances of high temperature decompression documented at Bearpaw Lake in the Thor-Odin dome (Norlander et al. 2002; Hinchey et al. 2006).



5 cm

Figure 2.52 Garnet–biotite–plagioclase–gedrite amphibolite at Icebound Lake. This layer occurs as a boudinaged layer of amphibolite throughout the Icebound Lake area, unconformably overlying the dominant migmatitic gneiss.



Figure 2.53 Close-up view of a garnet–biotite–plagioclase–gedrite amphibolite in the Icebound Lake area. This view shows an area with a 2 cm garnet, and gedrite-anthophyllite crystals up to 5 cm long. Biotite, quartz and plagioclase make up the matrix of the rock.



2 cm

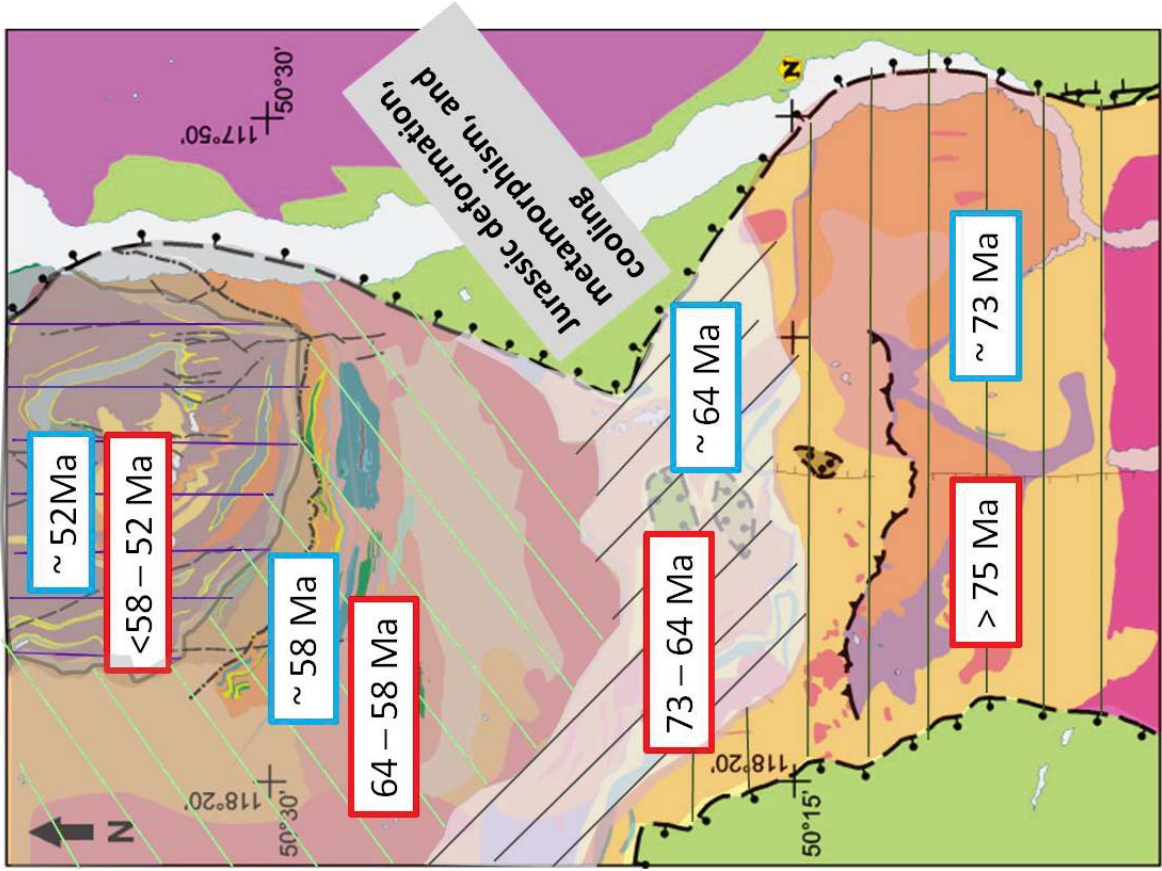
Figure 2.54 Gedrite–anthophyllite amphibolite with crystals up to 5 cm long in a matrix of quartz and plagioclase. The gedrite crystals are concentrated in layers, but not aligned within them.



Figure 2.55 Lens of chloritized garnets in the layer of migmatitic garnet–gedrite anthophyllite illustrated in Figures 2.51 – 2.53. This is interpreted as evidence for retrograde metamorphism in the Icebound Lake area.



Figure 2.56 Muscovite crystals in leucosomes at Cariboo Alp. These muscovite (1cm) crystals occur in pressure shadows of peritectic K-feldspar or plagioclase crystals in leucosome pods within the host migmatitic gneiss at Cariboo Alp. The muscovite is locally intergrown with chlorite, and interpreted as evidence for retrograde metamorphism. Both minerals are present as euhedral crystals 0.1 mm to 10 mm in diameter with sharp grain boundaries.



Infrastructure zones during the Lake Cretaceous to Eocene

- < 58 Ma
Thor-Odin dome
- ~ 64 – 58 Ma
North Fosthall, Mt. Symonds, Cariboo Alp
- ~ 73 – 64 Ma
Plant Creek – South Fosthall
- > 75 Ma
Whatshan Pinnacles

Based on the end of penetrative deformation, and deactivation of transposition foliation

Figure 2.57 Proposed locations for suprastructure/infrastructure zones preserved within the study area and their associated ages. Ages cited in boxes with blue borders indicate the time of ongoing metamorphism and penetrative deformation. Ages cited in boxes with red borders indicate the timing of the end of penetrative deformation.

3 Chapter: Age and provenance of marker quartzites in Thor-Odin dome:

Are apparent markers correlative and do Thor-Odin and Frenchman Cap

domes of the Monashee complex represent a single basement domain?

3.1 Introduction

The Thor-Odin and Frenchman Cap domes, together referred to as the Monashee Complex (Figure 1.1), are basement-cored tectonothermal culminations that form parts of the most deeply exposed structural levels in the Canadian Cordillera. These culminations are interpreted as exposures of Laurentian basement, based on correlation of magnetic and gravity anomalies (Ross 1991; Ross et al. 1991; Cook et al. 1995) and geochronology (Armstrong 1991; Parkinson 1991; Ross et al. 1991, 2005) which links age distinct basement domains on the Laurentian craton to rocks in the core of the Cordilleran orogen. They comprise Paleoproterozoic “basement” rocks (Armstrong et al. 1991; Parkinson 1991) consisting of orthogneiss and paragneiss in the core of the domes; and cover rocks consisting of paragneiss and other metasedimentary rocks, unconformably overlying the basement (Wheeler 1965 Reesor and Moore 1971; Brown 1980; Crowley 1997). These are tectonically overlain by pericratonic and accreted terranes; for example, the Kootenay, Slide Mountain, Cache Creek, and Quesnel terranes (see sections 2.2 – 2.5).

Throughout the Thor-Odin dome, and in the upper structural levels of the Frenchman Cap dome, the basement and cover rocks are complexly infolded and have experienced multistage Cretaceous to Eocene deformation and metamorphism (Reesor and Moore 1971; Brown 1980; Crowley 1997; Williams and Jiang 2005; Hinchey et al. 2006; Gervais et al. 2010) and Eocene exhumation (Parrish et al. 1988; Vanderhaeghe et al. 2003).

Geological maps of the Thor-Odin and Frenchman Cap domes show a single quartzite marker at the base of the cover rocks, which, in map view, delineates the shape of the domes (Read 1980; Kruse 2007; Gervais et al. 2010) (Figure 3.1). This quartzite marker has been interpreted as: i) having been unconformably deposited on Paleoproterozoic basement rocks, ii) a marker unit that can be used to identify infolds or repetitions of basement and cover rocks in the Thor-Odin dome (McNicoll and Brown 1995; Williams and Jiang 2005; Kruse 2007), and iii) the same unit in both domes (Read 1980; Spark 2001; Kruse 2007; Gervais et al. 2010).

The quartzite marker has formed the basis for correlations between the two domes (Read 1980) and has been generally accepted that the two domes form part of the same basement domain, contained within the Monashee Complex (Figure 3.2). Some workers argue that the roof of the complex is bounded by top to the northeast to east ductile thrust termed the Monashee décollement (Brown et al. 1986, 1992; McNicoll and Brown 1995; Brown and Gibson 2006; Williams et al. 2006) and that the two domes have a

shared tectonothermal history from the Proterozoic through the Eocene. We question this interpretation based on the following: (i) notable differences in lithology and age of basement rocks in the two domes, (ii) mapping evidence from the Thor-Odin dome questioning the presence of Monashee décollement at the upper boundary of the dome and reinterpreting the rocks as a continuous structural section without a structural break (McNicoll and Brown 1995; Spark 2001; Kuiper 2003; Kruse and Williams 2005, 2007) and, (iii) differences between timing of deformation and tectonothermal history within the two domes (Hinchey et al. 2006; Gervais et al. 2010; this study Chapter 2 and 5).

This study presents U-Pb detrital zircon ages from samples of the Thor-Odin dome (Mount Thor, Icebound Lake and Cariboo Alp; Figure 3.3) that were collected in order to test the hypotheses that: i) the quartzites within the Thor-Odin dome are correlative and share a common provenance; and ii) the basal quartzites in the Thor-Odin and Frenchman Cap domes are also correlative and shared a Proterozoic history.

3.2 Tectonic setting of the southeastern Canadian Cordillera and a brief history of the evolution of the Laurentian margin in the Thor-Odin – Pinnacles area

The focus of this chapter is on the metasedimentary rocks that occur within the internal zone of the orogen, within basement and cover rocks of the Thor-Odin dome as well as

on the overlying southern flank of the dome. The origins and original affinities of these highly deformed and metamorphosed rocks are crucial in understanding the tectonic evolution of the area. The miogeoclinal rocks deposited on the western margin of the Laurentian craton prior to Cordilleran orogenesis are preserved in the external and internal zones of the orogeny (see Chapter 2, section 2.6). Supracrustal rocks include those of the Proterozoic Belt Purcell Supergroup (Ross et al. 1992 and references therein), the Windermere Supergroup (Ross et al. 1992 and references therein), Neoproterozoic to Cambrian Hamill, Badshot and Mohican Groups (Colpron et al. 2002 and references therein), and the overlying Paleozoic Lardeau and Milford Groups (Fritz et al. 1991). In order to provide a basis for interpretation of detrital zircon ages, the following section briefly discusses detrital signatures and source terranes for each of the successions mentioned above.

The Belt-Purcell Supergroup of southeastern BC and northwestern United States is a 15 – 20 km thick siliciclastic and carbonate sedimentary succession, deposited mainly in an enclosed extensional basin setting with an active western margin (Ross et al. 1992).

Deposition of the Mesoproterozoic part of the Belt-Purcell Supergroup occurred between c. 1470 and 1400 Ma, based on U-Pb ages of intrusive igneous rocks within the Purcell sequences (Anderson and Davis 1995). Rocks of the eastern Belt-Purcell contain detrital zircons that range in age between c. 2700 to 1800 Ma while western Belt-Purcell rocks have additional detrital zircon populations with ages younger than c. 1800 Ma,

and as young as c. 1070 Ma (Ross et al. 1992; Ross and Villeneuve 2003). The younger populations do not have known sources within the western Laurentian craton but could be derived from the Grenville orogen. These populations overlap with the North American Magmatic Gap of 1610 to 1490 Ma (Ross et al. 1992; Ross and Villeneuve 2003). The Belt-Purcell rocks may be a source of second cycle zircons for some of the rocks discussed in this study.

The Windermere Supergroup is present throughout the Canadian Cordillera and the northwestern United States. The earliest rifting during the breakup of the supercontinent Rodinia occurred between c. 755 and 700 Ma (Powell et al. 1993; Windgate and Giddings 2000) and deposition of the Windermere Supergroup began between c. 740 and 723 Ma (Ross et al. 1995). The Windermere Supergroup records the first of two rifting events in the Neoproterozoic that formed what would eventually become the western passive margin of Laurentia (Colpron et al. 2002). The main Windermere strata present in southeastern British Columbia are the Horsethief Creek and Kaza Groups, the detrital signatures of which are both dominated by Laurentian-derived sediment with zircon age populations between c. 2160 and 1650 Ma, older than c. 2500 Ma, and a younger population with ages of c. 700 Ma (Ross and Bowring 1990; Ross and Parrish 1991; Smith and Gehrels 1991).

Rocks of the Hamill – Gog groups unconformably overlie the Neoproterozoic Windermere Supergroup rocks in southeastern BC, and in some areas directly overlie rocks of the Mesoproterozoic Belt-Purcell Supergroup (Colpron et al. 2002 and references therein). The Hamill Group contains shallow marine, fluvial and volcanic rocks (Gehrels and Ross 1998), interpreted as having been deposited in fault-bounded basins formed during crustal extension and rifting (Erdmer et al. 2001; Colpron et al. 2002 and references therein). Rifting along the western margin of Laurentia has been documented within the Hamill Group, where syn-rift volcanic rocks have been dated (U-Pb zircon) at 569.6 ± 5.3 Ma (Colpron et al. 2002), consistent with a previous 575 ± 25 Ma estimate of continental rifting based on evidence from analyses of tectonic subsidence (Bond 1997).

Overlying the Hamill Group in all areas of southeastern British Columbia is the Badshot Group, a Lower Cambrian carbonate sequence considered to be miogeoclinal, which includes a distinctive unit of archaeocyathid limestone-marble (Fritz et al. 1991). The Lardeau Group is part of the Kootenay terrane, a pericratonic terrane linked to the North American passive margin (Colpron and Price 1995). The Kootenay terrane is partly autochthonous with respect to the Laurentian margin, but also contains outboard volcanic terranes and associated oceanic sediments (Smith and Gehrels 1992; Colpron and Price 1995). The contact between the Badshot limestone and the lower Cambrian Lardeau Group rocks of the Kootenay terrane, as exposed in south-eastern British

Columbia, has been interpreted as a sheared fault contact (Smith and Gehrels 1992).

The Lower Paleozoic Kootenay terrane rocks typically contain detrital zircon populations that indicate sources dominated by Laurentian derived sediment (Smith and Gehrels 1991).

East of the Monashee complex in the Purcell Mountains and Rocky Mountain Main Ranges, Cambrian to Ordovician rocks of the Lardeau Group are shelf and shallow water sequences. In contrast, the Selkirk Mountains and Kootenay Arc contain Lardeau Group rocks that include metamorphosed deep basinal, sedimentary and volcanic rocks of the Kootenay terrane (Price and Colpron 1995; Colpron et al. 2002). Extensive basalt units, with alkali and within-plate tholeiitic composition (Smith and Gehrels 1992), and coarse clastic material in this sequence has been interpreted to be the result of crustal extension continuing after the Cambrian, linking the Lardeau Group (and by implication the Kootenay terrane) to the North American passive margin as a pericratonic terrane (Colpron and Price 1995). In contrast, earlier interpretations suggested that the deep water and volcanic units in the Kootenay terrane were part of an allochthonous terrane (Wheeler 1965; Monger and Price 2000).

Allochthonous terranes identified in south-eastern British Columbia, include the Paleozoic Slide Mountain terrane, the primarily Mesozoic Quesnellia terrane, the Harper Ranch, Cache Creek, and Stikinia terranes (Gabrielse et al. 1991; Ross et al. 1997). The

Slide Mountain terrane is a Permian marginal ocean basin that developed adjacent to the Laurentian margin, and is preserved as oceanic crust obducted over the pericratonic Kootenay terrane (Gabrielse et al. 1991). The Quesnellia terrane primarily consists of Triassic to Jurassic volcanic arc rocks and arc-related sediments that are all associated with juvenile oceanic crust, and are interpreted as having formed outboard of the Laurentian craton (Gabrielse et al. 1991; Parrish and Monger 1992), or alternatively on attenuated Laurentian crust (Erdmer et al. 2002; Thompson et al. 2006). In this study area (Figures 1.2, and 2.1) the Nicola, Slokan and Rossland Groups are part of the Quesnellia terrane (Carr 1991a; Gabrielse et al. 1991; Lemieux et al. 2003, 2004).

3.3 Monashee Complex and Monashee décollement terminology and interpretations

In current usage, the Monashee Complex (Figure 3.2) refers to two structural culminations, the Frenchman Cap dome to the north, and the Thor-Odin dome to the south (Reesor and Moore 1971; Höy and Brown 1980; Parrish et al. 1988) and has also been referred to as the Monashee Terrane (cf. Scammell and Brown 1990). It has generally been accepted that the two domes are part of the same basement domain, known as the Monashee Complex, and that the roof of the complex is bounded by a ductile thrust termed the Monashee décollement (Brown et al. 1986, 1992; McNicoll and Brown 1995; Brown and Gibson, 2006; Williams et al. 2006).

The Monashee décollement was originally described in the Frenchman Cap dome (Read 1979; Höy 1980; Brown 1980). It is a crustal scale top to the east to northeast thrust-sense ductile shear zone expressed as a northeast verging mylonitic shear zone juxtaposing Kootenay terrane rocks (referred to as Selkirk Allochthon) over the Monashee complex (Brown et al. 1986). The Selkirk Allochthon or hanging wall of the décollement contains age-equivalent rocks to the cover rocks in the footwall, including Windermere Supergroup rocks, Hamill-Badshot equivalents and Lardeau Group rocks (Journey 1986; Scammell 1993). Figures 3.4a and 3.4b illustrate the location of the Monashee décollement and some of the major stratigraphic correlations within the Thor-Odin and Frenchman Cap domes, respectively. The quartzite marker unit interpreted as the “basal” quartzite of both culminations has formed a basis for correlating the two domes (Read 1980).

The interpretations regarding the Monashee décollement were extended to include the Thor-Odin dome when McNicoll and Brown (1995) interpreted a zone of high strain in the Cariboo Alp area, on the southwestern flank of the Thor-Odin dome, as the detachment. The Cariboo Alp area was originally mapped by Reesor and Moore (1971) as a “contorted zone”, later found to be coincident with a zone of strong southwest dipping seismic reflections in Lithoprobe Lines 6 and 7 (Cook et al. 1992). McNicoll and Brown (1995) described the zone as a series of ductile thrust slices composed of F3 folds with sheared-out lower limbs, intercalating basement and cover rocks in a ductile

duplex. Recent studies have proposed that there is no lithological or structural break between the basement and cover rocks in the Thor-Odin dome, and that the Monashee décollement does not exist in the Thor-Odin dome (Spark, 2001; Kuiper, 2003; Williams et al. 2006). Other authors refer to the southwestern and southern margin of the dome as the Thor-Odin high strain zone, and interpret it as an extensional structure (Kruse and Williams 2005, 2007). It has also been proposed that the Monashee décollement in both domes is the lower boundary of a Cretaceous to Paleocene mid-crustal channel (Johnston et al. 2000; Brown and Gibson, 2006; Williams et al. 2006; Kuiper et al. 2006; Gervais et al. 2011).

In both the Thor-Odin dome and the upper structural levels of the Frenchman Cap dome the basement and cover rocks are complexly infolded and have experienced multistage deformation and metamorphism as discussed in sections 2.4 – 2.6 (Reesor and Moore 1971; Brown 1980; Crowley 1997; Williams and Jiang 2005; Hinchey 2005). Infolds of basement and cover rocks were mapped in the Thor-Odin dome at Pingston Creek, Mount Begbie, Mount Thor, Icebound Lake, Mount Skade, and at Cariboo Alp (Figure 1.3, 3.3). Quartzites at the previously interpreted locations for basement/cover contacts at Mount Thor, Icebound Lake, and Cariboo Alp were sampled for analyses in order to determine whether it is geologically permissible to interpret them as correlative.

3.3.1 Basement rocks: Thor-Odin and Frenchman Cap domes

This section presents an overview of the lithology and age constraints on basement rocks in the Thor-Odin dome. Basement rocks comprise migmatitic paragneiss and orthogneiss. Basement orthogneiss mainly consist of migmatitic hornblende–biotite–quartzofeldspathic gneiss with subordinate quartz monzonite gneiss (Reesor and Moore 1971). Basement paragneiss in the Thor Odin dome contain migmatitic garnet–sillimanite–quartzofeldspathic gneiss (\pm cordierite); migmatitic cordierite–biotite–quartzofeldspathic gneiss; minor calc-silicate gneiss, marble, and quartzite, with local amphibolites and distinct lenses of cordierite–gedrite rocks (Reesor and Moore 1971; Duncan 1984; Hinchey and Carr 2007). Basement orthogneiss and paragneiss are lithologically distinct with generally concordant contacts, but are commonly interlayered at meter scale as a result of folding and transposition. Some intrusive contacts between orthogneiss and paragneiss have been documented (Parkinson 1992; Spark 2001; Hinchey 2005). The contact relationships between units may be complicated by the migmatitic nature of the basement rocks and the abundance of leucosome derived from partial melting (Spark 2001; Hinchey 2005).

The Frenchman Cap dome basement rocks include granitic to dioritic orthogneiss, kyanite–sillimanite schist, migmatitic sillimanite paragneiss and biotite–hornblende paragneiss, and pelitic and semi-pelitic schist (Read 1979; Crowley 1997, 1999). In contrast to the Thor-Odin dome, cordierite–gedrite amphibolites are not present in the

Frenchman Cap dome. In the Thor-Odin dome the basement rocks are dominated by paragneiss whereas in the Frenchman Cap dome, orthogneiss is the dominant rock type and paragneiss is restricted to minor interlayers within the orthogneiss, and an a 0.5 km thick paragneiss layer structurally above the basement orthogneiss (Crowley 1997).

The Thor-Odin and Frenchman Cap (Monashee Complex) basement rocks are considered to be correlative with Paleoproterozoic exposures of North American cratonic rocks based on age (Armstrong et al. 1991; Parkinson 1991; Crowley 1997; Hinchey et al. 2006; Crowley et al. 2008). This correlation is also supported by similarities to the Paleoproterozoic craton with respect to Sm/Nd ratios and geochemistry as reported by Parkinson (1991) and Ross et al. (1995). Figure 3.5 summarizes the known ages of protoliths for the rocks in the Thor-Odin and Frenchman Cap domes. U-Pb zircon crystallization ages for orthogneisses in Thor-Odin dome are c. 1930 Ma (granodioritic augen orthogneiss) and c. 1870 Ma (granitic gneiss) (Parkinson 1991). In Frenchman Cap dome the known U-Pb crystallization ages of the dominant orthogneiss bodies are c. 2300 Ma (dioritic gneiss; Crowley 1999), c. 2270 – 2070 Ma (Armstrong et al. 1991), c. 2100Ma (granitic orthogneiss; Crowley 1999), c. 2080 Ma (K-feldspar augen granitic gneiss; Crowley 1999), and c. 1860 Ma (granitic orthogneiss; Crowley 1997). Other Paleoproterozoic basement gneisses in the southern Canadian Cordillera have similar ages including the Malton Gneiss at c. 1990 – 1870 Ma

(McDonough and Parrish, 1991), the Gold Creek gneiss at c. 2090 Ma (Murphy et al. 1991) and the Sifton Gneiss at c. 1850 Ma (Evenchick et al. 1984).

The paragneisses in both domes are assumed to be older than the intrusive orthogneiss bodies. In Thor-Odin dome detrital zircons from the paragneiss were dated between c. 2200 – 2000 Ma, suggesting deposition of the paragneiss protolith began after c. 2000 Ma (Parkinson 1992) and ended by c. 1870 Ma based on the intrusive orthogneiss crystallization age (Parkinson 1991, 1992). Deposition of paragneiss protoliths in other areas of Thor-Odin may have continued locally to c. 1800 Ma based on the youngest detrital zircons reported in basement paragneiss in the area of Blanket Mountain (Kuiper 2003). In Frenchman Cap dome the deposition of paragneiss protoliths had to have occurred before the growth of metamorphic monazite within the paragneiss at c. 2100 Ma (Crowley and Parrish 1999). Deposition most likely predated the intrusion of a c. 2300 Ma dioritic orthogneiss (Crowley 1999) but no other age constraints on the paragneiss in either dome exist. In a study of the leucosomes contained in the basement paragneiss by Hinchey et al. (2006), it was found that most zircons within the leucosomes had inherited Precambrian cores that ranged in age from 2564 ± 6 Ma to 1865 ± 12 , consistent with the age of zircons in the host paragneiss. (See Figures 3.4 and 3.5 for illustrations of the relationships between map units and the available geochronology data.)

3.3.2 Cover rocks: Thor-Odin and Frenchman Cap domes

The cover rocks of Thor-Odin dome consist of migmatitic paragneiss, quartzite, marble, calc-silicate gneiss, amphibolite, pelitic schist, and other variably metamorphosed sedimentary and volcanic rocks (Reesor and Moore 1971; Parkinson 1992; Spark 2001; Hinchey 2005). The cover rocks are only exposed within the traditional confines of the Monashee Complex in the mapped infolds of basement and cover rocks at Pingston Creek, Mount Begbie, Mount Thor, Icebound Lake, Mount Skade, and at Cariboo Alp (Figures 1.3, 3.2 and 3.3). It has been proposed that the Thor-Odin dome cover rocks should also include the rocks structurally above the margin of the dome at the Monashee décollement (or Thor-Odin high strain zone), including all the rocks in the footwall of the Columbia River fault and the Beaven or Okanagan Valley – Eagle River fault zone (Thompson et al. 2004, 2006). However, this is not considered as viable alternative in this study because the proposed “cover” rocks, as interpreted by Thompson et al. (2004, 2006), include a number of units (i.e. Lardeau Group rocks with ultramafic units in the Mount Symonds and Twin Peaks areas) that were tectonically emplaced and obducted over Laurentian margin sediments (Okulitch 1984; Carr 1990), and therefore do not fit the definition of cover rocks as being deposited directly on cratonic basement.

In the Frenchman Cap dome, the cover sequence is a laterally extensive, 2 – 3 km thick succession (Figure 3.4b), with some units continuing up to 150 km along strike

(Scammell and Brown 1990; Crowley 1999). The cover sequence is not in contact with the basement orthogneiss, but the cover-basement paragneiss contact is interpreted as an unconformity, where quartzite, or in some areas, pebble conglomerate is the basal unit (Crowley 1999). In Frenchman Cap the basal quartzite is the lowermost unit of three upward fining sequences that make up the cover succession of metasedimentary and metavolcanic rocks (Journey 1986). Each of the three sequences has a basal quartzite, overlain by semi-pelitic and calcareous schist, pelitic and semipelitic schist, calc-silicate gneiss, amphibolite gneiss and marble, with generally conformable gradational contacts between rock types (Journey 1986). The ages of the three cover divisions are as follows: the lowermost sequence begins with the basal quartzite on basement and contains a sequence of rocks up to the c. 740 Ma intrusive Mount Copeland and Mount Grace syenitic orthogneisses (Crowley 1997; Parrish and Scammell 1988); the middle part begins above the aforementioned gneiss and continues to a stratiform Pb-Zn horizon interpreted to be Early Cambrian in age (described by Höy and Godwin 1988); and, the upper part begins above the Pb-Zn horizon and may be as young as c. 350 Ma, based on preliminary U-Pb zircon ages from intrusive carbonatites in the cover sediments (Millonig et al. 2012) (see also Figures 3.5). There may be significant unconformities that are not recognized, or structural complications like repetition or omission of strata.

The Gold Creek gneiss of the Malton Complex north of the Monashee Complex is the only Cordilleran gneiss body where the original depositional contact between basement and cover rocks is unambiguously preserved (Murphy et al. 1991). In all other cases the contacts are transposed, folded or difficult to interpret (Crowley and Parrish 1999, Spark 2001; Hinchey 2005, Williams and Jiang, 2005). The cover sequences of Frenchman Cap and Thor-Odin domes have been correlated based on the presence of an interpreted “basal” quartzite in both domes (Figures 3.1, 3.2, 3.4). In the case of Frenchman Cap dome the cover sequence is interpreted as comprising the units that occur above the first occurrence of quartzite and where orthogneiss is absent (Höy and Brown 1980; Crowley 1997).

The Frenchman Cap basal quartzite (and overlying cover sequence) was mapped by Wheeler (1965), Read (1979), Höy (1980), and others (Scammell and Brown 1990 and references therein). The contact between basement and cover rocks was interpreted as an erosional unconformity (Journeay 1986) which in different areas of the dome displays sheared, gradational or sharp contact relationships. In some areas the base of the quartzite is associated with a conglomerate layer (Ross and Parrish 1991) which contains cobbles of the underlying paragneiss, supporting the hypothesis that the contact is erosional.

A similar apparent unconformable relationship exists between the basement paragneiss and the basal quartzite unit of the cover rocks in Thor-Odin as mapped by Reesor and Moore (1971) and subsequent workers (e.g. Duncan 1984; Spark 2001). However, in the Thor-Odin dome the affinity of the rocks at this complexly infolded boundary between the basement and supracrustal rocks remains poorly constrained because the stratigraphy in Thor-Odin dome is transposed and attenuated, and lacks the datable igneous rocks and distinctive marker units present in Frenchman Cap dome. The only age constraint on the upper part of the cover in Thor-Odin dome comes from an intrusive carbonatite at Mount Hall, 359 ± 45 Ma (Parrish 1995), implying that at least part of the upper division of the cover sequence is older than this carbonatite.

In Thor-Odin dome the relationship between the basement paragneiss and the structurally lowest quartzite units is less clear than in the Frenchman Cap dome. The Thor-Odin basement gneiss and cover sequence rocks have concordant gneissosity and foliations (Spark 2001), most likely as a result of transposition during deformation, or evidence that they were deformed together. The contact between the basal quartzite of the cover sequence and the basement gneiss of the Thor-Odin dome has been interpreted as a Paleoproterozoic erosional unconformity (Duncan 1982; Parkinson 1992; Spark 2001) based on the presence of gedrite amphibolites, interpreted as evidence for the presence of a paleoregolith horizon. However, there is no documented angular unconformity between the quartzite and the basement orthogneiss (Spark

2001) and it is possible that the contact is tectonic and the result of transposition during deformation, or that there may be unrecognized cover rocks under the quartzite. In addition, the interpretation of the gedrite amphibolites as evidence for a paleoregolith horizon is ambiguous, as discussed in the next paragraph.

In the Frenchman Cap dome the basal quartzite occurs locally above an interpreted paleoweathering horizon, consisting of aluminum-rich amphibolites, in the upper sections of basement paragneiss (Journeay 1986). This horizon is not present in all the basal quartzite-paragneiss contacts, and where it is absent it is interpreted to have been removed prior to quartzite deposition due to erosion along the unconformity (Ross and Parrish 1991). However, in the Thor-Odin dome, the cordierite–gedrite amphibolite rocks that could represent this paleoweathering horizon have been reinterpreted, on the basis of geochemistry studies, as being derived from volcanic rocks which were hydrothermally altered on the seafloor (Hinchey and Carr 2007). The differences in the interpretations of the origin of the aluminum-rich amphibolites in the two domes (paleoweathering horizon in the Frenchman Cap dome vs. hydrothermally altered seafloor horizon in the Thor-Odin dome) imply that they have not been interpreted correctly or were not formed in equivalent environments. In some areas of Frenchman Cap dome the basal quartzite overlies a quartz pebble metaconglomerate derived from the basement paragneiss and directly overlying the paleoweathering horizon (Ross and Parrish 1991). No metaconglomerate units are known to exist in association with the

basal quartzite in the Thor-Odin dome (Reesor and Moore 1971; Duncan 1984; Spark 2001).

3.3.3 Basal quartzite age in the Thor-Odin dome

Previous U-Pb detrital zircon ID-TIMS studies of the quartzite unit at Cariboo Alp, reported ages ranging c. 2100 – 1750 Ma for three zircon grains (Coleman 1990). Figure 3.5a shows the known protolith ages for the Thor-Odin dome. A preliminary detrital zircon study of a quartzite on Blanket Mountain, interpreted as the basal quartzite of the cover sequence in Thor-Odin dome (Kuiper 2003), yielded a range of discordant Paleoproterozoic ages (2763 ± 2 , 2506 ± 4 , 1825 ± 6 Ma), similar to those described in Frenchman Cap by Crowley (1997). This quartzite is not in contact with any clearly identified basement rocks; therefore, the results are not particularly helpful in constraining the depositional history of the area. A subsequent study of different quartzites in the Blanket Mountain area documented zircons (3 out of several hundred analyses) with U-Pb ages between 570 and 780 Ma in addition to Proterozoic detrital populations. This suggests that the base of the cover sequence at Blanket Mountain may be considerably younger than the Proterozoic age proposed for other quartzites of Thor-Odin and Frenchman Cap domes (Shields and Kuiper 2008).

3.3.4 Basal quartzite age in the Frenchman Cap dome

Preliminary detrital zircon data available from the basal quartzite in the Frenchman Cap dome are as follows: n=8 from basal conglomerate (at Perry River) in Ross and Parrish (1991); and n=8 from the basal quartzite (at Pettipiece Pass) in Crowley (1997). Figure 3.5b shows the known protolith ages for the Frenchman Cap dome. The youngest detrital zircon reported is c. 1990 Ma, with the main populations ranging c. 2020 – 1990 Ma and c. 2040 – 2260 Ma. Basement domains (some from exposed Canadian Shield and other known in the Alberta subsurface) corresponding to these ages include Thelon-Taltson (2000 – 1920 Ma), and Buffalo Head, Chinchiga, Wabuman or Thorsby (2400 – 2000 Ma) domains (Gehrels and Ross 1998; Ross and Villeneuve 2003, Ross et al. 2005). The Kirbyville gneiss which is c. 1860 Ma, is the youngest orthogneiss body known in Frenchman Cap dome that occurs in the basement but not in the cover rocks, and can further constrain this quartzite as being younger than 1860 Ma (Crowley 1997). The core of the Frenchman Cap dome preserves evidence for a major intrusive event at c. 1850 Ma in the Bourne granite, a variably deformed, syn-tectonic leucogranite that intruded into basement paragneiss (Crowley et al. 2008; Gervais et al. 2010). The Bourne granite preserves Proterozoic structure and was not pervasively overprinted by Cordilleran deformation (Crowley et al. 2008; Gervais et al. 2010).

The upper age limit for the Frenchman Cap basal quartzite has been proposed to be 1852 ± 4 Ma based on the interpreted U-Pb ID-TIMS zircon crystallization age of a

pegmatite reported in the cover rocks that stratigraphically overlies the basal quartzite (Sample s341, Crowley 1997). This pegmatite is foliated and folded concordantly with the host paragneiss and is interpreted to share at least part of the deformation history with the lower part of the cover sequence into which it was intruded (Crowley 1997). The interpreted crystallization age is based on an 1852 ± 4 Ma upper intercept of a discordia line defined by 5 out of 7 single grain zircon analyses (MSWD of 9.8) with a lower intercept of 149 ± 20 Ma. A deformed leucogranite reported higher up in the lower cover sequence has a U-Pb zircon age of 1762 ± 6 Ma and may similarly represent an inherited population (Sample 180, Crowley 1997). The interpreted crystallization age is based on a 1762 ± 6 Ma upper intercept of a discordia line (MSWD = 2.8) defined by 5 out of 12 single grain zircon analyses. The deposition of the basal quartzite overlaps with the range of the Bourne granite U-Pb zircon crystallization ages of c. 1850 Ma (Crowley et al. 2008). If the data discussed above is correct, the Frenchman Cap basal quartzite records Pre-Belt Purcell sedimentary deposition on Laurentian basement.

U-Pb Sensitive High Resolution Ion Microprobe (SHRIMP) dating of zircons in the Thor-Odin dome by Hinchey et al. (2006) illustrated how complex Pb inheritance patterns can be in zircons from leucosomes and pegmatites within the basement and cover rocks of the Thor-Odin dome. This suggests that the Frenchman Cap samples should be re-evaluated by an in-situ dating method to refine the age interpretation discussed above.

However, in the absence of more robust analysis, the timing constraints discussed are accepted as geologically valid and are used in interpretations.

3.3.5 Metamorphism and deformation in the domes

In Thor-Odin dome all the rocks experienced pervasive deformation and metamorphism during the Paleocene-Eocene Cordilleran orogeny which overprinted all earlier histories (see sections 2.4 and 2.6). Eocene migmatization and leucosome generation in the orthogneisses and paragneisses of Thor-Odin dome has been dated at c. 56 – 52 Ma (Vanderhaeghe et al. 1999; Hinchey 2005; Hinchey et al. 2006).

In the core of Frenchman Cap dome Proterozoic penetrative ductile deformation is preserved in the Bourne granite within the basement rocks below the base of Cordilleran deformation (Crowley 1999; Crowley et al. 2001, 2008; Gervais et al. 2010). Crowley et al. (2008) document the presence of c. 1900 Ma magmatic zircons (based on extensive imaging and geochemical study of zircons) in leucosomes, granite sheets and undeformed pegmatites that crosscut gneissosity within the basement rocks. There is a thermal overprint in the upper levels of the Proterozoic core of the dome where c. 50 Ma old monazite grains are present, indicating Eocene metamorphism (Crowley et al. 2008). This thermal overprint is limited to the structurally highest Bourne granite intrusions, indicating that Paleoproterozoic structures and anatexis are preserved despite Tertiary metamorphism. This suggests that the Frenchman Cap basement rocks

were not heated for long enough during the Cordilleran orogeny to overprint all of the Proterozoic thermal histories (Gervais et al. 2010), unlike in the Thor-Odin dome where all structural levels are pervasively overprinted by Tertiary metamorphism and deformation (Hinchey et al. 2006; this study Chapter 4 and 5).

3.3.6 Geology of specific study areas

There are three study areas where the proposed “basal quartzite” of the Thor-Odin dome was sampled. These are Mount Thor and Icebound Lake (within the Thor-Odin dome) and Cariboo Alp (on the south-western flank of dome), shown on Figure 3.3 and also projected into the stratigraphic columns of Figures 3.4 and 3.5. Below are descriptions of each of the three study areas (see section 2.4.3 and 2.4.4 for more detail).

3.3.6.1 Mount Thor

The quartzite sample from Mount Thor is the structurally lowest quartzite in this study. The quartzite has been interpreted as the basal quartzite of the cover succession in Thor-Odin dome (Figure 3.6; Reesor and Moore 1971; Hinchey 2005) because it unconformably overlies migmatitic hornblende–biotite gneiss interpreted as basement orthogneiss (Hinchey 2005). It is proposed that it represents the earliest preserved deposition of sediments on the Pre-Cambrian basement of Thor-Odin dome.

The quartzite is overlain by metapelitic sillimanite–garnet–biotite schist and a heterogeneous package of rocks typical of the cover sequences for both Thor-Odin and Frenchman Cap domes, including: marble, diopside calc-silicate gneiss, and sillimanite–garnet–biotite schist interlayered with calc-silicate (Hinchey 2005). The cover rocks are crosscut by granitic pegmatites containing accessory garnet and tourmaline (Hinchey 2005).

3.3.6.2 Icebound Lake

The map area around the Icebound Lake (Figure 3.3) sample sites comprises primarily migmatitic garnet–biotite quartzofeldspathic paragneiss and amphibolite, migmatitic cordierite–sillimanite–garnet–biotite schist and biotite–quartzofeldspathic paragneiss at uncertain age. Regionally, they are infolded with migmatitic, polydeformed Proterozoic paragneiss typical of the basement rocks in core of the dome. The quartzite sampled is in concordant contact with the dominant migmatitic garnet–biotite–quartzofeldspathic gneiss below and in concordant contact with a garnet–sillimanite–biotite paragneiss above (Figure 3.7). There is no evidence to suggest the quartzite is conformable or unconformable with the associated paragneiss.

Within the dominant migmatitic paragneiss of the area there is a thin (~10 m thick) package of metamorphosed ultramafic rocks that occurs in elongate lenses of 10 – 30 m along strike of the predominant foliation surfaces in the overlying quartzite and

paragneiss. Within this package the dominant rock type is gedrite–anthophyllite–tremolite amphibolite, with minor lenses of garnet–plagioclase–gedrite–biotite schist. Amphibolite boudins, pods and lenses are also contained within the dominant paragneiss. Rocks in this area are K-feldspar–sillimanite-bearing upper amphibolite facies and the paragneiss shows evidence for extensive anatexis and at least three phases of deformation. See section 2.4.4 for more details.

3.3.6.3 Cariboo Alp

Prominent structures at Cariboo Alp include a moderately southwest dipping composite transposition foliation with intrafolial rootless folds, concordant leucosome, granitoid lenses and boudinaged layers, northeast verging folds and west and southwest plunging mineral and stretching lineations. Northeast directed kinematic indicators such as shear bands, S-C fabrics and fold vergence indicate progressive northeastward flow (sections 2.4 and 2.6, also Reesor and Moore 1971; McNicoll and Brown 1995).

The rocks at Cariboo Alp form bands of “rusty” orange-coloured sillimanite–garnet–biotite gneiss and “grey” migmatitic gneiss (Figure 3.8). They have been correlated with rocks within Thor-Odin dome, specifically supracrustal cover rocks and Paleoproterozoic North American basement rocks, respectively. The rusty gneiss is mainly migmatitic garnet–sillimanite–biotite–quartzofeldspathic gneiss, with lenses and layers of

metamorphosed pelitic, siliciclastic and carbonate rocks. It contains predominantly lens-shaped stromatic leucosome that makes up < 20% of the rock.

The “grey” gneiss, a migmatitic biotite–hornblende–quartzofeldspathic gneiss (Figure 2.38) with minor interlayers of amphibolite and calc-silicate, is a metamorphosed greywacke characterized by extensive stromatic and phenocrystic vein leucosome that make up 30 – 60% of the rock. The presence of calc-silicate layers and cordierite–gedrite rocks within the grey gneiss could suggest that it is part of the basement assemblage since these rock types have been documented within the basement gneiss of Thor-Odin dome (Norlander et al. 2002; Hinchey and Carr 2007). However, both calc-silicate and ultramafic lithologies occur in the cover sequences as well, so lithological correlation of basement and cover is problematic.

The quartzite sampled at Cariboo Alp (Figure 3.9) represents the lowermost exposure of quartzite in the high strain zone, and has previously been interpreted to be part of the basal quartzite unit of the Thor-Odin dome, as exposed at Mount Thor and Icebound Lake (Reesor and Moore 1971). At Cariboo Alp all units are isoclinally folded and interlayered. The quartzite is underlain by grey migmatitic garnet–biotite orthogneiss and overlain by migmatitic garnet–sillimanite–biotite paragneiss. Lenses of cordierite–gedrite rocks occur above and below the quartzite in the surrounding gneisses. It is

important to determine whether this quartzite is equivalent to the “basal quartzite” that occurs within Thor-Odin dome.

3.4 Methods

3.4.1 Sample preparation

Each sample consisted of roughly 20 kg of quartzite, collected at several stratigraphic levels within each quartzite layer. This sampling strategy of collecting from a number of places within each quartzite layer was done in order to minimize the effect of natural sorting within the units or variation in zircon populations at different levels of the unit (DeGraaff-Surpless et al. 2003).

Quartzite samples were crushed using a jaw crusher and ground to a grain size of <250 μm using a mill grinder. Heavy minerals were separated using a Rodgers™ Gold Table. After standard heavy liquid separation, magnetic and non-magnetic minerals were separated from the heavy mineral fractions using a Frantz™ Magnetic separator with 10° forward slope and 10° side slope, starting at 0.25 Amp to 1.8 Amp. Zircons (~200 per sample) were picked from the non-magnetic fraction, under ethanol using a binocular microscope. In order to avoid introducing any artificial age bias based on zircon morphology, representative zircons were picked from all populations present in each sample. Representative crystals from all samples were photographed in reflected and transmitted light using a petrographic microscope. Sample preparation and zircon

picking was done at Carleton University. Preparation, polishing and imaging of grain mounts as well as all analyses and data reduction was done at the Inco Innovation Centre, Memorial University of Newfoundland (MUN). Isotopic data were collected using laser ablation-inductively coupled plasma-mass spectrometry (LA-ICP-MS).

For this study, ~100 crystals were analyzed from each sample. Standard practice in detrital zircon geochronology suggests that analyzing ~60 zircon grains (>100 preferred) from a sedimentary rock produces a 95% chance of identifying all the age populations present in a sample (Fedó et al. 2003; Vermeesch 2004; Andersen 2005). Andersen (2005) suggests that it is advisable to analyze a random sample of zircons (35 – 70 grains) to represent the typical age populations in a sample, as well as a number of grains selected non-randomly for particular characteristics such as unusual shapes or sizes to increase the chances that any population missed in the random sampling may be identified.

To accommodate the 40 μ m laser spot size, only size fractions with grains >50 μ m were used. The 75 – 125 μ m size fraction contained examples from all zircon morphologies in each sample, except for sample DC490 where a grain size of <80 μ m is the representative size. Gehrels (2000) suggests that using only larger grains (>100 μ m) introduces a bias towards coarse grained granitoids in provenance interpretation. Using these 75 – 125 μ m grain sizes for all samples follows the recommendations by Morton

(1996), who suggests that using a common grain size for detrital samples makes for a more valid comparison between samples.

Zircon crystals were mounted in 25 mm diameter epoxy resin grain mounts and ground to expose the cores of the zircons in order to analyze the sections of zircon that are least likely to have experienced Pb loss (Krogh 1982). The surfaces were polished to a 0.25 μ m finish and carbon coated for scanning electron microscope (SEM) imaging. All grains were imaged prior to analysis using backscattered electron mode (BSE) to document any zoning or core/rim structure within the crystals. The FEI Quanta 400 SEM, at Memorial University, equipped with a solid-state, twin-segment BSE detector was operated under high vacuum of 6×10^{-4} Pa with an accelerating potential of 25 kV and a beam current of 10 nA.

Sample mounts were ultrasonically cleaned in de-ionized water before being washed with double-distilled 8N HNO₃ and rinsed with purified Milli-Q H₂O before being loaded into the sample holder for LA-ICP-MS analysis. The grain mounts were placed in a sealed sample chamber on a computer-controlled movable stage. Zircon crystals were ablated using a 10 μ m laser beam, while moving the sample under the laser to produce a 40 x 40 μ m square ablation pit. This procedure minimizes the depth of the ablation pit and reduces laser-induced element fractionation at the ablated surface (Kořler 2008). Ablation sites were chosen to sample homogenous BSE domains.

3.4.2 Analytical Methods

U/Pb and Pb/Pb isotopic ratios were measured using a Finnigan ELEMENT XR double focusing magnetic sector field ICP-MS. Zircons were ablated using a Lambda Physik COMPexPro 110 ArF excimer laser operating at a deep UV wavelength of 193 nm and a pulse width of 20 ns. The 10 μm laser beam using an energy density of $3 \text{ J}\cdot\text{cm}^{-2}$ and fired at a 10 Hz repetition rate was delivered to the sample surface by an automated GeoLas Pro optical beam delivery system.

The ablated sample material was extracted from the sample chamber and transported to the ICP-MS system by flushing the sample chamber with helium carrier gas. An internal laboratory standard tracer solution containing natural Tl ($^{205}\text{Tl}/^{203}\text{Tl} = 2.3871$) and enriched ^{233}U , ^{209}Bi and ^{237}Np (concentrations of ca. 10 ppb per isotope) was nebulized simultaneously with the ablated sample material and used to correct for instrumental mass bias. Blanks were measured using the helium carrier gas and tracer solution before the inclusion of the ablated sample material. Time-resolved data were acquired in 180 second experiments preceded by a 20 – 30 second measurement of the helium gas blank and the tracer solution alone prior to the addition of the ablated sample material.

Data for U, Pb and tracer isotopes were acquired in time resolved peak-jumping, pulse counting mode with one point measured per peak. The masses measured for each analysis were: ^{204}Hg , ^{203}Tl , ^{205}Tl , ^{206}Pb , ^{207}Pb , ^{209}Bi , ^{232}Th , ^{233}U , ^{237}Np , ^{238}U . Three oxide masses, ^{233}UO , ^{237}NpO and ^{238}UO were measured to correct for oxide formation. The presence of ^{204}Hg in the He- Ar carrier gas prevents the accurate measurement of ^{204}Pb , so the instrumental ^{204}Hg background was monitored. The laboratory practice is to exclude any analyses with ^{204}Hg higher than the measured gas blank from the final data set. None of the analyses had ^{204}Hg measurements higher than the gas blank so there were no corrections applied for common ^{204}Pb . Raw counts were corrected for electron multiplier dead time (20 ns) and gas blank.

Following standard procedure at the MUN laboratory, natural zircon laboratory standards Zircon 91500 and Plešovice zircon were used. The U-Pb and Pb-Pb ages for these standards had been previously determined by ID TIMS to be 1065 ± 3 Ma for 91500 (Wiedenbeck et al. 1995) and 337.13 ± 0.37 Ma for PL, the Plešovice zircon (Sláma et al. 2008). Both standards were analyzed before and after every seven unknown samples to monitor instrumental drift or variability in operating conditions throughout sessions, as well as to monitor the efficiency of mass bias and laser induced fractionation corrections applied to the data. Concentrations of Th and U for the zircons were calibrated using known data from zircon 91500.

Raw U and Pb isotopic data were reduced using LAMDATE (Kořler et al. 2008). For each analysis $^{207}\text{Pb}/^{206}\text{Pb}$, $^{206}\text{Pb}/^{238}\text{U}$ and $^{207}\text{Pb}/^{235}\text{U}$ ratios were calculated and blank corrected. Laser-induced fractionation of U and Pb isotopes was corrected using the intercept method of Sylvester and Ghaderi (1997). Time resolved data reduced and displayed by LAMDATE were inspected for each analysis and the flat, stable part of each signal was picked to use for age calculation, using the average ratios produced by each ablation step (average $^{207}\text{Pb}/^{206}\text{Pb}$ ratio for each rather than intercept corrected). U-Pb ages were calculated using the present day $^{238}\text{U}/^{235}\text{U}$ of 137.88 with decay constants of $1.55125 \times 10^{-10} \text{ a}^{-1}$ for ^{238}U and $9.8485 \times 10^{-10} \text{ a}^{-1}$ for ^{235}U (Steiger and Jäger 1977). The Concordia ages for all analyses of Zircon 91500 and Pleřovice zircon performed over the course of this study (each analyzed at least 10 times per sample) were $1064 \pm 3 \text{ Ma}$ and $338 \pm 1 \text{ Ma}$ respectively (95% confidence interval, with decay-constant errors included).

Final ages, concordia diagrams, probability plots and cumulative distribution plots were produced using the Isoplot/Excel macro by Ludwig (2003). For plotting the cumulative probability plots in Isoplot (Ludwig 2003), and to enhance comparison between samples, bin sizes were set at 50 Ma for all samples. Changing bin sizes (e.g. 100 Ma, 25 Ma) did not change the distribution patterns significantly.

Lead loss can result in an underestimation of $^{207}\text{Pb}/^{206}\text{Pb}$ ages. It is common practice in detrital studies to report U-Pb ages to demonstrate the degree of concordance, and

then to use $^{207}\text{Pb}/^{206}\text{Pb}$ ages that are within 5 – 10% of being concordant to plot age histograms and cumulative probability plots (Fedo et al. 2003). Using $^{207}\text{Pb}/^{206}\text{Pb}$ ages is considered adequate for provenance studies within this cut-off (Sircombe 2000). However, this 10% cut-off may still include some truly discordant data, so in order to confirm any results obtained from using this 10%, we use data with 1% of concordance as an additional filter, and base maximum depositional ages on ages that are 100% concordant.

In detrital zircon provenance studies, $^{206}\text{Pb}/^{238}\text{U}$ ages are often used to generate cumulative probability plots for grains that are younger than 1 Ga, and $^{207}\text{Pb}/^{206}\text{Pb}$ ages for grains older than 1 Ga (Pollock et al. 2009). In the younger, <1 Ga grains the $^{206}\text{Pb}/^{238}\text{U}$ ages are more precise since there is more ^{206}Pb to measure than ^{207}Pb . Another approach is to use concordia ages (of grains that are >90% concordant) to generate cumulative probability plots. By using concordia ages one can avoid the need for this division and make use of all the isotopic ratios generated, making the ages obtained this way more precise than single U-Pb or Pb-Pb ages (Pollock et al. 2009). In this study concordia ages are used for all cumulative probability plots and interpretations of the ages of the youngest zircons are based on calculated concordia ages.

3.5 Results

Results for all samples are presented on concordia plots and as probability distributions in Figures 3.10 – 3.15. Data tables for all samples are included in appendix A.

3.5.1 DA224 – Mount Thor, Thor-Odin dome

The sample is a yellowish white, coarse-grained polycrystalline quartzite containing up to 15% feldspar locally, interpreted as detrital based on the rounded grain shapes, with minor (< 5%) biotite and accessory zircon, monazite, and rutile. It also contains thin (<2mm) layers of biotite–sillimanite schist. There is locally occurring subgrain development in the quartz and deformation twinning in the feldspars.

The zircons are clear, primarily rounded with metamorphic overgrowths (due to lack of internal oscillatory zoning), and low uranium concentration, based on BSE imaging (Figure 3.10). Almond shaped faceted grains typically exhibit a rounded core and a rim (typically < 10 μm) seen in backscatter electron (BSE) images. Internal oscillatory zoning, interpreted as magmatic, is preserved in the cores of the grains as apparent in cathodoluminescence (CL) images. The grains range in size from <75 μm to 150 μm , with most in the 80 – 100 μm size fraction.

Out of 98 analyses, 89 were within 90% concordant. The dominant age population in this sample is c. 1600 – 1900 Ma, with minor populations between c. 2000 – 2800 Ma,

with a peak at c. 2600 Ma (Figure 3.11). There is a minor Archean component at c. 3100 – 3400 Ma. The concordia ages of the youngest grains in this sample are 1662 ± 58 Ma (> 90% concordant) and 1769 ± 37 Ma (100% concordant).

3.5.2 DC422 – Icebound Lake, Thor-Odin dome

The Icebound Lake quartzite is a white, coarse-grained polycrystalline quartzite with <5% feldspars, biotite, and accessory rutile and monazite. The quartzite is in unconformable contact with the migmatitic garnet–biotite–quartzofeldspathic gneiss below and in conformable contact with a garnet–sillimanite–biotite paragneiss above it. The contacts are parallel to foliation and may be transposed. The dominant foliation in the garnet–sillimanite–biotite paragneiss parallel to the contact with the quartzite, and is interpreted as bedding parallel foliation, on average 130/30 SW. The 2 m thick quartzite is massive, with no evidence of relict bedding.

The detrital zircons in this sample are similar in morphology to the grains from sample DA224 (Figure 3.12). The zircons are clear, primarily rounded with metamorphic overgrowths. Almond shaped faceted grains typically exhibit rounded cores and rims (typically < 10 μm) seen in BSE. Internal oscillatory zoning interpreted as magmatic is preserved in the cores of the grains as apparent in CL images. The grains range in size from <75 μm to 150 μm , with most in the 80 – 100 μm size fraction.

Out of 104 zircon analyses 61 were >90% concordant. The age distribution in the sample includes a major population from c. 1700 – 1900 Ma, and a minor one from c. 2200 – 2700 Ma. There were no concordant Archean grains in this sample (Figure 3.13). The concordia ages of the youngest grains in this sample were 1725 ± 22 Ma (> 90% concordant) and 1842 ± 32 Ma (100% concordant).

3.5.3 DC165 – Cariboo Alp, Thor-Odin dome south-western flank

The quartzite is a pinkish grey to white quartzite with minor biotite. There are lineations defined by rare sillimanite needles and graphitic spots on surfaces. Heavy mineral bands in outcrop are not consistently aligned, nor continuous throughout the unit. The quartzite is unconformably underlain by grey migmatitic garnet–biotite orthogneiss and conformably overlain by migmatitic garnet–sillimanite–biotite paragneiss. Contacts are parallel to the orientation of the main quartzite layer of 116/40 SW. Lineations of sillimanite and elongated quartz grains are parallel to strike direction (~116). There are at least 4 discrete parallel quartzite layers within 100 m (measured perpendicular to strike) – this sample was collected from the lowermost and thickest layer (3 – 5 m).

The zircons from this sample are primarily clear, to light yellow, almond shaped faceted grains (Figure 3.14). The sample also contains rounded grains with metamorphic overgrowths, and rounded grains with no visible overgrowths. Almond shaped faceted grains typically exhibit rounded cores and faceted rims (typically < 10 μ m) seen in BSE.

The grains range in size from <75 μm to 150 μm , with most in the 80 – 100 μm size fraction.

Of 98 zircons analyzed 63 were >90% concordant. The age distribution in this sample includes a major population at c. 1700 – 1900 Ma and minor populations of c. 1100 Ma, 1300 – 1400 Ma, 2000, 2400, 2600 and 3000 Ma (Figure 3.15). The concordia ages of the youngest zircons were 1082 ± 35 Ma (>90% concordant) and 1097 ± 18 Ma (100% concordant). For comparison of the probability distributions of different age populations in all three samples analyzed see Figure 3.16.

3.6 Discussion

3.6.1 Thor-Odin quartzites, Mount Thor and Icebound Lake

The sampled quartzites from Mount Thor and Icebound Lake have similar detrital populations. They each have major detrital zircon age populations between c. 1900 and 1650 Ma and minor populations spanning c. 2800 – 2200 Ma. However, the peak between c. 1700 and 1900 Ma for the Icebound Lake sample (DC422) is older than in the Mount Thor (DA224) sample (Figure 3.16). There are no grains >3000 Ma in the DC422 sample.

The detrital zircon populations in these two samples are typical of those found in sedimentary rocks with Laurentian cratonic basement source rocks. The largest

populations in these two samples match the Rimbey (c. 1850 – 1790 Ma), Trans-Hudson (c. 1900 – 1800 Ma), Thelon-Taltson (c. 2000 – 1920 Ma) and Medicine Hat (c. 3300 – 2600 Ma) sub-surface domains in the Alberta basement (Gehrels and Ross 1998; Ross and Villeneuve 2003 and references therein). The populations in the c. 2400 – 2000 Ma range could be derived from the Buffalo Head, Chinchiga, Wabuman or Thorsby domains (Ross and Villeneuve 2003). There were no zircons in these samples with ages in the 1610 – 1490 Ma, North American Magmatic Gap, age range, supporting the hypothesis that the rocks were deposited in proximity to the basement domains represented in Laurentia.

The ages and provenance results for the quartzites in the Thor-Odin basement at Mount Thor and Icebound Lake are consistent with previously published studies of rocks of the Windermere Supergroup (Ross and Gehrels 1998; Smith and Gehrels 1991) in southeastern British Columbia that show that the oldest sedimentary rocks of the southern Omineca Belt commonly contain c. 1700 – 1900, 1900 – 2100 and 2500 – 2700 Ma zircon populations, with rare instances of zircon grains older than c. 3000 Ma. There are no known basement domains in the Canadian Shield that match the c. 1750 – 1650 Ma populations in the Mount Thor sample (Gehrels and Ross 1998). It is possible that there are unrecognized sub-surface basement domains that match that age range (Gehrels and Ross 1998). There are areas in the North American Cordillera where zircons of those ages are found – for example, the Priest River complex has basement rocks of

that age range (Doughty and Price 1999 and references therein). Other domains where those ages are common are in the Yavapai and Mazatzal orogenic belts (Ross et al. 2005 and references therein). Long-range transport of zircons across Laurentia is not uncommon and has been demonstrated for zircons from the Grenville Province and the Yavapai-Mazatzal orogen (Rainbird et al. 2003; Rainbird and Davis 2007).

Lewis et al. (2010) report that Neo-Proterozoic metasedimentary rocks of the Priest River Complex were derived from Belt-Purcell rocks and not the underlying Laurentian basement rocks. They also suggest that some of the younger Cambrian rocks in the area were derived from the Windermere Supergroup. The authors stress that it is not always true that sedimentary sequences on basement rocks have to contain detrital material from those basement rocks, but rather they could represent second cycle sedimentary deposits.

Based on the ages of the youngest concordant zircons, the Mount Thor quartzite has to be younger than c. 1650 Ma, and the Icebound Lake quartzite has to be younger than c. 1820 Ma. There are concordant Archean age zircons in the Mount Thor sample; however, there are apparently none in the Icebound Lake sample. There are about 3 times more grains less than 90% concordant in the Icebound Lake sample, possibly as a result of Pb loss. Based on detrital data alone we cannot distinguish between these two quartzite samples, but adding detrital data to interpretations based on the geology of

the study areas, the presence of similar basement gneisses in both areas, and the association with gedrite-anthophyllite units from the basement it is permissible that they may be correlated.

Data reported from Blanket Mountain on the western flank of the Thor-Odin dome suggested that the youngest detrital zircon age found in the Thor-Odin basal quartzite is younger than c. 540 Ma (Shields and Kuiper 2008). It is likely that the Blanket Mountain sample is part of a quartzite not related to the basal quartzites in the Thor-Odin dome, and that it does not represent an equivalent to either the Cariboo Alp or Thor-Odin quartzites. The Blanket Mountain quartzite in question is probably related to the rifting of the Laurentian margin resulting in the deposition of sedimentary rocks at the base of the Hamill Group (Colpron et al. 2002). It has similar detrital zircon ages as a quartzite in the Mount Symonds area, south of the Thor-Odin dome, discussed in section 4.4.

The detrital zircon ages from the Thor-Odin basal quartzite samples are only partly consistent with detrital zircon populations (c. 2170, 2050, 2040, 2010 – 1990 Ma) from the basal quartzite in Frenchman Cap obtained by Crowley (1997) and Ross and Parrish (1991), because the Thor-Odin quartzites all contain younger detrital zircons. The lowermost part of the Frenchman Cap cover sequence was deposited between c. 1990 Ma (based on the youngest zircons in the basal units) and c. 1850 Ma (Crowley 1997). The basal quartzite in Thor-Odin dome at Mount Thor and Icebound Lake, now

constrained to be younger than 1701 ± 28 Ma (> 90% concordant zircon) or 1769 ± 37 Ma (100% concordant zircon), can therefore not be the equivalent unit to the Frenchman Cap basal quartzite. It is possible that the Thor-Odin basal quartzite could be equivalent to the middle part of the Frenchman Cap cover sequence, and that the older part of the cover was removed by erosion, or not deposited at all. While Frenchman Cap and Thor-Odin may have some broad similarities with respect to rock types, they differ with respect to large scale metamorphic and deformational history, and there is evidence that the two domes were exhumed from different levels within the crust (Hinchey et al. 2006; Gervais 2009; this study, Chapter 2 and 5). This is the first indication that the “basal quartzite” units in the two domes may not be equivalent and therefore may have different histories as early as the Proterozoic.

There are no modern detrital zircon studies of the Frenchman Cap basal quartzite that have enough data to be comparable to this study. The current estimates of the depositional age for the Frenchman Cap basal quartzite are based on bulk ID-TIMS U-Pb zircon analyses (Crowley 1997) and somewhat ambiguous igneous zircon U-Pb ages. As discussed earlier, the cover stratigraphy in the Thor-Odin dome is also not as well preserved as in the Frenchman Cap dome, so correlations based only on rock types should be used with caution.

The hypothesis that there is a shared quartzite marker unit in the Frenchman Cap and Thor-Odin domes that represents the same basal quartzite (Read 1980; Spark 2001; Kruse 2007; Gervais et al. 2010) is still permissible if one considers only the northern parts of the Thor-Odin dome. In the northern part of the Thor-Odin dome there are thick successions of quartzite at the base of rocks interpreted to belong to the Thor-Odin cover rocks (Kruse 2007). Specifically, the quartzite layers at Mount Begbie, mapped as a series of shallowly northeast plunging recumbent isoclinal folds (Kruse 2007) are stratigraphically more similar to the Frenchman Cap basal quartzite stratigraphy, and could reasonably be linked to it. This interpretation does not require that the quartzites at Blanket Mountain, or the ones in the southern part of the Thor-Odin dome in this study, be included in such a basal quartzite. However, the Begbie quartzites were not originally interpreted as being part of the basal quartzite because they were thought to be higher up in the cover stratigraphy (Kruse 2007). In addition, the structures on the southern flank of the Frenchman Cap dome project beneath the northern flank of the Thor-Odin dome (Carr and Simony 2012). However, the Mount Begbie quartzites do outline the folds that are interpreted to represent the shape of the basal quartzite and the basement/cover contact (Read 1980; Kruse 2007). The only way to resolve this would be to do a complete detrital zircon study of the Frenchman Cap basal quartzite, and possible correlative units in the northern part of the Thor-Odin dome.

3.6.2 Cariboo Alp

The Cariboo Alp quartzite has major detrital zircon age populations from c. 1900 – 1650 Ma and c. 1100 Ma, and minor populations between c. 1200 – 1400 Ma. The youngest zircons indicate that the quartzite is younger than c. 1100 Ma. The older (> 1750 Ma) zircon ages are mostly typical of sediments derived from Laurentian cratonic sources. These zircons could be from the same basement sources as found in Mount Thor and Icebound Lake quartzites (e.g. the Alberta basement sub-surface Rimbey, Thelon-Taltson, Trans-Hudson, Buffalo Head, Chinchiga, Wabuman, Thorsby, and Medicine Hat domains; Ross and Villeneuve 2003). There are no known basement domains in the western Canadian Shield that match the c. 1750 – 1650 Ma populations. Similar to the zircons from the Thor-Odin dome quartzite samples, they could be from unrecognized basement areas or have the same source as rocks like the Priest River complex, or the Yavapai-Mazatzal domains (Doughty and Price 1999).

Zircons with ages in the 1100 – 1200 Ma range are not found in known exposed or sub-surface basement domains in the western Canadian Shield. They could be derived from regions within the Grenville Orogen or from 1100 – 1200 Ma igneous rocks in Colorado (e.g. Pikes Peak granite) or Wyoming (Gehrels and Ross 1998). It is also possible that the zircons could be from unrecognized or presently unexposed igneous rocks within the Cordillera. There is evidence for the presence of rocks of such c. 1000 – 1300 Ma age in the Cordillera. Detrital zircons in the c. 1000 – 1300 Ma age range have been reported in

sedimentary rocks of the Windermere Supergroup (e.g. Horsethief Creek Group at Howser Creek) and younger miogeoclinal successions (Gehrels and Ross 1998). For example, Grenville age zircons have been recovered from Ordovician quartzite in the Mount Wilson Formation and from miogeoclinal sedimentary rocks in southeastern British Columbia and southwestern Alberta (Ross and Gehrels 1998 and 2000). They interpreted the Grenville age populations as the result of two igneous pulses at c. 1050 and 1030 Ma, and proposed that igneous rocks of that age are present in the Cordillera but not currently exposed. Zircons with ages c. 1100 – 1200 Ma have also been found in xenocrysts within diatremes: for example, in the Elk River diatremes of the Columbia Ice field on the edge of the Medial basin (Parrish and Reichenbach 1991); in the Mesozoic Ice River carbonatite complex (Parrish 1995); and in rocks at Coates Lake (Jefferson and Parrish 1989, Mortensen and Colpron 1998).

Zircons of c. 1100 Ma age have also been recovered from granite cobbles in conglomerates (large clasts interpreted to have a nearby source) in the Triassic Spa Creek area and Bob Lake Assemblages in southeastern British Columbia to the west of the Thor-Odin dome area (Erdmer et al. 2001, 2002). These zircons and cobbles have been interpreted as evidence that there is Proterozoic continental crust beneath the Triassic Nicola Group and that it is not part of the Quesnel terrane, rather, that it was deposited onto attenuated Laurentian crust. The xenocrysts and cobbles mentioned above are all granitic in composition, suggesting that there may have been unrecognized

granitic plutons that sourced these zircons (Jefferson and Parrish 1989; Parrish and Reichenbach 1991; Mortensen and Colpron 1998; Erdmer et al. 2001, 2002).

The Cariboo Alp quartzite may be correlative to older parts of the Windermere Supergroup, or to Succession B of the northern Canadian Cordillera, based on the characteristic detrital population with Grenville ages documented in Succession B (Rainbird et al. 2003; Rainbird and Davis 2007). This is consistent with lithological correlations of the Fawn Lakes Assemblage (which overlies Cariboo Alp) with the semi-pelite-amphibolite member of the Horsethief Creek Group of the Windermere (Pell and Simony 1987; Carr 1991).

The Cariboo Alp quartzite is likely younger than the so-called basal quartzites in both the Thor-Odin and Frenchman Cap domes (Figure 3.16). The Cariboo Alp quartzite also has a different provenance than the quartzite samples at Mount Thor and Icebound Lake.

There are currently no data from crosscutting igneous rocks to use to bracket the upper end of the depositional age range for any of the Thor-Odin and Cariboo Alp quartzites.

In the southern Thor-Odin dome the only dated igneous rocks are those belonging to the Paleocene-Eocene Ladybird granite suite (Carr 1991); a peraluminous anatectic granite generated from partial melting of the basement rocks (Hinchey et al. 2006) and emplaced at upper structural levels as dykes, sills, and plutons (section 2.3.3).

Based on detrital zircon data alone it could be permissible that the Mount Thor and Icebound Lake quartzites are as young as the Cariboo Alp quartzite, or could be the same unit. However, this is not considered a viable interpretation because the younger (< 1400 Ma) age populations in the Cariboo Alp sample, particularly those in the c. 1100 Ma range, make up a significant portion of the total grains analyzed (at least 10%) and are generally concordant. If this population is present in the Mount Thor or Icebound Lake samples it is unlikely to have been missed. Based on detrital zircons alone we cannot conclusively state that the Mount Thor and Icebound Lake quartzites are older than the < 1100 Ma quartzite at Cariboo Alp. However, the structural context in which the Cariboo Alp rocks overlie those within the dome is consistent with this interpretation.

3.6.3 The Thor-Odin cover sequence and Monashee décollement

As illustrated in Figures 3.2, 3.4 and 3.5, the Monashee décollement has traditionally been interpreted to represent the roof of the Monashee Complex by some workers (cf. Brown et al. 1986, 1992; McNicoll and Brown 1995). In this interpretation, the extent of the so-called “cover rocks” of the Monashee Complex is defined by the position of the décollement because they are defined as rocks that occur inside the Monashee Complex. This creates a situation where correlative rocks (e.g. Cambrian Pb-Zn deposits) in both domes are on different sides of the proposed décollement. For example, the Cambrian Pb-Zn deposits and associated rocks in Frenchman Cap dome occur at Kneb,

Cottonbelt, and Jordan River (Höy 2000), locations which are all in the footwall of the Monashee décollement; the same association occurs at Mount Symonds (Big Ledge deposit), south of the Thor-Odin dome and in hanging wall of the Monashee décollement (or Thor-Odin high strain zone) (Figures 1.2, 3.4, and 3.5). This is not a problem if the décollement is viewed as a Cretaceous structure imposed on a pre-existing geometry (see section 2.6), but becomes difficult to reconcile with stratigraphic interpretations (Figures 3.4 and 4.5) when the Cretaceous structure is used as a defining feature for which Proterozoic rocks should be assigned to the “cover” sequence in both domes.

Thompson et al. (2006) suggest that the sequence between the “basal quartzite” up to above the Pb-Zn horizons (see Figures 3.2 and 3.4) are common to the Frenchman Cap and Thor-Odin dome areas. One problematic aspect of correlating the cover rocks of the two domes is that the distinct rift-related “cover” rocks, such as the extrusive carbonatites described in the Frenchman Cap dome (Scammell and Brown 1990; Crowley 1999; Millonig et al. 2012), do not occur in cover rocks of the Thor-Odin dome. The only known carbonatite in the Thor-Odin area is described on Mount Hall, and dated at 359 ± 45 Ma (Parrish 1995). Thompson et al. (2006) proposed this carbonatite as an equivalent to the Frenchman Cap carbonatites in the cover rocks and used it to suggest that the carbonatite–marble–Pb-Zn–calc-silicate–pelitic schist association traced

in the Frenchman Cap cover rocks is the same as the cover rocks of the Thor-Odin dome in the Mount Symonds area.

Structural data show that foliations and lineations in the southern part of Frenchman Cap dome dip and plunge to the south (Höy 1988; Journeay 1986; Scammell 1993), projecting under the Thor-Odin dome (Simony and Carr 2012). As drawn on Figure 3.2, it is permissible that the Monashee décollement projects under the Thor-Odin dome (Carr and Simony 2012). It is possible that the basal quartzite of the Frenchman Cap dome is linked to the quartzite layers at Mount Begbie, mapped as a series of shallowly northeast plunging recumbent isoclinal folds (Kruse 2007).

The interpretation presented above is consistent with interpretations proposed by Kruse and Williams (2007) suggesting that the Monashee décollement as mapped and defined in the Frenchman Cap dome does not exist in the Thor-Odin dome. This implies that it is not required that the quartzite at Cariboo Alp be the same basal quartzite unit as the Frenchman Cap basal quartzite, consistent with the results shown in this study.

However, they also proposed that there was no thrust sense component to the high strain zone on the southern flank of the Thor-Odin dome. This is inconsistent with structures documented in Cariboo Alp, which include northeast verging folds and southwest dipping composite foliations with northeast directed kinematic indicators such as shear bands, S-C fabrics and fold vergence (see section 2.4.3 for more discussion

on Cariboo Alp). This study agrees with earlier interpretations (McNicoll and Brown 1995) that the Cariboo Alp area and the Thor-Odin high strain zone represent a primarily ductile thrust sense shear or flow zone. However, it is suggested here that the Frenchman Cap dome represents a deeper structural level than the Thor-Odin dome, and was still being penetratively deformed in the infrastructure at c. 52 – 51 Ma when the Thor-Odin dome was structurally deactivated and cooling in the suprastructure (see section 2.6).

3.6.4 Implications of two quartzites in Thor-Odin dome

The < 1100 Ma Cariboo Alp quartzite is interpreted to be younger than the < 1650 Ma quartzites from Mount Thor and Icebound Lake, and has a different provenance. These quartzite marker units should not be correlated and drawn as the same unit in maps or cross sections, and repetition of the basal quartzite in Thor-Odin dome at Cariboo Alp is not required when constructing tectonic models of the evolution of the area. Based on the data presented it is also permissible that the basal quartzite in the Frenchman Cap dome is older than the quartzites in the Thor-Odin dome. It is therefore permissible to propose that: (a) the basement rocks and the associated “basal quartzites” may represent different basement domains, and that, (b) these basement domains were juxtaposed as a result of the crustal shortening after the deposition of the quartzites.

3.7 Conclusions and implications

The Mount Thor and Icebound Lake quartzites have: major detrital zircon age populations between c. 1900 and 1650 Ma; minor populations spanning 2200 – 2800 Ma; and minor populations >3000 Ma in the Mount Thor quartzite. The Cariboo Alp quartzite has major detrital zircon age populations from 1900 – 1650 Ma and c. 1100 Ma, and minor populations between 1200 – 1100 Ma. The Cariboo Alp quartzite is therefore not part of the Thor-Odin dome “basal quartzite”, as it has been previously mapped. All the quartzites have detrital zircons that could be derived from sources within the western Laurentian craton. The Cariboo Alp quartzite has an additional source that has to include Grenville age rocks (c. 1100 – 1200 Ma). The younger depositional age and provenance for the Cariboo alp quartzite means that it is not correlative with the Mount Thor or Icebound Lake quartzites, and should not be drawn as the same unit in maps or cross sections, and that infolding of the cover/basement rocks at Cariboo Alp is not required when constructing tectonic models of the evolution of the area.

The quartzites at Mount Thor and Icebound Lake may be correlative to the Muskwa Assemblage of the Northern Canadian Cordillera; however, the Muskwa Assemblage lacks the c. 1650 Ma detrital zircon populations (Ross et al. 2002) prominent in the Thor-Odin quartzites. The 1650 Ma ages are not known to be present in the Proterozoic or Cambrian rocks of the Windermere or Hamill-Gog Groups and their provenance is

enigmatic. They may be derived from the rocks in the Yavapai-Mazatzal orogen or represent sediments derived from the Belt-Purcell Supergroup.

The Cariboo Alp quartzite may be correlative to the older parts of the Windermere Supergroup, or to the Succession B of the northern Canadian Cordillera, based on the characteristic detrital population with Grenville ages documented in Succession B (Rainbird et al. 2003; Rainbird and Davis 2007). This is consistent with lithological correlations of the Fawn Lakes Assemblage (which overlies Cariboo Alp) with the semi-pelite-amphibolite member of the Horsethief Creek Group of the Windermere (Pell and Simony 1987; Carr 1991).

The Frenchman Cap basal quartzite is constrained to be older than ~ 1.78 Ga, and younger than ~ 1.85 Ga (Crowley 1997). Based on those data, and the new data presented in this chapter for two quartzite samples of the Thor-Odin dome, the “basal quartzites” of the Thor-Odin and Frenchman Cap domes have different minimum depositional ages and source terranes, and therefore the quartzites are not likely to be directly correlative. It is therefore permissible to propose that: (a) the basement rocks and the associated “basal quartzites” may represent different basement domains, and (b) these basement domains were juxtaposed after the deposition of the quartzites.

Based on geochronology and stratigraphic correlations (see Figures 3.4 and 3.5), the rocks at Cariboo Alp and Fawn Lakes that overlie the Thor-Odin dome are equivalent in age to rocks above the Monashee décollement in the Frenchman Cap dome. It is therefore permissible to propose that the Monashee décollement wraps around the south end of the Frenchman Cap dome and projects beneath the Thor-Odin dome as suggested by Simony and Carr (2011) and as drawn on Figure 3.2. The differences between the two domes in the geology of their basement rocks, the depositional history of their cover rocks suggest that it would be more appropriate to refer to them as separate structural culminations and not a “complex”.

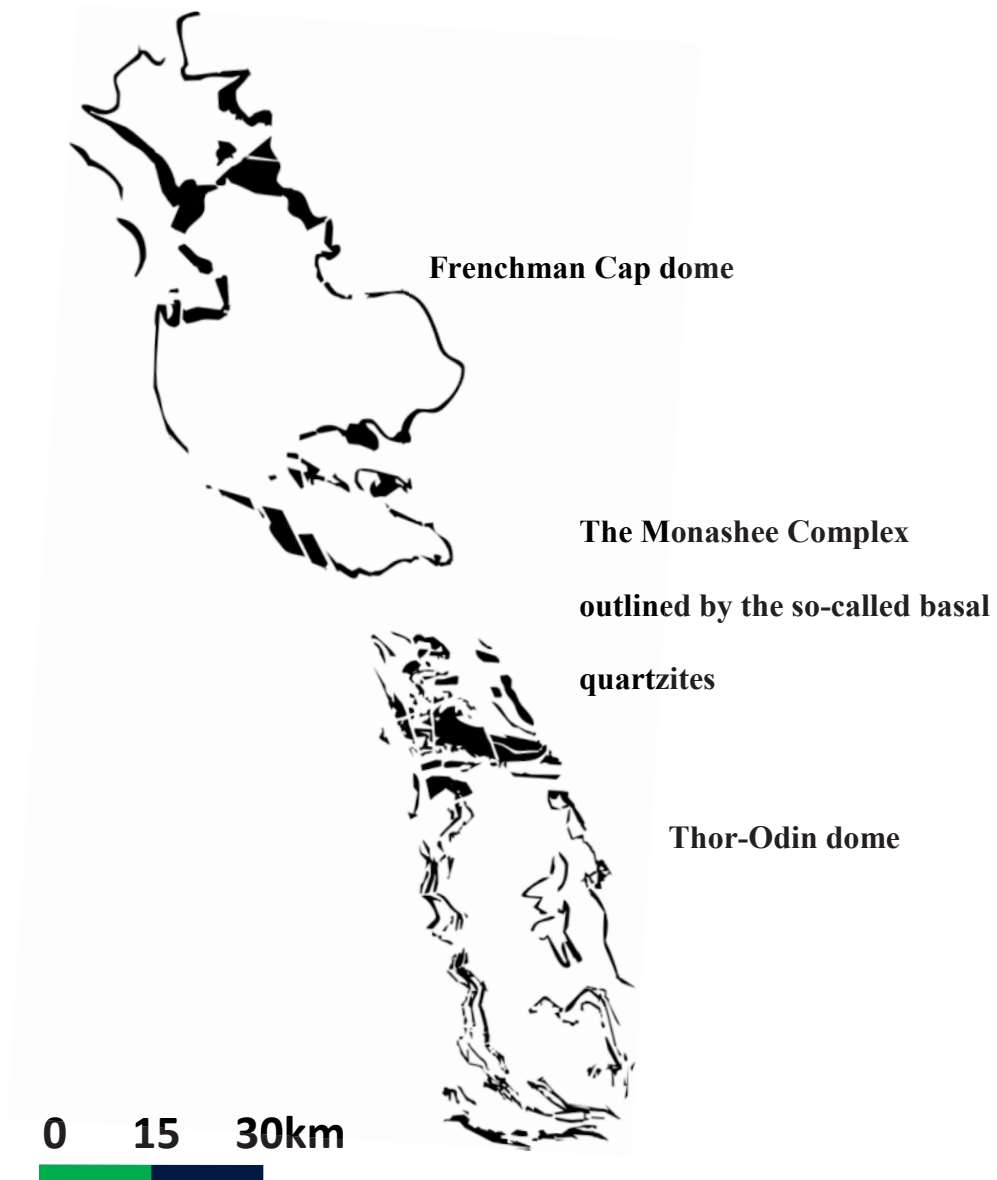


Figure 3.1 The Monashee Complex made up of the Frenchman Cap dome and the Thor-Odin dome, outlined by the basal quartzites. (Modified from Kruse 2007.)

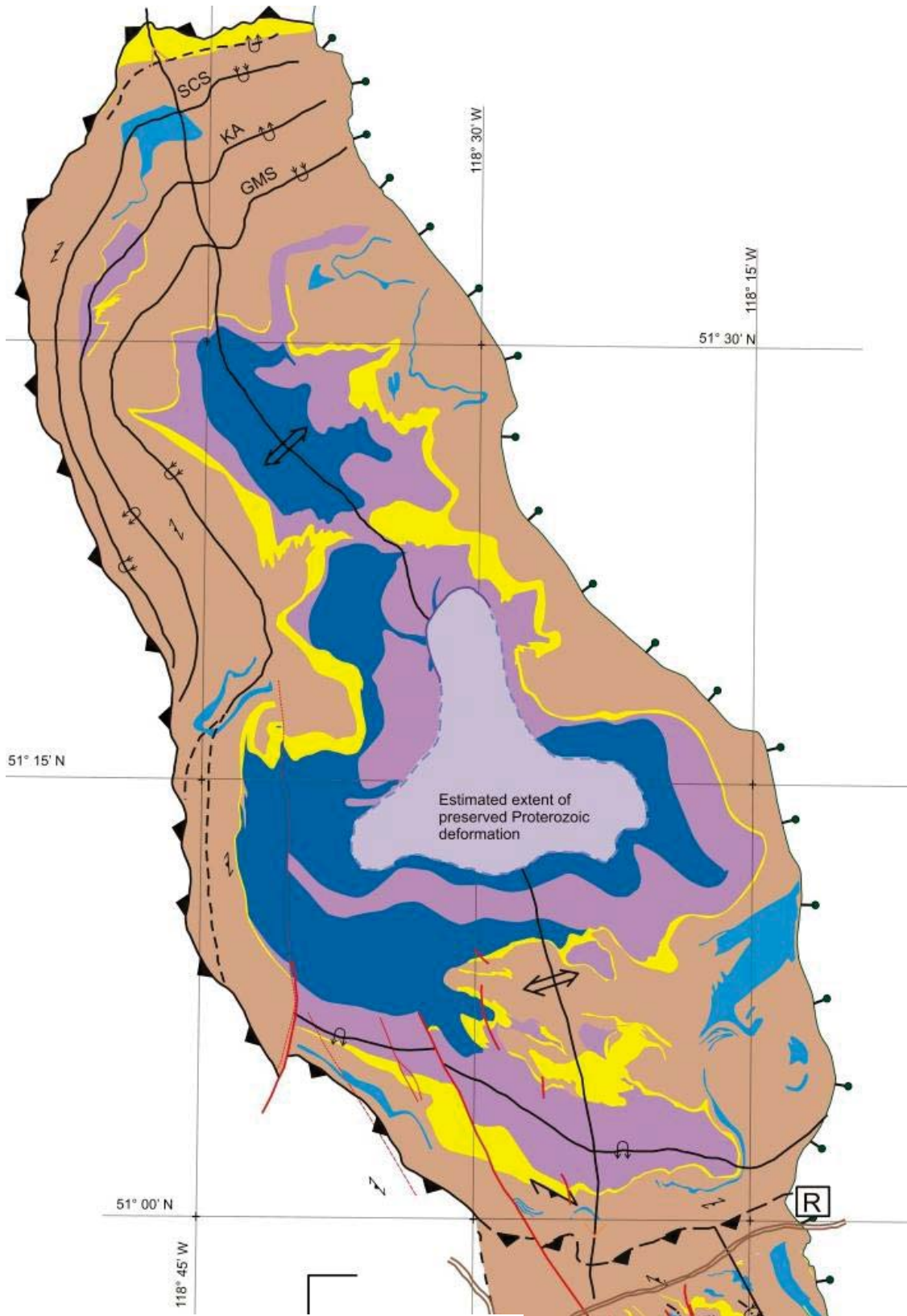


Figure 3.2a: The Frenchman Cap dome

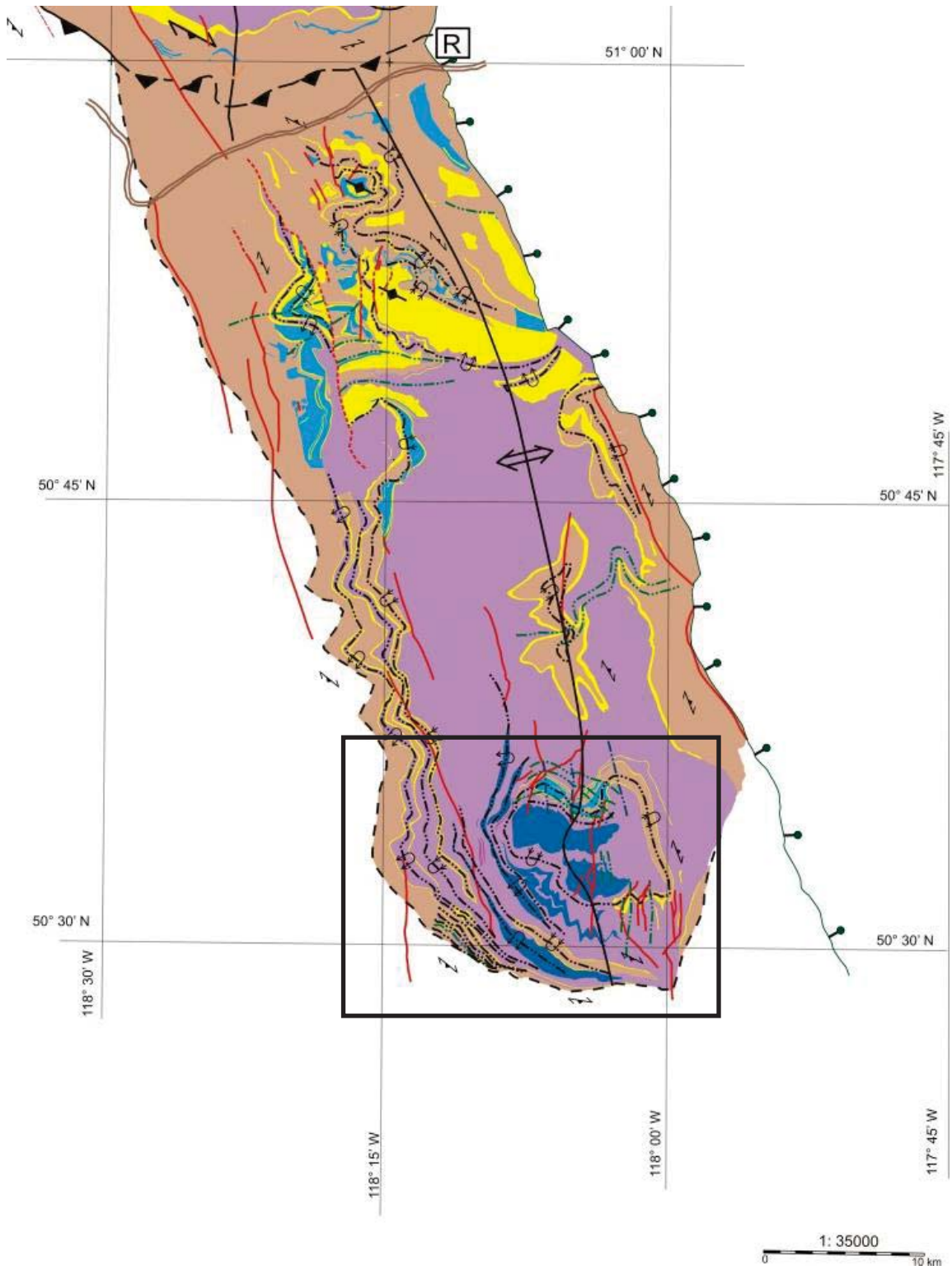


Figure 3.2b: Thor-Odin dome

Legend - Thor-Odin and Frenchman Cap Domes

Cover rocks

-  Cover calc-silicate gneiss
-  Cover pelitic schist, paragneiss
-  Quartzite

Basement rocks

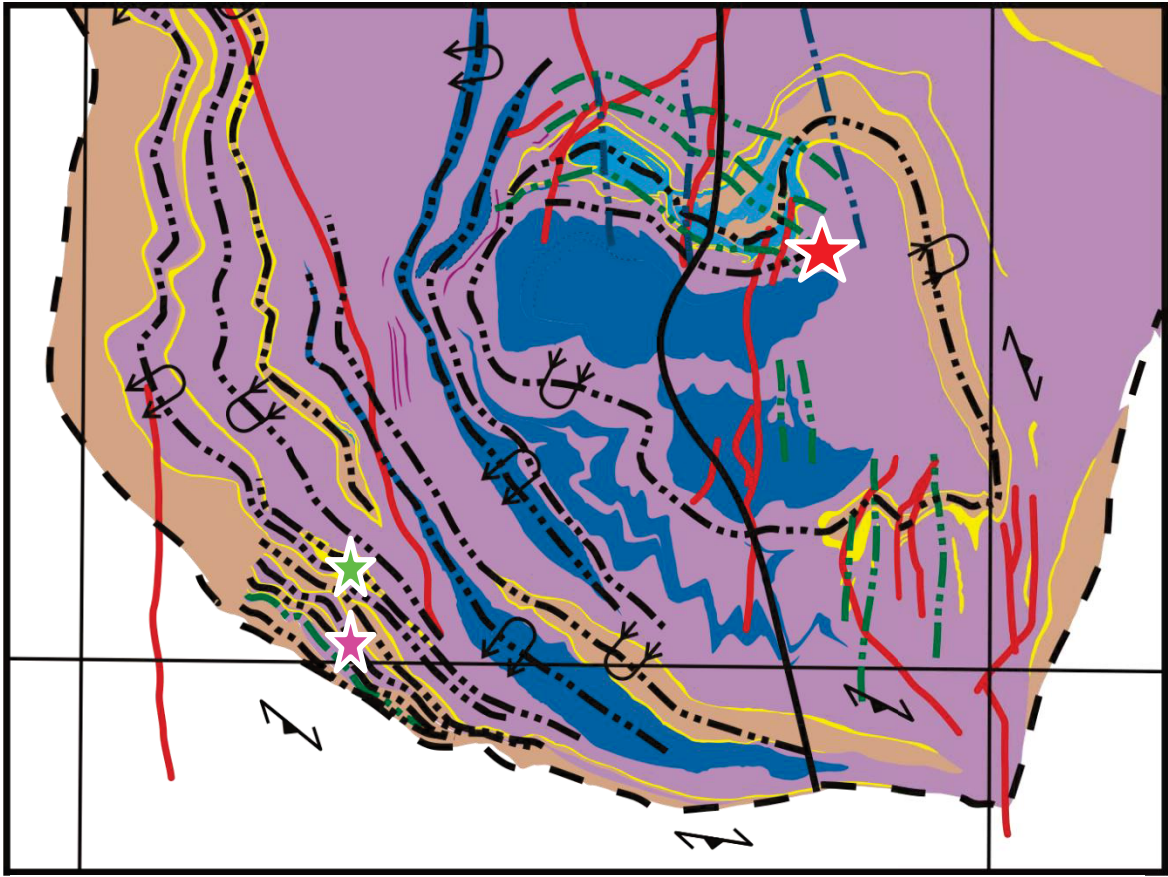
-  Basement paragneis
-  Basement orthogneiss

-  Axial trace of upright folds
-  Axial trace of NE verging asymmetric folds
-  Axial trace of overturned syncline
-  Overturned anticline
-  Trace of the Monashee Decollement
-  Transposition foliation, inclined, horizontal
-  Normal faults, Eocene or younger
-  Columbia River Fault

Figure 3.2 The Frenchman Cap (a) and Thor-Odin (b) domes, making up the Monashee Complex.

Modified from Kruse et al. (2004), Carr (1990), Höy (1977, 1988, 2000), Reesor and Moore (1971). The quartzites that separate the cover rocks from the basement rocks are interpreted to be part of a basal quartzite unit that outlines the shape of the domes and has been used to correlate the rocks of the cover sequence stratigraphy of the domes. R = Revelstoke with the Trans-Canada Highway indicated in brown double line.

Note: Figure 3.2a and b are separated only for clarity, they are at the same scale, and some overlap is included in each figure to show where they would be connected. For details of the structures in the Thor-Odin dome, see Figure 3.3.



★ ★ ★
 Cariboo Alp Icebound Lake Mount Thor

Figure 3.3 Southern flank of the Thor-Odin dome with the locations of the study areas at Mount Thor, Icebound Lake and Cariboo Alp marked. (See Figure 3.2 for legend) The repeated quartzite layers at Cariboo Alp, Icebound Lake and Mount Thor have been interpreted to be part of the 'basal' quartzite unit of the cover sequence rocks of the Thor-Odin dome, deposited onto basement rocks of Laurentian affinity. Modified from Kruse et al. (2004), Carr (1990) and Reesor and Moore (1971). The red lines represent steep Eocene and younger strike-slip and normal faults (Kruse et al. 2004).

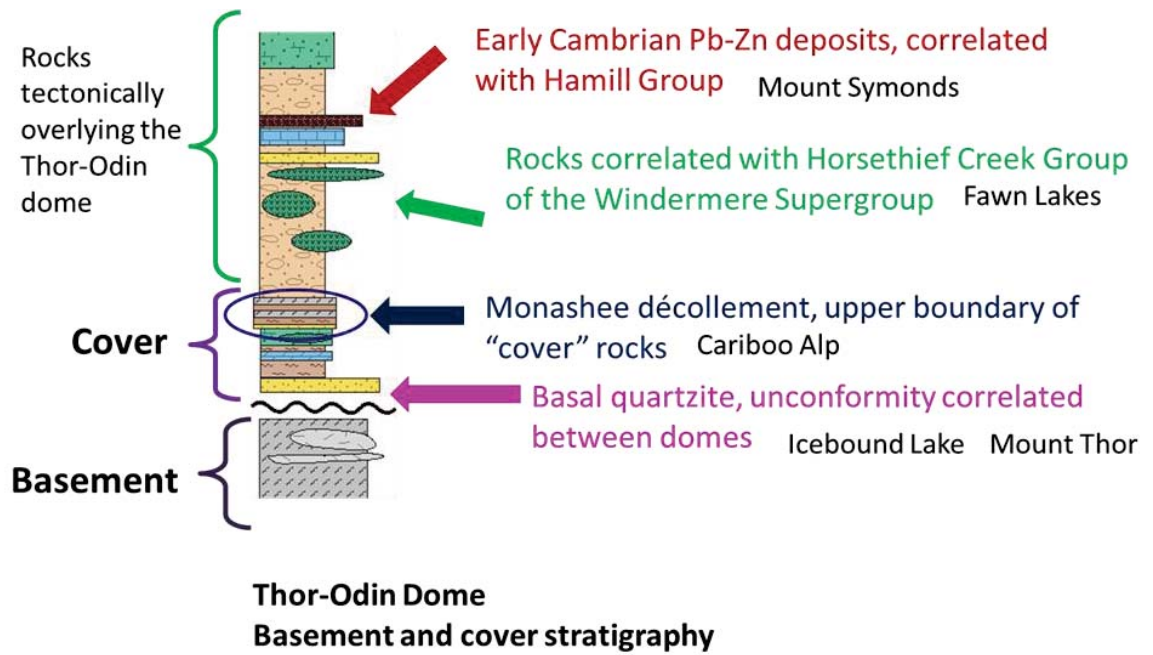


Figure 3.4a

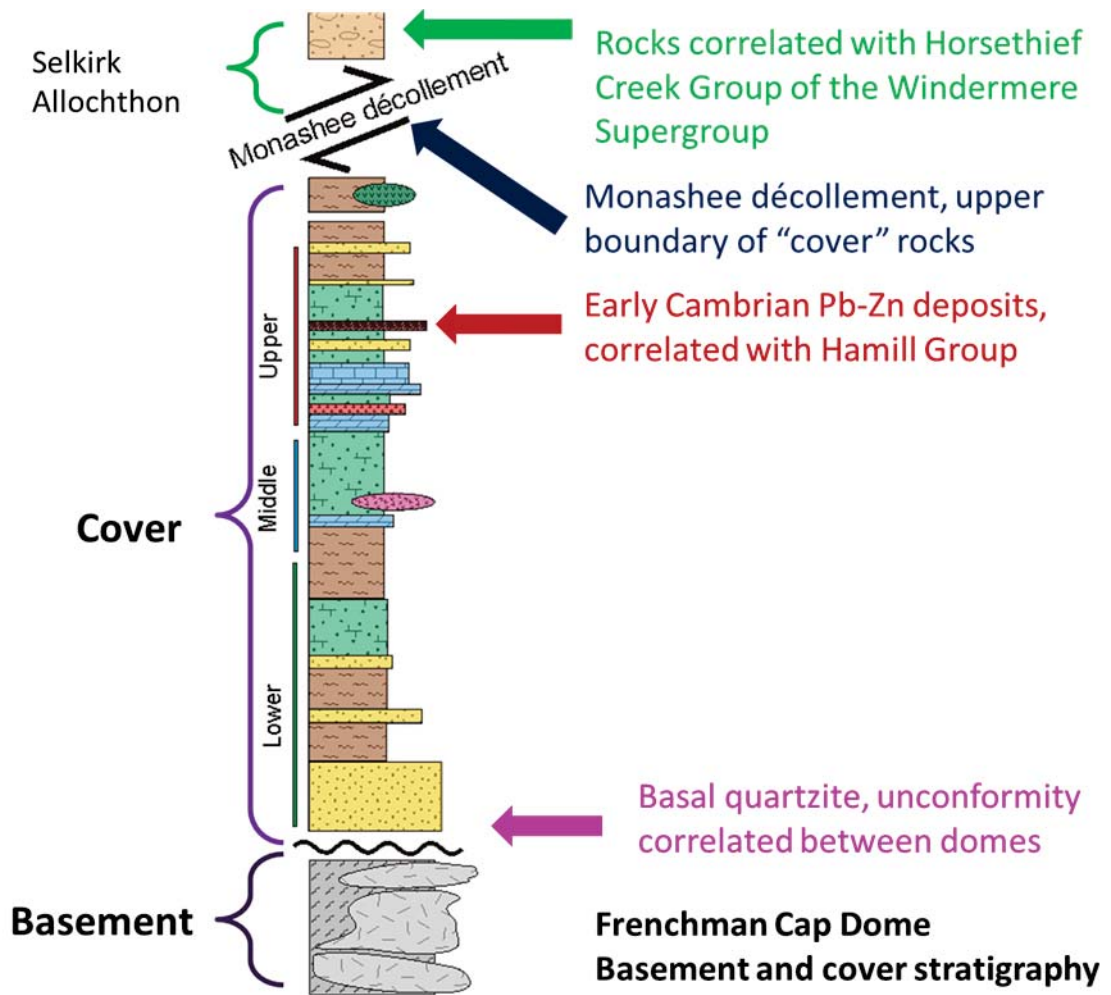


Figure 3.4b

Legend for stratigraphic column

-  Semipelitic/pelitic schist/gneiss
-  Metavolcanics, amphibolites
-  Pb-Zn horizon
-  Syenite (Mt. Copeland)
-  Calcite marble
-  Dolomitic marble
-  Pelitic/calc-silicate schist/gneiss
-  Granitic pegmatite
-  Pelitic schist/gneiss
-  Quartzite
-  Basal unconformity
-  Basement orthogneiss
-  Basement paragneiss

Figure 3.4 Simplified stratigraphy in the Thor-Odin and Frenchman Cap domes.

(a) Simplified stratigraphy of the Thor-Odin dome and overlying rocks showing some of the major divisions and correlations for comparison with those of the Frenchman Cap dome (Figure 3.3b). The stratigraphic columns show the basement rocks unconformably overlain by the basal quartzite which is repeated by a ductile shear zone at Cariboo Alp. This is the interpreted location of the Monashee décollement in the Thor-Odin dome (McNicoll and Brown 1995). Note that in this interpretation the rocks above Cariboo Alp are not considered to be part of the “cover sequence” rocks in the Thor-Odin dome, but in others (e.g. Thompson et al. 2006) the cover sequence extends structurally above Cariboo Alp. Based on Coleman (1990), and the template for Frenchman Cap stratigraphy after Scammell (1993) and Höy (2000).

(b) Simplified stratigraphy of the Frenchman Cap dome and overlying rocks showing some of the major divisions and correlations within the Thor-Odin dome (Figure 3.3a). The Monashee décollement in the Frenchman Cap dome transported rocks of the Selkirk Allochthon over the cover rocks of the Frenchman Cap dome (Brown et al. 1992). Modified from Scammell (1993), Crowley (1997), Höy (1987, 2000).

Note: In the legend for the stratigraphic columns used in Figures 3.4 and 3.5, the rock types are generalized so as to be comparable between the Thor-Odin and Frenchman Cap domes. Designations of rocks belonging to the cover or basement sequences of each dome are indicated in Figure 3.3a and 2.3b, and protolith ages for both domes are

summarized on Figures 2.4a and 2.4b. See text for discussion of cover and basement divisions.

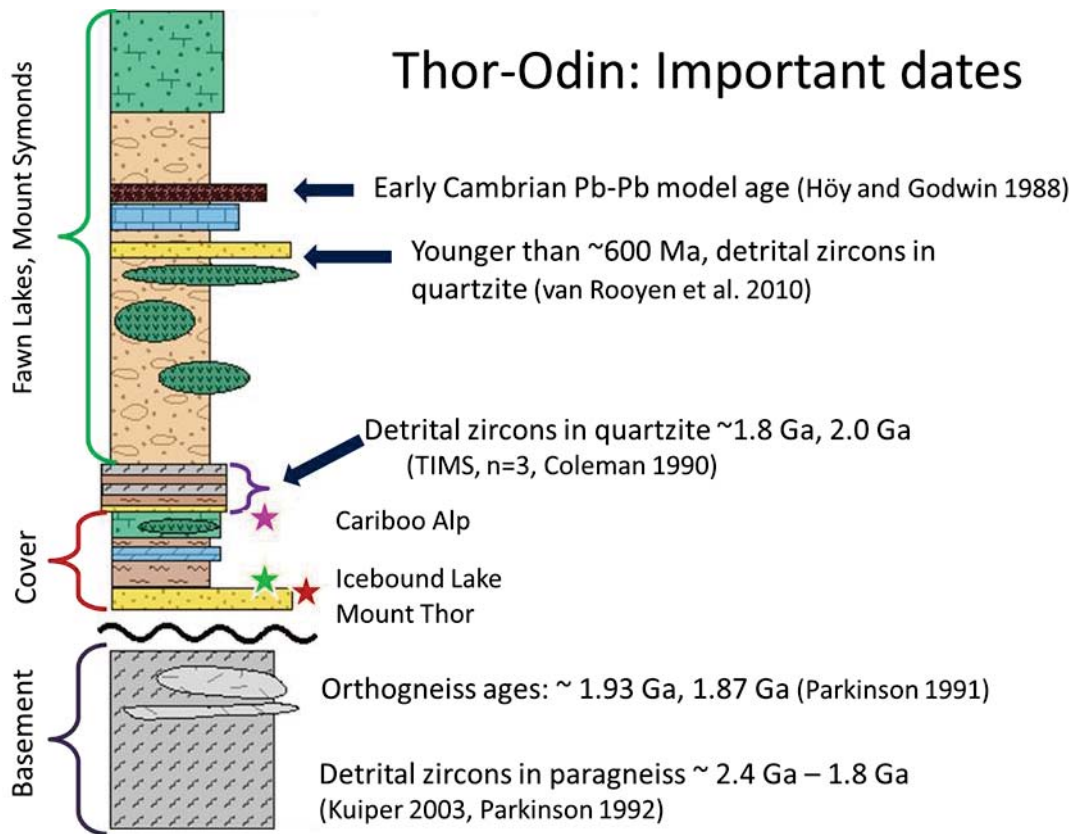


Figure 3.5a

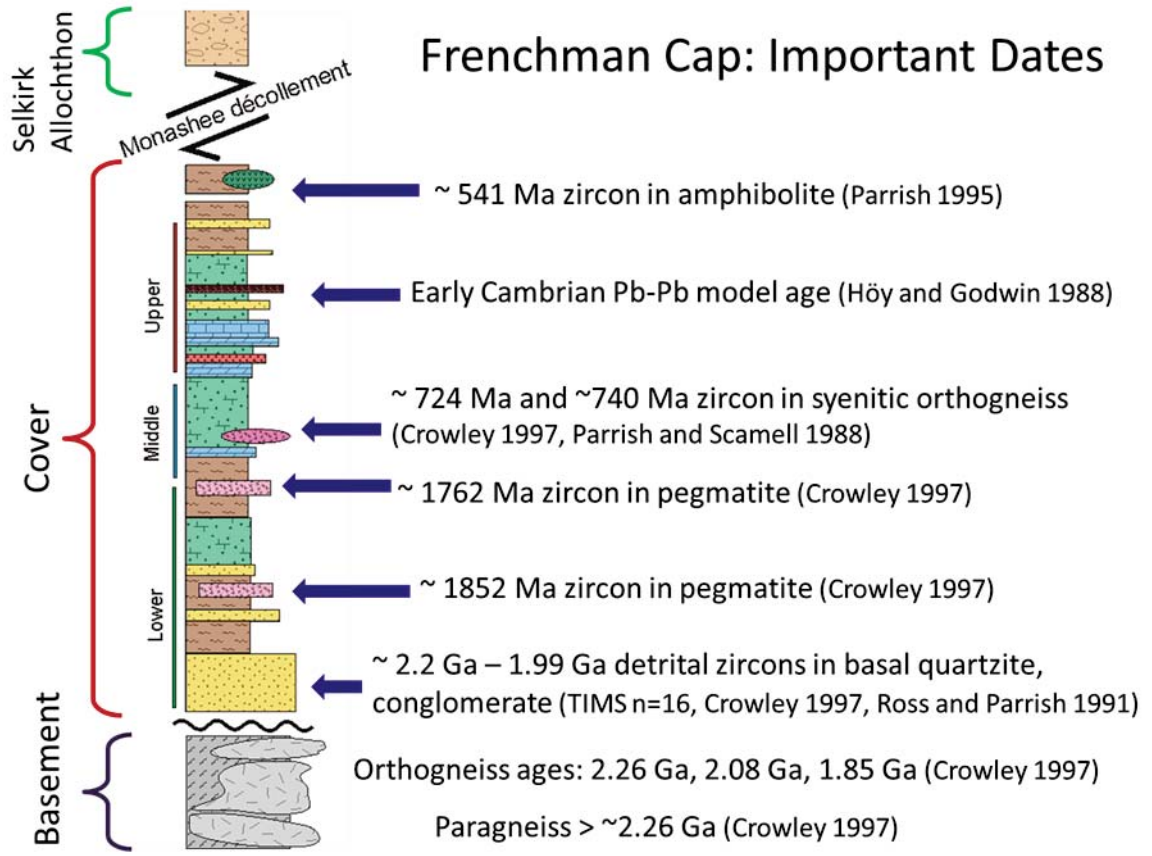


Figure 3.5b

Figure 3.5 Stratigraphy of the Thor-Odin and Frenchman Cap domes with known protolith ages.

(a) Simplified stratigraphy of the Thor-Odin dome and overlying rocks showing the known protolith ages of important units in the study. The study areas at Mount Thor, Icebound Lake and Cariboo Alp are located within the stratigraphic column. Data are from Coleman (1990), Parkinson (1991, 1992), Kuiper (2003) and this study (Chapter 3).

(b) Simplified stratigraphy of the Frenchman Cap dome and overlying rocks showing the known protolith ages of important units in the study. Data from Höy and Godwin (1988), Parrish and Scammell (1988), Ross and Parrish (1991), Parrish (1995), Crowley (1997) and Crowley et al. (2008).



Figure 3.6 Basal quartzite outlined in yellow at Mount Thor, looking north-northeast (from Hinchey 2005).

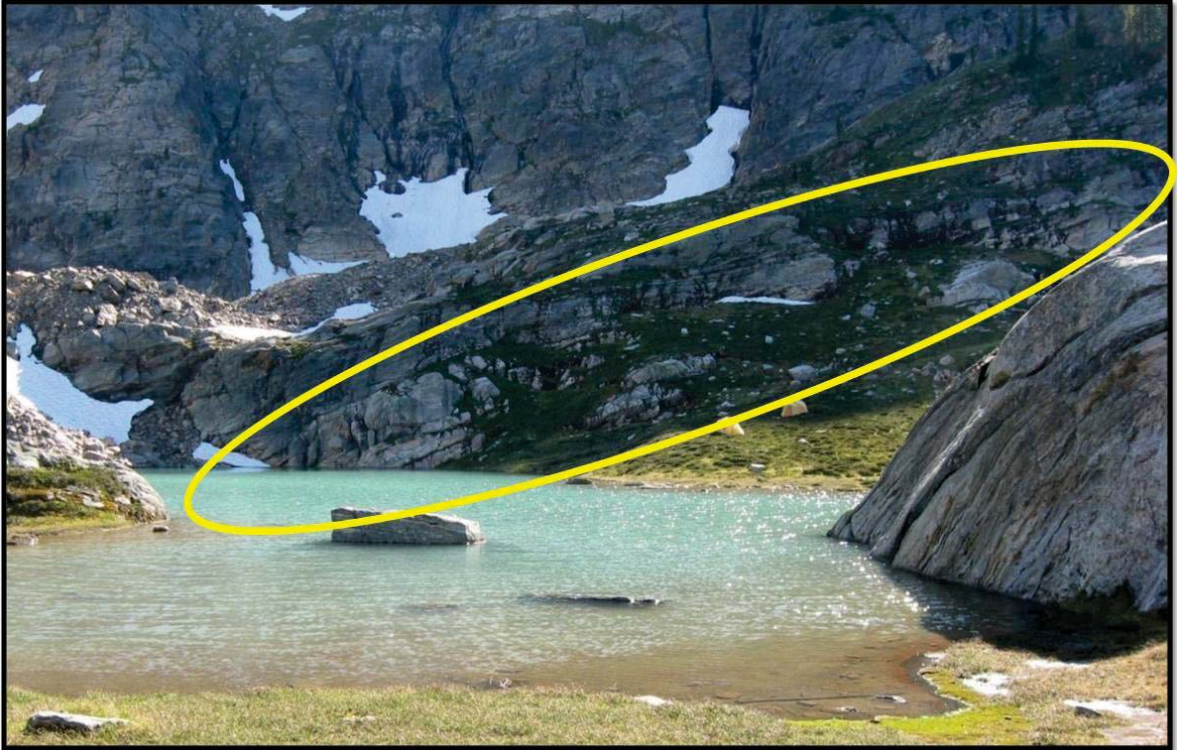


Figure 3.7 Basal quartzite at Icebound Lake. This quartzite is part of a moderately southwest dipping package of metasedimentary rocks unconformably overlying garnet–biotite–quartzofeldspathic diatexite migmatite. The yellow dots below the quartzite are tents for scale.

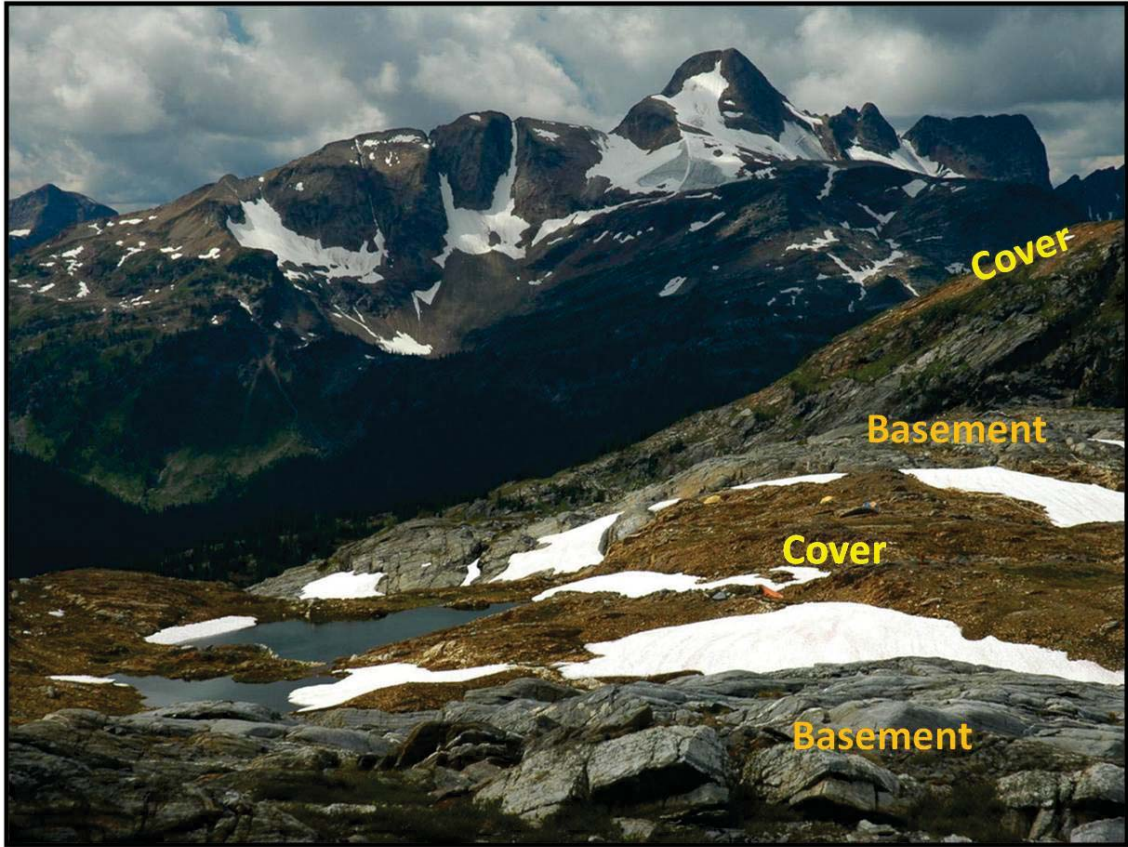
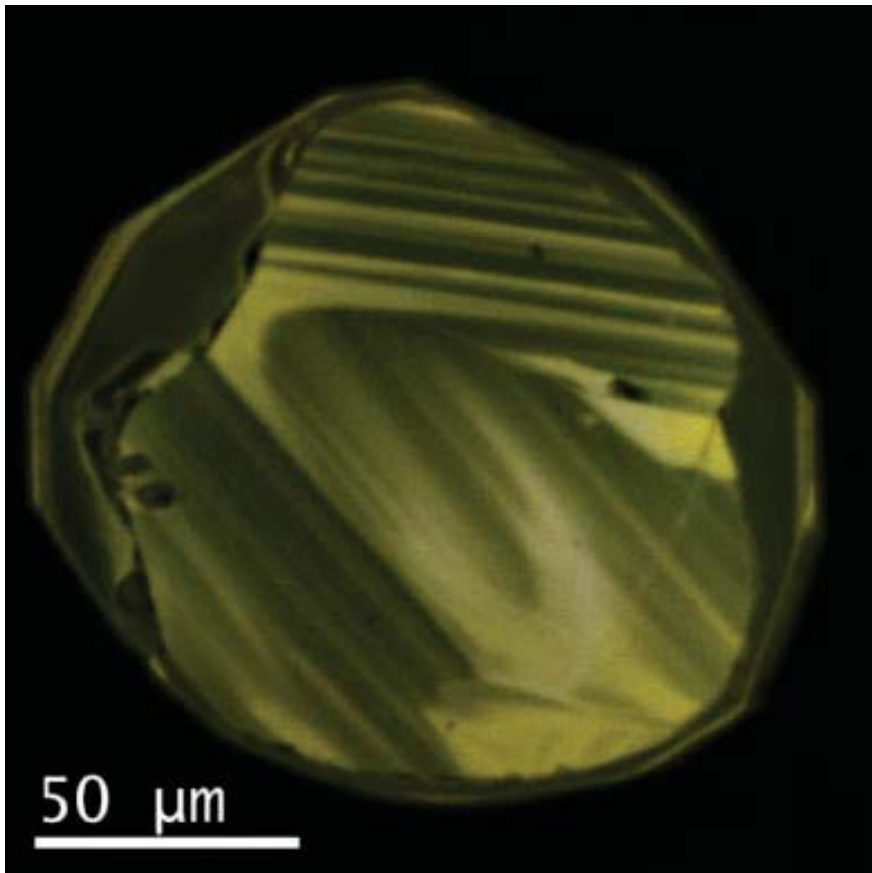
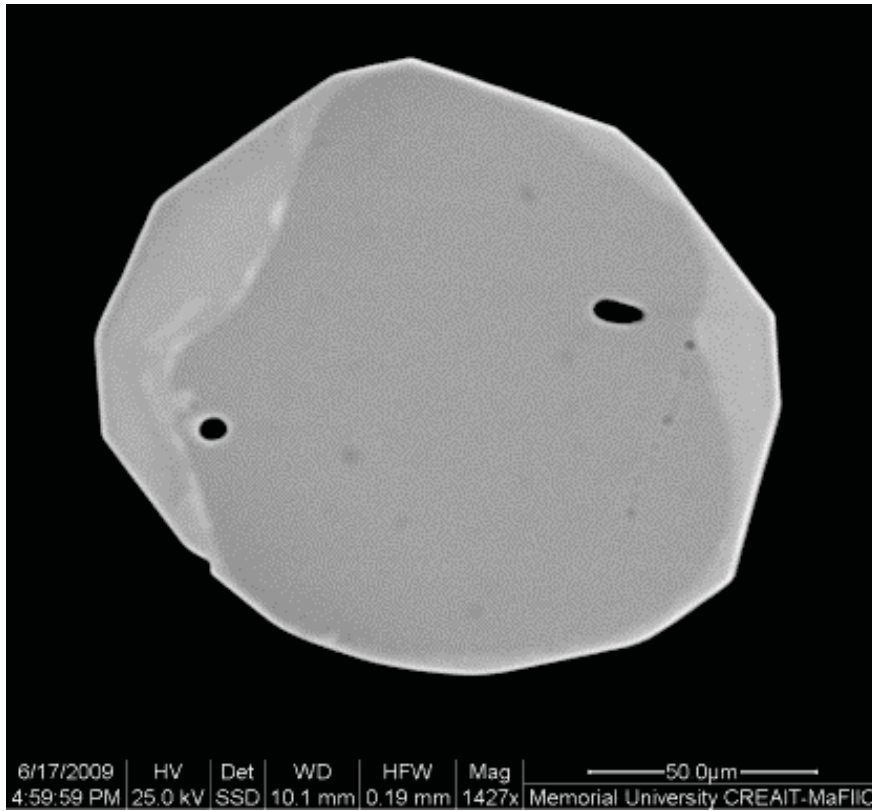


Figure 3.8 View of the Cariboo Alp area looking at Mount Fosthall to the southwest. The alternating belts of grey and rusty gneiss, interpreted as basement and cover rocks, respectively, are indicated. The yellow dots and orange dots in the middle cover section are tents for scale.



Figure 3.9 The basal quartzite at Cariboo Alp (DC165). This quartzite is a 10 m thick, moderately southwest dipping layer.



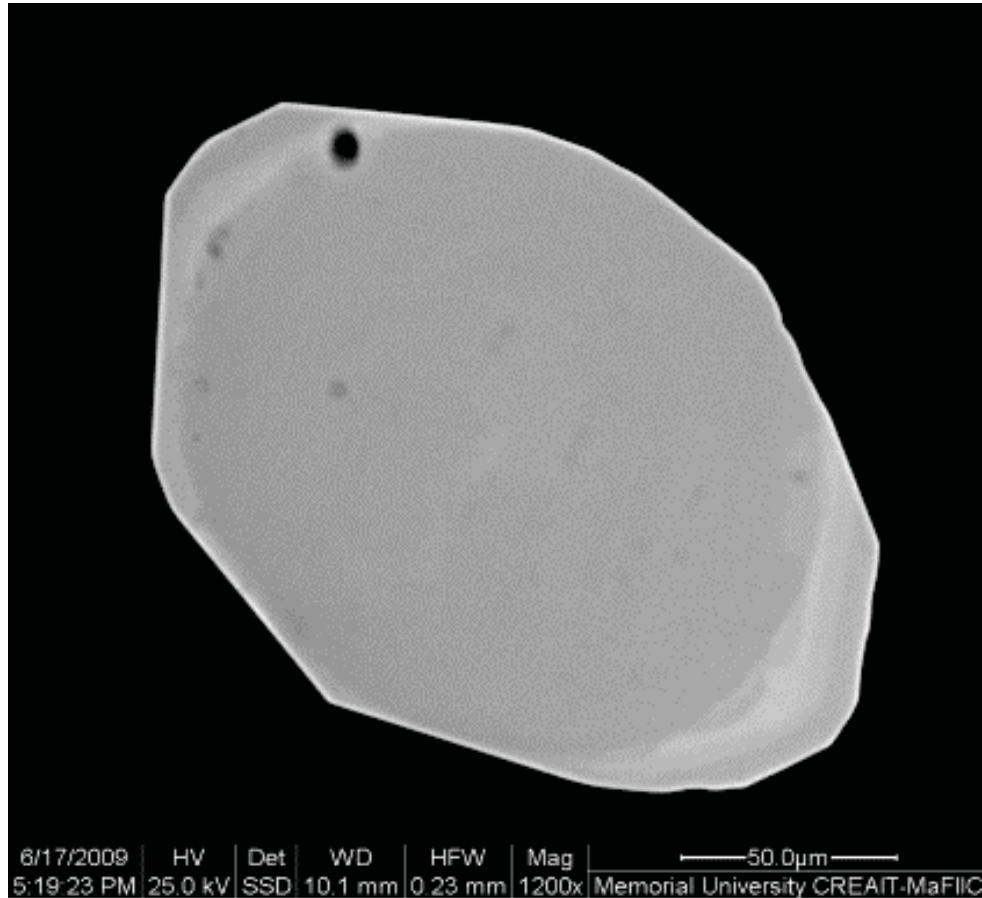


Figure 3.10 Detrital zircons from the Mount Thor quartzite (DA224).

Typical rounded zircons from the unit in BSE images. Zircons have internally zoned, rounded cores with metamorphic overgrowths and are interpreted as detrital zircons that have been transported.

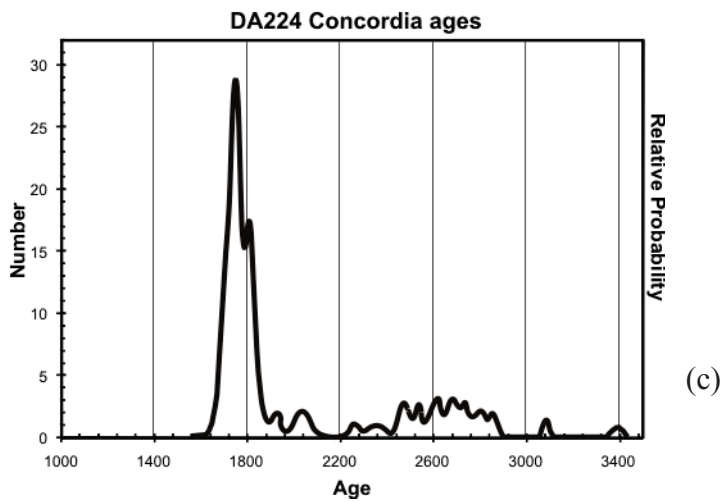
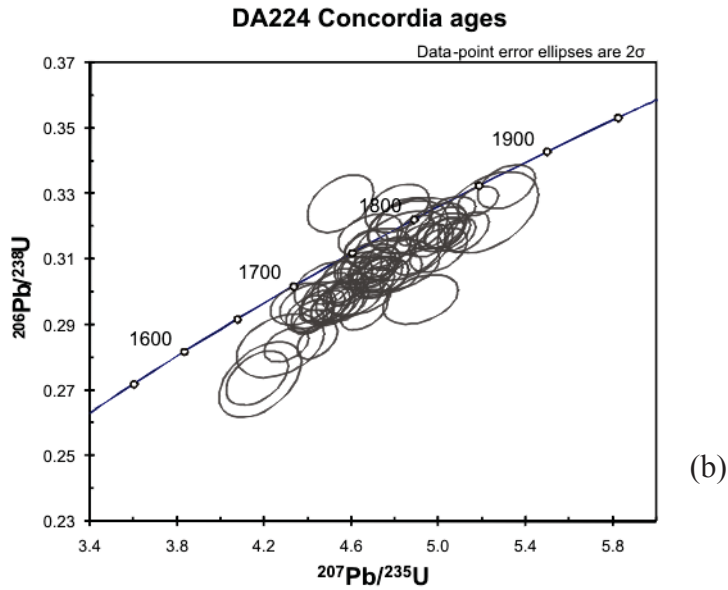
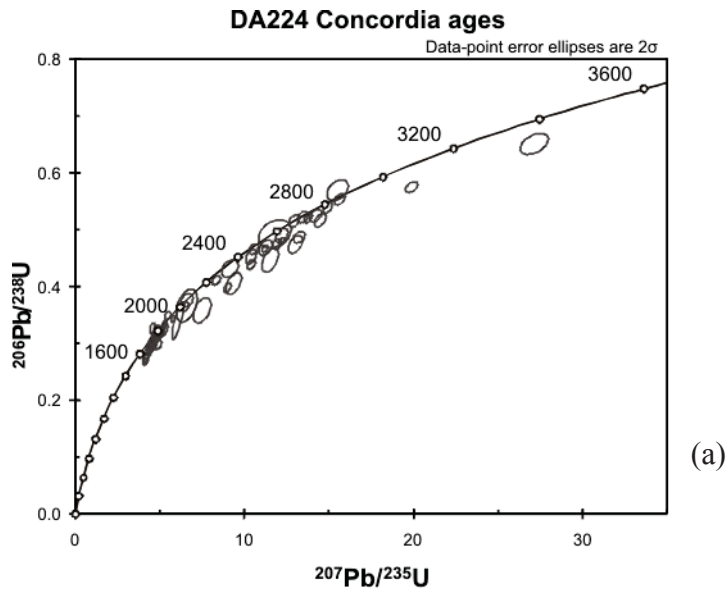
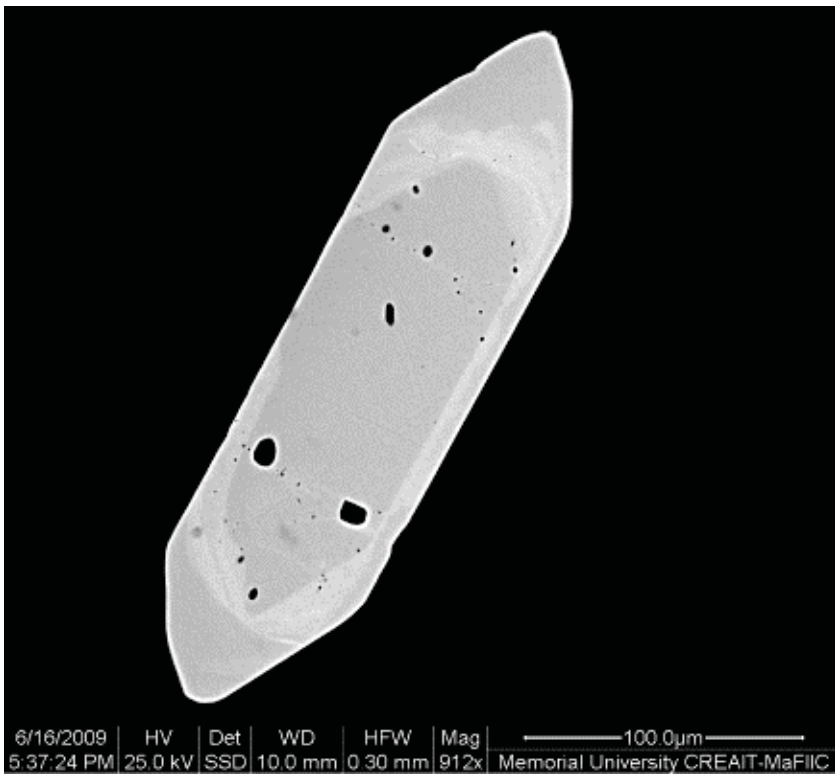
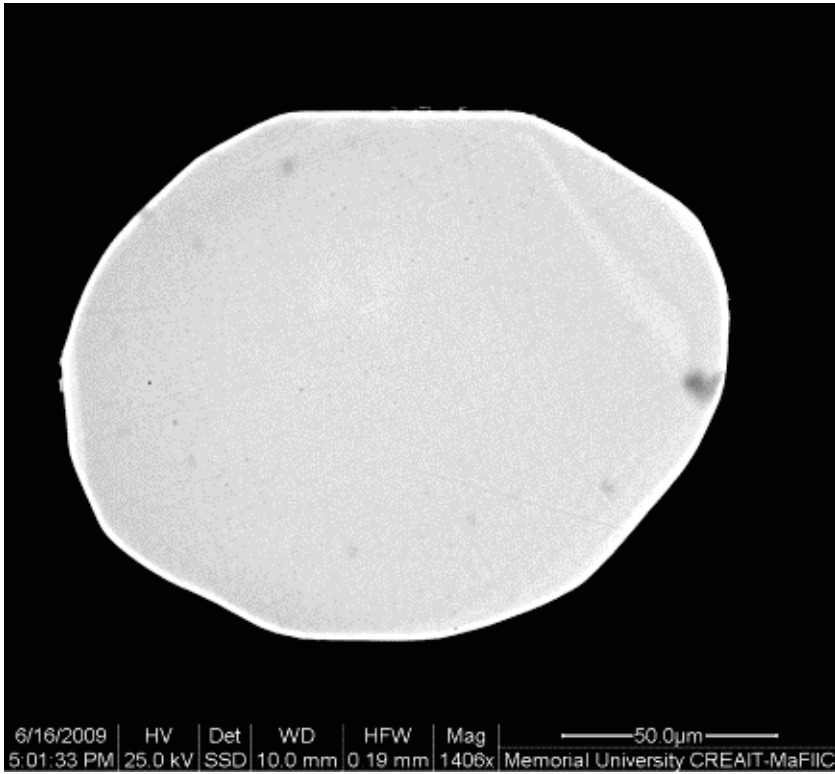


Figure 3.11 Detrital zircon U-Pb ages for Mount Thor quartzite (DA224).

(a) Concordia plot showing all grains more than 90% concordant.

(b) Concordia plot for all the grains between c. 1600 and 1900 Ma.

(c) Probability distributions using Concordia ages.



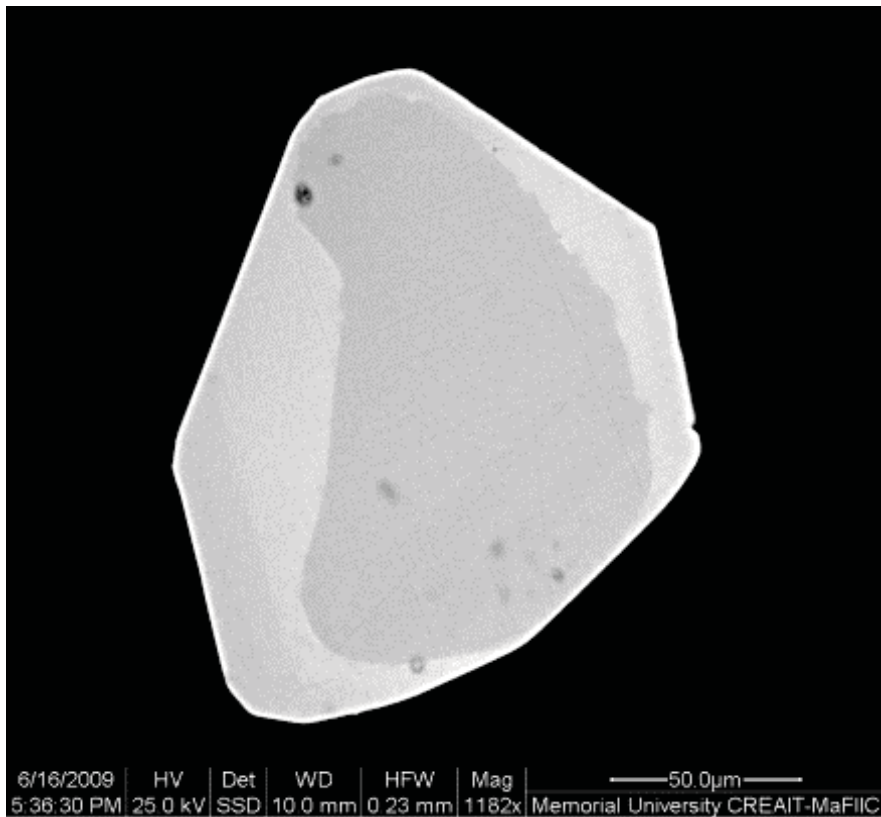
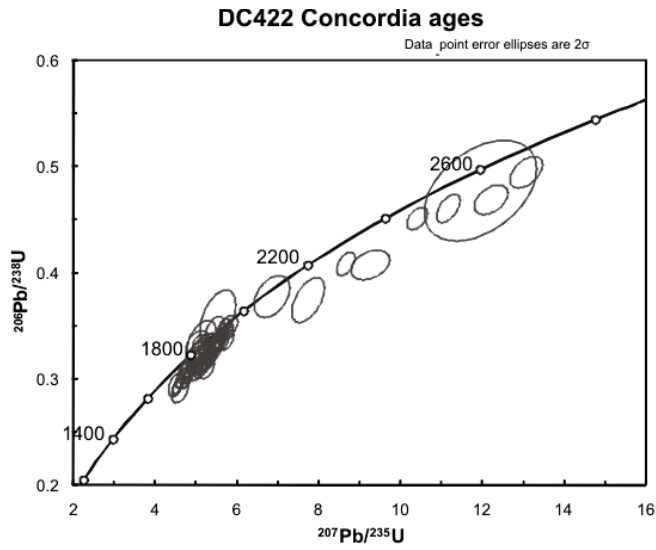
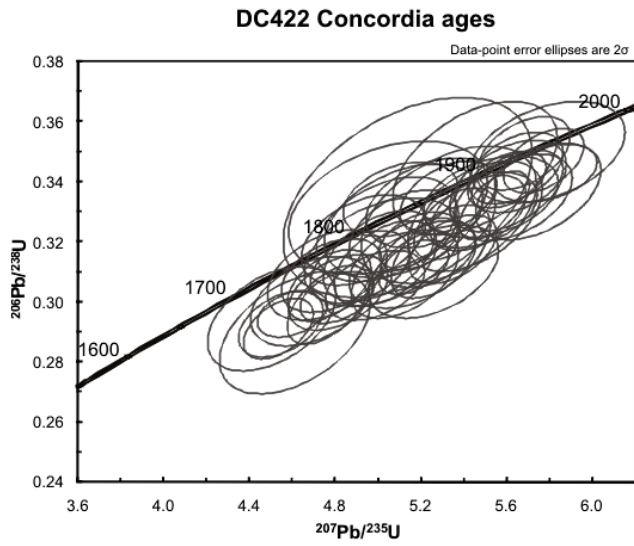


Figure 3.12 Detrital zircons from the Icebound Lake quartzite (DC422).

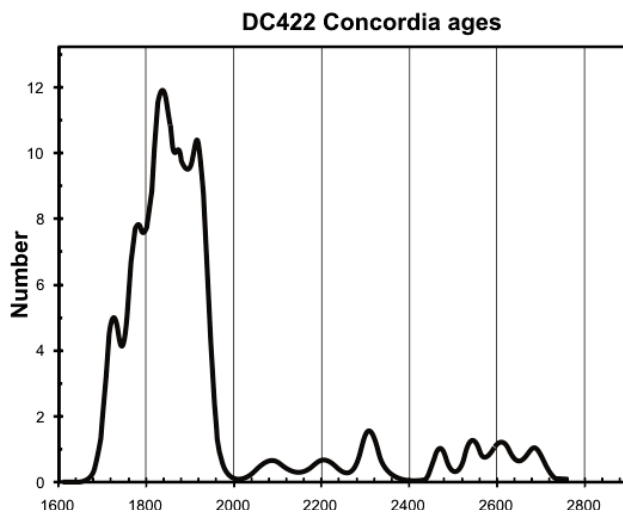
These are typical rounded zircons from the unit in BSE images. Zircons have rounded cores with metamorphic overgrowths and are interpreted as detrital zircons that have been rounded during transport.



(a)



(b)



(c)

Figure 3.13 Detrital zircon U-Pb ages from the Icebound Lake quartzite (DC422).

(a) Concordia plot showing all grains more than 90% concordant.

(b) Concordia plot for all the grains between c. 1600 and 1900 Ma.

(c) Probability distributions using Concordia ages.

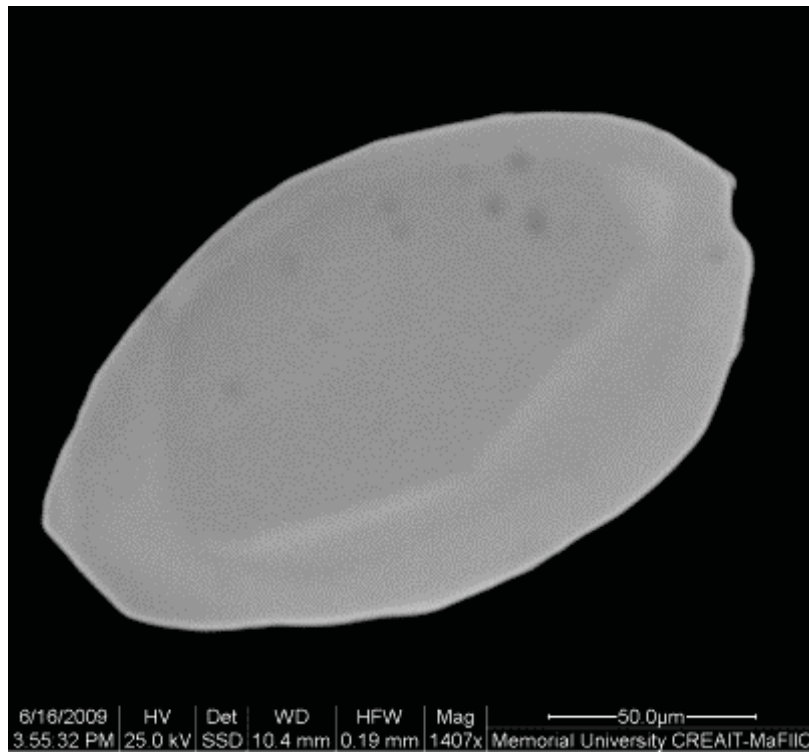
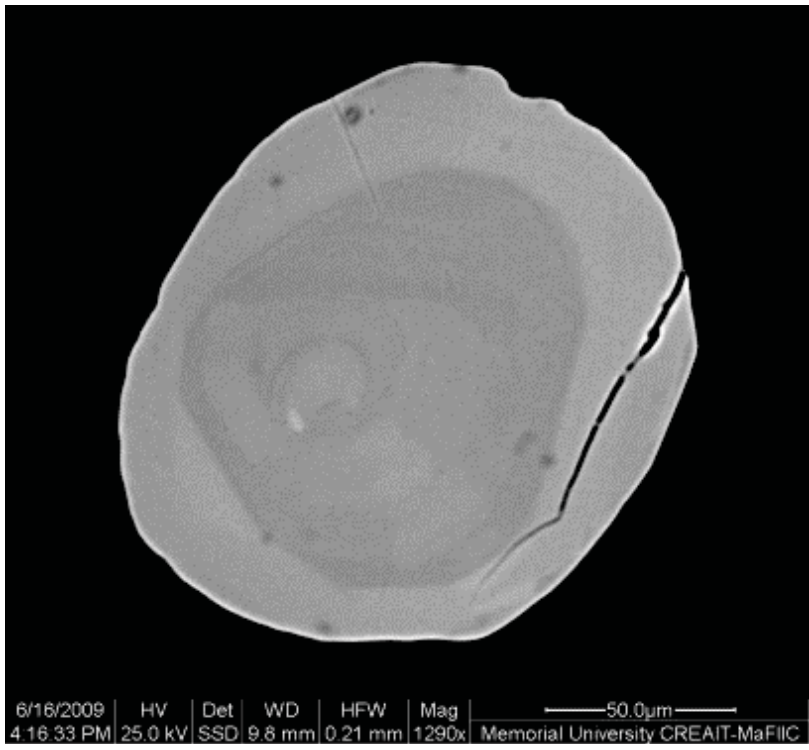
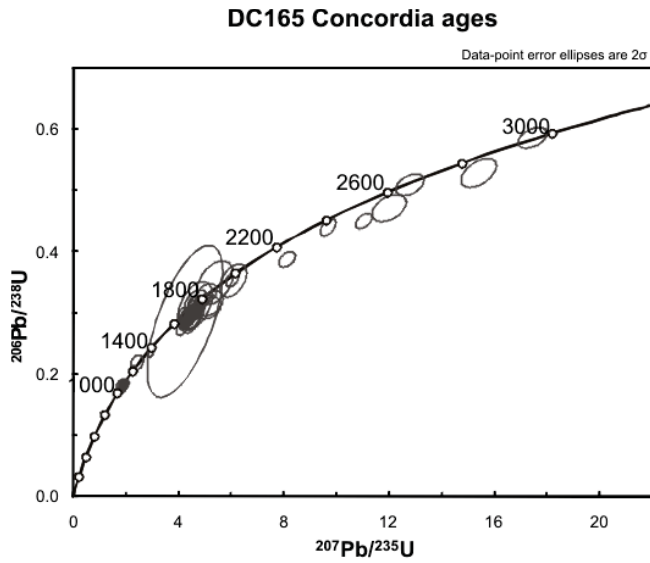
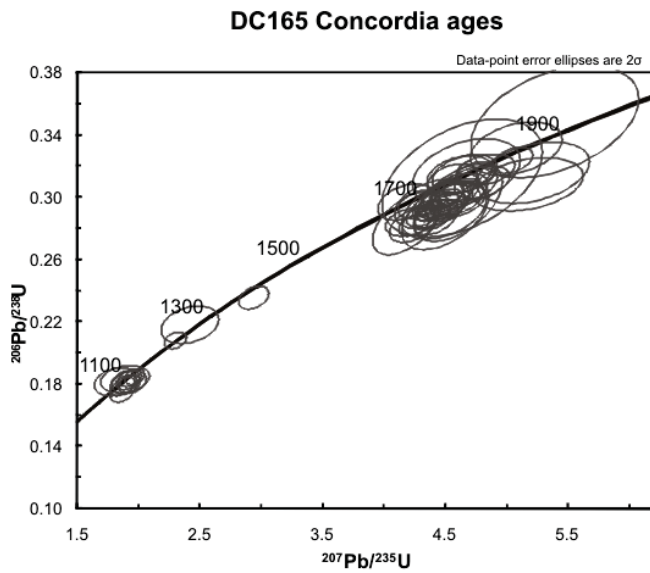


Figure 3.14 Detrital zircons from the Cariboo Alp quartzite (DC165).

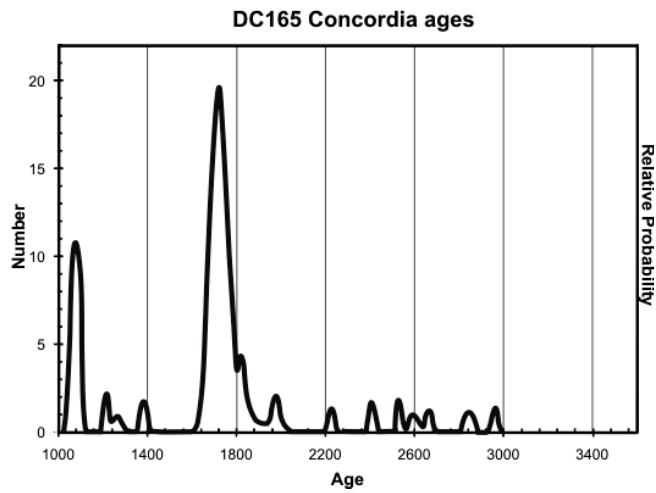
Rounded zircons from the unit shown in BSE images. Zircons have internally zoned, rounded cores with metamorphic overgrowths and are interpreted as detrital zircons that have been rounded during transport.



(a)



(b)



(c)

Figure 3.15 Detrital zircon U-Pb ages from the Cariboo Alp (DC165).

(a) Concordia plot showing all grains more than 90% concordant.

(b) Concordia plot for all the grains between c. 1000 and 1900 Ma.

(c) Probability distributions using Concordia ages.

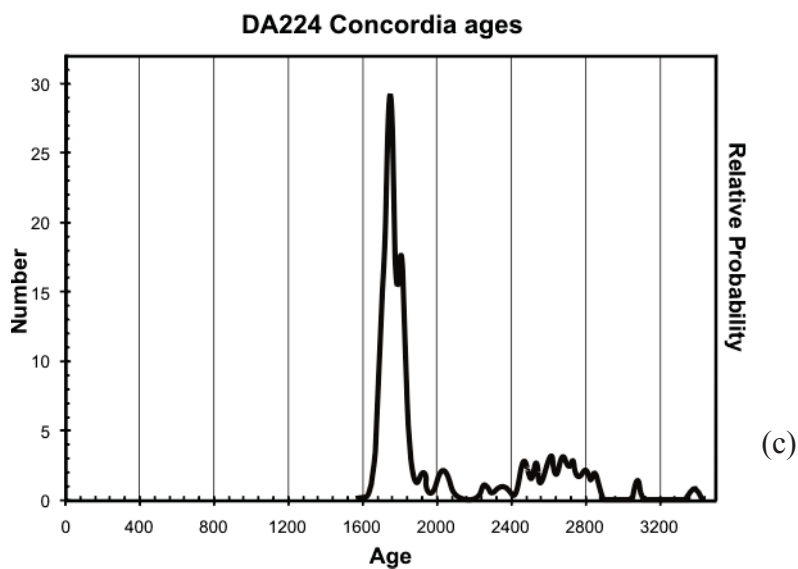
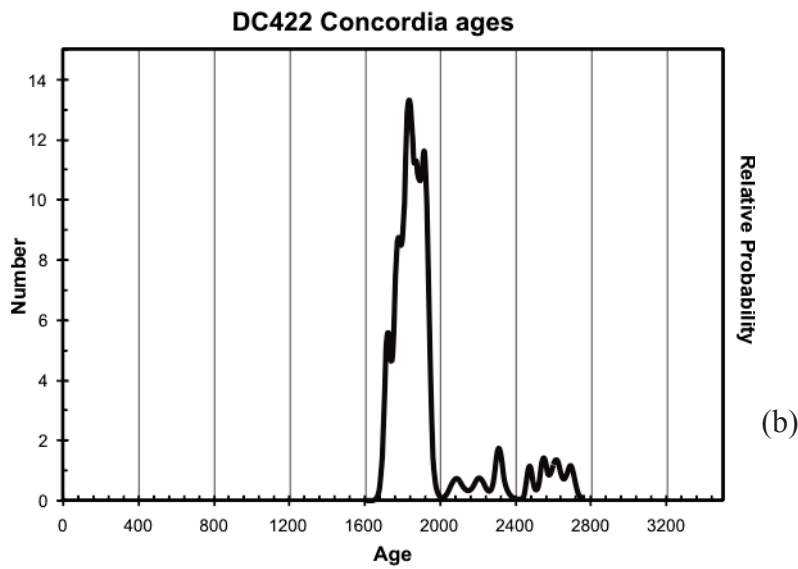
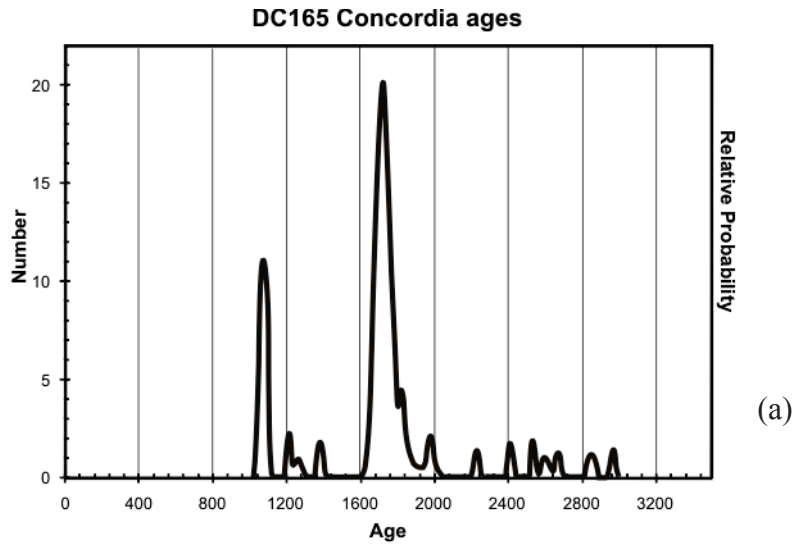


Figure 3.16 Comparison of the detrital zircon populations in samples from Mount Thor, Icebound Lake and Cariboo Alp. These probability distributions for detrital zircon U-Pb ages in samples from (a) Cariboo Alp (DC165), (b) Icebound Lake (DC422), and (c) Mount Thor (DA224) show the distinct c. 1100 Ma population in the Cariboo Alp sample that is absent in the other two. We interpret the Cariboo Alp quartzite to be younger than the Mount Thor and Icebound Lake samples.

4 Chapter: LA-ICP-MS detrital zircon results from two quartzites in the Thor-Odin – Pinnacles area: Constraints on age and provenance of the metasedimentary and metavolcanic rocks overlying the Thor-Odin dome; Implications for interpretations of accreted or autochthonous terranes.

4.1 Introduction

This study addresses the protolith age and depositional history of a panel of mid to upper amphibolite polydeformed supracrustal rocks from the metamorphic core of the southeastern Canadian Cordillera overlying the Thor-Odin dome in southeastern British Columbia, using detrital zircon U-Pb geochronology. The rocks are located west of Upper Arrow Lake in the Gold Range of the Monashee Mountains located within a 7 km thick, generally southwest dipping panel of rocks that lies structurally above the dome and extends south along Upper Arrow Lake (Figure 1.1, 1.2).

This panel of metamorphic rocks is exposed in the footwall of the east-dipping Columbia River fault zone (Figures 1.1, 1.2), an Eocene normal fault (Brown and Read 1983; Parrish et al. 1988). The Columbia River fault juxtaposed primarily greenschist facies rocks with generally pre-Middle Jurassic deformation and Jurassic – Early Cretaceous cooling histories against amphibolite facies rocks with Late Cretaceous to Eocene metamorphic and deformation histories (Read and Brown 1981; Brown and Read 1983; Archibald et al. 1983; Parrish et al. 1988) and Paleocene to Eocene cooling histories (see

Chapter 5, this study). The Okanagan Valley – Eagle River fault system is a shallowly west-dipping ductile-brittle normal fault, also active in the Eocene (Brown 2010 and references therein) (see section 2.3).

There are two contrasting interpretations of the origin of the rocks in this panel. In one interpretation, the lower part of the succession, which includes the rocks of Mount Symonds, is correlated with the Windermere Supergroup and Hamill Group (Carr 1991a and references therein). These rocks were likely deposited outboard relative to the present day location of Thor-Odin basement rocks and were structurally emplaced on and/or infolded with the basement rocks of the dome (McNicoll and Brown 1995; Williams and Jiang 2005; Carr and Simony 2006). In this interpretation, the upper part of the panel, as represented by the Plant Creek study area, contains Paleozoic and Mesozoic rocks, correlative with para-autochthonous Kootenay terrane and allochthonous Slide Mountain and Quesnel terranes (Carr 1991a). Allochthonous rocks were juxtaposed against para-autochthonous or Laurentian and pericratonic rocks during Paleozoic basin inversion, and Mesozoic terrane accretion and orogenesis (Evenchick et al. 2007 and references therein).

In contrast, another hypothesis interprets the rocks throughout the panel to be composed of a succession of Proterozoic to Paleozoic rocks unconformably overlain by Devonian to Jurassic rocks. In this interpretation the Proterozoic rocks were

unconformably deposited on the basement and the Paleozoic to Mesozoic rocks deposited in an in situ basin (Thompson et al. 2004, 2006). In this interpretation the Columbia River fault zone as well as the west-dipping Okanagan Valley – Eagle River fault zone are considered to be minor tectonic elements of the history of the area, and proposes that they have displacements of less than 1 km in contrast to the 20 – 90 km of displacement previously documented (Tempelman-Kluit 1986, Read and Brown 1981, Parrish et al. 1988). This model is inconsistent with the disparate thermal histories of the hanging wall vs. foot wall rocks (section 2.1 and 2.3). The controversy concerning the displacements on the Okanagan Valley – Eagle River fault zone was addressed by Brown (2010), who concluded that the large displacement hypothesis is correct, and that the apparent continuity of Devonian and Jurassic rocks in the Vernon area is due to corrugations in the fault surface of the Okanagan Valley – Eagle River fault zone, and not a result of unconformable deposition.

This study addresses the hypotheses described above by examining the protolith ages of the quartzites in question in order to determine minimum depositional ages for the metasedimentary packages that host them. The detrital zircon data in combination with structural data will determine whether the protoliths are Proterozoic or younger, and also constrain the source areas for the sediments, making it possible to discriminate between rocks with a Laurentian affinity or rocks of the Quesnellia terrane.

4.2 Geological setting of the Thor-Odin – Pinnacles area in the southeastern

Canadian Cordillera

The Thor-Odin – Pinnacles area (Figure 1.1, 1.2) is located on the western side of Upper Arrow Lake in southeastern British Columbia. The Thor-Odin dome consists of Paleoproterozoic basement orthogneiss and paragneiss, and is infolded with Paleoproterozoic cover paragneiss (Reesor and Moore 1971; Parkinson 1991). The panel of rocks overlying the Thor-Odin dome comprises rocks with protolith ages ranging from Late Proterozoic to Mesozoic (Reesor and Moore 1971; Carr 1991a and references therein; this study Chapter 2). The commonly held interpretation is that some of these rocks were deposited on the margin of Laurentia while others are part of pericratonic and allochthonous assemblages accreted to the Laurentian margin (Evenchick et al. 2007 and references therein).

Important successions of miogeoclinal rocks deposited on the western margin of the Laurentian craton, preserved in the external and internal zones, are exposed in southeastern British Columbia including rocks of the Proterozoic Belt Purcell Supergroup (Ross et al. 1992 and references therein), the Windermere Supergroup (Ross et al. 1992 and references therein), Neoproterozoic to Cambrian Hamill, Badshot and Mohican Groups (Colpron et al. 2002 and references therein), and the overlying Paleozoic Lardeau and Milford Groups (Fritz et al. 1991). See Chapter 3 for an introduction to the Laurentian passive margin successions important in southeastern British Columbia.

Accreted terranes include the Paleozoic Slide Mountain terrane and the Mesozoic Quesnellia terrane (Gabrielse et al. 1991; Ross et al. 1997).

Allochthonous terranes identified in southeastern British Columbia include the Paleozoic Slide Mountain terrane and the primarily Mesozoic Quesnellia terrane, in addition to the Harper Ranch, Cache Creek, and Stikinia terranes (Gabrielse et al. 1991; Ross et al. 1997). The Slide Mountain terrane is a Permian marginal ocean basin that developed adjacent to the Laurentian margin, and is preserved as oceanic crust obducted over the pericratonic Kootenay terrane (Gabrielse et al. 1991). The Quesnellia terrane primarily consists of Triassic to Jurassic volcanic arc rocks and arc-related sediments. These sediments were deposited on juvenile oceanic crust, and are interpreted as having formed adjacent to or outboard of the Laurentian craton (Gabrielse et al. 1991; Parrish and Monger 1992), or alternatively on attenuated Laurentian crust (Erdmer et al. 2002; Thompson et al. 2006). The Jurassic and Triassic rocks belonging to Quesnellia in the southeastern and south central Canadian Cordillera have been documented to contain detrital zircon populations derived from volcanic rocks in the Quesnellia terrane reflecting that Jurassic and Triassic volcanic material was a major source of detrital sediments and that there was only a minor influence from continental sediments (Petersen et al. 2004). In this study area the Nicola, Slokan and Rossland Groups are part of the Quesnellia terrane (Klepacki and Wheeler 1985; Carr 1991a; Gabrielse et al. 1991; Lemieux et al. 2003, 2004).

4.2.1 Quesnellia terrane rocks in the Thor-Odin – Pinnacles area

Rocks correlated with the Quesnellia terrane, in the Thor-Odin Pinnacles area, are generally considered to be confined to the hanging walls of Eocene normal faults such as the Columbia River fault (See Figure 1.1). These include parts of the Slocan Group in the Arrow Lake area and the hanging wall rocks of the Columbia River fault (Carr 1991a; Lemieux et al. 2003, 2004). In the center of the map there are three klippen soled by the Columbia River fault, containing rocks of the Rossland and Slocan Groups (Read and Brown 1981; Brown and Read 1983; Carr 1991a). Slocan Group rocks are also exposed in the hanging wall of the west-dipping Beaven fault in the southwest part of the map (Carr 1991a; Thompson et al. 2004).

The Slocan Group rocks in the hanging wall of the Columbia River fault are fine grained slates, argillites, and phyllites. Sections of the metamorphosed footwall rocks have also been correlated with the Slocan Group (Carr 1991), for example, the Silver Creek schist near Viddler Ridge (Figure 1.2), metamorphosed in the Late Cretaceous to sillimanite–muscovite-bearing amphibolite facies, with local staurolite (Glombick 2005). The Rossland Group rocks in this map area are exposed in the klippen of the Columbia River fault zone (Read and Brown 1981) and include porphyritic augite basalt flows and volcanoclastic sediments (Lemieux et al. 2003, 2004).

4.2.2 Geology of specific study areas

4.2.2.1 Mount Symonds

On Mount Symonds (Figure 4.1), there are two distinct quartzites within a heterogeneous package of amphibolite, paragneiss and marble. These rocks were penetratively deformed at upper amphibolite facies conditions in the Late Cretaceous – Paleocene (Carr 1991; Chapter 2), and intruded by the Ladybird granite suite (Carr 1990). The upper quartzite structurally underlies the Empress Marble, and together, they form a distinctive marker that is continuous for over 20 km along strike from Mount Symonds westward to Mount Fosthall, and beyond (Reesor and Moore 1971). This study focuses on the lower quartzite (DC395), a southwest dipping marker exposed in an isoclinal fold closure that straddles the peak of the mountain (Figure 4.1). The 2 – 10 m thick quartzite is white to light grey with dark heavy mineral bands (Figure 4.2).

Reesor and Moore (1971) mapped the Mount Symonds quartzite as part of the mantling gneiss zone on the flanks of the Thor-Odin dome, as Units M3 – M8. Höy and Godwin (1988) proposed a Lower Cambrian age for the Empress marble and an associated Pb-Zn deposit (Big Ledge), based on common-Pb model ages and a correlation with similar stratabound Pb-Zn deposits in Frenchman Cap. Carr (1991) included the rocks on Mount Symonds in the “Symonds quartzite-bearing Unit” (Map unit 5) and suggested that they may correlate with the Hamill Group. Based on lithology and stratigraphic relationships, Carr (1991) correlated the structurally underlying Fawn Lakes assemblage, a >1700 m

thick aluminum-poor semi-pelitic schist, with the semipelite-amphibolite division of the Horsethief Creek Group of the Windermere Supergroup (Pell and Simony 1987). Carr (1991) also correlated the overlying Empress Marble and its associated quartzite with the Badshot and Mohican groups. The Hamill Group is considered to be Late Proterozoic to Lower Cambrian in age. The Badshot and Mohican groups are Lower Cambrian (Fritz et al. 1991).

Thompson et al. (2004) mapped the Mount Symonds area and its quartzites as Paleo- to Mesoproterozoic, and as part of a larger unit which includes sillimanite–garnet–biotite schist, calc-silicate, marble, and biotite–quartz–K-feldspar paragneiss. However, Thompson et al. (2004) did not suggest any specific correlation, except to propose that the Pb-Zn deposits on Mt. Symonds are the same as in Frenchman Cap, and Late Proterozoic in age (Thompson et al. 2006). The assignment of map unit ages is, in part, supported by U-Pb detrital zircon ages from a study by Lemieux et al. (2007) which suggested that the Saddle Mountain area (Figure 1.2) have detrital zircon populations consistent with a Proterozoic protolith age.

4.2.2.2 Plant Creek

A quartzite (DC 490) from the headwaters of Plant Creek is exposed along Plant Creek Road, and associated with amphibolites and garnet–sillimanite–biotite schists (Figure 4.3). The metamorphic rocks of the surrounding assemblage are K-feldspar–sillimanite-

bearing amphibolite facies rocks. All the rocks in this panel are penetratively deformed and intruded by the Paleocene-Eocene Ladybird granite suite (Carr 1991b; Hinchey et al. 2006). This sample (Figure 4.4) lies structurally below greenschist facies meta-sedimentary and meta-volcanic rocks of the Triassic Nicola and Jurassic Rossland Groups of the Quesnellia terrane. These greenschist facies rocks are interpreted to be a klippe of the Columbia River fault (Parrish et al. 1988; Monger and Price 2000) or part of an unconformably deposited sedimentary assemblage (Thompson et al. 2004, 2006). The latter hypothesis was supported by U-Pb detrital zircon ages from a study by Lemieux et al. (2007) which documented a Devonian or younger protolith age for a calcareous quartzite in the Arrow Lakes area at the top of the stratigraphic section interpreted by Thompson et al. (2006) as Proterozoic to Paleozoic, the Chase Quartzite. In the same study, detrital zircon data from Saddle Mountain were consistent with a Proterozoic protolith ages.

Reesor and Moore (1971) mapped the Plant Creek area as part of the “fringe zone” surrounding the Thor-Odin dome, containing meta-sedimentary rocks with abundant leucogranite. However, they did not propose specific correlations since it was not directly relevant to their study of the Thor-Odin dome. Carr (1991a) mapped the assemblage containing this quartzite as occurring in the upper part of the Mount Fosthall Composite unit, a psammite-semipelite unit which includes rusty semi-pelitic gneiss, amphibolite gneiss, calc-silicate schist, marble and quartzite. Carr (1991a)

correlated the psammite-semipelite assemblage with the Milford Group which is interpreted to be Upper Mississippian to Lower Pennsylvanian in age (Fritz et al. 1991). The Milford Group is overlain by the Kaslo and Slocan Groups and was also described in the hanging wall of the Columbia River fault in the Nelson and Lardeau Map areas (Klepacki and Wheeler 1985).

4.3 Methods

Refer to Section 3.3 for methods. All sample preparation techniques for extraction and selection of zircon, analytical LA-ICP-MS methods, data reduction and data interpretation parameters are the same as those discussed in section 3.3.

4.4 Results

4.4.1 DC395 – Mount Symonds

The Mount Symonds quartzite is white to light grey with dark heavy mineral bands and muscovite foliations spaced 2 cm apart (Figure 4.2). It contains 90% polycrystalline, metamorphic quartz, 5% muscovite, and <5 % plagioclase feldspar, interpreted as detrital because of its rounded grain shapes. The quartzite layer is in conformable contact with garnet–biotite–sillimanite paragneiss above and below, and part of a heterogeneous succession of amphibolite, paragneiss and marble. It is the structurally lowest quartzite exposed on Mount Symonds and forms an isoclinal synform with limbs oriented 090/40 S.

The zircon grains in this sample have rounded cores and rims typically < 10 μm visible in BSE images (Figure 4.5). The cores show faint internal oscillatory zoning interpreted as magmatic, but are all well-rounded, interpreted as evidence that they are detrital in nature and have undergone transport from their source area. The rims give the grains a faceted appearance and are interpreted as metamorphic overgrowths.

Of 97 zircons analyzed, 48 were >90% concordant. The age populations present in this sample are clustered at 500 – 650 Ma, 1100 – 1200 Ma and 1600 – 1800 Ma (Figure 4.6). The youngest zircon within 10% concordance is 514 ± 18 Ma, and within 1% the youngest grain is 608 ± 35 Ma. Nine out of the 48 grains within 10% of concordance grains were < 700 Ma.

4.4.2 DC490 – Plant Creek

The Plant Creek quartzite is a light grey to yellow quartzite with indistinct cm-scale layering and does not contain heavy mineral bands (Figure 4.4). It contains 80 % quartz and 15% plagioclase feldspar interpreted as detrital because of grain rounding. It contains accessory (<5%) biotite and titanite. It is exposed along Plant Creek Road and is oriented 085/14 S. Zircons from this sample are generally small (<100 μm) and euhedral with bipiramidal terminations, and are not visibly abraded or rounded (Figure 4.7), and oscillatory zoning (in BSE images). There are very few rounded grains, and more than

half the grains have fractures or are broken. Less than 10% of grains have noticeable overgrowths or core and rim shapes.

In total, 8 out of the 24 grains within 90% concordance were younger than 200 Ma (Figure 4.8). The youngest grain within 90% concordance is 151 ± 6 Ma, and the youngest grain within 1% discordance is 184 ± 18 Ma. There are two grains with Proterozoic ages around 1800 Ma. Because about a third of the zircons in this sample are younger than 200 Ma, and all but 2 are Paleozoic or younger, both concordia ages as well as the $^{206}\text{Pb}/^{238}\text{U}$ ages are used to determine the age populations present in this sample for plotting age histograms (Figure 4.8). Both methods produced the same age distributions for the Upper Paleozoic and Mesozoic populations, but the plot of $^{206}\text{Pb}/^{238}\text{U}$ ages include discordant zircons of 800, 1100, and 1400 Ma that were excluded from the plot of Concordia ages (Figure 4.8).

4.5 Discussion

The Mount Symonds quartzite has to be younger than ~500 Ma because the youngest detrital zircon is 514 ± 18 Ma. A correlation of the Mount Symonds rocks with the Hamill Group is consistent, and is incompatible with the Paleo- or Mesoproterozoic age for these rocks as suggested by Thompson et al. (2004, 2006). Other detrital zircon samples in southern British Columbia where 600-700 Ma zircons have been dated include Spa Creek (Erdmer et al. 2001), the McHardy and Slide Mountain assemblages (Roback et al.

1994) and Grand Forks Quartzite (Ross and Parrish 2003). The dates between 500 and 650 Ma are consistent with syn-rift volcanic units documented within the Hamill Group (Colpron et al. 2002 and references therein), and the presence of amphibolite layers within the sedimentary units on Mount Symonds supports the correlation with Hamill Group rocks based on lithological similarities.

The largest populations of grains in the Mount Symonds sample are between 1600 and 1800 Ma in age, indicating that the predominant sediment sources were Laurentian basement rocks or recycled sedimentary rocks derived from them, such as the Belt-Purcell or Windermere supergroups (Parrish 1991; Gehrels and Ross 1998; Ross et al 2005). Smith and Gehrels (1991) report detrital zircon data from the Horsethief Creek and Hamill Groups where detrital zircons indicate sources of 700, 1700 – 1800, 1900 – 2100 and 2500 – 2700 Ma, consistent with sources in the North American cratonic basement or recycled sedimentary rocks derived from the basement. The detrital results from the Mount Symonds quartzite are therefore consistent with a correlation of the lower Mount Symonds quartzite with the Hamill Group, or younger rocks, that have a North American provenance. The grains with dates around 1100 Ma represent a Grenville source, similar to those found elsewhere in the Cordillera (Gehrels and Ross 1998). Given that the Mount Symonds quartzite lies structurally below the Pb-Zn deposit proposed to be Cambrian in age (Figures 3.4 and 3.5), a Lower Cambrian age for the unit is geologically permissible. It is also possible as an alternative interpretation that the

Mount Symonds quartzite could contain recycled sediments derived from the Neo-Proterozoic Windermere Supergroup as proposed for Cambrian quartzites in Idaho by Lewis et al. (2010). The Windermere Supergroup in southeastern British Columbia and northwestern USA contains several of the detrital signatures found in the Mount Symonds quartzite (e.g. 700; 1100, 1700 – 1900 Ma).

Given that the Mount Symonds quartzite lies structurally below the Pb-Zn deposit proposed to be Cambrian in age (Figures 3.4 and 3.5), a Lower Cambrian age for the unit is geologically permissible. It is also possible that the Mount Symonds quartzite could contain recycled sediments derived from the Neo-Proterozoic Windermere Supergroup as proposed for Cambrian quartzites in Idaho by Lewis et al. (2010). The Windermere Supergroup in southeastern British Columbia and northwestern USA contains several of the detrital signatures found in the Mount Symonds quartzite (e.g. 700; 1100, 1700 – 1900 Ma).

The Plant Creek sample has a younger maximum depositional age and different provenance than the Mount Symonds quartzite. Based on the 184 ± 18 Ma detrital zircon age that is 99% concordant, the deposition of the protolith of the Plant Creek quartzite has to be Middle Jurassic or younger. However, the youngest grain that is >90% concordant is 151 ± 6 Ma, so the quartzite protolith could be as young as Late Jurassic. Other detrital zircon ages seen in this sample are clustered between 300 and

450 Ma. Based on the euhedral crystal shapes and oscillatory zoning patterns (Corfu et al. 2003) these zircons are interpreted as being derived from an immature, igneous source, proximal to the depositional area. This is consistent with data from Petersen et al. (2004) which indicates that Jurassic volcanic material was an important sediment source for supracrustal rocks in the Quesnel terrane.

The age distribution of the zircon populations in the Plant Creek sample are inconsistent with a dominantly cratonic provenance, rather, Paleozoic and Mesozoic sources of detrital zircons in the Plant Creek quartzite are more likely to be arc dominated terranes to the west. Possibilities include the Cache Creek and Quesnel terranes, including the Nicola and Rossland groups which contain Triassic to Jurassic volcanic rocks (Erdmer et al. 2002; Petersen et al. 2004, and references therein). There is only a minimal contribution from Proterozoic rocks. This is consistent with data from Middle to Late Jurassic sedimentary rocks in the Bowser Basin where western and south-western sources from the Cache Creek and Quesnel terranes contributed dominantly Triassic to Jurassic zircons into the basin and only minor Proterozoic zircons (Evenchick et al. 2007). It is also consistent with geochemical data presented by Petersen et al. (2004) suggesting a minor continental influence on the chemistry and Nd model ages of supracrustal sedimentary rocks in the southeastern Canadian Cordillera, either as a result of sediments directly derived from Proterozoic age continental sources, or the

incorporation of recycled sediments from younger strata such as the Slide Mountain or Kootenay terranes.

These new data confirm previous interpretations regarding the Late Proterozoic to Early Cambrian protolith age of the Mount Symonds rocks (Pell and Simony 1987; Höy and Godwin 1988; Carr 1991). This study is the first to report Late Jurassic or younger protolith ages for the Plant Creek rocks. Previous correlations of the rocks around Plant Creek with Mississippian (Carr 1991), Devonian or Proterozoic rocks need to be reevaluated. Figure 4.9 and 4.10 illustrate the proposed distribution of protolith ages in the Thor-Odin – Pinnacles area (Figure 4.9) and shows where previously unrecognized rocks of the Quesnellia terrane may be present in the footwall of the Columbia River fault (Figure 4.10).

The juxtaposition of a Late Jurassic or younger quartzite, situated in a Cretaceous – Paleocene K-feldspar–sillimanite–melt-bearing assemblage, with structurally overlying Jurassic rocks of greenschist facies supports the interpretation that there is a fault contact between the two units, in this case the Columbia River fault zone, and that unconformable deposition of the now greenschist facies rocks is not a viable model. Data regarding the fault displacement of 10 – 30 km (Read and Brown 1981; Carr 1990) and the detrital zircon data presented here, indicate that the age, provenance and probable correlations for this quartzite are all inconsistent with the Thompson et al.

(2004, 2006) hypothesis of unconformable deposition. Rather, they support interpretations of a transposed terrane boundary within the metamorphic package.

This study concludes that the Mesozoic rocks of the Quesnellia terrane in the Thor-Odin Pinnacles area that preserve Jurassic deformation and metamorphic histories are separated from high grade rocks with Late Cretaceous to Eocene deformation and metamorphic histories (sections 2.3 and 2.4) by faults rather than unconformities. This relationship is documented elsewhere in the southeastern Canadian Cordillera. Acton et al. (2002) described the nature of the basement-Quesnellia contact in the Kettle – Grand Forks area and determined that the Jurassic age Quesnellia strata were juxtaposed over Laurentian basement rocks along thrust faults and not as a result of unconformable deposition onto exposed basement. Through mapping and structural analysis Brown (2010) determined that the apparent continuity of Jurassic age, greenschist facies strata across the Okanagan Valley – Eagle River fault zone is the result of an uneven, corrugated fault surface, and not unconformable deposition of Jurassic age rocks as proposed by Glombick (2005 and Thompson et al. (2004, 2006).

By the Late Jurassic, orogenic activity had initiated major sedimentation in the foreland basin. The sedimentary record in the foreland basin records three major pulses of sedimentation (Ross et al. 2005): i) the Late Jurassic Kootenay Group (152 – 144 Ma), ii) the Lower Cretaceous Blairmore Group (115 – 103 Ma), and iii) the Late Cretaceous to

Tertiary sedimentary rocks of the Alberta Group as young as the Porcupine Hills Formation (98 – 58 Ma; Ross et al. 2005 and references therein). The youngest sediments of the Porcupine Hills Formation were deposited at the same time as the onset of regional extension in the internal zone of the orogen (Parrish et al. 1988). Like the Plant Creek sample, the Kootenay Group has detrital zircon signatures and provenance indicators that indicate sediment was derived from uplifted miogeoclinal strata (Ross et al. 2005). In the foreland basin, the Lower Cretaceous Blairmore Group of the same age also contains detrital zircons (and other provenance indicators) that show sediments were derived from igneous rocks in the Quesnel terrane (particularly prominent in the Beaver Mines Formation) as well as miogeoclinal strata (Ross et al. 2005).

The data showing the Jurassic protolith age of the Plant Creek sample discussed here is also consistent with work by Eisbacher (1985) which proposed that the southeastern Canadian Cordillera preserves evidence for syn-orogenic peri-collisional strike-slip basins that developed during the compressional phases of the orogen. On the hinterland side of the orogen, some Quesnel-derived detrital material was deposited in basins proximal to the igneous sources in the Late Jurassic, and metamorphosed in the Early Cretaceous (Lemieux 2006) at amphibolite facies conditions (Figure 2.14). Therefore detrital material from Quesnellia can be found in the hanging walls of the Columbia River and Okanagan Valley – Eagle River fault systems (and other normal faults in the

southeastern Canadian Cordillera as shown on Figure 1.1), in the footwall of the Columbia River fault zone in the Thor-Odin – Pinnacles area (Figure 4.10) and in the Alberta foreland basin.

4.6 Conclusions and implications

The quartzite at Mount Symonds is younger than ~500 Ma, based on the ages of the youngest zircons. This quartzite has age populations between 500 – 650 Ma and 1600 – 1900 Ma, and minor populations between 1100 – 1200 Ma and 2200 – 2800 Ma. The age of the youngest detrital zircon and distributions and ages of the Archean and Proterozoic zircons in the lower Mount Symonds quartzite are consistent with the correlation of the lower Mount Symonds quartzite with the Hamill Group or younger rocks that have a North American provenance. The minimum depositional age of ~500 Ma for the Mount Symonds quartzite rules out any interpretations where it is considered to be the same age as the quartzites from the Thor-Odin dome basement or Cariboo Alp discussed in Chapter 3 of this study.

The quartzite at Plant Creek has major detrital zircon populations between 150 – 200 Ma and 300 – 450 Ma, and minor populations between 1700 – 1900 Ma. Paleozoic and Mesozoic sources of detrital zircons in the Plant Creek quartzite are more likely to be juvenile arc dominated terranes such as the Cache Creek and Quesnel terranes,

including the Nicola and Rossland groups which contain Triassic to Jurassic volcanic rocks (Petersen et al. 2004 and references therein). The outboard Quesnellia terrane was providing sediments into a basin during the Late Jurassic; this basin was incorporated into the Cordilleran orogen and metamorphosed by the early Cretaceous (Lemieux 2006) in a generally compressive tectonic setting and parts of it are now exposed in the footwall of the Columbia River fault zone in the Thor-Odin – Pinnacles area (Figure 4.10).

The Jurassic or younger protolith age of the Plant Creek sample supports the interpretation that the greenschist facies Jurassic and Triassic rocks of the Rossland and Slocan groups in the Plant Creek area are separated from the Jurassic to Cretaceous – Paleocene K-feldspar-sillimanite and K-feldspar-muscovite-bearing rocks beneath them by a fault, not an unconformity. This supports the interpretation that the outliers of greenschist facies rocks are klippen of the Columbia River fault, and that unconformable deposition of the protoliths of greenschist facies rocks, as proposed by Thompson et al. (2004, 2006), is not a viable model.

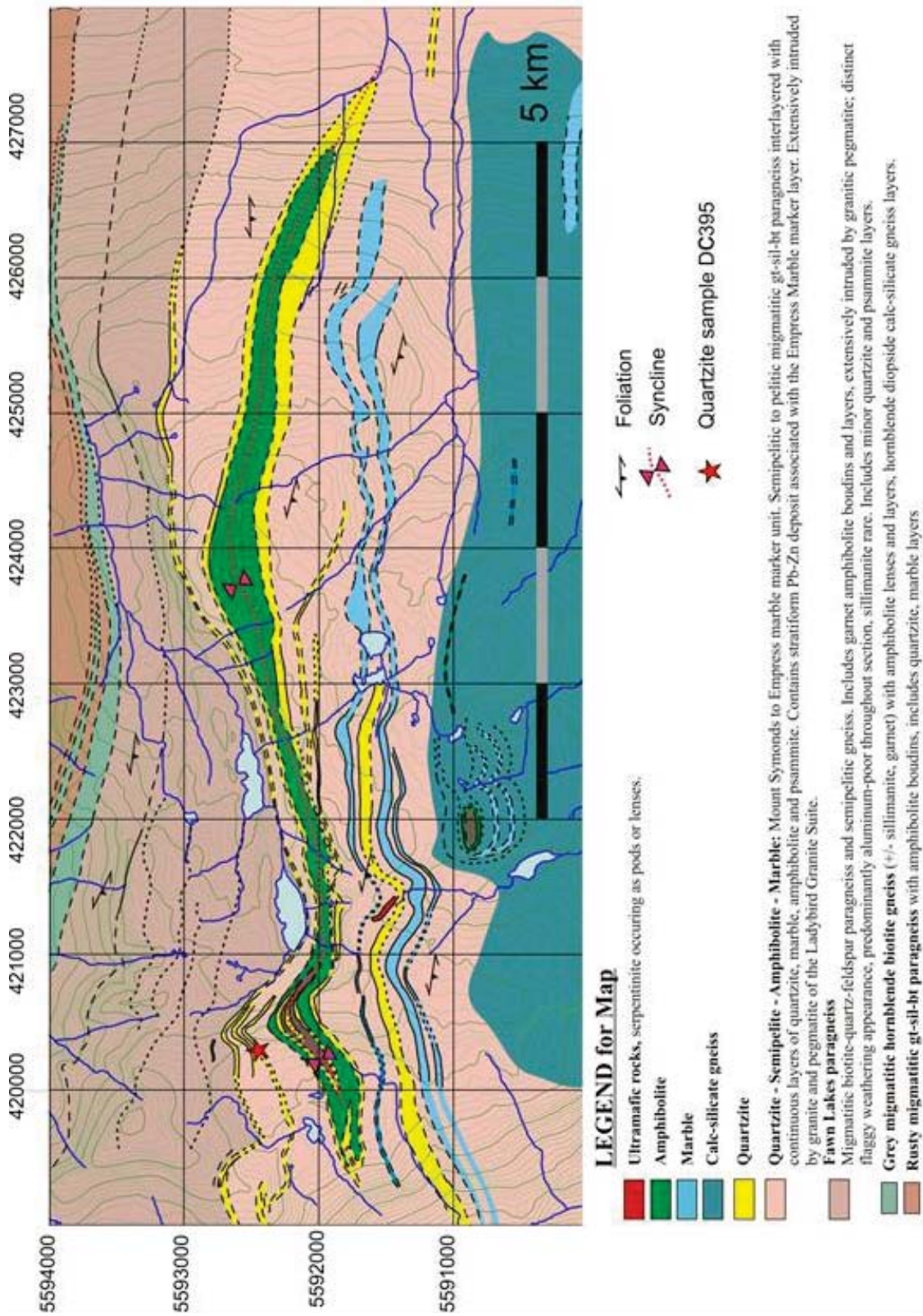
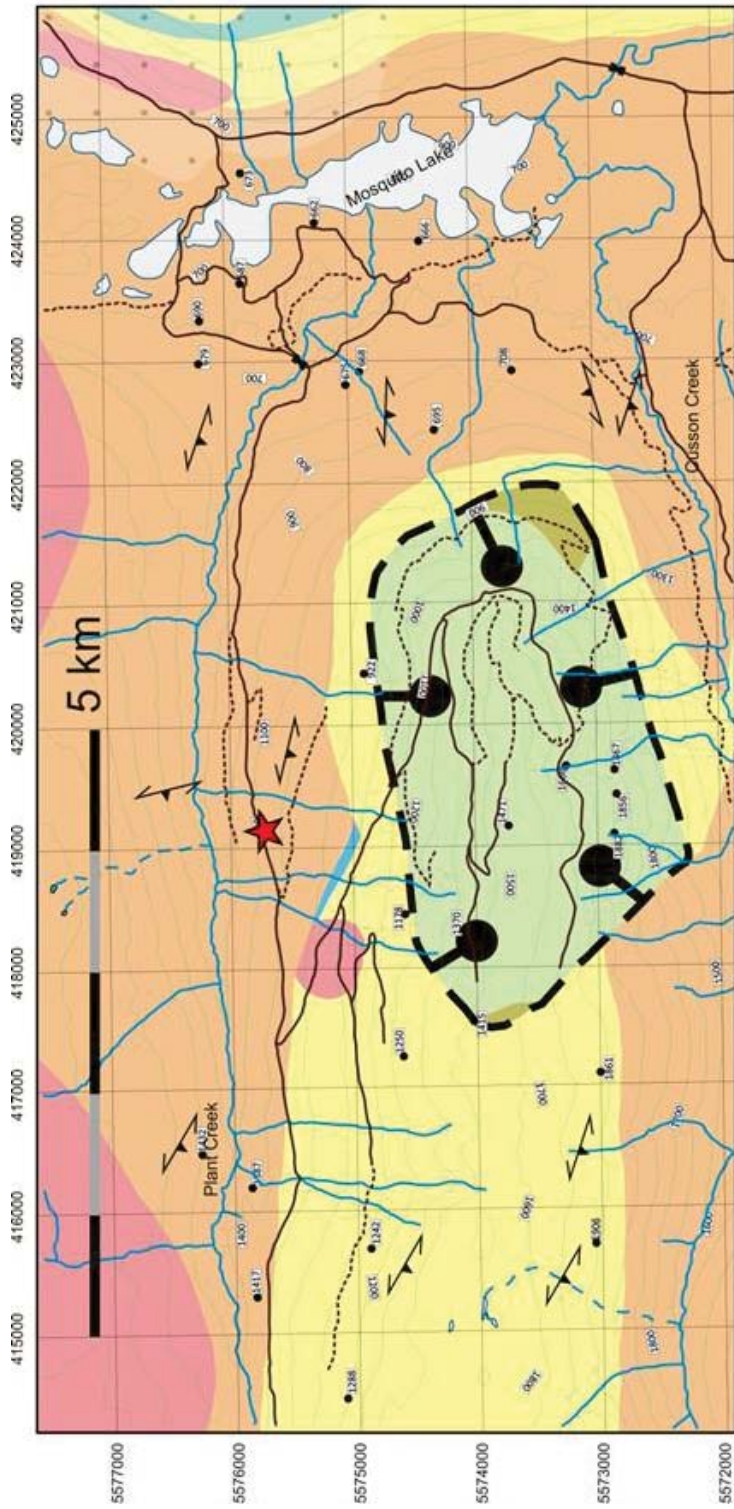


Figure 4.1 Map of the Mount Symonds area. Location of sample DC395 quartzite in a heterogeneous package of metasedimentary and metavolcanic rocks, metamorphosed in the Late Cretaceous to Paleocene at amphibolite facies conditions. Modified from Reesor and Moore (1971), Carr (1990), Kruse et al. (2004) and Thompson et al. (2004).



1 m

Figure 4.2 Steeply south to southwest dipping quartzite layers of sample DC395 in the Mount Symonds area. The quartzite has dark mineral bands (visible in outcrop), and muscovite on parting surfaces.



LEGEND

- Rosland Group** metavolcanic rocks including breccia, tuff, basalt, augite porphyry. (Lower Jurassic)
 - Slocan Group** siliciclastic rocks including phyllite, argillite, quartzite and minor volcaniclastic tuffs. (Upper Triassic)
 - Ladybird Granite Suite** – Late Paleocene to Eocene ca. 62 – 55 Ma (Carr 1992)
 - Arrow Lake garnet sillimanite muscovite biotite schist**
Muscovite-biotite schist +/- garnet, sillimanite, local staurolite, kyanite. Includes micaceous quartzite, minor psammitic gneiss, marble and amphibolite layers. Local carbonaceous schist and staurolite schist.
 - Staurolite schist**
 - Calcareous quartzite**
 - Undivided semipelite - Pelite - Amphibolite**: South of South Fossil Pluton, includes Saddle Mountain, Viddler Ridge, continuing to Pinnacles. Psammitic, semi-pelitic, pelitic schists and gneisses; contains sillimanite and garnet; contains lenses and layers of calc-silicate schist or gneiss, marble, amphibolite or quartzite. Extensively intruded by granite and pegmatite of the Ladybird Granite Suite.
- Rocks in the hanging wall of the Columbia River Fault** ★ Plant Creek quartzite (DC490)
- Rocks in the footwall of the Columbia River Fault** ↔ Foliation

Figure 4.3 Map of the Plant Creek area. Location of sample DC490 in a package of heterogeneous rocks metamorphosed at amphibolite facies conditions in the Late Cretaceous. In the klippe of the Columbia River fault the rocks were metamorphosed at greenschist facies conditions in the Jurassic. Modified from Reesor and Moore (1971), Carr (1990), Kruse et al. (2004) and Thompson et al. (2004).



1 m

Figure 4.4 Moderately southwest dipping quartzite at of the Plant Creek area. This quartzite has 5 – 10 cm thick beds but no distinct heavy mineral banding, containing 30% detrital feldspar grains and minor biotite.

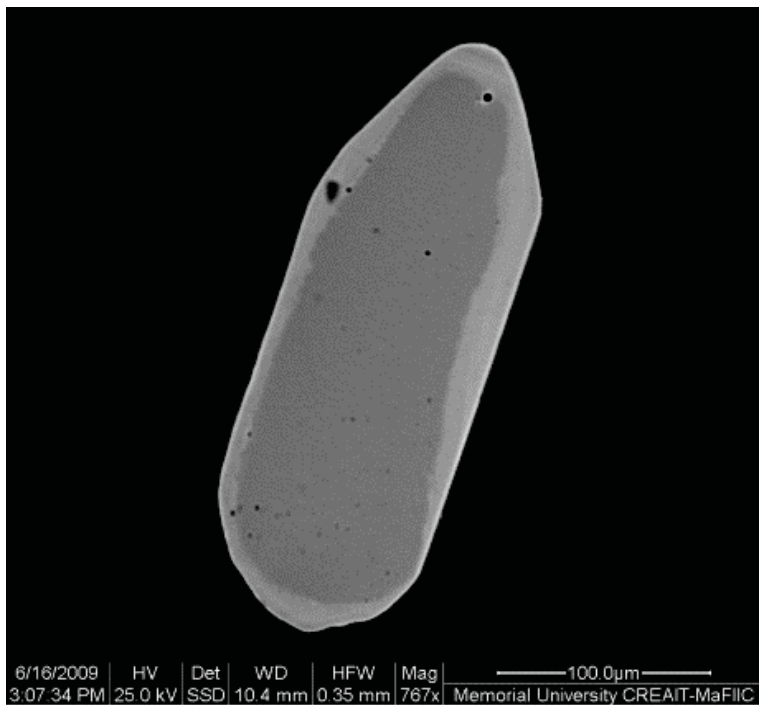
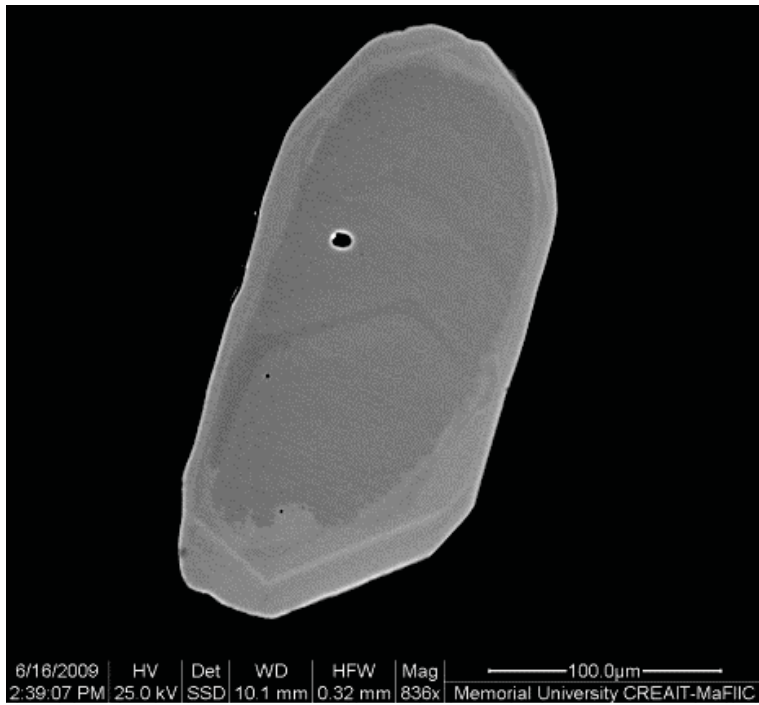
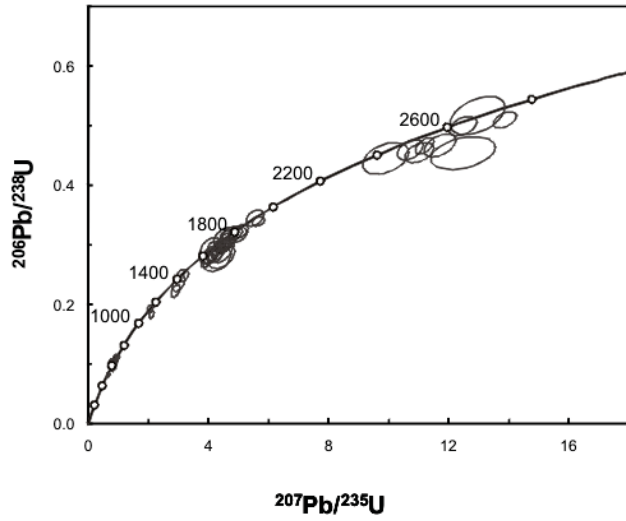


Figure 4.5 Zircon morphology from the Mount Symonds quartzite. These zircons have rounded cores with oscillatory zoning and metamorphic overgrowths.

DC395 Grains Concordia Ages

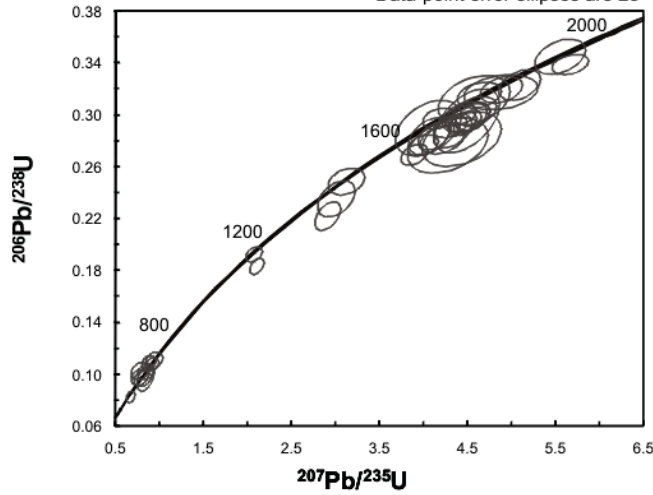
Data-point error ellipses are 2σ



(a)

DC395 Grains < 1.8 Ga

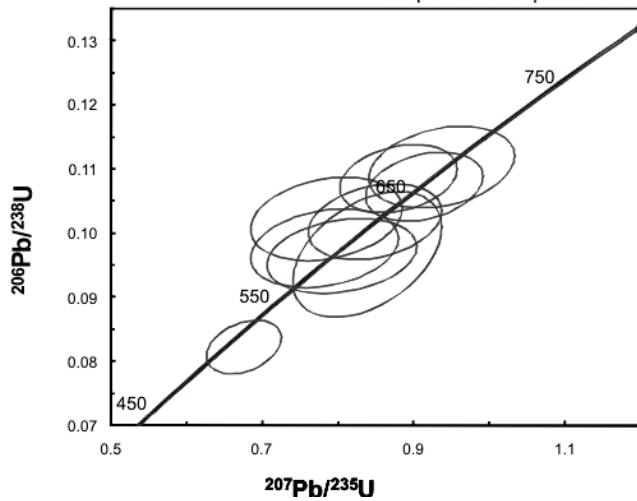
Data-point error ellipses are 2σ



(b)

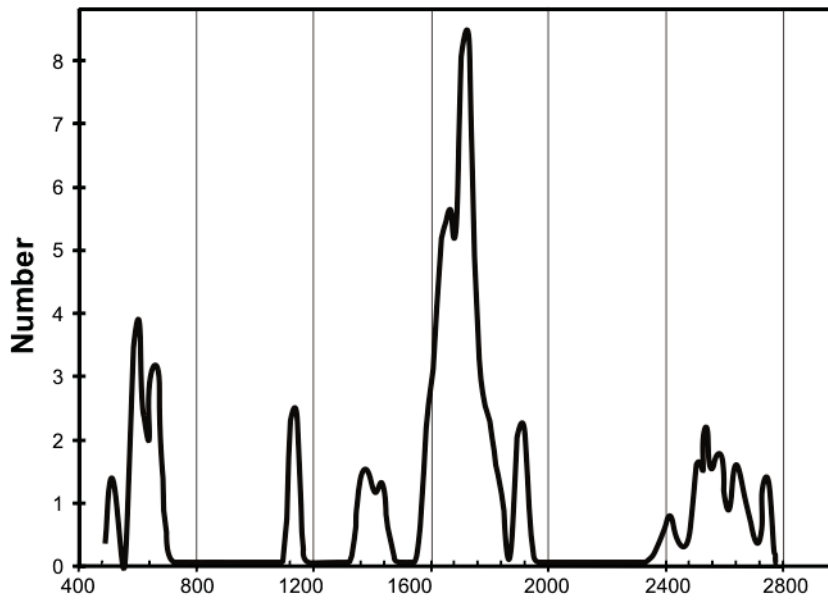
DC395 Grains < 650 Ma

Data-point error ellipses are 2σ



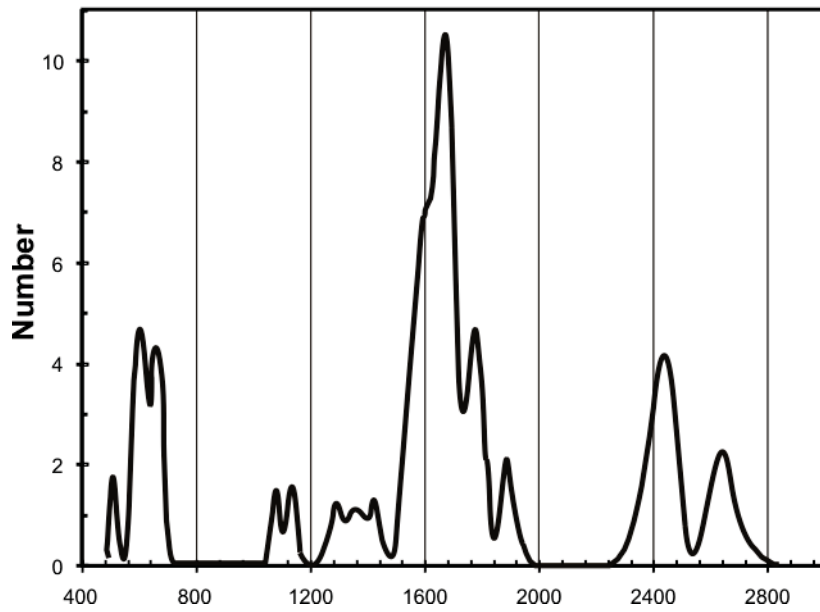
(c)

DC395 Concordia Ages (within 10% of concordance)



(d)

DC395 $^{206}\text{Pb}/^{238}\text{U}$ ages within 10% of concordance



(e)

Figure 4.6 Detrital zircon U-Pb data for sample DC395, Mount Symonds.

(a) Concordia plot showing all grains more than 90% concordant.

(b) Concordia plot for all the grains younger than 1800 Ma.

(c) Concordia plot for all the grains younger than 650 Ma.

(d) Probability distributions using Concordia ages.

(e) Probability distributions using $^{206}\text{Pb}/^{238}\text{U}$ ages within 10 % of concordance.

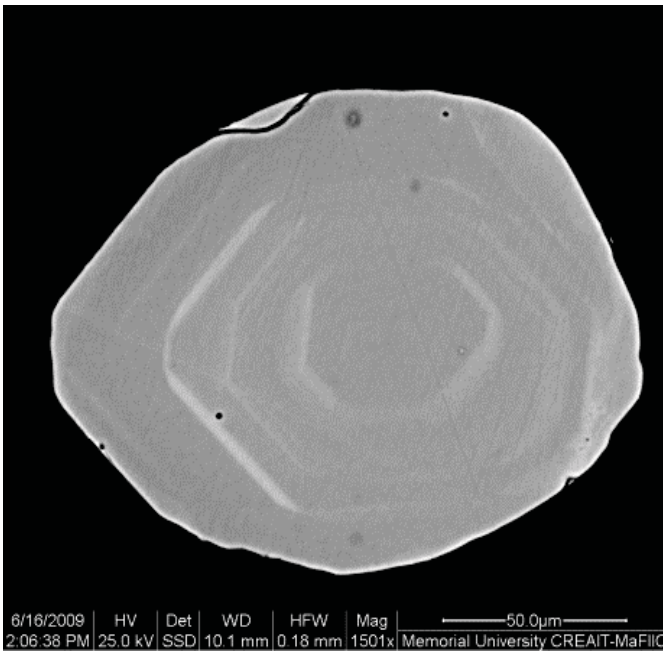
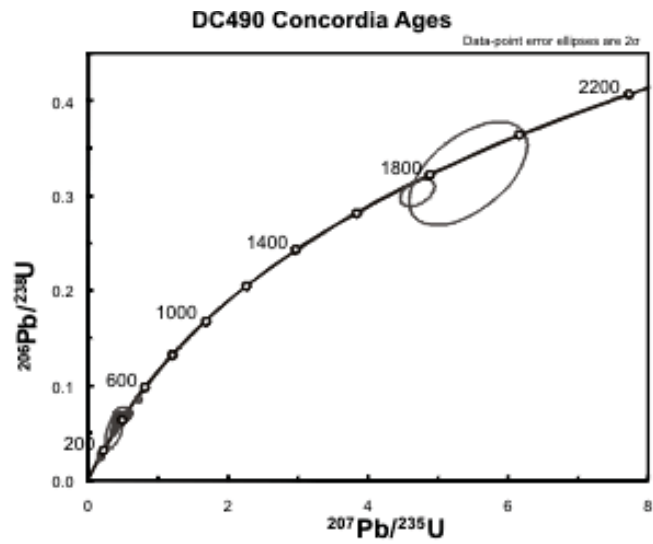
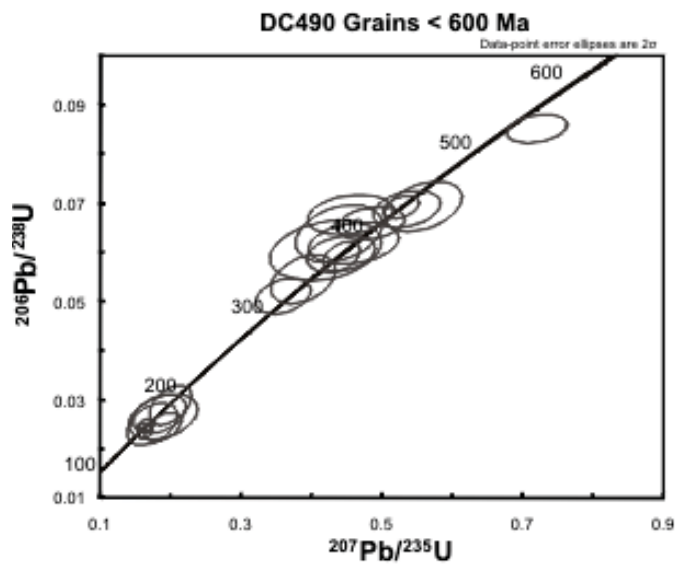


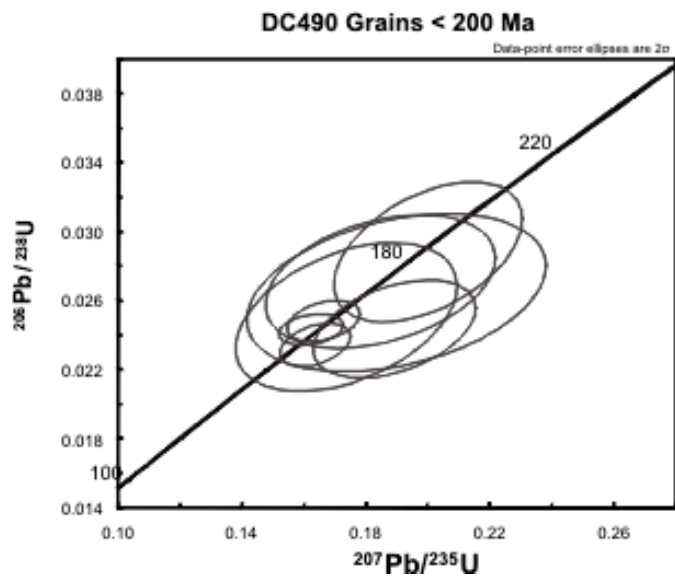
Figure 4.7 Typical zircons from the Plant Creek quartzite unit. The zircons are euhedral, small (<50µm), show oscillatory zoning throughout, and have no metamorphic overgrowths. These are interpreted as being from an immature source, and not transported far from their source.



(a)

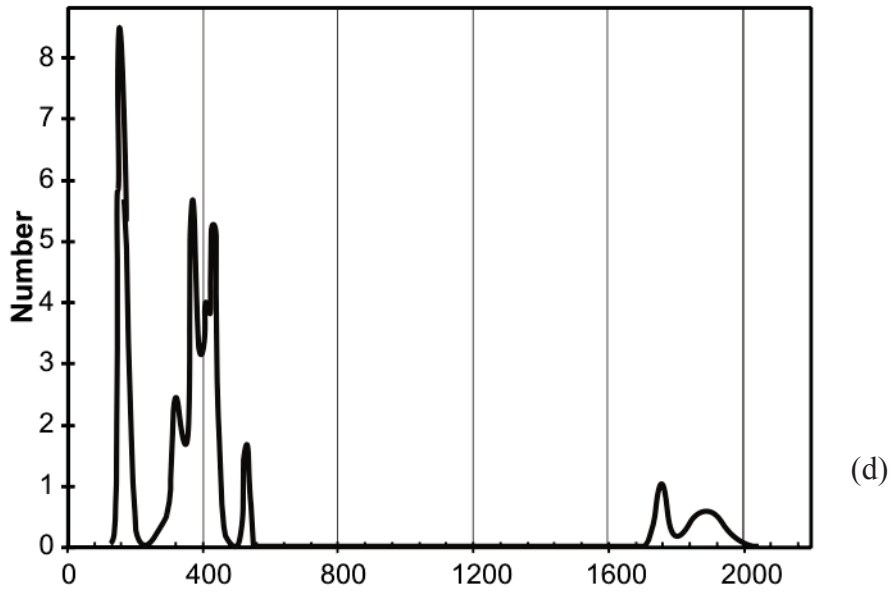


(b)



(c)

DC490 Concordia Ages (within 10% of concordance)



DC490 $^{206}\text{Pb}/^{238}\text{U}$ ages, all data

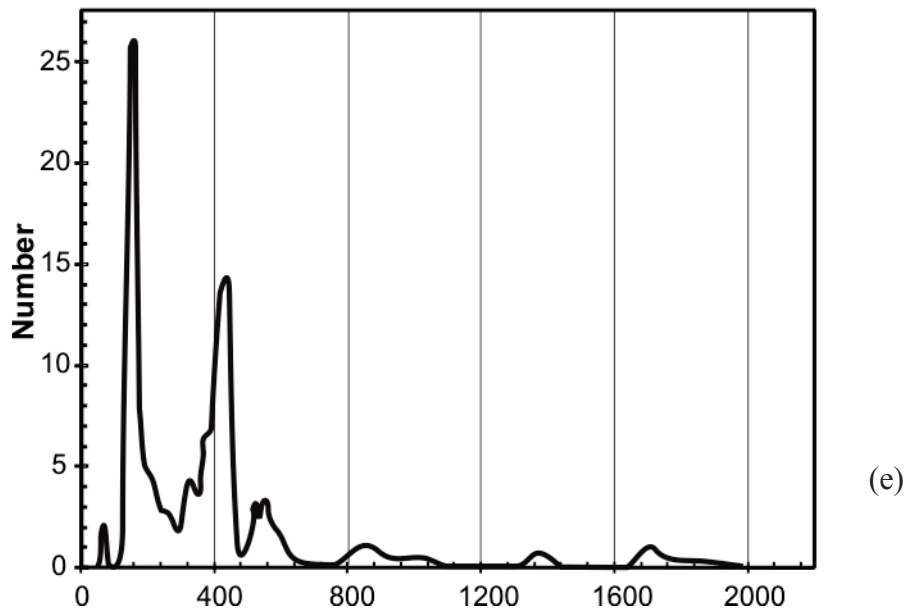


Figure 4.8 Detrital zircon U-Pb data for sample DC490, Plant Creek.

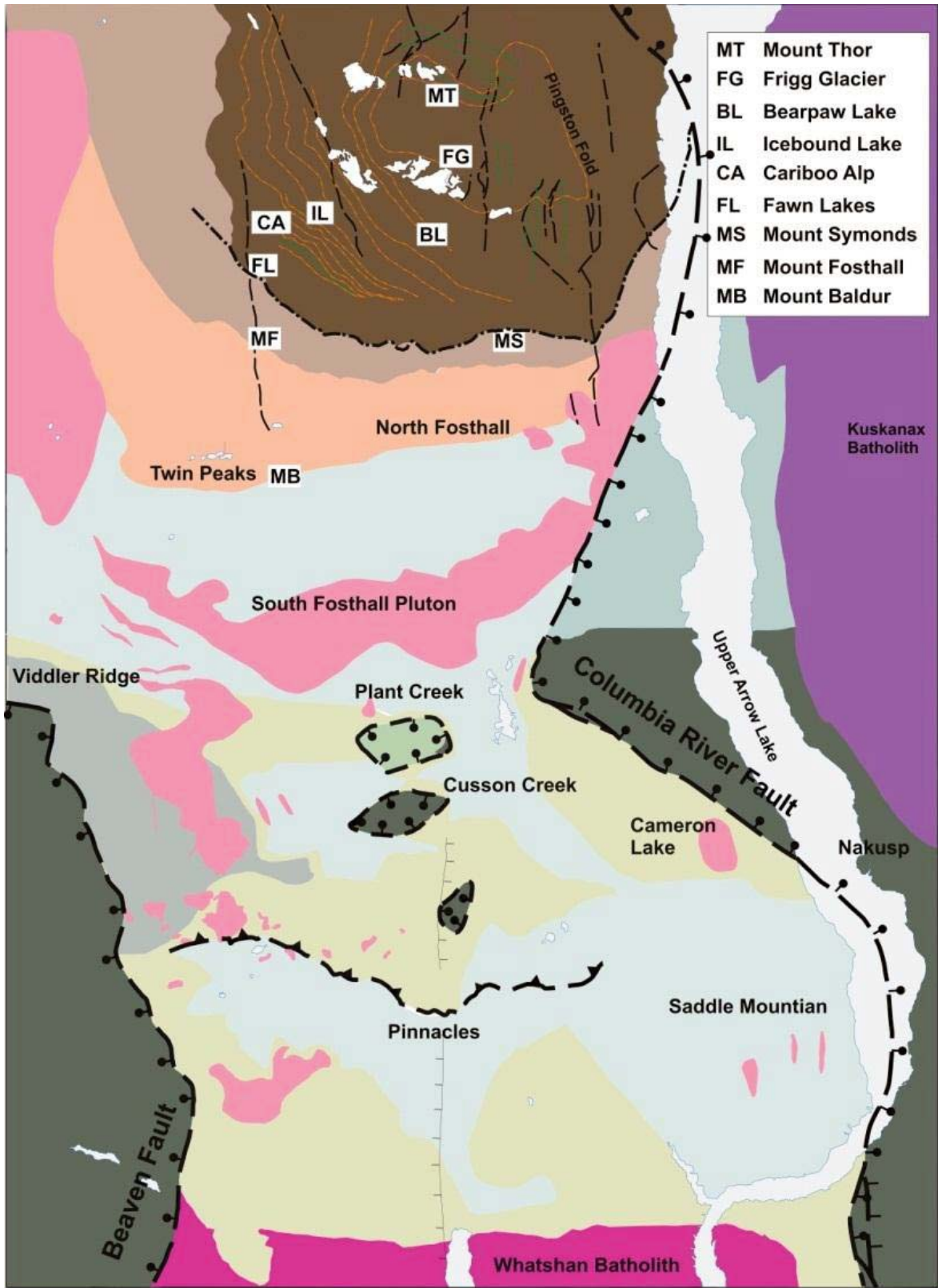
(a) Concordia plot showing all grains more than 90% concordant.

(b) Concordia plot for all the grains younger than 600 Ma.

(c) Concordia plot for all the grains younger than 200 Ma.

(d) Probability distributions using Concordia ages.

(e) Probability distributions using $^{206}\text{Pb}/^{238}\text{U}$ ages from all data.



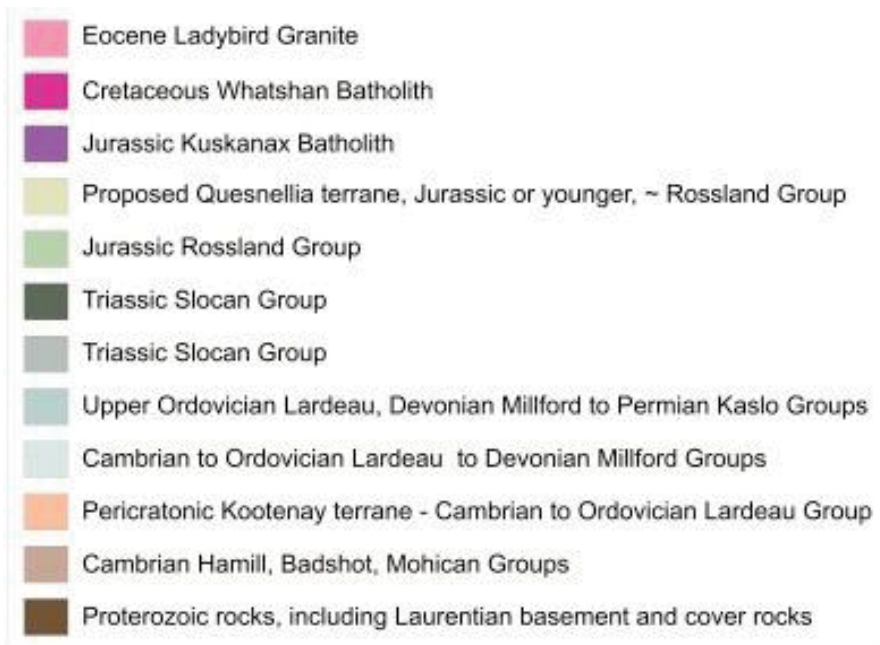


Figure 4.9 Interpreted protoliths for the rocks in the Thor-Odin – Pinnacles area, in the hanging walls and footwalls of the normal fault systems. Data from this study have been added to previous correlations of protoliths compiled from Little (1960), Fyles and Eastwood (1962), Fyles (1964), Reesor and Moore (1971), Read (1973), Reesor (1973), Zwanzig (1973), Read and Wheeler (1976), (Höy 1977), Klepacki (1985), Gehrels and Smith (1987), Raeside and Simony (1983), Pell and Simony (1987), Johnson (1994), Scammell (1990), Fritz (1991), Carr (1991a), Kruse et al. (2004) and Thompson et al. (2004).

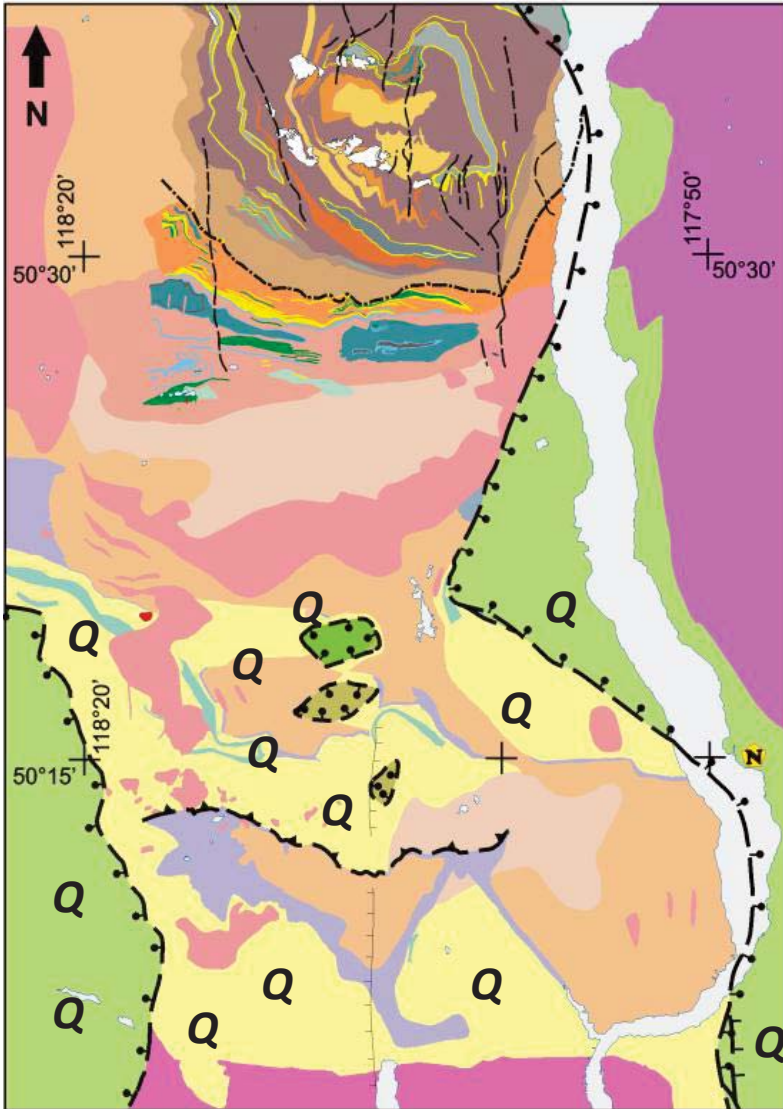


Figure 4.10 New interpretation of possible Middle Jurassic Quesnellia rocks as protoliths for the metamorphic rocks in the footwall of the Columbia River fault. In this interpretation the Middle Jurassic Quesnellia terrane and accreted island arc rocks are not restricted to the hanging walls of the Eocene normal faults. The accreted island arc terranes were incorporated into the Cordilleran Orogen and metamorphosed in the Early to Late Cretaceous.

5 Chapter: $^{40}\text{Ar}/^{39}\text{Ar}$ thermochronology studies of the Thor-Odin – Pinnacles area, southeastern British Columbia: tests of structural models.

5.1 Introduction

The focus of this chapter is a $^{40}\text{Ar}/^{39}\text{Ar}$ thermochronology study of metamorphic rocks that were penetratively deformed in the mid-crust during the Late Cretaceous to Eocene, and exhumed, during progressive Cretaceous to Eocene orogenesis in the core of the southeastern Canadian Cordillera (Figures 1.1, 1.2, 1.3, and 2.56). The results of this study have implications for thermochronology studies in complex metamorphic rocks, as well as for reinterpretation of the Late Cretaceous to Eocene structural setting of the Thor-Odin dome and surrounding area. Refer to Chapter 2 for a complete discussion of the geology of the study area and interpretations regarding the timing of deformation and metamorphism.

This thermochronology study encompasses a 20 x 50 km area that includes the interior of the Thor-Odin dome and the structurally overlying rocks to the south of the dome extending to Cusson Creek (Figure 1.2). These rocks comprise a 12 km-thick, tilted structural section as illustrated in Figure 1.3. Note that that the Thor-Odin to Cusson Creek section is the lower 12 km structural thickness of the complete Thor-Odin to Whatshan section which comprises 17 km of rocks. We present cooling histories obtained by step-heating $^{40}\text{Ar}/^{39}\text{Ar}$ thermochronology of hornblende, biotite and

muscovite from all structural levels within the study area. In combination with published U-Pb geochronology results on metamorphic and deformation events, these thermochronology data provide information about the cooling history over the temperature range between ~600 °C and 280 °C. Thermochronology data have not been previously available from flanks of the dome and the area to the south of the dome, making it difficult to link the cooling history within the dome with that of the overlying structural levels.

These new $^{40}\text{Ar}/^{39}\text{Ar}$ cooling ages from the interior of the Thor-Odin dome and the overlying structural panels, together with geological constraints, are used to re-evaluate the viability of structural and tectonic models proposed to explain the significance of penetratively deformed high grade rocks with Paleocene and Eocene cooling histories. This study addresses the nature of the so-called upper boundary of basement rocks in the Thor-Odin dome, at Cariboo Alp on the southwestern flank of the dome, which has been interpreted in multiple ways, including: as an intensely folded and contorted zone (Reesor and Moore 1971; Duncan 1984), ductile duplex within a ductile thrust-sense shear zone termed the Monashee décollement (McNicoll and Brown 1995), deformed zone within a wider channel (Williams and Jiang 2005) or ductile extensional fault (Kruse and Williams 2007). It also addresses the timing and evolution of west- or east-dipping Eocene ductile-brittle extensional faults that bound the tectonothermal culmination on

the East and West sides, and their role in the tectonic denudation of the metamorphic rocks.

This study addresses: (i) the high-temperature cooling histories of the mid-crustal rocks in the southern Thor-Odin dome and the structurally overlying rocks located in the footwall of the Columbia River fault; (ii) whether there are different thermal domains with sharp boundaries between them that could indicate the presence of syn- or post-tectonic faults, specifically at Cariboo Alp; (iii) the cooling history of the suprastructure-infrastructure zones described in Chapter 2 (Figure 2.56) in relation to the timing of penetrative deformation; and (iv) implications for the timing of activity on the Columbia River fault system.

5.2 Tectonic and geological setting

This study is concerned with rocks that were in the mid-crust during Cretaceous to Eocene and are now exposed in the western internal zone of the orogen (Figure 1.1, Figure 2.2). In particular, this study addresses the time period between c. 62 and 50 Ma coinciding with the final stages of crustal shortening in a transpressional regime and the transition to transtension manifested by the end of thrust faulting in the foreland and the onset of extensional faulting and exhumation in the internal zone. Contractional deformation in the Cordilleran orogen continued through the Paleocene-Eocene when the southern Canadian Cordillera experienced a period of strike slip faulting (Struik

1983) due to changes in the relative motion of the Kula plate subducting under Laurentia (Andronicos et al. 2003; Lonsdale 1988). This change from transtension to transpression resulted in Eocene crustal thinning, localized in the western internal zone of southeastern British Columbia and northern Washington and Idaho (Engebretson et al. 1985; Parrish et al. 1988). This extension was accommodated by mainly north-south striking normal faults (Parrish et al. 1988) and synchronous east-west strike-slip faults in transfer zones that root into extensional faults (Johnson 2006), resulting in the exhumation of high grade rocks in the core zone of the orogen (Armstrong 1982; Okulitch 1984; Parrish et al. 1988; Bardoux and Mareschal 1994; Lorencak et al. 2001; Vanderhaeghe et al. 2003; Kruse and Williams 2005; Carr and Simony 2006).

It has been suggested that the Paleocene upper crust, (up to 15 km depth), the area that is now the internal zone, had a geothermal gradient as steep as 60°C/km, either related to high heat-flow or intrusion of anatectic granites (Vanderhaeghe 1999). Thermal modeling by Callahan (2008) and Crider (2011) suggest a similar gradient of 50°C/km at 60 Ma, about double the average crustal geotherm of 25°C/km, suggesting that the overlapping processes of orogenic scale anatexis, plutonism and extension are all related to the crustal heat budget in the Cordillera in the Late Cretaceous to Eocene.

Thermochronology studies in the high grade rocks in and around the southern Cordillera have reported K-Ar and $^{40}\text{Ar}/^{39}\text{Ar}$ mica cooling ages ranging from Jurassic to Cretaceous,

and Paleocene-Eocene ages between c. 53 – 48 Ma (Armstrong 1981; Scammell 1993; Bardoux 1993; Johnson 1994; Sanborn 1996; Spark 2001; Kuiper 2003; Vanderhaeghe et al. 2003; Mulch and Cosca 2004; Ghent and Villeneuve 2006; Brown et al. 2012; Cubley et al. 2012). Generally the Late Cretaceous and Paleocene-Eocene ages are confined to the structural culminations and associated tracts of high grade rocks in the western internal zone of the core (Figure 1.1), and the Jurassic to Early Cretaceous ages are confined to the suprastructure or hanging walls of the extensional fault systems, discussed earlier Chapter 2. However, all the above studies also reported significant problems in the interpretation of $^{40}\text{Ar}/^{39}\text{Ar}$ data from hornblende and mica, particularly in the highest grade rocks within the Thor-Odin and Frenchman Cap domes because the “cooling dates” obtained by some studies (Scammell 1993; Spark 2001; Kuiper 2003) were older than the known timing of anatexis in the areas studied.

As is the case in many high grade terranes in orogenic belts worldwide, particularly in migmatitic rocks, the $^{40}\text{Ar}/^{39}\text{Ar}$ thermochronology data available for the Thor-Odin dome and surrounding area are in some cases complicated by disturbed argon systematics and equivocal cooling dates. In the Thor-Odin dome, Spark (2001), Kuiper (2003), and Vanderhaeghe et al. (2003) have reported cases where Early Cretaceous to Paleocene $^{40}\text{Ar}/^{39}\text{Ar}$ cooling dates (particularly in hornblende) are older than Paleocene-Eocene U-Pb zircon crystallization dates in leucosomes. These leucosome are interpreted to have crystallized at higher temperatures than that of the closure temperature of argon in

hornblende, within penetratively deformed rocks from the same areas (Spark 2001; Kuiper 2003; Vanderhaeghe et al. 2003; Hinchey et al. 2006). Similar problems have been documented in the high grade migmatitic rocks immediately north of the Thor-Odin dome in the Frenchman Cap dome (Scammell 1993; Johnson 1994; Sanborn 1996) and in other high grade terranes worldwide, including (but not limited to) Norway (Boundy et al. 1996, 1997), the Grenville orogen (Smith et al. 1994), and the Himalayas (Reddy et al. 1997). Some of the samples from this study show that excess argon is a factor in the Thor-Odin area, particularly when hornblende cooling dates are considered. The approaches taken to minimize these problems are discussed in section 5.3 (Methods) and 5.4 (Results).

5.2.1 Study locations and map area

The study area in which thermochronology was carried out extends from the core of the Thor-Odin dome in the north, to south of the Cusson Creek area. It includes only rocks in the footwall of the Columbia River fault. All study areas are fully described in Chapter 2, and illustrated in Figures 1.2 to 1.4.

5.2.2 Diachronous metamorphism, deformation and suprastructure-infrastructure transitions.

The following presents a brief summary of the main conclusions of Chapter 2 in order to illustrate the thermal state of the rocks in the study area before the onset of cooling. The rock in the study area experienced protracted, but not necessarily continuous, deformation and metamorphism throughout the Cretaceous to Paleocene, which may have overprinted Early Cretaceous or older events (Carr 1990, 1991, 1992; Hinchey et al. 2006; Lemieux 2006; Glombick 2005). Being able to constrain the metamorphic history provides the background necessary to make interpretations regarding the cooling history of the area.

Chapter 2 (sections 2.4 and 2.6; Figures 2.14 and 2.56) illustrates the times at which belts of rocks were being penetratively deformed in the infrastructure, and when they were deactivated, cooled, and translated in the suprastructure. In the area between the Thor-Odin dome and the Whatshan batholith there are four belts of rocks which can be discussed as tectonothermal domains. Each of these domains experienced regional metamorphism and deformation at different times (Figure 2.56). In general, the timing of tectonothermal events young downwards from the Whatshan – Pinnacles area into the structurally deeper Thor-Odin dome and the metamorphic grade generally increases downwards throughout the structural section into the dome. The end of penetrative ductile deformation marks the transition of specific structural levels from infrastructure to suprastructure. In summary, the Whatshan Pinnacles area made the transition from infrastructure to suprastructure before c. 75 Ma, the Plant Creek – South Fosthall area

became suprastructure by 64 – 62 Ma, the North Fosthall – Mount Symonds – Cariboo Alp area became suprastructure by c. 58 Ma, and the Thor-Odin dome remained in the infrastructure until c. 52 Ma. For more details, refer to section 2.4 – 2.6. Within this framework of infrastructure-suprastructure transitions, the cooling history presented in this chapter provides the data

5.2.3 Recent work relating to the cooling history of the Thor-Odin – Pinnacles area

Vanderhaeghe et al. (1999, 2003) presented hornblende, biotite and K-feldspar $^{40}\text{Ar}/^{39}\text{Ar}$ and K-Ar thermochronology data from the Thor-Odin dome and overlying/surrounding rocks. Some samples are interpreted by the authors as having been contaminated by excess argon (because of saddle shaped release spectra) as well as geologically unreasonable dates (i.e. too old relative data from robust geochronology studies). For example; the dates from hornblendes from amphibolite boudins from Mount Odin and Mount Thor that are 70.3 ± 1.1 and 118 ± 1.3 Ma respectively; and hornblende from an amphibolite boudin in Mount Symonds with an apparent age of 64.5 ± 0.9 Ma are all geologically inconsistent with the known timing of high grade metamorphism and anatexis in these rocks at c. 58 – 54 Ma (Vanderhaeghe et al. 1999; Hinchey et al. 2006). In cases where robust plateau dates were obtained, hornblende cooling dates from amphibolite boudins at a structural level comparable to Cariboo Alp, Mount Symonds and the North Fosthall/Twin Peaks areas range between c. 59 and 54 Ma. Biotite cooling ages in that study range between c. 48 and 52 Ma (Vanderhaeghe et al. 2003).

Muscovite ages of c. 49 and 47.5 Ma, from the western and eastern detachments of the Shuswap complex, respectively (Vanderhaeghe et al. 2003), were interpreted as cooling ages. Mulch and Cosca (2004) documented ages for white micas within the Thor-Odin dome at Mount Hall (Figure 1.3) in a laser probe study of white micas in the immediate footwall of the Columbia River fault. Ages of c. 49 – 48 Ma were interpreted as crystallization ages for muscovites that grew below their closure temperature (Mulch and Cosca 2004), and used as a date for the end of ductile deformation and subsequent recrystallization in the Columbia River fault after ductile extension (Teyssier et al. 2005).

5.2.4 Excess argon

$^{40}\text{Ar}/^{39}\text{Ar}$ cooling ages that are older than independent geochronological constraints are usually attributed to the presence of excess radiogenic ^{40}Ar (McDougall and Harrison 1999; Kelley 2002). Excess argon has long been known as a complicating factor in thermochronology (Lanphere and Dalrymple 1976) and has been repeatedly documented in many different tectonic environments (Dallmeyer and Rivers 1983; Smith et al. 1994; McDougall and Harrison 1999; Kelley 2002). Excess argon is defined as radiogenic ^{40}Ar that is not generated from in-situ decay of ^{40}K in the matrix of the mineral or system in question (McDougall and Harrison 1999; Kelley 2002). This definition does not include “inherited” argon which refers to argon from an older argon component incorporated within the mineral or system in question. Inherited argon can

also be a sign of partially reset cooling ages where rocks are reheated during metamorphic episodes, fluid incursion, high heat flow or heat sources such as plutons, after their initial cooling through closure temperature (T_c). The main distinction is that inherited argon is generated within the system, while excess argon is from outside the system (Kelley 2002). However, it is not possible to distinguish between the two purely on the basis of step-heating release spectra since both can generate cooling dates that are too old, so the term “excess argon” is used here to include both cases.

Excess argon is commonly present in metamorphic rocks with old protoliths or long-lived tectonothermal histories (Cumbest et al. 1994; Arnaud and Kelley 1995; Scaillet 1996; Sherlock et al. 1999). Hydrous minerals (biotite, hornblende) are known for taking up excess argon easily (Cumbest et al. 1994; Kelley 2002). Excess argon can be located within melt inclusions, fluid inclusions (interpreted as excess radiogenic argon) or within solid inclusions of older minerals (inherited argon). The distribution of excess argon within migmatitic or high grade terranes depends on rock type (Baxter et al. 2002; Scaillet 1996), the presence of melt phases (Baxter 2003), the protolith ages (Arnaud and Kelley 1995) and the cooling rate (Kelley and Wartho 2000; Wartho and Kelley 2003).

Researchers who have studied the Thor-Odin dome area have used different approaches to deal with excess argon problems. In samples without plateau ages, or in

saddle-shaped spectra, Vanderhaeghe et al. (2003) interpreted the steps with the youngest ages in the release spectra as representing a possible maximum cooling age for the sample. Kuiper recalculated $^{40}\text{Ar}/^{39}\text{Ar}$ data from Spark (2001) using inverse isochron plots to get cooling ages from hornblende samples that did not have plateau ages. Based on the O and H isotopic composition of the minerals studied, "old" (c. 100 – 70 Ma, mid- to Late Cretaceous) argon dates were reinterpreted as geologically correct and it was proposed that the Paleocene-Eocene U-Pb zircon dates were not crystallization ages, but rather, represented alteration and Pb loss due to interaction with meteoric water (Kuiper 2003). It was also suggested that Paleocene $^{40}\text{Ar}/^{39}\text{Ar}$ dates are the result of argon loss due to interaction of meteoric water and hornblendes. Subsequent U-Pb zircon geochronology studies have discounted this hypothesis by showing that the zircons are in fact magmatic, and formed during anatexis at c. 56 Ma (Hinchey et al. 2006) during decompression melting of the Thor-Odin dome rocks (Norlander et al. 2002).

Both these approaches (interpreting the youngest step in a step heating spectrum as a maximum cooling age or using inverse isochron ages) may produce dates which are geologically reasonable, but there is no way to tell which results may be meaningful, so additional data are needed from an independent method in order to make meaningful geological interpretations. Therefore, in this study we exclude samples that do not produce very conservatively defined plateaus (section 5.3.4).

5.3 Methods

Samples for $^{40}\text{Ar}/^{39}\text{Ar}$ thermochronology were collected at all structural levels, from all lithologies present, in order to have as complete a transect across the study area as possible (Chapter 2). Sample locations and rock types are presented along with results in Tables 1 and 2. In total, 41 hornblende samples, 29 biotite samples and 11 muscovite samples were analyzed. Lithologies include amphibolites, various types of paragneiss, calc-silicate gneiss, psammite, and granitic pegmatites from all structural levels distributed throughout the study area.

5.3.1 Petrography and geochemistry studies

Thin sections of rocks were examined with a petrographic microscope to determine the metamorphic assemblages. Petrographic examination also determined whether the minerals (hornblende, biotite and muscovite) were free of obvious fractures, inclusions, overgrowths, or chloritization indicating retrograde metamorphism. Samples with evidence for multiple generations of growth for one mineral were not included to eliminate the possibility of mixtures of ages from different mineral grains in the same sample.

Representative samples were analyzed, using the Camebax MBX Electron Microprobe at Carleton University to determine K and Ca content of the minerals before selection for

further analysis. The chemical composition of individual amphiboles does not affect the retention of excess argon to any great degree (Cosca and O'Nions 1994; Leake et al. 1988) so microprobe examination of amphibole grains was limited to determining whether they were free of internal alteration, obvious inclusions, and chloritization or overgrowths not visible under binocular microscope and ensuring that they contained at least 0.5% K_2O and contain enough radiogenic argon to be successfully analyzed.

5.3.2 Sample picking and preparation

Samples were crushed using a jaw crusher and sieved to obtain grain sizes close to the predominant grain size in the original sample. Samples were washed in distilled water and ethanol and sieved into size fractions of $<100\mu m$, $100 - 250 \mu m$ and $>250 \mu m$. Hornblende and biotite grains were separated using a Frantz magnetic separator at 0.25 Amp, 10° forward slope and 10° side slope. Grains were picked under ethanol using a binocular microscope. Grains were selected to be representative of the predominant grain size in the rock, determined from petrography, and free of visible cracks, inclusions, overgrowths or obvious alteration. In samples where multiple grain sizes were present, several mineral populations of different grain sizes were picked. For pegmatitic samples, biotite or muscovite grains were picked directly out of the rock. Depending on the grain size of each sample, between 10 and 50 grains were selected for analysis.

5.3.3 Irradiation and analysis

Grains that were selected for analysis were washed in ethanol in an ultrasonic bath for 5 minutes and dried under a heat lamp before being packed in Al-foil folded into 1 cm diameter disks. The disks were packed into an aluminium container (11.5 cm long, 2 cm diameter) for irradiation at the McMaster Nuclear Reactor in Hamilton, Ontario. The sample containers were irradiated with fast neutrons in position 5C of the reactor for 10 hours at 30 MWH.

Groups of flux monitors were located at approximately centimetre spacing along the container in order to monitor the neutron flux at vertical different locations. Horizontal neutron flux gradients are considered to be negligible (Archibald, pers. comm. 2008, 2009) in the core of the reactor so no attempts were made to monitor or correct for this. J-values for the individual samples were determined by second-order polynomial interpolation between replicate analyses of splits for each position in the capsule. Typically, J-values are between c. 0.003 and 0.03 and vary by <10% over the length of the capsule.

Irradiated samples and monitors were placed in pits in an aluminium sample holder of a bakeable stainless steel chamber connected to an ultra-high vacuum gas purification system in the argon laboratory at Queen's University in Kingston, ON. The sample holder is situated on a manually controlled movable sample stage and can be observed with a

binocular microscope and video system through the sapphire view port. Samples were heated with an 8W Loxel 3500 continuous argon-ion laser, using a sharply focussed beam for total fusion analyses and a defocused beam for step-heating to ensure even heating of the whole sample. Samples were heated for 3 minutes at each power setting and fused once melting was observed in any part of the sample, usually at 6.5 -7 W. Hornblende samples were heated starting at 2 – 3 W, biotite and muscovite starting at 0.25 W.

The gas released was purified using an SAES C50 getter (c. 5 minutes) and then released into an online MAP 216 mass spectrometer with a Baur-Signer source and an electron multiplier, set to a gain of 100 over the Faraday collector. Blanks, measured routinely, were subtracted from the subsequent sample gas-fractions. The extraction blanks are typically $<10 \times 10^{-13}$, $<0.5 \times 10^{-13}$, $<0.5 \times 10^{-13}$, and $<0.5 \times 10^{-13} \text{ cm}^{-3}$ STP for masses 40, 39, 37, and 36, respectively. Measured argon-isotope peak heights are extrapolated to zero-time, normalized to the accepted $^{40}\text{Ar}/^{36}\text{Ar}$ atmospheric ratio (295.5) using measured values of atmospheric argon, and corrected for neutron-induced ^{40}Ar from potassium, ^{39}Ar and ^{36}Ar from calcium using production ratios of Onstott and Peacock (1987), and ^{36}Ar from chlorine (Roddick 1983).

Dates and errors were calculated using formulae given in Dalrymple et al. (1981), and the constants recommended by Steiger and Jäger (1977). Isotope correlation analysis

used the formulae and error propagation of Hall (1981) and the regression of York (1969). Errors shown in Tables 2 and 3 represent the analytical precision at 2σ , assuming that the errors in the ages of the flux monitors are zero. This is suitable for comparing within-spectrum variation and determining which steps form a plateau (McDougall and Harrison 1999). A conservative estimate of this error in the J-value is 0.5% is added for inter-sample comparison (Table 2). The dates and J-values for the in-house laboratory standard MAC-83 biotite at 24.36 Ma (Sandeman et al. 1999) are referenced to TCR sanidine at 28.34 Ma and Fish Canyon Tuff FCT sanidine at 28.02 Ma (Renne et al. 1998).

5.3.4 Step-heating and the definition of plateaus

Plateau dates, and correlation and integrated dates were calculated using in-house software from the Queen's University laboratory written in Corel QuattroPro. Weighted mean ages for different groupings of samples (e.g. muscovite population, groups of samples from the same areas etc.) were calculated using Isoplot (Ludwig, 2003). Robust plateau dates are defined here as those that include at least 80% of ^{39}Ar released in 5 or more contiguous steps during step heating. This is very restrictive compared to most published definitions of plateau ages (McDougall and Harrison 1999), but is considered to be appropriate here given the sample density and the 1 or 2 million year age resolution required in this study. The results of samples that do not meet the above criteria are excluded from our interpretations.

Spectra that show obvious signs of excess argon were similarly not included in analyses or interpretations. Signs of excess argon include saddle shaped spectra (particularly for hornblendes), disturbed spectra where no plateau can be obtained, and spectra that consistently increase or decrease in age throughout the step heating process. Biotite release spectra are less useful to distinguish excess argon because the biotite lattice breaks down when heated, erasing the internal variations in argon isotopic composition, producing a flat spectrum that looks like a plateau age (McDougall and Harrison 1999).

Excess argon contributions to plateau in release spectra can be reduced by very careful sampling and picking grains to avoid contamination or visible inclusions, cleaning of grains and by following conservative step-heating procedures, but cannot be completely eliminated without in-vacuo crushing and analysis to eliminate fluid or mineral inclusions. To increase the data quality in step-heating experiments it is necessary to use small steps during heating (e.g. 0.5 W laser power increments), to use several lower temperature steps to degas possible excess argon (e.g. starting heating at 0.25 W for biotites) and to proceed to total fusion steps only once melt appears in the sample to avoid homogenizing the last steps of gas released. These methods generally increase the chance of being able to identify the presence of excess argon in the release spectra. Samples with variable K/Ca or K/Cl contents are not used in interpretations. Changes in

the K/Ca content within chemically zoned amphiboles correspond to differences in the argon dates obtained from chemical zones (Villa et al. 2000).

5.3.5 Closure temperatures

A range of closure temperatures (T_c) for minerals in this study are calculated using Dodson's (1973) equation relating the T_c of a mineral to various diffusive parameters and physical characteristics of the minerals. Diffusion rate is strongly dependent on temperature. As the temperature drops, diffusion slows down and more argon is retained in the mineral than is lost. This temperature is known as the T_c for the mineral in question.

$$\frac{Q}{RT_c} = \ln \left[\frac{ART_c^2 (D_0/a^2)}{Q(dT/dt)} \right] \quad \text{Eq. 1}$$

Where:

Q = Activation Energy (kcal/mol)

R = Gas constant (1.98717×10^{-03} kcal/mol/K)

T_c = Closure temperature (K)

A = Geometric factor (slab 8.7, cylinder 27, sphere 55)

D_0 = Diffusive coefficient (cm^2/s)

a = Grain radius (cm; converted from μm)

(dT/dt) = Cooling rate ($^\circ\text{C}/\text{s}$; converted from $^\circ\text{C}/1\text{Ma}$)

Values used:

Hornblende: A = 55, Q = 64.11 kcal/mol, $D_0 = 0.024 \text{ cm}^2/\text{s}$ (Harrison 1981)

Muscovite: $A = 27$, $Q = 521$ kcal/mol, $D_0 = 0.077$ cm²/s (Hames and Bowring 1994)

Biotite: $A = 27$, $Q = 47.1$ kcal/mol, $D_0 = 0.04$ cm²/s (Harrison et al. 1985)

Equation [1] can be solved iteratively when an estimated T_c is entered for the first iteration (set at 273.15 K for a spreadsheet calculation) and calculating subsequent T_c values that converge towards the effective T_c , generally within 2-3 iterations. The terms in the equation that have the largest effects on the calculated T_c are the grain radii of the samples, the activation energy and the diffusion coefficient of the mineral in question. The grain size is determined by examining the samples. Values for Q and D_0 have been experimentally determined. The cooling rate also affects the T_c , but is of secondary importance (Lee 2000), and varying the cooling rate between 5 °C/Ma and 200 °C/Ma generally produces generally about 50 °C difference in T_c between the lower and upper range of cooling rates. The closure temperatures calculated for hornblende, biotite and muscovite samples with different grain sizes (a =average grain radius reported in μm) in this study are presented in Figure 5.2, using a range of cooling rates from 5 °C/Ma and 200 °C/Ma. Closure temperatures for intermediate cooling rates of 20, 40, 60, 80, 100 and 150 °C/Ma are shown.

5.3.6 Limitations of the closure temperature concept

The above method of calculating closure temperatures is a good first approximation of the temperature range over which a mineral can provide useful information about

cooling times. However, there are some limitations to this approach that should be considered when making interpretations of cooling regimes. The concept of T_c for argon in minerals was originally described for slow cooling rate settings such as igneous plutons (Dodson 1973). The original Dodson equation does provide the option of evaluating variable cooling rates. Faster cooling rates increase the calculated closure temperatures by 50 to 100 °C, depending on grain size. In rapidly cooled rocks argon may be retained in the mineral at high temperature because it does not have sufficient time to diffuse through the mineral lattice. In these cases the argon date obtained would approach the actual crystallization age rather than a cooling age as would be the case in a slowly cooling system (Lee 2009).

The T_c equation is also designed to assume a constant cooling rate throughout the cooling history of the mineral in question. This is not geologically realistic, especially in rapidly exhumed terranes such as the Thor-Odin dome, since it has been documented that cooling rates change over time (Hinchey et al. 2006; Norlander et al. 2002; this study). If the changes in cooling rate occur over the temperature range around the T_c of the mineral involved then it may not be realistic to assume that the T_c calculated for a constant cooling rate is correct.

Diffusion behaviour of argon is most strongly controlled by mineral composition and structure (Dahl 1996a, 1996b), and secondarily by crystal defects and diffusion pathways

in the minerals (Lee 1995). Also, the closure temperatures calculated this way only account for volume diffusion through the whole mineral and do not consider the effects of other diffusion pathways such surface diffusion along grain boundaries, or diffusion along fractures or cleavage planes. Volume diffusion is the slowest mechanism of diffusion and models using volume diffusion as the dominant process would therefore predict lower closure temperatures than other diffusion mechanisms. However, closure temperatures calculated using the above equations are still considered to be, at the very least, reasonable approximations of the temperature at times obtained from $^{40}\text{Ar}/^{39}\text{Ar}$ analyses and should be used with caution when making interpretations about thermal and tectonic histories of particular areas (Kelley 2002; Lee 2009).

5.4 Results

$^{40}\text{Ar}/^{39}\text{Ar}$ dates were obtained from hornblende, biotite and muscovite from a range of rock types and structural levels. The thermochronology data presented here are applicable to the temperature range between ~600 °C and 280 °C (Figure 5.2). Sample locations (UTM) and lithology are listed in Table 5.1. Argon data are shown in Table 5.2 (samples that yielded plateau dates) and Table 5.3 (samples that did not yield plateau dates). All data are presented in the text following this standardized format: the plateau date followed by corresponding information in brackets (a number corresponding to location on Table 5.2; sample number; percentage of ^{39}Ar included in plateau).

5.4.1 Hornblende plateau ages from a range of rock types and thermotectonic domains

5.4.1.1 Hornblende samples from the Thor-Odin dome

Hornblende samples from the Thor-Odin dome at Frigg Glacier (AH-02-003H and AH-02-004H), Bearpaw Lake (AH-03-024-1, AH-03-024-2, AH-03-029-1, AH-03-029-2) and Icebound Lake (DC446, DC423) did not produce any plateau dates that included 80% or more ^{39}Ar in the step-heating plateaus. Some of the step-heating release spectra have pronounced saddle shapes indicating the presence of excess argon, or are completely disturbed with no contiguous steps. In addition, the integrated and correlation dates calculated for these samples are not within error of each other, or within error of the pseudo-plateau dates (in cases of plateaus that have less than 80% ^{39}Ar), and therefore the data did not meet our definition of a valid plateau date.

The Thor-Odin samples from Frigg Glacier and Bearpaw Lake are from garnet amphibolites in migmatitic paragneiss (Hinchey 2005). The garnet amphibolites are not foliated and do not contain visible chlorite. There is evidence for extensive decompression reactions in the anthophyllite-gedrite mafic rocks of the area (Norlander et al. 2002; Hinchey et al. 2006) including garnet replacement by cordierite, and kyanite replaced by sillimanite (Norlander et al. 2002). These samples are not described here because they form parts of previous work already published. This study used garnet

amphibolites in the same areas because the anthophyllite-gedrite units do not have enough K for argon thermochronology.

Amphibolites from Icebound Lake (DC446 and DC423) represent the upper structural levels of the Thor-Odin dome. Sample DC446 is from a garnet amphibolite boudin shown in Figure 5.3, which illustrates the extensive anatexis of the host paragneiss in which the amphibolites of Icebound Lake are located. The garnet amphibolite contains a pre-existing foliation defined by a weak alignment of hornblende and plagioclase crystals that pre-dates the migmatitic structures indicating a previous deformation event of uncertain age. The garnet amphibolite DC423 (Figures 5.4 to 5.6) has the same mineralogy as DC464 (hornblende, garnet, plagioclase, quartz, and titanite) and is also surrounded by migmatitic-garnet-biotite-quartzofeldspathic gneiss. Figure 5.6 shows a reaction rim around the garnet, with the possible reaction $Grt = Sil + Bt + Plg$ indicating breakdown of garnet and some of the hornblende grains have small amounts of chlorite on their grain boundaries.

5.4.1.2 Cariboo Alp

Samples from Cariboo Alp (CA) on the southwest flank of Thor-Odin dome (Figure 1.2) are the structurally lowest samples that produced robust hornblende plateau dates.

Hornblende crystals from an amphibolite boudin in rusty weathering garnet-sillimanite-biotite paragneiss show distinctive amphibolite cleavage patterns without alteration

minerals in grain boundaries or cleavage planes as illustrated in Figure 5.7. Also, these hornblende crystals do not show any retrograde reactions at their boundaries or cleavage planes, and are not chloritized. They produced a plateau date of 57.3 ± 0.8 Ma (**10**; DC169-2; 82.9%). Hornblende crystals from a calc-silicate amphibolite layer in grey sillimanite–biotite quartzofeldspathic paragneiss (Figure 5.8) are also not chloritized. The amphibolite consists primarily of hornblende with minor (10 – 15 %) plagioclase and quartz along with trace amounts of titanite and opaque minerals. They produced a plateau date of 53.6 ± 0.4 Ma (**12**; DC176-1; 87.4%).

Sample DC186 contains hornblende, quartz, plagioclase with some sericite alteration and trace amounts of titanite (not pictured), as illustrated in Figure 5.9. Two hornblende fractions from this amphibolite layer in grey sillimanite–biotite–quartzofeldspathic paragneiss produced plateau dates of 56.2 ± 0.6 Ma for a 250 μm size fraction of hornblendes (**17**; DC186-2H; 94.8%), and 50.8 ± 1.3 Ma for a 350 μm piece of a 2cm hornblende crystal (**18**; DC186-LH; 92.4%). Sample DC188 from a plagioclase amphibolite boudin (Figure 5.10, not the garnet amphibolite in the foreground) in rusty weathering garnet–sillimanite paragneiss consists of 50% hornblende, 35% plagioclase, 10% quartz and minor titanite. The amphibolite contains a poorly developed foliation defined by hornblende crystals. Hornblende crystals have minor chlorite alteration on their grain boundaries and cleavage plains as illustrated in Figure 5.11. This sample produced a plateau date of 56.1 ± 1.0 Ma (**22**; DC188; 93.1%).

5.4.1.3 Fawn Lakes and Mount Symonds

The Fawn Lakes and Mount Symonds study areas structurally overlie the Cariboo Alpr rocks (Figure 1.2, 2.1). Sample DC320 is a garnet–plagioclase–quartz amphibolite within the western part of the Fawn Lake Assemblage paragneiss. This sample consists of 55% hornblende, 25% quartz, 10% plagioclase and 10% garnet with a weakly developed foliation defined by hornblende. Hornblende crystals produced a plateau age of 61.3 ± 0.6 Ma (**30**; DC320; 82%). Hornblende crystals from a quartz–plagioclase–garnet amphibolite with similar mineralogy in different proportions (60% hornblende, 25% garnet, 10% plagioclase and 10% quartz), in the eastern part of the same Fawn Lakes Assemblage paragneiss, just north of Mount Symonds (see Figure 1.2), produced a plateau age of 57.3 ± 0.5 Ma (**31**; DC342; 86%).

At Mount Symonds hornblende from three different amphibolite layers in transposed concordant contact with southwest dipping metasedimentary rocks including quartzite, migmatitic garnet–sillimanite–biotite paragneiss and marbles yielded plateau ages of 52.2 ± 0.7 Ma (**35**; DC 400; 92%), 55.4 ± 1.5 Ma (**36**; DC 414; 97.2%), and 55.7 ± 1.8 Ma (**37**; DC370; 85.1%), respectively. The amphibolite mineralogy for the three samples is similar, all containing hornblende (60 %), plagioclase (20 %) and quartz (20 %) with proportions of minerals varying by ~5 % in different locations. All the amphibolites contain a weakly developed foliation (Figure 5.14 and 5.15) defined by hornblende

crystals, concordant with the regional south to southwest dipping transposition foliation. Sample DC370 is located in the core of a syncline with a steeply south dipping axial plane (Figure 5.16). None of the amphibolites had significant chlorite content, and were not extensively intruded by crosscutting Ladybird granite, even though DC 414 contained concordant leucocratic layers and boudins (Figure 5.15). In contrast, sample DC397, an amphibolite with similar mineralogy but infolded (Figure 5.17) with pegmatites of the Ladybird granite did not produce a plateau date in either of the size fractions tested.

5.4.1.4 Twin Peaks and North Fosthall

In the Twin Peaks area, hornblende from three amphibolite samples all produced plateau ages between c. 55.0 Ma and 57.5 Ma. Sample DC476 is an amphibolite boudin surrounded by granitic pegmatite (Figure 5.18) of the Ladybird granite which contains 80% dark green to black hornblende, 20 % plagioclase with trace amounts of biotite and titanite. Plateau ages for DC476 are 57.3 ± 1.4 Ma for the $>250 \mu\text{m}$ fraction (**41**; DC476-2; 97.5%) and 57.5 ± 2.0 Ma for the 200-250 μm fraction (**42**; DC476-1; 99.3%). Sample DC473 is a calc-silicate amphibolite (Figure 5.19) consisting of 80 % hornblende, with minor plagioclase (10 %), quartz (5%) and diopside (5 %) with a weakly developed foliation defined by hornblende crystals, concordant with the moderately south to southwest dipping transposition foliation in the area. Plateau ages for this sample are 55.7 ± 0.5 Ma for the $>250 \mu\text{m}$ fraction (**43**; DC473-2; 82.9%) and 55.6 ± 0.6 Ma for the

200 – 250 μm fraction (**44**; DC473-1; 99.2%). For a plagioclase amphibolite plateau ages are 55.7 ± 0.8 Ma for the >250 μm fraction (**45**; DC469-2; 97.6%) and 55.3 ± 0.9 Ma for the 200 – 250 μm fraction (**46**; DC469-1; 93.7%). Samples DC457 and DC464 (Figure 5.20) did not produce plateau dates with 80% ^{39}Ar included in the plateau, but produced plateaus with dates of 57.3 ± 0.7 Ma (68.1% ^{39}Ar) and 56.3 ± 0.7 Ma (67.2% ^{39}Ar) respectively, within error of the dates indicated by the conservative plateau definition used in this study.

In the North Fosthall area, hornblende from a calc-silicate amphibolite (Figure 5.21) with a steeply south dipping foliation defined by layers of quartz and plagioclase, alternating with hornblende, diopside and minor biotite produced a plateau date of 55.0 ± 1 Ma for the 100 – 200 μm fraction (**39**; DC219-1; 98.9%) and slightly younger plateau date of 52.3 ± 0.7 Ma for the ~ 250 μm fraction (**38**; DC219-2; 86.8%), similar to sample DC400 from Mount Symonds. No significant chlorite alteration is visible in this sample (Figure 5.22). Hornblende from a plagioclase amphibolite gneiss (Figure 5.23) with shallow south dipping foliation defined by hornblende alternating with plagioclase and quartz layers yielded a plateau age of 55.8 ± 1.5 Ma (**40**; DC209; 99.5%). A similar calc-silicate amphibolite gneiss (Figure 5.24) containing hornblende, biotite, diopside, plagioclase and quartz produced a plateau age of 56.2 ± 1.1 Ma (**49**; DC239; 85.3%).

5.4.1.5 Plant Creek and Cusson Creek

The structurally highest samples used for this study are from Plant Creek and Cusson Creek areas. Plagioclase amphibolite DC048 from Plant Creek contains 55 % hornblende, 30% plagioclase and 15% quartz with traces of chlorite on fracture planes within hornblende crystals (Figure 5.25). Plateau dates from this sample are 58.1 ± 1.0 Ma (**52**; DC048-2; 99.7 %) from the ~ 250 μm fraction, and 60.1 ± 1.8 Ma (**53**; DC048-1; 96.4 %) from the 100 – 200 μm grain size fraction. Amphibolite from Cusson Creek, immediately south of Plant Creek (Figure 5.26), containing 40% hornblende, 20% biotite, 30% plagioclase, 15% quartz and 5% titanite with a weakly developed foliation defined by biotite and hornblende produced a date of 62.7 ± 0.7 Ma (**56**; DC080-H; 96.7%).

5.4.2 Biotite plateau ages from a range of rock types and structural levels

5.4.2.1 Thor-Odin dome

The rocks of the Thor-Odin dome were sampled in the Mount Thor (MT), Bearpaw Lake (BL), Frigg Glacier (FG), and Icebound Lake (IL) areas (Figure 1.2). At Mount Thor, biotite from the foliation planes of migmatitic sillimanite–garnet–muscovite–biotite schist produced a plateau date of 51.2 ± 0.5 Ma (**1**; AH-02-022; 99.9 %). At Bearpaw Lake, biotite from foliation planes in a migmatitic hornblende–quartz–K-feldspar–plagioclase paragneiss produced a plateau date of 52.3 ± 0.3 Ma (**3**; AH-03-021; 100 %). At Frigg Glacier, biotite from a phenocrystic leucosome crosscutting the host hornblende–biotite orthogneiss produced a plateau date of 54.8 ± 0.7 Ma (**2**; AH-02-013; 99.6%).

At Icebound Lake on the southwestern flank of the Thor-Odin dome two biotite samples about 250 m apart in a boudinaged layer of migmatitic garnet–gedrite–anthophyllite (Figure 5.27 and 5.28) produced plateau ages of 52.9 ± 0.3 Ma (**5**; DC536; 100%) and 56.9 ± 0.5 Ma (**8**; DC532; 96.5%). Another biotite sample taken from a garnet–biotite amphibolite lens (Figure 5.28) associated with the layer of migmatitic garnet–gedrite–anthophyllite that contained the previous two samples produced a plateau date of 54.7 ± 0.6 Ma (**6**; DC450; 99.4%). The dominant basement lithology in the Icebound Lake area is a migmatitic garnet–biotite–quartzofeldspathic paragneiss (Figure 5.3, Figure 5.29) consisting of plagioclase, quartz, K-feldspar, biotite and garnet. Biotite from sample DC439 produced a plateau date of 52.2 ± 0.4 Ma (**7**; DC439; 99.8%). Biotite from an apparently undeformed tourmaline bearing pegmatite which crosscuts the metasedimentary rock immediately overlying the migmatitic paragneiss of sample DC439, produced a plateau date of 51.0 ± 0.4 Ma (**9**; DC418; 99.8%).

5.4.2.2 Cariboo Alp

In the Cariboo Alp area, biotite from an amphibolite boudin (Figure 5.8) within the southwest dipping grey biotite–quartzofeldspathic paragneiss (Figure 5.30) produced a plateau date of 50.9 ± 0.4 Ma (**11**; DC176-2; 99.9%). The grey gneiss at Cariboo Alp is primarily biotite–quartzofeldspathic gneiss, with up to 5% garnet and 10% sillimanite present in some layers, and 5% diopside and 10 – 15 % hornblende in other layers

(Figure 5.30). The garnets in this gneiss do not show evidence for decompression reactions around the rims (Figure 5.31). Foliations are defined by biotite and sillimanite (Figure 5.32). Biotite defining the foliation in grey calc-silicate gneiss produced a plateau date of 51.1 ± 0.4 Ma (**16**; DC178; 97.3%). Biotite from the foliation planes in a southwest dipping diopside–hornblende–biotite calc-silicate gneiss (Figure 5.9) produced plateau dates of 50.7 ± 0.3 Ma for the 250 – 300 μm fraction (**19**; DC186-2B; 95.8%) and 51.2 ± 0.4 Ma for the 100 – 200 μm fraction (**20**; DC186-1B; 98.1%).

The second main paragneiss unit present at Cariboo Alp is a moderately southwest dipping rusty-weathering garnet–sillimanite–biotite paragneiss (Figure 5.33) in which foliations are defined by biotite and sillimanite. This rusty paragneiss (Figure 5.34) has more plagioclase (up to 40%) and less quartz (20%) than the grey gneiss, similar amounts of biotite (15%), more garnet and sillimanite (up to 15 % each), and hornblende and diopside are absent. Biotite sampled from the foliation planes of this garnet–sillimanite–biotite paragneiss produced a plateau date of 51.7 ± 0.6 Ma (**23**; DC193; 99.7%). Biotite from a moderately foliated garnet–biotite amphibolite (Figure 5.35) with large (>3 cm) garnets produced plateau dates of 51.6 ± 0.4 Ma for larger 2 x 3 x 0.7 mm crystals (**24**; DC191-L; 99.7%) and 51.6 ± 0.4 Ma for smaller 2 x 3 x 0.1 mm crystals (**25**; DC191-1; 99.2%).

5.4.2.3 Fawn Lakes

The semipelitic paragneiss at Fawn Lakes has a distinct flaggy weathering style (Figure 5.36) and contains plagioclase, quartz, biotite and garnet, with only rare sillimanite. In the Fawn Lakes area, which is structurally above Cariboo Alp, biotite from foliations in a biotite–quartz psammite (Figure 5.37) produced a plateau date of 52.2 ± 0.4 Ma (**28**; DC330; 98.2%). Biotite from the foliation planes in a typical exposure of southwest dipping migmatitic semipelitic paragneiss produced a plateau date of 52.6 ± 0.4 (**29**; DC326; 99.4%).

5.4.2.4 Mount Symonds

At Mount Symonds, biotite from a granitic pegmatite interpreted as part of the Ladybird suite which crosscuts the host migmatitic garnet–sillimanite–biotite paragneiss (Figure 5.38) produced a plateau date of 50.9 ± 0.3 Ma (**32**; DC395; 99.9%). Biotite (1 x 3 x 0.5 mm) from a granitic pegmatite concordant with the southwest-dipping layers of host paragneiss and amphibolites (Figure 5.17), also interpreted as part of the Ladybird suite, produced a single grain plateau date of 50.6 ± 0.4 Ma (**34**; DC398-1; 80.3%) and another grain (2 x 2 x 0.5 mm) produced a date of 50.2 ± 0.4 Ma (**33**; DC398-2; 82.4%) from multiple total fusion laser spots. These pegmatites are apparently undeformed but do not have any chilled margins, indicating that the country rocks were not cold at the time the pegmatites intruded.

5.4.2.5 North Fosthall

At Twin Peaks immediately to the west of Mount Baldur (see next sample) biotite from weakly developed foliations in a garnet–biotite calc-silicate amphibolite produced a plateau age of 52.0 ± 0.4 Ma (**47**; DC468; 83.6%). Biotite from the Ladybird granite at Mount Baldur produced a plateau date of 51.7 ± 0.4 Ma (**48**; AH-03-032; 99.8%). In the North Fosthall – Cameron Lake area, biotite from foliation planes in south dipping calc-silicate gneiss containing plagioclase, diopside, biotite and hornblende (Figure 5.39) produced a plateau date of 52.5 ± 0.5 Ma (**55**; DC299; 88.5%).

5.4.2.6 Plant Creek

In the Plant Creek area biotite from the foliation planes in a south southwest dipping sillimanite–garnet–biotite–muscovite schist (Figure 5.40) produced a plateau date of 52.1 ± 0.4 Ma (**51**; DC028; 99.7%). In the Plant Creek area two biotite samples from a weakly foliated plagioclase amphibolite, also used for hornblende analysis (Figure 5.26), produced plateau dates of 51.3 ± 0.3 Ma (**58**; DC080-B1; 97.8%) and 51.7 ± 1.1 Ma (**57**; DC080-B2; 100% TF). The last date represents a total fusion (TF) analysis and is therefore equivalent to a correlation age.

5.4.3 Muscovite plateau ages from a range of structural levels

5.4.3.1 Muscovite in leucosomes, Cariboo Alp

At Cariboo Alp muscovite only occurs in leucosomes and in pegmatites, not in the host gneisses. Muscovite samples were taken from both structural contexts for comparison. Muscovite occurs in boudinaged leucosomes (Figures 5.41 – 5.43) within the grey migmatitic paragneiss which makes up the dominant host rocks at Cariboo Alp. These muscovites, intergrown with chlorite (Figure 5.43), represent retrograde metamorphic minerals overprinting the main parageneses (section 2.5). Muscovite from boudinaged leucosomes sampled from the grey sillimanite–biotite–quartzofeldspathic migmatitic paragneiss at Cariboo Alp produced plateau dates of 50.6 ± 0.3 Ma (**13**; DC519; 100%), 50.5 ± 0.3 Ma (**14**; DC512; 100%), 50.9 ± 0.4 Ma (**15**; DC511; 100%), and 50.6 ± 0.3 Ma (**26**; DC515; 100%).

5.4.3.2 Muscovite in Ladybird granite pegmatites

At Icebound Lake, Cariboo Alp, and Plant Creek, muscovite was sampled from leucogranite pegmatites which are part of the Ladybird granite suite. These muscovites are part of the primary igneous mineralogy in the pegmatites. Muscovite crystals from a pegmatite that crosscuts the rusty garnet–sillimanite–biotite paragneiss (Figure 5.44) produced a plateau age of 51.3 ± 0.4 Ma (**21**; DC502; 100%). Muscovite crystals from a pegmatite that crosscuts the grey sillimanite–biotite–quartzofeldspathic migmatitic

paragneiss (Figure 2.8) produced a plateau age of 50.6 ± 0.4 Ma (**27**; DC528; 100%). Muscovite from a pegmatite crosscutting the dominant migmatitic quartzofeldspathic paragneiss (Figure 5.45) of the Icebound Lake area produced a plateau date of 50.6 ± 0.3 Ma (**4**; DC543; 98.6%). For comparison, the biotite cooling age of the host paragneiss (Figure 5.29) from sample DC439 is 52.2 ± 0.4 Ma, and the biotite cooling age from a pegmatite sample DC418 which crosscuts the metasedimentary rocks (Figure 5.46) structurally above the paragneiss is 51.0 ± 0.4 Ma.

In the plant Creek area garnet–muscovite bearing pegmatites of the Ladybird granite crosscut the foliation in the host rocks (garnet–sillimanite–biotite schist and psammite respectively). These pegmatites do not have chilled margins and do not have any internal foliation. In the sampled areas the pegmatites appear to be planar (unfolded) but due to lack of exposure they could not be traced further away. Muscovite from garnet–muscovite bearing granitic pegmatites in the Plant Creek – South Fosthall area (Figure 5.47) and the North Fosthall – Cameron Lake area (Figure 5.48), interpreted as being part of the Ladybird granite suite, produced plateau dates of 50.7 ± 0.3 Ma (**50**; DC058-1; 98.7%) and 50.9 ± 0.3 Ma (**54**; DC295P; 99.9%).

5.5 Discussion

All samples with $^{40}\text{Ar}/^{39}\text{Ar}$ thermochronology data are presented in Figure 5.49.

Interpretations and summary information are presented in Figure 5.50 and 5.51.

5.5.1 Hornblende

Hornblende samples from rocks within the Thor-Odin dome that have the oldest Proterozoic protoliths (Parkinson 1992) at Frigg Glacier, Bearpaw Lake and Icebound Lake did not produce plateau ages and showed signs of containing excess argon. This is likely the result of a combination of factors. These factors likely include: the Proterozoic ages of protoliths and long-lived tectonothermal histories (Arnaud and Kelley 1995; Scaillet 1996; Sherlock et al. 1999); the hydrous nature of some of the minerals used (Kelley 2002), or the presence of fluid or solid inclusions within the minerals (Kelley et al. 1986).

Excess argon is most commonly found in metamorphic rocks with Proterozoic or older protoliths or long-lived tectonothermal histories (Arnaud and Kelley 1995; Scaillet 1996; Sherlock et al. 1999) like the ones mentioned above. However, protolith age cannot be the main factor in determining whether a rock will have Ar_E since samples from rocks with Neoproterozoic protoliths (Fawn Lakes, Cariboo Alp) produced robust dates with no discernible excess argon. The thermal history and length of time the rocks spent at temperatures above or below their closure temperatures would have a much larger influence on the retention of excess argon. The amphibolites in the dome experienced significant decompression during anatexis (Norlander et al. 2002; Hinchey et al. 2006) in the Paleocene, but it is not known when prograde metamorphism began, or how long

the rocks spent at temperatures above T_c for argon in hornblende (~ 500 °C). The rocks of the Thor-Odin dome at the deepest structural levels are the source area for the anatectic melts emplaced at higher structural levels (Hinchey and Carr 2006). Therefore, it is possible that they did not remain at high temperatures for long enough in the Paleocene to Eocene to completely reset the hornblende cooling ages and reflect Eocene cooling.

Hornblende dates from Cariboo Alp, range between c. 57 and 53 Ma. These hornblende dates are interpreted as cooling ages. Regional metamorphism and penetrative deformation in the Cariboo Alp and overlying Fawn Lakes area was active between c. 62 – 58 Ma in the Late Cretaceous to Paleocene (Carr 1992, Coleman 1990). Therefore, the rocks would have cooled after regional metamorphism and deformation in the Paleocene to Eocene, as reflected in the above-mentioned cooling ages. The hornblende plateau dates from rocks at Fawn Lakes overlying the Cariboo Alp area are c. 62 and 57 Ma. As with the dates from Cariboo Alp, these are interpreted as cooling ages after regional metamorphism and accompanying deformation. The 50.8 ± 1.3 Ma for a ~ 350 μm piece of a >2 cm hornblende crystal from DC186 is interpreted as representing only a fragment of a crystal, not the main cooling ages for the area. It is however within error of the c. 53 Ma cooling age of other samples e.g. DC176.

The hornblende plateau dates from Mount Symonds range are c. 55 and 52 Ma. These hornblende dates can be interpreted in two different ways: (i) as reset cooling ages after reheating by the intrusion of Ladybird granite because the metamorphism in the area is interpreted to be older than ~62 Ma; and (ii) as a cooling age where the rocks remained above the approximate closure temperature (~500 °C) between the end of metamorphism (interpreted as c. 62 Ma) and the c. 55 and 52 Ma cooling date. The second interpretation, that these are cooling dates that represent the time the rock cooled through the closure temperature for Ar in hornblende is preferred here, since some of the 62 – 54 Ma Ladybird granite in this area is concordant with the regional foliation and (older than the deformation), and some crosscuts the foliation (younger than the deformation). However, the presence of extensive (~30%) Ladybird granites in this area would have contributed heat to the rocks and delayed cooling after metamorphism.

In the Twin Peaks area, hornblende from three amphibolite samples all produced plateau ages between c. 55.0 Ma and 57.5 Ma. All the hornblende dates from the Twin Peaks and North Fosthall areas can be interpreted as reset cooling ages after reheating by the intrusion of Ladybird granite, since prograde metamorphism in this area is interpreted to be older at c. 73 – 62 Ma, in the Late Cretaceous to Paleocene. However, like the Mount Symonds area discussed above, it is possible that the rocks remained above the approximate closure temperature for hornblende (~500 °C) between the end

of amphibolite facies metamorphism (interpreted as c. 64 – 62 Ma) and the cooling ages presented here are cooling ages. Many of the samples in this area are within the defined boundaries of the South Fosthall pluton. In areas where Ladybird granite makes up >50% of the rocks this extensive melt presence would have contributed heat to the rocks and delayed cooling after metamorphism. The cooling dates for all the biotite samples taken from the Ladybird pegmatites or granites are between c. 51 and 52 Ma, indicating that the Ladybird granite remained above ~300 °C until c. 52 Ma (see Biotite results, Section 5.4.3). It is therefore the favoured interpretation that the Ladybird granite contributed enough heat to the rocks that cooling after regional metamorphism was delayed. However, it is not realistic to attempt to separate the two possibilities (regional cooling without Ladybird contribution vs. Ladybird-induced resetting) without more precise dating of prograde metamorphic timing, further U-Pb dating of the granite and extensive thermal modeling, which are outside the scope of this project.

Hornblende plateau dates in the Plant Creek areas of c. 62 – 58 Ma are interpreted as cooling ages. Metamorphism in this area is documented between c. 100 – 80 Ma, Late Cretaceous, and likely continued to the period between c. 73 and 64 Ma (Carr 1992; Glombick 2005; Lemieux 2006). It is therefore possible that the rocks remained above the closure temperature for argon in hornblende (c. 500 °C) from the end of metamorphism to cooling through 500 °C at c. 62 – 58 Ma. The two areas that have the oldest hornblende cooling ages are Fawn Lakes (lower part of the section) and Plant

Creek (upper part). The hornblende cooling ages in these two areas are between c. 62 and 58 Ma. These cooling ages represent the time of cooling through 500 – 550 °C. The Plant Creek and Fawn Lakes areas have the least amount of Ladybird granite intrusion (<10 – 20%), in contrast to the areas in the central part of the study area around the South Fosthall pluton. While the penetrative deformation and metamorphism at Plant Creek is older (ended c. 64 Ma) than at Fawn Lakes (ended c. 58 Ma) it is geologically consistent to interpret these $^{40}\text{Ar}/^{39}\text{Ar}$ dates as cooling ages when compared to the timing of metamorphism.

The $^{40}\text{Ar}/^{39}\text{Ar}$ ages obtained from hornblende samples in the middle part of the structural section, North Fosthall, Twin Peaks and Mount Baldur, (all within or closely adjacent to the South Fosthall pluton), and Mount Symonds, all represent cooling ages which may have been reset by the presence of the anatectic Ladybird granite suite. In this area, the documented age of amphibolite facies metamorphism forming K-feldspar–sillimanite and K-feldspar–sillimanite–melt-bearing assemblages Late Cretaceous to Paleocene (Carr 1992; Glombick 2005; Lemieux 2006), coeval with the formation of the transposition foliation. Since penetrative deformation continued through c. 64 – 58 Ma in these areas it is also reasonable to suggest that the rocks in fact did remain above the range of closure temperatures for argon in hornblende between the end of deformation and the cooling ages presented here. The $^{40}\text{Ar}/^{39}\text{Ar}$ dates obtained from hornblende

samples from Cariboo Alp are interpreted as cooling ages after metamorphism and penetrative deformation which ended c. 58 Ma.

5.5.2 Biotite

Biotite samples from Mount Thor and Bearpaw Lake produced plateau ages of c. 52 and 51 Ma. Both samples were taken from the foliations within the dominant paragneiss lithology at Mount Thor and Bearpaw Lake, and are interpreted to be representative of the respective areas. These two dates are interpreted as cooling ages for the rocks in the area because documented amphibolite to granulite facies metamorphism is older than c. 56 Ma, and anatexis was ongoing at c. 56 Ma. At Frigg Glacier, biotite from a phenocrystic leucosome crosscutting the host hornblende–biotite orthogneiss produced an older plateau date of 54.8 ± 0.7 Ma (**2**; AH-02-013; 99.6%). Anatexis and decompression melting is documented to occur in the Thor-Odin dome at c. 56 Ma, therefore, this sample either represents an example of extremely fast cooling (from >650 °C to ~ 350 °C in <2 Ma), or can demonstrate that temperatures within the dome were not completely homogenous between c. 56 and 52 Ma.

Frigg Glacier is the structurally deepest sample within the dome; both with respect to the lithostratigraphic interpretation presented in Figure 2.1 based on the cross section in Figure 1.3, and with respect to its relative position in the footwall of the Columbia River fault, which cuts into progressively deeper rocks in the northern part of the study

area. It is therefore possible that anatexis in the Frigg Glacier area was not coeval with the anatexis documented at Bearpaw Lake. It is also possible that this biotite sample represents a partially reset argon date because the sampled biotite is likely a restitic biotite within the leucosome (Bea 1994).

At Icebound Lake a migmatitic garnet–biotite–quartzofeldspathic paragneiss that makes up the dominant basement rock in the area, produced a plateau date of 52.2 ± 0.4 Ma. This date is interpreted as an original cooling age for the migmatitic paragneiss in the area. It is consistent with the unit's metamorphic history as the amphibolite- to granulite facies metamorphism in Thor-Odin dome is older than c. 56 Ma, and anatexis was ongoing at c. 56 Ma. Biotite, from a tourmaline bearing pegmatite, cross-cutting the metasedimentary rocks immediately overlying the migmatitic paragneiss of sample DC439, produced a plateau date of 51.0 ± 0.4 Ma. Tourmaline-bearing pegmatites in this area are interpreted as the youngest representatives of Ladybird granite and this date is interpreted as a cooling age for biotite within the pegmatite, as representative of the Ladybird granite in Thor-Odin dome.

Biotite plateau dates, within and associated with a migmatitic layer of gedrite–anthophyllite amphiboles and chloritized garnets (Figure 5.27), from Icebound Lake are more difficult to interpret. A local boudinaged layer gives plateau ages of 52.9 ± 0.3 and 56.9 ± 0.5 Ma, while a garnet–biotite–amphibolite boudin, associated with this layer,

produced a plateau age of 54.7 ± 0.6 Ma. The biotite grains in these two samples have similar grain sizes, and are optically similar. Therefore, no differences in T_c or cooling history were expected. Although these two samples are within the same rock layer, they produced different plateau ages. This difference is inferred to be the result of inherited argon and/or partial resetting of argon. It is possible this rock layer was a significant conduit for melt (during migmatization) or fluid (during retrogression). The older argon dates may represent inherited restitic biotite or an argon system disturbed by fluid events. It is also possible that these biotite samples record different episodes of mineral growth as a result of mineral reactions during anatexis. Given the data we have it is not possible to distinguish among these possibilities.

Biotite from Frigg Glacier, Bearpaw Lake and Icebound Lake produced robust plateau dates even though hornblendes from the same areas did not. It is possible that this is the result of the relative K content of the respective minerals. The argon ages of minerals with low K contents are more likely to be affected by the presence of fluid inclusions. Comparatively, argon ages of minerals with high K contents can be significantly altered by the high presence of K (Kelley 2002). For example, fluid inclusions (0.1 to 10% by volume) containing 10 ppm Ar in a mineral with only 1% K may result in an order of magnitude age increase of 100 to 1000 Ma (Kelley 2002).

In addition, the distribution of excess argon within rock outcrops follows patterns governed by the diffusion behaviour of the gas within minerals, and the bulk rock diffusivity of the whole system (Baxter et al. 2002). In a case presented by Baxter (2002), the dates of biotite crystals from an amphibolite were different than those in a pelite in contact with each other. Biotite dates are apparently older in the amphibolite, and younger in the pelite, with a gradation across the contact. This distribution in dates is interpreted as a result of excess argon being trapped in the biotite within the amphibolite due to a K-poor rock matrix; relative to the biotite within the pelite, where excess argon diffused away, possibly into a local argon sink such as quartz. Excess argon is less likely to diffuse towards K-rich (and therefore Ar-rich) rocks on larger scales (Baxter et al. 2002). This could be used to explain the ages found in the rocks from Bearpaw Lake, where hornblende from amphibolites did not produce geologically meaningful ages and were strongly affected by excess argon, and biotite grains from adjacent paragneiss produced a robust plateau age (100% ^{39}Ar) of c. 52 Ma, that was geologically sound.

Biotite plateau ages from Cariboo Alp range c. 52.5 – 51 Ma are interpreted as primary cooling ages. The timing of amphibolite facies metamorphism in this area is documented between c. 62 and 58 Ma (Carr 1992), slightly older than the c. 56 Ma anatexis (Hinckey et al. 2006) in the structurally lower rocks of the interior of the Thor-Odin dome. Cooling through 300 °C between c. 52.5 – 51.0 Ma is therefore younger than the known timing

of regional metamorphism. Biotite plateau dates from Fawn Lakes, south of Cariboo Alp are 52.2 ± 0.4 Ma and 52.6 ± 0.4 . These biotite dates are interpreted as cooling ages, similar to those in Cariboo Alp, because they post-date documented amphibolite facies metamorphism, ongoing between c. 62 – 58 Ma.

Biotite samples from Mount Symonds were all collected from pegmatites of the Ladybird granite and produced plateau ages of c. 51 – 50 Ma. These ages are interpreted as cooling ages for the pegmatites, representative of pegmatites associated with the Ladybird granite in this southwest dipping package of rocks overlying the Thor-Odin dome. Biotite from the Ladybird granite, within the mapped/interpreted edges of the South Fosthall pluton at Mount Baldur, produced a plateau age of 51.7 ± 0.4 Ma, interpreted as a cooling age, representative of the Ladybird granite making up the South Fosthall pluton in this area.

Biotite dates from metamorphic country rocks in the North Fosthall and Plant Creek areas range from c. 52.5 to 51.3 Ma and are interpreted as cooling ages. These biotite dates are possibly reset by the intrusion of the Ladybird granite in the area. The documented metamorphism in this area is as old as c. 80 Ma, however, since penetrative deformation continued until c. 64 Ma, it is likely that metamorphism continued to that time as well. Similar to the North Fosthall area noted above, it is therefore possible that the rocks remained above the closure temperature for argon in

biotite between the end of metamorphism and the intrusion of the Ladybird granite. While the rocks at Plant Creek are at lower metamorphic grade (sillimanite–muscovite-bearing amphibolite facies rocks in the Plant Creek area, compared to sillimanite–K-feldspar–melt-bearing amphibolite facies rocks in North Fosthall), there is no significant greenschist facies overprint in Plant Creek, suggesting that the dates reported above are cooling ages.

The $^{40}\text{Ar}/^{39}\text{Ar}$ dates obtained from biotite samples in pegmatites both at Icebound Lake (within the dome) and Mount Symonds (within the overlying rocks) represent cooling ages for the Ladybird granite pegmatites of the area. It is also possible that these biotite ages represent crystallization ages for the pegmatites because in areas where rapid cooling took place, crystallization and cooling dates may be indistinguishable within error (McDougall and Harrison 1999). The biotite cooling ages of the country rocks into which the pegmatites intrude overlap within error with the cooling dates in the pegmatites, indicating that all the rocks were at or near a common isotherm at this time, and cooled together.

5.5.3 Muscovite

Muscovite from leucosomes in the migmatitic paragneiss at Cariboo Alp all produced plateau ages between c. 50.9 Ma and 50.5 Ma. As discussed in Chapter 2, the muscovite-chlorite association in these leucosomes are interpreted as retrograde

metamorphic minerals and not part of the prograde metamorphic assemblage in the host gneisses. These dates are therefore interpreted to represent the time of crystallization of retrograde metamorphic muscovite growing together with chlorite, below the normal range of closure temperatures for muscovite. These dates likely represent the timing of retrograde metamorphic overprints on these formerly high grade rocks occurring at c. 51 Ma.

Biotite has a lower T_c range for argon than muscovite does (Figure 5.2). For example, for equivalent grain sizes over the same range of cooling rates (e.g. 1000 μm grain radius, cooling rates from 5 $^{\circ}\text{C}/\text{Ma}$ to 200 $^{\circ}\text{C}/\text{Ma}$), biotite has a T_c range of 355 – 420 $^{\circ}\text{C}$, while muscovite has a T_c range of 430 – 510 $^{\circ}\text{C}$. It is therefore predicted that biotite cooling ages for the same rock or unit, within similar structural contexts, would be younger than the muscovite cooling ages. This is not the case in this study since the biotite samples (with cooling ages between c. 52.5 and 51.0 Ma) represent different structural contexts than the muscovite samples (ages between c. 51.0 and 50.5 Ma). There are no examples where biotite and muscovite from the same structural context (e.g. both lying in the same foliation) give contradictory ages.

Muscovite bearing pegmatites crosscutting the host gneisses at Icebound Lake and Cariboo Alp produced plateau dates of 50.6 ± 0.3 and 51.3 ± 0.4 Ma. Muscovite from garnet–muscovite bearing granitic pegmatites in the Plant Creek area, interpreted as

being part of the Ladybird granite suite, produced plateau dates of 50.7 ± 0.3 Ma and 50.9 ± 0.3 Ma. These pegmatites all crosscut the foliation in the host rocks (garnet–sillimanite–biotite schist and psammite, respectively), and do not have chilled margins or any internal foliation. The $^{40}\text{Ar}/^{39}\text{Ar}$ dates obtained from muscovite samples in pegmatites at Icebound Lake (the dome), Cariboo Alp (the structurally lowest rocks overlying the dome), and Plant Creek (the structurally highest rocks overlying the dome) represent cooling ages for the Ladybird pegmatites of the area of c. 51 – 50.5 Ma. It is also possible that these muscovite ages could be crystallization ages for the pegmatites because in areas where rapid cooling takes place crystallization and cooling dates may be indistinguishable within error (McDougal and Harrison 1999). Cooling rates for this area are discussed in section 5.4.5. The $^{40}\text{Ar}/^{39}\text{Ar}$ dates obtained from muscovite samples in leucosomes at Cariboo Alp (the structurally lowest rocks overlying the dome) represent crystallization ages for greenschist facies retrograde metamorphic assemblages in the formerly migmatitic K-feldspar–sillimanite–melt-bearing amphibolite facies rocks at c. 51 – 50.5 Ma.

5.5.4 Cooling ages versus reset ages

Some of the above mentioned $^{40}\text{Ar}/^{39}\text{Ar}$ dates from the metamorphic rocks hosting Ladybird granite can be interpreted as being reset by the intrusion of the Ladybird granite, or as representing dates where the cooling was delayed by the presence of the Ladybird granite. This is seen in the hornblende samples from the Mount Symonds,

North Fosthall, Mount Baldur, Twin Peaks and Cariboo Alp. These areas are either within the boundaries of the South Fosthall pluton, or in areas with voluminous granite intrusions as discussed in section 2.2.3. It is likely that at least part of the Ladybird granite intrusion history occurred when the country rock temperature was above greenschist facies conditions. Evidence for this interpretation includes a lack of greenschist facies overprint on the main metamorphic assemblages, a lack of chilled margins in Ladybird pegmatites, and the ductile nature of post-transposition northeast directed folding in these rocks.

The closure temperatures of argon in hornblende, in this study are between 490 and 550 °C (sections 5.3.5 and 5.4.1). This study proposes that the pluton introduced enough heat into the surrounding rocks to delay the cooling of hornblende through its T_c. This is likely since the end of upper amphibolite facies metamorphism overlapped with or shortly preceded the intrusion of the first phases of Ladybird granite. The hornblende ⁴⁰Ar/³⁹Ar dates are therefore appropriate cooling ages, with the qualifying statement that it reflects a thermal regime heavily influenced by intrusive activity and does not only reflect cooling after initial upper amphibolite facies metamorphism.

It is important to note that even through the ⁴⁰Ar/³⁹Ar ages we interpret as being reset, or influenced by the thermal regime of the Ladybird granite, these ages still have geological significance because they provide information on the thermal state of the

rocks in this structural section during the Paleocene – Eocene. All the biotite ages in this study, whether we interpret them as reset, reheated biotite cooling ages or cooling ages through T_c are all within the 52.5 – 51.0 Ma range. This is interpreted as evidence for widespread cooling through 300 °C over the entire structural section at this time.

5.5.5 Cooling rates

In some samples, where robust $^{40}\text{Ar}/^{39}\text{Ar}$ plateau dates were obtained from hornblende and biotite, cooling rates for rocks are estimated using closure temperatures (Figure 5.2) of 500 °C for hornblende and the corresponding (i.e. same cooling rate input) 300 °C for biotite. Closure temperatures for the mineral pairs change in the same proportions when cooling rates vary (see Figure 5.2); therefore, it can be assumed that relative temperature differences between the mineral pairs remains constant, with varying cooling rates.

DC080-H from Cusson Creek produced a hornblende cooling age of 62.7 ± 0.7 Ma, and biotites from the same rock produced a cooling age of 51.3 ± 0.3 Ma giving a calculated cooling rate of 20 °C/Ma. This cooling rate is still valid, regardless of the hornblende age being interpreted as a reset cooling age, because the reheated rocks would have cooled from above their hornblende closure temperatures after the intrusion of the Ladybird granite. In sample DC186, a migmatitic hornblende–biotite calc-silicate gneiss from Cariboo Alp, hornblende from the matrix produced a plateau age of 56.2 ± 0.6 Ma for

the 250 – 300 μm fraction (plateau includes 94.8% ^{39}Ar), and biotite from the gneissic bands produced ages of $51.2 \pm 0.4 \text{ Ma}$ (100 – 200 μm) and $50.7 \pm 0.3 \text{ Ma}$ (250 μm), giving a calculated cooling rate of $\sim 40 \text{ }^\circ\text{C}/\text{Ma}$. The faster cooling rate for the Cariboo Alp sample reflects the fact that the Cariboo Alp rocks have hornblende cooling ages that are younger than those at Cusson Creek, but that both areas have the same biotite cooling ages. Therefore, the rocks at Cariboo Alp cooled faster than those higher in the structural section at Cusson Creek.

Using the $^{40}\text{Ar}/^{39}\text{Ar}$ thermochronology data reported in this study we have constructed cooling rates for different structural levels in the study area. The cooling ages of hornblende, biotite and muscovite provide information on cooling histories and cooling rates for the temperature range between $\sim 600 \text{ }^\circ\text{C}$ and $280 \text{ }^\circ\text{C}$. Zircon, monazite and titanite ages provide constraints on the timing of anatexis, intrusions, and thermal peak metamorphism as well as deformation as outlined in Chapter 2. Cooling ages in pegmatites are not included since they may not accurately reflect the thermal state of the country rocks into which they intrude.

The rocks at Plant Creek cooled from $500 \text{ }^\circ\text{C}$ (c. 62 Ma to 58 Ma; upper and lower end of hornblende cooling age range) to $300 \text{ }^\circ\text{C}$ (c. 52 Ma), a difference of $200 \text{ }^\circ\text{C}$ in 10 million years or 6 million years. This is a cooling rate of between $20 - 33 \text{ }^\circ\text{C}/\text{Ma}$. The rocks at Fawn Lakes cooled from $500 \text{ }^\circ\text{C}$ ($\sim 58 \text{ Ma}$) – $300 \text{ }^\circ\text{C}$ (52 Ma), a difference of $200 \text{ }^\circ\text{C}$ in 6

million years, giving a cooling rate of 33 °C/Ma. The rocks at Cariboo Alp on the upper margin of the Thor-Odin dome cooled from 500 °C (55 Ma) to 300 °C (52 Ma), a difference of 200 °C in 3 million years, giving a cooling rate of 66 °C/Ma. In the absence of hornblende cooling dates from the dome, the timing of peak metamorphism and anatexis by Norlander et al. (2002) and Hinchey et al. (2006) can be used to estimate cooling rates. Using peak metamorphism of 650 °C at c. 56 Ma, with the biotite cooling age of c. 52 Ma, a change of 450 °C in 4 million years occurred, giving a cooling rate of ~112 °C/Ma or higher. These calculated ranges of cooling rates support the hypothesis that the cooling rate in the lower structural level towards the Thor-Odin dome is faster than in the overlying panel of rocks, and was fastest in the northern areas of the study where the Columbia River fault cuts deeper into the structural section.

Rapid cooling rates of >100 °C/Ma from high temperature conditions >650 °C like the ones documented in this study and in other studies of the Thor-Odin dome (Norlander et al. 2002; Vanderhaeghe et al. 2003; Hinchey et al. 2006) have also been documented in the Grand Forks Complex (Cubley et al. 2013a, 2013b), Valhalla Complex (Gordon et al. 2008; Hallett and Spear 2011) and Okanogan Dome (Kruckenberg et al. 2008).

Kruckenberg et al. (2008) document biotite cooling ages of c. 48 – 47 Ma in the Okanogan Dome (Figure 1.1), and U-Pb zircon crystallization ages from migmatites between c. 61 Ma to 49 Ma. These ages show that anatexis and melt crystallization at high temperatures, >650 °C, happened over a protracted time period in the Paleocene –

Eocene and that cooling to ~300 °C (biotite cooling) was a rapid process. This is similar to previously reported data (this study, Vanderhaeghe et al. 2003; Hinchey et al. 2006); however, these studies also highlight that partial melting and the associated diapiric ascent of melt is not the only driving force behind cooling and exhumation of basement rocks. In Frenchman Cap dome, doming is proposed to be a result of channel flow up a pre-existing basement ramp along the Monashee décollement (Gervais and Brown 2011). A similar process of transport of rocks over a basement ramp (Hallett and Spear 2011) and decompression melting in pelitic rocks (Carr and Simony 2006) is likely responsible for the structural culmination in the Valhalla dome. In Thor-Odin dome decompression melting (Norlander et al. 2002) and anatexis occurred during northeast directed transport before c. 56 Ma and the dome had cooled through 300 °C by c. 52 – 51 Ma, indicating that the transition between thermal peak metamorphism and cooling in the structurally deepest rocks of the Thor-Odin dome occurred very rapidly.

5.5.6 The nature of the boundary between the Thor-Odin dome and overlying rocks at Cariboo Alp

The structural history at Cariboo Alp (Figures 1.2, 1.3, and 3.2) and the nature of the margin between the dome and overlying rocks has been interpreted a number of different ways, e.g. a Cretaceous to Paleocene ductile thrust fault (McNicoll and Brown 1995), the border of a Paleocene to Eocene diapir (Fayon et al. 2004; Norlander et al.

2002), or an Eocene ductile extensional shear zone involved in the exhumation of the rocks in the interior of the Thor-Odin dome (Kruse and Williams 2007).

Biotite $^{40}\text{Ar}/^{39}\text{Ar}$ cooling ages are the same (c. 52.5 – 51.0 Ma) regardless of lithology or structural level on both sides of the proposed extensional shear zone (Kruse and Williams 2007) at Cariboo Alp. This shows that the rocks structurally above and below Cariboo Alp cooled through biotite closure temperature at the same time. The geometry of the southwest dipping package of rocks with their southwest dipping transposition foliation in Cariboo Alp (Figures 1.3 and 2.14) and the similar southwest dipping rocks, with the same transposition foliation, were therefore all created before the Paleocene to Eocene cooling and exhumation of the dome. This interpretation is also supported by the muscovite thermochronology data. Muscovite cooling and crystallization ages (section 5.4.3), at and below Cariboo Alp are identical (c. 51 – 50.5 Ma). The muscovite crystallization ages date the onset of retrograde greenschist facies metamorphism at the same time structurally above and below Cariboo Alp, and the evidence of greenschist facies overprint is not penetrative throughout the rocks but is limited to structures interpreted as extension-related (section 2.5).

The Cariboo Alp area did not accommodate km-scale extension or significant reactivation related to exhumation during the Eocene because there is no gap between the biotite and muscovite cooling ages above, below or at Cariboo Alp. Based on these

cooling and metamorphic histories there is no evidence for a significant post-cooling or post-metamorphic break between the rocks of the dome and the rocks overlying the dome at Cariboo Alp such as the Thor-Odin high strain zone proposed by Kruse and Williams (2007) or the border of a diapir (Norlander et al. 2002; Vanderhaeghe et al. 2003) on the flank of the Thor-Odin dome. If Cariboo Alp represents a shear zone, any movement along it must have taken place at temperatures higher than 550 °C (hornblende T_c), and before c. 58 Ma (end of transposition foliation), after which rocks on both sides equilibrated and cooled together to 300 °C by c. 52 Ma. This would make the Cariboo Alp High Strain Zone of Kruse and Williams (2007) older than the Columbia River fault, inconsistent with the proposed link between them.

5.5.7 Contribution of the Columbia River fault to cooling and exhumation of high grade rocks

Based on the ⁴⁰Ar/³⁹Ar thermochronology data presented here, and the integration of structural studies, U-Pb geochronology and metamorphic studies, we can make some general conclusions about the timing of major crustal scale events in the Thor-Odin – Pinnacles area. The 62 – 55 Ma timing of regional cooling below 500 °C, in Mount Symonds, North Fosthall and Plant Creek, in part predates the previously documented period of Columbia River fault activity at c. 55 Ma (Parrish et al. 1988). Ductile deformation in the Ladybird granites is recorded at c. 55 Ma, indicating syn-tectonic emplacement and is attributed to the initiation of movement on the Columbia River

fault (Parrish et al. 1988). It is also possible that earlier estimates of c. 55 Ma motion may be related to the formation of east-west stretching lineations during syn-deformational emplacement of granite. This process was described in the Paleocene to Eocene Pukeashun granite in the Adams – North Thompson segment of the Okanagan Valley – Eagle River fault system by Johnson (2006), and was attributed to the localization of granite in a step-over between normal faults. He proposed that the Ladybird granite in the South Fosthall pluton occurs in a similar structural context. His model of syntectonic granite emplacement and strain localization matches the interpretations of Carr (1992), proposing that the extent of mylonitic rocks described in the South Fosthall pluton (Carr 1992) suggests that the deformation does need a crustal scale fault to explain the intensity and extent of deformation.

Before c. 52.5 Ma it is likely that the Columbia River fault zone was already active (as documented by Parrish et al. 1988) but was limited to the structural levels of < 15 km depth where granite was being emplaced and had not propagated down to the level of the Thor-Odin dome rocks. This phase of activity on the Columbia River fault would correspond to early phases of extensional faulting due to gravitational collapse where normal faults involving only the mid-crust are coeval with thrusting in the foreland, in an overall compressional setting. The lower structural levels (e.g. the rocks of the Thor-Odin dome) were undergoing penetrative deformation while the upper levels (e.g. Plant Creek) were cooling. This is consistent with the interpretations in Chapter 2 that

propose the rocks of the Thor-Odin – Pinnacles area preserve several suprastructure-infrastructure transitions that occurred at different times.

By c. 52.5 – 51.0 Ma all structural levels were cooling through the closure temperature for argon in biotite, reflecting the change from regional compression to crustal scale extension. We propose that the main period of activity on the Columbia River fault falls between c. 52.5 and 50.5 Ma and is represented by: (i) biotite cooling ages; (ii) initiation of greenschist facies metamorphism documented by muscovite crystallization ages in the rocks at Cariboo Alp and Icebound Lake; and (iii) by cooling ages of muscovite in Ladybird pegmatites at Plant Creek, Cariboo Alp and Icebound Lake.

The preservation of at least four suprastructure-infrastructure transitions in the Thor-Odin – Pinnacles area (Chapter 2) with a generally downward younging progression of metamorphism and deformation documented throughout this structural section shows that neither metamorphism nor deformation was synchronous over the section. As the deformation front progressed downward, the upper levels were deactivated, and exhumation and cooling in the upper parts of the section were ongoing during transposition and folding in lower parts. The Columbia River fault dissects all four of these suprastructure-infrastructure transitions, and post-dates all of them.

Exhumation and cooling of the upper structural level in this study area is attributed to extension on the Columbia River fault zone in combination with erosion. Cooling and exhumation of the deeper structural levels, within Thor-Odin dome, is attributed to a component of buoyancy driven decompression. It is also possible that there is a complex extensional fault system with a ductile component at deeper levels (which would form shear bands). The contribution of the west-dipping Okanagan Valley – Eagle River fault system to the cooling and exhumation of the rocks in this study area cannot be ignored. Given the known displacements of 30 – 90 km on this fault system (Tempelman-Kluit 1989; Brown 2010) the upper plate could be restored as far east as this study area. Given that the timing of activity on the Okanagan Valley – Eagle River fault system (Brown 2010) overlaps the major c. 52.5 – 51.0 Ma cooling period described here, it is permissible to propose that this study area is cooled and exhumed partly through a west-directed extensional fault in combination with the east dipping Columbia River fault.

It has been noted that the Columbia River fault experienced periodic pulses of movement in its later history up to 35 Ma (Lorenca et al. 2001), so it is not unreasonable that its early activity should also indicate different stages of movement. By c. 48 Ma, crustal extension was extensive, as indicated by the intrusion of mantle derived lamprophyre and syenite, which cross-cut rocks in all structural levels, and are associated with brittle faulting throughout the study area. This phase of cooling and

extension would correspond to extension in which normal faulting occurs on a crustal scale once thrusting and compressional deformation has largely ended (Fossen 2000). The thermochronology data presented in this study, specifically the biotite and muscovite cooling and crystallization ages, therefore helps to place additional constraints on the timing of the regional switch from transpression to transtension in this part of the Cordillera.

The cooling history proposed in this study is consistent with recent work in the Grand Forks Complex bound by the Kettle River and Granby faults, and the western margin of the Shuswap Complex bound by the Okanagan Valley – Eagle River fault system (Brown 2010; Cubley et al. 2012, 2013a). Cubley et al. (2012, 2013a) report cooling ages in the Grand Forks Complex that indicate cooling through 500 – 550 °C at c. 54 Ma, and through 280 – 300 °C at c. 51 Ma. The authors propose a 2-stage cooling history based on apatite fission track data, showing an initial fast phase of cooling (before c. 51 Ma) followed by 15 million years of slower cooling and exhumation. This two stage history is also proposed for the Okanagan Valley – Eagle River fault by Brown (2010) who reported biotite cooling ages between c. 51 and 48 Ma. These interpretations are similar to the proposed rates and timing for Thor-Odin dome by Lorenca et al. (2001). In the case of Thor-Odin dome the thermochronology presented here also helps to place robust constraints on the timing of the regional switch from transpression to transtension in

the Eocene evolution of the Thor-Odin – Pinnacles area of the southern Cordillera at c. 52.5 – 51 Ma.

5.6 Conclusions and implications

Cooling histories of different structural levels were examined using U-Pb zircon, monazite and titanite geochronology data in conjunction with new hornblende, biotite and muscovite $^{40}\text{Ar}/^{39}\text{Ar}$ data (Figure 5.49 and 5.50). All data, with locations, are presented in Figure 5.51. Hornblende cooling ages between c. 62 and 58 Ma represent cooling after regional metamorphism and penetrative deformation. Hornblende cooling ages between c. 58 and 55 Ma represent reset cooling ages, strongly affected by the thermal regime of the Ladybird granite suite, particularly in the vicinity of the South Fosthall pluton. Biotite cooling ages between c. 52.5 and 51.0 Ma across the entire study area represent a major cooling event, both in the metamorphic country rock and in pegmatites of the Ladybird granite suite.

Muscovite ages of c. 51 Ma represent the cooling age for muscovite in granitic pegmatites of the Ladybird granite suite. In these pegmatites the cooling age is likely close to the crystallization age because of the fast cooling rates documented in this area, at this time. Muscovite ages of c. 51.0 – 50.5 Ma, documented in greenschist facies metamorphic assemblages, represent muscovite growth below closure temperatures, and date the onset of retrograde metamorphism.

It is necessary to integrate $^{40}\text{Ar}/^{39}\text{Ar}$ thermochronology data with other data sets (i.e. structural, metamorphic and U-Pb geochronology studies) in order to understand whether the dates represent cooling of regional metamorphism through T_c , reheating or sporadic intrusions and local heating. By integrating the $^{40}\text{Ar}/^{39}\text{Ar}$ thermochronology results with previous work on the timing of regional metamorphism and deformation, this work has documented progressively deeper zones preserving the transition between suprastructure and infrastructure (see Chapter 2, this study). This study shows that the upper structural levels of the study area were cooling through the hornblende closure temperature of 550°C while lower structural levels were still being penetratively deformed. The narrow range of biotite cooling ages from all structural levels indicate a regional cooling event which shows that all of the rocks involved cooled through biotite closure temperatures over a 1.5 million year period between 52.5 and 51.0 Ma. This suggests that either all the rocks were at a similar crustal level (i.e. at a similar isotherm), or that cooling rates across the area were rapid, recording the same range of cooling dates over different structural levels.

There is no syn- or post-metamorphic break at Cariboo Alp on the southwestern flank of the Thor-Odin dome, proving it is not an Eocene age extensional shear zone (Kruse and Williams 2007). Similarly, Cariboo Alp does not represent the border of a diapir

(Vanderhaeghe et al. 1999, 2003), because the structures in the area are northeast verging compressional structures and do not indicate any component of flattening away from the Thor-Odin dome that would be expected in a diapir. Cariboo Alp is best interpreted as a zone of infrastructural flow (see Chapter 4 of this study) being penetratively deformed before c. 58 Ma, in a compressional shear zone or flow zone that transported rocks with Proterozoic protoliths (see Chapter 2 of this study) over Laurentian margin basement and cover rocks during the youngest Eocene compressional phase of the Cordilleran orogeny. The tilted geometry of the southwest dipping panel at Cariboo Alp juxtaposed with rocks of the Thor-Odin dome was created before cooling, and was in place before the Paleocene – Eocene period discussed here.

The 62 – 58 Ma hornblende cooling ages from the Plant Creek and South Fosthall areas are not related to motion on the Columbia River fault because they predate the c. 58 – 55 Ma age range suggested for the initiation of motion (Parrish et al. 1988). The period between c. 52.5 – 51.0 Ma, defined by the biotite cooling ages across the whole study area, is interpreted as a major period of regional cooling as a result of exhumation due to motion on the Columbia River fault extensional fault system, with erosional contributions. This is a major period of motion on the fault. This is consistent with similar cooling ages (c. 52 – 50 Ma) across the Okanagan Valley – Eagle River fault system to the west of our study area, which provides evidence for a regional scale extensional regime. The growth of retrograde metamorphic minerals (muscovite

crystallization ages, c. 51 – 50.5 Ma) is further evidence for widespread cooling and crustal scale extension. The thermochronology data presented in this study therefore helps to place robust constraints on the timing of the regional switch from transpression to transtension in the Thor-Odin – Pinnacles area of the southeastern Cordillera at c. 52.5 – 51 Ma.

Table 5.1 Sample locations and rock types for thermochronology.

Sample	Northing	Easting	Location	Rock
DC004	5578185	421973	North Plant Rd	Plagioclase amphibolite
DC028	5573777	413370	Plant Rd, Sp A, Br 30	Garnet–muscovite–biotite schist
DC048	5573508	410254	Plant Rd, Sp A, Br 30	Amphibolite
DC058	5574477	412261	Plant Rd, Sp A, Br 30	Ladybird pegmatite
DC080	5571584	415929	South Cusson Rd	Calc-silicate amphibolite
DC169	5597854	416000	Cariboo Alp	Amphibolite
DC176	5597846	415957	Cariboo Alp	Calc-silicate gneiss
DC178	5597357	415648	Cariboo Alp	Biotite–quartzofeldspathic gneiss
DC186	5597310	415626	Cariboo Alp	Calc-silicate gneiss
DC188	5597266	415554	Cariboo Alp	Plagioclase amphibolite
DC191	5597218	415496	Cariboo Alp	Garnet amphibolite
DC193	5597218	415496	Cariboo Alp	Garnet–sillimanite–biotite paragneiss
DC195	5597218	415496	Cariboo Alp	Amphibolite
DC209	5588095	417457	Bear Lake Rd, N. Fosthall	Plagioclase amphibolite
DC219	5588920	417587	Bear Lake Rd, N. Fosthall	Calc-silicate amphibolite
DC239	5584816	427976	N Fosthall, Br 30	Calc-silicate gneiss
DC295P	5572965	426367	Cameron Lake Rd, Br 5	Ladybird pegmatite
DC299	5572143	426826	Cameron Lake Rd, Br 5	Calc-silicate gneiss
DC320	5595822	414378	Fawn Lakes	Garnet amphibolite
DC326	5596366	415415	Fawn Lakes	Biotite semipelite
DC330	5596684	415500	Fawn Lakes/Cariboo Alp	Biotite–quartzofeldspathic gneiss
DC342	5592908	420255	Mount Symonds	Garnet amphibolite
DC370	5591819	419742	Mount Symonds	Amphibolite in core of fold
DC395P	5592410	419823	Mount Symonds	Ladybird pegmatite
DC397	5592410	419823	Mount Symonds	Amphibolite next to pegmatite DC398
DC398	5592410	419823	Mount Symonds	Ladybird pegmatite
DC400	5592142	419627	Mount Symonds	Amphibolite
DC414	5591957	420696	Mount Symonds	Amphibolite infolded with paragneiss and granite

Sample	Northing	Easting	Location	Rock
DC418	5598435	415757	Icebound Lake	Ladybird pegmatite
DC423	5598524	416071	Icebound Lake	Garnet amphibolite
DC439	5598537	416071	Icebound Lake	Migmatitic biotite–garnet–quartzofeldspathic gneiss
DC446	5598579	415951	Icebound Lake	Boudin of amphibolite in layer within migmatite
DC450	5598537	416071	Icebound Lake	Biotite layer in gedrite–anthophyllite amphibolite
DC457	5586605	409858	Twin Peaks	Calc-silicate amphibolite
DC464	5587098	411440	Twin Peaks	Garnet amphibolite
DC468	5587274	410993	Twin Peaks	Garnet calc-silicate amphibolite
DC469	5587283	410739	Twin Peaks	Plagioclase amphibolite
DC473	5587415	409940	Twin Peaks	Calc-silicate amphibolite
DC476	5587944	410064	Twin Peaks	Amphibolite
DC502	5597301	415520	Cariboo Alp	Tourmaline muscovite pegmatite
DC510	5597598	415797	Cariboo Alp	Leucosome in biotite–quartzofeldspathic gneiss
DC511	5597598	415797	Cariboo Alp	Leucosome in biotite–quartzofeldspathic gneiss
DC512	5597598	415797	Cariboo Alp	Leucosome in biotite–quartzofeldspathic gneiss
DC515	5597198	415444	Cariboo Alp	Leucosome in biotite–quartzofeldspathic gneiss
DC519	5597598	415797	Cariboo Alp	Leucosome in biotite–quartzofeldspathic gneiss
DC528	5507180	415450	Cariboo Alp	Leucosome in biotite–quartzofeldspathic gneiss
DC532	5598459	416085	Icebound Lake	Gedrite anthophyllite
DC536	5598550	415841	Icebound Lake	Garnet–biotite–plagioclase anthophyllite
DC538	5598550	415988	Icebound Lake	Muscovite pegmatite in quartzofeldspathic gneiss
DC543	5598562	415995	Icebound Lake	Muscovite pegmatite in quartzofeldspathic gneiss
AH-02-003	5600049	423426	Frigg Glacier	Folded garnet amphibolite
AH-02-004	5600302	423299	Frigg Glacier	Folded garnet amphibolite
AH-02-013	5600386	423453	Frigg Glacier	Crosscutting phenocrystic granitic leucosome
AH-02-022	5605064	423568	Mt. Thor	Sillimanite–garnet–muscovite–biotite schist
AH-03-021	5598790	419186	Bearpaw Lake	Hornblende–K-feldspar–plagioclase paragneiss
AH-03-024	5598068	418812	Bearpaw Lake	Garnet amphibolite
AH-03-029	5598511	418497	Bearpaw Lake	Garnet amphibolite
AH-03-032	5586113	416111	Mt Baldur	Ladybird garnet–muscovite biotite granite

Table 5.2 $^{40}\text{Ar}/^{39}\text{Ar}$ data for samples from all study areas which include 80% or more ^{39}Ar in a robust plateau age. Numbers in column 1 correspond to numbers in Figure 5.51.

Sample	Location	Mineral	Size μm	Integrated Age	Error	Correlation Age	Error	% ^{39}Ar	Plateau Age	Error	% ^{39}Ar	
58	DC080-H	Plant Creek	hbl	100-250	64.3	0.8	62.8	1.8	96.7	62.7	0.7	96.7
57	DC080-B2	Plant Creek	bt	>250	51.7	1.1	TF		51.7	1.1		
56	DC080-B1	Plant Creek	bt	100-250	51.2	0.3	51.4	0.4	93.9	51.3	0.3	97.8
55	DC058-1	Plant Creek	ms	>250	50.7	0.3	50.8	0.2	100	50.7	0.3	98.7
54	DC048-2	Plant Creek	hbl	>250	58.2	1.0	56.8	3.7	99.7	58.1	1.0	99.7
53	DC048-1	Plant Creek	hbl	100-250	60.4	1.8	60.9	8.6	91.5	60.1	1.8	96.4
52	DC028	Plant Creek	bt	100-250	52.1	0.4	52.1	0.3	100	52.1	0.4	99.7
51	DC299	North Fosthall (CL)	bt	>250	52.1	0.5	52.4	0.3	96.9	52.4	0.5	88.5
50	DC295P	North Fosthall (CL)	ms	>250	50.9	0.3	50.8	0.2	99.9	50.9	0.3	99.9
49	DC239	North Fosthall	hbl	>250	72.4	1.2	51.7	10.2	85.3	56.2	1.1	85.3
48	DC219-2	North Fosthall	hbl	>250	53.4	0.9	52.1	0.7	100	52.3	0.7	86.8
47	DC219-1	North Fosthall	hbl	100-250	55.4	1.1	54.2	2.0	100	55.0	1.0	98.9
46	DC209	North Fosthall	hbl	200-250	56.8	1.6	54.2	2.9	100	55.8	1.6	99.5
45	AH-03-032	North Fosthall (MB)	bt	>250	51.7	0.4	51.6	0.3	99.8	51.7	0.4	99.8
44	DC476-2	Twin Peaks	hbl	>250	60.3	1.7	54.0	7.4	99.2	57.3	1.4	97.5
43	DC476-1	Twin Peaks	hbl	200-250	58.9	2.1	55.1	8.0	99.3	57.5	2.0	99.3
42	DC473-2	Twin Peaks	hbl	>250	59.1	0.6	54.9	1.0	98.7	55.7	0.5	82.9
41	DC473-1	Twin Peaks	hbl	200-250	57.1	0.6	54.3	2.6	75.6	55.6	0.6	99.2
40	DC469-2	Twin Peaks	hbl	>250	58.1	0.9	55.0	3.1	93.1	55.7	0.8	97.6
39	DC469-1	Twin Peaks	hbl	100-250	56.4	0.9	55.8	1.6	93.7	55.3	0.9	93.7
38	DC468	Twin Peaks	bt	200-250	51.8	0.4	51.9	0.2	100	52.0	0.4	83.6
37	DC414	Mount Symonds	hbl	200-250	57.1	1.7	54.2	7.1	97.2	55.4	1.5	97.2
36	DC400	Mount Symonds	hbl	>250	53.2	0.8	52.2	1.8	92.0	52.2	0.7	92.0
35	DC398-2	Mount Symonds	bt S	2X2 mm	49.9	0.4	50.3	0.4	100	50.2	0.4	82.4
34	DC398-1	Mount Symonds	bt	1X3 mm	50.4	0.4	50.5	0.6	70.6	50.6	0.4	80.3
33	DC395	Mount Symonds	bt	>250	50.9	0.3	50.6	0.4	99.9	50.9	0.3	99.9
32	DC370	Mount Symonds	hbl	200-250	59.0	1.8	54.1	3.1	100	55.7	1.8	85.1
31	DC342	Fawn Lakes	hbl	>250	60.2	0.5	55.9	0.7	99.2	57.3	0.5	86.1
30	DC330	Fawn Lakes	bt	>250	52.0	0.4	52.3	0.2	98.2	52.2	0.4	98.2
29	DC326	Fawn Lakes	bt	>250	52.5	0.3	52.7	0.1	99.4	52.6	0.3	99.4
28	DC320	Fawn Lakes	hbl	>250	63.5	0.6	60.0	1.3	99.0	61.3	0.6	81.9

Sample	Location	Mineral	Size μm	Integrated Age	Error	Correlation Age	Error	% ^{39}Ar	Plateau Age	Error	% ^{39}Ar	
27	DC528	Cariboo Alp	ms	>250	50.6	0.4	50.8	0.5	100	50.6	0.4	100
26	DC519	Cariboo Alp	ms	>250	50.6	0.3	50.2	1.1	100	50.6	0.3	100
25	DC515	Cariboo Alp	ms	>250	50.6	0.3	50.5	0.4	100	50.6	0.3	100
24	DC512	Cariboo Alp	ms	>250	50.5	0.3	50.2	0.6	100	50.5	0.3	100
23	DC511	Cariboo Alp	ms	>250	50.0	0.4	51.0	1.2	100	50.9	0.4	100
22	DC502	Cariboo Alp	ms	>250	51.3	0.4	51.4	2.2	100	51.3	0.4	100
21	DC193	Cariboo Alp	bt	200-250	51.8	0.7	51.5	0.9	99.7	51.7	0.6	99.7
20	DC191-L	Cariboo Alp	bt R	2x3x0.7mm	51.6	0.4	51.8	0.4	99.3	51.6	0.4	99.7
19	DC191-1	Cariboo Alp	bt	2x3x0.1mm	51.6	0.4	51.2	1.1	99.2	51.6	0.4	99.2
18	DC188	Cariboo Alp	hbl	100-250	59.1	1.1	50.5	9.2	93.1	56.1	1.0	93.1
17	DC186-2H	Cariboo Alp	hbl	>250	64.0	0.7	54.6	2.3	98	56.2	0.6	94.8
16	DC186-LH	Cariboo Alp	hbl	>250	58.1	1.5	51.6	16.6	18.1	50.8	1.3	92.4
15	DC186-2B	Cariboo Alp	bt	>250	50.6	0.3	50.8	0.4	85.8	50.7	0.3	95.8
14	DC186-1B	Cariboo Alp	bt	100-250	51.1	0.4	51.2	0.3	98.1	51.2	0.4	98.1
13	DC178	Cariboo Alp	bt	200-250	51.1	0.4	51.3	0.2	100	51.1	0.4	97.3
12	DC176-2	Cariboo Alp	bt	>250	50.9	0.4	50.9	0.9	100	50.9	0.4	99.9
11	DC176-1	Cariboo Alp	hbl	200-250	54.1	0.4	52.6	0.8	87.4	53.6	0.4	87.4
10	DC169-2	Cariboo Alp	hbl	>250	63.5	0.9	53.9	4.8	91.4	57.3	0.8	82.9
9	DC450	Icebound Lake	bt	4X3 mm	54.6	0.7	54.9	0.5	100	54.7	0.6	99.4
8	DC543	Icebound Lake	ms	>250	50.6	0.3	50.0	1.9	100	50.6	0.3	98.6
7	DC536	Icebound Lake	bt	>250	53.0	0.3	53.1	0.5	100	52.9	0.3	100
6	DC532	Icebound Lake	bt	>250	57.1	0.5	57.5	0.8	96.6	56.9	0.5	96.5
5	DC439	Icebound Lake	bt	>250	52.2	0.4	52.2	0.2	100	52.2	0.4	99.8
4	DC418	Icebound Lake	bt	200-250	51.0	0.4	51.8	0.6	99.8	51.0	0.4	99.8
3	AH-03-021	Bearpaw Lake	bt	>250	52.3	0.3	52.2	0.3	100	52.3	0.3	100
2	AH-02-022	Mt. Thor	bt	>250	51.2	0.5	51.4	0.5	99.9	51.9	0.5	99.9
1	AH-02-013	Frigg Glacier	bt	>250	54.7	0.8	54.9	1.5	99.6	54.8	0.8	99.6

Table 5.3 $^{40}\text{Ar}/^{39}\text{Ar}$ data for samples from all study areas which are not considered robust because they do not include 80% or more ^{39}Ar in a plateau age.

Sample	Location	Mineral	Size μm	Integrated Age	Error	Correlation Age	Error	% ^{39}Ar	Plateau Age	Error	% ^{39}Ar
DC004-1	Plant Creek	hbl	100-250	71.4	0.7	58.5	3.5	55.2	62.1	0.7	46.9
DC004-2	Plant Creek	hbl	>250	64.2	0.6	57.8	1.8	72.1	59.4	0.6	72.1
DC457	Twin Peaks	hbl	200-250	68.9	0.7	55.4	2.2	99.8	57.3	0.7	68.1
DC464	Twin Peaks	hbl	200-250	58.0	0.7	54.5	2.2	92.7	56.3	0.7	67.2
DC397-1	Mount Symonds	hbl	100-200	93.3	1.2	55.3	6.0	89.1	69.6	2.3	19.7
DC397-2	Mount Symonds	hbl	>250	72.0	2.9	62.2	5.3	63.3	61.9	3.3	63.3
DC510	Cariboo Alp	ms	>250	52.6	0.4	48.8	0.7	67.8	50.5	0.4	75.3
DC195	Cariboo Alp	hbl	>250	57.9	0.8	53.6	1.2	99.3	55.2	0.8	75.8
DC186-1H	Cariboo Alp	hbl	100-250	65.3	0.9	57.4	1.5	76.9	57.4	0.9	67.0
DC169-1	Cariboo Alp	hbl	100-250	60.1	1.4	49.3	19.6	60.5	53.1	1.8	60.5
DC538	Icebound Lake	ms	>250	52.4	0.5	48.6	1.9	52.0	50.6	0.7	38.8
DC423	Icebound Lake	hbl	>250	62.5	0.7	47.0	18.4	73.6	57.6	0.7	72.0
DC446	Twin Peaks	hbl	>250	70.9	0.7	51.9	12.7	98.2	62.9	0.8	48.5
AH-03-024-1	Bearpaw Lake	hbl	100-250	85.5	1.1	74.5	2.8	59.9	74.4	1.0	59.9
AH-03-024-2	Bearpaw Lake	hbl	>250	89.4	0.7	77.1	2.7	71.1	77.9	0.7	54.7
AH-03-029-1	Bearpaw Lake	hbl	100-250	108.4	1.6	70.7	6.6	61.2	83.9	1.6	60.9
AH-03-029-2	Bearpaw Lake	hbl	>250	110.8	0.9	75.2	7.4	36.3	82.7	1.0	36.3
AH-02-003B	Frigg Glacier	bt	>250	65.5	0.6	65.3	7.8	50.0	65.9	0.6	77.9
AH-02-003H	Frigg Glacier	hbl	100-200	97.1	2.0	71.3	12.9	62.2	78.4	2.6	62.2
AH-02-004B	Frigg Glacier	bt	>250	57.6	0.6	53.6	10.4	64.9	60.1	0.7	64.9
AH-02-004H	Frigg Glacier	hbl	200-250	68.5	0.7	58.8	3.8	31.3	59.8	0.8	76.9

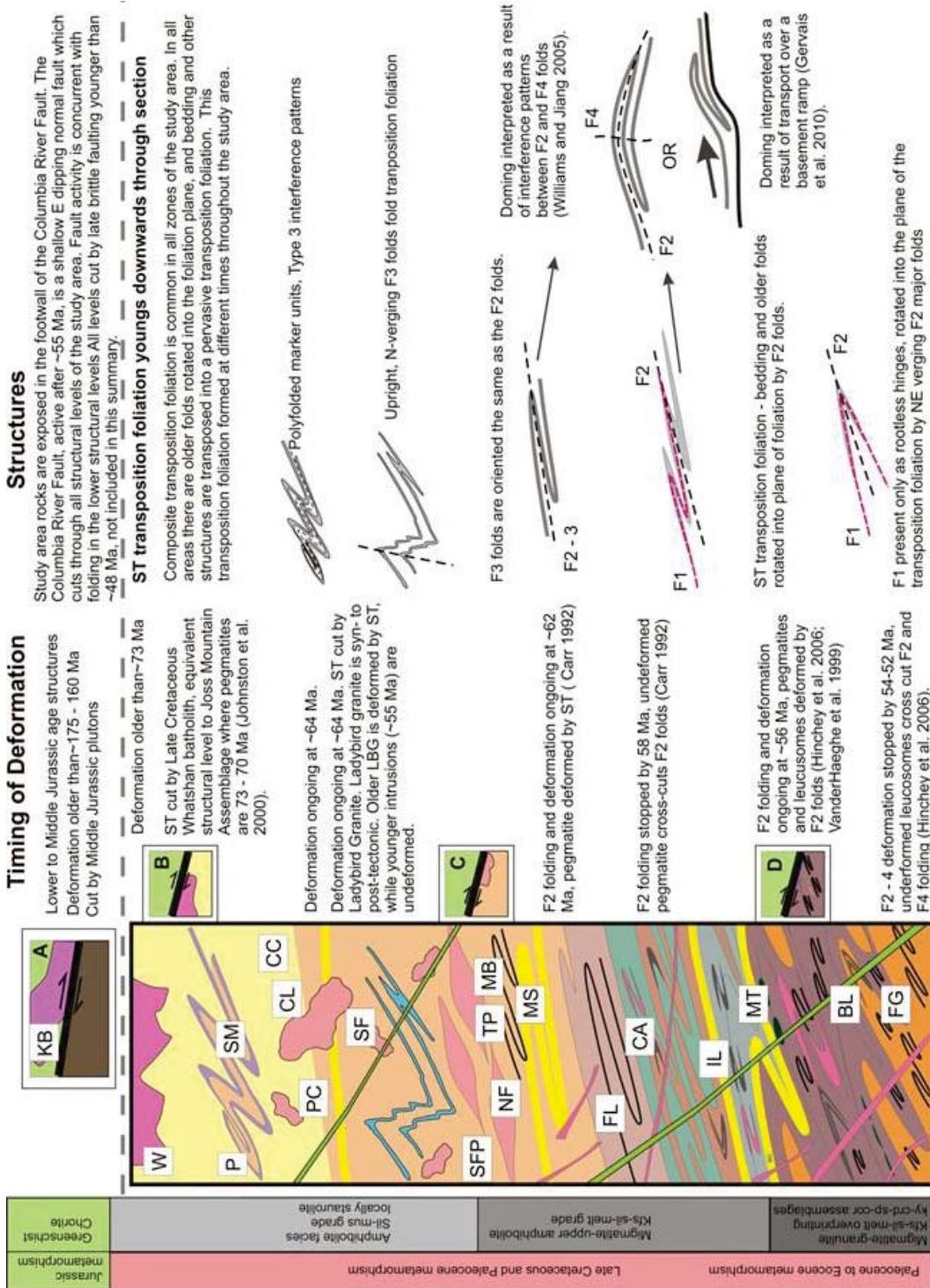


Figure 5.1 Structural styles and timing of deformation in the Thor-Odin – Pinnacles area.

Generalized tectonostratigraphic column of Thor-Odin – Pinnacles area showing the relative structural positions and structural styles of the different study areas, along with a summary of the ages of metamorphism and deformation as discussed in section 2.4. Total structural thickness is 15 – 17 km; repetitions of units are not illustrated here. The Columbia River fault cuts across structural levels in its footwall and the small boxes show the hanging wall and footwall geological relationships at different places along the trace of the fault. Specific areas discussed in the text are Bearpaw Lake (BL), Cameron Lake (CL), Cariboo Alp (CA), Cusson Creek (CC), Fawn Lakes (FL), and Frigg Glacier (FG). Icebound Lake (IL), Mount Baldur (MB), Mount Symonds (MS), Mount Thor (MT), North Fosthall (NF), Plant Creek (PC), Pinnacles (P), Saddle Mountain (SM), South Fosthall (SF), South Fosthall pluton (SFP), Twin Peaks (TP), and Whatshan batholith (W). (Data are from Read and Wheeler 1976; Archibald et al. 1983; Parrish and Wheeler 1983; Parrish and Armstrong 1987; Parrish et al. 1988; Coleman 1990; Fritz et al. 1991; Parkinson 1991; Carr 1990, 1991, 1992, 1995; Colpron et al. 1996; Vanderhaeghe et al. 1999; Johnston et al. 2000; Norlander et al. 2002; Gibson et al. 2003; Kuiper 2003; Thompson et al. 2004; Kruse et al. 2004; Adams et al. 2005; Glombick 2005; Hinchey et al. 2006, 2007; Lemieux 2006; and this study.)

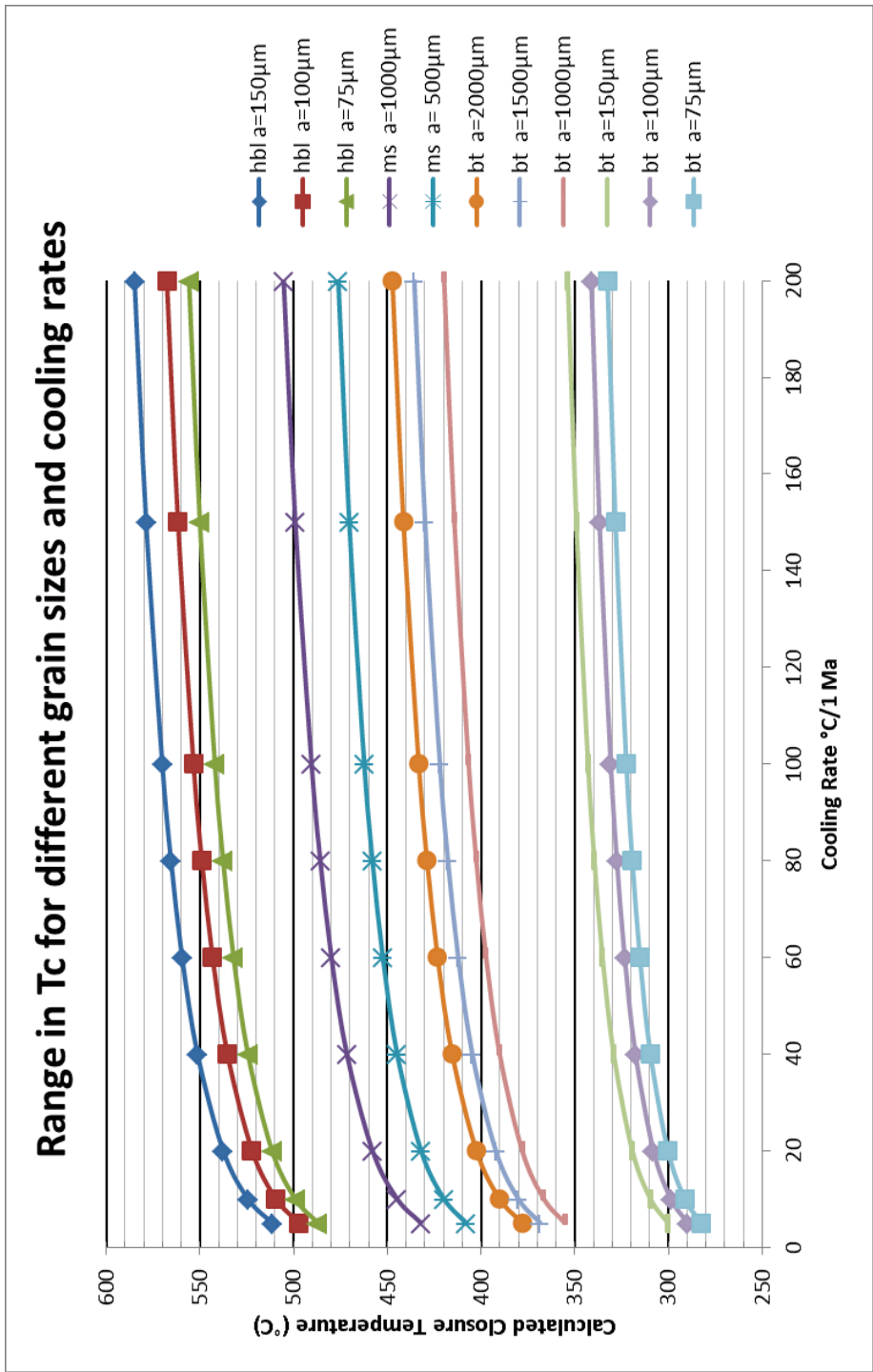


Figure 5.2 Range of closure temperatures for argon in hornblende, biotite and muscovite in this study. The grain radius and cooling rate are the most important variables in the calculation of closure temperatures.



50 cm

Figure 5.3 Garnet amphibolite DC446 boudin in migmatitic garnet–biotite–quartzofeldspathic gneiss at Icebound Lake. This photograph illustrates the migmatitic nature of the Thor-Odin dome basement gneiss. Hornblende from this sample did not produce a plateau date, most likely as a consequence of the Proterozoic protolith age of the host rock in which the amphibolite boudin is located.



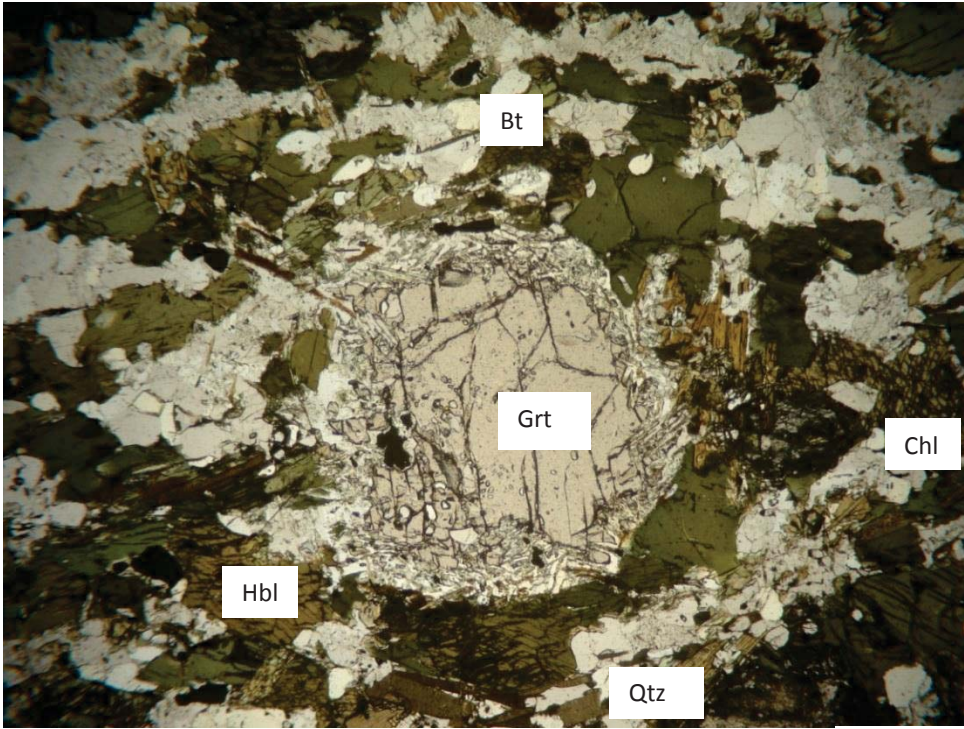
1 m

Figure 5.4 Garnet amphibolite layer DC423 in migmatitic garnet–biotite–quartzofeldspathic gneiss. The garnet amphibolite layers vary in thickness from 1 to 30 m and are surrounded by migmatitic gneiss. This amphibolite has the same mineralogy as sample DC446 in Figure 5.3 (Hbl–Grt–Plg–Qtz–Bt–Ttn) and is in the same host paragneiss.



10 cm

Figure 5.5 Details of garnet amphibolite DC423. Garnets range between 0.1 and 1 cm and some show reaction rims containing biotite, sillimanite and plagioclase. There are leucocratic layers of melt within the amphibolite.



0.5 mm

Figure 5.6a

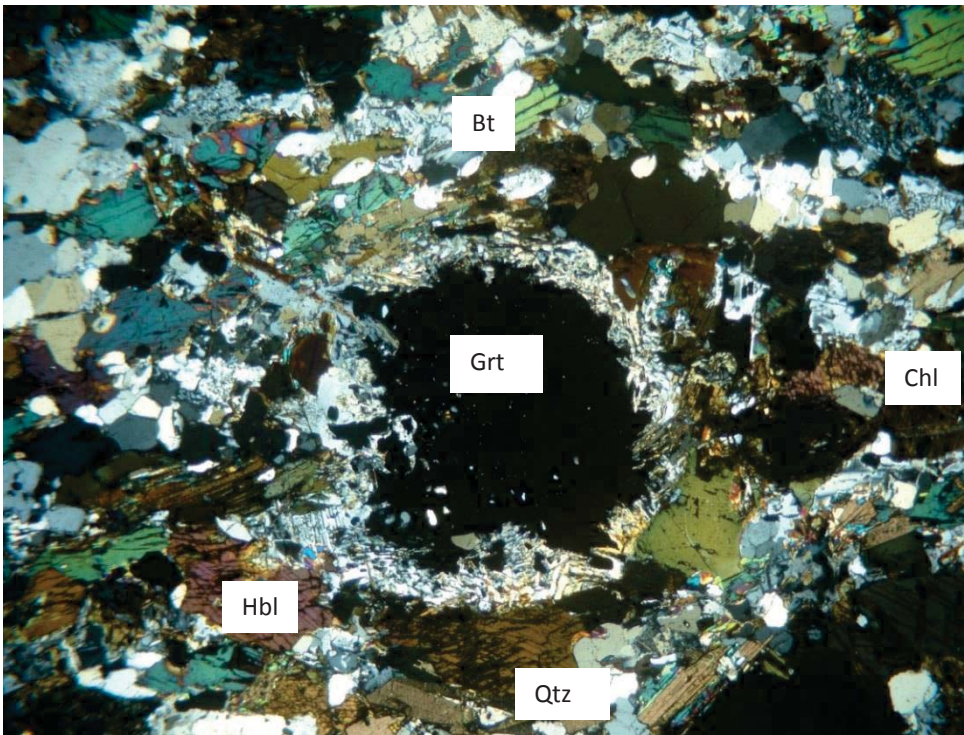


Figure 5.6b

Figure 5.6 Photomicrograph of garnet amphibolite DC423 in plane polarized light (a) and in cross polarized light (b). The photograph shows a reaction rim around the garnet, interpreted as a decompression reaction. The reaction $\text{Grt} = \text{Sil} + \text{Bt} + \text{Plg}$ indicates breakdown of garnet. This sample did not produce a plateau date. Some of the hornblende grains have small amounts of chlorite on their grain boundaries as pictured above.

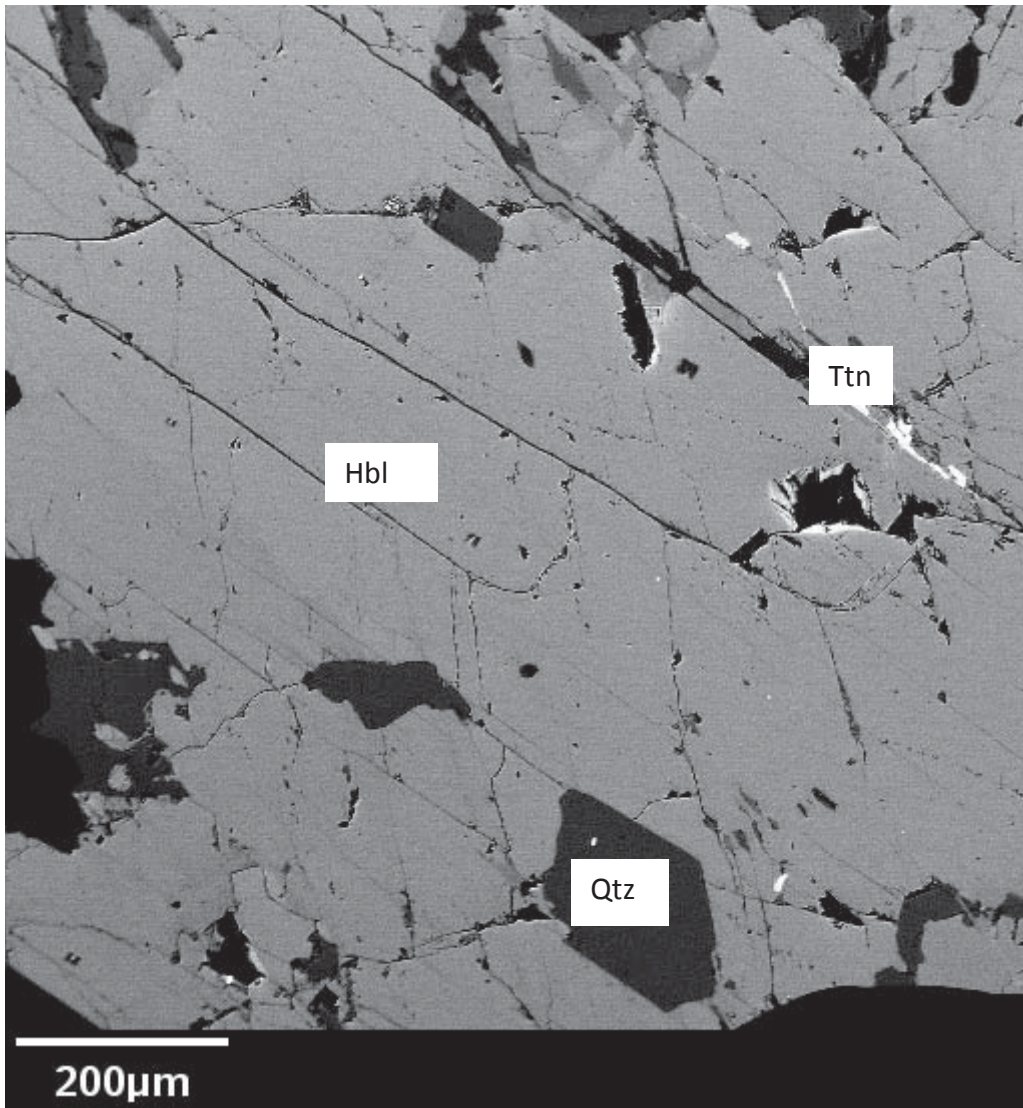
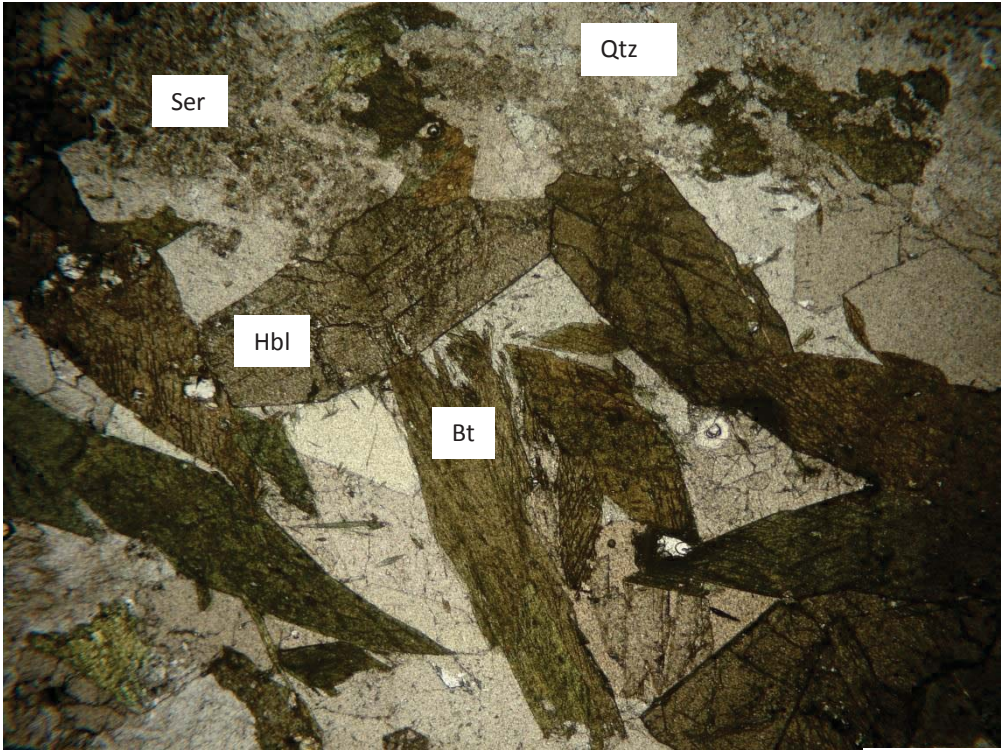


Figure 5.7 Electron microprobe image of a hornblende grain from sample DC169. This view shows distinctive amphibolite cleavage patterns without alteration minerals in grain boundaries or cleavage planes. This sample produced a plateau date of 57.3 ± 0.8 Ma.



50 cm

Figure 5.8 Calc-silicate amphibolite layer DC176 in grey sillimanite–biotite–quartzofeldspathic paragneiss at Cariboo Alp. The foliation in the amphibolite is concordant with the moderately dipping south to southwest dipping foliation in the host gneiss. This sample produced a plateau date of 53.6 ± 0.4 Ma, interpreted as a cooling age for the amphibolite and paragneiss. Biotite grains from the same amphibolite produced a plateau date of 50.9 ± 0.4 Ma.



0.5 mm

Figure5.9a

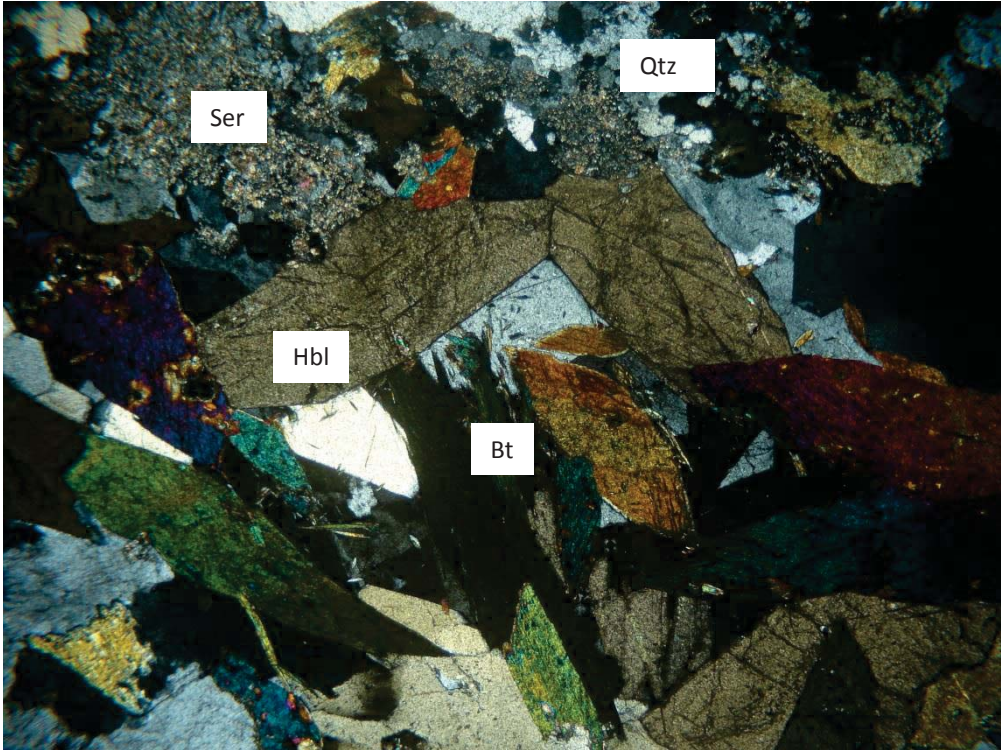
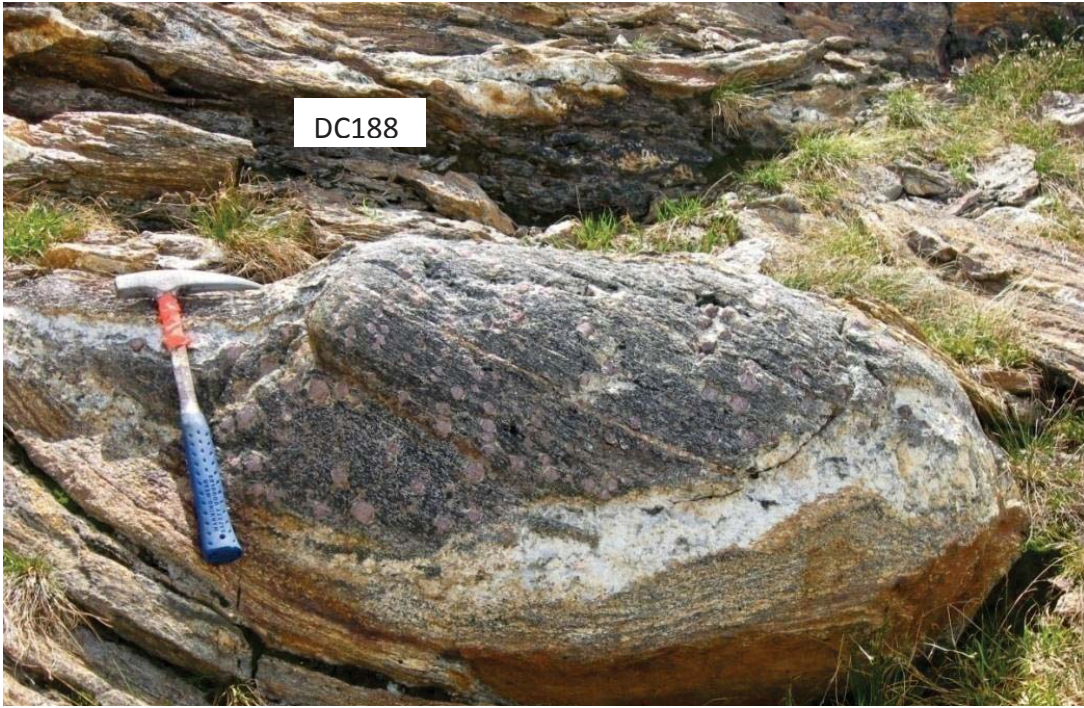


Figure 5.9b

Figure 5.9 Photomicrograph of amphibolite DC186 in plane polarized light (a) and in cross polarized light (b). Hornblende crystals appear unaltered, with clear grain boundaries. Sericitic alteration of feldspar is shown in the top left corner. This sample produced plateau dates of 56.2 ± 0.6 Ma for a 250 μm size fraction of hornblendes shown in the photograph, and 50.8 ± 1.3 Ma for a 350 μm piece of a 2cm hornblende crystal not pictured. The latter date is interpreted as representing only a fragment of a crystal, and is not representative of the main cooling ages for the area. It is within error of the c. 53 Ma cooling age of DC176 above. This sample also produced biotite plateau dates of 50.7 ± 0.3 Ma and 51.2 ± 0.4 Ma.



20 cm

Figure 5.10 Garnet amphibolite boudin in rusty garnet–sillimanite–biotite paragneiss at Cariboo Alp. The location of plagioclase amphibolite Sample DC188 is indicated. The transposition foliation in the paragneiss dips moderately to the southwest. The amphibolite boudin in the foreground contains a preexisting foliation dipping shallowly to the west. This sample produced a plateau date of 56.1 ± 1.0 Ma.

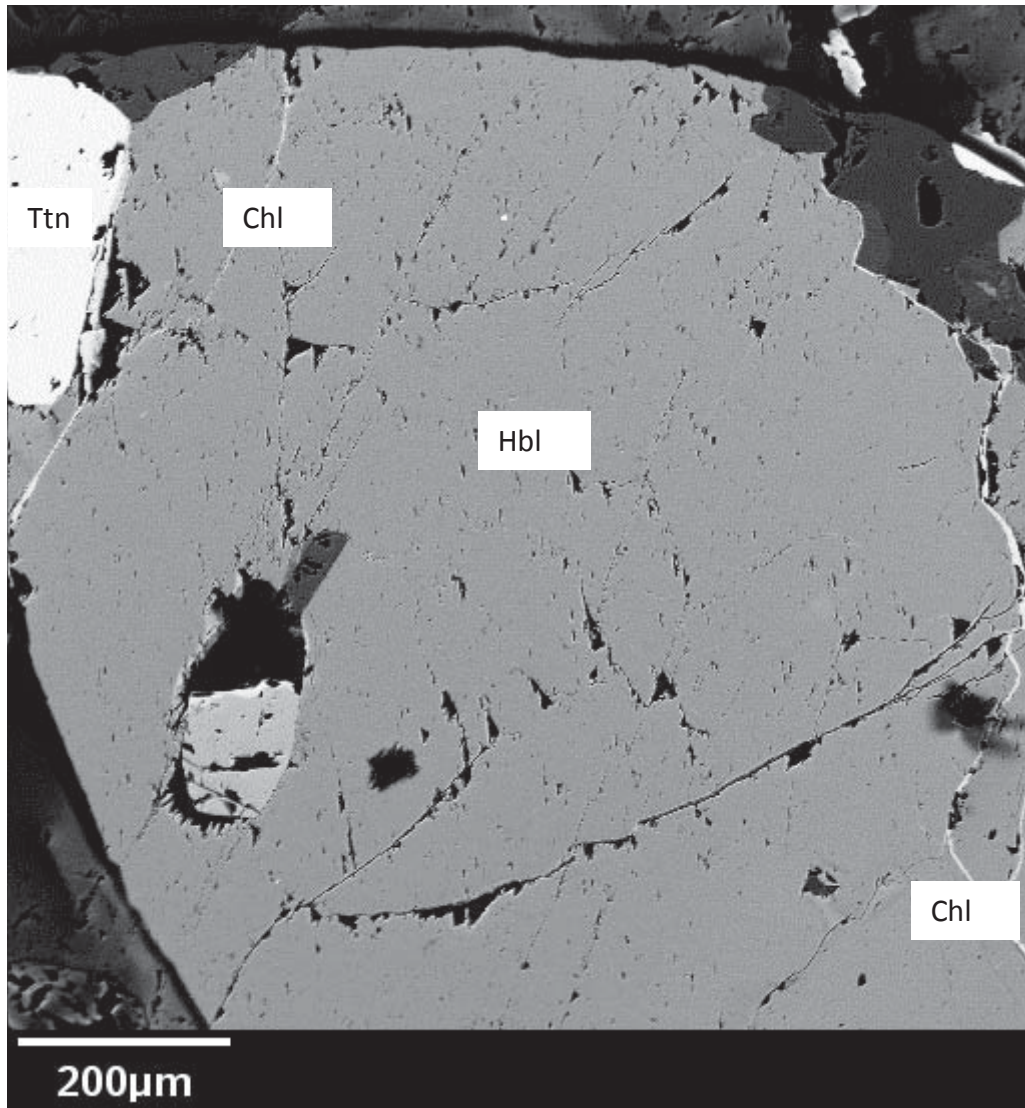


Figure 5.11 Electron microprobe image of a hornblende grain from sample DC188 showing minor chlorite alteration in some fracture planes.



5 cm

Figure 5.12 Garnet amphibolite sample DC320 in the western Fawn Lakes Assemblage south of Cariboo Alp. This sample consists of 55 % hornblende, 25 % quartz, 10% plagioclase and 10 % garnet. Hornblende crystals produced a plateau age of 61.3 ± 0.6 Ma. The Fawn Lakes Assemblage is a semi-pelitic paragneiss that extends from south of Cariboo Alp to the Mount Symonds area. Sample DC342, a garnet amphibolite from the same structural level pictured in Figure 5.13 is from the eastern part near Mount Symonds.



1 m

Figure 5.13 Garnet amphibolite DC342 in the Fawn Lakes Assemblage north of Mount Symonds. This sample is a quartz–plagioclase–garnet amphibolite (60 % hornblende, 25 % garnet, 10% plagioclase and 10 % quartz) and produced a plateau date of 57.3 ± 0.5 Ma.



10 cm

Figure 5.14 Amphibolite sample DC400 at Mount Symonds. This sample contains hornblende (60 %), plagioclase (20 %) and quartz (20 %). The weakly developed foliation is defined by hornblende crystals and is concordant with the regional south southwest dipping transposition foliation. This sample produced a plateau date of 52.2 ± 0.7 Ma, interpreted as a cooling age, possibly reset by the intrusion of the Ladybird granite in the area.



Figure 5.15a

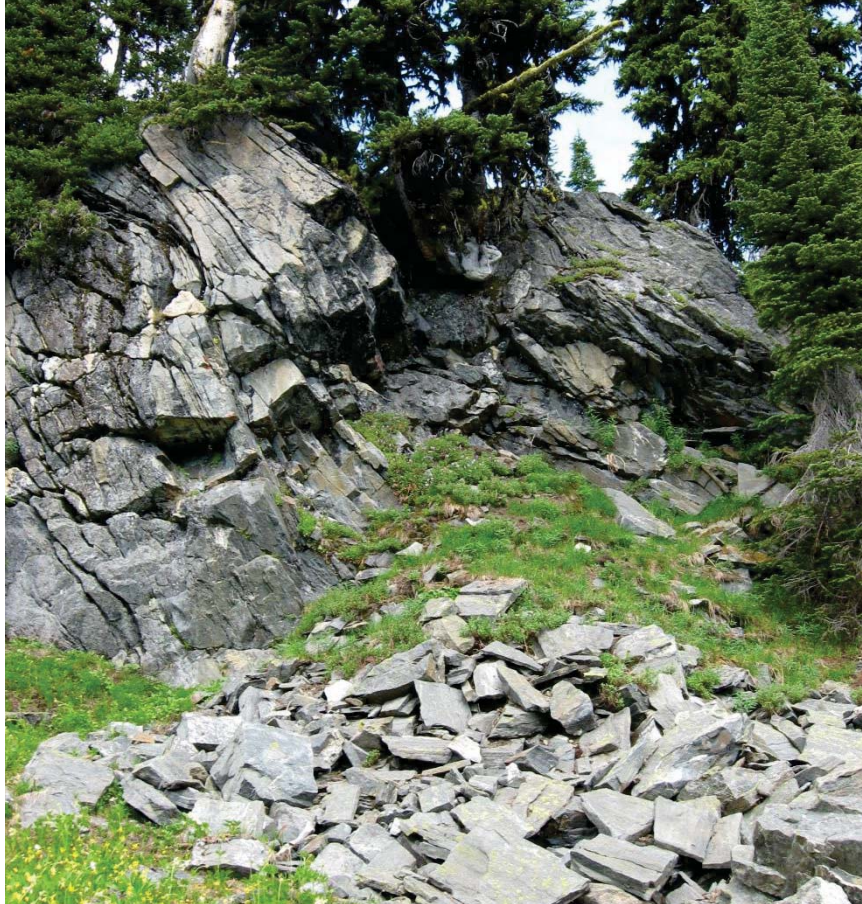
10 cm



Figure 5.15b

20 cm

Figure 5.15 Plagioclase amphibolite sample DC414 infolded with south dipping in garnet–sillimanite–biotite paragneiss and pegmatite of the Ladybird granite. This granite is deformed concordantly with the host paragneiss, indicating pre- or syntectonic granite intrusion. This sample produced a plateau age of 55.4 ± 1.5 Ma.



1 m



Figure 5.16 Amphibolite sample DC370 at Mount Symonds. This amphibolite forms the core of a syncline with a steeply south dipping axial plane. This sample produced a plateau age of 55.7 ± 1.8 Ma.



20 cm

Figure 5.17 Pegmatite and amphibolite interleaved along the south-southwest dipping transposition foliation at Mount Symonds. The pegmatites are deformed concordantly with the host paragneiss, indicating pre- or syntectonic intrusion. This amphibolite and surrounding paragneiss units are also shown in Figure 5.14. This sample of amphibolite did not produce a plateau age. The concordant pegmatite is sample DC395 that produced a biotite plateau ages of 50.6 ± 0.4 Ma and 50.2 ± 0.4 Ma.

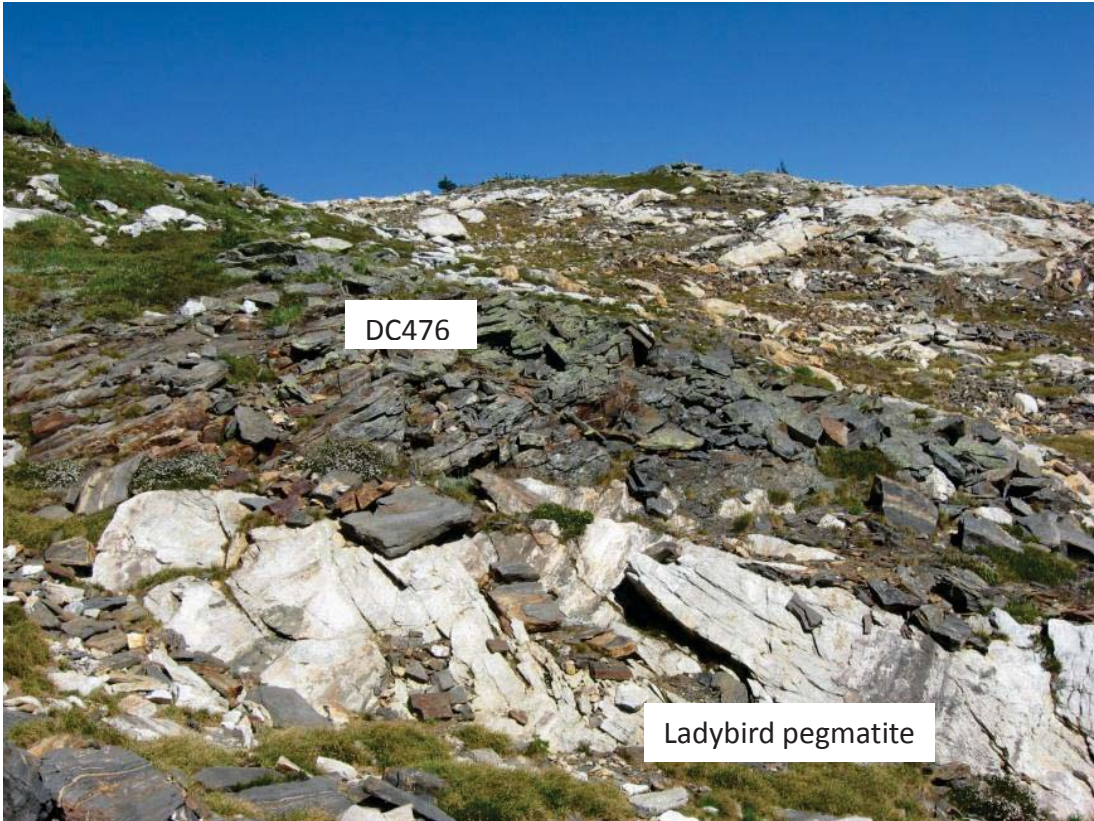


Figure 5.18 Pegmatite of the Ladybird granite crosscutting amphibolite at Twin Peaks.

This pegmatite is interpreted as a post-tectonic intrusion. The amphibolite contains 80% dark green to black hornblende, 20 % plagioclase and quartz in varying proportions throughout the outcrop, with trace amounts of biotite and titanite. This view looks toward the north, and the regional transposition foliation dips moderately south-southwest. This amphibolite sample produced hornblende plateau ages of 57.3 ± 1.4 Ma and 57.5 ± 2.0 Ma.



50 cm

Figure 5.19 Calc-silicate amphibolite DC473 at Twin Peaks. This sample consists of 80 % hornblende, with minor plagioclase (10 %), quartz (5%) and diopside (5 %). It is surrounded and crosscut by post-tectonic pegmatite of the Ladybird granite. The foliation in the amphibolite is concordant with the moderately south-southwest dipping transposition foliation in the area. This sample produced plateau dates of 55.7 ± 0.5 Ma and 55.6 ± 0.6 Ma.



Figure 5.20a

10 c m



Figure 5.20b

1 m

Figure 5.20 Amphibolites at Twin Peaks which did not produce plateau dates. Calc-silicate amphibolite DC457 (a) and garnet amphibolite DC464 (b) did not produce plateau dates with 80 % ^{39}Ar included in the plateau, but produced plateaus with dates of $57.3 \pm 0.7 \text{ Ma}$ (68.1% ^{39}Ar) and $56.3 \pm 0.7 \text{ Ma}$ (67.2% ^{39}Ar) respectively, within error of the dates indicated by the conservative plateau definition used in this study.



10 cm

Figure 5.21 Calc-silicate amphibolite gneiss DC219 in North Fosthall. This sample has a steeply south dipping foliation defined by layers of quartz and plagioclase, alternating with hornblende, diopside and minor biotite. This sample produced plateau dates of 55.0 ± 1 Ma and 52.3 ± 0.7 Ma.

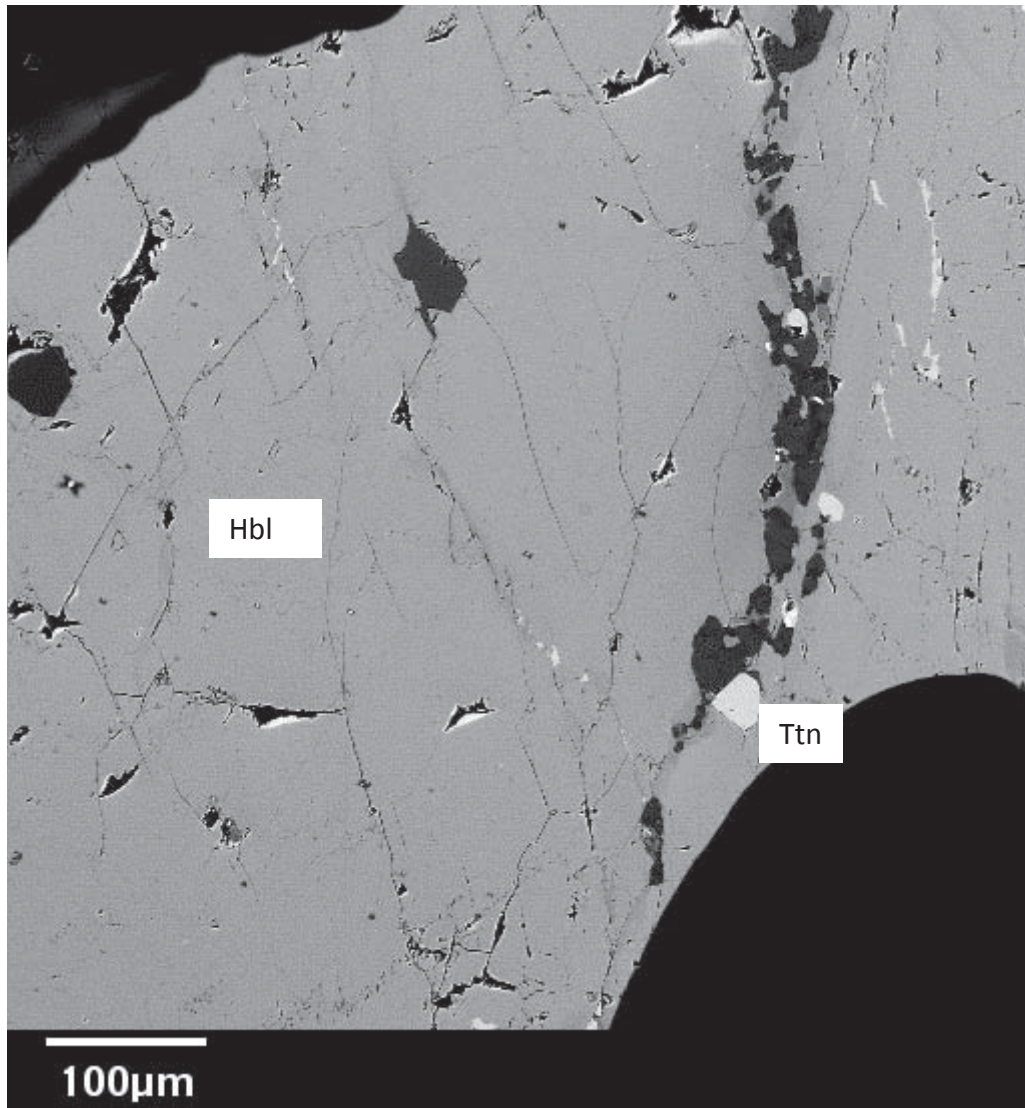


Figure 5.22 Electron microprobe image of hornblende in calc-silicate amphibolite gneiss DC219 showing fractures with a small titanite grain. Chlorite alteration is not visible in fracture planes or on grain boundaries.



10 cm

Figure 5.23 Exposure of foliated plagioclase amphibolite gneiss DC209 in the North Fosthall area. Foliation in the amphibolite is defined by hornblende and biotite alternating with plagioclase and quartz layers and dips shallowly to the south. The photograph also shows the relationship between the amphibolite and pegmatites of the Ladybird granite, boudinaged along the foliation planes, interpreted as indicating pre- or syn-deformational intrusion of pegmatites. This sample produced a plateau age of 55.8 ± 1.5 Ma.



1 m

Figure 5.24 Calc-silicate amphibolite gneiss in the North Fosthall area DC239 showing moderately south-southwest dipping foliation defined by gneissic banding of hornblende, diopside and biotite layers alternating with plagioclase and quartz layers. This sample produced a plateau age of 56.2 ± 1.1 Ma.

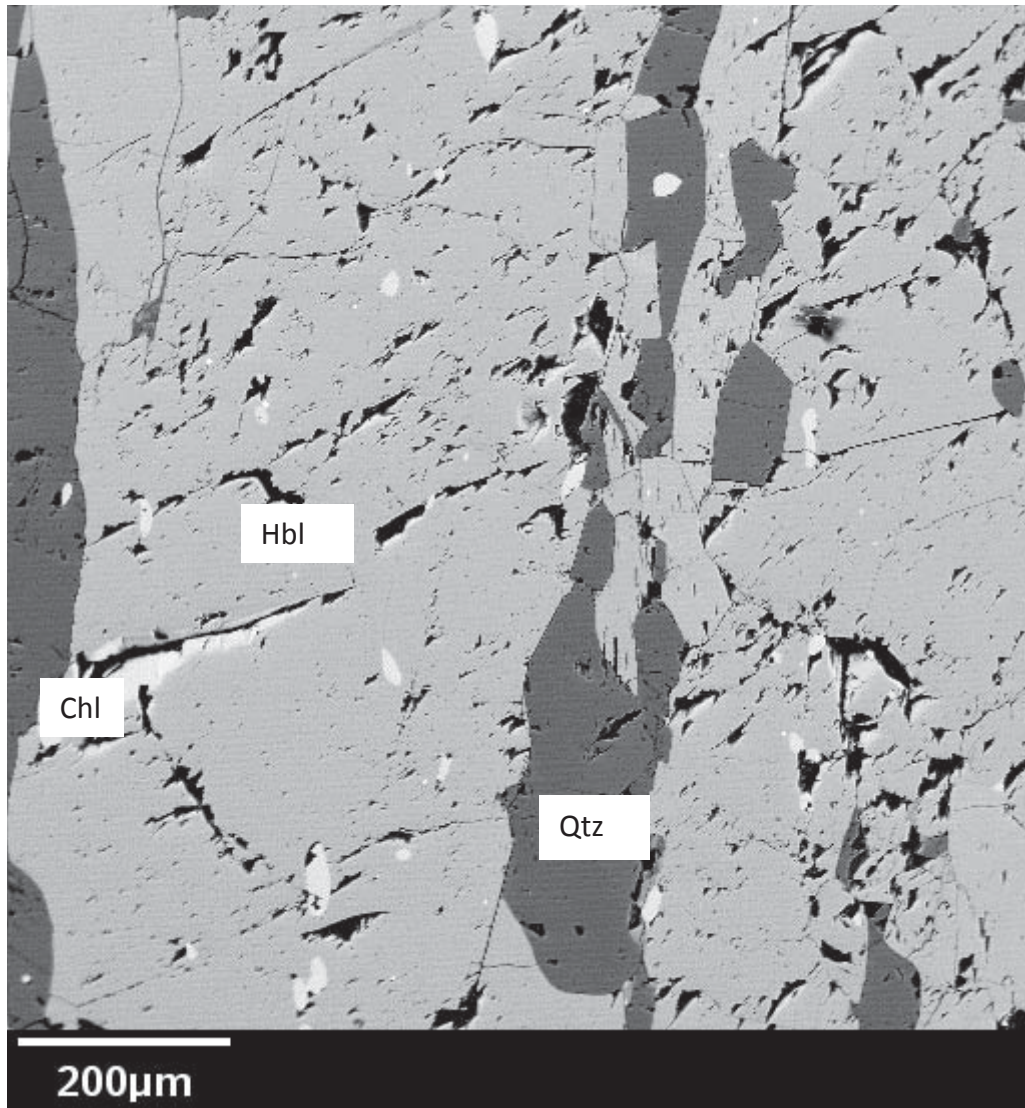


Figure 5.25 Electron microprobe photograph of hornblende grain from plagioclase amphibolite DC048 from Plant Creek which contains ~55 % hornblende, 30% plagioclase and 15% quartz with traces of chlorite on fracture planes within hornblende crystals.

Plateau dates from this sample are 58.1 ± 1.0 Ma and 60.1 ± 1.8 Ma.

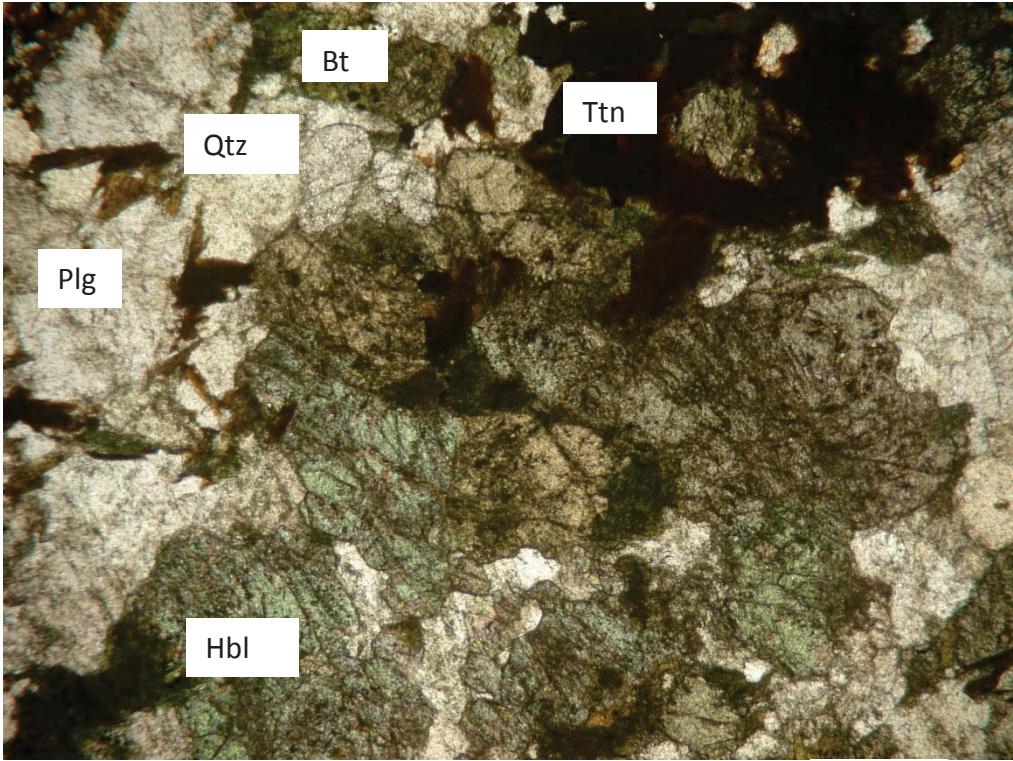


Figure 5.26a

0.5 mm

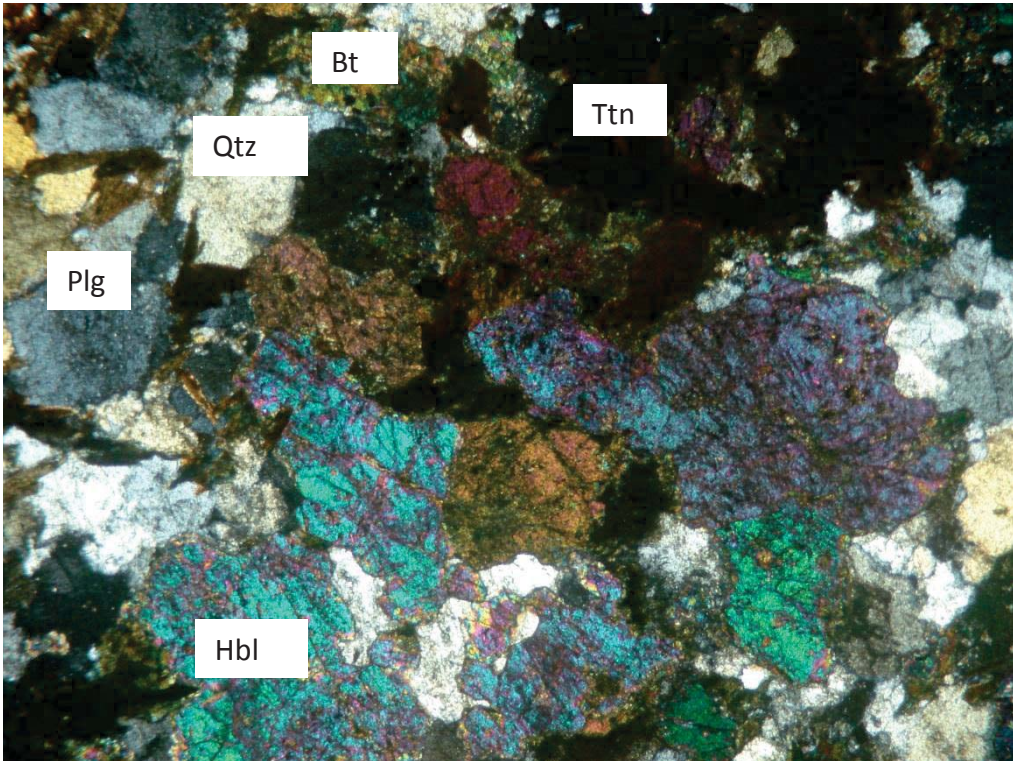


Figure 5.26b

Figure 5.26 Photomicrograph of plagioclase amphibolite DC080 in plane polarized light

(a) and in cross polarized light (b). This amphibolite DC080 from the Cusson Creek

immediately south of Plant Creek area contains ~40 % hornblende, 20 % biotite, 30 %

quartz, 15 % plagioclase and ~5 % titanite produced a date of 62.7 ± 0.7 Ma for

hornblende and plateau dates for biotite of 51.3 ± 0.3 Ma and 51.7 ± 1.1 Ma.



10 cm

Figure 5.27 : Exposure of a boudinaged layer of migmatitic garnet–gedrite–anthophyllite amphibolite containing sample DC536. This amphibolite consists of alternating bands of plagioclase and quartz with garnet, and layers containing biotite, gedrite and anthophyllite. Garnets range between 0.5 and 2 cm, and show evidence of chlorite alteration around the rims. Biotite from this sample produced a plateau age of 52.9 ± 0.3 Ma.



10 cm

Figure 5.28 Gedrite and anthophyllite crystals up to 5 cm long in a boudinaged layer of migmatitic garnet–gedrite–anthophyllite amphibolite containing samples DC536 and DC532. The yellow arrow points to a garnet–biotite amphibolite lens associated with the layer of migmatitic garnet–gedrite–anthophyllite amphibolite. Sample DC450 from this garnet–biotite amphibolite layer produced a plateau date of 54.7 ± 0.6 Ma. While the gedrite and anthophyllite crystals are contained in layers, they are not aligned within the layers.



10 cm

Figure 5.29 Example of a migmatitic garnet–biotite–quartzofeldspathic paragneiss that makes up the dominant basement rock in the Icebound Lake area. Biotite from this sample produced a plateau date of 52.2 ± 0.4 Ma, interpreted as a cooling age representative of the basement rocks in this area.



2 cm

Figure 5.30 Details of the southwest dipping grey calc-silicate gneiss at Cariboo Alp. This shows the southwest dipping foliation defined by biotite alignment and layering in quartz and plagioclase. Diopside and hornblende are present (< 10 %) and garnet is present in some layers (not pictured here). Biotite from an amphibolite boudin in this gneiss (Figure 5.8) produced a plateau date of 50.9 ± 0.4 Ma.

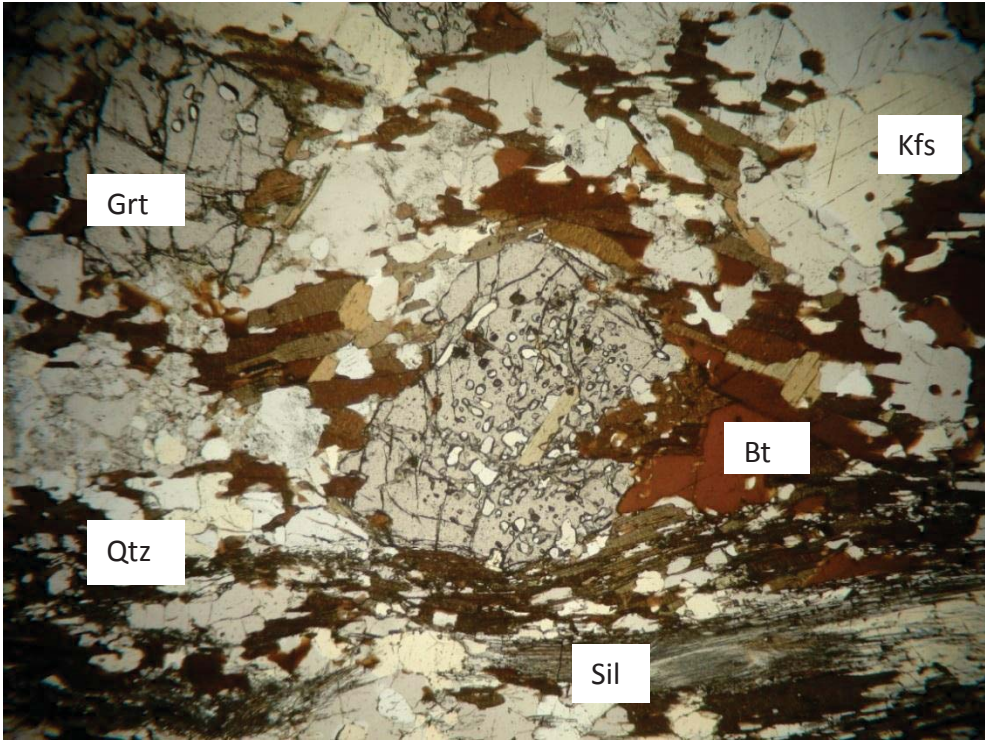


Figure 5.31a

0.5 mm

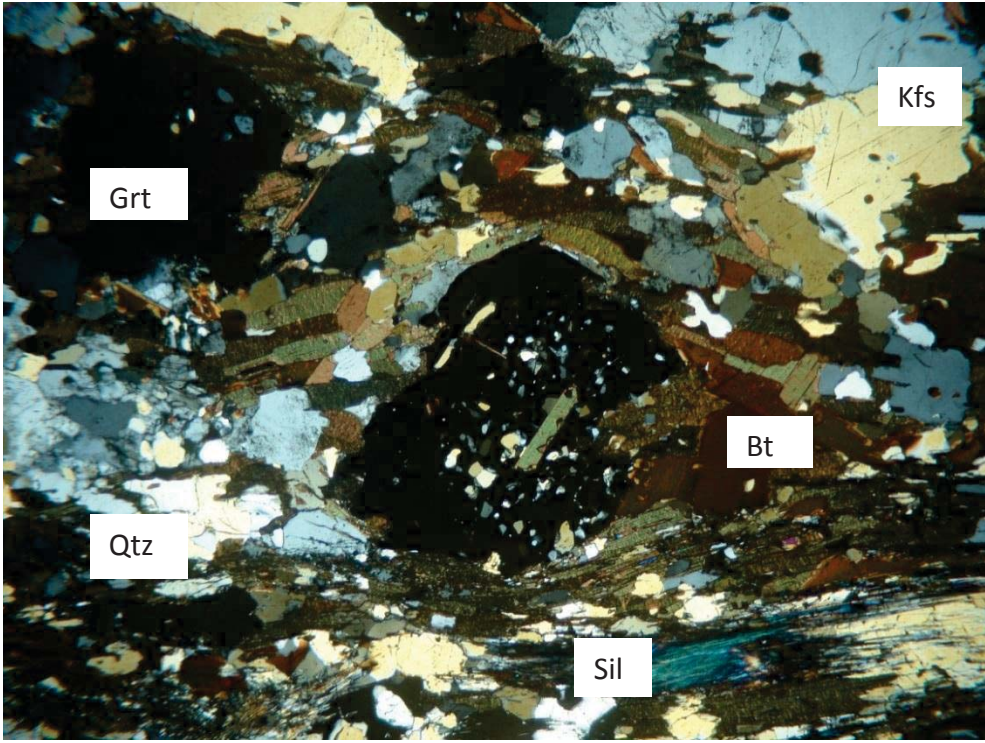
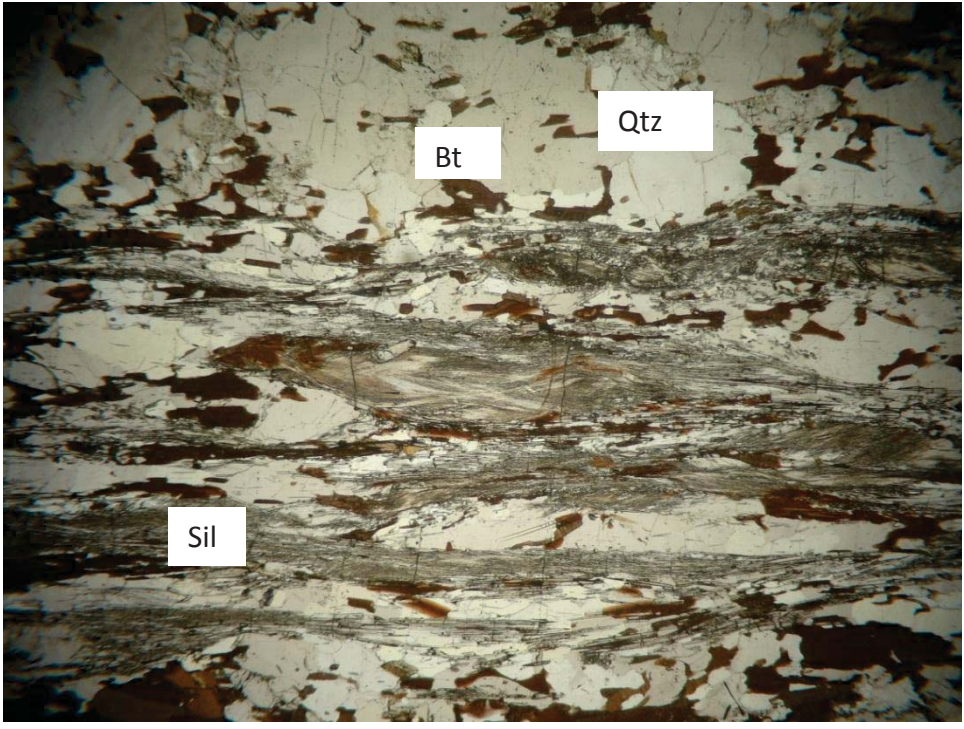


Figure 5.31b

Figure 5.31 Photomicrograph of garnet–biotite–quartzofeldspathic gneiss DC178 in plane polarized light (a) and in cross polarized light (b). The grey gneiss at Cariboo Alp is primarily biotite–quartzofeldspathic gneiss, with garnet and sillimanite present in some layers, and diopside and hornblende in other layers. Biotite defining the foliation in the grey gneiss produced a plateau date of 51.1 ± 0.4 Ma.



0.5 mm

Figure 5.32a

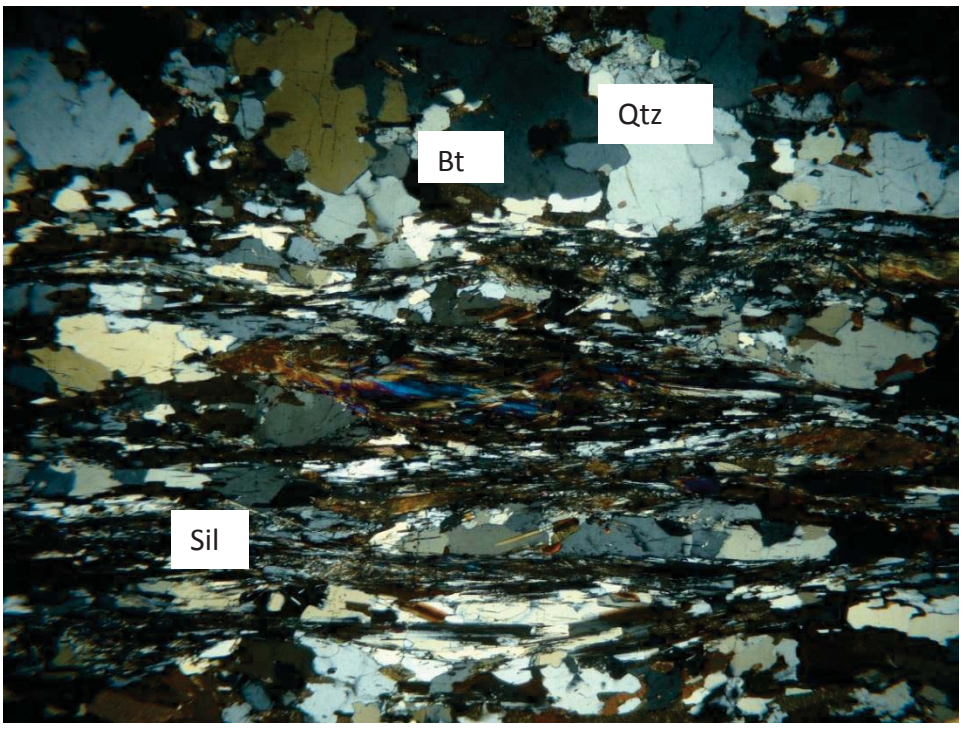


Figure 5.32b

Figure 5.32 Photomicrograph of garnet–biotite–quartzofeldspathic gneiss DC178 in plane polarized light (a) and in cross polarized light (b). This foliation is the regional southwest dipping transposition foliation. In this section the foliation is defined by sillimanite and biotite. Quartz is polycrystalline and shows subgrain development in about 50% of the quartz grains. Biotite from this sample produced a plateau date of 51.1 ± 0.4 Ma.



1 m

Figure 5.33 Moderately southwest dipping rusty-weathering garnet–sillimanite–biotite paragneiss DC193 at Cariboo Alp. All the paragneiss layers at Cariboo Alp are concordant with the regional southwest dipping transposition foliation. This sample produced a biotite plateau date of 51.7 ± 0.6 Ma.



1 cm

Figure 5.34 Details of the rusty-weathering garnet–sillimanite–biotite paragneiss DC193 at Cariboo Alp. In close-up pictures the foliation does not seem to be well-defined, but on outcrop scale (as in Figure 5.33) it is more distinct. This sample produced a biotite plateau date of 51.7 ± 0.6 Ma.



2 cm

Figure 5.35 Moderately foliated garnet–plagioclase–biotite amphibolite at Cariboo Alp.

This amphibolite contains large (1 – 3 cm) garnets that have plagioclase and quartz in pressure shadows around the garnet crystals. This sample produced biotite plateau ages of 51.6 ± 0.4 Ma and 51.6 ± 0.4 Ma.



1 m

Figure 5.36 Typical exposure of the moderately southwest dipping migmatitic semipelitic biotite paragneiss at Fawn Lakes. This photograph shows the characteristic flaggy weathering style of the paragneiss in the Fawn Lakes Assemblage, a sillimanite poor paragneiss unit interleaved with amphibolite layers.



2 cm

Figure 5.37 Semipelitic garnet–biotite paragneiss of sample DC330 in the Fawn Lakes area. This sample illustrates well-developed southwest dipping foliations defined by layers of biotite alternating with plagioclase and quartz. This sample produced a biotite plateau date of 52.2 ± 0.4 Ma.



1 m

Figure 5.38 Pegmatite of the Ladybird granite crosscutting garnet–biotite paragneiss at Mount Symonds. This pegmatite illustrates the post-tectonic intrusion of pegmatites at Mount Symonds, in contrast to the pre- or syn-tectonic intrusions illustrated in Figure 5.17. This sample produced a biotite plateau date of 50.9 ± 0.3 Ma, interpreted as a cooling date for Ladybird pegmatites in the area.

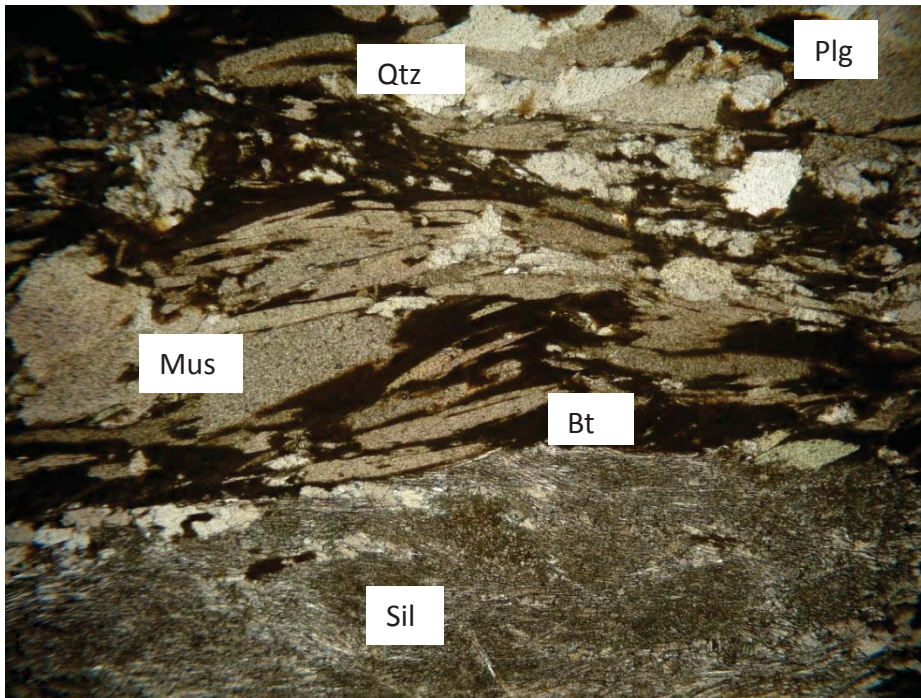


Figure 5.39 a

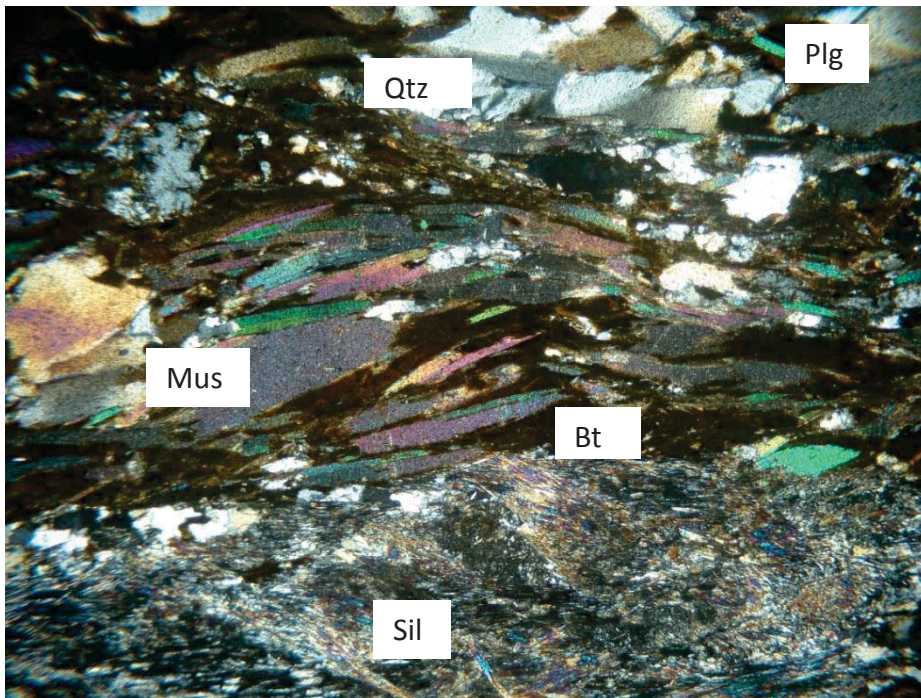


Figure 5.39b

Figure 5.39 Photomicrograph of garnet–muscovite–biotite schist DC028 in plane polarized light (a) and in cross polarized light (b). (Note: garnet is not pictured in this section.) Foliations are defined by muscovite and biotite, and sillimanite occurs as fibrous clumps of up to 1 cm in diameter. This sample is typical of the non-migmatitic gneiss or schists found in the Plant Creek and South Fosthall areas. Biotite from this sample produced a plateau date of 52.1 ± 0.4 Ma.



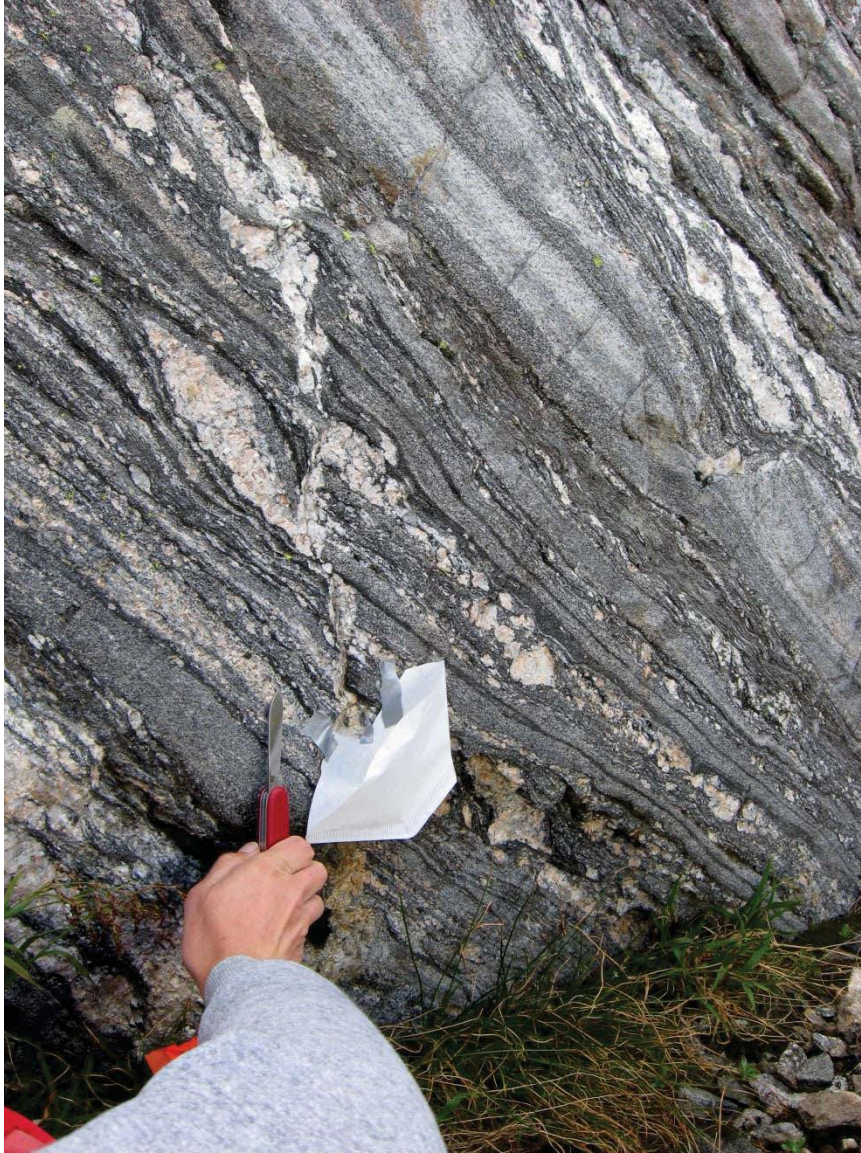
1 m

Figure 5.40 Calc-silicate amphibolite DC299 showing transposition foliation dipping steeply to the south. This sample is typical of amphibolites in the North Fosthall area and contains small lenses and veins of leucosome. This amphibolite produced a biotite plateau date of 52.4 ± 0.5 Ma.



1 m

Figure 5.41 Migmatitic grey biotite gneiss at Cariboo Alp. This exposure shows boudinaged pegmatites elongated in a northeast-southwest direction along the southwest dipping foliation planes as well as coarse-grained granitic leucosomes crosscutting the transposition foliation. Muscovite samples DC512, DC511, DC515, DC519 and DC528 are from this type of exposure and produced plateau dates of 50.9 to 50.5 Ma with errors of 0.4 to 0.3 Ma.



10 cm

Figure 5.42 Detail of migmatitic grey biotite gneiss with coarse-grained granitic leucosomes crosscutting the transposition foliation.



2 cm

Figure 5.43 Detailed view of a boudinaged leucosome in migmatitic gneiss at Cariboo Alp. This photograph shows muscovite (1 cm) crystals in pressure shadows of peritectic K-feldspar or plagioclase crystals in leucosome pods within the host migmatitic gneiss. The muscovite is locally intergrown with chlorite, interpreted as retrograde metamorphic minerals. Both minerals are present as euhedral crystals 0.1 mm to 10 mm in diameter with sharp grain boundaries and are not part of the main parageneses of the migmatitic gneiss.



10 cm

Figure 5.44 Conjugate Ladybird pegmatites crosscutting the transposition foliation in the rusty garnet sillimanite paragneiss at Cariboo Alp. These pegmatites are slightly deformed, unlike their counterparts in the grey gneiss illustrated in Figure 2.8. The pegmatites are interpreted as post-transposition intrusions. Muscovite from this sample (DC502) produced a plateau age of 51.3 ± 0.4 Ma.



1 m

Figure 5.45 Ladybird pegmatite sample DC543 at Icebound Lake. This pegmatite is deformed concordantly with the host migmatitic gneiss, indicating pre- or syntectonic intrusion. This pegmatite produced a muscovite plateau age of 50.6 ± 0.3 Ma.



1 m

Figure 5.46 Ladybird pegmatite DC418 at Icebound Lake. This pegmatite is structurally higher than the one in Figure 5.45 pictured above, and crosscuts the metasedimentary succession that structurally overlies the migmatitic garnet biotite paragneiss (DC439) interpreted to be part of the Thor-Odin basement rocks. This pegmatite produced a biotite plateau age of 51.0 ± 0.4 Ma compared to the muscovite plateau date of 50.6 ± 0.3 Ma in pegmatite DC543.



2 cm

Figure 5.47 Typical appearance of the undeformed Ladybird pegmatite. Sample DC058 in the Plant Creek area contains primary igneous muscovite and garnet. This sample produced a muscovite plateau age of 50.7 ± 0.3 Ma.



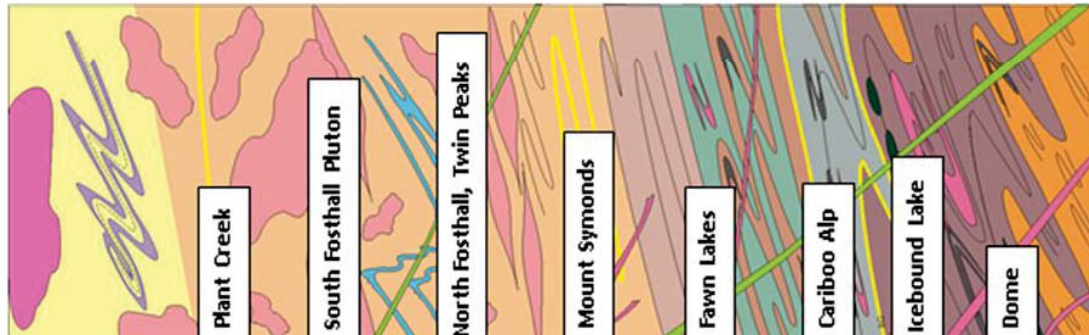
1 m

Figure 5.48 Pegmatite crosscutting moderately dipping metasedimentary country rocks at sample DC295P. This pegmatite produced a muscovite plateau age of 50.9 ± 0.3 Ma, identical to those from South Fosthall, North Fosthall, Cariboo Alp and Icebound Lake. This is interpreted as evidence that the muscovite-bearing Ladybird pegmatites sampled in the South Fosthall, Cariboo Alp and Icebound Lake areas all cooled at the same time, indicating a major cooling trend at 50.5 to 51 Ma.

DC543; 50.6 ± 0.3 Ma	Muscovite plateau age
DC418; 51.0 ± 0.4 Ma	Biotite plateau age
DC239; 56.2 ± 1.1 Ma	Hornblende plateau
DC423 NA	Sample with no plateau age

Figure 5.49 $^{40}\text{Ar}/^{39}\text{Ar}$ thermochronology results with sample locations. It follows the same classification of samples as Figure 5.50; blue boxes are for muscovite, brown are for biotite and green for hornblende. Samples that did not produce robust plateau dates are labeled NA.

This figure only shows the relevant section of the larger map in Figure 1.2 and Appendix. For clarity some map information is omitted.



Hornblende

Tc 490°C – 510 °C,
23 dates

~62- 58 Ma

Cooling age, reset by LBG

~58 – 55 Ma

Cooling age, reset by LBG

~55 Ma

Cooling age, reset by LBG

~62- 58 Ma

Original cooling age

~57 - 54 Ma

Original cooling age

< 54 Ma predicted, no
plateau ages

Biotite

Tc 280°C – 300 °C,
22 dates

(*4 not included, see Discussion)

~51 – 52.5 Ma

Cooling age, reset by LBG
OR Original cooling age?

~51 Ma

Cooling age for LBG in SFP

~51 – 52.5 Ma

Cooling age, reset by LBG
OR Original cooling age?

~51 Ma

Cooling age for Ladybird pegmatites

~51 – 52.5 Ma

Original cooling age

~51 – 52.5 Ma

Original cooling age

~51 Ma

Cooling age for
Ladybird pegmatites

~51 – 52.5 Ma

Original cooling age

Muscovite

Tc 400°C – 500 °C,
9 dates

~50.8 Ma

Cooling age for Ladybird pegmatites

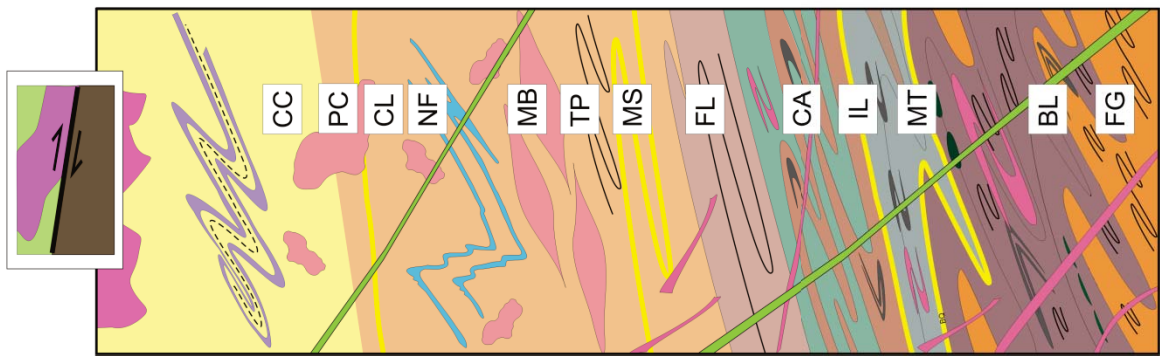
~50.7 Ma

Cooling age for Ladybird pegmatites
Crystallization age for muscovite in
retrograde metamorphism

~50.6 Ma

Cooling age for Ladybird pegmatites

Figure 5.50 Summary of all $^{40}\text{Ar}/^{39}\text{Ar}$ hornblende, biotite and muscovite cooling ages organized by structural level and location throughout the study area. The hornblende cooling dates reflect cooling after peak metamorphism as well as reheating by the Ladybird granite). Biotite and muscovite dates reflect a major period of cooling attributed to motion on the Columbia River fault between ~52.5 and 51 Ma. See text for discussion.



Arranged according to age in Ma, and by structural position
 Numbers on bars correspond to numbering in Sample Table

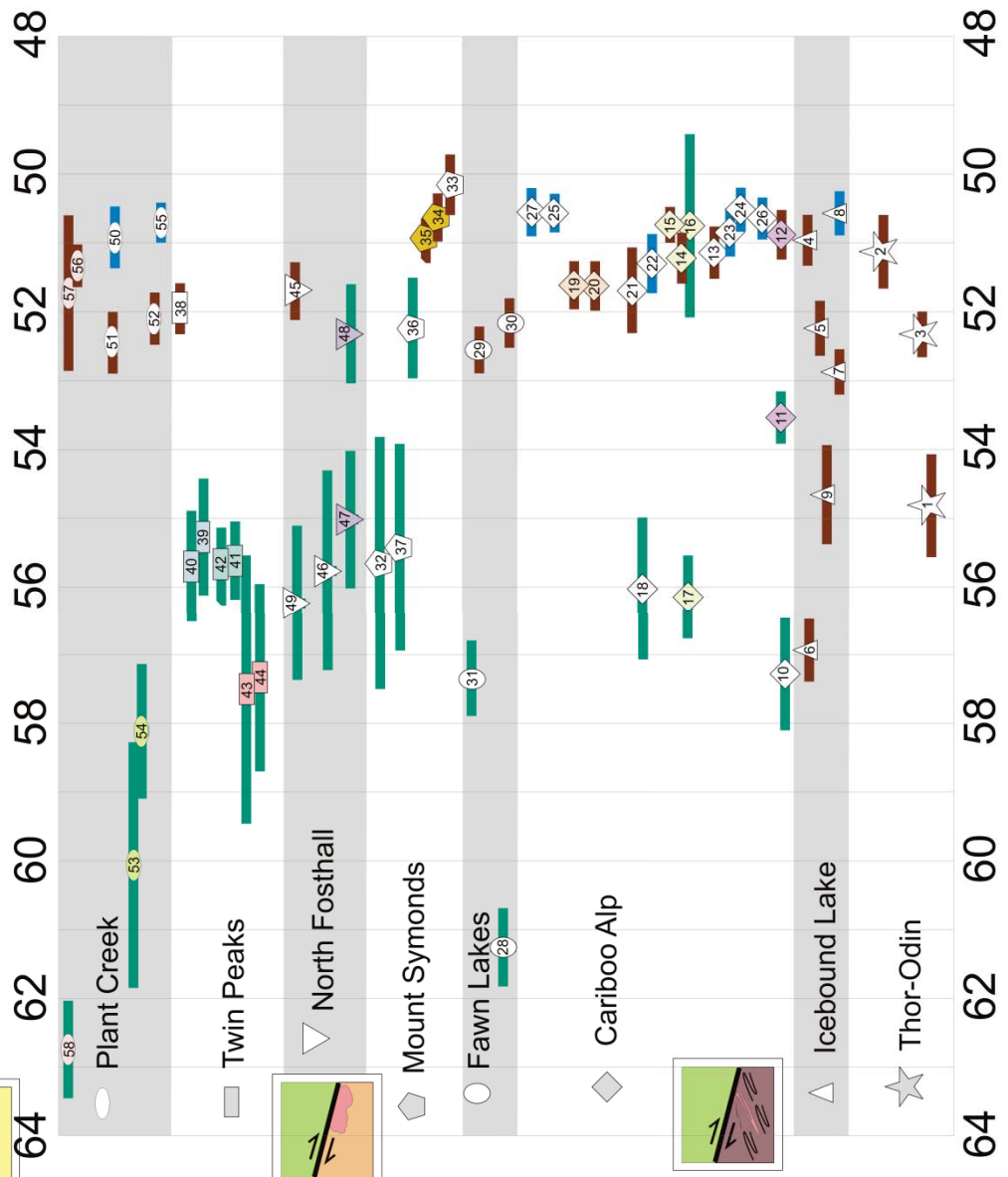


Figure 5.51 Summary of all $^{40}\text{Ar}/^{39}\text{Ar}$ hornblende, biotite and muscovite ages, presented as individual sample ages with error bars. The results are organized by structural level and location throughout the study area. Sample numbers correspond to Table 5.2. The hornblende cooling dates reflect cooling after peak metamorphism as well as reheating by the Ladybird granite (see section 5.5.4 for discussion), and the biotite and muscovite dates reflect a major period of cooling attributed to motion on the Columbia River fault between 52.5 and 51.0 Ma.

Note: Symbols correspond to the sample area (e.g. Thor-Odin dome samples have stars and Icebound Lake samples have triangles). Samples which have the same colour inside the symbol refer to replicates or a mineral pair (e.g. 14, 15, and 16 from Cariboo Alp).

6 Chapter: Implications for the tectonic evolution of the Thor-Odin – Pinnacles area

6.1 Introduction

This chapter presents the conclusions of this thesis with results from all chapters as well as a discussion of the tectonic evolution of the Thor-Odin dome with reference specifically to events that occurred in the Late Cretaceous to Eocene. Section 6.2 presents conclusions from Chapters 3 and 4, dealing with the detrital zircon U-Pb geochronology part of this study. Subsequent sections (6.3, 6.4, and 6.5) integrate conclusions regarding the Late Cretaceous to Eocene tectonothermal history of the Thor-Odin – Pinnacles area from Chapters 2 and 5 in order to discuss tectonic models. Section 6.6 presents suggestions for future work.

6.2 Detrital zircon U-Pb geochronology studies: new interpretations of protolith ages and provenance of the rocks in the Thor-Odin – Pinnacles area

The detrital zircon U-Pb geochronology presented in this study includes LA-ICP-MS U-Pb data from five marker quartzite units in the Thor-Odin – Pinnacles area (Figures 1.1 and 1.2). There are two groups of samples; the first includes samples from Mount Thor, Icebound Lake and Cariboo Alp from the interior and southwestern flank of the Thor-Odin dome (Figure 3.3) and the second group includes quartzites from rocks that structurally overlie the dome at Mount Symonds and Plant Creek (Figures 4.1 and 4.3).

Data from these quartzites (see sections 3.3, 3.4, 4.3, and 4.4 for detailed methods and results for each sample) provide constraints on the maximum depositional ages and provenance of the rocks within the Thor-Odin dome and the rocks overlying the dome.

The basal quartzite unit of the Thor-Odin dome in the Mount Thor area (section 3.4; Figures 3.2 and 3.3) has a maximum depositional age of c. 1650 Ma, on the basis of the U-Pb LA-ICP-MS age of the youngest zircon (Figure 3.11). It contains a primary detrital zircon population with ages between c. 1900 and 1650, and minor age populations that are > 3000 Ma, and between c. 2800 and 2200 Ma. The Icebound Lake quartzite detrital zircon age populations are similar (section 3.4; Figure 3.13), and based on the distribution of ages, it is permissible that the Mount Thor and Icebound Lake quartzites are correlative. They were both derived primarily from source areas present in western Laurentia; however, the c. 1650 Ma zircons may have been derived from the Yavapai – Mazatzal orogen, or represent sources derived from the Belt-Purcell Supergroup. The Thor-Odin dome basal quartzite is here interpreted as younger than the basal quartzite of the Frenchman Cap dome to the north, which is interpreted as being older than ~1780 Ma, and younger than ~1850 Ma (Crowley 1997; Figures 3.4 and 3.5). This difference in depositional ages and source terranes implies that the basement rocks and the associated “basal quartzites” of the Thor-Odin and Frenchman Cap domes may represent different basement domains. It is therefore permissible that these basement

domains were not necessarily contiguous during the Proterozoic and may have been juxtaposed after the deposition of the quartzites.

The quartzite at Cariboo Alp on the southwestern flank of the Thor-Odin dome (section 3.4; Figures 3.2 and 3.3) is not part of the Thor-Odin dome basal quartzite unit because it is younger, on the basis of a Grenville age population of zircons with ages between 1200 and 1100 Ma (Figure 3.14) in addition to the older western Laurentian populations present in the samples from the dome. Based on this interpretation, it is not required that the Cariboo Alp quartzite be drawn on maps and cross sections as an infolded segment of the basal quartzite, and tectonic models do not need to account for repetition of the Thor-Odin basal quartzite at Cariboo Alp. The Cariboo Alp quartzite is most likely correlative to the older units of the Windermere Supergroup (Figure 4.9).

The quartzite at Mount Symonds (section 4.4, Figure 4.1) is younger than ~500 Ma and has detrital zircon age populations between 500 – 650 Ma and 1600 – 1900 Ma, with minor populations between 1100 Ma and 1200 Ma, and spanning 2200 – 2800 Ma (Figures 4.5 and 4.6). The populations older than 1600 Ma are consistent with those in the Thor-Odin dome quartzites derived from western Laurentian sources, and the 1100 – 1200 Ma Grenville age populations match those in the Cariboo Alp quartzite. The population with ages between 500 and 650 Ma are the same ages as syn-rift volcanic units documented within the Hamill Group (Colpron et al. 2002, and references therein).

The detrital zircon populations in the Mount Symonds quartzite are consistent with the interpretation that the package of rocks at Mount Symonds is Cambrian in age and equivalent to the pericratonic Hamill Group (Figure 3.4, 3.5, and 4.9). The Mount Symonds quartzite is not related to or correlative to the basal quartzite of the Thor-Odin dome.

The Plant Creek quartzite (section 4.4, Figure 4.3) has the youngest protolith of all the samples in this study. It contains major detrital zircon age populations between 150 – 200 Ma and 300 – 450 Ma (Figures 4.7 and 4.8). There is a notable lack of Proterozoic dates as there are only a few grains with ages between 1700 and 1900 Ma. The quartzite is Late Jurassic or younger based on the age of the youngest zircons. The age distributions and the zircon morphology (i.e. oscillatory igneous zoning, euhedral grains with bipiramidal terminations showing lack of transport and abrasion; Figure 4.7) suggest that the source area for this quartzite was an immature proximal source, unlike the dominantly cratonic sources documented in the other quartzites studied. This quartzite has Paleozoic and Mesozoic sources of detrital zircons and could be derived from juvenile volcanic arc terranes like the Cache Creek and Quesnel terranes, which include the Nicola and Rosslund groups comprising Triassic to Jurassic volcanic rocks (Petersen et al. 2004 and references therein).

The Late Jurassic detrital zircon populations in this sample support the interpretation that the greenschist facies Jurassic and Triassic rocks of the Rossland and Slocan groups in the Plant Creek area are separated from the Jurassic to Cretaceous – Paleocene K-feldspar–sillimanite and K-feldspar–muscovite bearing amphibolite facies rocks beneath them by a fault, not an unconformity. The greenschist facies rocks in the Plant Creek area are klippen of the Columbia River fault, which, as discussed in Chapter 2, is an Eocene structure imposed on rocks with older thermal and tectonic histories. However, in addition to the Jurassic age greenschist facies rocks of the Quesnellia terrane in the klippen of the Columbia River fault, there are also amphibolite facies rocks with Jurassic protoliths and Quesnellia terrane affinity in the footwall of the Columbia River fault between the Thor-Odin dome and the Whatshan – Pinnacles area (Figures 4.9 and 4.10).

6.3 Exhumation mechanisms

Mechanisms to account for extension-related exhumation of mid-crustal rocks in the Canadian Cordillera can be divided into two broad categories. The first involves exhumation during post-convergent gravitational collapse and includes: (i) core complex models where exhumation post-dates convergence and buoyant crustal material rises in the footwall of low-angle outward dipping shear zones (Coney and Harms, 1984); (ii) large-scale extension models where large tracts of mid-crustal rocks are exhumed in the footwalls of extensional faults (Parrish et al., 1988); (iii) and vertical flow models in which diapiric ascent of partial melts play a large role (Vanderhaeghe et al. 1999;

Norlander et al. 2002; Whitney et al. 2004; Teyssier et al. 2005). The second broad category of extrusion mechanisms involves ductile extrusion and channel flow (Johnston et al. 2000; Williams and Jiang 2005; Brown and Gibson 2006; Glombick et al. 2006; Kuiper et al. 2006) in which mid-crustal rocks flow in a channel and are bound by two opposite verging shear zones at the top and base, active at the same time. The following sections discuss how the data presented in this study relate to the models mentioned above.

6.3.1 Suprastructure-infrastructure transitions in the Thor-Odin – Pinnacles area related to core complex models.

The classical core complex model states that a core complex is formed by the exhumation of high grade metamorphic rocks along shallowly dipping extensional faults which are younger than the polydeformed structures that form in the high grade rocks during orogenesis, and that the lower plate is quenched concomitantly with motion on the bounding extensional shear zone (Ewing, 1980; Coney, 1980; Armstrong, 1982; Coney and Harms, 1984; Tempelman-Kluit and Parkinson, 1986). In the Thor-Odin – Pinnacles area (Figures 1.1 and 1.2) there is evidence for multiple, complex periods of metamorphism and deformation, and as discussed in Chapter 2, it is clear that not all structural levels were affected by every event. This section briefly discusses the interpretations made in this study regarding timing of deformation and metamorphism and the implications for discussing this area in terms of an infrastructure-suprastructure

association in the Late Cretaceous to Eocene. The area represents a structural section through c. 17 km of rocks exposed in the footwall of the Columbia River fault (Figures 2.1 and 2.2). The penetratively deformed Thor-Odin dome represents the deepest part of the section. On the southern flank of the Thor-Odin dome the section is exposed as a south to southwest dipping tilted panel of transposed rocks (Figure 1.3), and the Plant Creek to Whatshan – Pinnacles area preserves polyfolded, non-transposed structures (Figure 2.14).

Based on data regarding the timing of metamorphism, deformation, anatexis in basement rocks, and intrusion of leucogranites (sections 2.2 – 2.5; Figure 2.14), there are at least four belts of rocks, or tectonothermal domains, in the footwall of the Columbia River fault in the Thor-Odin – Pinnacles area that experienced regional metamorphism, deformation and high temperature cooling (below ~650 °C) at different times between the Late Cretaceous and the Eocene (Figure 2.56). In general terms, the timing of tectonothermal events youngs structurally downwards from the Pinnacles – Whatshan area towards the Thor-Odin dome, and the metamorphic grade of the rocks generally increases towards the dome, or downward into the structural section (Figure 2.14). This is interpreted as a reflection of a downward migration of the suprastructure-infrastructure boundary through time (section 2.6).

The timing of the transitions between suprastructure and infrastructure for the different belts of rocks in the study area are summarized in Figure 2.56, and form the basis of the interpretations presented in figure 6.1. The rocks of the Whatshan – Pinnacles area were polyfolded in the Late Cretaceous (pre c. 75 Ma) and represent the infrastructure before c. 75 Ma. At c. 73 – 64 Ma, the Whatshan – Pinnacles area rocks were deactivated and acted as suprastructure to the underlying Plant Creek – South Fosthall area rocks, from the central part of the tract structurally above the South Fosthall pluton. This central part of the section was being penetratively deformed within the infrastructure at this time. After c. 64 Ma, the Plant Creek-South Fosthall area rocks became part of the suprastructure, as evidence by the timing of the end of penetrative deformation. Rocks in the lowest part of the tract, below the South Fosthall pluton (i.e. Mount Symonds-Cariboo Alp area), continued to be deformed after c. 64 Ma. After ~58 Ma, the lowest part of the tract, the Mount Symonds-Cariboo Alp area, was no longer active and lay in suprastructure relative to the infrastructure now comprised of the deforming rocks in the Thor-Odin dome. The Thor-Odin dome rocks remained in the infrastructure until c. 52 Ma when they cooled through ~300 °C (section 5.4.2).

The Columbia River fault zone crosscuts the trace of these aforementioned belts of rocks, and the fossil suprastructure-infrastructure boundaries. Therefore, the Columbia River fault is a younger, Eocene structure imposed on footwall rocks that preserve

crustal belts that underwent deformation and metamorphism at different times, including some that have a thermal history that is older than that of the shear zone. This crustal section in the footwall of the Columbia River fault zone does not represent a continuous mid-crustal zone (c.f. Carr 1991a). It can be better described as a tilted crustal section representing multiple thermotectonic domains, with a complex and progressive history involving progressive folding and transposition during northeastward directed compression. This is inconsistent with previous interpretations of these rocks as a simple lower plate of a Cordilleran metamorphic core complex that were penetratively deformed and then quenched during Eocene extensional exhumation (Brown and Reid 1983; Coney and Harms, 1984; Parrish et al. 1988; Vanderhaeghe et al. 2003; Teyssier et al. 2005).

Therefore, the rocks between the Whatshan – Pinnacles area and the interior of the Thor-Odin dome record Cretaceous metamorphism and cooling in the upper structural levels, and three stages of infrastructural flow at progressively deeper crustal levels in the Late Cretaceous, Paleocene and Eocene. The generally downward younging progression of metamorphism and deformation, as well as the structural style and transposition foliation in the lower part of the section, is consistent with a model in which rocks were progressively heated and deformed during compressional transport, possibly up a basement ramp which facilitated doming and exhumation.

6.3.2 Late Cretaceous to Eocene thermal history of the Thor-Odin – Plant Creek area related to exhumation and extension.

Chapter 5 presents a discussion of the cooling history (from c. 550 °C to <300 °C) of this area from c. 62 – 50 Ma based on $^{40}\text{Ar}/^{39}\text{Ar}$ cooling ages from 58 samples of hornblende, biotite and muscovite. These samples represent all major rock types in the study area, and were taken throughout the structural section from the Thor-Odin dome to the uppermost structural level at Cusson Creek, specifically targeted at crossing proposed tectonic boundaries such as the margin of the Thor-Odin dome at Cariboo Alp, the boundaries of the South Fosthall Pluton, and the boundaries of the suprastructure-infrastructure zones discussed in section 2.6 (Figure 5.6 for locations and summary). The following is a short summary of the thermochronology data (section 5.4 and 5.5; Table 5.2), relating the cooling history to the suprastructure-infrastructure divisions discussed above. The cooling history is illustrated in Figure 6.1, along with the downward younging progression of tectonothermal events and migrating belts of suprastructure-infrastructure mentioned in sections 2.6 and 6.3.

The time of cooling through 500 – 600 °C, based on hornblende $^{40}\text{Ar}/^{39}\text{Ar}$ cooling dates (section 5.4.1) varies throughout the structural section: (i) Plant Creek – South Fosthall area, c. 62 – 58 Ma; (ii) Twin Peaks – Fosthall Pluton area, c. 57 – 56 Ma; and (iii) upper margin of the dome at Cariboo Alp c. 55 – 53 Ma. We interpret the c. 62 – 55 Ma

hornblende cooling ages in the Twin Peaks – South Fosthall Pluton area to be mostly related to reheating and resetting during emplacement of the Ladybird Granite suite, which played a significant role in heating since the granites and pegmatites post-date the estimated time for peak metamorphism. However, it is also permissible that the rocks stayed above the predicted closure temperatures for 5 – 10 Ma between the end of metamorphism and the above-mentioned cooling dates. The younger hornblende dates of c. 55 – 53 Ma at Cariboo Alp on the SW margin of the Thor-Odin dome are interpreted as post-metamorphic cooling ages. This is consistent with our interpretation of migrating suprastructure-infrastructure transitions because it shows that cooling in upper suprastructural levels (e.g. Plant Creek – South Fosthall cooling at c. 58 Ma) was coeval with penetrative ductile deformation in the lower infrastructural levels (e.g. Thor-Odin dome deforming in the infrastructure at the same time).

Biotite cooling ages (section 5.4.2), for closure temperatures of 280 – 350 °C, are between c. 52.5 to 51.0 Ma throughout the entire area regardless of structural level. Similarly, muscovite dates (section 5.4.3) throughout the structural section are the same at c. 51.0 – 51.5 Ma, representing both cooling ages (in pegmatites, for closure temperatures of 400 – 450 °C) and retrograde metamorphic crystallization ages (at temperatures below biotite closure temperatures of 280 – 350 °C) in migmatitic gneiss. There is no syn- or post-metamorphic structural break at the southwestern margin of the Thor-Odin dome at Cariboo Alp as described by Kruse and Williams (2007),

indicating that the tilted geometry (Figure 1.3) of the southwest dipping panel that lies above the Thor-Odin dome and juxtaposition with underlying rocks of the dome occurred before cooling, and was in place before the Paleocene – Eocene period of cooling and exhumation.

The biotite and muscovite cooling ages acquired from samples between Plant Creek and the Thor-Odin dome (sections 5.4.2 and 5.4.3) indicate that there was a major period of cooling and exhumation c. 52.5 to 51.0 Ma. We interpret this as a time of significant motion on the Columbia River fault system (Figure 1.2) and possibly its western counterpart, the Okanagan Valley – Eagle River fault system (Figure 1.1). The Columbia River fault zone has a history of periodic reactivation from c. 55 Ma to 35 Ma. Major displacement at c. 52 – 51 Ma on the extensional fault systems was responsible for cooling of all footwall rocks below 300 °C at every structural level discussed here. At this time, the penetrative ductile deformation related to northeast directed compression had stopped, extension in the region had been initiated and the entire crustal section exposed in the study area underwent exhumation and cooled below ~300 °C. In addition, these data suggest any structural breaks that may be present at Cariboo Alp must predate this cooling and therefore be older (i.e. pre-Paleocene), for example, the equivalent of the Late Cretaceous Gwillim Creek shear zone in the Valhalla Complex (Simony and Carr 2011).

The Columbia River fault zone cannot have been responsible for the high temperature cooling within the footwall section (Figures 5.50, 5.51; 6.1), since, at least the upper part of the section (Whatshan to South Fosthall) cooled through hornblende closure temperatures (500 – 600 °C) before the activation of the Columbia River fault zone. Thus, the Columbia River fault zone is best interpreted as an Eocene structure imposed on an area with a pre-existing tectonothermal history. It is not concordant with the Eocene isotherms, and is not the upper boundary of an active zone of mid-crustal flow. In addition, the footwall rocks preserve a protracted deformation history which includes suprastructure-infrastructure transitions in the Cretaceous, Paleocene and Eocene, which are not consistent with the existence of a zone of mid-crustal flow in the Paleocene to Eocene. These data are also inconsistent with previous interpretations suggesting that the Thor-Odin dome is the lower plate of a Cordilleran metamorphic core complex that was penetratively deformed and then cooled during Eocene extensional exhumation.

6.3.3 Diapirism within the Thor-Odin dome related to core complex models

There are certainly aspects of the evolution of the Thor-Odin dome – Pinnacles area that resemble the core complex model as described in section 1.3. For example, the Columbia River fault does separate high grade metamorphic rocks in its footwall from low grade rocks in the hanging wall, and there are migmatites in the Thor-Odin dome linked to decompression melting (Vanderhaeghe et al. 1999, 2003; Norlander et al.

2002; Fayon et al. 2004; Teyssier et al. 2005). However, as discussed in sections 6.3.1 and 6.3.2, the complexity of the suprastructure-infrastructure transitions and the cooling history of the rocks in the footwall are not consistent with a core complex model. Similarly, interpretation of the Thor-Odin dome as a diapir, with or without being coupled with a core complex model is not appropriate. When the rocks exposed in the footwall of the Columbia River fault are considered, the formation of transposition foliation and northeast directed folds in the Thor-Odin dome is coeval with cooling in the upper structural levels, (e.g. in the North Fosthall area) (Chapter 5) and the age of deformation young downwards into the structural section.

Evidence for decompression melting in the Thor-Odin dome (specifically the Bearpaw Lake area, Figures 1.2, 2.14) was reported by Norlander et al. (2002). Rocks underwent decompression from 8 – 10 kbar in the kyanite zone to 4 – 5 kbar in the sillimanite-cordierite zone, which equates to exhumation from ~25 – 30 km to ~ 15 km depth. The authors suggest that this occurred as isothermal or near-isothermal decompression with coeval anatexis, based on reaction textures, mineral assemblages and the extensive presence of anatectic melt in the rocks. It is proposed that the driving force for the exhumation of Thor-Odin dome was gravitational instability created by the presence of anatectic melt and the subsequent ascent of partially molten crust in the core of the dome as a diapir (Vanderhaeghe et al. 1999, 2003; Norlander et al. 2002; Fayon et al. 2004; Teyssier et al. 2005). However, the polyphase folding of the leucosomes in Thor-

Odin dome (McNeill 2002; Hinchey et al. 2006) precludes this interpretation. The dome is a fold interference structure, perhaps amplified by some buoyancy effect, but the preservation of NE-directed compressional structures is not consistent with that of a diapir (Williams and Jiang 2005; Hinchey et al. 2006).

Models for the Thor-Odin dome invoking diapirism delineated Cariboo Alp (Vanderhaeghe et al. 1999; Teyssier et al. 2005) as a possible boundary along which the dome is exhumed. The data in this study strongly contradicts this interpretation (Vanderhaeghe et al. 1999; Teyssier et al. 2005). Not only is the Cariboo Alp area not a major extensional shear zone (Chapter 2), it was also not involved in the exhumation of the dome, as discussed above. In thermochronological studies of core complexes, as well as in numerical modeling, cooling ages always young towards the extensional shear zone (Sullivan et al. 2007; Tirel et al. 2006, 2008). The data presented in this study show that the cooling ages through 300 °C are the same through a 12 km thick structural package that contains the Cariboo Alp, and that the structural section was tilted and assembled before cooling, which strongly argues against a diapir model for the Thor-Odin dome.

6.3.4 Crustal flow in the Thor-Odin and Frenchman Cap domes

Gervais et al. (2010) document an absence of Cordilleran strain and metamorphism in the deepest exposed basement rocks of the Frenchman Cap dome, approximately 1.5

km structurally below the basal quartzite of the cover rocks (Figure 3.1). There is no equivalent base of Cordilleran deformation in Thor-Odin dome. However, it is possible that there is a basal limit to the Cordilleran deformation in the Thor-Odin dome, either unexposed, or not identified because most of the geochronology on Cordilleran strain (Vanderhaeghe et al. 1999; Johnston et al. 2000; Norlander et al. 2002; Hinchey et al. 2006) were done on rocks less than 1.5 km below the Thor-Odin basal quartzite. Deeper areas (such as Frigg Glacier) may preserve the Proterozoic structural history as seen in Frenchman Cap (Gervais et al. 2010). However, several studies suggest that Thor-Odin dome was penetratively deformed in all exposed areas, and that the deformation is Cordilleran in age (Vanderhaeghe et al. 1999; Johnston et al. 2000; Norlander et al. 2002; Hinchey et al. 2006; Kruse and Williams 2007). The preservation of Proterozoic deformation in the core of the Frenchman Cap dome indicates that it could not have formed as a result of vertical diapiric rise of partially molten crust (Crowley et al. 2008; Gervais et al. 2010) as proposed for the Thor-Odin dome (Vanderhaeghe et al. 1999, 2003; Norlander et al. 2002; Whitney et al. 2004; Teyssier et al. 2005) and the Okanogan dome (Kruckenberg et al. 2008). As is the case in the Frenchman Cap dome, the folded and refolded migmatites in the Thor-Odin dome are inconsistent with diapirism.

Instead, Gervais and Brown (2011) propose a model of formation for the Frenchman Cap dome that is based in the sequential extrusion of mid-crustal material up a basement ramp, in which the Monashee décollement represents the lower boundary of

a mid-crustal channel and the Okanagan Valley – Eagle River Fault represents the upper boundary, or lid, of the channel. In this model, the rocks of the Lower Selkirk Allochthon (taken to be equivalent to the rocks between Thor-Odin and Pinnacles) were exhumed while the underlying Monashee Complex rocks were being buried. Movement on the east-verging Monashee décollement in the Frenchman Cap dome was coeval with amphibolite facies metamorphism (forming kyanite and K-feldspar) and penetrative ductile deformation between c. 60 and 55 Ma (Parrish 1995; Crowley and Parrish 1999; Crowley et al. 2001; Gibson et al. 2003). The main period of formation for north-northeast directed folds and transposition foliations in a top-to-the-east shear zone in the Frenchman Cap dome was between c. 53 and 49 Ma (Crowley et al. 2001; Gervais et al. 2010).

6.4 A hybrid model for the evolution of the Thor-Odin dome in the Late Cretaceous to Eocene and implications for the tectonic history of the southeastern Canadian Cordillera

Despite documented differences in the pressures, temperatures, and deformation histories of the Frenchman Cap dome and the Thor-Odin dome discussed above (see sections 6.3.4, 2.4.4, 3.2) (Hinchey 2005; Gervais et al. 2010), there are some aspects of the evolution of the Thor-Odin dome that are broadly similar in the Frenchman Cap dome. Specifically, the thermochronology data showing that the upper structural levels (e.g. Plant Creek area) are being cooled through 500 °C while the lower levels are being

penetratively deformed, followed by crustal scale extension over the whole area, is kinematically consistent with the channel flow model for Frenchman Cap discussed by Gervais and Brown (2011). However, Carr and Simony (2006) argue against a full model of channel flow in the southeastern Canadian Cordillera and have suggested instead that channel flow occurs for a short duration and was arrested before extrusion occurred. Alternatively, the Gwillim Creek shear zone is known to have transported rocks over a basement ramp (Hallett and Spear 2011) and it was suggested by Simony and Carr (2011) that this type of transport is a mechanism that can be extended to the Thor-Odin dome.

The preferred model for the evolution of the Thor-Odin – Pinnacles area suggested by this study is therefore a hybrid model in which the primary tectonic process driving deformation and metamorphism is crustal thickening in a convergent setting. The rocks of the Thor-Odin – Pinnacles were progressively heated and deformed as they were transported to the east to northeast over a basement ramp in the Late Cretaceous to Paleocene (cf. Gervais et al. 2010; Hallett and Spear 2011). The suprastructure-infrastructure boundary, marking the division between rocks in which penetrative deformation has ended and actively deforming rocks, migrated structurally downward into the crust as rocks were structurally deactivated at the top of the section while deformation continued at lower structural levels. The top of the section (Whatshan to Pinnacles to South Fosthall) was the first to be penetratively deformed, and also the first

to be deactivated. The structural style in the Whatshan – Pinnacles area is sufficiently different from that in the Plant Creek to Mount Symonds areas that the Whatshan – Pinnacles area is interpreted here as representative of a period of thickening of the orogen in the Late Cretaceous, which is required to insulate the rocks beneath them. This thickening then allowed for the heating, deformation, and flow of the rocks beneath, here represented by the South Fosthall to Mount Symonds areas. The hot rocks were then transported up a basement ramp during Paleocene northeast directed compression. As discussed by Simony and Carr (2011) the Gwillim Creek shear zone represents a major ductile shear zone and represents the top of a series of Late Cretaceous to Eocene belts of younging downward infrastructure, consistent with the transitions documented in this study. The structurally lowest part of the section in the core of the Thor-Odin dome hosts the youngest penetrative deformation, and was the last to be deactivated.

Channel flow can form a minor component of the transport but this channel flow had to be limited in time and space (cf. Carr and Simony 2006) and did not extrude in the Thor-Odin dome. Likewise, diapirism and gravity driven buoyant exhumation of deep crustal rocks may be a factor (Norlander et al. 2002); however, the structural styles in the rocks dictate that it was limited in duration and spatial extent to areas in the core of the Thor-Odin dome. The initial cooling to below c. 500 °C between 62 and 58 Ma in the upper part of the section (Pinnacles to South Fosthall) occurred as a result of syn-convergent

exhumation of the suprastructure. The switch to cooling across the whole area, linked to crustal scale extension, occurred only when the Columbia River fault cut across the entire crustal section, when all the rocks in the Thor-Odin – Pinnacles area cooled through c. 300 °C as a unit between c. 52.5 to 51 Ma. This crustal scale extension marked the beginning of a period of intrusion by mantle-derived igneous rocks throughout the southeastern Canadian Cordillera (Adams et al. 2005) in an extensional tectonic regime.

This study demonstrates how integrated data sets can be used in geologically complex areas. It is particularly relevant to regions where seemingly contrasting tectonic histories can be constructed in adjacent areas where only some datasets are used. It is necessary to compare tectonothermal culminations in the Cordillera using similar and complementary data sets in order to determine whether or not they have common histories.

This study also demonstrates the influence of basement architecture on tectonic processes in the Thor-Odin dome as illustrated by the basement ramp component to the geometry of the Cariboo Alp area. This is an important factor in determining the final shape of tectonothermal culminations,, and can be extrapolated to other tectonothermal culminations since the influence of basement ramps has also been

illustrated in both the Frenchman Cap dome (Gervais et al 2010) and Valhalla Complex (Hallett and Spear 2011).

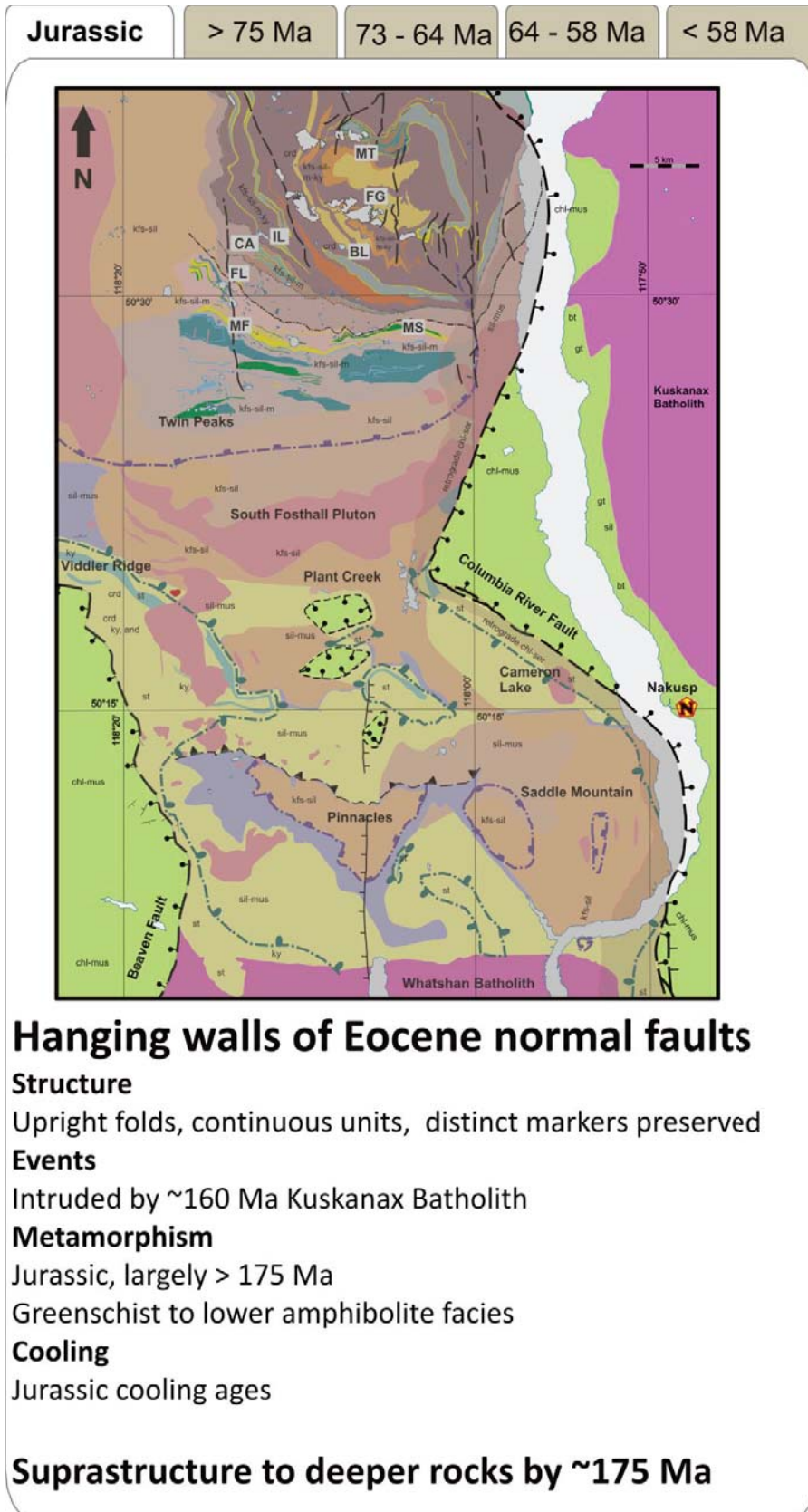
This is the first study to discuss this area in terms of suprastructure-infrastructure transitions to explain contrasting histories in different parts of the Thor-Odin – Pinnacles area. This suprastructure-infrastructure framework makes it possible to explain seemingly conflicting geological histories in adjacent areas while linking the different histories into an internally consistent geological model.

6.5 Future work

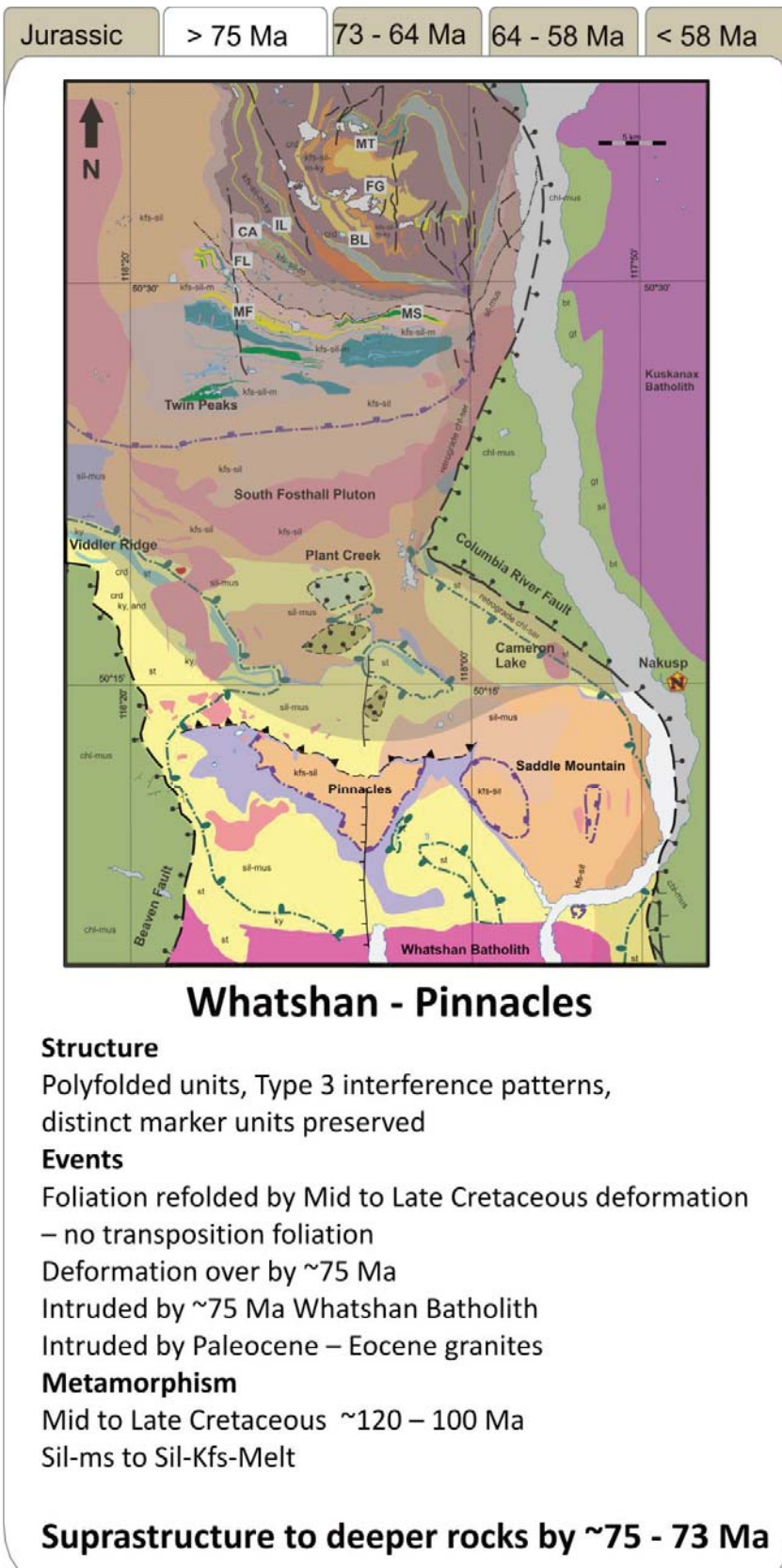
One problem that is only partially solved is the relationship between the basal quartzite in the Thor-Odin dome with the basal quartzite of the Frenchman Cap dome; this should be addressed with a complete LA-ICP-MS detrital zircon study of the Frenchman Cap dome's basal quartzite. Additional dating targets should be the Begbie quartzite in the Thor-Odin dome in order to have better constraints on the origin of the rocks in the northern part of the dome.

Future work in this area should be focused on detailed geochronology combined with thermobarometry, since the timing of prograde metamorphism is the least well constrained problem in the Thor-Odin – Pinnacles area. The pressure, temperature, time and deformation data from all structural levels will make it possible to unravel more of

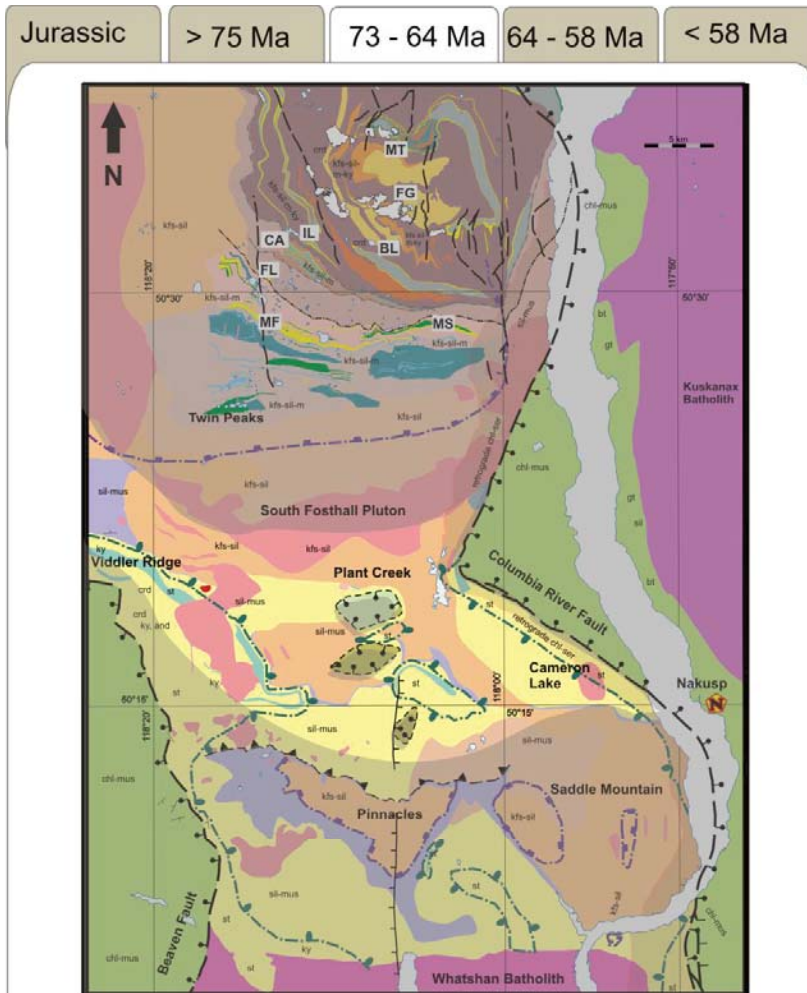
the complex histories discussed in this study. The Twin Peaks and North Fosthall areas would be of particular interest since these areas are the ones that are least well constrained in terms of metamorphic timing and conditions. A detailed thermobarometry – geochronology study following the same strategy used in the thermochronology portion of this study (sampling across boundaries to document discontinuities) will make it possible to prove or disprove the hypothesis presented here that rocks are progressively heated up during burial and transport, and if combined with monazite geochronology will place more precise timing constraints on the proposed suprastructure-infrastructure transitions proposed here.



a)



b)



Plant Creek - South Fosthall

Structure

Transposition foliation, refolded by NE verging folds

Events

Transposed, folded rocks cut by ~62 – 54 Ma Ladybird Suite

Deformation ongoing at ~62, over by ~55 Ma

Metamorphism

Late Cretaceous ~100 - 80 Ma, and younger

Sil-ms ± St to Sil-Kfs

$^{40}\text{Ar}/^{39}\text{Ar}$

Hbl ~62 – 58 Ma ($T_c \sim 500^\circ\text{C}$)

Bt ~52 – 51.5 Ma ($T_c \sim 300^\circ\text{C}$)

Ms ~50.7 Ma ($T_c \sim 450^\circ\text{C}$)

Cooling age, reset by
Ladybird leucogranite

Cooling age, reset by
Ladybird leucogranite

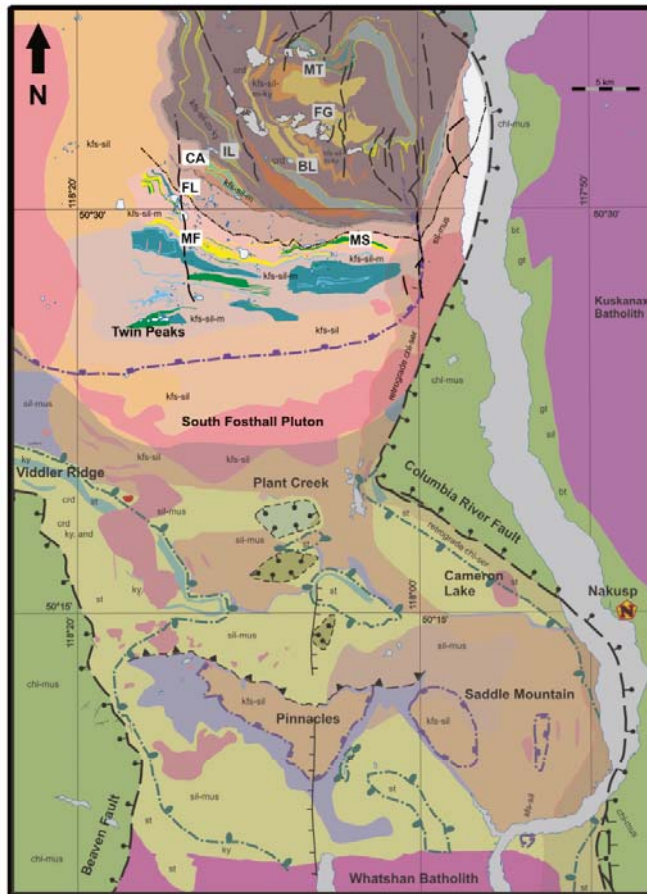
Cooling age for Ladybird pegmatites

Crystallization age for retrograde metamorphism

Suprastructure to deeper rocks by ~64 Ma

c)

Jurassic > 75 Ma 73 - 64 Ma **64 - 58 Ma** < 58 Ma



North Fosthall - Cariboo Alp

Structure

Pervasive transposition, refolded by NE verging folds

Events

Transposition foliation Late Cretaceous to Paleocene

Deformation ongoing before ~60 Ma

Deformation over by ~ 58 Ma

Metamorphism

Late Cretaceous to Paleocene ~73 to 62 , up to ~58 Ma at CA

Sil-Kfs-Melt, migmatites

⁴⁰Ar/³⁹Ar

Hbl ~58 – 55 Ma (Tc ~ 500°C)

Bt ~52 – 51.5 Ma (Tc ~ 300°C)

Ms ~50.7 Ma (Tc ~ 450°C)

Cooling age, reset by
Ladybird leucogranite

Cooling age, reset by
Ladybird leucogranite

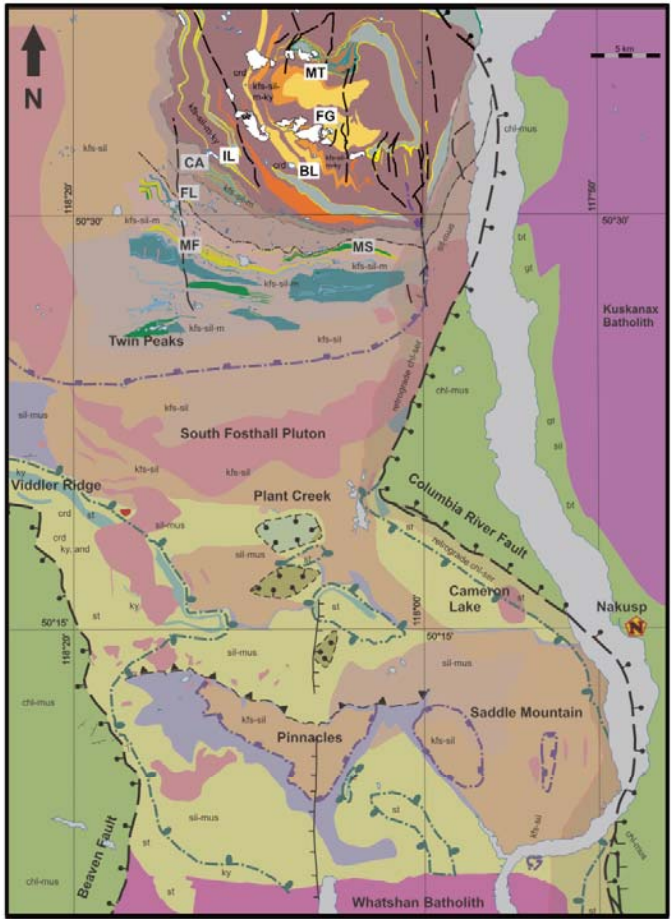
Cooling age for Ladybird pegmatites

Crystallization age for retrograde metamorphism

Suprastructure to deeper rocks by ~58 Ma

d)

Jurassic > 75 Ma 73 - 64 Ma 64 - 58 Ma < 58 Ma



Thor-Odin Dome

Structure

Pervasive NE verging transposition foliation

Events

Transposition foliation Paleocene to Eocene

Deformation ongoing ~ 56 – 54 Ma

Deformation over by ~ 54 – 52.5 Ma

Metamorphism

Paleocene to Eocene ~ 65 to 56 Ma

Sil-Kfs-Melt, ± Ky, Crd, migmatites, anatexis

⁴⁰Ar/³⁹Ar Cooling age

Bt ~ 52 – 51.5 Ma (Tc ~ 300°C)

Ms ~ 50.7 Ma (Tc ~ 450°C)

Cooling age for Ladybird pegmatites
Crystallization age for retrograde metamorphism

Suprastructure to deeper rocks by ~52 Ma?

e)

Figure 6.1 Summary of interpretations of the thermotectonic evolution of the Thor-Odin – Pinnacles area as presented in this study. In each panel the rocks that are highlighted are those being actively deformed in the time period indicated. See text for discussion.

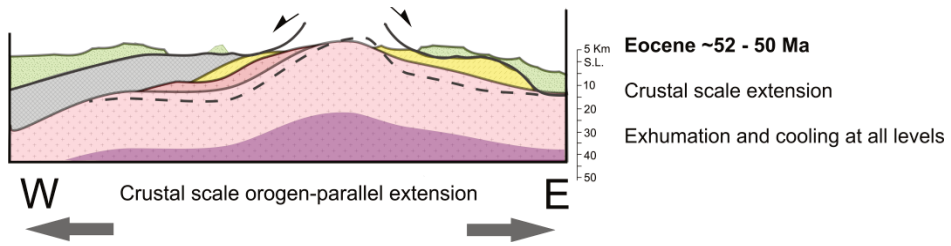
a) Hanging walls of the Columbia River and Beaven faults

b) Whatshan – Pinnacles area

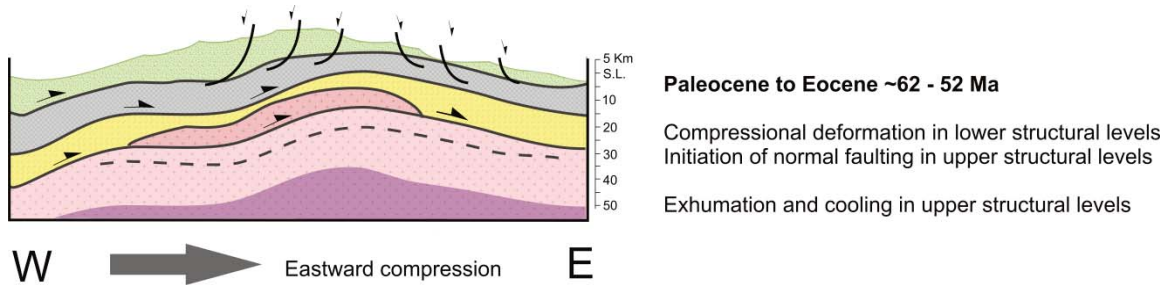
c) Plant Creek area

d) North Fosthall to Cariboo Alp

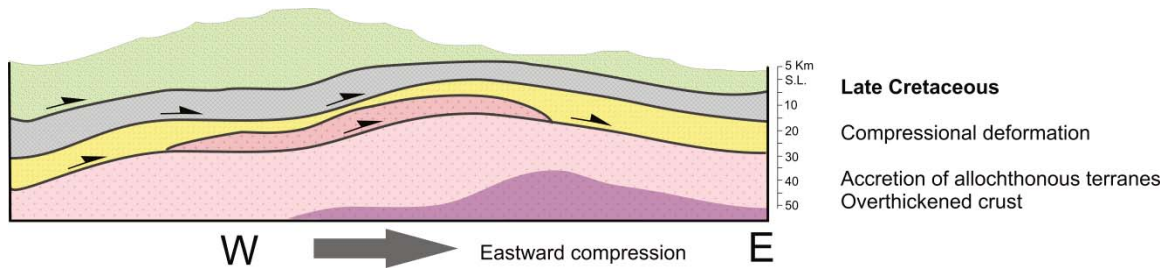
e) The Thor-Odin dome



c)



b)



a)

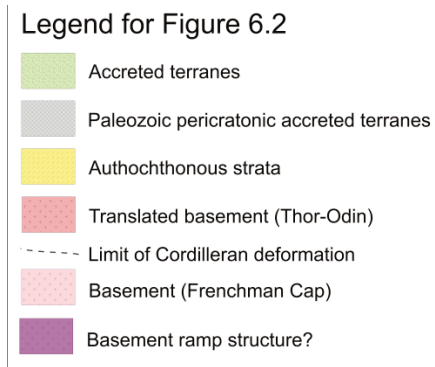


Figure 6.2 Model for the Late Cretaceous to Eocene evolution of the Thor-Odin dome as proposed in this study. The Thor-Odin – Pinnacles area is part of a thrust sheet transported over a basement ramp while being penetratively deformed during the Jurassic to Paleocene shortening in the Cordillera. Rocks were progressively buried and heated during northeast to easterly compression. Cooling and exhumation began first as syn-compressional normal faulting in the upper parts of the structural section, overlapping with penetrative deformation in the lower sections. The major period of movement on the Columbia River fault at c. 52 Ma initiated the crustal scale extension that is active in all areas by c. 51 Ma.

References

Acton S.L., Simony P.S. and Heaman L.M. 2002. Nature of the basement to Quesnel Terrane near Christina Lake, southeastern British Columbia. *Canadian Journal of Earth Sciences* 39: 65-78.

Adams, M.G., Lentz, D.R., Shaw, C.S.J., Williams, P.F., Archibald, D.A., and Cousens, B. 2005. Eocene shoshonitic mafic dykes intruding the Monashee Complex, British Columbia: A petrogenetic relationship with the Kamloops Group volcanic sequence? *Canadian Journal of Earth Sciences*, **42**: 11-24.

Andersen, T. 2005. Detrital zircons as tracers of sedimentary provenance: Limiting conditions from statistics and numerical simulation. *Chemical Geology*, **216**: 249-270.

Anderson, H.E. and Davis, D.W. 1995. U-Pb geochronology of the Moyie Sills, Purcell Supergroup, southeastern British Columbia: Implications for the Mesoproterozoic geological history of the Purcell (Belt) basin. *Canadian Journal of Earth Sciences*, **32**: 1180-1193.

Andronicos, C.L., Chardon, D.H., Hollister, L.S., Gehrels, G.E., and Woodsworth, G.J. 2003. Strain partitioning in an obliquely convergent orogen, plutonism, and syn-orogenic collapse: Coast Mountains batholith, British Columbia, Canada. *Tectonics*, **22**: 1-7.

Archibald, D.A., Glover, J.K., A., P.R., Farrar, E., and Carmichael, D.M. 1983.

Geochronology and tectonic implications of magmatism and metamorphism, southern Kootenay Arc and neighboring regions, southeastern British Columbia. Part I: Jurassic to Mid-Cretaceous. *Canadian Journal of Earth Sciences*, **20**: 1891-1913.

Archibald, D.A., Krogh, T.E., Armstrong, R.L., and Farrar, E. 1984. Geochronology and tectonic implications of magmatism and metamorphism, southern Kootenay Arc and neighboring regions, southeastern British Columbia. Part II: Mid-Cretaceous to Eocene. *Canadian Journal of Earth Sciences*, **21**: 567-583.

Armstrong, R.L. 1982. Cordilleran metamorphic core complexes -- from Arizona to southern Canada. *Annual Review of Earth and Planetary Sciences*, **10**: 129-154.

Armstrong, R.L., Parrish, R.R., P. Van Der Heydenscott, K., Runkle, D., and Brown, R.L. 1991. Early Proterozoic basement exposures in the southern Canadian Cordillera: Core gneiss of Frenchman Cap, Unit I of the Grand Forks Gneiss, and the Vaseaux Formation. *Canadian Journal of Earth Sciences*, **28**: 1169-1201.

Arnaud, N.O. and Kelley, S.P. 1995. Evidence for excess argon during high pressure metamorphism in the Dora Maira Massif (western Alps, Italy), using an ultra-violet laser ablation microprobe $^{40}\text{Ar}/^{39}\text{Ar}$ technique. *Contributions to Mineralogy and Petrology*, **121**: 1-11.

Bardoux, M. 1993. The Okanagan Valley normal fault from Penticton to Enderby, south-central British Columbia. Ph.D. thesis. Carleton University, Ottawa, Canada.

Bardoux, M. and Mareschal, J.C. 1994. Extension in south-central British Columbia: Mechanical and thermal controls. *Tectonophysics*, **238**: 451-470.

Baxter, E.F., DePaolo, D.J., and Renne, P.R. 2002. Spatially correlated anomalous $^{40}\text{Ar}/^{39}\text{Ar}$ "age" variations in biotites about a lithologic contact near Simplon Pass, Switzerland: A mechanistic explanation for excess Ar. *Geochimica et Cosmochimica Acta*, **66**: 1067-1083.

Bea, F., Pereira, M.D., and Stroh, A. 1994. Mineral/leucosome trace-element partitioning in a peraluminous migmatite (a laser ablation-ICP-MS study). *Chemical Geology*, **117**: 291-312.

Bond, G. 1997. New constraints on Rodinia breakup ages from revised tectonic subsidence curves. *Geological Society of America Abstracts with Programs*, **29**: 280.

Boundy, T.M., Hall, C.M., Li, G., Essene, E.J., and Halliday, A.N. 1997. Fine-scale isotopic heterogeneities and fluids in the deep crust: An $^{40}\text{Ar}/^{39}\text{Ar}$ laser ablation and TEM study of muscovite from a granulite-eclogite transition zone. *Earth and Planetary Science Letters*, **148**: 223-242.

Boundy, T.M., Essene, E.J., Hall, C.M., Austrheim, H., and Halliday, A.N. 1996. Rapid exhumation of lower crust during continent-continent collision and late extension:

Evidence from $^{40}\text{Ar}/^{39}\text{Ar}$ incremental heating of hornblendes and muscovites, Caledonian Orogen, Western Norway. *Geological Society of America Bulletin*, **108**: 1425-1437.

Brown, R.L. 1980. Frenchman Cap Dome, Shuswap Complex, British Columbia: A progress report. Current Research, part A: Geological Survey of Canada Paper, **80-1A**: 47-51.

Brown, R.L. and Gibson, H.D. 2006. An argument for channel flow in the southern Canadian Cordillera and comparison with Himalayan tectonics. *In: Channel Flow, Ductile Extrusion and Exhumation in Continental Collision Zones. Edited by: Law, R. D., Searle, M. P. and Godin, L.* Geological Society, London, Special Publications, **268**: 543-559.

Brown, R.L. and Journeay, J.M. 1987. Tectonic denudation of the Shuswap metamorphic terrane of southeastern British Columbia. *Geology*, **15**: 142-146.

Brown, R.L. and Read, P.B. 1983. Shuswap terrane of British Columbia: A Mesozoic "core complex. *Geology*, **11**: 164-168.

Brown, R.L., Journey, J.M., Lane, L.S., Murphy, D.C., and Rees, C.J. 1986. Obduction, backfolding and piggyback thrusting in the metamorphic hinterland of the southeastern Canadian Cordillera. *Journal of Structural Geology*, **8**: 225-268.

Brown, R.L., Carr, S.D., Johnson, B.J., Coleman, V.J., Cook, F.A., and Varsek, J.L. 1992. The Monashee décollement of the southern Canadian Cordillera: A crustal scale shear zone

linking the Rocky Mountain foreland belt to lower crust beneath accreted terranes. *In*: Thrust Tectonics: London, Chapman and Hall, 357-364.

Brown, S.R. 2010. Geology and geochronology of the southern Okanagan Valley Shear Zone, southern Canadian Cordillera, British Columbia. Ph.D. thesis, Simon Fraser University, Vancouver, British Columbia, Canada.

Brown, S.R., Gibson, H.D., Andrews, G.D.M., Thorkelson, D.J., Marshall, D.D., Vervoort, J.D. and Rayner, N., 2012. New constraints on Eocene extension within the Canadian Cordillera and identification of Phanerozoic protoliths for footwall gneisses of the Okanagan Valley shear zone. *Lithosphere* **4**: 354-377.

Callahan, O. 2008. An elevated geothermal gradient prior to early Cenozoic collapse of the North American Cordillera: Evidence and implications.

Carr, S.D. 1990. Late Cretaceous-Early Tertiary tectonic evolution of the southern Omineca belt, Canadian Cordillera. Ph.D. thesis, Carleton University, Ottawa, Canada.

Carr, S.D. 1991a. Three crustal zones in the Thor-Odin – Pinnacles area, southern Omineca belt, British Columbia. *Canadian Journal of Earth Sciences*, **28**: 2003-2023.

Carr, S.D. 1991b. U-Pb zircon and titanite ages of three Mesozoic igneous rocks south of the Thor-Odin– Pinnacles area, southern Omineca belt, British Columbia. *Canadian Journal of Earth Sciences*, **28**: 1877-1882.

Carr, S.D. 1992. Tectonic setting and U-Pb geochronology of the Early Tertiary Ladybird Leucogranite suite, Thor-Odin – Pinnacles area, southern Omineca belt, British Columbia. *Tectonics*, **11**: 258-278.

Carr, S.D. 1995. The southern Omineca Belt, British Columbia: New perspectives from the LITHOPROBE Geoscience Program. *Canadian Journal of Earth Sciences*, **32**: 1720-1739.

Carr, S.D. and Simony, P.S. 2006. Ductile thrusting versus channel flow in the southeastern Canadian Cordillera: Evolution of a coherent crystalline thrust sheet. *In: Channel Flow, Ductile Extrusion and Exhumation in Continental Collision Zones. Edited by: Law, R. D., Searle, M. P. and Godin, L. Geological Society, London, Special Publications*, **268**: 561-587.

Carr, S.D. and Simony, P.S. 2012. Cretaceous to Eocene evolution of the southeastern Canadian Cordillera: Continuity of Rocky Mountain thrust systems with zones of “in-sequence” mid-crustal flow. *In: Cordilleran Tectonics Workshop, Victoria BC, February 24 – 26, 2012.*

Carr, S.D., Parrish, R.R., and Brown, R.L. 1987. Eocene structural development of the Valhalla Complex, southeastern British Columbia. *Tectonics*, **6**: 175-196.

Coleman, V.J. 1990. The Monashee Décollement at Cariboo Alp and regional kinematic indicators, southeastern British Columbia. M.Sc. thesis, Carleton University, Ottawa, Canada.

Colpron, M. and Price, R.A. 1995. Tectonic significance of the Kootenay terrane, southeastern Canadian Cordillera: An alternative model. *Geology*, **23**: 25-28.

Colpron, M., Logan, J.M., and Mortensen, J.K. 2002. U-Pb zircon age constraint for late Neoproterozoic rifting and initiation of the Lower Paleozoic passive margin of western Laurentia. *Canadian Journal of Earth Sciences*, **39**: 133-143.

Colpron, M., Price, R.A., Archibald, D.A., and Carmichael, D.M. 1996. Middle Jurassic exhumation along the western flank of the Selkirk Fan structure: Thermobarometric and thermochronometric constraints from the Illecillewaet Synclinorium, southeastern British Columbia. *Geological Society of America Bulletin*, **108**: 1372-1392.

Coney, P.J. 1980. Cordilleran metamorphic core complexes: An overview. *In*: Cordilleran metamorphic core complexes. Edited by M. Crittenden, P. Coney, P. and G. Davis, G. Geological Society of America Memoir, **153**: 7-31.

Coney, P.J. and Harms, T.A. 1984. Cordilleran metamorphic core complexes: Cenozoic extensional relics of Mesozoic compression. *Geology*, **12**: 550-554.

Cook, F.A. 1995. Lithospheric processes and products in the southern Canadian Cordillera: A LITHOPROBE perspective. *Canadian Journal of Earth Sciences*, **32**: 1803-1824.

Cook, F.A., Varsek, J.L., Clowes, R.M., Kanasewich, E.R., Spencer, C.S., Parrish, R.R., Brown, R.L., Carr, S.D., Johnson, B.J., and Price, R.A. 1992. LITHOPROBE crustal reflection structure of the southern Canadian Cordillera 1, Foreland Thrust and Fold belt to Fraser River fault. *Tectonics*, **11**: 12-35.

Corfu, F., Hanchar, J.M., Hoskin, P.W.O., and Kinny, P. 2003. Atlas of zircon textures. Mineralogical Society of America, *Reviews in Mineralogy and Geochemistry*, **53**: 469-500.

Cosca, M.A. and O'Nions, R.K. 1994. A re-examination of the influence of composition on argon retentivity in metamorphic calcic amphiboles. *Chemical Geology*, **112**: 39-56.

Crider, J.G. 2011. Persistently high geothermal gradient above the Okanogan detachment: Thermal weakening is a cause but not trigger of orogenic collapse. GSA Annual Meeting, Minneapolis, USA.

Crowley, J.L. 1997. U-Pb geochronologic constraints on the cover sequence of the Monashee Complex, Canadian Cordillera: Paleoproterozoic deposition on basement. *Canadian Journal of Earth Sciences*, **34**: 1008-1022.

Crowley, J.L. 1999. U-Pb geochronologic constraints on Paleoproterozoic tectonism in the Monashee Complex, Canadian Cordillera: Elucidating an overprinted geologic history. *Geological Society of America Bulletin*, **111**: 560-577.

Crowley, J.L. and Parrish, R.R. 1999. U-Pb isotopic constraints on diachronous metamorphism in the northern Monashee Complex, southern Canadian Cordillera. *Journal of Metamorphic Geology*, **17**: 483-502.

Crowley, J.L., Brown, R.L., and Parrish, R.R. 2001. Diachronous deformation and a strain gradient beneath the Selkirk Allochthon, northern Monashee Complex, southeastern Canadian Cordillera. *Journal of Structural Geology*, **23**: 1103-1121.

Crowley, J.L., Brown, R.L., Gervais, F., and Gibson, H.D. 2008. Assessing inheritance of zircon and monazite in granitic rocks from the Monashee Complex, Canadian Cordillera. *Journal of Petrology*, **49**: 1915-1929.

Cubley, J.F. and Pattison, D.R.M. 2012. Metamorphism and deformation of the Grand Forks complex: implications for the exhumation history of the Shuswap core complex, southern British Columbia. *Canadian Journal of Earth Sciences*. **49**: 1329-1363.

Cubley J.F., Pattison D.R.M., Archibald D.A. and Jolivet M. 2013a. Thermochronological constraints on the Eocene exhumation of the Grand Forks complex, British Columbia, based on $^{40}\text{Ar}/^{39}\text{Ar}$ and apatite fission track geochronology. *Canadian Journal of Earth Sciences* **50**: 576-598.

Cubley, J.F., Pattison, D.R.M., Tinkham D.K., Fanning, C.M. 2013b. U-Pb geochronological constraints on the timing of metamorphism and high-T exhumation in the Grand Forks complex, British Columbia. *Lithos* **156**: 241-267.

Culshaw, N.G., Beaumont, C., and Jamieson, R.A. 2006. The orogenic superstructure-infrastructure concept: Revisited, quantified, and revived. *Geology* **34**: 733-736.

Cumbest, R.J., Johnson, E.L., and Onstott, T.C. 1994. Argon composition of metamorphic fluids: Implications for $^{40}\text{Ar}/^{39}\text{Ar}$ geochronology. *Geological Society of America Bulletin*, **106**: 942-951.

Dahl, P.S. 1996b. The effects of composition on retentivity of argon and oxygen in hornblende and related amphiboles: A field-tested empirical model. *Geochimica et Cosmochimica Acta*, **60**: 3687-3700.

Dahl, P.S. 1996a. The crystal-chemical basis for Ar retention in micas: Inferences from interlayer partitioning and implications for geochronology. *Contributions to Mineralogy and Petrology*, **123**: 22-39.

Dallmeyer, D. and Rivers, T. 1983. Recognition of excess ^{40}Ar through incremental-release $^{40}\text{Ar}/^{39}\text{Ar}$ analysis of biotite and hornblende across the Grenvillian metamorphic gradient in southwestern Labrador. *Geochimica et Cosmochimica Acta*, **47**: 413-428.

Dalrymple, G.B., Alexander Jr, E.C., Lanphere, M.A., and Kraker, G.P. 1981. Irradiation of samples for $^{40}\text{Ar}/^{39}\text{Ar}$ dating using the Geological Survey TRIGA reactor. U.S. Geological Survey Professional Paper **1176**.

DeGraaff-Surpless, K., Mahoney, J.B., Wooden, J.L., and McWilliams, M.O. 2003. Lithofacies control in detrital zircon provenance studies: Insights from the Cretaceous Methow Basin, southern Canadian Cordillera. Geological Society of America Bulletin, **115**: 899-915.

Dodson, M.H. 1973. Closure temperature in cooling geochronological and petrological systems. Contributions to Mineralogy and Petrology, **40**: 259-274.

Doughty, P.T. and Price, R.A. 1999. Tectonic evolution of the Priest River Complex, northern Idaho and Washington: A reappraisal of the Newport fault with new insights on metamorphic core complex formation. Tectonics, **18**: 375-393.

Duncan, I.J. 1984. Structural evolution of the Thor-Odin gneiss dome. Tectonophysics, **101**: 87-130.

Duncan, I.J. 1982. The evolution of the Thor-Odin gneiss dome and related geochronological studies. Ph.D., University of British Columbia, Vancouver, Canada.

Eisbacher, G.H. 1985. Pericollisional strike-slip faults and synorogenic basins, Canadian Cordillera. Society of Economic Paleontologists and Mineralogists Special Publication **37**: 1-256.

Engebretson, D.C., Cox, A., and Gordon, R.G. 1985. Relative motions between oceanic and continental plates in the Pacific basin. Special Paper, Geological Society of America, **206**: 1-59.

Erdmer, P., Heaman, L., Creaser, R.A., Thompson, R.I., and Daughtry, K.L. 2001. Eocambrian granite clasts in southern British Columbia shed light on Cordilleran hinterland crust. Canadian Journal of Earth Sciences, **38**: 1007-1016.

Erdmer, P., Moore, J.M., Heaman, L., Thompson, R.I., Daughtry, K.L., and Creaser, R.A. 2002. Extending the ancient margin outboard in the Canadian Cordillera: Record of Proterozoic crust and Paleocene regional metamorphism in the Nicola Horst, southern British Columbia. Canadian Journal of Earth Sciences **39**: 1605-1623.

Evenchick, C.A., Parrish, R.R., and Gabrielse, H.G. 1984. Precambrian gneiss and Late Proterozoic sedimentation in north-central British Columbia. Geology, **12**: 233-237.

Evenchick, C.A., McMechan, M.E., McNicoll, V.J., and Carr, S.D. 2007. A synthesis of the Jurassic–Cretaceous tectonic evolution of the central and southeastern Canadian Cordillera: Exploring links across the orogen. Geological Society of America Special Papers, **433**: 117-145.

Ewing, T.E. 1980. Paleogene tectonic evolution of the Pacific northwest. The Journal of Geology, **88**: 619-638.

Fayon, A.K., Whitney, D.L., and Teyssier, C. 2004. Exhumation of orogenic crust; diapiric ascent versus low-angle normal faulting. Special Paper, Geological Society of America, **380**: 129-139.

Fedo, C.M., Sircombe, K.N., and Rainbird, R.H. 2003. Detrital zircon analysis of the sedimentary record. *Reviews in Mineralogy and Geochemistry*, **53**: 277-303.

Fermor, P.R., 1999. Aspects of the three-dimensional structure of the Alberta Foothills and front ranges. *Geological Society of American Bulletin* **111**: 317-346.

Fossen, H. 2000. Extensional tectonics in the Caledonides: Synorogenic or postorogenic? *Tectonics*, **19**: 213-224.

Fritz, W.H., Cecile, M.P., Norford, B.S., Morrow, D., and Geldsetzer, H. 1991. Cambrian to Middle Devonian assemblages. *In* *Geology of the Cordilleran Orogen in Canada. Edited by H.G. Gabrielse and C.J. Yorath.*, Geological Survey of Canada, Ottawa, Canada. *Geology of Canada Series* **4**: 151-218.

Fyles, J.T. 1964. *Geology of the Duncan Lake area, Lardeau District, British Columbia.* *Geology of the Duncan Lake area, Lardeau District, British Columbia.* British Columbia Department of Mines and Petroleum Resources, *Bulletin* **49**.

Fyles, J.T. and Eastwood, G.E.P. 1962. *Geology of the Ferguson area, Lardeau District, British Columbia.* British Columbia Department of Mines and Petroleum Resources, *Bulletin* **45**.

Gabrielse, H., Monger, J.W.H., Wheeler, J.O., and Yorath, C.J. 1991. Tectonic synthesis. *In* *Geology of the Cordilleran Orogen in Canada. Edited by H.G. Gabrielse and C.J. Yorath.* Geological Survey of Canada, Ottawa, Canada. *Geology of Canada Series 4*: 679-705.

Gehrels, G.E. 2000. Introduction to detrital zircon studies of Paleozoic and Triassic strata in western Nevada and northern California. *Geological Society of America Special Papers*, **347**: 1-17.

Gehrels, G.E. and Ross, G.M. 1998. Detrital zircon geochronology of Neoproterozoic to Permian miogeoclinal strata in British Columbia and Alberta. *Canadian Journal of Earth Sciences*, **35**: 1380-1401; 1380.

Gervais, F. 2009. Pressure-temperature-time-deformation paths of former mid-crustal rocks, northern Monashee Complex of the southeastern Canadian Cordillera: A model of synconvergent exhumation by sequential ductile extrusion. Ph.D. thesis, Carleton University, Ottawa, Canada.

Gervais, F. and Brown, R.L. 2011. Testing modes of exhumation in collisional orogens: Synconvergent channel flow in the southeastern Canadian Cordillera. *Lithosphere*, **3**: 55-75.

Gervais, F., Brown, R.L., and Crowley, J.L. 2010. Tectonic implications for a Cordilleran orogenic base in the Frenchman Cap dome, southeastern Canadian Cordillera. *Journal of Structural Geology*, **32** 941-959.

Ghent, E. and Villeneuve, M. 2006. $^{40}\text{Ar}/^{39}\text{Ar}$ dates on hornblende, muscovite, and biotite from the Mica Creek area, British Columbia: Regional metamorphic and tectonic implications. *Canadian Journal of Earth Sciences*, **43**: 83-100.

Gibson, H.D., Brown, R.L., and Carr, S.D. 2008. Tectonic evolution of the Selkirk Fan, southeastern Canadian Cordillera: A composite middle Jurassic–Cretaceous orogenic structure. *Tectonics*, **27**: TC6007.

Gibson, H.D., Carr, S.D., Hamilton, M.A., and Brown, R.L. 2004. Correlating yttrium zones and age domains in monazite with metamorphic reactions involving major pelitic phases: An integration of ID-TIMS and SHRIMP geochronology with Y-Th-U X-ray mapping. *Chemical Geology*, **211**: 237-260.

Glombick, P.M. 2005. Mesozoic to Early Tertiary tectonic evolution of the Shuswap metamorphic complex in the Vernon area, southeastern Canadian Cordillera. Ph.D. thesis, University of Alberta, Edmonton.

Glombick, P., Thompson, R.I., Erdmer, P., and Daughtry, K.L., 2006. A reappraisal of the tectonic significance of early Tertiary low-angle shear zones exposed in the Vernon map area (82 L), Shuswap metamorphic complex, southeastern Canadian Cordillera: *Canadian Journal of Earth Sciences* **43**: 245-268.

Gordon, S.M., Whitney, D.L., Teyssier, C., Grove, M., and Dunlap, W.J. 2008. Timescales of migmatization, melt crystallization, and cooling in a Cordilleran gneiss dome: Valhalla complex, southeastern British Columbia. *Tectonics*, **27**: TC4010.

Hall, C.M. 1981. The application of K-Ar and $^{40}\text{Ar}/^{39}\text{Ar}$ methods to the dating of recent volcanics and the Laschamp event. Ph.D. thesis, University of Toronto, Toronto, Canada.

Hallett, B.W. and Spear, F.S. 2011. Insight into the cooling history of the Valhalla Complex, British Columbia. *Lithos*, **125**: 809-824.

Hames, W.E. and Bowring, S.A. 1994. An empirical evaluation of the argon diffusion geometry in muscovite. *Earth and Planetary Science Letters*, **124**: 161-169.

Harrison, T.M. 1981. Diffusion of ^{40}Ar in hornblende. *Contributions to Mineralogy & Petrology*, **78**: 324-331.

Harrison, T.M., Duncan, I., and McDougall, I. 1985. Diffusion of ^{40}Ar in biotite: Temperature, pressure and compositional effects. *Geochimica et Cosmochimica Acta*, **49**: 2461-2468.

Hinchey, A.M. 2005. Thor-Odin dome: Constraints on Paleocene-Eocene anatexis and deformation, leucogranite generation and the tectonic evolution of the southern Omineca belt, Canadian Cordillera. Ph.D. thesis, Carleton University, Ottawa, Ontario, Canada.

Hinchey, A.M. and Carr, S.D. 2006. The S-type ladybird leucogranite suite of southeastern British Columbia: Geochemical and isotopic evidence for a genetic link with migmatite formation in the North American basement gneiss of the Monashee Complex. *Lithos*, **90**: 223-248.

Hinchey, A.M. and Carr, S.D. 2007. Protolith composition of cordierite-gedrite basement rocks and garnet amphibolite of the Bearpaw Lake area of Thor-Odin dome, Monashee Complex, British Columbia. *The Canadian Mineralogist*, **45**: 607-629.

Hinchey, A.M., Carr, S.D., and Rayner, N. 2007. Bulk compositional controls on the preservation of age domains within metamorphic monazite: A case study from quartzite and garnet-cordierite-gedrite gneiss of Thor-Odin dome, Monashee Complex, Canadian Cordillera. *Chemical Geology*, **240**: 85-102.

Hinchey, A.M., Carr, S.D., McNeill, P.D., and Rayner, N. 2006. Paleocene-Eocene high-grade metamorphism, anatexis and deformation in the Thor-Odin dome, Monashee Complex, southeastern British Columbia. *Canadian Journal of Earth Sciences*, **43**: 1341-1365.

Höy, T. 1977. Big ledge (82L/8E). *Geology in British Columbia*. British Columbia Ministry of Mines and Petroleum Resources, **75**: G18-G29.

Höy, T. 1987. *Geology of the Cottonbelt lead-zinc-magnetite layer, carbonatites and alkalic rocks in the Mount Grace area, Frenchman Cap dome, southeastern British*

Columbia. British Columbia Ministry of Energy, Mines, and Petroleum Resources Bulletin **80**: 99 p.

Höy, T. 2000. Sedex and Broken Hill-type deposits, northern Monashee Mountains, southern British Columbia. BC Ministry of Energy and Mines, Geological Fieldwork 2000, Paper **2001-1**: 85-114.

Höy, T. and Brown, R.L. 1980. Geology of the eastern margin of Frenchman Cap dome. British Columbia Ministry of Energy, Mines and Petroleum Resources Bulletin, Preliminary Map **No. 43**.

Höy, T. and Godwin, C.I. 1988. Significance of a Cambrian date from galena lead-isotope data for the stratiform Cottonbelt deposit in the Monashee Complex, southeastern British Columbia. Canadian Journal of Earth Sciences, **25**: 1534-1541.

Langenberg, C.W., Beaton, A., Berhane, H., 2002. Regional evaluation of the Coalbed methane potential of the Foothills/Mountains of Alberta. Alberta Geological Survey, Earth Sciences Report 74.

Lerbekmo, J.F., Heaman, L.M., Baadsgaard, H., Muehlenbachs, K., Evans, M.E., Sweet, A.R., 2008. Normal polarity magnetosubchrons in 24r and the age of the Paleocene - Eocene boundary. Canadian Journal of Earth Sciences **45**: 781-793.

Jefferson, C. and Parrish, R. 1989. Late Proterozoic stratigraphy, U-Pb zircon ages, and rift tectonics, Mackenzie Mountains, northwestern Canada. *Canadian Journal of Earth Sciences*, **26**: 1784-1801.

Johnson, B.J. 1994. Structure and tectonic setting of the Okanagan Valley fault system in the Shuswap Lake area, southern British Columbia. Ph.D. thesis, Carleton University, Ottawa, Canada.

Johnson, B.J. 2006. Extensional shear zones, granitic melts, and linkage of overstepping normal faults bounding the Shuswap metamorphic core complex, British Columbia. *Geological Society of America Bulletin*, **118**: 366-382.

Johnson, B.J. and Brown, R.L. 1996. Crustal structure and early Tertiary extensional tectonics of the Omineca belt at 51°N latitude, southern Canadian Cordillera. *Canadian Journal of Earth Sciences*, **33**: 1596-1611.

Johnston, D.H., Williams, P.F., Brown, R.L., Crowley, J.L., and Carr, S.D. 2000. Northeastward extrusion and extensional exhumation of crystalline rocks from the Monashee Complex, southeastern Canadian Cordillera. *Journal of Structural Geology*, **22**: 603-625.

Journey, J.M. 1986. Stratigraphy, internal strain, and thermotectonic evolution of northern Frenchman Cap dome, an exhumed basement duplex structure, Omineca

hinterland, southeastern Canadian Cordillera. Ph. D. thesis, Queen's University, Kingston, Canada.

Kelley, S. 2002. Excess argon in K–Ar and Ar–Ar geochronology. *Chemical Geology*, **188**: 1-22.

Kelley, S., Turner, G., Butterfield, A.W., and Shepherd, T.J. 1986. The source and significance of argon isotopes in fluid inclusions from areas of mineralization. *Earth and Planetary Science Letters*, **79**: 303-318.

Kelley, S.P. and Wartho, J.A. 2000. Rapid kimberlite ascent and the significance of Ar–Ar ages in xenolith phlogopites. *Science*, **289**: 609-611.

Klepacki, D. and Wheeler, J. 1985. Stratigraphic and structural relations of the Milford, Kaslo, and Slocan Groups, Goat Range, Lardeau and Nelson map areas, British Columbia: Geological Survey of Canada, Paper **85-1A**: 277-286.

Klepacki, D.W. 1985. Stratigraphy and structural geology of the Goat Range area, southeastern British Columbia. Ph.D. thesis, Massachusetts Institute of Technology, Boston, USA.

Košler, J. 2008. Laser ablation sampling strategies for concentration and isotope ratio analyses by ICP-MS. *In: Laser ablation ICP-MS in the Earth sciences: current practices and outstanding issues. Edited by P. Sylvester. Mineralogical Association of Canada, Short Course Series, 40*: 79-92.

Košler, J., Forst, L., and Sláma, J. 2008. LamDate and LamTool: Spreadsheet-based data reduction for laser ablation ICP-MS. *In: Laser ablation ICP-MS in the Earth Sciences: current practices and outstanding issues: Edited by P. Sylvester.* Mineralogical Association of Canada, Short Course Series, **40**: 315-317.

Kretz, R. 1983. Symbols for rock-forming minerals. *American Mineralogist*, **68**: 77-279.

Krogh, T. 1982. Improved accuracy of U-Pb zircon ages by the creation of more concordant systems using an air abrasion technique. *Geochimica et Cosmochimica Acta*, **46**: 637-649.

Kruse, S. 2007. Structural evolution of the northern Thor–Odin culmination, Monashee Complex, southern Canadian Cordillera. Ph.D. thesis, University of New Brunswick, Fredericton, Canada.

Kruse, S. and Williams, P.F. 2005. Brittle faulting in the Thor-Odin culmination, Monashee Complex, southern Canadian Cordillera: Constraints on geometry and kinematics. *Canadian Journal of Earth Sciences*, **42**: 2141-2160.

Kruse, S. and Williams, P.F. 2007. The Monashee reflection: Re-examination of a LITHOPROBE crustal-scale seismic reflection in the southern Canadian Cordillera. *Geosphere*, **3**: 26-41.

Kruse, S., McNeill, P.D., and Williams, P.F. 2004. A geological compilation map of the Thor–Odin dome. Provided by personal communication.

Kuiper, Y. 2003. Isotopic constraints on timing of deformation and metamorphism in the Thor-Odin dome, Monashee Complex, southeastern British Columbia. Ph.D. thesis, University of New Brunswick, Fredericton, Canada.

Kuiper, Y.D., Williams, P.F., and Kruse, S. 2006. Possibility of channel flow in the southern Canadian Cordillera; a new approach to explain existing data. *In: Channel Flow, Ductile Extrusion and Exhumation in Continental Collision Zones. Edited by: Law, R. D., Searle, M. P. and Godin, L. Geological Society of London, Special Publication 268: 589-611.*

Lanphere, M.A. and Brent Dalrymple, G. 1976. Identification of excess ^{40}Ar by the $^{40}\text{Ar}/^{39}\text{Ar}$ age spectrum technique. *Earth and Planetary Science Letters*, **32**: 141-148.

Leake, B.E., Elias, E.M., and Farrow, C.M. 1988. The relationship of argon retentivity and chemical composition of hornblende. *Geochimica et Cosmochimica Acta*, **52**: 2165.

Lee, J.K.W. 1995. Multipath diffusion in geochronology. *Contributions to Mineralogy and Petrology*, **120**: 60-82.

Lee, J.K.W. 2000. Empirical constraints on closure temperature from a single diffusion coefficient. *Contributions to Mineralogy and Petrology*, **139**: 526-540.

Lee, J.K.W. 2009. Using argon as a temporal tracer of large-scale geologic processes. *Chemical Geology*, **266**: 104-112.

Lemieux, Y. 2006. Structure, geochronology and thermobarometry of the eastern flank of the Shuswap metamorphic complex in the Upper Arrow Lake area, southeastern British Columbia. Ph.D. thesis, University of Alberta, Edmonton, Canada.

Lemieux, Y., Thompson, R.I., and Erdmer, P. 2003. Stratigraphy and structure of the Upper Arrow Lake area, southeastern British Columbia: New perspectives for the Columbia River fault zone. Geological Survey of Canada, Current Research **2003-A7**: 1-9.

Lemieux, Y., Thompson, R.I., and Erdmer, P. 2004. Stratigraphic and structural relationships across the Columbia River fault zone, Vernon and Lardeau map areas, British Columbia. Geological Survey of Canada, Current research **2004-A3**: 1-8.

Lemieux, Y., Thompson, R.I., Erdmer, P., Simonetti, A., and Creaser, R.A. 2007. Detrital zircon geochronology and provenance of Late Proterozoic and Mid-Paleozoic successions outboard of the miogeocline, southeastern Canadian Cordillera. Canadian Journal of Earth Sciences, **44**: 1675-1693.

Lewis, R.S., Vervoort, J.D., Burmester, R.F. and Oswald, P.J. 2010. Detrital zircon analysis of Mesoproterozoic and Neoproterozoic metasedimentary rocks of north-central Idaho: implications for development of the Belt–Purcell basin. Canadian Journal of Earth Sciences, **47**: 1383-1404

Little, H.W. 1960. Nelson map-area, west half, British Columbia. Geological Survey of Canada, Memoir **308**.

Lonsdale, P.F. 1988. Paleogene history of the Kula plate; offshore evidence and onshore implications. *Geological Society of America Bulletin*, **100**: 733-754.

Lorencak, M., Seward, D., Vanderhaeghe, O., Teyssier, C., and Burg, J.-. 2001. Low-temperature cooling history of the Shuswap metamorphic core complex, British Columbia; constraints from apatite and zircon fission-track ages. *Canadian Journal of Earth Sciences* **38**: 1615-1625.

Ludwig, K.R. 2003. User's manual for Isoplot 3.00. Berkeley Geochronology Center, CA.

McDonough, M.R. and Parrish, R.R. 1991. Proterozoic gneisses of the Malton Complex, near Valemount, British Columbia: U–Pb ages and Nd isotopic signatures. *Canadian Journal of Earth Sciences*, **28**: 1202-1216.

McDougall, I. and Harrison, T.M. 1999. *Geochronology and thermochronology by the $^{40}\text{Ar}/^{39}\text{Ar}$ method*. Oxford University Press, New York.

McMechan, M.E., 1995. *Geology of rocky mountain foothills and front ranges in Kananaskis country, west of Fifth Meridian, Alberta*. Geological Survey of Canada. Map 1865A.

McMechan, M.E., 2001. Large scale duplex structures in the McConnell thrust sheet, Rocky Mountains, Southwest Alberta. *Bulletin of Canadian Petroleum Geology* **49**: 408-425.

McMillan, W.J. 1973. Petrology and structure of the west flank, Frenchman's Cap dome, near Revelstoke, British Columbia. Geological Survey of Canada, Paper **71-29**: 1-29.

McNeill, P.D. 2002. Structural evolution of migmatites of the Thor-Odin area of the Monashee Complex, southern British Columbia, Canada. *In* 2002 GSA Denver Annual Meeting.

McNicoll, V.J. and Brown, R.L. 1995. The Monashee décollement at Cariboo Alp, southern flank of the Monashee Complex, southern British Columbia, Canada. *Journal of Structural Geology*, **17**: 17-30.

Millonig, L.J., Gerdes, A., and Groat, L.A. 2012. U-Th-Pb geochronology of meta-carbonatites and meta-alkaline rocks in the southern Canadian Cordillera: A geodynamic perspective. *Lithos*, **152**: 202-217.

Monger, J. and Journeay, J. 1994. Basement geology and tectonic evolution of the Vancouver region. Geological Survey of Canada, Bulletin, **481**: 3-25.

Monger, J. and Price, R.A. 2000. A transect of the southern Canadian Cordillera from Canadian Cordillera Vancouver to Calgary. Natural Resources Canada.

Monger, J.W.H., Price, R.A., and Tempelman-Kluit, D.J. 1982. Tectonic accretion and the origin of the two major metamorphic and plutonic belts in the Canadian Cordillera. *Geology*, **10**: 70-75.

Monger, J., Wheeler, J., Tipper, H., Gabrielse, H., Harms, T., Struik, L., Campbell, R., Dodds, C., Gehrels, G., and O'Brien, J. 1991. Part B. Cordilleran terranes: Upper Devonian to Middle Jurassic assemblages. *In* *Geology of the Cordilleran Orogen in Canada*. Edited by H.G. Gabrielse and C.J. Yorath. Geological Survey of Canada, Ottawa, Canada. *Geology of Canada Series* **4**: 281-327.

Mortensen, J. and Colpron, M. 1998. Geochronological and geochemical studies of the Coates Lake diatreme, southern Mackenzie Mountains, western NWT. *Lithoprobe, Report*, **64**: 1-278.

Morton, A., Cloué-Long, J., and Berge, C. 1996. Factors influencing heavy mineral suites in the Statfjord Formation, Brent Field, North Sea: Constraints provided by SHRIMP U–Pb dating of detrital zircons. *Journal of the Geological Society, London*, **153**: 911-929.

Mulch, A. and Cosca, M.A. 2004. Recrystallization or cooling ages: In situ UV-laser $^{40}\text{Ar}/^{39}\text{Ar}$ geochronology of muscovite in mylonitic rocks. *Journal of the Geological Society*, **161**: 573-582.

Murphy, D.C., 1987. Suprastructure/infrastructure transition, east-central Cariboo Mountains, British Columbia: geometry, kinematics and tectonic implications. *Journal of Structural Geology* **9**: 13-29.

Murphy, D.C., Walker, R.T., and Parrish, R.R. 1991. Age and geological setting of Gold Creek gneiss, crystalline basement of the Windermere Supergroup, Cariboo Mountains, British Columbia. *Canadian Journal of Earth Sciences*, **28**: 1217-1231.

Norlander, B.H., Whitney, D.L., Teyssier, C., and Vanderhaeghe, O. 2002. Partial melting and decompression of the Thor-Odin dome, Shuswap metamorphic core complex, Canadian Cordillera. *Lithos*, **61**: 103-125.

Okulitch, A.V. 1984. The role of the Shuswap metamorphic complex in Cordilleran tectonism: A review. *Canadian Journal of Earth Sciences*, **21**: 1171-1193.

Onstott, T.C. and Peacock, M.W. 1987. Argon retentivity of hornblendes: A field experiment in a slowly cooled metamorphic terrane. *Geochimica et Cosmochimica Acta*, **51**: 2891-2903.

Parkinson, D. 1991. Age and isotopic character of early Proterozoic basement gneisses in the southern Monashee Complex, southeastern British Columbia. *Canadian Journal of Earth Sciences*, **28**: 1159-1168.

Parkinson, D. 1992. Age and evolution of the southern Monashee Complex, southeastern British Columbia; a window into the deep crust. Ph.D. thesis, University of California, Santa Barbara, USA.

Parrish, R.R. 1990. U-Pb dating of monazite and its application to geological problems. *Canadian Journal of Earth Sciences*, **27**: 1431-1450.

Parrish, R. 1992. U-Pb ages of Jurassic–Eocene plutonic rocks in the vicinity of Valhalla complex, southeast British Columbia. *Radiogenic age and isotopic studies: Report*, **5**: 91 – 92.

Parrish, R.R. 1995. Thermal evolution of the southeastern Canadian Cordillera. *Canadian Journal of Earth Sciences*, **32**: 1618-1642.

Parrish, R.R. and Armstrong, R.L. 1987. The ca. 162 ma galena bay stock and its relationship to the Columbia River fault zone, southeast British Columbia. *Radiogenic age and isotopic studies: Report*, **1**: 87 – 2.

Parrish, R. and Reichenbach, I. 1991. Age of xenocrystic zircon from diatremes of western Canada. *Canadian Journal of Earth Sciences*, **28**: 1232-1238.

Parrish, R. and Scammell, R. 1988. The age of the Mount Copeland syenite gneiss and its metamorphic zircons, Monashee Complex, southeastern British Columbia. *Radiogenic age and isotopic studies: Report*, **2**: 88 – 82.

Parrish, R.R. and Wheeler, J.O. 1983. U-Pb zircon age of the Kuskanax batholith, southeastern British Columbia. *Canadian Journal of Earth Sciences*, **20**: 1751-1756.

Parrish, R.R., Carr, S.D., and Parkinson, D.L. 1988. Eocene extensional tectonics and geochronology in the southern Omineca belt, British Columbia and Washington. *Tectonics*, **7**: 181-212.

Pell, J. and Simony, P. 1987. New correlations of Hadrynian strata, south-central British Columbia. *Canadian Journal of Earth Sciences*, **24**: 302-313.

Petersen, N.T., Smith, P.L., Mortensen, J.K., Creaser, R.A., and Tipper, H.W. 2004. Provenance of Jurassic sedimentary rocks of south-central Quesnellia, British Columbia: Implications for paleogeography. *Canadian Journal of Earth Sciences*, **41**: 103-125.

Pollock, J.C., Hibbard, J.P., and Sylvester, P.J. 2009. Early Ordovician rifting of Avalonia and birth of the Rheic ocean: U–Pb detrital zircon constraints from Newfoundland. *Journal of the Geological Society*, **166**: 501-515.

Powell, C.M., Li, Z., McElhinny, M., Meert, J., and Park, J. 1993. Paleomagnetic constraints on timing of the Neoproterozoic breakup of Rodinia and the Cambrian formation of Gondwana. *Geology*, **21**: 889-892.

Price, R.A. 1994. Cordilleran tectonics and the evolution of the Western Canada sedimentary basin. Canadian Society of Petroleum Geologists - Alberta Research Council, Calgary.

Price, R.A., 2007. Fault dating in the Canadian Rocky Mountains: evidence for late Cretaceous and early Eocene orogenic pulses: Comment. *Geology*. doi:10.1130/G23592C.1.

Price, R.A. and Mountjoy, E. 1970. Geologic structure of the Canadian Rocky Mountains between Bow and Athabasca rivers; a progress report. *In*: Structure of the southern Canadian Cordillera: Geological Association of Canada, Special Publication, **6**: 7-25.

Raeside, R.P. and Simony, P.S. 1983. Stratigraphy and deformational history of the Scrip Nappe, Monashee Mountains, British Columbia. Canadian Journal of Earth Sciences, **20**: 639-650.

Rainbird, R. and Davis, W. 2007. U-Pb detrital zircon geochronology and provenance of the Late Paleoproterozoic Dubawnt Supergroup: Linking sedimentation with tectonic reworking of the western Churchill Province, Canada. Geological Society of America Bulletin, **119**: 314-328.

Rainbird, R., Hadlari, T., Aspler, L., Donaldson, J., LeCheminant, A., and Petersen, T. 2003. Sequence stratigraphy and evolution of the Paleoproterozoic intracontinental Baker Lake and Thelon basins, western Churchill province, Nunavut, Canada. Precambrian Research, **125**: 21-53.

Rainbird, R.H., McNicoll, V., Theriault, R., Heaman, L., Abbott, J., Long, D., and Thorkelson, D. 1997. Pan-continental river system draining Grenville orogen recorded by U-Pb and Sm-Nd geochronology of Neoproterozoic quartzarenites and mudrocks, northwestern Canada. The Journal of Geology, **105**: 1-17.

Read, P.B. 1973. Petrology and structure of Poplar Creek map-area, British Columbia. Geological Survey of Canada, Bulletin **193**.

Read, P. 1975. Lardeau group, Lardeau map-area, west half (82K west half), British Columbia. Current research, part A. Geological Survey of Canada, Paper, 75- 1, Part A: 29-30.

Read, P. 1979. Relationship between the Shuswap metamorphic complex and Kootenay Arc, Vernon east-half, southern British Columbia. Current research, part A. Geological Survey of Canada, Paper, **79-1A**: 37-40.

Read, P.B. 1980. Stratigraphy and structures: Thor-Odin to Frenchman Cap “domes”, Vernon east-half, southern British Columbia. Current Research, Part A: Geological Survey of Canada Paper, **79-1A**: 33-34.

Read, P.B. and Brown, R.L. 1981. Columbia River fault zone: Southeastern margin of the Shuswap and Monashee Complexes, southern British Columbia. Canadian Journal of Earth Sciences, **18**: 1127-1145.

Read, P.B. and Wheeler, J.O. 1976. Geology of Lardeau west-half map area. Geological Survey of Canada, Open file Map 432.

Reddy, S.M., Kelley, S.P., Magennis, L., 1997. A microstructural and argon laserprobe study of shear zone development at the western margin of the Nanga Parbat–Haramosh Massif, western Himalaya. Contributions to Mineralogy and Petrology **128**: 16-29.

Reesor, J. 1970. Some aspects of structural evolution and regional setting in part of the Shuswap metamorphic complex. *In: Structure on the southern Canadian Cordillera.*

Edited by J.O. Wheeler, Geological Association of Canada, Special Paper, 6: 73-86.

Reesor, J.E. and Moore, J.M. 1971. Petrology and structure of Thor-Odin gneiss come, Shuswap metamorphic complex. *Geological Survey of Canada Bulletin, 195.*

Renne, P. R., Swisher, C. C., Deino, A. L., Karner, D. B., Owens, T. L., and DePaolo, D. J.

1998. Intercalibration of standards, absolute ages and uncertainties in $^{40}\text{Ar}/^{39}\text{Ar}$ dating.

Chemical Geology, 145: 117–152.

Roback, R.C., Sevigny, J.H., and Walker, N.W. 1994. Tectonic setting of the Slide

Mountain terrane, southern British Columbia. *Tectonics, 13: 1242-1258.*

Roddick, J.C. 1983. High precision intercalibration of $^{40}\text{Ar}/^{39}\text{Ar}$ standards. *Geochimica et Cosmochimica Acta, 47: 887-898.*

Ross, G.M. 1991. Precambrian basement in the Canadian Cordillera: An introduction.

Canadian Journal of Earth Sciences, 28: 1133-1139.

Ross, G.M. 2002. Evolution of Precambrian continental lithosphere in western Canada:

Results from LITHOPROBE studies in Alberta and beyond. *Canadian Journal of Earth*

Sciences, 39: 413-437.

Ross, G.M. and Bowring, S.A. 1990. Detrital zircon geochronology of the Windermere Supergroup and the tectonic assembly of the southern Canadian Cordillera. *Journal of Geology*, **98**: 879-893.

Ross, G.M. and Parrish, R.R. 1991. Detrital zircon geochronology of metasedimentary rocks in the southern Omineca belt, Canadian cordillera. *Canadian Journal of Earth Sciences*, **28**: 1254-1270.

Ross, G.M. and Villeneuve, M. 2003. Provenance of the Mesoproterozoic (1.45 Ga) Belt basin (western North America): Another piece in the pre-Rodinia paleogeographic puzzle. *Geological Society of America Bulletin*, **115**: 1191-1217.

Ross, G.M., Gehrels, G.E., and Patchett, P.J. 1997. Provenance of Triassic strata in the Cordilleran miogeocline, western Canada. *Bulletin of Canadian Petroleum Geology*, **45**: 461-473.

Ross, G., Parrish, R., Villeneuve, M., and Bowring, S. 1991. Geophysics and geochronology of the crystalline basement of the Alberta basin, western Canada. *Canadian Journal of Earth Sciences*, **28**: 512-522.

Ross, G.M., Parrish, R.R., and Winston, D. 1992. Provenance and U-Pb geochronology of the Mesoproterozoic Belt Supergroup (northwestern United States): Implications for age of deposition and pre-Panthalassa plate reconstructions. *Earth and Planetary Science Letters*, **113**: 57-76.

Ross, G.M., Patchett, P.J., Hamilton, M., Heaman, L., DeCelles, P.G., Rosenberg, E., and Giovanni, M.K. 2005. Evolution of the Cordilleran orogen (southwestern Alberta, Canada) inferred from detrital mineral geochronology, geochemistry, and Nd isotopes in the foreland basin. *Geological Society of America Bulletin*, **117**: 747-763.

Rubatto, D., Williams, I.S., and Buick, I.S. 2001. Zircon and monazite response to prograde metamorphism in the Reynolds Range, central Australia. *Contributions to Mineralogy and Petrology*, **140**: 458-468.

Sanborn, N. 1996. Constraints on the timing and conditions of Cordilleran tectonism in Frenchman Cap dome, Monashee Complex, southeastern British Columbia from $^{40}\text{Ar}/^{39}\text{Ar}$ geochronology. B.Sc. thesis, Queen's University, Kingston, Canada.

Sandeman, H.A., Archibald, D.A., Grant, J., Villeneuve, M.E., and Ford, F. 1999. Characterization of the composition and calibration of the age of MAC-83 biotite: A potential 24.06 ma laser $^{40}\text{Ar}/^{39}\text{Ar}$ geochronological standard. *Radiogenic Age and Isotopic Studies: Geological Survey of Canada, Report*, **12**: 13-26.

Scaillet, S. 1996. Excess ^{40}Ar transport scale and mechanism in high-pressure phengites: A case study from an eclogitized metabasite of the Dora Maira nappe, western Alps. *Geochimica et Cosmochimica Acta*, **60**: 1075-1090.

Scammell, R.J. 1993. Mid-Cretaceous to Tertiary thermotectonic history of former mid-crustal rocks, southern Omineca belt, Canadian Cordillera. Ph.D. thesis, Queen's University, Kingston, Canada.

Scammell, R.J. and Brown, R.L. 1990. Cover gneisses of the Monashee terrane: A record of synsedimentary rifting in the North American Cordillera. *Canadian Journal of Earth Sciences*, **27**: 712-726; 712.

Sears, J.W., 2001. Emplacement and denudation history of the Lewis – Eldorado – Hoadley thrust slab in the northern Montana Cordillera, USA: implications for steady state orogenic processes. *American Journal of Science* **301**: 354-373.

Sherlock, S., Kelley, S., Inger, S., Harris, N., and Okay, A. 1999. $^{40}\text{Ar}/^{39}\text{Ar}$ and Rb-Sr geochronology of high-pressure metamorphism and exhumation history of the Tavsanli zone, NW turkey. *Contributions to Mineralogy and Petrology*, **137**: 46-58.

Shields, C. and Kuiper, Y.D. 2008. New detrital and metamorphic zircon ages from cover rocks of the Monashee complex, southeastern Canadian Cordillera. *In* GSA, Northeastern Section 43rd Annual Meeting, Vol. 40, pp. 19.

Simony, P.S. and Carr, S.D. 2011. Cretaceous to Eocene evolution of the southeastern Canadian Cordillera: Continuity of rocky mountain thrust systems with zones of "in-sequence" mid-crustal flow. *Journal of Structural Geology*, **33**: 1417-1434.

Sircombe, K.N. 2000. Quantitative comparison of large sets of geochronological data using multivariate analysis: A provenance study example from Australia. *Geochimica et Cosmochimica Acta*, **64**: 1593-1616.

Sláma, J., Košler, J., Condon, D.J., Crowley, J.L., Gerdes, A., Hanchar, J.M., Horstwood, M.S., Morris, G.A., Nasdala, L., and Norberg, N. 2008. Plešovice zircon—a new natural reference material for U–Pb and Hf isotopic microanalysis. *Chemical Geology*, **249**: 1-35.

Smith, M.T. and Gehrels, G.E. 1992. Structural geology of the Lardeau Group near Trout Lake, British Columbia: Implications for the structural evolution of the Kootenay Arc. *Canadian Journal of Earth Sciences*, **29**: 1305-1319.

Smith, M.T. and Gehrels, G.E. 1991. Detrital zircon geochronology of Upper Proterozoic to Lower Paleozoic continental margin strata of the Kootenay Arc: Implications for early Paleozoic tectonic development of the eastern Canadian Cordillera. *Canadian Journal of Earth Sciences*, **28**: 1271-1284.

Smith, P.E., York, D., Easton, R.M., Özdemir, Ö., and Layer, P.W. 1994. A laser $^{40}\text{Ar}/^{39}\text{Ar}$ study of minerals across the Grenville front: Investigation of reproducible excess Ar patterns. *Canadian Journal of Earth Sciences*, **31**: 808-817.

Spark, R.N. 2001. Crustal thickening and tectonic denudation within the Thor-Odin culmination, Monashee Complex, southern Canadian Cordillera. Ph.D. thesis, University of New Brunswick, Fredericton, Canada.

Spear, F.S. 1993. Metamorphic phase equilibria and pressure-temperature-time paths. Mineralogical Society of America, Washington D.C.

Steiger, R.H. and Jäger, E. 1977. Subcommittee on geochronology: Convention on the use of decay constants in geo- and cosmochronology. Earth and Planetary Science Letters, **36**: 359-362.

Stockmal, G.S., Issler, D.R., Lebel, D., 1997. Early to Middle Eocene thrusting, outer Foothills belt, southern Alberta: Evidence from apatite fission track data. *In* Canadian Society of Petroleum Geologists e Society of Economic Paleontologists and Mineralogists, Abstracts, vol. 269.

Struik, L.C. 1993. Intersecting intracontinental Tertiary transform fault systems in the North American Cordillera. Canadian Journal of Earth Sciences, **30**: 1262-1274.

Sullivan, W.A. and Snoke, A.W. 2007. Comparative anatomy of core-complex development in the northeastern Great Basin, USA. Rocky Mountain Geology, **42**: 1-29.

Sylvester, P.J. and Ghaderi, M. 1997. Trace element analysis of scheelite by Excimer laser ablation-inductively coupled plasma-mass spectrometry (ELA-ICP-MS) using a synthetic silicate glass standard. Chemical Geology, **141**: 49-65.

Tempelman-Kluit, D. 1989. Geology, Penticton, British Columbia. Geological Survey of Canada, Map 1736A.

Tempelman-Kluit, D. and Parkinson, D. 1986. Extension across the Eocene Okanagan crustal shear in southern British Columbia. *Geology*, **14**: 318-321.

Teyssier, C., Ferré, E., Whitney, D.L., Norlander, B., Vanderhaeghe, O., and Parkinson, D. 2005. Flow of partially molten crust and origin of detachments during collapse of the Cordilleran orogen. *In: High-Strain Zones: Structure and Physical Properties. Edited by: Bruhn, D. & Burlini, L. Geological Society, London, Special Publications, 245: 39-64.*

Thompson, R.I., Glombick, P., and Lemieux, Y. 2004. *Geology, Mount Fosthall, British Columbia: Geological Survey of Canada, Open File 4377.*

Thompson, R.I., Glombick, P., Erdmer, P., Heaman, L., Lemieux, Y., and Daughtry, K.L. 2006. Evolution of the ancestral Pacific margin, southern Canadian Cordillera: Insights from new geologic maps. *In: Paleozoic evolution and metallogeny of pericratonic terranes at the ancient Pacific margin of North America, Canadian and Alaskan Cordillera. Edited by M. Colpron and J.A. Nelson. Geological Association of Canada, Special Paper 45: 433-482.*

Tirel, C., Brun, J., and Sokoutis, D. 2006. Extension of thickened and hot lithospheres: Inferences from laboratory modeling. *Tectonics*, **25**: TC1005.

Tirel, C., Brun, J., and Burov, E. 2008. Dynamics and structural development of metamorphic core complexes. *Journal of Geophysical Research*, **113**: B04403.

Van der Pluijm, B.A., Vrolijk, P., Pevear, D., Hall, C.M., and Solum, J., 2006. Fault dating in the Canadian Rocky Mountains; evidence for late Cretaceous and early Eocene orogenic pulses. *Geology* **34**, 837-840.

Vanderhaeghe, O. 1999. Pervasive melt migration from migmatites to leucogranite in the Shuswap metamorphic core complex, Canada: Control of regional deformation. *Tectonophysics*, **312**: 35-55.

Vanderhaeghe, O., Teysier, C., McDougall, I., and Dunlap, W.J. 2003. Cooling and exhumation of the Shuswap metamorphic core complex constrained by $^{40}\text{Ar}/^{39}\text{Ar}$ thermochronology. *Geological Society of America Bulletin*, **115**: 200-216.

Vanderhaeghe, O., Teysier, C., and Wysoczanski, R. 1999. Structural and geochronological constraints on the role of partial melting during the formation of the Shuswap metamorphic core complex at the latitude of the Thor-Odin dome, British Columbia. *Canadian Journal of Earth Sciences*, **36**: 917-943.

Varsek, J.L. and Cook, F.A. 1994. Three-dimensional crustal structure of the eastern Cordillera, southwestern Canada and northwestern United States. *Geological Society of America Bulletin*, **106**: 503-823.

Vermeesch, P. 2004. How many grains are needed for a provenance study? *Earth and Planetary Science Letters*, **224**: 441-451.

Villa, I.M., Hermann, J., Muntener, O., Trommsdorff, V., Wijbrans, J.R., and McDougall, I.M. 2000. $^{40}\text{Ar}/^{39}\text{Ar}$ dating of multiply zoned amphibole generations (Malenco, Italian Alps). *Contributions to Mineralogy and Petrology*, **140**: 363-381.

Wartho, J.A. and Kelley, S.P. 2003. $^{40}\text{Ar}/^{39}\text{Ar}$ ages in mantle xenolith phlogopites: Determining the ages of multiple lithospheric mantle events and diatreme ascent rates in southern Africa and Malaita, Solomon Islands. *Geological Society, London, Special Publications* **220**: 231-248.

Wheeler, J.O. 1965. Big Bend map-area, British Columbia. *Geological Survey of Canada Paper*, **64-32**.

Wheeler, J.O. and McFeely, P. 1991. Tectonic assemblage map of the Canadian Cordillera and adjacent parts of the United States of America. *Geological Survey of Canada Map*, **1712A**.

Whitney, D.L., Teyssier, C., Rey, P., Buck and W.R., 2013. Continental and oceanic core complexes. *Geological Society of America Bulletin* **125**: 273-29.

Whitney, D.L., Teyssier, C., and Vanderhaeghe, O. 2004. Gneiss domes and crustal flow. *In: Gneiss domes in orogeny. Edited by: Whitney, D.L., Teyssier, C., and Siddoway, C.S. Special Paper, Geological Society of America*, **380**: 15-33.

Wiedenbeck, M., Alle, P., Corfu, F., Griffin, W., Meier, M., Oberli, F., Quadt, A.V., Roddick, J., and Spiegel, W. 1995. Three natural zircon standards for U-Th-Pb, Lu-Hf, trace element and REE analyses. *Geostandards Newsletter*, **19**: 1-23.

Williams, P.F. and Jiang, D. 2005. An investigation of lower crustal deformation: Evidence for channel flow and its implications for tectonics and structural studies. *Journal of Structural Geology*, **27**: 1486-1504.

Williams, P.F., Jiang, D., and Lin, S. 2006. Interpretation of deformation fabrics of infrastructure zone rocks in the context of channel flow and other tectonic models. *In: Channel Flow, Ductile Extrusion and Exhumation in Continental Collision Zones. Edited by: Law, R. D., Searle, M. P. and Godin, L. Geological Society. London. Special Publications. 268*: 221-235.

York, D. 1969. Least squares fitting of a straight line with correlated errors. *Earth and Planetary Science Letters*, **5**: 320-324.

Table A1. LA-ICP-MS U-Pb isotopic analyses of detrital zircons, Mount Thor (DA224).

Measured Isotopic Ratios										Calculated Ages										
207Pb /235U	1s error	206Pb /238U	1s error	Rho	207Pb /206Pb	1s error	207Pb /235U	1s	206Pb /238U	1s	207Pb /206Pb	1s	U-Pb /Pb-Pb (% conc)	Concordia age (Ma)	2s	MSWD (of concordance)	Probability	ppm 232Th	ppm 238U	Ratio Th/U
2.1461	0.1626	0.1427	0.0108	0.4991	0.1061	0.0008	1164	52	860	61	1733	15	50	1011	104	27.18	0.000	616	689	0.895
3.1903	0.1832	0.2107	0.0111	0.4608	0.1079	0.0007	1455	44	1232	59	1764	11	70	1386	88	16.17	0.000	52	209	0.250
7.5060	0.4145	0.3579	0.0179	0.4525	0.1441	0.0015	2174	49	1972	85	2277	18	87	2150	100	7.09	0.008	35	65	0.542
9.0228	0.1828	0.3978	0.0074	0.4567	0.1604	0.0005	2340	19	2159	34	2459	6	88	2326	37	36.48	0.000	142	351	0.404
4.1678	0.1144	0.2736	0.0067	0.4461	0.1080	0.0007	1668	22	1559	34	1766	12	88	1647	44	12.20	0.000	58	206	0.280
4.6277	0.1270	0.2984	0.0045	0.2752	0.1167	0.0007	1754	23	1683	22	1906	11	88	1716	37	6.63	0.010	71	440	0.160
4.1815	0.1538	0.2732	0.0094	0.4670	0.1074	0.0005	1670	30	1557	48	1755	8	89	1654	60	7.12	0.008	52	384	0.135
11.5278	0.4220	0.4460	0.0167	0.5100	0.1822	0.0010	2567	34	2377	74	2673	9	89	2571	68	9.04	0.003	49	129	0.383
4.9181	0.1399	0.2977	0.0062	0.3652	0.1143	0.0013	1805	24	1680	31	1868	21	90	1762	45	16.00	0.000	35	41	0.853
9.3920	0.3886	0.4048	0.0162	0.4841	0.1580	0.0015	2377	38	2191	74	2435	16	90	2372	76	8.37	0.004	36	76	0.474
4.4438	0.0760	0.2852	0.0046	0.4755	0.1096	0.0005	1721	14	1617	23	1793	9	90	1709	28	25.06	0.000	48	381	0.127
13.0113	0.3655	0.4738	0.0126	0.4751	0.1928	0.0025	2680	26	2500	55	2766	21	90	2678	53	14.08	0.000	4	13	0.311
4.3032	0.0814	0.2836	0.0043	0.3992	0.1082	0.0005	1694	16	1610	22	1769	9	91	1671	30	16.29	0.000	84	197	0.428
4.2754	0.1637	0.2835	0.0080	0.3681	0.1081	0.0008	1689	32	1609	40	1767	13	91	1662	58	3.81	0.051	64	174	0.367
4.6613	0.0885	0.2945	0.0050	0.4502	0.1116	0.0005	1760	16	1664	25	1826	8	91	1746	31	17.88	0.000	74	366	0.203
13.2666	0.2884	0.4874	0.0085	0.3990	0.1951	0.0017	2699	21	2560	37	2786	14	92	2682	41	16.90	0.000	13	30	0.429
4.5580	0.1001	0.2972	0.0050	0.3815	0.1111	0.0008	1742	18	1677	25	1818	14	92	1723	35	6.86	0.009	70	95	0.733
10.3991	0.1940	0.4385	0.0074	0.4527	0.1682	0.0006	2471	17	2344	33	2540	6	92	2464	35	18.63	0.000	143	345	0.416
19.8838	0.2870	0.5744	0.0075	0.4492	0.2475	0.0010	3086	14	2926	31	3169	6	92	3084	28	35.26	0.000	24	185	0.128
4.4045	0.0584	0.2907	0.0031	0.3960	0.1082	0.0005	1713	11	1645	15	1770	8	93	1695	21	21.17	0.000	68	354	0.192
27.1419	0.6799	0.6501	0.0151	0.4638	0.2954	0.0006	3389	25	3228	59	3446	3	94	3392	49	9.60	0.002	171	528	0.324
4.4212	0.0792	0.2924	0.0042	0.4036	0.1076	0.0006	1716	15	1653	21	1759	10	94	1701	28	9.61	0.002	81	252	0.319
4.6185	0.1080	0.2991	0.0055	0.3940	0.1093	0.0005	1753	20	1687	27	1788	8	94	1736	37	6.09	0.014	19	536	0.036
4.5732	0.0724	0.2961	0.0043	0.4616	0.1083	0.0004	1744	13	1672	22	1771	7	94	1735	26	14.20	0.000	45	494	0.092
4.8263	0.0789	0.3056	0.0048	0.4763	0.1112	0.0005	1789	14	1719	24	1820	9	94	1783	27	11.48	0.001	11	256	0.041
4.7630	0.1961	0.3080	0.0066	0.2600	0.1120	0.0025	1778	35	1731	33	1832	40	94	1752	54	1.35	0.246	21	26	0.834
4.5164	0.0843	0.2955	0.0048	0.4377	0.1078	0.0006	1734	16	1669	24	1763	10	95	1723	30	8.68	0.003	86	272	0.316
5.0005	0.1072	0.3126	0.0056	0.4181	0.1132	0.0008	1819	18	1754	28	1851	14	95	1807	35	6.52	0.011	58	115	0.506
11.9431	0.2177	0.4745	0.0075	0.4339	0.1787	0.0008	2600	17	2503	33	2640	8	95	2594	34	10.69	0.001	71	163	0.436
4.4102	0.0912	0.2933	0.0047	0.3885	0.1070	0.0006	1714	17	1658	23	1748	10	95	1699	32	6.00	0.014	64	254	0.252
4.4323	0.1320	0.2960	0.0058	0.3262	0.1077	0.0006	1718	25	1672	29	1761	11	95	1699	43	2.26	0.133	83	253	0.329
6.0775	0.2978	0.3393	0.0271	0.8142	0.1217	0.0008	1987	43	1883	130	1981	12	95	2016	64	1.12	0.289	25	273	0.093
4.4927	0.0649	0.2957	0.0040	0.4672	0.1074	0.0003	1730	12	1670	20	1756	6	95	1723	24	11.41	0.001	167	613	0.273
14.5050	0.2806	0.5158	0.0096	0.4808	0.1988	0.0010	2783	18	2681	41	2816	8	95	2785	37	8.23	0.004	98	86	1.138

207Pb /235U	1s error	206Pb /238U	1s error	Rho	207Pb /206Pb	1s error	207Pb /235U	1s Ma	206Pb /238U	1s Ma	207Pb /206Pb	1s Ma	U-Pb (% conc)	Concordia age (Ma)	2s Ma	MSWD (of concordance)	Probability	ppm 232Th	ppm 238U	Ratio Th/U
6.5283	0.1850	0.3647	0.0067	0.3223	0.1305	0.0017	2050	25	2005	31	2104	22	95	2034	45	1.83	0.176	23	32	0.712
12.2528	0.1604	0.4791	0.0057	0.4564	0.1789	0.0007	2624	12	2523	25	2642	6	95	2621	25	20.87	0.000	230	192	1.195
4.7600	0.0859	0.3049	0.0041	0.3733	0.1098	0.0008	1778	15	1715	20	1796	13	95	1760	28	9.46	0.002	46	120	0.382
4.4890	0.0953	0.2968	0.0053	0.4198	0.1073	0.0004	1729	18	1676	26	1754	8	96	1718	34	4.65	0.031	145	415	0.350
4.3705	0.1147	0.2963	0.0053	0.3405	0.1071	0.0007	1707	22	1673	26	1751	11	96	1694	39	1.49	0.222	81	195	0.414
4.4438	0.0675	0.2956	0.0039	0.4352	0.1069	0.0005	1721	13	1670	19	1747	9	96	1712	25	8.03	0.005	215	311	0.693
11.2159	0.1580	0.4661	0.0058	0.4387	0.1723	0.0009	2541	13	2467	25	2580	9	96	2537	26	10.79	0.001	91	122	0.744
4.7035	0.0612	0.3035	0.0032	0.4040	0.1090	0.0006	1768	11	1709	16	1783	10	96	1754	21	15.43	0.000	69	201	0.344
4.6806	0.0774	0.3063	0.0035	0.3484	0.1098	0.0005	1764	14	1722	17	1796	8	96	1750	25	5.26	0.022	82	434	0.188
11.2321	0.3378	0.4677	0.0112	0.3997	0.1713	0.0013	2543	28	2473	49	2571	12	96	2534	55	2.29	0.131	92	69	1.337
4.7391	0.0635	0.3069	0.0031	0.3747	0.1096	0.0005	1774	11	1726	15	1793	8	96	1760	21	10.27	0.001	297	361	0.822
4.8416	0.1845	0.3140	0.0087	0.3622	0.1115	0.0010	1792	32	1760	43	1825	16	96	1783	59	0.55	0.460	40	94	0.431
4.5089	0.0719	0.3009	0.0040	0.4144	0.1075	0.0004	1733	13	1696	20	1757	7	96	1725	26	3.96	0.047	219	281	0.780
10.3895	0.2502	0.4522	0.0106	0.4885	0.1635	0.0010	2470	22	2405	47	2492	10	96	2471	45	2.52	0.112	58	137	0.420
4.6998	0.0785	0.3059	0.0039	0.3855	0.1090	0.0007	1767	14	1721	19	1783	12	97	1755	27	5.97	0.015	45	112	0.399
4.5170	0.1178	0.2986	0.0070	0.4513	0.1067	0.0005	1734	22	1684	35	1744	9	97	1727	43	2.50	0.114	232	378	0.615
5.0833	0.0724	0.3173	0.0041	0.4509	0.1123	0.0006	1833	12	1777	20	1837	9	97	1826	24	9.89	0.002	71	209	0.340
4.7303	0.1098	0.3042	0.0052	0.3675	0.1082	0.0009	1773	19	1712	26	1769	16	97	1754	36	5.49	0.019	52	115	0.452
4.7062	0.0730	0.3028	0.0039	0.4116	0.1078	0.0005	1768	13	1705	19	1762	9	97	1755	25	12.18	0.000	98	294	0.333
5.1312	0.0823	0.3181	0.0050	0.4922	0.1124	0.0008	1841	14	1781	25	1839	13	97	1838	27	8.09	0.004	51	111	0.461
5.0268	0.0755	0.3178	0.0039	0.4092	0.1121	0.0005	1824	13	1779	19	1834	9	97	1815	25	6.19	0.013	311	281	1.104
5.0257	0.1002	0.3180	0.0049	0.3849	0.1121	0.0008	1824	17	1780	24	1834	13	97	1813	32	3.55	0.060	23	111	0.208
5.0284	0.0748	0.3179	0.0039	0.4134	0.1121	0.0007	1824	13	1780	19	1834	12	97	1816	24	6.10	0.014	42	108	0.388
9.1486	0.3993	0.4310	0.0126	0.3353	0.1525	0.0014	2353	40	2310	57	2374	16	97	2342	75	0.56	0.455	36	48	0.745
12.2116	0.3192	0.4889	0.0106	0.4149	0.1782	0.0010	2621	25	2566	46	2636	10	97	2616	49	1.72	0.190	136	107	1.271
6.6276	0.5119	0.3659	0.0235	0.4159	0.1275	0.0011	2063	68	2010	111	2064	16	97	2055	134	0.26	0.607	57	85	0.666
4.6387	0.0830	0.3071	0.0040	0.3613	0.1083	0.0007	1756	15	1726	20	1772	12	97	1747	28	2.27	0.132	70	164	0.427
4.9570	0.0738	0.3156	0.0041	0.4355	0.1109	0.0007	1812	13	1768	20	1814	12	97	1806	25	5.63	0.018	51	133	0.386
8.3609	0.1916	0.4107	0.0071	0.3784	0.1438	0.0010	2271	21	2218	33	2274	12	98	2261	40	2.87	0.090	60	92	0.651
4.5915	0.0703	0.3008	0.0042	0.4542	0.1063	0.0006	1748	13	1695	21	1737	10	98	1741	25	7.85	0.005	94	163	0.577
4.7244	0.0892	0.3048	0.0050	0.4332	0.1074	0.0007	1772	16	1715	25	1756	11	98	1762	31	6.13	0.013	74	169	0.441
4.5716	0.1012	0.3037	0.0059	0.4424	0.1069	0.0006	1744	18	1709	29	1746	10	98	1739	36	1.66	0.197	86	357	0.241
5.7805	0.0994	0.3430	0.0046	0.3900	0.1190	0.0005	1943	15	1901	22	1942	8	98	1934	29	3.94	0.047	233	326	0.713
4.4938	0.1275	0.3017	0.0061	0.3583	0.1062	0.0008	1730	24	1700	30	1736	14	98	1720	43	0.94	0.331	70	130	0.537
4.6997	0.0885	0.3078	0.0043	0.3721	0.1080	0.0008	1767	16	1730	21	1766	14	98	1757	29	3.07	0.080	55	106	0.515
5.2298	0.1872	0.3241	0.0101	0.4335	0.1126	0.0008	1857	31	1810	49	1842	13	98	1851	60	1.13	0.288	70	103	0.677
4.7899	0.0873	0.3115	0.0043	0.3752	0.1088	0.0008	1783	15	1748	21	1779	13	98	1774	29	2.81	0.094	62	113	0.545
4.8862	0.1714	0.3201	0.0071	0.3176	0.1112	0.0012	1800	30	1790	35	1819	19	98	1796	52	0.07	0.797	71	61	1.159

207Pb /235U	1s error	206Pb /238U	1s error	Rho	207Pb /206Pb	1s error	207Pb /235U	1s Ma	206Pb /238U	1s Ma	207Pb /206Pb	1s Ma	U-Pb /Pb-Pb (% conc)	Concordia age (Ma)	2s Ma	MSWD (of concordance)	Probability	ppm 232Th	ppm 238U	Ratio Th/U
4.7214	0.1238	0.3131	0.0050	0.3033	0.1089	0.0007	1771	22	1756	24	1782	12	99	1765	37	0.30	0.584	81	134	0.603
4.6885	0.1112	0.3078	0.0055	0.3778	0.1073	0.0006	1765	20	1730	27	1754	10	99	1756	37	1.73	0.189	43	291	0.148
14.2330	0.3059	0.5252	0.0094	0.4154	0.1915	0.0013	2765	20	2721	40	2755	11	99	2763	41	1.49	0.222	85	59	1.446
5.0163	0.0952	0.3194	0.0053	0.4345	0.1105	0.0007	1822	16	1787	26	1808	12	99	1817	32	2.23	0.135	85	143	0.591
5.0639	0.0856	0.3246	0.0036	0.3237	0.1121	0.0007	1830	14	1812	17	1833	12	99	1823	25	0.94	0.333	152	143	1.059
6.6009	0.2845	0.3764	0.0099	0.3059	0.1287	0.0020	2059	38	2059	46	2080	27	99	2059	67	0.00	0.997	48	27	1.806
4.7299	0.0757	0.3089	0.0038	0.3842	0.1072	0.0007	1773	13	1735	19	1752	12	99	1763	25	4.17	0.041	53	142	0.374
11.8123	0.7748	0.4920	0.0201	0.3116	0.1748	0.0013	2590	61	2579	87	2604	13	99	2587	114	0.01	0.909	11	62	0.172
14.9248	0.2209	0.5385	0.0080	0.5018	0.1965	0.0013	2810	14	2777	34	2798	11	99	2812	28	1.33	0.249	42	68	0.610
10.5634	0.2082	0.4655	0.0072	0.3919	0.1621	0.0012	2485	18	2464	32	2477	13	99	2483	36	0.52	0.469	19	44	0.438
13.7775	0.1860	0.5201	0.0075	0.5320	0.1868	0.0011	2735	13	2700	32	2714	10	99	2737	25	1.67	0.196	27	62	0.443
5.1822	0.0752	0.3276	0.0036	0.3786	0.1122	0.0006	1850	12	1827	17	1835	10	100	1844	23	1.79	0.181	111	208	0.533
4.9880	0.1129	0.3199	0.0059	0.4044	0.1098	0.0007	1817	19	1789	29	1796	12	100	1812	37	1.08	0.300	78	114	0.683
4.8118	0.1190	0.3255	0.0060	0.3699	0.1113	0.0011	1787	21	1816	29	1821	17	100	1794	39	1.05	0.305	83	90	0.916
5.3125	0.1094	0.3320	0.0055	0.4001	0.1129	0.0009	1871	18	1848	26	1847	15	100	1866	34	0.81	0.369	53	83	0.633
12.9665	0.2622	0.5157	0.0086	0.4113	0.1829	0.0017	2677	19	2681	36	2679	15	100	2677	38	0.01	0.909	5	30	0.162
4.6869	0.1198	0.3172	0.0053	0.3267	0.1083	0.0009	1765	21	1776	26	1772	14	100	1769	38	0.16	0.693	71	120	0.586
13.4724	0.2455	0.5220	0.0079	0.4150	0.1846	0.0016	2713	17	2708	33	2694	14	100	2713	34	0.04	0.851	41	33	1.249
15.6543	0.2525	0.5541	0.0084	0.4695	0.2002	0.0011	2856	15	2842	35	2828	9	101	2856	31	0.20	0.651	75	87	0.859
4.9064	0.1050	0.3130	0.0063	0.4724	0.1067	0.0009	1803	18	1755	31	1744	16	101	1799	36	3.04	0.081	70	70	1.001
4.8595	0.1505	0.3198	0.0065	0.3303	0.1083	0.0012	1795	26	1789	32	1771	20	101	1793	46	0.04	0.846	36	44	0.825
4.8966	0.0710	0.3188	0.0038	0.4106	0.1077	0.0007	1802	12	1784	19	1762	11	101	1798	24	1.06	0.303	59	93	0.635
15.5156	0.5240	0.5693	0.0147	0.3828	0.2048	0.0024	2847	32	2905	60	2865	19	101	2852	63	1.03	0.311	5	13	0.388
4.6707	0.0817	0.3137	0.0040	0.3655	0.1061	0.0006	1762	15	1759	20	1734	10	101	1761	27	0.03	0.870	136	222	0.614
5.4894	0.1411	0.3486	0.0056	0.3133	0.1142	0.0013	1899	22	1928	27	1867	20	103	1909	39	1.00	0.318	68	66	1.021
4.8441	0.1052	0.3221	0.0055	0.3935	0.1065	0.0008	1793	18	1800	27	1741	14	103	1794	35	0.08	0.782	28	75	0.374

Table A2. LA-ICP-MS U-Pb isotopic analyses of detrital zircons, Icebound Lake (DC422).

Measured Isotopic Ratios					Calculated Ages															
207Pb /235U	1s error	206Pb /238U	1s error	Rho	207Pb /206Pb	1s error	207Pb /235U	1s 206Pb /238U	1s	207Pb /206Pb	1s	U-Pb /Pb-Pb (% conc)	Concordia age (Ma)	2s	MSWD	Probability	ppm	ppm	Ratio	
							Ma	Ma	Ma	Ma	Ma	Ma		Ma	(of concordance)		232Th	238U	Th/U	
2.1219	0.2129	0.1022	0.0099	0.4823	0.1492	0.0014	1156	69	627	58	2337	17	27	635	116	46.13	0.00	77	259	0.297
0.8200	0.1292	0.0621	0.0120	0.6114	0.0896	0.0031	608	72	388	73	1417	66	27	461	137	11.11	0.00	8	26	0.330
1.1678	0.2132	0.0858	0.0150	0.4794	0.0979	0.0011	786	100	531	89	1584	21	34	592	170	6.18	0.01	67	262	0.254
2.1572	0.3150	0.1338	0.0190	0.4858	0.1102	0.0009	1167	101	809	108	1803	16	45	936	197	10.38	0.00	172	813	0.211
2.1101	0.1055	0.1365	0.0063	0.4592	0.1084	0.0004	1152	34	825	36	1772	7	47	939	65	73.81	0.00	179	1298	0.138
1.8172	0.1345	0.1325	0.0100	0.5106	0.0943	0.0007	1052	48	802	57	1514	15	53	939	96	21.88	0.00	214	359	0.595
2.4142	0.1120	0.1579	0.0070	0.4768	0.1089	0.0003	1247	33	945	39	1781	4	53	1098	66	63.33	0.00	117	1881	0.062
2.6786	0.2558	0.1776	0.0154	0.4543	0.1078	0.0009	1323	71	1054	84	1762	15	60	1202	138	10.51	0.00	83	136	0.606
3.5191	0.1205	0.2117	0.0070	0.4863	0.1173	0.0004	1532	27	1238	37	1915	6	65	1446	55	75.49	0.00	309	719	0.429
3.3300	0.2231	0.2155	0.0137	0.4736	0.1127	0.0007	1488	52	1258	73	1843	11	68	1425	105	12.09	0.00	370	404	0.916
3.6388	0.0806	0.2332	0.0052	0.5049	0.1105	0.0003	1558	18	1351	27	1807	5	75	1526	36	76.83	0.00	86	1552	0.056
3.8073	0.0575	0.2416	0.0037	0.5121	0.1114	0.0003	1594	12	1395	19	1822	5	77	1570	25	143.38	0.00	120	1032	0.116
3.4246	0.1278	0.2298	0.0079	0.4592	0.1065	0.0008	1510	29	1334	41	1740	14	77	1466	58	21.60	0.00	48	122	0.392
4.3741	0.1113	0.2638	0.0066	0.4889	0.1169	0.0003	1707	21	1509	33	1909	5	79	1679	42	45.79	0.00	387	983	0.393
4.5209	0.1616	0.2687	0.0098	0.5097	0.1171	0.0007	1735	30	1534	50	1912	11	80	1716	60	22.34	0.00	179	195	0.917
4.6619	0.1278	0.2747	0.0072	0.4784	0.1185	0.0004	1760	23	1565	36	1933	7	81	1731	46	36.98	0.00	212	507	0.419
7.9062	0.2325	0.3581	0.0093	0.4427	0.1532	0.0008	2220	27	1973	44	2382	9	83	2184	54	38.55	0.00	72	283	0.256
4.2520	0.1423	0.2659	0.0092	0.5187	0.1120	0.0005	1684	28	1520	47	1833	9	83	1673	55	16.99	0.00	128	248	0.514
7.3105	0.1500	0.3525	0.0067	0.4644	0.1466	0.0007	2150	18	1946	32	2306	8	84	2130	37	52.16	0.00	153	376	0.409
5.2664	0.0664	0.3196	0.0044	0.5417	0.1313	0.0139	1863	11	1788	21	2116	185	85	1865	21	17.93	0.00	119	179	0.667
4.3885	0.0861	0.2756	0.0052	0.4827	0.1130	0.0005	1710	16	1569	26	1848	8	85	1693	32	36.90	0.00	81	637	0.128
7.3727	0.4710	0.3529	0.0256	0.5678	0.1447	0.0006	2158	57	1948	122	2284	8	85	2171	112	4.44	0.04	149	267	0.560
4.4893	0.0681	0.2893	0.0044	0.5043	0.1174	0.0078	1729	13	1638	22	1917	119	85	1724	25	22.92	0.00	109	227	0.479
4.2294	0.0635	0.2719	0.0042	0.5128	0.1109	0.0006	1680	12	1551	21	1814	9	85	1671	25	50.89	0.00	97	431	0.225
8.0602	0.2717	0.3706	0.0098	0.3904	0.1525	0.0009	2238	30	2032	46	2374	10	86	2189	60	22.00	0.00	128	281	0.455
5.9918	0.1040	0.3284	0.0043	0.3750	0.1321	0.0006	1975	15	1831	21	2126	8	86	1932	29	49.06	0.00	174	333	0.522
4.8803	0.0965	0.2926	0.0055	0.4765	0.1174	0.0005	1799	17	1655	27	1918	8	86	1782	33	35.46	0.00	68	210	0.325
4.3071	0.0895	0.2773	0.0053	0.4580	0.1112	0.0006	1695	17	1578	27	1820	10	87	1676	34	23.57	0.00	222	309	0.719
4.3725	0.0831	0.2773	0.0053	0.5062	0.1109	0.0004	1707	16	1578	27	1814	7	87	1698	32	31.33	0.00	140	804	0.174
7.8669	0.3061	0.3730	0.0117	0.4014	0.1491	0.0007	2216	35	2043	55	2336	8	87	2181	69	11.22	0.00	232	751	0.309
9.6432	0.1908	0.4100	0.0073	0.4502	0.1667	0.0013	2401	18	2215	33	2524	13	88	2386	37	39.65	0.00	36	61	0.594
4.5024	0.1189	0.2840	0.0073	0.4886	0.1121	0.0006	1731	22	1612	37	1834	9	88	1720	44	13.93	0.00	198	238	0.832
10.4955	0.4402	0.4276	0.0158	0.4414	0.1740	0.0014	2480	39	2295	71	2596	13	88	2464	78	8.38	0.00	54	129	0.418
5.0889	0.1280	0.3050	0.0061	0.3986	0.1179	0.0006	1834	21	1716	30	1925	9	89	1804	41	16.45	0.00	147	269	0.548
4.4283	0.0605	0.2851	0.0037	0.4777	0.1108	0.0004	1718	11	1617	19	1813	6	89	1706	23	37.30	0.00	32	1042	0.031
4.5818	0.1107	0.2898	0.0068	0.4829	0.1124	0.0007	1746	20	1640	34	1838	11	89	1736	40	12.68	0.00	204	306	0.667
4.6128	0.1438	0.2896	0.0083	0.4602	0.1117	0.0005	1752	26	1640	42	1828	8	90	1735	52	9.01	0.00	122	432	0.283
5.1261	0.1025	0.3091	0.0060	0.4854	0.1184	0.0005	1840	17	1736	30	1932	8	90	1832	34	16.24	0.00	137	623	0.221

207Pb /235U	1s error	206Pb /238U	1s error	Rho	207Pb /206Pb	1s error	207Pb /235U Ma	1s 206Pb Ma	238U /206Pb Ma	1s Ma	207Pb /206Pb Ma	1s Ma	U-Pb /Pb-Pb (% conc)	Concordia age (Ma)	2s Ma	MSWD (of concordance)	Probability	ppm 232Th	ppm 238U	Ratio Th/U
5.2595	0.1233	0.3101	0.0063	0.4344	0.1186	0.0009	1862	20	1741	31	1936	13	90	1841	40	17.97	0.00	74	97	0.768
4.7671	0.0777	0.2988	0.0054	0.5511	0.1145	0.0006	1779	14	1686	27	1872	9	90	1781	27	17.94	0.00	223	320	0.697
9.2618	0.3120	0.4072	0.0095	0.3445	0.1576	0.0011	2364	31	2202	43	2431	12	91	2317	59	13.76	0.00	90	400	0.225
5.1663	0.0663	0.3115	0.0037	0.4601	0.1182	0.0005	1847	11	1748	18	1929	8	91	1835	22	37.40	0.00	108	362	0.299
7.7371	0.2667	0.3742	0.0138	0.5353	0.1426	0.0006	2201	31	2049	65	2259	8	91	2206	62	7.88	0.01	144	237	0.608
11.9513	0.9101	0.4773	0.0311	0.4284	0.1925	0.0055	2601	71	2515	136	2764	47	91	2595	143	0.48	0.49	0	3	0.120
5.1613	0.1201	0.3128	0.0062	0.4239	0.1180	0.0005	1846	20	1755	30	1926	7	91	1829	39	10.54	0.00	344	538	0.640
4.8082	0.0700	0.3013	0.0035	0.4025	0.1139	0.0006	1786	12	1698	17	1863	10	91	1765	24	27.75	0.00	196	259	0.757
4.6903	0.1171	0.3001	0.0061	0.4058	0.1135	0.0011	1766	21	1692	30	1856	18	91	1748	40	6.49	0.01	55	72	0.764
4.9860	0.0941	0.3053	0.0048	0.4131	0.1150	0.0007	1817	16	1718	24	1880	11	91	1795	31	19.94	0.00	54	135	0.402
4.5365	0.0661	0.2909	0.0041	0.4848	0.1101	0.0006	1738	12	1646	21	1801	10	91	1729	24	25.88	0.00	105	350	0.300
5.3481	0.0835	0.3174	0.0047	0.4714	0.1190	0.0007	1877	13	1777	23	1941	10	92	1867	27	24.25	0.00	113	209	0.538
4.5055	0.1216	0.2943	0.0072	0.4507	0.1106	0.0006	1732	22	1663	36	1810	9	92	1722	44	4.57	0.03	186	385	0.484
4.5473	0.0814	0.2925	0.0044	0.4246	0.1095	0.0005	1740	15	1654	22	1792	9	92	1722	29	17.08	0.00	145	347	0.418
4.8140	0.0940	0.3030	0.0052	0.4352	0.1128	0.0006	1787	16	1706	25	1845	9	92	1774	32	11.89	0.00	67	216	0.308
8.6644	0.1460	0.4078	0.0072	0.5237	0.1533	0.0043	2303	15	2205	33	2383	48	93	2307	31	12.43	0.00	89	155	0.570
12.2142	0.2730	0.4688	0.0091	0.4325	0.1828	0.0013	2621	21	2478	40	2679	12	93	2611	42	15.91	0.00	28	74	0.376
5.2915	0.0949	0.3167	0.0064	0.5636	0.1174	0.0005	1867	15	1773	31	1916	8	93	1872	30	13.31	0.00	266	706	0.377
5.2357	0.0904	0.3158	0.0045	0.4163	0.1168	0.0006	1858	15	1769	22	1908	9	93	1841	29	18.34	0.00	204	272	0.748
4.6016	0.0665	0.2960	0.0032	0.3687	0.1101	0.0006	1750	12	1671	16	1800	11	93	1725	22	24.19	0.00	41	134	0.307
13.0720	0.2669	0.4946	0.0099	0.4881	0.1913	0.0018	2685	19	2590	43	2753	15	94	2687	38	6.56	0.01	24	47	0.502
5.5425	0.0657	0.3321	0.0046	0.5902	0.1203	0.0023	1907	10	1848	22	1960	33	94	1913	20	10.30	0.00	313	847	0.370
4.7704	0.0797	0.3053	0.0049	0.4804	0.1113	0.0006	1780	14	1718	24	1821	10	94	1775	28	8.51	0.00	65	266	0.245
5.0343	0.0970	0.3127	0.0058	0.4839	0.1136	0.0005	1825	16	1754	29	1858	8	94	1820	33	8.10	0.00	208	324	0.642
4.9163	0.0952	0.3114	0.0050	0.4104	0.1129	0.0006	1805	16	1747	24	1847	10	95	1793	32	6.25	0.01	126	117	1.074
5.6286	0.1126	0.3346	0.0059	0.4410	0.1207	0.0022	1920	17	1861	29	1966	33	95	1913	34	5.29	0.02	196	237	0.827
5.7813	0.0971	0.3429	0.0040	0.3503	0.1232	0.0036	1944	15	1901	19	2003	52	95	1931	27	4.75	0.03	113	194	0.583
5.0180	0.1475	0.3165	0.0073	0.3943	0.1141	0.0013	1822	25	1772	36	1866	20	95	1811	48	2.07	0.15	59	50	1.198
11.1692	0.1917	0.4606	0.0087	0.5491	0.1712	0.0007	2537	16	2442	38	2570	7	95	2544	31	8.76	0.00	131	328	0.399
5.4667	0.0916	0.3294	0.0051	0.4648	0.1181	0.0005	1895	14	1836	25	1927	8	95	1890	29	7.31	0.01	162	376	0.430
5.1886	0.0749	0.3203	0.0040	0.4284	0.1149	0.0006	1851	12	1791	19	1878	10	95	1841	24	11.12	0.00	121	192	0.630
5.7463	0.1194	0.3365	0.0065	0.4640	0.1203	0.0005	1938	18	1870	31	1961	8	95	1932	36	6.07	0.01	160	305	0.526
4.7617	0.1139	0.3088	0.0062	0.4181	0.1110	0.0011	1778	20	1735	30	1816	18	96	1770	39	2.32	0.13	49	96	0.507
5.4715	0.1100	0.3305	0.0052	0.3907	0.1181	0.0010	1896	17	1841	25	1927	15	96	1884	33	5.18	0.02	26	61	0.422
5.3571	0.0782	0.3258	0.0049	0.5128	0.1163	0.0005	1878	12	1818	24	1900	8	96	1877	25	8.72	0.00	341	600	0.569
5.4512	0.1281	0.3283	0.0075	0.4891	0.1171	0.0009	1893	20	1830	37	1912	14	96	1890	40	3.85	0.05	34	85	0.399
6.8489	0.2897	0.3775	0.0129	0.4041	0.1343	0.0024	2092	37	2065	60	2155	31	96	2088	73	0.23	0.63	7	8	0.929
5.5260	0.1277	0.3349	0.0055	0.3576	0.1190	0.0009	1905	20	1862	27	1941	14	96	1892	37	2.50	0.11	71	131	0.540
5.0038	0.1062	0.3151	0.0062	0.4637	0.1124	0.0007	1820	18	1766	30	1839	11	96	1815	36	3.99	0.05	189	209	0.906
10.4084	0.1685	0.4511	0.0068	0.4682	0.1636	0.0008	2472	15	2400	30	2493	8	96	2470	30	7.18	0.01	63	125	0.507
5.6512	0.0874	0.3400	0.0043	0.4106	0.1184	0.0008	1924	13	1886	21	1933	12	98	1917	26	3.69	0.05	108	147	0.732
5.1185	0.1509	0.3269	0.0078	0.4031	0.1138	0.0013	1839	25	1823	38	1861	21	98	1836	48	0.20	0.66	50	46	1.083

207Pb /235U	1s error	206Pb /238U	1s error	Rho	207Pb /206Pb	1s error	207Pb /235U Ma	1s Ma	206Pb /238U Ma	1s Ma	207Pb /206Pb Ma	1s Ma	U-Pb /Pb-Pb (% conc)	Concordia age (Ma)	2s Ma	MSWD (of concordance)	Probability	ppm 232Th	ppm 238U	Ratio Th/U
5.1207	0.1036	0.3233	0.0056	0.4300	0.1120	0.0007	1840	17	1806	27	1833	11	99	1835	34	1.76	0.18	156	184	0.847
4.9327	0.1183	0.3203	0.0062	0.4016	0.1111	0.0010	1808	20	1791	30	1818	16	99	1805	39	0.33	0.57	63	69	0.902
5.6056	0.1104	0.3384	0.0062	0.4666	0.1164	0.0005	1917	17	1879	30	1901	8	99	1914	34	2.02	0.16	316	488	0.648
5.0385	0.1341	0.3241	0.0071	0.4097	0.1118	0.0012	1826	23	1809	34	1829	20	99	1823	44	0.25	0.62	63	89	0.707
5.7732	0.0772	0.3468	0.0044	0.4750	0.1189	0.0005	1942	12	1919	21	1940	7	99	1941	23	1.55	0.21	410	565	0.726
5.6018	0.0746	0.3406	0.0039	0.4259	0.1167	0.0007	1916	11	1889	19	1906	11	99	1913	23	2.48	0.12	97	201	0.483
4.7844	0.0961	0.3086	0.0050	0.4045	0.1069	0.0008	1782	17	1734	25	1748	14	99	1772	33	4.23	0.04	71	141	0.500
5.6432	0.0902	0.3445	0.0048	0.4401	0.1177	0.0008	1923	14	1908	23	1921	12	99	1921	27	0.47	0.49	99	150	0.660
5.3300	0.1667	0.3289	0.0094	0.4562	0.1127	0.0010	1874	27	1833	46	1844	17	99	1870	53	1.00	0.32	76	73	1.048
5.7899	0.1467	0.3497	0.0069	0.3882	0.1189	0.0012	1945	22	1933	33	1939	18	100	1943	42	0.14	0.71	35	70	0.493
5.0462	0.1904	0.3311	0.0091	0.3637	0.1130	0.0014	1827	32	1844	44	1849	23	100	1831	59	0.14	0.70	32	30	1.052
5.6792	0.0882	0.3494	0.0050	0.4585	0.1185	0.0007	1928	13	1932	24	1933	10	100	1928	27	0.03	0.86	171	261	0.654
5.2482	0.1249	0.3328	0.0061	0.3854	0.1130	0.0012	1860	20	1852	30	1848	19	100	1859	39	0.09	0.76	69	55	1.241
5.3270	0.0928	0.3345	0.0050	0.4274	0.1132	0.0010	1873	15	1860	24	1851	15	100	1871	29	0.36	0.55	92	128	0.718
5.1030	0.1093	0.3340	0.0051	0.3562	0.1115	0.0010	1837	18	1858	25	1825	17	102	1842	34	0.72	0.40	44	57	0.775
5.1399	0.2375	0.3347	0.0136	0.4393	0.1109	0.0012	1843	39	1861	66	1814	20	103	1845	77	0.10	0.76	43	40	1.066
5.4531	0.1558	0.3445	0.0091	0.4601	0.1115	0.0012	1893	25	1909	43	1823	19	105	1894	49	0.15	0.69	23	46	0.503
5.5442	0.2906	0.3571	0.0175	0.4671	0.1137	0.0011	1907	45	1969	83	1859	18	106	1910	90	0.68	0.41	85	107	0.797

Table A3. LA-ICP-MS U-Pb isotopic analyses of detrital zircons, Cariboo Alp (DC165).

Measured Isotopic Ratios							Calculated Ages													
207Pb /235U	1s error	206Pb /238U	1s error	Rho	207Pb /206Pb	1s error	207Pb /235U	1s	206Pb /238U	1s	207Pb /206Pb	1s	U-Pb /Pb-Pb (% conc)	Concordia age (Ma)	2s	MSWD	Probability	ppm	ppm	Ratio
							Ma	Ma	Ma	Ma	Ma	Ma			Ma	(of concordance)		232Th	238U	Th/U
1.5016	0.1130	0.1028	0.0067	0.4313	0.1118	0.0064	931	46	631	39	1829	104	34	690	75	37.34	0.00	112	298	0.375
3.1072	0.1636	0.2243	0.0108	0.4584	0.1112	0.0013	1434	40	1305	57	1819	21	72	1404	79	6.12	0.01	26	43	0.604
3.5764	0.0931	0.2336	0.0058	0.4752	0.1068	0.0006	1544	21	1354	30	1746	11	78	1503	41	49.36	0.00	117	290	0.405
3.3434	0.1032	0.2298	0.0062	0.4338	0.1046	0.0011	1491	24	1333	32	1707	19	78	1444	47	26.28	0.00	186	431	0.431
3.4385	0.0772	0.2368	0.0045	0.4188	0.1060	0.0007	1513	18	1370	23	1732	12	79	1468	34	40.26	0.00	60	401	0.150
1.7049	0.0754	0.1598	0.0039	0.2786	0.0800	0.0010	1010	28	956	22	1198	25	80	973	39	3.10	0.08	29	69	0.422
12.0730	0.4576	0.4309	0.0150	0.4581	0.2035	0.0012	2610	36	2310	67	2855	10	81	2589	72	26.02	0.00	115	230	0.498
4.2146	0.1436	0.2670	0.0064	0.3505	0.1152	0.0007	1677	28	1525	32	1883	10	81	1611	51	18.78	0.00	156	446	0.350
3.7400	0.2244	0.2495	0.0159	0.5303	0.1080	0.0009	1580	48	1436	82	1766	16	81	1571	97	4.36	0.04	134	219	0.611
10.6283	0.7302	0.4078	0.0345	0.6164	0.1835	0.0014	2491	64	2205	158	2684	13	82	2528	119	5.19	0.02	59	253	0.234
5.4744	0.2519	0.3069	0.0093	0.3290	0.1300	0.0010	1897	39	1725	46	2098	13	82	1820	71	11.63	0.00	45	336	0.135
6.5574	0.0671	0.3327	0.0032	0.4745	0.1406	0.0005	2054	9	1852	16	2235	6	83	2034	18	218.05	0.00	117	497	0.235
3.9164	0.0604	0.2573	0.0039	0.4879	0.1074	0.0005	1617	12	1476	20	1756	8	84	1598	25	65.34	0.00	289	366	0.790
3.9909	0.0961	0.2620	0.0047	0.3764	0.1090	0.0011	1632	20	1500	24	1782	18	84	1583	36	28.42	0.00	50	170	0.293
1.7364	0.0728	0.1692	0.0041	0.2860	0.0788	0.0016	1022	27	1008	22	1168	39	86	1013	39	0.23	0.63	15	21	0.697
4.0630	0.0608	0.2672	0.0037	0.4635	0.1078	0.0004	1647	12	1527	19	1763	6	87	1627	24	50.20	0.00	155	615	0.253
3.9690	0.0711	0.2643	0.0040	0.4271	0.1068	0.0005	1628	15	1512	21	1745	8	87	1600	28	35.60	0.00	58	331	0.176
3.9309	0.0708	0.2649	0.0039	0.4078	0.1068	0.0004	1620	15	1515	20	1745	6	87	1590	28	30.11	0.00	134	484	0.277
4.1156	0.0965	0.2796	0.0053	0.4054	0.1108	0.0010	1657	19	1589	27	1813	16	88	1640	37	6.94	0.01	89	225	0.397
4.0855	0.1092	0.2743	0.0068	0.4608	0.1083	0.0006	1651	22	1562	34	1770	10	88	1638	43	8.35	0.00	320	748	0.427
4.2079	0.0535	0.2771	0.0031	0.4378	0.1088	0.0004	1676	10	1577	16	1779	6	89	1656	20	46.98	0.00	159	704	0.225
4.3749	0.0913	0.2843	0.0048	0.4011	0.1109	0.0006	1708	17	1613	24	1813	10	89	1682	33	16.76	0.00	171	376	0.456
4.5014	0.0948	0.2864	0.0053	0.4363	0.1113	0.0006	1731	18	1624	26	1821	9	89	1710	34	19.48	0.00	76	332	0.228
3.9834	0.0736	0.2705	0.0038	0.3823	0.1057	0.0008	1631	15	1543	19	1726	14	89	1602	28	20.26	0.00	63	294	0.214
4.1255	0.0940	0.2731	0.0054	0.4345	0.1065	0.0005	1659	19	1557	27	1741	9	89	1638	36	16.27	0.00	160	778	0.206
4.1849	0.0704	0.2790	0.0034	0.3598	0.1084	0.0006	1671	14	1586	17	1773	10	89	1640	25	23.02	0.00	59	178	0.332
8.1320	0.1277	0.3875	0.0051	0.4194	0.1496	0.0007	2246	14	2111	24	2341	8	90	2227	28	38.07	0.00	52	162	0.321
5.1721	0.1848	0.3081	0.0071	0.3219	0.1173	0.0009	1848	30	1731	35	1915	14	90	1797	54	9.19	0.00	119	821	0.145
5.2162	0.1878	0.3155	0.0082	0.3605	0.1197	0.0017	1855	31	1768	40	1952	26	91	1827	57	4.60	0.03	9	33	0.259
4.5018	0.1450	0.2891	0.0093	0.5005	0.1104	0.0006	1731	27	1637	47	1807	10	91	1725	54	5.50	0.02	49	147	0.331
4.3943	0.0601	0.2864	0.0031	0.3946	0.1089	0.0005	1711	11	1623	15	1782	8	91	1687	22	33.60	0.00	45	268	0.167
4.2466	0.0490	0.2821	0.0028	0.4329	0.1075	0.0004	1683	9	1602	14	1757	7	91	1667	19	37.94	0.00	169	342	0.495
4.4279	0.0752	0.2870	0.0045	0.4653	0.1088	0.0005	1718	14	1627	23	1780	8	91	1706	28	20.08	0.00	52	321	0.161
4.5081	0.0846	0.2990	0.0042	0.3765	0.1127	0.0050	1732	16	1686	21	1844	81	91	1719	29	4.91	0.03	28	106	0.260
4.2371	0.0789	0.2820	0.0046	0.4392	0.1068	0.0004	1681	15	1601	23	1746	8	92	1667	30	13.95	0.00	150	335	0.447
11.0518	0.1274	0.4498	0.0052	0.5007	0.1747	0.0006	2528	11	2395	23	2603	6	92	2530	21	45.11	0.00	125	246	0.508

207Pb /235U	1s error	206Pb /238U	1s error	Rho	207Pb /206Pb	1s error	207Pb /235U Ma	1s Ma	206Pb /238U Ma	1s 207Pb /206Pb Ma	1s Ma	U-Pb /Pb-Pb (% conc)	Concordia age (Ma)	2s Ma	MSWD (of concordance)	Probability	ppm 232Th	ppm 238U	Ratio Th/U	
4.2163	0.0825	0.2840	0.0037	0.3337	0.1072	0.0009	1677	16	1611	19	1752	15	92	1650	28	10.59	0.00	80	247	0.325
4.2500	0.5914	0.2850	0.0508	0.6399	0.1072	0.0009	1684	114	1617	255	1752	15	92	1693	220	0.11	0.74	177	424	0.417
4.4927	0.1400	0.2917	0.0076	0.4159	0.1087	0.0007	1730	26	1650	38	1777	12	93	1712	50	5.00	0.03	161	252	0.639
4.5235	0.0503	0.2916	0.0029	0.4426	0.1085	0.0005	1735	9	1649	14	1775	8	93	1721	18	42.81	0.00	98	379	0.259
4.5965	0.0948	0.2982	0.0045	0.3631	0.1105	0.0009	1749	17	1682	22	1807	15	93	1727	32	8.58	0.00	17	208	0.080
4.3138	0.0546	0.2880	0.0029	0.3989	0.1072	0.0006	1696	10	1632	15	1752	10	93	1680	20	20.78	0.00	83	165	0.504
4.6050	0.1466	0.2963	0.0101	0.5344	0.1096	0.0008	1750	27	1673	50	1793	13	93	1750	53	3.36	0.07	43	134	0.322
1.8916	0.0805	0.1830	0.0037	0.2348	0.0785	0.0014	1078	28	1083	20	1160	36	93	1082	36	0.03	0.87	42	89	0.474
4.4679	0.0777	0.2954	0.0039	0.3779	0.1091	0.0006	1725	14	1668	19	1784	11	93	1709	27	8.70	0.00	72	179	0.402
4.3951	0.0601	0.2893	0.0037	0.4661	0.1071	0.0006	1711	11	1638	18	1751	11	94	1702	22	19.94	0.00	76	201	0.377
4.5122	0.0667	0.2945	0.0036	0.4135	0.1088	0.0006	1733	12	1664	18	1779	9	94	1718	24	16.55	0.00	212	304	0.695
12.0103	0.2655	0.4710	0.0090	0.4343	0.1807	0.0014	2605	21	2488	40	2660	13	94	2598	41	10.83	0.00	71	92	0.775
4.3805	0.0466	0.2909	0.0026	0.4203	0.1074	0.0005	1709	9	1646	13	1756	8	94	1696	17	26.30	0.00	63	303	0.207
4.3575	0.0520	0.2912	0.0026	0.3764	0.1072	0.0005	1704	10	1648	13	1753	8	94	1687	18	18.79	0.00	87	222	0.392
15.4079	0.2786	0.5280	0.0096	0.5041	0.2087	0.0011	2841	17	2733	41	2896	9	94	2845	34	9.56	0.00	83	77	1.075
4.6050	0.0870	0.2993	0.0045	0.3973	0.1093	0.0008	1750	16	1688	22	1787	13	94	1735	30	8.39	0.00	136	108	1.264
4.3901	0.1234	0.2957	0.0065	0.3887	0.1081	0.0010	1710	23	1670	32	1768	16	94	1700	44	1.66	0.20	77	249	0.308
4.4290	0.0727	0.2953	0.0034	0.3490	0.1079	0.0006	1718	14	1668	17	1765	10	94	1700	25	8.09	0.00	154	180	0.860
4.1857	0.1144	0.2832	0.0083	0.5332	0.1041	0.0007	1671	22	1607	41	1698	12	95	1671	45	3.34	0.07	70	141	0.498
4.6319	0.0877	0.3041	0.0045	0.3929	0.1104	0.0005	1755	16	1711	22	1806	8	95	1744	30	4.04	0.04	103	261	0.394
4.8027	0.0928	0.3095	0.0043	0.3614	0.1110	0.0008	1785	16	1738	21	1815	14	96	1771	30	4.71	0.03	112	201	0.557
1.9076	0.0348	0.1810	0.0019	0.2872	0.0769	0.0006	1084	12	1072	10	1118	16	96	1077	18	0.70	0.40	85	178	0.476
2.9426	0.0497	0.2354	0.0029	0.3700	0.0896	0.0006	1393	13	1363	15	1418	13	96	1382	23	3.60	0.06	77	133	0.576
4.4814	0.0648	0.3002	0.0035	0.4049	0.1077	0.0006	1728	12	1692	17	1760	10	96	1720	23	4.43	0.04	85	228	0.374
4.5546	0.0675	0.3028	0.0030	0.3338	0.1084	0.0007	1741	12	1705	15	1773	11	96	1728	22	5.06	0.02	92	176	0.520
9.6707	0.1234	0.4396	0.0057	0.5092	0.1584	0.0010	2404	12	2349	26	2439	10	96	2406	23	6.31	0.01	85	213	0.398
4.4832	0.0674	0.3019	0.0036	0.3912	0.1075	0.0006	1728	12	1701	18	1758	11	97	1721	24	2.51	0.11	65	146	0.447
4.6705	0.1792	0.3158	0.0087	0.3606	0.1115	0.0014	1762	32	1769	43	1824	22	97	1764	59	0.03	0.87	74	103	0.715
4.7055	0.0910	0.3082	0.0045	0.3806	0.1091	0.0006	1768	16	1732	22	1785	10	97	1759	31	2.74	0.10	231	241	0.958
6.0805	0.2133	0.3525	0.0112	0.4546	0.1232	0.0009	1987	31	1946	54	2003	14	97	1984	61	0.73	0.39	105	104	1.010
1.8739	0.0434	0.1762	0.0032	0.3892	0.0750	0.0007	1072	15	1046	17	1069	18	98	1062	27	1.96	0.16	41	132	0.309
4.5734	0.0837	0.3029	0.0050	0.4482	0.1063	0.0006	1744	15	1706	25	1738	11	98	1739	30	3.02	0.08	191	139	1.380
1.9241	0.0362	0.1799	0.0022	0.3317	0.0755	0.0007	1089	13	1066	12	1081	18	99	1077	20	2.58	0.11	81	222	0.366
1.8261	0.0753	0.1812	0.0037	0.2490	0.0756	0.0013	1055	27	1073	20	1085	35	99	1067	36	0.40	0.53	25	57	0.444
4.8328	0.0972	0.3176	0.0041	0.3212	0.1094	0.0011	1791	17	1778	20	1789	18	99	1786	30	0.35	0.55	36	51	0.718
4.2851	0.0684	0.2954	0.0037	0.3878	0.1030	0.0007	1690	13	1668	18	1678	12	99	1685	25	1.52	0.22	62	139	0.448
6.0289	0.0970	0.3541	0.0046	0.4013	0.1206	0.0010	1980	14	1954	22	1965	14	99	1975	27	1.57	0.21	40	91	0.440
4.7496	0.0672	0.3149	0.0033	0.3671	0.1083	0.0006	1776	12	1765	16	1772	11	100	1773	22	0.49	0.48	70	177	0.395
5.0540	0.0665	0.3236	0.0034	0.4022	0.1105	0.0006	1828	11	1807	17	1808	9	100	1824	21	1.80	0.18	135	188	0.718

207Pb /235U	1s error	206Pb /238U	1s error	Rho	207Pb /206Pb	1s error	207Pb /235U Ma	1s Ma	206Pb /238U Ma	1s 207Pb /206Pb Ma	1s Ma	U-Pb /Pb-Pb (% conc)	Concordia age (Ma)	2s Ma	MSWD (of concordance)	Probability	ppm 232Th	ppm 238U	Ratio Th/U	
2.4201	0.0962	0.2180	0.0050	0.2875	0.0831	0.0009	1249	29	1271	26	1271	22	100	1261	44	0.47	0.49	60	73	0.830
5.0815	0.1535	0.3307	0.0070	0.3504	0.1125	0.0014	1833	26	1842	34	1839	22	100	1836	47	0.07	0.80	15	27	0.547
1.9661	0.0328	0.1845	0.0020	0.3254	0.0758	0.0005	1104	11	1091	11	1089	13	100	1097	18	0.97	0.33	112	268	0.418
5.3904	0.2788	0.3487	0.0147	0.4063	0.1179	0.0030	1883	44	1929	70	1924	46	100	1890	86	0.47	0.49	2	13	0.172
1.9323	0.0375	0.1834	0.0022	0.3142	0.0754	0.0007	1092	13	1086	12	1079	18	101	1089	20	0.21	0.65	92	120	0.761
12.7873	0.2157	0.5094	0.0072	0.4215	0.1776	0.0011	2664	16	2654	31	2631	10	101	2664	32	0.13	0.72	39	74	0.529
4.6617	0.1071	0.3148	0.0051	0.3528	0.1069	0.0009	1760	19	1764	25	1746	16	101	1762	35	0.02	0.88	33	55	0.605
4.6360	0.2663	0.3122	0.0156	0.4355	0.1061	0.0017	1756	48	1751	77	1733	29	101	1755	94	0.00	0.95	13	74	0.176
4.1748	0.0897	0.2970	0.0048	0.3752	0.1019	0.0008	1669	18	1676	24	1659	15	101	1671	33	0.10	0.76	44	81	0.551
4.6188	0.1091	0.3140	0.0051	0.3410	0.1064	0.0008	1753	20	1760	25	1739	13	101	1755	35	0.09	0.77	86	95	0.910
4.5555	0.0839	0.3107	0.0043	0.3718	0.1053	0.0008	1741	15	1744	21	1719	14	101	1742	29	0.02	0.90	86	213	0.402
17.4464	0.2243	0.5863	0.0070	0.4667	0.2128	0.0009	2960	12	2974	29	2927	7	102	2959	25	0.33	0.56	86	114	0.758
2.3026	0.0372	0.2077	0.0022	0.3306	0.0796	0.0005	1213	11	1216	12	1188	12	102	1215	19	0.06	0.81	170	249	0.682
1.8709	0.0415	0.1801	0.0033	0.4119	0.0738	0.0006	1071	15	1067	18	1036	15	103	1070	27	0.04	0.84	67	241	0.280
1.9261	0.0588	0.1807	0.0030	0.2696	0.0739	0.0010	1090	20	1071	16	1038	28	103	1078	29	0.73	0.39	28	73	0.377

Table A4. LA-ICP-MS U-Pb isotopic analyses of detrital zircons, Mount Symonds (DC395).

Measured Isotopic Ratios							Calculated Ages													
207Pb /235U	1s error	206Pb /238U	1s error	Rho	207Pb /206Pb	1s error	207Pb /235U	1s	206Pb /238U	1s	207Pb /206Pb	1s	U-Pb /Pb-Pb (% conc)	Concordia age (Ma)	2s	MSWD (of concordance)	Probability	ppm	ppm	Ratio
							Ma	Ma	Ma	Ma	Ma	Ma			Ma		(%)	232Th	238U	Th/U
0.4420	0.0936	0.0327	0.0060	0.4367	0.0961	0.0009	372	66	207	38	1549	18	13	213	75	6.52	0.01	49	733	0.067
0.1435	0.0583	0.0193	0.0072	0.4601	0.0555	0.0006	136	52	123	46	432	25	28	128	83	0.07	0.80	87	954	0.092
1.1114	0.2700	0.0742	0.0185	0.5140	0.0997	0.0010	759	130	461	111	1619	19	29	505	218	5.23	0.02	51	346	0.148
2.8251	0.4750	0.1476	0.0180	0.3619	0.1468	0.0012	1362	126	887	101	2309	14	38	942	197	10.15	0.00	131	916	0.143
0.4707	0.0818	0.0513	0.0071	0.3974	0.0652	0.0014	392	56	323	43	781	44	41	340	82	1.47	0.22	63	164	0.386
2.0177	0.1851	0.1347	0.0103	0.4177	0.1066	0.0007	1121	62	815	59	1742	11	47	903	109	19.69	0.00	362	534	0.677
6.1965	0.4568	0.2274	0.0155	0.4627	0.1901	0.0010	2004	64	1321	81	2743	8	48	1546	148	70.66	0.00	84	208	0.405
5.5128	0.3436	0.2173	0.0121	0.4453	0.1727	0.0061	1903	54	1268	64	2584	59	49	1459	118	90.31	0.00	66	398	0.165
1.4344	0.0892	0.1111	0.0064	0.4649	0.0860	0.0008	903	37	679	37	1339	18	51	765	67	31.77	0.00	120	334	0.359
2.1238	0.1429	0.1509	0.0090	0.4426	0.1032	0.0010	1157	46	906	50	1682	18	54	1020	87	22.76	0.00	52	116	0.448
2.3771	0.3284	0.1606	0.0196	0.4424	0.1054	0.0009	1236	99	960	109	1722	16	56	1087	187	5.98	0.01	101	285	0.352
2.5447	0.1191	0.1655	0.0088	0.5693	0.1030	0.0006	1285	34	987	49	1678	10	59	1223	70	54.96	0.00	65	238	0.274
3.5301	0.4543	0.2034	0.0267	0.5095	0.1230	0.0026	1534	102	1193	143	2001	37	60	1437	211	7.36	0.01	81	99	0.814
3.6812	0.1297	0.2218	0.0060	0.3870	0.1149	0.0008	1567	28	1291	32	1878	13	69	1428	53	65.38	0.00	77	240	0.319
2.9772	0.1143	0.2023	0.0064	0.4150	0.1050	0.0006	1402	29	1188	35	1713	10	69	1308	55	37.04	0.00	88	365	0.241
3.2113	0.1393	0.2137	0.0091	0.4900	0.1053	0.0008	1460	34	1249	48	1720	14	73	1412	68	24.20	0.00	43	169	0.251
0.9812	0.0366	0.1069	0.0022	0.2785	0.0690	0.0012	694	19	654	13	899	36	73	664	24	4.02	0.04	60	91	0.656
2.0525	0.1076	0.1699	0.0079	0.4464	0.0879	0.0009	1133	36	1012	44	1379	21	73	1089	68	8.16	0.00	52	151	0.344
3.6983	0.1378	0.2328	0.0070	0.4047	0.1121	0.0006	1571	30	1349	37	1834	10	74	1482	57	35.85	0.00	120	213	0.562
3.0782	0.0930	0.2134	0.0057	0.4398	0.1038	0.0005	1427	23	1247	30	1692	8	74	1368	45	39.12	0.00	131	492	0.266
8.7600	0.4007	0.3514	0.0146	0.4545	0.1770	0.0010	2313	42	1941	70	2625	10	74	2254	86	36.29	0.00	99	167	0.592
3.2979	0.0863	0.2127	0.0041	0.3711	0.1023	0.0008	1481	20	1243	22	1666	15	75	1353	37	95.01	0.00	55	151	0.364
2.9429	0.1864	0.2149	0.0097	0.3567	0.1015	0.0011	1393	48	1255	52	1652	20	76	1324	84	5.85	0.02	77	75	1.017
3.3247	0.1682	0.2219	0.0093	0.4128	0.1022	0.0009	1487	39	1292	49	1665	17	78	1411	75	15.96	0.00	137	187	0.734
8.7157	0.2380	0.3638	0.0098	0.4917	0.1702	0.0007	2309	25	2000	46	2560	7	78	2290	50	61.23	0.00	89	204	0.435
3.1655	0.1703	0.2193	0.0114	0.4837	0.1005	0.0006	1449	42	1278	60	1633	11	78	1413	83	10.03	0.00	85	406	0.209
9.3469	0.2078	0.3710	0.0080	0.4863	0.1716	0.0009	2373	20	2034	38	2573	8	79	2349	41	110.15	0.00	247	246	1.006
3.5826	0.2689	0.2392	0.0164	0.4577	0.1066	0.0008	1546	60	1382	85	1742	14	79	1508	118	4.34	0.04	71	153	0.463
1.8186	0.0853	0.1594	0.0068	0.4578	0.0800	0.0011	1052	31	953	38	1196	27	80	1018	58	7.36	0.01	65	87	0.749
3.5374	0.1599	0.2470	0.0084	0.3776	0.1077	0.0010	1536	36	1423	44	1760	18	81	1493	66	6.30	0.01	60	124	0.486
3.6801	0.0810	0.2388	0.0045	0.4315	0.1035	0.0007	1567	18	1381	24	1688	13	82	1510	34	68.41	0.00	110	203	0.542
9.7133	0.4020	0.3875	0.0131	0.4096	0.1720	0.0010	2408	38	2111	61	2577	9	82	2348	77	27.55	0.00	110	200	0.547
11.3566	0.6194	0.4144	0.0187	0.4140	0.1876	0.0011	2553	51	2235	85	2722	10	82	2498	104	16.59	0.00	201	127	1.582
4.0364	0.1115	0.2645	0.0053	0.3658	0.1119	0.0006	1642	22	1513	27	1830	9	83	1591	41	20.59	0.00	53	324	0.164
10.1269	0.2363	0.4253	0.0079	0.3968	0.1904	0.0168	2446	22	2285	36	2746	145	83	2420	43	23.64	0.00	83	111	0.751
9.9604	0.3107	0.4019	0.0118	0.4714	0.1760	0.0010	2431	29	2178	54	2616	9	83	2416	58	28.81	0.00	62	122	0.508

207Pb /235U	1s error	206Pb /238U	1s error	Rho	207Pb /206Pb	1s error	207Pb /235U	1s	206Pb /238U	1s	207Pb /206Pb	1s	U-Pb /Pb-Pb (% conc)	Concordia age (Ma)	2s	MSWD (of concordance)	Probability	ppm	ppm	Ratio
							Ma	Ma	Ma	Ma	Ma	Ma			Ma			232Th	238U	Th/U
3.9043	0.1135	0.2528	0.0050	0.3419	0.1064	0.0008	1615	23	1453	26	1738	14	84	1536	42	31.70	0.00	150	162	0.925
3.4387	0.0753	0.2413	0.0041	0.3887	0.1018	0.0008	1513	17	1393	21	1657	14	84	1469	32	30.61	0.00	33	98	0.338
19.6707	0.5785	0.5299	0.0154	0.4943	0.2606	0.0022	3075	28	2741	65	3250	13	84	3082	56	36.91	0.00	9	42	0.220
9.7501	0.2010	0.4019	0.0074	0.4462	0.1716	0.0008	2411	19	2178	34	2573	8	85	2388	38	59.64	0.00	112	235	0.476
16.2145	0.2720	0.5063	0.0081	0.4746	0.2344	0.0040	2890	16	2641	34	3082	27	86	2888	32	69.68	0.00	50	101	0.500
4.5134	0.0844	0.2950	0.0060	0.5404	0.1184	0.0105	1733	16	1666	30	1933	159	86	1734	31	7.27	0.01	74	251	0.296
10.9615	0.2098	0.4365	0.0074	0.4406	0.1856	0.0068	2520	18	2335	33	2704	61	86	2505	36	39.44	0.00	176	328	0.538
10.2540	0.1900	0.4186	0.0070	0.4539	0.1753	0.0011	2458	17	2254	32	2609	11	86	2443	35	52.16	0.00	62	90	0.683
3.6705	0.0718	0.2448	0.0047	0.4864	0.1004	0.0005	1565	16	1411	24	1632	10	86	1541	31	52.10	0.00	143	319	0.448
4.1735	0.1720	0.2667	0.0078	0.3568	0.1074	0.0009	1669	34	1524	40	1755	14	87	1608	62	11.64	0.00	51	151	0.336
4.3775	0.2417	0.2773	0.0140	0.4568	0.1109	0.0007	1708	46	1578	71	1814	12	87	1686	91	4.16	0.04	165	269	0.613
3.8164	0.1019	0.2555	0.0043	0.3142	0.1018	0.0008	1596	21	1467	22	1657	15	88	1528	36	25.19	0.00	50	154	0.326
0.8550	0.0586	0.0989	0.0032	0.2376	0.0622	0.0010	627	32	608	19	680	33	89	612	36	0.34	0.56	51	109	0.468
4.2796	0.1866	0.2764	0.0088	0.3639	0.1066	0.0008	1689	36	1573	44	1743	13	90	1646	66	6.42	0.01	90	195	0.464
12.4735	0.4396	0.4535	0.0112	0.3510	0.1817	0.0014	2641	33	2411	50	2668	13	90	2581	65	22.07	0.00	111	94	1.175
4.4386	0.1844	0.2809	0.0087	0.3706	0.1079	0.0010	1720	34	1596	44	1765	16	90	1676	64	7.73	0.01	74	135	0.548
2.9081	0.0599	0.2218	0.0045	0.4879	0.0899	0.0006	1384	16	1291	24	1423	13	91	1369	31	19.74	0.00	85	195	0.434
0.6760	0.0203	0.0822	0.0017	0.3437	0.0588	0.0007	524	12	509	10	560	25	91	514	18	1.36	0.24	282	279	1.010
3.8958	0.0624	0.2691	0.0033	0.3865	0.1034	0.0006	1613	13	1536	17	1686	11	91	1589	24	20.63	0.00	69	197	0.348
3.1215	0.0839	0.2483	0.0042	0.3120	0.0964	0.0054	1438	21	1430	22	1555	105	92	1434	34	0.11	0.74	42	85	0.492
0.8054	0.0404	0.0965	0.0024	0.2472	0.0611	0.0007	600	23	594	14	642	26	92	595	26	0.07	0.80	182	329	0.554
4.2091	0.1020	0.2809	0.0045	0.3299	0.1056	0.0008	1676	20	1596	23	1725	14	93	1641	35	10.41	0.00	41	112	0.366
0.7820	0.0399	0.0976	0.0025	0.2519	0.0613	0.0010	587	23	600	15	648	33	93	597	27	0.33	0.57	61	110	0.555
11.7022	0.2093	0.4659	0.0078	0.4698	0.1785	0.0009	2581	17	2466	34	2639	9	93	2579	34	14.65	0.00	93	169	0.549
2.1082	0.0339	0.1828	0.0026	0.4455	0.0784	0.0004	1152	11	1082	14	1158	11	93	1131	21	25.85	0.00	234	917	0.256
3.9921	0.0720	0.2761	0.0034	0.3436	0.1030	0.0007	1633	15	1572	17	1678	13	94	1609	26	10.89	0.00	77	193	0.401
4.8755	0.1709	0.3173	0.0056	0.2513	0.1161	0.0072	1798	30	1776	27	1897	111	94	1786	45	0.38	0.54	39	43	0.900
4.3316	0.0889	0.2873	0.0053	0.4524	0.1064	0.0006	1699	17	1628	27	1738	11	94	1689	33	8.69	0.00	93	207	0.451
4.4412	0.0645	0.2928	0.0038	0.4424	0.1079	0.0006	1720	12	1656	19	1764	10	94	1710	24	14.02	0.00	51	130	0.393
11.0110	0.1931	0.4543	0.0072	0.4514	0.1713	0.0008	2524	16	2414	32	2571	7	94	2519	33	15.00	0.00	118	194	0.607
0.8487	0.0359	0.1018	0.0024	0.2810	0.0616	0.0007	624	20	625	14	660	26	95	625	26	0.00	0.96	177	213	0.830
4.4996	0.0649	0.2940	0.0039	0.4588	0.1066	0.0006	1731	12	1662	19	1742	11	95	1722	24	15.80	0.00	68	130	0.518
13.8647	0.1552	0.5087	0.0056	0.4898	0.1940	0.0007	2741	11	2651	24	2776	6	95	2743	21	18.81	0.00	148	184	0.803
4.0671	0.0984	0.2830	0.0059	0.4316	0.1032	0.0007	1648	20	1606	30	1682	13	95	1640	38	2.24	0.13	54	126	0.428
4.3032	0.0760	0.2907	0.0036	0.3489	0.1055	0.0008	1694	15	1645	18	1723	14	96	1677	26	6.78	0.01	42	130	0.319
4.4959	0.1513	0.2948	0.0102	0.5118	0.1066	0.0008	1730	28	1666	51	1742	14	96	1728	56	2.23	0.14	54	137	0.395
4.4833	0.0990	0.2980	0.0048	0.3620	0.1075	0.0008	1728	18	1681	24	1758	14	96	1713	34	3.73	0.05	92	108	0.849
5.6668	0.0854	0.3385	0.0033	0.3222	0.1204	0.0009	1926	13	1879	16	1962	14	96	1909	23	7.68	0.01	157	215	0.732
4.1197	0.0744	0.2830	0.0043	0.4230	0.1029	0.0006	1658	15	1606	22	1677	10	96	1648	29	6.48	0.01	116	310	0.374
4.4795	0.1109	0.2980	0.0050	0.3422	0.1070	0.0009	1727	21	1681	25	1749	15	96	1710	37	3.02	0.08	62	122	0.507

207Pb /235U	1s error	206Pb /238U	1s error	Rho	207Pb /206Pb	1s error	207Pb /235U	1s	206Pb /238U	1s	207Pb /206Pb	1s	U-Pb /Pb-Pb (% conc)	Concordia age (Ma)	2s	MSWD (of concordance)	Probability	ppm	ppm	Ratio
							Ma	Ma	Ma	Ma	Ma	Ma			Ma			232Th	238U	Th/U
11.1863	0.1209	0.4655	0.0055	0.5479	0.1700	0.0006	2539	10	2464	24	2557	6	96	2544	20	13.58	0.00	57	211	0.272
9.8944	0.3144	0.4445	0.0111	0.3931	0.1598	0.0011	2425	29	2371	50	2454	11	97	2417	58	1.35	0.24	90	99	0.910
10.7184	0.1782	0.4592	0.0067	0.4410	0.1663	0.0011	2499	15	2436	30	2521	11	97	2496	31	5.55	0.02	30	86	0.347
4.5572	0.0790	0.2979	0.0045	0.4334	0.1062	0.0004	1741	14	1681	22	1736	7	97	1731	28	8.69	0.00	179	426	0.420
3.0138	0.0870	0.2349	0.0058	0.4243	0.0887	0.0006	1411	22	1360	30	1398	13	97	1398	42	3.14	0.08	124	191	0.649
4.4571	0.0583	0.2999	0.0031	0.3923	0.1058	0.0005	1723	11	1691	15	1728	9	98	1715	21	4.73	0.03	115	352	0.327
4.5913	0.0985	0.3026	0.0046	0.3546	0.1064	0.0008	1748	18	1704	23	1738	13	98	1733	33	3.46	0.06	46	128	0.355
4.5718	0.1667	0.3107	0.0078	0.3452	0.1084	0.0015	1744	30	1744	38	1773	26	98	1744	55	0.00	1.00	29	42	0.690
5.0969	0.0977	0.3229	0.0048	0.3900	0.1116	0.0007	1836	16	1804	24	1826	12	99	1828	31	1.96	0.16	71	174	0.409
4.6353	0.1041	0.3148	0.0042	0.2945	0.1089	0.0011	1756	19	1764	20	1780	18	99	1759	31	0.13	0.71	52	77	0.676
12.9442	0.3758	0.5162	0.0133	0.4433	0.1847	0.0017	2676	27	2683	56	2696	15	100	2676	55	0.02	0.88	24	36	0.662
12.4719	0.1903	0.4989	0.0067	0.4422	0.1765	0.0010	2641	14	2609	29	2620	9	100	2640	29	1.48	0.22	96	100	0.957
4.0516	0.1529	0.2895	0.0088	0.4019	0.1012	0.0011	1645	31	1639	44	1646	20	100	1643	58	0.02	0.89	40	112	0.358
4.1748	0.0732	0.2966	0.0032	0.3116	0.1028	0.0007	1669	14	1675	16	1676	13	100	1671	24	0.09	0.76	105	185	0.569
0.8390	0.0401	0.0967	0.0040	0.4318	0.0597	0.0007	619	22	595	23	593	24	100	608	39	0.96	0.33	52	178	0.294
4.8861	0.0966	0.3187	0.0042	0.3367	0.1081	0.0008	1800	17	1783	21	1767	13	101	1794	30	0.57	0.45	95	101	0.934
5.5496	0.1175	0.3444	0.0055	0.3791	0.1147	0.0009	1908	18	1908	27	1876	14	102	1908	35	0.00	0.99	29	49	0.595
2.0740	0.0376	0.1920	0.0024	0.3482	0.0765	0.0006	1140	12	1132	13	1108	16	102	1137	21	0.31	0.58	103	195	0.531
0.9365	0.0393	0.1103	0.0026	0.2796	0.0616	0.0010	671	21	674	15	659	34	102	673	27	0.02	0.88	25	60	0.413
0.8800	0.0315	0.1085	0.0022	0.2796	0.0613	0.0007	641	17	664	13	648	26	102	657	23	1.66	0.20	73	177	0.412
0.7846	0.0409	0.1022	0.0027	0.2495	0.0597	0.0008	588	23	627	16	591	31	106	617	28	2.62	0.11	109	188	0.578
0.9142	0.0315	0.1072	0.0022	0.2979	0.0598	0.0009	659	17	657	13	598	32	110	657	23	0.02	0.88	32	60	0.534

Table A5. LA-ICP-MS U-Pb isotopic analyses of detrital zircons, Plant Creek (DC490).

Measured Isotopic Ratios							Calculated Ages													
207Pb /235U	1s error	206Pb /238U	1s error	Rho	207Pb /206Pb	1s error	207Pb /235U	1s	206Pb /238U	1s	207Pb /206Pb	1s	U-Pb /Pb-Pb (% conc)	Concordia age (Ma)	2s	MSWD	Probability	ppm	ppm	Ratio
							Ma	Ma	Ma	Ma	Ma	Ma		(Ma)	Ma	(of concordance)		232Th	238U	Th/U
0.0990	0.0071	0.0109	0.0006	0.3829	0.0685	0.0025	96	7	70	4	883	77	8	73	8	16.82	0.00	1	58	0.020
0.3805	0.0997	0.0372	0.0056	0.2867	0.0784	0.0019	327	73	235	35	1157	47	20	242	69	1.54	0.22	196	1108	0.177
0.4497	0.0670	0.0439	0.0043	0.3320	0.0717	0.0016	377	47	277	27	979	45	28	288	53	4.45	0.03	948	1814	0.522
0.1847	0.0149	0.0255	0.0018	0.4389	0.0555	0.0008	172	13	162	11	434	33	37	166	20	0.58	0.45	322	989	0.326
1.2139	0.1978	0.0934	0.0129	0.4252	0.0939	0.0011	807	91	576	76	1506	23	38	629	145	5.86	0.02	93	448	0.208
0.1543	0.0057	0.0221	0.0006	0.3520	0.0528	0.0005	146	5	141	4	322	20	44	142	7	0.83	0.36	5290	3592	1.473
0.2152	0.0416	0.0270	0.0046	0.4414	0.0536	0.0009	198	35	172	29	355	40	48	180	53	0.59	0.44	61	787	0.078
0.1705	0.0071	0.0250	0.0005	0.2200	0.0527	0.0006	160	6	159	3	315	25	51	159	6	0.01	0.91	1214	2467	0.492
0.2264	0.0191	0.0324	0.0023	0.4193	0.0537	0.0005	207	16	205	14	359	20	57	206	25	0.01	0.92	369	1348	0.274
0.1614	0.0100	0.0241	0.0007	0.2362	0.0515	0.0008	152	9	154	4	265	36	58	153	9	0.04	0.84	519	1739	0.299
0.3956	0.0287	0.0516	0.0029	0.3862	0.0584	0.0006	338	21	324	18	545	21	59	329	32	0.44	0.51	197	709	0.278
2.4241	0.1916	0.1681	0.0111	0.4192	0.1017	0.0007	1250	57	1001	61	1656	14	60	1115	105	14.41	0.00	81	271	0.298
0.1752	0.0182	0.0252	0.0020	0.3834	0.0513	0.0005	164	16	161	13	255	22	63	162	23	0.05	0.83	1643	2710	0.606
0.5601	0.0444	0.0681	0.0035	0.3236	0.0601	0.0011	452	29	425	21	607	40	70	432	39	0.80	0.37	95	237	0.400
0.1830	0.0089	0.0259	0.0006	0.2547	0.0508	0.0009	171	8	165	4	232	39	71	166	8	0.54	0.46	302	677	0.447
0.2855	0.0219	0.0402	0.0026	0.4162	0.0536	0.0006	255	17	254	16	354	27	72	254	28	0.00	0.95	192	644	0.298
0.4067	0.0274	0.0524	0.0031	0.4373	0.0561	0.0005	347	20	329	19	458	21	72	337	33	0.71	0.40	288	760	0.379
0.5303	0.0356	0.0697	0.0023	0.2486	0.0597	0.0012	432	24	434	14	592	43	73	434	26	0.01	0.92	66	149	0.446
1.4583	0.0876	0.1374	0.0058	0.3494	0.0766	0.0006	913	36	830	33	1110	17	75	862	57	4.36	0.04	121	1000	0.121
0.2296	0.0233	0.0344	0.0022	0.3206	0.0520	0.0007	210	19	218	14	287	31	76	216	26	0.17	0.68	881	1205	0.731
0.5616	0.0189	0.0707	0.0012	0.2477	0.0589	0.0008	453	12	440	7	563	28	78	442	13	0.97	0.32	131	254	0.517
0.4185	0.0248	0.0565	0.0021	0.3121	0.0559	0.0007	355	18	354	13	449	28	79	355	23	0.00	0.98	139	464	0.299
0.7966	0.0547	0.0913	0.0051	0.4055	0.0630	0.0011	595	31	563	30	708	37	79	578	51	0.92	0.34	45	70	0.651
0.2235	0.0127	0.0311	0.0015	0.4352	0.0512	0.0006	205	11	198	10	248	28	80	201	17	0.45	0.50	125	1173	0.107
0.1620	0.0094	0.0245	0.0007	0.2421	0.0500	0.0007	152	8	156	4	195	32	80	155	8	0.16	0.69	2866	5191	0.552
0.1577	0.0040	0.0237	0.0004	0.3177	0.0498	0.0003	149	4	151	2	186	16	81	150	4	0.34	0.56	2053	3946	0.520
0.5002	0.0362	0.0652	0.0034	0.3591	0.0571	0.0007	412	25	407	21	497	28	82	409	37	0.03	0.86	39	354	0.109
0.5277	0.0170	0.0694	0.0011	0.2539	0.0579	0.0007	430	11	432	7	527	25	82	432	13	0.03	0.86	79	364	0.218
3.4286	0.1056	0.2362	0.0065	0.4435	0.1009	0.0007	1511	24	1367	34	1641	13	83	1474	47	20.89	0.00	131	200	0.653
0.6650	0.0406	0.0834	0.0029	0.2837	0.0603	0.0006	518	25	516	17	614	22	84	517	32	0.00	0.95	493	525	0.939
0.5586	0.0415	0.0703	0.0028	0.2712	0.0577	0.0013	451	27	438	17	517	51	85	441	32	0.20	0.65	70	118	0.593
0.4478	0.0247	0.0616	0.0016	0.2406	0.0560	0.0009	376	17	385	10	454	35	85	384	19	0.30	0.59	83	198	0.418
0.5005	0.0295	0.0650	0.0025	0.3225	0.0563	0.0009	412	20	406	15	465	37	87	408	27	0.08	0.78	69	141	0.488
1.4867	0.0595	0.1452	0.0062	0.5363	0.0723	0.0006	925	24	874	35	994	17	88	917	48	2.90	0.09	12	383	0.030
0.1457	0.0155	0.0223	0.0014	0.2877	0.0493	0.0005	138	14	142	9	160	22	89	142	16	0.09	0.76	249	3575	0.070

207Pb /235U	1s error	206Pb /238U	1s error	Rho	207Pb /206Pb	1s error	207Pb /235U	1s	206Pb /238U	1s	207Pb /206Pb	1s	U-Pb /Pb-Pb (% conc)	Concordia age (Ma)	2s	MSWD	Probability	ppm	ppm	Ratio
							Ma	Ma	Ma	Ma	Ma	Ma			Ma	(of concordance)		232Th	238U	Th/U
0.5353	0.0195	0.0687	0.0015	0.3058	0.0566	0.0007	435	13	429	9	474	27	90	430	17	0.26	0.61	84	260	0.325
0.1892	0.0107	0.0244	0.0012	0.4244	0.0495	0.0008	176	9	155	7	172	39	90	162	14	5.29	0.02	566	671	0.843
0.4601	0.0262	0.0618	0.0017	0.2464	0.0553	0.0011	384	18	386	11	426	44	91	386	20	0.01	0.91	56	135	0.416
0.1736	0.0146	0.0251	0.0018	0.4185	0.0495	0.0004	163	13	160	11	171	20	93	161	20	0.06	0.81	3278	2775	1.181
5.4307	0.3432	0.3233	0.0222	0.5421	0.1184	0.0010	1890	54	1806	108	1933	15	93	1892	108	0.86	0.35	96	131	0.733
0.3721	0.0504	0.0522	0.0077	0.5437	0.0534	0.0009	321	37	328	47	346	40	95	323	71	0.03	0.86	78	426	0.182
4.7038	0.1013	0.3032	0.0058	0.4403	0.1090	0.0007	1768	18	1707	28	1782	11	96	1759	35	5.40	0.02	64	130	0.493
0.1846	0.0152	0.0271	0.0016	0.3533	0.0496	0.0007	172	13	173	10	176	34	98	172	18	0.00	0.97	223	1324	0.168
0.4428	0.0107	0.0592	0.0012	0.4167	0.0540	0.0004	372	8	370	7	373	16	99	371	12	0.05	0.83	1246	1627	0.766
0.2000	0.0124	0.0288	0.0017	0.4692	0.0498	0.0006	185	10	183	10	184	26	99	184	18	0.03	0.86	135	1197	0.113
0.5591	0.0225	0.0692	0.0021	0.3732	0.0554	0.0010	451	15	432	13	430	40	100	439	22	1.59	0.21	90	255	0.353
0.4554	0.0248	0.0677	0.0017	0.2262	0.0552	0.0010	381	17	422	10	421	39	100	414	19	5.36	0.02	54	127	0.428
0.4201	0.0322	0.0604	0.0025	0.2734	0.0541	0.0013	356	23	378	15	376	54	101	373	28	0.85	0.36	45	105	0.424
0.3887	0.0187	0.0545	0.0020	0.3792	0.0531	0.0006	333	14	342	12	333	27	103	339	21	0.35	0.55	176	428	0.410
0.1663	0.0047	0.0248	0.0005	0.3511	0.0491	0.0003	156	4	158	3	154	13	103	157	6	0.17	0.68	1926	4026	0.478
0.5277	0.0103	0.0692	0.0010	0.3591	0.0552	0.0004	430	7	431	6	419	16	103	431	10	0.02	0.88	725	870	0.833
0.7198	0.0175	0.0851	0.0012	0.2823	0.0575	0.0005	551	10	527	7	510	20	103	532	13	4.88	0.03	340	433	0.785
0.1622	0.0042	0.0243	0.0004	0.2890	0.0490	0.0004	153	4	155	2	148	20	105	155	4	0.43	0.51	348	1997	0.174
0.4850	0.0197	0.0658	0.0014	0.2551	0.0545	0.0008	401	13	411	8	391	31	105	409	15	0.47	0.49	131	384	0.342
0.1900	0.0197	0.0265	0.0019	0.3425	0.0492	0.0004	177	17	168	12	159	18	106	170	22	0.24	0.62	2855	5636	0.506
0.4422	0.0198	0.0596	0.0015	0.2864	0.0535	0.0007	372	14	373	9	350	30	107	373	17	0.01	0.92	138	361	0.383
0.1637	0.0046	0.0234	0.0005	0.3896	0.0488	0.0003	154	4	149	3	139	15	107	151	6	1.25	0.26	2541	4716	0.539
0.4940	0.0568	0.0693	0.0034	0.2156	0.0547	0.0011	408	39	432	21	401	44	108	428	39	0.38	0.54	210	252	0.834
0.4394	0.0251	0.0638	0.0024	0.3284	0.0538	0.0006	370	18	399	14	363	27	110	388	26	2.39	0.12	106	311	0.340
0.3599	0.0161	0.0510	0.0015	0.3294	0.0521	0.0007	312	12	321	9	292	32	110	318	17	0.50	0.48	63	277	0.227
0.1659	0.0042	0.0247	0.0004	0.3248	0.0489	0.0003	156	4	157	3	142	15	111	157	5	0.13	0.72	2088	3651	0.572
0.7207	0.0167	0.0896	0.0012	0.2793	0.0572	0.0005	551	10	553	7	498	21	111	553	13	0.04	0.85	247	341	0.725
0.4895	0.0172	0.0652	0.0012	0.2653	0.0539	0.0008	405	12	407	7	366	33	111	407	14	0.04	0.84	93	216	0.432
0.1555	0.0078	0.0231	0.0009	0.3674	0.0487	0.0004	147	7	147	5	131	21	112	147	10	0.00	0.95	1987	2859	0.695
0.5157	0.0197	0.0673	0.0015	0.2985	0.0540	0.0006	422	13	420	9	373	26	113	421	17	0.02	0.87	196	397	0.494
0.1529	0.0055	0.0218	0.0006	0.3788	0.0485	0.0006	144	5	139	4	122	27	114	141	7	1.30	0.25	61	1220	0.050
0.5108	0.0150	0.0699	0.0011	0.2746	0.0542	0.0007	419	10	436	7	381	27	114	431	13	2.51	0.11	115	291	0.395
0.5413	0.0188	0.0715	0.0012	0.2349	0.0545	0.0007	439	12	445	7	390	30	114	444	13	0.24	0.62	121	296	0.411
0.1628	0.0034	0.0236	0.0003	0.3363	0.0486	0.0003	153	3	151	2	130	16	116	151	4	0.73	0.39	1654	3615	0.458
0.1678	0.0038	0.0249	0.0004	0.3716	0.0487	0.0003	157	3	158	3	136	14	117	158	5	0.05	0.82	2169	4201	0.516
0.4710	0.0153	0.0645	0.0011	0.2572	0.0533	0.0007	392	11	403	7	340	29	118	400	12	0.99	0.32	134	309	0.433
0.5275	0.0145	0.0697	0.0011	0.2748	0.0539	0.0005	430	10	434	6	366	21	119	433	12	0.19	0.66	256	591	0.434
0.1703	0.0044	0.0246	0.0005	0.3729	0.0487	0.0003	160	4	156	3	131	14	119	157	5	0.73	0.39	1566	4928	0.318
0.2290	0.0362	0.0335	0.0053	0.5046	0.0496	0.0003	209	30	213	33	176	15	120	211	54	0.01	0.92	3630	4474	0.811

207Pb /235U	1s error	206Pb /238U	1s error	Rho	207Pb /206Pb	1s error	207Pb /235U	1s Ma	206Pb /238U	1s Ma	207Pb /206Pb	1s Ma	U-Pb /Pb-Pb (% conc)	Concordia age (Ma)	2s Ma	MSWD (of concordance)	Probability	ppm 232Th	ppm 238U	Ratio Th/U
0.4844	0.0199	0.0667	0.0014	0.2564	0.0533	0.0008	401	14	416	8	340	34	122	413	16	1.17	0.28	55	265	0.206
0.6859	0.0530	0.0934	0.0045	0.3141	0.0558	0.0011	530	32	576	27	446	45	129	558	46	1.73	0.19	120	211	0.569
0.1698	0.0058	0.0248	0.0006	0.3481	0.0484	0.0004	159	5	158	4	119	20	133	158	7	0.08	0.77	634	2183	0.290
0.1556	0.0060	0.0239	0.0005	0.2553	0.0481	0.0007	147	5	152	3	105	35	144	151	6	0.95	0.33	39	552	0.071
0.1539	0.0049	0.0226	0.0006	0.4309	0.0480	0.0003	145	4	144	4	97	14	148	145	7	0.07	0.79	1751	4862	0.360
0.1575	0.0051	0.0227	0.0007	0.4483	0.0479	0.0003	149	4	145	4	93	14	156	146	7	0.71	0.40	2572	6037	0.426
0.1567	0.0053	0.0232	0.0007	0.4452	0.0475	0.0005	148	5	148	4	77	26	193	148	8	0.00	0.98	85	933	0.091

TABLE B1: Major and trace element data from XRF analysis

Sample	SiO2	Al2O3	CaO	K2O	MgO	MnO	Na2O	P2O5	Fe2O3(T)	TiO2	
DC004	61.34	16.80	5.09	2.22	3.08	0.09	4.27	0.14	6.18	0.57	
DC025	74.79	14.39	1.72	3.31	3.31	0.21	0.02	4.25	0.01	1.09	0.11
DC028	64.85	19.31	0.23	5.70	1.78	0.04	0.70	0.06	6.30	0.82	
DC048	48.44	15.78	10.82	0.31	7.85	0.19	3.04	0.09	11.96	1.39	
DC058	73.55	15.34	1.28	4.00	0.23	0.18	3.61	0.08	1.38	0.06	
DC080	62.55	15.34	4.66	2.50	3.02	0.11	4.04	0.18	6.56	0.57	
DC081	66.43	15.10	3.09	2.58	2.56	0.06	2.89	0.15	5.69	0.74	
DC130	51.84	14.74	10.60	0.89	7.19	0.18	2.01	0.28	11.27	0.78	
DC132	49.82	14.69	12.52	0.72	8.44	0.19	2.15	0.26	10.33	0.73	
DC139	47.78	13.17	13.83	0.98	8.28	0.19	1.50	0.27	13.01	0.77	
DC164	54.15	17.51	0.10	0.14	23.02	0.02	0.30	0.04	3.65	0.88	
DC166	66.64	14.13	0.07	0.15	16.16	0.01	0.53	0.02	1.52	0.68	
DC167	64.47	14.02	0.07	2.95	15.96	0.00	0.54	0.02	1.40	0.47	
DC169	49.94	14.05	11.16	0.45	10.28	0.24	1.28	0.64	10.24	1.52	
DC176	81.31	6.80	2.34	1.56	1.94	0.05	1.15	0.09	4.05	0.51	
DC178	67.81	13.11	0.82	4.75	2.93	0.11	1.13	0.11	8.02	0.99	
DC179	68.94	13.21	0.75	4.02	2.90	0.12	0.97	0.11	7.80	0.99	
DC186	75.03	6.93	6.08	1.68	4.73	0.11	0.73	0.10	3.90	0.54	
DC188	54.28	15.52	6.67	0.43	3.86	0.20	3.96	0.52	11.96	2.39	
DC195	45.90	12.27	10.47	0.68	11.49	0.23	1.64	0.52	14.12	2.47	
DC209	47.84	17.57	12.30	0.20	7.62	0.15	2.61	0.10	10.40	1.05	
DC219	50.18	13.96	10.44	0.56	8.28	0.17	2.83	0.16	11.87	1.35	
DC237	49.87	15.27	6.08	3.02	4.12	0.18	2.60	0.98	14.57	3.08	
DC286	71.65	9.91	4.46	1.99	4.83	0.08	1.23	0.13	5.01	0.46	
DC299	61.90	16.39	1.81	1.72	4.17	0.16	3.86	0.14	8.81	0.90	
DC320	50.26	15.13	12.30	0.72	9.70	0.18	1.41	0.04	9.60	0.49	
DC326	86.39	6.41	1.04	0.61	0.90	0.07	1.54	0.03	2.71	0.21	
DC330	60.49	16.10	1.76	3.42	4.00	0.20	1.25	0.11	11.16	1.29	
DC342	60.50	16.11	1.75	3.42	4.01	0.20	1.25	0.11	11.13	1.30	
DC370	48.91	14.67	8.04	0.46	4.43	0.23	3.84	0.34	15.72	3.21	
DC397	47.87	15.18	8.60	0.41	7.24	0.23	3.49	0.33	13.75	2.74	
DC400	47.66	13.93	9.40	0.81	6.20	0.23	3.71	0.31	14.72	2.87	
DC414	48.46	16.27	9.04	0.69	5.48	0.21	3.66	0.21	13.31	2.52	
DC418	73.67	15.12	1.42	5.47	0.33	0.01	2.34	0.10	1.26	0.13	
DC423	48.83	14.57	8.90	1.24	6.57	0.29	0.93	0.30	16.57	1.70	
DC427	50.77	10.01	12.37	0.90	16.18	0.14	1.04	0.03	8.14	0.35	
DC428	59.15	9.73	5.67	0.56	18.65	0.13	0.68	0.07	4.97	0.33	
DC429	56.03	8.38	9.73	0.14	19.13	0.18	0.71	0.07	5.27	0.29	
DC432	55.90	13.88	0.92	0.60	13.17	0.04	1.18	0.59	11.77	1.81	
DC439	69.87	13.77	2.07	3.06	1.85	0.11	2.63	0.23	5.65	0.59	
DC444	64.65	9.80	4.06	0.53	14.36	0.05	0.91	0.12	5.04	0.38	
DC446	47.87	15.76	9.30	0.77	7.38	0.26	1.57	0.25	15.48	1.23	
DC456	51.31	15.74	7.71	1.86	7.21	0.14	3.57	0.80	9.90	1.42	
DC457	45.87	12.16	11.81	0.94	12.54	0.21	1.17	0.18	13.40	1.50	
DC458	44.31	2.42	2.06	1.15	40.53	0.12	-0.23	0.02	9.01	0.08	
DC459	43.78	18.65	14.91	0.56	14.21	0.12	1.63	0.02	5.73	0.13	
DC464	53.87	14.94	9.57	1.07	5.83	0.18	1.00	0.11	11.91	1.40	
DC468	65.56	14.54	3.17	4.21	4.05	0.09	1.29	0.10	6.03	0.74	
DC469	48.20	14.30	10.11	0.64	7.22	0.18	2.67	0.32	13.40	2.80	
DC473	45.11	12.33	15.83	1.23	9.33	0.16	1.30	0.24	12.31	1.97	
DC475	51.38	15.72	7.49	2.00	7.16	0.15	3.76	0.72	9.87	1.42	
DC476	47.10	10.96	12.01	0.27	13.41	0.16	1.58	0.22	12.14	1.97	
DC477	57.79	0.97	8.67	0.07	27.55	0.08	-0.04	0.01	4.51	0.03	
DC478	47.47	4.47	8.68	0.14	27.58	0.16	0.53	0.14	9.89	0.59	

TABLE B2: Trace element data from XRF analysis

Sample	Zn	Ba	Ce	Co	Cr	Ga	La	Nb	Nd	Ni	Pb	Rb	Sr	Th	U	V	Y	Zr
DC004	82	1191	29	17	114	18	29	6	17	17	7	58	453	2	-1	100	19	124
DC025	43	481	6	3	129	16	8	12	0	3	30	104	188	6	4	-1	5	21
DC028	82	881	80	14	156	26	33	16	39	35	14	206	54	24	12	110	27	170
DC048	88	213	8	39	241	19	-7	2	7	86	6	7	126	7	4	315	32	88
DC058	22	293	33	0	199	16	3	9	11	8	64	103	140	6	8	9	23	55
DC080	71	3578	13	13	198	10	18	3	18	101	14	55	282	9	6	122	17	86
DC081	192	5858	9	19	169	14	26	5	22	30	25	65	225	4	0	127	26	139
DC130	118	840	7	30	194	15	6	3	14	66	-1	19	541	-4	-1	282	22	57
DC132	93	216	0	33	249	12	1	4	11	86	-3	16	521	-7	-5	266	19	40
DC139	79	276	18	43	206	15	28	3	6	42	-10	19	1202	-17	-15	326	13	32
DC164	23	32	179	3	156	16	125	23	47	16	14	18	3	54	19	46	16	717
DC166	6	22	62	0	242	12	16	15	24	16	5	16	14	26	9	37	15	334
DC167	6	52	30	4	224	10	36	11	8	14	10	100	12	24	10	35	11	251
DC169	153	27	54	34	829	23	48	33	30	106	14	11	62	15	7	281	30	194
DC176	41	942	28	6	243	7	14	5	21	19	11	53	240	7	2	66	14	158
DC178	92	741	70	22	272	15	47	16	32	70	29	170	76	23	10	109	39	297
DC179	90	682	78	21	320	15	47	15	31	53	21	157	58	22	4	107	40	305
DC186	50	584	32	11	266	9	18	8	21	16	14	59	88	14	9	63	24	165
DC188	97	159	139	19	111	18	77	80	61	4	3	10	741	3	-4	287	33	277
DC195	131	95	81	52	533	16	68	53	35	258	13	15	124	18	13	211	36	224
DC209	74	372	-17	44	325	14	-2	8	1	100	-1	8	305	-2	-2	234	26	67
DC219	97	487	19	45	471	18	34	16	15	126	5	9	321	7	4	251	21	88
DC237	111	1106	98	31	47	17	53	75	44	15	3	153	291	4	3	127	37	244
DC286	121	1086	-11	17	508	10	5	4	13	204	16	62	248	9	7	174	19	81
DC299	87	524	16	23	257	16	13	5	11	53	27	48	130	15	10	176	26	109
DC320	79	72	-4	34	811	15	24	4	6	96	8	14	100	5	3	208	24	38
DC326	30	89	4	3	340	6	15	2	2	23	16	30	88	14	6	23	13	112
DC330	114	540	100	28	294	20	33	33	41	52	14	160	84	29	7	135	70	306
DC342	117	580	110	28	297	21	63	32	46	60	13	160	83	29	8	143	69	306
DC370	123	43	54	49	76	21	17	30	36	62	3	7	227	6	2	362	35	220
DC397	117	68	57	48	187	19	30	33	30	97	4	10	402	7	5	266	29	190
DC400	153	165	67	51	50	20	-2	29	43	56	4	13	279	2	-1	332	34	205
DC414	119	102	11	44	142	20	6	23	8	66	-3	7	364	0	-2	287	30	151
DC418	13	522	50	4	255	16	8	7	26	21	53	140	139	13	11	6	20	38
DC423	132	83	23	48	210	21	29	13	20	90	10	38	140	4	5	255	41	120
DC427	92	45	50	26	53	15	26	4	29	63	6	16	92	12	3	95	23	121
DC428	85	32	41	11	118	11	13	10	22	13	7	26	12	12	3	43	21	92
DC429	89	79	47	6	89	10	25	8	22	13	4	9	15	14	5	34	21	83
DC432	144	124	127	28	164	31	67	29	71	15	4	28	16	28	10	137	33	398
DC439	87	468	90	12	210	19	41	22	31	13	27	160	173	20	10	75	22	122
DC444	64	74	81	11	228	12	37	16	31	17	7	24	21	22	11	46	39	91
DC446	150	98	13	53	251	15	40	6	12	157	14	21	178	7	4	208	36	97
DC456	96	1177	102	38	279	15	50	21	38	105	-10	55	1000	-10	-11	177	25	199
DC457	138	113	21	63	789	14	17	23	14	434	5	24	176	6	1	197	18	106
DC458	111	48	-21	102	2497	1	5	2	-10	2092	8	114	13	8	6	36	3	4
DC459	87	88	-10	39	1624	9	-6	2	-3	451	6	19	268	-2	-3	114	7	7
DC464	122	263	9	36	94	20	24	9	8	10	8	62	176	8	2	289	29	118
DC468	79	1027	72	16	166	16	63	14	32	34	34	160	109	23	9	89	36	207
DC469	97	143	8	40	296	19	13	24	24	124	7	11	201	5	1	284	34	183
DC473	109	313	33	51	494	13	39	27	18	268	3	31	263	3	3	162	21	114
DC475	108	1176	80	37	290	15	46	19	40	118	-11	37	988	-11	-12	182	27	205
DC476	98	12	18	61	502	14	3	16	9	314	4	11	224	7	5	214	22	140
DC477	131	38	-29	69	1685	1	-4	1	-3	1489	4	7	77	5	4	19	6	7
DC478	134	53	13	73	1614	3	28	25	8	1196	2	6	157	9	0	98	17	75

Table B3: Trace element data from ICP.MS for selected samples

Element Units	Ba ppm	Be ppm	Bi ppm	Cd ppm	Ce ppm	Co ppm	Cr ppm	Cs ppm	Cu ppm	Dy ppm	Er ppm	Eu ppm	Ga ppm	Gd ppm	Hf ppm
Detect Limit	0.9	0.06	0.009	0.01	0.2	0.1	24	0.006	2	0.02	0.02	0.005	0.05	0.02	0.09
DC139	257.4	0.69	0.018	0.06	16.6	45.2	226	0.445	137	2.4	1.23	0.933	14.63	2.78	1.08
DC146	255.5	0.58	0.027	0.05	16.7	44.8	231	0.468	135	2.5	1.26	0.959	14.77	2.87	1.1
DC164	15.6	0.48	0.012	0.11	155.5	3.6	144	0.969	5	3.6	2	1.278	15.76	4.45	13.19
DC427	44.8	3.12	0.178	0.07	49.1	25.2	55	0.429	7	3.2	1.71	0.985	15.79	3.8	2.14
DC428	27.7	1.99	0.215	0.04	40	7.7	131	0.975	3	2.9	1.6	0.829	12.02	3.3	2.11
DC429	55.4	2.21	0.253	0.05	43.4	6.3	94	0.114	3	2.8	1.66	0.94	12.14	3.24	1.74
DC432	125.7	5.01	0.01	0.07	129.7	24.4	184	0.704	7	7.3	2.94	2.665	32.02	11.2	5.58
DC444	51	2.44	0.092	0.04	82.9	7.5	238	1.241	5	5.7	2.92	1.447	11.82	6.5	2.3
DC456	1167.7	2.11	0.477	0.08	108.6	31	287	1.586	40	4.8	2.29	2.214	16.61	6.74	4.36
DC458	36	0.37	0.948	0.04	1.5	104	>600	21.068	6	0.2	0.13	0.063	2.18	0.21	<0.09
DC459	62.7	2.29	0.184	0.07	1.6	39.3	>600	1.066	10	0.7	0.42	0.623	8.71	0.5	0.15
DC475	1197	2	0.036	0.11	103.8	30.1	297	0.579	33	4.8	2.31	2.217	16.34	6.42	4.42
DC477	32.5	0.1	1.43	0.34	1.7	71.5	>600	0.209	4	0.4	0.25	0.272	1.95	0.31	0.18
DC478	27.6	0.42	0.544	0.24	36.9	73	>600	0.495	40	2.6	1.16	0.684	6.4	3.21	1.13
DC559	60.7	2.34	0.208	0.07	1.7	39.6	>600	1.145	10	0.6	0.42	0.601	8.89	0.51	0.14

Element Units	Ho ppm	La ppm	Li ppm	Lu ppm	Mo ppm	Nb ppm	Nd ppm	Ni ppm	Pb ppm	Pr ppm	Rb ppm	Sb ppm	Sc ppm	Sm ppm	Sn ppm
Detect Limit	0.003	0.09	0.2	0.002	0.03	0.04	0.08	3	0.4	0.02	0.2	0.04	0	0.02	0.08
DC139	0.471	7.61	7.4	0.174	1.17	2.18	11.27	46	3.4	2.3	23.5	0.47	44.9	2.86	0.7
DC146	0.472	7.79	7.3	0.18	1.2	2.18	11.02	46	3.5	2.38	23.5	0.45	43.6	2.88	0.74
DC164	0.708	101.1	134.2	0.343	1.13	26.77	43.19	21	0.7	13.47	5.2	0.12	4.2	5.83	1.87
DC427	0.642	23.32	6.9	0.259	0.37	3.69	22.9	64	6.1	5.81	10.5	0.06	12.5	4.3	2.31
DC428	0.586	19.73	24.3	0.234	0.9	8.45	19.74	19	3	5.02	21.3	0.06	8	3.79	1.2
DC429	0.588	20.38	6.6	0.272	0.7	7.06	21.03	16	2	5.41	2.8	0.06	7.1	3.75	1.16
DC432	1.27	57.71	107.6	0.348	1.94	29.95	69.49	17	1.3	16.26	21.4	0.1	17.5	13.97	4.79
DC444	1.157	44.33	15.8	0.375	1.57	14.14	37.12	22	1.7	9.77	17.7	0.11	8.9	6.65	1.84
DC456	0.898	55.37	35.2	0.321	1.92	19.83	49.69	114	3.1	12.54	57.9	0.12	18.8	8.3	3.72
DC458	0.043	0.76	8.7	0.025	0.7	1.25	0.82	1961	0.4	0.18	106.3	0.06	8	0.2	0.51
DC459	0.145	0.96	14.7	0.063	0.47	0.94	1.05	441	5.5	0.23	15.8	0.07	28.8	0.36	4.96
DC475	0.906	53.77	10.6	0.319	2.08	19.83	47.1	112	8.3	12.1	40.1	0.07	18.6	7.9	1.22
DC477	0.088	1.13	3.2	0.05	0.89	0.37	0.83	1491	1.1	0.2	0.8	0.74	4.7	0.25	0.37
DC478	0.476	18.17	3.8	0.143	2.16	23.25	17.35	1230	4.2	4.34	0.8	0.11	11.5	3.49	1.88
DC559	0.149	1.03	15.2	0.064	0.53	0.94	1.14	441	5.2	0.25	15.9	0.06	29.8	0.39	4.94

Element Units	Sr ppm	Ta ppm	Tb ppm	Th ppm	Ti ppm	Tl ppm	Tm ppm	U ppm	V ppm	W ppm	Y ppm	Yb ppm	Zn ppm	Zr ppm
Detect Limit	2	0.2	0.003	0.09	26	0.005	0.002	0.02	10	0.5	0.08	0.009	8	3
DC139	1166	<0.2	0.423	1.07	3763	0.062	0.19	0.48	347	0.6	13.59	1.179	73	33
DC146	1163	<0.2	0.44	1.16	3716	0.061	0.19	0.49	344	0.7	13.52	1.174	71	33
DC164	5	1.6	0.697	21.51	4336	0.035	0.327	3.95	40	2.7	19.57	2.15	25	501
DC427	86	0.3	0.578	8.79	1626	0.056	0.263	1.6	92	<0.5	19.29	1.689	79	62
DC428	11	0.6	0.508	6.21	1555	0.109	0.238	1.55	39	0.6	18.14	1.564	75	71
DC429	14	0.5	0.5	5.73	1318	0.018	0.266	1.66	33	<0.5	19.23	1.742	79	58
DC432	17	1.9	1.504	12.67	9216	0.1	0.406	2.26	132	2.6	33.69	2.448	138	215
DC444	17	1.2	0.997	13.76	1765	0.082	0.43	3.17	46	1	34.38	2.591	56	79
DC456	964	0.9	0.935	5.51	6686	0.505	0.352	1.34	178	0.7	26.29	2.139	89	195
DC458	10	<0.2	0.035	0.15	325	0.88	0.021	0.06	37	0.8	1.22	0.14	95	3
DC459	254	<0.2	0.097	0.15	561	0.143	0.065	0.44	123	0.9	4.09	0.392	74	4
DC475	933	1	0.919	5.5	6622	0.213	0.335	1.63	173	0.6	25.63	2.126	97	193
DC477	72	<0.2	0.06	0.17	75	0.027	0.044	0.67	24	<0.5	2.59	0.298	113	5
DC478	147	0.8	0.484	4.96	2676	0.036	0.166	0.57	102	0.7	12.98	1.018	119	45
DC559	258	<0.2	0.095	0.15	569	0.14	0.065	0.24	132	0.9	4.19	0.409	73	4

TABLE B4: Sr and Nd isotopic ratios from TIMS analysis

Sample	Rock	⁸⁷ Sr/ ⁸⁶ Sr	¹⁴³ Nd/ ¹⁴⁴ Nd	Sr XRF	Nd XRF	Sr ICP	Nd ICP
DC004	Amphibolite	0.70833	0.51259	453	17		
DC048	Amphibolite	no data	0.51306	126	7		
DC080	Amphibolite	0.70842	0.51264	282	18		
DC081	Amphibolite	0.71172	0.51257	225	22		
DC125	Amphibolite	0.74122	0.51130	no data	no data		
DC130	Volcaniclastic	0.70418	0.51285	18	18		
DC132	Volcaniclastic	0.70375	0.51287	22	22		
DC139	Volcaniclastic	0.70350	0.51285	1202	6	1166	11.27
DC164	Gedrite	0.74692	0.51120	3	47	5	43.19
DC166	Gedrite	0.73155	no data	14	24		
DC167	Gedrite	0.77222	no data	12	8		
DC169	Amphibolite	0.72899	0.51237	62	30		
DC179	sil-bt-paragneiss	0.80827	0.51187	58	31		
DC186	sil-bt-paragneiss	0.74030	0.51192	88	21		
DC188	Amphibolite	0.71586	0.51230	741	61		
DC218	Amphibolite	0.70521	no data	no data	no data		
DC219	Amphibolite	0.70670	0.51254	321	15		
DC320	Amphibolite	0.74393	0.51208	100	6		
DC326	Quartzite	0.76459	0.51135	88	2		
DC330	Amphibolite	0.76731	0.51197	84	41		
DC342	Amphibolite	0.73445	no data	83	46		
DC397	Amphibolite	0.70543	no data	402	30		
DC400	Amphibolite	0.70565	no data	279	43		
DC414	Amphibolite	0.70619	no data	364	8		
DC423	Amphibolite	0.74289	0.51187	139	26		
DC427	Gedrite	0.72931	0.51162	140	20	86	22.9
DC428	Gedrite	0.76284	0.51151	92	29	11	19.74
DC429	Gedrite	0.75518	0.51149	12	22	14	21.03
DC432	Gedrite	0.72649	0.51188	15	22	17	69.49
DC439	sil-bt-paragneiss	0.79191	0.51142	16	71		
DC444	Gedrite	0.74307	0.51146	173	31	17	37.12
DC446	Amphibolite	0.74453	0.51175	21	31		
DC456	sil-bt-paragneiss	0.70549	0.51253	178	12	964	49.69
DC457	Amphibolite	0.70629	no data	1000	38		
DC458	Ultramafic	0.74773	0.51144	13	-10	10	0.82
DC459	Ultramafic	0.71171	0.51258	268	-3	254	1.05
DC464	Amphibolite	0.72418	no data	176	8		
DC468	Amphibolite	0.77583	no data	109	32		
DC469	Amphibolite	0.70689	no data	201	24		
DC473	Amphibolite	0.71162	no data	263	18		
DC475	Lamprophyre	no data	0.51253	988	40	933	47.1
DC476	Amphibolite	0.70572	no data	224	9		
DC477	Ultramafic	0.71045	0.51278	77	-3	72	0.83
DC478	Ultramafic	0.71001	0.51272	157	8	147	17.35

TABLE C1: Hornblende thermochronology data

Watts	40Ar/39Ar	±	38Ar/39Ar	±	37Ar/39Ar	±	36Ar/39Ar	±	40Ar*/39ArK	±	%40Ar atm % 39Ar	Age	±	Ca/K	Cl/K	
AH-02-003H	Hornblende	HP	J= 0.003692±0.000018													
2.00	55.063	0.014	0.4	0.03	0.056	0.014	0.066	0.091	53.31	2.06	7.80	6.58	324.1	11.5	12.892	0.085
2.50	13.209	0.007	0.389	0.015	0.027	0.006	0.014	0.078	12.75	0.35	3.51	31.20	83	2.2	12.892	0.085
2.75	12.537	0.007	0.388	0.015	0.03	0.007	0.02	0.076	11.82	0.46	5.25	22.12	77	3	12.892	0.085
3.00	12.448	0.011	0.382	0.019	0.035	0.01	0.026	0.083	11.6	0.68	5.56	15.18	75.6	4.4	12.892	0.083
3.50	14.241	0.017	0.388	0.034	0.064	0.016	0.067	0.092	11.53	2.01	16.05	5.44	75.2	12.8	12.892	0.083
4.00	17.612	0.018	0.405	0.045	0.083	0.016	0.093	0.092	13.62	2.86	21.05	3.71	88.5	18.1	12.892	0.086
6.00	13.475	0.008	0.408	0.018	0.035	0.008	0.026	0.111	12.54	0.88	6.14	15.78	81.7	5.6	12.892	0.089
AH-02-004H	Hornblende	HP	J= 0.003695±0.000018													
2.00	15.275	0.004	0.483	0.009	0.022	0.004	0.008	0.067	14.974	0.171	2.78	22.81	97.15±	1.08	12.733	0.107
2.50	28.836	0.038	0.456	0.087	0.192	0.037	0.289	0.112	13.003	13.48	59.67	0.27	84.66	85.74	12.733	0.094
3.00	9.424	0.004	0.481	0.007	0.02	0.004	0.006	0.051	9.121	0.092	3.75	45.66	59.8	0.59	12.733	0.106
3.25	9.228	0.008	0.48	0.014	0.03	0.007	0.017	0.101	8.969	0.539	0.88	6.13	58.82	3.48	12.733	0.106
3.50	9.434	0.009	0.481	0.017	0.033	0.008	0.023	0.097	8.714	0.676	4.96	4.76	57.18	4.37	12.733	0.106
4.00	9.498	0.008	0.479	0.016	0.03	0.007	0.018	0.093	9.019	0.529	3.11	5.91	59.14	3.41	12.733	0.106
4.50	9.619	0.009	0.476	0.016	0.035	0.008	0.023	0.092	9.353	0.649	0.02	4.51	61.29	4.18	12.733	0.105
6.00	9.269	0.007	0.481	0.012	0.026	0.006	0.011	0.093	9.369	0.327	-1.90	9.96	61.4	2.11	12.733	0.107
AH-03-024-1	Hornblende	100-250um	J= 0.003729±0.000040													
1.00	1745.887	0.15	0.992	0.245	3.424	0.169	2.575	0.161	1172.413	208.673	37.98	0.04	3033.01	261.33	14.218	0.116
2.00	571.809	0.081	0.456	0.232	2.649	0.099	0.71	0.136	419.798	45.079	27.82	0.09	1699.68	118.21	12.578	0.069
3.00	35.098	0.007	0.25	0.018	2.006	0.01	0.065	0.024	17.478	0.473	50.36	8.37	113.91	2.99	11.139	0.051
3.50	21.82	0.005	0.236	0.016	1.983	0.008	0.037	0.024	12.093	0.268	44.74	15.19	79.57	1.72	11.027	0.049
3.75	19.559	0.008	0.235	0.02	2.014	0.01	0.025	0.053	13.534	0.403	30.46	6.76	88.83	2.58	11.185	0.050
4.00	13.652	0.009	0.233	0.018	2.005	0.011	0.008	0.092	12.139	0.251	10.58	9.66	79.87	1.61	11.151	0.050
4.25	14.39	0.012	0.235	0.033	2.006	0.015	0.015	0.148	11.429	0.694	17.55	2.90	75.3	4.48	11.096	0.050
5.00	15.511	0.004	0.234	0.01	1.992	0.007	0.017	0.025	11.274	0.138	27.68	35.21	74.29	0.89	11.099	0.050
5.50	12.937	0.006	0.228	0.018	1.961	0.009	0.009	0.094	11.227	0.264	12.47	8.68	73.99	1.71	10.909	0.048
6.00	12.158	0.005	0.245	0.017	2.07	0.008	0.006	0.099	11.315	0.182	6.54	13.10	74.56	1.18	11.534	0.053
AH-03-024-2	Hornblende	HP	J= 0.003601±0.000024													
1.00	778.147	0.114	0.69	0.17	0.399	0.123	1.569	0.122	1042.158	281.973	39.86	0.04	2812.1	385.42	11.100	0.079
2.00	299.841	0.05	0.386	0.125	0.244	0.156	0.573	0.073	328.775	29.673	26.44	0.11	1409.21	88.27	11.100	0.039
3.00	24.182	0.007	0.302	0.016	0.025	0.068	0.022	0.055	21.592	0.396	11.53	5.13	135.09	2.39	11.100	0.064

Watts	40Ar/39Ar	±	38Ar/39Ar	±	37Ar/39Ar	±	36Ar/39Ar	±	40Ar*/39ArK	±	%40Ar atm	% 39Ar	Age	±	Ca/K	Cl/K
3.50	19.06	0.005	0.243	0.011	0.019	0.036	0.021	0.024	14.641	0.17	23.86	16.94	92.69	1.05	11.100	0.051
3.75	14.54	0.006	0.239	0.015	0.023	0.051	0.016	0.051	12.891	0.255	11.61	6.66	81.86	1.58	11.100	0.050
4.00	16.413	0.004	0.24	0.011	0.019	0.032	0.018	0.027	13.001	0.155	21.42	16.46	82.54	0.96	11.100	0.051
4.25	13.056	0.007	0.243	0.022	0.026	0.061	0.017	0.058	12.212	0.305	6.17	4.58	77.64	1.9	11.100	0.051
4.50	13.453	0.007	0.242	0.017	0.023	0.061	0.016	0.063	12.221	0.307	9.11	5.62	77.7	1.91	11.100	0.051
5.00	13.085	0.007	0.243	0.02	0.027	0.065	0.02	0.063	11.778	0.389	9.46	3.85	74.94	2.42	11.100	0.051
5.50	13.739	0.009	0.247	0.026	0.032	0.106	0.027	0.079	12.242	0.655	10.08	2.76	77.83	4.07	11.100	0.051
6.50	12.609	0.004	0.245	0.011	0.018	0.03	0.005	0.05	12.302	0.09	3.25	37.85	78.2	0.56	11.100	0.052
AH-03-029-1	Hornblende	100-250um	J= 0.003732±0.000038													
2.00	830.626	0.081	0.345	0.196	2.449	0.101	1.143	0.104	546.07	53.36	36.17	0.27	2004.7	118.3	11.181	0.034
3.00	32.569	0.011	0.128	0.042	2.916	0.014	0.019	0.134	28.95	0.81	10.96	9.74	185.1	5	16.513	0.026
3.50	14.626	0.01	0.123	0.038	2.911	0.012	0.009	0.168	13.66	0.46	5.04	11.69	89.7	3	16.490	0.025
4.00	18.47	0.009	0.124	0.03	2.926	0.011	0.01	0.115	16.8	0.39	8.72	17.38	109.7	2.5	16.585	0.025
4.25	13.831	0.008	0.122	0.035	2.934	0.011	0.009	0.144	12.72	0.4	6.45	12.28	83.7	2.6	16.620	0.024
4.75	13.411	0.008	0.124	0.03	2.891	0.01	0.008	0.117	12.25	0.31	7.96	19.98	80.7	2	16.406	0.025
5.25	17.034	0.014	0.127	0.062	2.973	0.016	0.018	0.186	13.78	1.01	15.43	5.07	90.5	6.5	16.788	0.025
5.75	16.15	0.013	0.125	0.051	2.922	0.015	0.014	0.185	13.8	0.79	12.25	8.09	90.6	5.1	16.531	0.025
6.00	14.022	0.009	0.124	0.027	2.946	0.011	0.01	0.117	12.55	0.36	9.49	15.50	82.6	2.3	16.732	0.025
AH-03-029-2	Hornblende	HP	J= 0.003607±0.000022													
2.00	83.366	0.011	0.104	0.056	0.041	0.011	0.09	0.038	67.18	1.3	22.36	3.57	391.4	6.8	16.550	0.015
3.00	27.872	0.007	0.114	0.024	0.032	0.007	0.019	0.057	26.9	0.38	5.12	7.46	167.1	2.3	16.550	0.021
3.50	19.538	0.007	0.129	0.022	0.033	0.007	0.018	0.07	18.69	0.4	5.41	7.56	117.7	2.4	16.550	0.025
4.00	15.356	0.004	0.127	0.016	0.028	0.004	0.011	0.048	14.47	0.17	6.66	19.11	91.8	1	16.550	0.025
4.50	18.369	0.005	0.13	0.021	0.029	0.005	0.012	0.059	17.47	0.24	5.96	14.75	110.3	1.4	16.550	0.026
4.75	15.726	0.005	0.131	0.019	0.03	0.005	0.014	0.062	14.91	0.27	5.93	11.27	94.5	1.6	16.550	0.025
5.00	13.692	0.004	0.129	0.015	0.029	0.004	0.012	0.047	12.83	0.18	6.99	14.63	81.6	1.1	16.550	0.025
5.50	13.831	0.005	0.127	0.018	0.029	0.005	0.013	0.057	12.76	0.24	8.36	13.16	81.2	1.5	16.550	0.025
6.50	15.338	0.005	0.135	0.022	0.032	0.005	0.019	0.066	13.65	0.39	11.58	8.49	86.7	2.4	16.550	0.026
DC004-1	Hornblende	100-250um	J= 0.003741±0.000030													
2.00	176.023	0.018	0.225	0.042	1.301	0.023	0.279	0.03	98.36	2.69	44.42	1.41	565.2	13.3	7.260	0.037
3.00	12.791	0.004	0.205	0.012	1.461	0.007	0.01	0.036	10.34	0.12	19.39	19.86	68.4	0.8	8.310	0.043
3.25	10.037	0.005	0.199	0.014	1.385	0.008	0.004	0.081	9.28	0.12	7.43	14.44	61.5	0.8	7.873	0.042
3.50	10.143	0.005	0.195	0.014	1.37	0.008	0.004	0.098	9.45	0.13	6.71	14.31	62.7	0.9	7.789	0.041
3.75	10.331	0.007	0.194	0.019	1.368	0.009	0.006	0.114	9.35	0.2	8.76	7.93	62	1.3	7.768	0.041
4.00	10.658	0.007	0.197	0.019	1.383	0.01	0.007	0.113	9.49	0.23	9.96	6.37	62.9	1.5	7.850	0.042
4.50	10.563	0.009	0.203	0.026	1.408	0.013	0.008	0.166	9.17	0.4	11.14	3.89	60.9	2.6	7.972	0.043
5.00	11.072	0.006	0.201	0.016	1.377	0.009	0.007	0.092	9.72	0.2	11.69	8.25	64.4	1.3	7.823	0.043

Watts	40Ar/39Ar	±	38Ar/39Ar	±	37Ar/39Ar	±	36Ar/39Ar	±	40Ar*/39ArK	±	%40Ar atm	% 39Ar	Age	±	Ca/K	Cl/K
5.50	10.687	0.009	0.201	0.02	1.388	0.013	0.007	0.127	9.22	0.28	12.38	5.26	61.2	1.9	7.881	0.043
6.00	9.659	0.005	0.202	0.013	1.378	0.008	0.004	0.095	9.11	0.11	5.59	18.28	60.5	0.7	7.852	0.043
DC004-2	Hornblende	HP	J= 0.003624±0.000018													
2.00	63.036	0.011	0.147	0.046	0.035	0.011	0.123	0.034	37.54	1.33	42.43	2.24	230.1	7.7	7.950	0.022
3.00	11.225	0.004	0.195	0.01	0.014	0.004	0.009	0.035	9.72	0.11	13.60	25.62	62.5	0.7	7.950	0.041
3.50	9.844	0.004	0.193	0.01	0.014	0.004	0.007	0.053	9.08	0.12	7.79	23.23	58.4	0.7	7.950	0.040
3.75	10.237	0.006	0.184	0.017	0.018	0.006	0.013	0.066	9.06	0.27	10.53	8.81	58.3	1.7	7.950	0.038
4.00	11.764	0.008	0.192	0.022	0.021	0.007	0.021	0.069	9.44	0.44	18.56	5.57	60.7	2.8	7.950	0.039
4.50	12.106	0.008	0.194	0.024	0.024	0.007	0.026	0.072	9.52	0.58	19.73	4.20	61.2	3.7	7.949	0.039
5.00	11.313	0.006	0.187	0.019	0.019	0.005	0.018	0.067	9.49	0.37	14.97	6.37	61	2.3	7.949	0.038
6.00	9.909	0.004	0.192	0.01	0.014	0.004	0.007	0.05	9.27	0.11	6.58	23.96	59.6	0.7	7.951	0.040
DC048-1	Hornblende	100-250um	J= 0.003734±0.000036													
2.00	28.945	0.025	0.047	0.204	3.811	0.029	0.078	0.105	10.27	2.45	62.38	3.62	67.9	15.9	21.474	0.004
3.00	10.37	0.006	0.023	0.056	4.215	0.008	0.009	0.076	9.1	0.22	12.07	52.01	60.3	1.4	24.059	0.002
3.25	13.204	0.018	0.025	0.16	4.067	0.02	0.022	0.178	9.27	1.18	24.79	7.64	61.4	7.7	23.098	0.001
3.75	10.7	0.011	0.022	0.12	4.101	0.013	0.011	0.156	9.23	0.54	11.23	18.08	61.1	3.5	23.381	0.001
4.25	14.069	0.023	0.03	0.279	4.245	0.024	0.031	0.197	8.13	1.83	35.58	4.84	54	11.9	24.052	0.002
5.00	12.027	0.018	0.027	0.165	4.334	0.019	0.02	0.2	8.65	1.23	22.11	7.32	57.4	8	24.662	0.002
5.50	21.287	0.04	0.038	0.541	4.446	0.042	0.072	0.243	8.08	5.25	52.66	1.73	53.6	34.3	24.810	0.003
6.00	14.072	0.025	0.028	0.294	4.327	0.026	0.028	0.224	9.72	1.87	22.22	4.74	64.3	12.2	24.539	0.003
DC048-2	Hornblende	HP	J= 0.003613±0.000022													
2.00	49.393	0.039	0.218	0.193	0.223	0.038	0.387	0.088	10.28	14.19	82.90	0.34	65.8	89.2	24.498	0.003
3.00	11.177	0.011	0.034	0.106	0.049	0.01	0.029	0.079	9.12	0.71	15.95	7.36	58.5	4.5	24.500	0.001
3.50	10.772	0.007	0.03	0.077	0.045	0.006	0.021	0.078	9.26	0.49	12.83	12.07	59.4	3.1	24.500	0.001
4.00	10.003	0.006	0.027	0.051	0.041	0.006	0.014	0.064	9.09	0.29	8.55	18.97	58.3	1.8	24.500	0.001
4.50	10.566	0.006	0.029	0.059	0.042	0.006	0.018	0.058	9.06	0.33	13.54	15.54	58.1	2.1	24.500	0.001
5.00	11.769	0.008	0.033	0.075	0.046	0.007	0.028	0.071	8.96	0.62	22.44	9.24	57.5	3.9	24.500	0.001
5.50	12.577	0.01	0.038	0.088	0.05	0.01	0.036	0.076	9.21	0.85	24.80	6.53	59.1	5.3	24.500	0.001
6.50	9.793	0.005	0.026	0.043	0.039	0.005	0.012	0.047	8.96	0.17	8.64	29.96	57.4	1.1	24.500	0.001
DC080-H	Hornblende	100-250um	J= 0.003744±0.000028													
2.00	56.087	0.012	0.053	0.081	0.9	0.02	0.142	0.03	16.51	1.19	70.54	3.27	108.2	7.6	5.101	0.003
2.75	11.963	0.006	0.035	0.056	1.905	0.009	0.012	0.074	9.35	0.27	21.40	10.44	62.1	1.8	10.993	0.004
3.25	10.21	0.004	0.035	0.029	1.887	0.007	0.005	0.07	9.43	0.11	7.87	29.96	62.6	0.7	10.903	0.005

Watts	40Ar/39Ar	±	38Ar/39Ar	±	37Ar/39Ar	±	36Ar/39Ar	±	40Ar*/39ArK	±	%40Ar atm % 39Ar	Age	±	Ca/K	Cl/K	
3.50	10.046	0.006	0.035	0.036	1.803	0.009	0.005	0.114	9.44	0.17	5.74	16.20	62.7	1.1	10.411	0.005
3.75	10.231	0.008	0.035	0.051	1.873	0.01	0.005	0.138	9.62	0.23	5.20	10.48	63.8	1.5	10.816	0.005
4.00	10.481	0.008	0.035	0.066	1.831	0.01	0.007	0.173	9.47	0.36	8.42	7.60	62.8	2.3	10.564	0.005
4.50	11.986	0.011	0.036	0.074	1.829	0.014	0.013	0.127	9.43	0.51	19.61	4.84	62.6	3.3	10.530	0.004
5.00	11.562	0.01	0.036	0.095	1.885	0.013	0.011	0.18	9.56	0.61	14.86	3.91	63.5	4	10.865	0.004
5.50	10.996	0.011	0.036	0.087	1.85	0.014	0.01	0.188	9.66	0.56	9.53	4.17	64.1	3.6	10.673	0.005
6.50	10.364	0.007	0.033	0.057	1.653	0.011	0.007	0.133	9.32	0.28	9.11	9.13	61.9	1.8	9.546	0.004
DC169-1	Hornblende	HP	J= 0.003639±0.000016													
2.00	129.029	0.028	0.175	0.111	0.115	0.028	0.415	0.047	52.43	6.16	65.61	1.54	315	34	17.850	0.005
3.00	14.466	0.007	0.044	0.068	0.037	0.007	0.033	0.056	10.33	0.56	28.03	14.75	66.6	3.5	17.850	0.004
3.50	10.31	0.006	0.039	0.049	0.034	0.005	0.018	0.064	8.7	0.36	14.68	23.23	56.2	2.3	17.850	0.004
4.00	10.826	0.007	0.044	0.06	0.038	0.007	0.027	0.072	8.21	0.6	22.30	14.29	53.1	3.8	17.850	0.004
4.50	10.359	0.007	0.042	0.066	0.035	0.006	0.023	0.062	8.18	0.44	19.53	17.49	52.9	2.8	17.850	0.004
5.00	11.043	0.008	0.047	0.059	0.039	0.007	0.03	0.062	8	0.57	25.65	12.87	51.7	3.7	17.850	0.004
6.00	11.405	0.008	0.046	0.063	0.037	0.007	0.027	0.058	8.41	0.48	24.97	15.83	54.4	3.1	17.850	0.004
DC169-2	Hornblende	>250um	J= 0.003747±0.000028													
2.00	269.91	0.02	0.181	0.069	2.05	0.025	0.753	0.027	58.46	4.62	78.59	1.42	357.3	25.6	11.704	0.006
3.00	33.749	0.019	0.035	0.223	1.844	0.025	0.061	0.116	20.07	2.13	38.79	1.50	130.8	13.4	10.484	0.003
3.50	11.045	0.008	0.032	0.075	2.794	0.011	0.011	0.143	9.25	0.48	14.79	6.92	61.5	3.1	16.207	0.004
4.00	9.454	0.006	0.03	0.039	2.88	0.008	0.006	0.105	8.71	0.2	7.69	18.38	57.9	1.3	16.735	0.003
4.25	9.216	0.007	0.031	0.053	3.05	0.009	0.007	0.102	8.53	0.21	6.92	14.91	56.8	1.4	17.730	0.004
4.50	9.183	0.007	0.031	0.047	2.962	0.009	0.006	0.12	8.48	0.24	6.93	12.54	56.4	1.6	17.225	0.004
4.75	12.77	0.015	0.034	0.168	2.973	0.018	0.022	0.216	9.37	1.41	21.61	2.08	62.2	9.2	17.234	0.004
5.25	9.387	0.007	0.031	0.052	2.998	0.009	0.006	0.115	8.72	0.22	6.59	14.45	58	1.5	17.450	0.004
5.50	9.591	0.008	0.031	0.066	3.053	0.01	0.008	0.141	8.58	0.36	9.22	8.65	57.1	2.4	17.768	0.004
6.00	9.029	0.008	0.031	0.062	3.026	0.01	0.007	0.14	8.4	0.28	5.73	9.93	55.9	1.9	17.604	0.003
6.25	11.871	0.016	0.036	0.269	3.041	0.019	0.021	0.233	8.87	1.5	19.16	1.99	59	9.8	17.598	0.004
7.00	9.765	0.01	0.04	0.061	3.672	0.013	0.009	0.165	8.91	0.46	7.13	7.22	59.2	3	21.416	0.006
DC176-1	Hornblende	200-250um	J= 0.003807±0.000022													
2.00	157.06	0.052	0.171	0.258	0.654	0.091	0.422	0.088	43.07	9.38	72.22	0.11	273.9	55.4	3.282	0.017
3.00	14.211	0.008	0.156	0.029	0.843	0.014	0.021	0.075	8.92	0.48	36.66	2.27	60.2	3.2	5.659	0.032
3.50	8.304	0.005	0.15	0.013	0.834	0.008	0.002	0.119	8.01	0.09	3.53	10.25	54.2	0.6	5.646	0.031
4.00	8.015	0.003	0.162	0.009	0.822	0.007	0.002	0.087	7.89	0.05	1.91	34.78	53.4	0.3	5.568	0.034
4.25	7.987	0.004	0.156	0.012	0.806	0.007	0.002	0.143	7.87	0.08	1.52	12.46	53.2	0.6	5.454	0.032
4.50	8.242	0.005	0.149	0.016	0.797	0.009	0.003	0.18	7.92	0.15	3.56	6.52	53.6	1	5.391	0.031
5.00	8.162	0.005	0.158	0.015	0.804	0.008	0.002	0.176	7.94	0.12	2.52	8.17	53.7	0.8	5.441	0.033
5.50	8.778	0.007	0.149	0.026	0.821	0.01	0.005	0.165	8	0.24	8.02	3.90	54.1	1.6	5.542	0.031

Watts	40Ar/39Ar	±	38Ar/39Ar	±	37Ar/39Ar	±	36Ar/39Ar	±	40Ar*/39ArK	±	%40Ar atm	% 39Ar	Age	±	Ca/K	Cl/K
6.00	8.606	0.007	0.163	0.024	0.832	0.011	0.004	0.224	7.94	0.28	6.51	3.16	53.7	1.9	5.612	0.034
7.50	8.131	0.004	0.152	0.009	0.785	0.007	0.002	0.107	7.97	0.06	2.18	18.37	53.9	0.4	5.325	0.032
DC186-1H	Hornblende	100-250um	J= 0.003756±0.000024													
2.00	92.975	0.014	0.134	0.056	0.86	0.02	0.178	0.034	43.79	1.79	53.14	2.48	274.7	10.4	4.914	0.020
2.50	26.881	0.012	0.191	0.037	2.298	0.015	0.046	0.075	15.33	1.03	42.89	3.28	101	6.6	13.476	0.038
2.75	12.298	0.009	0.172	0.034	1.861	0.012	0.014	0.126	9.3	0.53	23.68	5.27	61.9	3.5	10.912	0.036
3.00	11.63	0.006	0.184	0.018	1.914	0.009	0.011	0.076	9.22	0.27	20.80	12.03	61.4	1.8	11.274	0.038
3.25	10.025	0.006	0.165	0.024	1.603	0.009	0.008	0.15	8.66	0.35	13.28	9.95	57.7	2.3	9.420	0.034
3.50	10.294	0.008	0.161	0.022	1.609	0.01	0.008	0.112	8.87	0.27	13.63	11.12	59.1	1.8	9.467	0.033
3.75	9.938	0.007	0.156	0.023	1.52	0.009	0.007	0.103	8.68	0.22	12.57	14.60	57.9	1.4	8.952	0.032
4.00	9.806	0.007	0.142	0.026	1.278	0.011	0.008	0.157	8.35	0.36	14.26	8.65	55.7	2.4	7.508	0.029
4.25	10.36	0.009	0.139	0.029	1.218	0.012	0.009	0.125	8.64	0.36	16.00	7.83	57.6	2.4	7.139	0.028
4.50	9.799	0.01	0.155	0.033	1.349	0.014	0.008	0.221	8.38	0.55	13.43	5.97	55.9	3.6	7.915	0.032
5.00	9.509	0.009	0.167	0.03	1.554	0.013	0.007	0.202	8.19	0.45	13.01	6.44	54.6	3	9.142	0.035
6.50	15.25	0.006	0.166	0.02	1.56	0.009	0.025	0.042	8.78	0.32	42.52	12.37	58.5	2.1	9.196	0.034
DC186-2H	Hornblende	HP	J= 0.003647±0.000016													
2.00	136.654	0.016	0.142	0.058	0.037	0.144	0.303	0.029	65.71	2.58	54.52	1.98	387.6	13.7	1.805	0.013
3.00	21.068	0.01	0.131	0.046	0.029	0.084	0.06	0.057	11.67	1.05	44.15	3.26	75.2	6.7	6.787	0.022
3.50	12.298	0.009	0.179	0.03	0.028	0.077	0.032	0.073	8.85	0.71	25.92	4.64	57.3	4.5	9.692	0.035
4.00	9.997	0.005	0.173	0.015	0.018	0.005	0.011	0.056	8.69	0.2	12.57	16.86	56.3	1.3	9.850	0.035
4.50	10.085	0.006	0.152	0.018	0.02	0.006	0.015	0.076	8.69	0.34	12.56	10.43	56.3	2.2	9.850	0.030
5.00	11.411	0.007	0.154	0.023	0.024	0.007	0.024	0.071	8.79	0.51	21.22	6.62	56.9	3.3	9.850	0.030
5.50	9.545	0.004	0.132	0.013	0.016	0.004	0.008	0.048	8.69	0.12	8.89	28.43	56.3	0.8	9.850	0.026
6.50	9.205	0.004	0.139	0.011	0.017	0.004	0.007	0.052	8.57	0.12	6.76	27.78	55.5	0.7	9.850	0.028
DC186-LH	Hornblende	HP	J= 0.003647±0.000016													
2.00	163.17	0.03	0.251	0.099	0.134	0.029	0.496	0.048	81.98	8.05	60.10	1.05	471.9	40.8	9.850	0.016
2.50	51.899	0.027	0.28	0.074	0.102	0.027	0.247	0.063	16.53	5.22	72.11	1.43	105.6	32.4	9.850	0.046
3.00	34.133	0.012	0.314	0.03	0.045	0.012	0.117	0.039	12.81	1.4	63.58	5.12	82.4	8.8	9.851	0.062
4.00	13.838	0.004	0.243	0.01	0.017	0.004	0.026	0.022	7.76	0.18	44.26	75.39	50.3	1.1	9.850	0.051
4.50	10.573	0.009	0.176	0.026	0.031	0.009	0.03	0.071	8.85	0.65	14.15	9.20	57.3	4.2	9.850	0.034
5.00	17.173	0.019	0.265	0.069	0.079	0.018	0.119	0.08	7.21	3.15	56.88	2.17	46.8	20.2	9.850	0.049
5.50	17.732	0.022	0.328	0.061	0.101	0.021	0.151	0.076	6.14	3.88	63.93	1.58	40	25	9.850	0.063
6.50	12.468	0.014	0.277	0.042	0.052	0.013	0.066	0.09	7.71	1.9	35.02	4.06	50	12.1	9.850	0.055
DC188	Hornblende	100-250um	J= 0.003749±0.000026													

Watts	40Ar/39Ar	±	38Ar/39Ar	±	37Ar/39Ar	±	36Ar/39Ar	±	40Ar*/39ArK	±	%40Ar atm % 39Ar	Age	±	Ca/K	Cl/K	
2.00	264.263	0.043	0.214	0.155	2.6	0.051	0.695	0.064	76.61	10.79	71.05	0.54	455.5	56.7	14.476	0.017
2.75	12.96	0.011	0.025	0.118	2.943	0.013	0.018	0.127	9.73	0.68	23.23	6.40	64.6	4.4	17.134	0.002
3.00	9.586	0.008	0.023	0.072	3.045	0.01	0.008	0.133	8.64	0.33	8.99	14.22	57.5	2.2	17.757	0.002
3.25	9.398	0.007	0.022	0.08	2.989	0.009	0.008	0.177	8.5	0.42	8.55	14.18	56.6	2.7	17.432	0.002
3.50	9.821	0.009	0.023	0.096	2.906	0.011	0.01	0.145	8.58	0.43	10.62	8.92	57.1	2.8	16.938	0.001
3.75	9.375	0.009	0.024	0.1	2.822	0.011	0.008	0.172	8.36	0.44	8.93	9.90	55.7	2.9	16.448	0.002
4.00	9.803	0.011	0.024	0.116	2.747	0.013	0.01	0.179	8.45	0.55	11.05	7.21	56.3	3.6	15.985	0.002
4.50	9.128	0.008	0.021	0.095	2.921	0.01	0.007	0.171	8.33	0.38	7.28	11.96	55.5	2.5	17.043	0.001
4.75	11.372	0.017	0.026	0.176	2.842	0.019	0.02	0.227	8.19	1.35	22.58	3.17	54.6	8.8	16.490	0.002
5.25	9.897	0.009	0.024	0.104	2.843	0.012	0.01	0.162	8.43	0.51	12.72	8.10	56.1	3.3	16.603	0.002
6.00	9.224	0.007	0.023	0.076	2.974	0.01	0.008	0.143	8.17	0.34	10.56	15.40	54.4	2.2	17.388	0.002
DC195 Hornblende >250um J= 0.003811±0.000026																
2.00	266.714	0.029	0.178	0.125	0.681	0.05	0.8	0.039	42.38	6.45	84.25	0.68	270.1	38.2	4.113	0.004
3.00	37.067	0.03	0.042	0.492	1.464	0.041	0.105	0.122	10.06	3.77	71.74	0.74	67.8	25	9.530	0.001
3.50	27.147	0.02	0.035	0.332	2.136	0.025	0.062	0.15	12.1	2.75	53.71	1.20	81.3	18.1	14.223	0.001
4.00	10.936	0.005	0.021	0.049	2.199	0.008	0.011	0.049	8.67	0.16	20.97	21.61	58.6	1.1	14.999	0.001
4.50	8.936	0.004	0.02	0.038	2.222	0.007	0.006	0.071	8.19	0.12	8.71	32.30	55.5	0.8	15.174	0.001
5.00	8.519	0.005	0.02	0.056	2.227	0.008	0.005	0.11	8.06	0.16	5.53	22.72	54.6	1.1	15.207	0.001
5.50	8.956	0.009	0.021	0.116	2.289	0.01	0.007	0.216	8.06	0.49	8.78	6.91	54.6	3.2	15.606	0.001
6.00	8.851	0.008	0.021	0.16	2.264	0.01	0.006	0.245	8.11	0.46	7.21	7.77	54.9	3.1	15.448	0.001
7.50	9.488	0.011	0.025	0.12	2.793	0.012	0.009	0.251	8.48	0.68	9.35	6.07	57.3	4.5	19.110	0.002
DC209 Hornblende 200-250um J= 0.003812±0.000026																
2.00	338.6	0.087	0.299	0.268	3.132	0.092	1.094	0.099	39.48	17.04	88.60	0.51	253	101.8	20.400	0.016
3.00	17.289	0.015	0.15	0.054	3.481	0.017	0.038	0.114	8.7	1.3	48.59	6.26	58.9	8.7	23.731	0.029
3.50	8.929	0.006	0.147	0.023	3.405	0.008	0.008	0.117	8.09	0.27	9.18	27.21	54.8	1.8	23.372	0.030
4.00	8.87	0.007	0.148	0.026	3.401	0.009	0.007	0.125	8.16	0.29	7.80	26.57	55.2	1.9	23.348	0.031
4.50	9.596	0.01	0.15	0.031	3.429	0.011	0.011	0.161	7.97	0.54	15.87	14.80	54	3.6	23.518	0.031
5.00	12.902	0.018	0.157	0.07	3.497	0.02	0.026	0.224	8.17	1.79	33.22	4.08	55.3	11.9	23.914	0.032
5.50	11.989	0.017	0.146	0.099	3.493	0.018	0.023	0.186	8.28	1.29	28.03	5.22	56.1	8.6	23.934	0.029
6.00	11.356	0.013	0.154	0.046	3.466	0.015	0.018	0.212	8.58	1.15	21.71	6.38	58.1	7.7	23.773	0.031
7.50	12.528	0.011	0.258	0.029	4.038	0.013	0.022	0.122	8.77	0.8	28.77	8.96	59.3	5.3	27.731	0.055
DC219-1 Hornblende 100-250um J= 0.003737±0.000032																
2.00	65.288	0.031	0.094	0.188	1.777	0.038	0.2	0.081	13.72	4.56	78.08	1.08	90.2	29.3	9.505	0.009
3.00	9.79	0.006	0.07	0.031	2.398	0.009	0.009	0.079	8.2	0.21	15.79	29.69	54.4	1.4	13.395	0.013
3.25	9.231	0.008	0.055	0.043	2.528	0.01	0.007	0.121	8.27	0.25	9.16	20.14	54.9	1.7	14.122	0.009
3.50	9.369	0.009	0.057	0.049	2.447	0.012	0.008	0.168	8.38	0.39	7.90	11.45	55.6	2.6	13.648	0.009

Watts	40Ar/39Ar	±	38Ar/39Ar	±	37Ar/39Ar	±	36Ar/39Ar	±	40Ar*/39ArK	±	%40Ar atm % 39Ar	Age	±	Ca/K	Cl/K	
4.00	9.952	0.01	0.059	0.048	2.48	0.012	0.01	0.137	8.32	0.4	14.01	12.49	55.2	2.6	13.849	0.010
4.50	10.275	0.014	0.064	0.094	2.511	0.017	0.012	0.216	8.73	0.77	8.95	5.62	57.9	5.1	13.992	0.011
5.00	11.238	0.016	0.079	0.091	2.51	0.019	0.018	0.23	8.17	1.24	20.27	3.75	54.3	8.1	13.947	0.014
6.00	9.276	0.009	0.057	0.046	2.514	0.011	0.007	0.156	8.24	0.35	8.83	15.77	54.7	2.3	14.065	0.009
DC219-2 Hornblende HP J= 0.003618±0.000020																
2.00	233.532	0.031	0.268	0.093	0.123	0.031	0.874	0.039	24.73	7.6	91.27	0.68	154.6	45.5	13.950	0.009
3.00	52.871	0.032	0.193	0.164	0.159	0.031	0.332	0.073	7.85	9	87.41	0.44	50.5	57.1	13.950	0.009
3.50	31.778	0.021	0.172	0.105	0.093	0.021	0.174	0.081	8.26	4.7	74.67	1.02	53.1	29.8	13.950	0.021
4.00	12.192	0.006	0.132	0.023	0.028	0.006	0.025	0.045	8.44	0.35	30.19	11.05	54.2	2.2	13.950	0.025
4.50	8.944	0.004	0.129	0.014	0.024	0.004	0.009	0.06	8.27	0.17	7.29	27.09	53.2	1	13.950	0.026
4.75	9.149	0.005	0.112	0.019	0.025	0.005	0.012	0.072	8.17	0.26	9.94	17.78	52.6	1.7	13.950	0.021
5.00	9.002	0.005	0.103	0.015	0.024	0.004	0.011	0.055	8.1	0.18	9.57	22.69	52.1	1.1	13.950	0.019
5.50	9.101	0.005	0.078	0.02	0.025	0.005	0.012	0.067	7.95	0.25	11.91	19.25	51.2	1.6	13.950	0.013
DC239 Hornblende >250um J= 0.003813±0.000028																
2.00	1151.288	0.091	0.529	0.399	3.037	0.108	1.008	0.126	912.55	90.1	22.62	0.19	2705.3	138.4	18.472	0.073
3.00	141.63	0.045	0.172	0.344	1.193	0.071	0.103	0.264	119.6	9.81	16.03	0.54	677.8	46.3	7.291	0.028
3.50	10.031	0.007	0.107	0.035	1.255	0.011	0.004	0.284	9.44	0.36	5.99	13.95	63.8	2.4	8.633	0.021
4.00	8.6	0.006	0.111	0.024	1.256	0.009	0.003	0.227	8.29	0.22	3.74	20.50	56.2	1.5	8.650	0.022
4.50	8.64	0.008	0.102	0.035	1.235	0.011	0.003	0.424	8.25	0.4	4.47	13.24	55.9	2.7	8.493	0.020
5.00	9.012	0.006	0.126	0.029	1.225	0.01	0.004	0.247	8.57	0.29	4.97	15.53	58	1.9	8.433	0.026
5.50	8.808	0.007	0.188	0.022	1.191	0.01	0.004	0.304	8.35	0.36	5.19	13.94	56.5	2.4	8.189	0.040
6.00	8.752	0.008	0.175	0.029	1.235	0.012	0.005	0.333	8.04	0.51	8.02	10.85	54.5	3.4	8.495	0.037
6.50	9.208	0.015	0.166	0.068	1.235	0.019	0.009	0.487	7.94	1.37	12.19	3.52	53.8	9.1	8.416	0.035
7.50	9.042	0.01	0.157	0.039	1.216	0.013	0.006	0.441	8.33	0.76	7.46	7.75	56.4	5.1	8.357	0.032
DC320 Hornblende >250um J= 0.003759±0.000024																
2.00	286.871	0.039	0.184	0.165	1.024	0.08	0.672	0.059	103.56	9.87	64.20	0.23	593.1	48.2	5.325	0.009
3.00	26.78	0.021	0.14	0.078	1.392	0.028	0.058	0.126	12.32	2.19	53.17	0.80	81.7	14.2	8.002	0.025
3.50	12.865	0.009	0.149	0.03	1.446	0.014	0.012	0.11	10.39	0.4	18.96	3.86	69.1	2.6	8.513	0.030
4.00	10.304	0.005	0.143	0.015	1.41	0.008	0.004	0.088	9.58	0.13	7.29	13.17	63.8	0.8	8.330	0.029
4.25	9.473	0.005	0.15	0.015	1.386	0.008	0.003	0.128	9.26	0.11	2.54	15.01	61.7	0.7	8.189	0.031
4.50	9.631	0.007	0.145	0.026	1.39	0.01	0.004	0.193	9.12	0.26	4.85	5.52	60.8	1.7	8.197	0.030
4.75	9.713	0.008	0.143	0.025	1.404	0.011	0.005	0.237	9.2	0.34	4.89	5.20	61.3	2.2	8.281	0.029
5.00	9.246	0.005	0.139	0.013	1.386	0.007	0.002	0.151	9.07	0.12	2.19	16.19	60.5	0.8	8.199	0.028
5.25	9.757	0.006	0.14	0.018	1.364	0.008	0.004	0.138	9.04	0.19	7.47	10.55	60.3	1.2	8.067	0.029
5.50	10.487	0.008	0.135	0.027	1.404	0.011	0.007	0.14	9.09	0.32	12.95	4.86	60.6	2.1	8.290	0.027
6.00	11.679	0.007	0.135	0.023	1.414	0.01	0.01	0.091	9.56	0.27	18.10	6.85	63.7	1.8	8.361	0.027
6.50	10.795	0.011	0.147	0.038	1.499	0.014	0.008	0.216	9.49	0.56	11.08	2.69	63.2	3.6	8.846	0.030

Watts	40Ar/39Ar	±	38Ar/39Ar	±	37Ar/39Ar	±	36Ar/39Ar	±	40Ar*/39ArK	±	%40Ar atm	% 39Ar	Age	±	Ca/K	Cl/K
7.00	9.724	0.005	0.145	0.013	1.475	0.008	0.004	0.098	9.2	0.12	5.71	15.09	61.3	0.8	8.744	0.030
DC342	Hornblende	>250um	J= 0.003768±0.000026													
2.00	211.681	0.025	0.161	0.101	0.525	0.049	0.479	0.04	78.69	4.87	63.04	0.41	468.5	25.5	2.738	0.012
3.00	35.628	0.021	0.134	0.11	0.986	0.033	0.072	0.129	17.79	2.78	49.08	0.42	117	17.7	5.532	0.025
4.00	10.583	0.005	0.164	0.014	1.391	0.007	0.006	0.057	9.38	0.11	11.73	13.03	62.6	0.7	8.254	0.034
4.25	8.724	0.003	0.169	0.011	1.367	0.006	0.002	0.096	8.59	0.07	1.98	22.70	57.5	0.5	8.117	0.035
4.50	8.523	0.004	0.171	0.01	1.374	0.007	0.002	0.113	8.44	0.07	1.29	19.07	56.5	0.5	8.160	0.036
4.75	8.775	0.005	0.165	0.013	1.365	0.008	0.003	0.139	8.5	0.13	3.32	10.40	56.8	0.8	8.101	0.035
5.00	9.888	0.006	0.174	0.016	1.372	0.009	0.005	0.132	9.1	0.2	7.97	6.54	60.8	1.3	8.141	0.036
5.25	8.757	0.006	0.157	0.015	1.371	0.009	0.003	0.176	8.44	0.17	3.54	7.51	56.5	1.1	8.137	0.032
5.50	8.964	0.007	0.159	0.021	1.366	0.01	0.004	0.196	8.54	0.23	4.50	5.22	57.1	1.5	8.107	0.033
5.75	9.49	0.01	0.153	0.028	1.381	0.013	0.006	0.216	8.57	0.4	8.92	2.91	57.3	2.6	8.180	0.032
6.00	9.295	0.008	0.154	0.028	1.376	0.012	0.005	0.258	8.71	0.42	5.36	2.80	58.2	2.8	8.151	0.032
6.50	9.013	0.007	0.153	0.023	1.373	0.01	0.004	0.224	8.54	0.3	4.69	4.04	57.1	1.9	8.142	0.031
7.50	9.1	0.006	0.182	0.017	1.422	0.009	0.004	0.185	8.62	0.24	5.06	4.94	57.6	1.6	8.451	0.038
DC370	Hornblende	200-250um	J= 0.003815±0.000032													
2.00	192.82	0.044	0.224	0.335	2.967	0.054	0.511	0.085	55.35	11.61	71.64	0.73	345.6	66	19.513	0.024
3.00	12.355	0.009	0.134	0.039	1.666	0.011	0.014	0.138	9.35	0.59	24.38	14.12	63.2	3.9	11.510	0.027
3.50	8.92	0.006	0.152	0.022	1.66	0.009	0.005	0.165	8.27	0.25	7.54	31.01	56	1.7	11.483	0.031
4.00	9.13	0.008	0.169	0.028	1.732	0.011	0.007	0.278	8.24	0.55	9.80	17.24	55.8	3.7	11.972	0.035
4.50	8.756	0.01	0.164	0.04	1.67	0.014	0.007	0.355	7.9	0.73	9.31	12.37	53.6	4.8	11.526	0.034
5.00	10.893	0.019	0.145	0.149	1.681	0.024	0.019	0.53	8.02	3.08	23.99	2.99	54.4	20.6	11.373	0.029
5.50	9.957	0.016	0.135	0.09	1.64	0.02	0.013	0.436	8.61	1.65	11.83	5.04	58.3	11	11.193	0.028
6.00	11.986	0.031	0.135	0.224	1.725	0.038	0.027	0.471	9.75	3.86	14.46	1.82	65.9	25.6	11.527	0.026
7.50	9.127	0.014	0.14	0.052	1.685	0.02	0.007	0.299	8.03	0.61	11.85	14.67	54.4	4.1	11.654	0.028
DC397	Hornblende	>250um	J= 0.003771±0.000026													
2.00	718.498	0.13	0.347	0.423	1.523	0.236	1.055	0.16	483.98	78.73	36.88	0.16	1873.6	189.6	5.586	0.029
3.00	9.048	0.008	0.058	0.053	1.444	0.012	0.006	0.225	8.07	0.39	8.49	10.75	54.1	2.6	8.621	0.010
3.50	58.686	0.009	0.042	0.073	3.214	0.012	0.091	0.028	34.56	0.79	41.71	11.14	221	4.7	19.387	0.003
4.00	19.046	0.007	0.024	0.064	3.245	0.009	0.02	0.043	14.42	0.28	24.61	19.75	95.6	1.8	19.592	0.001
4.50	11.897	0.007	0.022	0.087	3.513	0.009	0.01	0.091	10.3	0.28	13.25	18.18	68.7	1.9	21.222	0.001
5.00	10.694	0.009	0.022	0.123	3.439	0.011	0.01	0.126	9.35	0.37	11.48	12.16	62.5	2.5	20.766	0.001
5.50	10.38	0.012	0.022	0.15	3.539	0.013	0.011	0.154	8.5	0.53	16.04	8.14	56.9	3.5	21.385	0.001
6.00	14.29	0.012	0.024	0.217	3.387	0.014	0.02	0.138	10.17	0.85	26.71	5.45	67.9	5.6	20.396	0.001
7.50	12.252	0.007	0.026	0.089	3.614	0.01	0.011	0.103	10.52	0.35	13.63	14.27	70.2	2.3	21.868	0.002

Watts	40Ar/39Ar	±	38Ar/39Ar	±	37Ar/39Ar	±	36Ar/39Ar	±	40Ar*/39ArK	±	%40Ar atm	% 39Ar	Age	±	Ca/K	Cl/K
DC397-2	Hornblende	HP	J= 0.003703±0.000016													
2.00	289.472	0.107	0.168	0.493	1.373	0.15	0.548	0.149	158.23	26.34	47.04	0.55	832	110.9	15.839	0.008
3.00	13.541	0.01	0.023	0.115	1.304	0.021	0.012	0.107	11.47	0.39	15.34	36.14	75	2.5	18.543	0.001
3.50	11.806	0.024	0.024	0.272	1.308	0.037	0.012	0.242	9.69	0.89	17.10	21.18	63.6	5.7	18.556	0.002
4.00	10.632	0.017	0.023	0.247	1.405	0.026	0.01	0.225	9.38	0.68	9.58	13.37	61.6	4.4	19.895	0.001
4.50	10.803	0.02	0.029	0.196	1.386	0.029	0.011	0.261	9.69	0.92	6.86	9.87	63.6	5.9	19.599	0.003
5.50	10.92	0.024	0.022	0.258	1.349	0.033	0.014	0.239	9.16	1.03	11.37	7.02	60.2	6.6	18.933	0.001
7.00	49.55	0.015	0.049	0.125	1.4	0.029	0.148	0.044	8.91	1.84	82.07	11.87	58.6	11.9	19.829	0.001
DC400	Hornblende	>250um	J= 0.003776±0.000026													
2.00	130.213	0.309	0.204	1.87	2.541	0.399	0.554	0.613	17.85	94.97	80.29	0.04	117.7	606.1	7.760	0.056
2.50	34.098	0.045	0.085	0.531	1.53	0.061	0.088	0.307	15.01	8.11	50.63	0.42	99.5	52.3	9.004	0.013
3.00	12.083	0.009	0.066	0.05	1.456	0.012	0.012	0.135	9.33	0.5	21.90	7.50	62.4	3.3	9.286	0.011
3.50	8.215	0.004	0.061	0.02	1.43	0.007	0.003	0.099	7.84	0.1	4.65	39.36	52.6	0.7	9.157	0.011
3.75	8.016	0.005	0.059	0.027	1.4	0.008	0.003	0.185	7.78	0.16	2.71	24.89	52.2	1.1	8.963	0.010
4.00	8.527	0.008	0.058	0.059	1.415	0.012	0.005	0.345	7.71	0.57	7.63	7.48	51.7	3.8	9.027	0.010
5.00	8.678	0.008	0.064	0.042	1.435	0.012	0.006	0.24	7.57	0.43	11.28	9.22	50.9	2.9	9.173	0.011
7.00	8.496	0.008	0.062	0.042	1.48	0.011	0.005	0.233	7.77	0.32	7.47	11.09	52.1	2.1	9.467	0.011
DC414	Hornblende	200-250um	J= 0.003779±0.000026													
2.00	81.116	0.029	0.066	0.216	3.484	0.032	0.23	0.062	18.19	3.85	77.43	2.31	119.9	24.6	22.101	0.004
2.50	54.772	0.071	0.045	1.444	3.463	0.079	0.207	0.26	14.05	16.17	71.41	0.47	93.3	104.7	21.002	0.002
3.00	12.45	0.013	0.019	0.215	3.727	0.016	0.019	0.164	8.82	0.95	27.72	9.06	59.1	6.2	24.034	0.001
3.50	9.691	0.009	0.018	0.117	3.343	0.01	0.009	0.148	8.21	0.42	14.55	19.28	55.1	2.8	21.562	0.000
4.00	9.158	0.006	0.016	0.07	3.48	0.008	0.008	0.098	8.21	0.23	10.49	39.62	55.1	1.5	22.476	0.000
4.50	11.142	0.015	0.02	0.258	3.676	0.017	0.017	0.269	8.3	1.37	22.47	6.57	55.7	9	23.674	0.001
5.00	11.625	0.015	0.019	0.426	3.827	0.018	0.021	0.223	7.99	1.39	27.81	5.32	53.6	9.2	24.628	0.001
5.50	11.791	0.019	0.02	0.386	3.671	0.02	0.021	0.244	8.04	1.52	28.10	4.91	54	10	23.654	0.000
7.50	9.786	0.01	0.017	0.179	3.814	0.012	0.011	0.169	8.23	0.57	14.29	12.45	55.3	3.8	24.644	0.000
DC423	Hornblende	>250um	J= 0.003782±0.000026													
2.00	180.778	0.037	0.105	0.314	0.582	0.093	0.259	0.09	115.69	7.73	35.65	0.45	654.7	36.7	2.676	0.008
3.00	22.095	0.018	0.142	0.078	1.106	0.027	0.021	0.257	18.07	1.64	15.83	1.68	119.2	10.5	6.905	0.027
3.50	9.148	0.005	0.145	0.018	1.228	0.008	0.003	0.131	8.96	0.11	2.07	24.32	60.1	0.7	7.969	0.030
4.00	8.698	0.004	0.15	0.012	1.244	0.007	0.002	0.162	8.55	0.12	1.92	38.70	57.4	0.8	8.078	0.031
4.25	8.742	0.008	0.151	0.027	1.247	0.011	0.004	0.227	8.46	0.26	2.23	10.13	56.8	1.7	8.076	0.031
4.50	8.933	0.009	0.16	0.026	1.268	0.013	0.005	0.243	8.36	0.36	4.81	6.96	56.1	2.4	8.191	0.033
5.00	10.113	0.021	0.164	0.076	1.339	0.026	0.013	0.499	8.79	1.9	4.32	1.52	59	12.5	8.421	0.034

Watts	40Ar/39Ar	±	38Ar/39Ar	±	37Ar/39Ar	±	36Ar/39Ar	±	40Ar*/39ArK	±	%40Ar atm	% 39Ar	Age	±	Ca/K	Cl/K
7.00	9.019	0.006	0.177	0.018	1.401	0.009	0.003	0.173	8.79	0.17	2.26	16.24	59	1.1	9.107	0.037
DC446	Hornblende	>250um	J= 0.003786±0.000026													
2.00	232.75	0.024	0.164	0.119	0.543	0.048	0.478	0.038	99.6	4.91	57.37	0.76	577.2	24.4	3.094	0.013
3.00	42.236	0.019	0.236	0.061	1.298	0.027	0.048	0.161	31.69	2.41	24.20	1.01	204.4	14.7	8.185	0.048
3.50	12.377	0.009	0.309	0.022	1.889	0.012	0.007	0.181	11.36	0.42	7.28	4.64	76	2.7	12.273	0.067
4.00	10.163	0.004	0.303	0.011	1.862	0.007	0.004	0.119	9.87	0.13	3.30	21.83	66.2	0.9	12.150	0.066
4.50	10.101	0.005	0.305	0.009	1.823	0.007	0.004	0.095	9.81	0.11	3.31	23.30	65.8	0.7	11.896	0.067
5.00	9.562	0.005	0.3	0.012	1.651	0.008	0.004	0.145	9.23	0.16	3.50	15.75	62	1.1	10.766	0.065
5.50	9.635	0.006	0.305	0.014	1.856	0.009	0.004	0.178	9.4	0.2	2.55	14.34	63.1	1.3	12.119	0.067
6.00	10.007	0.008	0.31	0.021	1.836	0.011	0.006	0.208	9.5	0.36	4.01	5.57	63.7	2.4	11.952	0.067
7.50	9.697	0.006	0.366	0.016	1.85	0.008	0.004	0.12	9.43	0.15	2.77	12.80	63.3	1	12.079	0.081
DC457	Hornblende	200-250um	J= 0.003791±0.000026													
2.00	1275.17	0.094	0.602	0.211	1.516	0.113	1.345	0.102	907.63	87.75	28.56	0.17	2689.6	135.1	7.362	0.071
3.00	29.113	0.024	0.72	0.04	2.062	0.029	0.055	0.117	17.15	1.95	39.78	1.30	113.6	12.5	13.234	0.160
3.50	11.22	0.008	0.643	0.015	1.954	0.011	0.009	0.15	9.69	0.43	12.88	6.76	65.1	2.8	12.749	0.144
4.00	9.352	0.005	0.654	0.009	1.956	0.007	0.005	0.071	8.68	0.11	7.44	23.79	58.4	0.8	12.803	0.147
4.50	8.759	0.004	0.639	0.007	1.956	0.007	0.004	0.077	8.48	0.09	3.52	35.12	57.1	0.6	12.811	0.143
5.00	8.761	0.006	0.635	0.01	1.958	0.008	0.004	0.116	8.44	0.15	3.62	17.17	56.8	1	12.812	0.142
5.50	9.362	0.009	0.607	0.016	1.899	0.011	0.007	0.179	8.6	0.38	6.68	5.96	57.9	2.5	12.385	0.136
6.00	10.537	0.018	0.587	0.03	1.911	0.021	0.014	0.33	9.08	1.36	8.69	1.85	61.1	9	12.348	0.130
6.50	9.602	0.014	0.508	0.024	1.801	0.017	0.009	0.328	8.75	0.85	5.60	3.01	58.9	5.6	11.727	0.113
7.50	9.167	0.011	0.627	0.017	1.981	0.014	0.007	0.226	8.46	0.46	5.83	4.86	56.9	3	12.927	0.140
DC464	Hornblende	200-250um	J= 0.003793±0.000026													
2.00	16.825	0.009	0.173	0.028	1.181	0.013	0.026	0.061	10.3	0.48	38.52	6.48	69.2	3.2	7.677	0.035
2.50	16.576	0.026	0.176	0.125	1.223	0.036	0.033	0.257	10.27	2.52	32.28	0.82	69	16.6	7.586	0.036
3.00	10.02	0.007	0.173	0.022	1.183	0.01	0.006	0.174	9.08	0.3	8.99	10.78	61.1	2	7.723	0.036
3.50	9.001	0.006	0.174	0.017	1.187	0.008	0.003	0.157	8.61	0.17	4.08	14.69	58	1.1	7.767	0.037
4.00	8.511	0.005	0.171	0.014	1.158	0.008	0.003	0.127	8.31	0.11	2.37	23.79	56	0.7	7.581	0.036
4.50	8.592	0.005	0.168	0.014	1.145	0.008	0.003	0.182	8.36	0.14	2.73	22.64	56.3	1	7.495	0.035
5.00	9.14	0.008	0.17	0.023	1.14	0.011	0.005	0.206	8.37	0.31	7.58	8.62	56.4	2	7.449	0.035
5.50	9.627	0.014	0.174	0.054	1.184	0.019	0.008	0.262	8.5	0.66	8.38	3.09	57.3	4.4	7.653	0.036
7.50	8.84	0.007	0.173	0.022	1.192	0.01	0.004	0.194	8.4	0.23	4.05	9.10	56.6	1.5	7.794	0.036
DC469-1	Hornblende	100-250um	J= 0.003797±0.000026													

Watts	40Ar/39Ar	±	38Ar/39Ar	±	37Ar/39Ar	±	36Ar/39Ar	±	40Ar*/39ArK	±	%40Ar atm % 39Ar	Age	±	Ca/K	Cl/K	
2.00	363.579	0.06	0.315	0.186	1.454	0.1	1.168	0.079	46.36	18.64	87.37	0.31	292.5	108.6	6.174	0.022
3.00	12.841	0.012	0.079	0.059	2.035	0.015	0.018	0.137	8.96	0.76	27.56	6.04	60.3	5.1	11.527	0.014
3.75	8.452	0.004	0.074	0.019	1.961	0.007	0.003	0.098	8.23	0.1	2.67	60.52	55.5	0.6	11.203	0.014
4.25	8.873	0.008	0.076	0.033	1.947	0.01	0.005	0.158	8.18	0.25	6.58	18.61	55.2	1.7	11.107	0.014
4.75	9.962	0.012	0.079	0.059	1.941	0.015	0.011	0.181	7.9	0.61	16.72	6.41	53.3	4	11.007	0.015
5.50	11.262	0.017	0.084	0.077	1.982	0.019	0.018	0.258	8.18	1.36	21.49	3.78	55.2	9.1	11.197	0.015
6.50	10.656	0.014	0.08	0.071	1.984	0.017	0.014	0.232	8.19	0.97	17.49	4.34	55.3	6.4	11.220	0.015
DC469-2 Hornblende >250um J= 0.003799±0.000024																
2.00	425.177	0.053	0.292	0.241	1.121	0.097	1.1	0.075	120.04	18.3	70.74	0.24	677.8	86.1	5.443	0.023
3.00	32.968	0.042	0.092	0.451	1.59	0.056	0.084	0.363	22.09	8.96	22.82	0.41	145.4	56.6	9.143	0.022
3.50	13.557	0.02	0.089	0.132	1.767	0.024	0.02	0.333	10.52	1.95	17.58	1.80	70.7	12.9	11.491	0.017
4.00	8.714	0.004	0.081	0.022	1.686	0.007	0.004	0.133	8.36	0.15	4.19	28.53	56.4	1	11.183	0.015
4.50	8.454	0.005	0.081	0.025	1.699	0.008	0.003	0.222	8.32	0.21	1.25	19.21	56.2	1.4	11.259	0.015
5.00	8.338	0.005	0.078	0.02	1.691	0.008	0.003	0.189	8.21	0.16	1.44	24.96	55.4	1.1	11.218	0.015
5.25	8.98	0.01	0.08	0.075	1.691	0.013	0.007	0.363	8.12	0.81	6.88	5.17	54.8	5.4	11.136	0.015
5.50	8.924	0.013	0.079	0.071	1.686	0.015	0.007	0.355	8.24	0.74	4.74	4.87	55.6	4.9	11.097	0.015
6.00	8.514	0.009	0.078	0.043	1.665	0.011	0.005	0.328	8.11	0.49	3.17	8.59	54.7	3.2	11.011	0.014
7.50	8.856	0.01	0.088	0.052	1.923	0.012	0.007	0.32	8.05	0.63	7.02	6.22	54.3	4.2	12.721	0.017
DC473-1 Hornblende 200-250um J= 0.003800±0.000024																
2.00	188.585	0.045	0.235	0.204	1.008	0.076	0.411	0.099	78.32	11.24	56.90	0.23	470	59.4	5.261	0.037
2.50	44.935	0.054	0.395	0.213	0.932	0.096	0.112	0.439	31.51	14.28	16.56	0.16	204.1	87.4	4.267	0.090
3.00	17.75	0.031	0.402	0.081	0.948	0.047	0.038	0.468	13	5.32	15.21	0.41	87	34.8	5.580	0.089
3.50	10.339	0.011	0.248	0.035	0.813	0.017	0.01	0.386	8.59	1.11	13.49	2.25	58	7.3	5.271	0.053
4.00	8.937	0.007	0.192	0.02	0.783	0.011	0.003	0.275	8.53	0.28	3.61	8.05	57.6	1.9	5.170	0.041
4.50	8.335	0.004	0.144	0.014	0.755	0.007	0.002	0.238	8.17	0.13	1.79	19.45	55.2	0.9	5.007	0.030
5.00	8.295	0.004	0.126	0.014	0.749	0.008	0.002	0.295	8.23	0.15	0.60	17.91	55.5	1	4.966	0.026
5.50	8.306	0.004	0.131	0.015	0.728	0.007	0.002	0.213	8.17	0.11	1.53	22.05	55.2	0.7	4.835	0.027
6.00	8.55	0.008	0.126	0.026	0.729	0.012	0.003	0.446	8.32	0.42	1.17	5.93	56.1	2.8	4.798	0.026
7.50	8.351	0.004	0.128	0.014	0.747	0.007	0.002	0.22	8.21	0.12	1.72	23.55	55.4	0.8	4.964	0.026
DC473-2 Hornblende >250um J= 0.003802±0.000022																
2.00	230.145	0.034	0.272	0.119	1.009	0.052	0.428	0.062	111.39	7.53	50.36	0.35	637.1	36.3	5.906	0.043
3.00	40.515	0.029	0.403	0.1	0.932	0.044	0.057	0.295	28.85	5.02	23.66	0.38	187.8	31	5.461	0.087
3.50	15.236	0.026	0.443	0.055	0.902	0.042	0.031	0.347	10.14	3.25	26.52	0.59	68.3	21.5	5.605	0.099
4.00	11.066	0.01	0.243	0.03	0.811	0.016	0.01	0.219	9.22	0.65	14.85	3.07	62.2	4.3	5.323	0.052
4.50	8.911	0.005	0.149	0.015	0.73	0.009	0.003	0.224	8.56	0.17	3.68	12.75	57.8	1.2	4.849	0.031
5.00	8.329	0.004	0.118	0.012	0.717	0.007	0.001	0.201	8.26	0.09	0.87	25.14	55.8	0.6	4.774	0.024
5.50	8.48	0.004	0.116	0.013	0.701	0.007	0.002	0.127	8.22	0.08	3.13	28.07	55.5	0.6	4.667	0.023

Watts	40Ar/39Ar	±	38Ar/39Ar	±	37Ar/39Ar	±	36Ar/39Ar	±	40Ar*/39ArK	±	%40Ar atm % 39Ar	Age	±	Ca/K	Cl/K	
5.75	8.299	0.005	0.114	0.02	0.706	0.009	0.002	0.316	8.07	0.19	2.15	10.52	54.5	1.2	4.691	0.023
6.00	9.406	0.013	0.124	0.065	0.736	0.021	0.009	0.448	8.65	1.16	2.66	1.58	58.4	7.7	4.737	0.025
6.50	8.761	0.009	0.125	0.04	0.741	0.014	0.004	0.463	8.43	0.57	1.27	3.43	56.9	3.8	4.868	0.025
7.50	8.453	0.005	0.123	0.016	0.758	0.008	0.002	0.25	8.28	0.16	1.75	14.13	55.9	1	5.047	0.025
DC476-1	Homblende	200-250um	J= 0.003803±0.000022													
2.00	265.286	0.051	0.201	0.281	1.025	0.092	0.847	0.085	36.17	17.11	85.96	0.71	232.5	103.2	5.158	0.007
3.00	30.75	0.031	0.1	0.295	4.776	0.033	0.092	0.23	10.84	6.28	62.22	1.65	72.9	41.4	31.421	0.017
3.50	11.171	0.011	0.098	0.062	6.577	0.012	0.018	0.155	8.83	0.86	19.92	11.48	59.6	5.7	44.497	0.019
4.00	9.34	0.008	0.093	0.034	6.568	0.01	0.012	0.124	8.54	0.45	8.50	21.12	57.7	3	44.526	0.018
4.50	8.836	0.007	0.091	0.034	6.527	0.008	0.01	0.12	8.31	0.37	6.18	26.02	56.1	2.5	44.281	0.017
5.00	9.291	0.008	0.094	0.039	6.586	0.01	0.012	0.142	8.41	0.53	8.91	17.94	56.8	3.5	44.600	0.018
5.50	9.871	0.01	0.098	0.065	6.59	0.011	0.015	0.211	8.47	0.97	12.24	9.75	57.2	6.4	44.674	0.019
6.00	11.982	0.02	0.127	0.095	6.753	0.021	0.028	0.38	9.41	3.2	15.26	3.65	63.4	21.2	45.506	0.026
7.50	10.09	0.014	0.126	0.058	6.941	0.014	0.019	0.259	8.09	1.46	16.93	7.68	54.7	9.7	46.970	0.026
DC476-2	Homblende	>250um	J= 0.003805±0.000022													
2.00	403.091	0.046	0.292	0.147	1.203	0.064	1.268	0.055	48.77	11.95	88.17	0.80	307.1	69.2	7.215	0.007
3.00	35.731	0.026	0.088	0.256	4.333	0.029	0.092	0.179	15	4.96	56.53	1.74	100.2	32.2	29.138	0.011
3.50	13.729	0.014	0.091	0.075	6.194	0.016	0.025	0.17	9.62	1.3	28.65	6.27	64.9	8.6	42.401	0.017
4.00	9.651	0.007	0.088	0.026	6.373	0.008	0.012	0.067	8.39	0.26	13.84	30.62	56.7	1.7	43.677	0.016
4.50	9.834	0.008	0.092	0.033	6.497	0.009	0.013	0.093	8.45	0.38	14.44	21.07	57.1	2.5	44.562	0.017
5.00	8.91	0.008	0.095	0.034	6.722	0.009	0.011	0.105	8.23	0.36	7.79	19.38	55.6	2.4	46.178	0.018
5.50	9.271	0.01	0.098	0.063	6.688	0.011	0.013	0.183	8.59	0.73	6.19	10.76	58	4.8	45.950	0.019
6.00	9.936	0.014	0.102	0.068	6.748	0.014	0.017	0.169	8.17	0.9	15.31	6.73	55.3	6	46.400	0.020
7.50	13.487	0.023	0.283	0.071	8.962	0.024	0.036	0.214	9.46	2.36	24.85	2.63	63.8	15.6	62.066	0.062

TABLE C2: Biotite thermochronology data

Watts	40Ar/39Ar	±	38Ar/39Ar	±	37Ar/39Ar	±	36Ar/39Ar	±	40Ar*/39ArK	±	%40Ar atm % 39Ar	Age	±	Ca/K	Cl/K	
AH-02-003B Biotite		HP	J= 0.003690±0.000018													
0.50	52.599	0.086	0.131	0.475	0.29	0.392	0.203	0.253	9.66	14.96	78.93	0.17	63.2	96.2	0.000	0.019
1.00	12.407	0.01	0.086	0.063	0.006	0.312	0.011	0.117	9.69	0.39	21.20	9.23	63.4	2.5	0.011	0.016
1.50	10.641	0.01	0.085	0.06	0.004	0.409	0.004	0.169	9.87	0.2	6.58	12.66	64.6	1.3	0.000	0.016
2.00	10.332	0.008	0.085	0.038	0.004	0.332	0.002	0.291	10.03	0.18	2.46	15.60	65.6	1.2	0.000	0.016
2.50	10.334	0.01	0.086	0.038	0.006	0.283	0.002	0.311	10.1	0.2	1.53	12.29	66	1.3	0.022	0.016
3.00	10.391	0.012	0.088	0.055	0.009	0.261	0.002	0.366	10.14	0.27	1.30	8.92	66.3	1.7	0.050	0.017
4.00	10.249	0.01	0.085	0.046	0.006	0.334	0.002	0.368	10.05	0.21	1.16	11.83	65.7	1.4	0.026	0.016
5.00	10.155	0.009	0.086	0.038	0.006	0.195	0.001	0.4	10.05	0.16	0.57	16.49	65.7	1.1	0.039	0.016
6.00	10.469	0.017	0.088	0.072	0.015	0.309	0.003	0.544	10.22	0.51	-0.06	4.72	66.8	3.3	0.047	0.017
7.00	10.439	0.01	0.089	0.049	0.011	0.3	0.002	0.363	10.12	0.29	1.83	8.09	66.2	1.8	0.054	0.017
AH-02-004B Biotite		HP	J= 0.003694±0.000018													
0.50	45.27	0.028	0.135	0.121	0.045	0.266	0.158	0.078	1.95	3.48	95.56	0.81	12.9	23	0.000	0.021
0.75	24.658	0.019	0.108	0.065	0.015	0.235	0.074	0.06	3.95	1.27	83.71	2.73	26.1	8.3	0.000	0.018
1.00	14.201	0.015	0.093	0.083	0.009	0.294	0.024	0.097	7.71	0.71	44.87	3.99	50.7	4.6	0.000	0.017
1.50	9.551	0.005	0.09	0.028	0.002	0.237	0.003	0.113	8.86	0.1	7.19	27.53	58.1	0.7	0.004	0.017
1.75	9.493	0.007	0.089	0.031	0.002	0.327	0.002	0.185	9.08	0.12	4.13	19.90	59.5	0.8	0.007	0.017
2.00	9.864	0.011	0.091	0.055	0.006	0.253	0.003	0.316	9.26	0.29	5.17	7.60	60.7	1.9	0.009	0.017
2.50	9.87	0.01	0.091	0.049	0.005	0.293	0.003	0.273	9.24	0.27	5.45	8.13	60.6	1.7	0.012	0.017
3.00	9.461	0.009	0.09	0.046	0.004	0.233	0.002	0.282	9.02	0.19	3.99	10.65	59.1	1.3	0.012	0.017
3.50	9.626	0.012	0.09	0.06	0.009	0.241	0.003	0.535	9.18	0.49	2.59	4.22	60.1	3.2	0.001	0.017
4.25	9.733	0.017	0.091	0.079	0.011	0.284	0.003	0.507	9.27	0.49	2.51	4.07	60.7	3.1	0.030	0.017
5.00	10.227	0.018	0.094	0.08	0.018	0.216	0.005	0.469	9.23	0.78	6.27	2.48	60.5	5	0.070	0.018
7.00	9.686	0.01	0.088	0.043	0.014	0.146	0.002	0.416	9.34	0.27	2.47	7.90	61.2	1.8	0.122	0.017
AH-02-013 Biotite		HP	J= 0.003697±0.000018													
0.50	34.32	0.062	0.113	0.346	0.144	0.277	0.129	0.22	3.57	8.32	88.35	0.40	23.6	54.8	0.000	0.016
1.00	9.825	0.012	0.068	0.065	0.006	0.282	0.007	0.176	8.07	0.4	16.46	8.75	53	2.6	0.000	0.012
1.25	8.798	0.008	0.069	0.049	0.004	0.274	0.002	0.296	8.37	0.21	4.01	17.09	55	1.3	0.000	0.012
1.50	8.497	0.009	0.071	0.038	0.005	0.356	0.001	0.643	8.34	0.27	0.49	12.68	54.8	1.8	0.000	0.013
1.75	8.545	0.013	0.072	0.059	0.005	0.316	0.002	0.638	8.38	0.32	0.28	10.27	55	2	0.000	0.013
2.00	8.66	0.014	0.073	0.07	0.008	0.316	0.002	0.648	8.35	0.48	1.04	7.12	54.9	3.1	0.000	0.013
2.50	8.537	0.011	0.071	0.052	0.006	0.411	0.002	0.526	8.33	0.28	0.80	10.40	54.7	1.8	0.001	0.013
3.00	8.5	0.01	0.072	0.056	0.005	0.41	0.001	0.792	8.38	0.29	-0.04	12.05	55.1	1.9	0.000	0.013
4.00	8.508	0.012	0.071	0.043	0.005	0.32	0.001	0.659	8.39	0.27	-0.04	11.30	55.1	1.7	0.000	0.013
5.00	8.654	0.014	0.069	0.078	0.01	0.399	0.003	0.596	8.39	0.5	-0.04	5.87	55.1	3.2	0.000	0.012
6.00	9.212	0.027	0.068	0.125	0.025	0.247	0.005	0.778	8.5	1.24	-0.04	2.33	55.8	8	0.000	0.012
7.00	9.51	0.032	0.07	0.172	0.033	0.296	0.007	0.845	8.56	1.89	-0.05	1.75	56.2	12.2	0.015	0.012

Watts	40Ar/39Ar	±	38Ar/39Ar	±	37Ar/39Ar	±	36Ar/39Ar	±	40Ar*/39ArK	±	%40Ar atm	% 39Ar	Age	±	Ca/K	Cl/K
AH-02-022	Biotite	HP	J= 0.003698±0.000018													
0.50	44.435	0.089	0.071	1.327	0.316	0.39	0.181	0.328	9.92	17.8	72.07	0.10	65	114.5	0.000	0.005
0.75	16.276	0.022	0.041	0.208	0.021	0.285	0.033	0.161	8.07	1.56	48.58	1.59	53	10.1	0.000	0.004
1.00	8.264	0.005	0.024	0.035	0.001	0.318	0.002	0.143	7.73	0.1	6.46	39.46	50.8	0.6	0.002	0.002
1.25	7.986	0.015	0.019	0.118	0.007	0.399	0.002	0.666	7.8	0.43	-0.00	4.95	51.3	2.8	0.000	0.001
1.50	7.882	0.009	0.02	0.122	0.004	0.244	0.001	0.572	7.7	0.24	1.06	8.49	50.6	1.5	0.000	0.001
1.75	8.215	0.017	0.025	0.147	0.01	0.259	0.003	0.664	7.87	0.59	0.87	3.47	51.7	3.8	0.000	0.002
2.00	8.259	0.014	0.024	0.169	0.011	0.288	0.003	0.609	7.89	0.62	0.92	3.25	51.9	4	0.009	0.002
3.00	7.913	0.005	0.025	0.042	0.002	0.243	0.001	0.37	7.81	0.08	1.08	30.11	51.4	0.5	0.006	0.003
4.00	8.886	0.03	0.025	0.302	0.031	0.272	0.008	0.765	7.99	1.78	-0.01	1.15	52.6	11.6	0.000	0.002
7.00	8.139	0.01	0.026	0.099	0.005	0.244	0.002	0.493	7.84	0.27	2.23	7.42	51.6	1.8	0.002	0.003
AH-03-021	Biotite	HP	J= 0.003700±0.000018													
0.50	93.868	0.093	0.179	0.433	0.335	0.446	0.368	0.214	4.49	22.55	94.97	0.04	29.8	148.1	0.259	0.018
0.75	31.062	0.03	0.091	0.16	0.042	0.372	0.089	0.131	6.97	3.42	76.63	0.30	45.9	22.3	0.000	0.013
1.00	10.902	0.02	0.08	0.097	0.016	0.302	0.014	0.216	7.82	0.89	25.26	0.82	51.4	5.8	0.000	0.015
1.25	8.952	0.011	0.077	0.045	0.004	0.349	0.004	0.185	7.91	0.25	10.78	3.56	52	1.6	0.002	0.014
1.50	8.234	0.011	0.076	0.059	0.004	0.302	0.002	0.38	7.96	0.21	2.25	3.39	52.4	1.4	0.000	0.014
1.75	8.363	0.009	0.076	0.036	0.003	0.314	0.002	0.24	7.9	0.17	4.94	4.80	51.9	1.1	0.001	0.014
2.00	8.243	0.006	0.073	0.032	0.002	0.379	0.001	0.283	8.02	0.11	2.48	8.62	52.7	0.7	0.004	0.013
2.25	8.104	0.006	0.073	0.034	0.001	0.299	0.001	0.407	8.01	0.09	11.23	52.7	52.7	0.6	0.001	0.014
2.50	8.119	0.007	0.075	0.038	0.003	0.244	0.001	0.509	8	0.13	0.98	6.57	52.7	0.9	0.005	0.014
3.00	8.059	0.007	0.075	0.035	0.002	0.206	0.001	0.385	7.96	0.1	0.97	8.70	52.4	0.6	0.006	0.014
3.50	8.001	0.005	0.075	0.026	0.002	0.201	0	0.419	7.96	0.07	0.35	12.43	52.4	0.4	0.010	0.014
4.00	7.956	0.006	0.075	0.024	0.002	0.219	0	0.43	7.91	0.08	0.40	11.64	52.1	0.5	0.011	0.014
4.50	8.012	0.006	0.075	0.032	0.003	0.179	0	0.65	7.97	0.11	0.17	8.52	52.5	0.7	0.025	0.014
5.00	8.054	0.007	0.075	0.038	0.009	0.097	0.001	0.502	7.95	0.13	0.78	5.83	52.3	0.9	0.085	0.014
6.00	8.117	0.009	0.077	0.061	0.027	0.087	0.001	0.563	7.97	0.19	1.04	4.52	52.4	1.2	0.330	0.014
7.00	7.988	0.009	0.077	0.029	0.018	0.056	0.001	0.396	7.91	0.1	0.78	9.03	52	0.7	0.236	0.014
AH-03-032	Biotite	HP	J= 0.003701±0.000018													
0.50	43.622	0.067	0.2	0.261	0.125	0.346	0.154	0.152	5.22	6.43	87.00	0.18	34.5	42.1	0.000	0.036
1.00	10.426	0.01	0.214	0.029	0.003	0.332	0.01	0.091	7.76	0.28	25.08	7.73	51.1	1.8	0.000	0.045
1.25	14.78	0.015	0.214	0.047	0.008	0.344	0.026	0.078	7.72	0.61	47.08	2.96	50.8	4	0.000	0.045
1.50	8.112	0.005	0.212	0.016	0.001	0.46	0.002	0.157	7.77	0.08	3.98	18.71	51.2	0.5	0.000	0.045
1.75	7.866	0.005	0.211	0.017	0.001	0.306	0	0.51	7.8	0.08	0.64	20.27	51.3	0.5	0.001	0.045
2.00	8.034	0.011	0.211	0.028	0.004	0.361	0.001	0.458	7.92	0.18	0.39	6.72	52.1	1.2	0.002	0.045
2.50	8.074	0.011	0.211	0.032	0.005	0.319	0.001	0.555	7.93	0.25	0.33	5.12	52.2	1.6	0.001	0.045
3.00	8.072	0.009	0.209	0.035	0.004	0.267	0.001	0.44	7.91	0.18	1.01	6.98	52.1	1.2	0.004	0.045
3.50	8.048	0.011	0.207	0.036	0.004	0.464	0.001	0.41	7.9	0.19	0.67	6.21	52	1.2	0.000	0.044
4.00	8.076	0.01	0.211	0.03	0.005	0.308	0.001	0.441	7.98	0.2	-0.14	5.54	52.5	1.3	0.000	0.045
4.50	8.111	0.014	0.209	0.041	0.006	0.323	0.002	0.516	7.98	0.27	-0.15	4.32	52.5	1.8	0.002	0.044

Watts	40Ar/39Ar	±	38Ar/39Ar	±	37Ar/39Ar	±	36Ar/39Ar	±	40Ar*/39ArK	±	%40Ar atm	% 39Ar	Age	±	Ca/K	Cl/K
5.00	8.259	0.016	0.211	0.042	0.009	0.386	0.003	0.453	7.97	0.4	0.58	2.73	52.5	2.6	0.000	0.045
6.00	8.134	0.015	0.21	0.045	0.007	0.412	0.002	0.512	7.95	0.33	-0.15	3.37	52.3	2.1	0.000	0.045
7.00	7.95	0.008	0.212	0.02	0.003	0.306	0.001	0.527	7.9	0.14	-0.10	9.17	52	0.9	0.001	0.045
DC028	Biotite	200-250um	J= 0.003806±0.000022													
0.50	29.337	0.024	0.043	0.303	0.057	0.242	0.089	0.153	6.13	4	77.94	0.25	41.6	26.9	0.045	0.004
1.00	10.265	0.006	0.015	0.109	0.005	0.271	0.01	0.124	7.71	0.35	24.11	3.11	52.2	2.4	0.012	-0.000
1.50	8.187	0.004	0.013	0.066	0.001	0.284	0.002	0.189	7.63	0.13	6.58	10.08	51.6	0.8	0.001	-0.000
2.00	7.926	0.004	0.013	0.06	0.001	0.294	0.001	0.289	7.67	0.1	3.01	11.05	51.9	0.7	0.000	-0.000
2.25	7.944	0.006	0.013	0.084	0.002	0.324	0.001	0.46	7.72	0.17	2.30	5.93	52.2	1.2	0.001	-0.000
2.75	7.861	0.005	0.013	0.087	0.002	0.431	0.001	0.564	7.79	0.14	0.55	7.67	52.7	0.9	0.000	-0.000
3.25	7.84	0.004	0.013	0.068	0.002	0.33	0.001	0.428	7.72	0.11	1.21	9.21	52.2	0.7	0.002	-0.000
4.00	7.788	0.004	0.013	0.05	0.001	0.326	0.001	0.462	7.65	0.09	1.65	11.41	51.7	0.6	0.000	-0.000
5.00	7.768	0.004	0.013	0.04	0.001	0.318	0.001	0.388	7.68	0.07	1.02	16.31	52	0.5	0.000	-0.000
6.00	7.82	0.004	0.013	0.06	0.002	0.312	0.001	0.467	7.72	0.1	1.11	10.12	52.2	0.6	0.000	-0.000
7.00	7.908	0.006	0.013	0.081	0.003	0.324	0.001	0.64	7.8	0.18	0.75	5.53	52.8	1.2	0.004	-0.000
8.00	7.843	0.004	0.013	0.062	0.002	0.256	0.001	0.481	7.7	0.12	1.59	9.33	52.1	0.8	0.001	-0.000
DC080-B1	Biotite	HP	J= 0.003630±0.000018													
0.25	53.092	0.086	0.084	1.02	0.308	0.427	0.208	0.222	2.78	13.2	94.06	0.04	18.1	85.6	0.000	0.002
0.50	23.302	0.055	0.041	1.199	0.143	0.469	0.081	0.263	5.74	6.31	71.13	0.08	37.2	40.5	0.000	0.000
0.75	11.116	0.014	0.021	0.148	0.007	0.405	0.01	0.099	7.35	0.42	33.10	2.11	47.5	2.7	0.008	0.001
1.00	8.911	0.008	0.018	0.102	0.005	0.303	0.004	0.15	7.86	0.19	11.17	3.84	50.8	1.2	0.014	0.001
1.25	8.666	0.006	0.019	0.058	0.003	0.238	0.003	0.096	7.9	0.1	8.74	8.57	51	0.6	0.016	0.001
1.50	8.526	0.006	0.018	0.073	0.003	0.219	0.002	0.106	7.92	0.09	6.97	8.93	51.1	0.6	0.017	0.001
1.75	8.398	0.006	0.018	0.059	0.003	0.295	0.002	0.17	7.99	0.1	4.69	8.03	51.6	0.6	0.011	0.001
2.00	8.185	0.007	0.018	0.062	0.003	0.246	0.001	0.198	7.96	0.08	2.64	9.02	51.4	0.5	0.018	0.001
2.50	8.083	0.006	0.018	0.044	0.005	0.146	0.001	0.319	7.96	0.09	1.34	9.40	51.4	0.5	0.040	0.001
3.00	8.103	0.006	0.018	0.054	0.009	0.098	0.001	0.266	7.95	0.08	1.74	9.20	51.3	0.5	0.099	0.001
3.50	8.068	0.007	0.018	0.066	0.004	0.223	0.001	0.335	7.94	0.1	1.33	6.83	51.3	0.6	0.025	0.001
4.00	8.053	0.005	0.018	0.062	0.009	0.098	0.001	0.29	7.94	0.08	1.20	8.84	51.3	0.5	0.095	0.001
4.50	8.058	0.008	0.018	0.074	0.014	0.087	0.001	0.328	7.94	0.1	1.20	7.24	51.3	0.6	0.160	0.001
5.00	8.138	0.009	0.018	0.103	0.006	0.272	0.001	0.445	8.03	0.15	0.66	4.39	51.9	0.9	0.026	0.001
5.50	8.173	0.01	0.018	0.104	0.005	0.33	0.001	0.435	8	0.18	1.24	3.26	51.6	1.1	0.008	0.001
6.00	8.263	0.012	0.018	0.149	0.008	0.439	0.002	0.516	8.03	0.29	1.18	1.95	51.8	1.8	0.006	0.001
7.00	8.03	0.006	0.018	0.064	0.005	0.173	0.001	0.374	7.96	0.08	0.71	8.28	51.4	0.5	0.040	0.001
DC080-B2	Biotite	HP	J= 0.003733±0.000018													
7.00	8.877	0.007	0.02	0.067	0.003	0.006	0.006	0.085	7.79	0.17	10.33	100.00	51.7	1.1	0.001	0.001
DC176-2	Biotite	>250um	J= 0.003809±0.000024													

Watts	40Ar/39Ar	±	38Ar/39Ar	±	37Ar/39Ar	±	36Ar/39Ar	±	40Ar*/39ArK	±	%40Ar atm	% 39Ar	Age	±	Ca/K	Cl/K
0.50	82.448	0.036	0.108	0.288	0.098	0.312	0.287	0.067	6.55	5	92.00	0.13	44.4	33.5	0.187	0.006
1.00	14.228	0.011	0.051	0.076	0.011	0.284	0.026	0.068	7.3	0.53	47.66	1.16	49.5	3.5	0.033	0.007
1.50	9.086	0.008	0.047	0.05	0.005	0.219	0.006	0.134	7.39	0.26	17.80	3.07	50.1	1.8	0.012	0.007
1.75	8.028	0.005	0.046	0.029	0.003	0.25	0.002	0.158	7.52	0.11	5.82	5.47	50.9	0.8	0.009	0.007
2.00	7.89	0.004	0.046	0.022	0.002	0.221	0.002	0.122	7.5	0.07	4.67	8.78	50.8	0.5	0.007	0.007
2.25	7.808	0.006	0.046	0.058	0.005	0.211	0.002	0.37	7.6	0.18	1.37	3.14	51.5	1.2	0.018	0.007
2.50	7.732	0.006	0.046	0.045	0.004	0.279	0.001	0.333	7.6	0.14	0.73	3.84	51.5	1	0.014	0.007
3.00	7.711	0.004	0.046	0.04	0.003	0.224	0.001	0.255	7.55	0.08	1.55	6.26	51.2	0.6	0.012	0.007
3.50	7.681	0.004	0.046	0.033	0.003	0.207	0.001	0.307	7.53	0.09	1.52	7.34	51	0.6	0.012	0.007
4.00	7.719	0.005	0.045	0.031	0.004	0.2	0.001	0.255	7.5	0.1	2.31	5.76	50.8	0.7	0.018	0.007
4.50	7.711	0.005	0.046	0.027	0.003	0.213	0.001	0.249	7.5	0.09	2.30	6.43	50.8	0.6	0.012	0.007
5.00	7.707	0.005	0.045	0.031	0.003	0.269	0.001	0.323	7.57	0.1	1.24	6.17	51.3	0.6	0.013	0.007
6.00	7.564	0.004	0.045	0.02	0.002	0.246	0.001	0.293	7.49	0.06	0.83	11.37	50.7	0.4	0.006	0.007
7.00	7.55	0.004	0.045	0.021	0.002	0.194	0	0.352	7.48	0.06	0.80	13.07	50.7	0.4	0.006	0.007
8.00	7.586	0.004	0.046	0.021	0.002	0.182	0	0.276	7.51	0.05	0.97	18.01	50.9	0.3	0.009	0.007
DC178	Biotite	200-250um	J= 0.003810±0.000024													
0.50	48.825	0.029	0.05	0.634	0.062	0.43	0.162	0.098	5.39	4.55	88.86	0.19	36.7	30.6	0.003	-0.000
1.00	12.71	0.006	0.018	0.141	0.006	0.343	0.02	0.059	7.22	0.35	43.08	2.46	49	2.4	0.002	0.000
1.50	8.392	0.004	0.015	0.063	0.002	0.348	0.004	0.088	7.43	0.1	11.53	9.07	50.4	0.7	0.000	0.000
1.75	7.796	0.004	0.015	0.053	0.002	0.374	0.001	0.211	7.53	0.09	3.49	9.21	51	0.6	0.000	0.000
2.00	7.705	0.004	0.015	0.062	0.002	0.443	0.001	0.331	7.52	0.09	2.43	8.90	51	0.6	0.001	0.000
2.25	7.695	0.004	0.015	0.056	0.002	0.282	0.001	0.369	7.56	0.1	1.85	9.62	51.2	0.7	0.004	0.000
2.75	7.922	0.006	0.015	0.155	0.004	0.448	0.002	0.491	7.68	0.25	2.80	3.15	52.1	1.7	0.002	0.000
3.25	7.739	0.005	0.015	0.065	0.002	0.387	0.001	0.394	7.57	0.12	2.26	7.23	51.3	0.8	0.000	0.000
3.75	7.726	0.005	0.015	0.069	0.002	0.36	0.001	0.465	7.55	0.15	2.38	6.70	51.1	1	0.002	0.000
4.25	7.694	0.005	0.015	0.064	0.002	0.39	0.001	0.444	7.59	0.11	1.41	8.23	51.5	0.8	0.000	0.000
4.75	7.736	0.005	0.015	0.082	0.002	0.393	0.001	0.386	7.53	0.13	2.61	5.94	51.1	0.9	0.000	0.000
5.50	7.718	0.005	0.015	0.067	0.002	0.426	0.001	0.437	7.55	0.12	2.26	6.53	51.1	0.8	0.002	0.000
6.50	7.728	0.004	0.015	0.072	0.002	0.312	0.001	0.422	7.62	0.11	1.46	7.06	51.6	0.8	0.002	0.000
7.50	7.644	0.003	0.015	0.04	0.006	0.077	0.001	0.322	7.54	0.06	1.54	15.72	51.1	0.4	0.035	0.000
DC186-1B	Biotite	100-250um	J= 0.003748±0.000022													
0.50	40.956	0.027	0.074	0.253	0.079	0.225	0.134	0.089	2.69	3.43	93.22	0.23	18.1	22.9	0.170	0.007
1.00	12.879	0.01	0.046	0.072	0.012	0.191	0.021	0.082	7.11	0.51	44.07	1.66	47.5	3.3	0.009	0.006
1.50	9.117	0.005	0.046	0.031	0.003	0.222	0.006	0.108	7.58	0.18	16.63	6.36	50.5	1.2	0.008	0.007
1.75	8.593	0.006	0.046	0.032	0.003	0.174	0.004	0.116	7.58	0.14	11.52	6.41	50.5	0.9	0.004	0.007
2.00	8.85	0.005	0.046	0.042	0.004	0.208	0.004	0.141	7.71	0.19	12.50	4.88	51.4	1.2	0.010	0.007
2.25	8.445	0.006	0.045	0.041	0.004	0.199	0.003	0.208	7.69	0.19	8.41	4.58	51.3	1.2	0.006	0.007
2.50	8.212	0.006	0.047	0.036	0.004	0.194	0.002	0.223	7.71	0.14	5.76	5.72	51.4	0.9	0.012	0.007
3.00	8.209	0.005	0.047	0.038	0.004	0.178	0.002	0.295	7.8	0.16	4.50	4.90	52	1.1	0.007	0.007
3.50	8.011	0.004	0.047	0.024	0.003	0.156	0.001	0.203	7.73	0.08	3.32	9.13	51.5	0.5	0.011	0.008
4.00	8.17	0.006	0.047	0.039	0.004	0.199	0.002	0.357	7.77	0.19	4.39	5.01	51.8	1.3	0.013	0.007
5.00	7.977	0.005	0.046	0.034	0.005	0.133	0.001	0.262	7.65	0.1	3.84	7.82	51	0.7	0.025	0.007

Watts	40Ar/39Ar	±	38Ar/39Ar	±	37Ar/39Ar	±	36Ar/39Ar	±	40Ar*/39ArK	±	%40Ar atm	% 39Ar	Age	±	Ca/K	Cl/K
6.00	7.851	0.004	0.046	0.029	0.004	0.125	0.001	0.31	7.68	0.08	2.05	9.91	51.2	0.5	0.020	0.007
7.00	7.907	0.005	0.046	0.032	0.006	0.141	0.001	0.424	7.69	0.13	2.40	6.59	51.3	0.8	0.029	0.007
8.00	7.762	0.004	0.047	0.024	0.002	0.223	0	0.255	7.67	0.05	1.33	26.79	51.1	0.3	0.012	0.007
DC186-2B Biotite HP J= 0.003643±0.000016																
0.50	160.471	0.036	0.193	0.13	0.098	0.245	0.556	0.052	2.07	6.28	98.70	0.10	13.6	41	0.533	0.016
1.00	19.502	0.01	0.056	0.061	0.014	0.184	0.042	0.046	7.56	0.58	61.15	1.16	49	3.7	0.119	0.008
1.25	9.892	0.007	0.049	0.035	0.005	0.194	0.008	0.055	7.71	0.14	21.99	2.96	49.9	0.9	0.036	0.008
1.50	8.523	0.006	0.049	0.037	0.002	0.226	0.003	0.096	7.79	0.09	8.60	4.34	50.5	0.6	0.015	0.008
1.75	8.716	0.006	0.049	0.029	0.002	0.268	0.003	0.065	7.79	0.08	10.71	5.68	50.5	0.5	0.011	0.008
2.00	8.238	0.006	0.05	0.03	0.002	0.239	0.002	0.114	7.8	0.08	5.28	4.85	50.6	0.5	0.010	0.008
2.25	8.13	0.005	0.049	0.024	0.002	0.263	0.001	0.135	7.81	0.07	3.91	4.77	50.6	0.4	0.012	0.008
2.50	8.12	0.005	0.051	0.026	0.002	0.264	0.001	0.151	7.83	0.07	3.57	5.27	50.7	0.4	0.011	0.008
2.75	8.112	0.005	0.05	0.048	0.002	0.273	0.001	0.216	7.86	0.09	3.01	3.40	50.9	0.6	0.011	0.008
3.00	8.149	0.006	0.051	0.042	0.003	0.279	0.001	0.191	7.88	0.08	3.12	3.60	51.1	0.5	0.014	0.008
3.50	8.075	0.005	0.05	0.036	0.002	0.238	0.001	0.175	7.83	0.07	2.98	5.05	50.8	0.4	0.014	0.008
4.00	7.985	0.005	0.049	0.036	0.002	0.23	0.001	0.249	7.85	0.07	1.64	4.53	50.9	0.4	0.014	0.008
4.50	8.069	0.005	0.049	0.033	0.003	0.232	0.001	0.237	7.87	0.08	2.29	3.81	51	0.5	0.014	0.008
5.00	7.978	0.005	0.049	0.031	0.002	0.249	0.001	0.249	7.84	0.07	1.65	4.63	50.8	0.4	0.017	0.008
5.50	7.958	0.006	0.049	0.035	0.002	0.292	0.001	0.239	7.85	0.06	1.35	5.89	50.9	0.4	0.008	0.008
6.00	7.909	0.006	0.049	0.03	0.001	0.371	0.001	0.287	7.81	0.07	1.30	7.44	50.6	0.4	0.003	0.008
6.50	7.922	0.005	0.049	0.03	0.001	0.348	0.001	0.307	7.83	0.06	1.14	5.51	50.7	0.4	0.002	0.008
7.00	7.904	0.004	0.051	0.026	0.001	0.382	0	0.264	7.82	0.05	1.21	27.01	50.7	0.3	0.006	0.008
DC191-1 Biotite HP J= 0.003670±0.000016																
0.50	56.482	0.018	0.052	0.178	0.019	0.472	0.175	0.047	7.07	2.26	87.41	0.85	46.2	14.6	0.000	0.001
1.00	11.933	0.006	0.018	0.049	0.001	0.408	0.015	0.04	7.84	0.18	34.30	12.58	51.2	1.2	0.001	0.000
1.25	8.765	0.005	0.016	0.05	0.001	0.455	0.003	0.077	7.83	0.09	10.61	17.94	51.1	0.6	0.000	0.000
1.50	8.465	0.006	0.016	0.096	0.001	0.397	0.002	0.104	7.9	0.09	6.49	11.72	51.6	0.6	0.000	0.000
1.75	8.639	0.007	0.016	0.095	0.003	0.398	0.003	0.153	7.96	0.15	7.29	5.94	51.9	0.9	0.000	0.000
2.00	8.951	0.009	0.016	0.093	0.003	0.402	0.004	0.148	7.97	0.19	10.29	5.11	52	1.2	0.000	0.000
2.50	9.027	0.009	0.017	0.12	0.004	0.371	0.004	0.139	8.11	0.18	9.42	4.36	52.9	1.2	0.000	0.000
3.00	8.693	0.008	0.016	0.111	0.003	0.376	0.003	0.156	7.99	0.16	7.48	5.69	52.2	1	0.000	0.000
3.50	8.649	0.01	0.016	0.117	0.004	0.402	0.003	0.237	8.02	0.23	6.34	4.04	52.3	1.5	0.000	0.000
4.00	8.487	0.01	0.017	0.081	0.004	0.402	0.003	0.235	8.01	0.2	4.77	4.51	52.3	1.3	0.000	0.000
4.50	8.307	0.01	0.016	0.113	0.004	0.357	0.002	0.275	7.93	0.18	3.72	4.84	51.8	1.1	0.000	0.000
5.00	8.333	0.01	0.016	0.102	0.004	0.35	0.002	0.385	8	0.24	2.91	3.79	52.2	1.5	0.000	0.000
6.00	8.107	0.009	0.016	0.098	0.002	0.432	0.001	0.33	7.91	0.14	1.94	6.71	51.6	0.9	0.000	0.000
7.00	8.011	0.005	0.016	0.05	0.001	0.47	0.001	0.234	7.82	0.08	2.19	11.93	51	0.5	0.000	0.000
DC191-1 Biotite HP J= 0.003775±0.000018																
7.00	9.994	0.008	0.019	0.077	0.003	0.016	0.01	0.079	7.94	0.24	18.91	1.62	53.3	1.6	0.001	0.000

Watts	40Ar/39Ar	±	38Ar/39Ar	±	37Ar/39Ar	±	36Ar/39Ar	±	40Ar*/39ArK	±	%40Ar atm	% 39Ar	Age	±	Ca/K	Cl/K
7.00	9.015	0.006	0.017	0.056	0	0.006	0.005	0.06	7.76	0.1	13.42	11.61	52.1	0.6	0.001	0.000
7.00	9.501	0.005	0.018	0.042	0.001	0.008	0.007	0.059	7.7	0.12	18.42	7.50	51.7	0.8	0.001	0.000
7.00	10.09	0.005	0.018	0.04	0	0.006	0.009	0.053	7.65	0.14	23.84	13.13	51.3	0.9	0.001	0.000
7.00	9.919	0.006	0.018	0.049	0.001	0.007	0.008	0.054	7.7	0.14	21.95	10.37	51.7	0.9	0.001	0.000
7.00	10.762	0.005	0.018	0.051	0.001	0.006	0.012	0.05	7.63	0.18	28.59	5.84	51.2	1.2	0.001	0.000
0.50	22.14	0.014	0.033	0.113	0.013	0.014	0.062	0.059	7.66	1.09	64.50	0.40	51.4	7.2	0.001	0.000
1.00	9.533	0.007	0.019	0.073	0.003	0.013	0.009	0.081	7.79	0.22	16.56	1.68	52.3	1.5	0.001	0.000
7.00	8.628	0.005	0.018	0.041	0.001	0.005	0.004	0.074	7.71	0.11	9.47	3.52	51.8	0.7	0.001	0.000
0.50	71.407	0.018	0.073	0.128	0.02	0.018	0.246	0.034	4.95	2.21	93.09	0.26	33.4	14.8	0.001	0.001
1.00	15.196	0.007	0.022	0.056	0.002	0.007	0.028	0.032	7.49	0.27	50.28	3.06	50.3	1.8	0.001	0.000
2.00	9.634	0.006	0.017	0.059	0.001	0.007	0.007	0.054	7.65	0.13	20.13	11.10	51.4	0.8	0.001	0.000
3.00	8.612	0.005	0.017	0.055	0.001	0.005	0.004	0.088	7.75	0.1	9.34	7.04	52	0.7	0.001	0.000
7.00	8.254	0.005	0.017	0.045	0	0.007	0.002	0.09	7.68	0.07	6.48	22.85	51.6	0.5	0.001	0.001

DC193 Biotite HP J= 0.003702±0.000018

0.50	45.421	0.075	0.063	0.706	0.201	0.356	0.155	0.252	11.47	11.49	72.27	0.33	75	73.6	0.525	0.002
1.00	10.699	0.013	0.016	0.129	0.007	0.336	0.011	0.129	7.89	0.44	24.92	8.30	52	2.9	0.000	-0.000
1.50	7.973	0.008	0.015	0.085	0.003	0.34	0.001	0.312	7.82	0.13	1.16	22.34	51.5	0.8	0.000	0.000
1.75	8.013	0.011	0.015	0.154	0.005	0.332	0.002	0.442	7.86	0.24	0.39	12.11	51.7	1.6	0.000	-0.000
2.00	8.163	0.015	0.015	0.189	0.009	0.299	0.003	0.443	7.94	0.36	0.09	7.30	52.3	2.3	0.006	0.000
2.50	8.479	0.021	0.016	0.308	0.018	0.375	0.005	0.467	7.92	0.72	0.72	3.27	52.1	4.7	0.000	-0.000
3.00	8.222	0.014	0.015	0.214	0.011	0.312	0.003	0.515	7.74	0.54	2.47	5.62	51	3.5	0.000	0.000
4.00	8.035	0.012	0.015	0.165	0.005	0.317	0.002	0.447	7.87	0.24	0.58	12.19	51.8	1.6	0.000	0.000
5.00	7.969	0.012	0.015	0.104	0.005	0.414	0.001	0.504	7.81	0.23	0.66	13.71	51.4	1.5	0.000	-0.000
7.00	7.982	0.01	0.014	0.129	0.004	0.302	0.001	0.502	7.88	0.2	0.16	14.83	51.9	1.3	0.000	-0.000

DC299 Biotite >250um J= 0.003814±0.000030

0.50	158.86	0.027	0.126	0.175	0.07	0.231	0.559	0.042	-0.18	5.45	100.09	0.17	-1.2	37.5	0.000	-0.002
1.00	35.977	0.015	0.038	0.174	0.028	0.217	0.111	0.05	4.97	1.59	86.04	0.56	33.9	10.8	0.051	0.001
1.50	12.976	0.007	0.019	0.092	0.008	0.164	0.021	0.055	7.09	0.35	44.99	2.33	48.1	2.4	0.022	0.000
1.75	10.169	0.006	0.016	0.071	0.005	0.362	0.01	0.079	7.53	0.23	25.59	3.53	51.1	1.6	0.008	0.000
2.00	8.966	0.005	0.016	0.081	0.004	0.25	0.005	0.086	7.67	0.13	14.22	4.92	52	0.9	0.014	0.000
2.25	8.795	0.005	0.016	0.07	0.004	0.204	0.004	0.121	7.72	0.15	11.88	4.71	52.4	1	0.011	0.000
2.50	8.575	0.005	0.015	0.087	0.003	0.208	0.003	0.121	7.77	0.12	9.17	5.97	52.7	0.8	0.010	0.000
3.00	8.327	0.004	0.015	0.039	0.002	0.183	0.002	0.107	7.7	0.08	7.48	10.12	52.2	0.5	0.009	0.000
3.50	8.239	0.004	0.015	0.049	0.002	0.18	0.002	0.136	7.77	0.09	5.56	8.24	52.7	0.6	0.006	0.000
4.00	8.191	0.004	0.015	0.061	0.002	0.157	0.002	0.138	7.74	0.08	5.40	9.30	52.5	0.5	0.005	0.000
4.50	8.223	0.004	0.015	0.074	0.002	0.257	0.002	0.166	7.71	0.1	6.01	6.86	52.3	0.7	0.004	0.000
5.00	8.127	0.004	0.015	0.05	0.002	0.223	0.001	0.191	7.76	0.09	4.40	8.52	52.6	0.6	0.004	0.000
6.00	8.002	0.004	0.015	0.044	0.002	0.176	0.001	0.165	7.74	0.06	3.25	12.34	52.5	0.4	0.006	0.000
7.00	7.971	0.004	0.015	0.051	0.002	0.214	0.001	0.261	7.75	0.08	2.63	7.66	52.6	0.6	0.004	0.000
8.00	7.851	0.003	0.015	0.047	0.003	0.162	0.001	0.24	7.69	0.05	2.07	14.77	52.2	0.3	0.018	0.000

Watts	40Ar/39Ar	±	38Ar/39Ar	±	37Ar/39Ar	±	36Ar/39Ar	±	40Ar*/39ArK	±	%40Ar atm	% 39Ar	Age	±	Ca/K	Cl/K	
DC326	Biotite	>250um	J= 0.003759±0.000022														
0.50	87.188	0.026	0.08	0.228	0.063	0.431	0.305	0.045	3.21	3.45	96.30	0.10	21.6	23.1	0.135	-0.000	
1.00	27.085	0.011	0.03	0.132	0.011	0.385	0.072	0.038	7.28	0.79	72.89	0.52	48.7	5.2	0.023	0.000	
1.50	10.207	0.005	0.017	0.057	0.002	0.339	0.009	0.045	7.79	0.12	23.48	3.37	52.1	0.8	0.004	0.000	
2.00	8.667	0.004	0.016	0.044	0.001	0.373	0.003	0.072	7.81	0.07	9.85	7.28	52.2	0.5	0.000	0.000	
2.25	8.293	0.004	0.016	0.039	0.001	0.356	0.002	0.084	7.82	0.06	5.61	6.73	52.3	0.4	0.002	0.000	
2.50	8.072	0.004	0.016	0.04	0.001	0.417	0.001	0.189	7.85	0.07	2.70	6.68	52.5	0.4	0.000	0.000	
2.75	7.982	0.004	0.015	0.05	0.001	0.365	0.001	0.273	7.87	0.07	1.34	5.62	52.6	0.5	0.001	0.000	
3.00	7.995	0.004	0.015	0.046	0.001	0.437	0.001	0.294	7.9	0.07	0.94	4.84	52.8	0.4	0.002	0.000	
3.25	8.014	0.004	0.015	0.055	0.001	0.468	0.001	0.33	7.94	0.08	0.67	3.97	53	0.5	0.002	0.000	
3.50	8.112	0.004	0.015	0.068	0.002	0.275	0.001	0.365	7.93	0.12	1.84	3.04	53	0.8	0.003	0.000	
4.00	8.094	0.005	0.015	0.075	0.002	0.42	0.001	0.365	7.95	0.11	1.31	3.17	53.2	0.7	0.001	0.000	
5.00	8.063	0.004	0.016	0.056	0.001	0.278	0.001	0.204	7.87	0.07	2.27	5.11	52.6	0.4	0.003	0.000	
6.00	8.047	0.003	0.015	0.038	0.001	0.435	0.001	0.187	7.9	0.05	1.81	7.20	52.8	0.3	0.002	0.000	
7.00	7.986	0.004	0.015	0.036	0	0.495	0.001	0.352	7.85	0.07	1.79	12.58	52.5	0.5	0.000	0.000	
8.00	7.966	0.004	0.015	0.041	0	1.62	0	0.321	7.87	0.05	1.43	29.81	52.6	0.3	0.000	0.000	
DC330	Biotite	>250um	J= 0.003763±0.000024														
0.50	76.804	0.025	0.08	0.173	0.045	0.416	0.26	0.054	4.82	3.73	93.66	0.12	32.5	24.9	0.044	0.005	
1.00	11.662	0.148	0.025	0.159	0.003	0.432	0.017	0.157	6.85	1.08	40.91	1.71	45.9	7.1	0.004	0.002	
1.25	9.319	0.006	0.024	0.055	0.003	0.42	0.006	0.103	7.81	0.19	15.78	2.11	52.2	1.2	0.005	0.002	
1.50	8.765	0.004	0.025	0.04	0.002	0.257	0.004	0.072	7.74	0.09	11.51	4.18	51.8	0.6	0.006	0.002	
1.75	8.792	0.004	0.025	0.027	0.002	0.292	0.004	0.062	7.74	0.08	11.87	5.30	51.8	0.5	0.005	0.002	
2.00	8.283	0.004	0.024	0.036	0.001	0.331	0.002	0.126	7.75	0.08	6.29	4.88	51.9	0.6	0.003	0.002	
2.25	8.891	0.004	0.024	0.045	0.002	0.346	0.004	0.085	7.8	0.11	12.16	3.75	52.2	0.8	0.002	0.002	
2.50	8.289	0.004	0.024	0.047	0.002	0.442	0.002	0.137	7.79	0.09	5.74	3.71	52.2	0.6	0.001	0.002	
2.75	8.252	0.004	0.025	0.042	0.001	0.595	0.002	0.148	7.81	0.09	5.19	3.91	52.3	0.6	0.002	0.002	
3.00	8.038	0.004	0.024	0.04	0.002	0.399	0.001	0.324	7.86	0.11	2.03	3.77	52.6	0.7	0.002	0.002	
3.25	8.032	0.004	0.024	0.041	0.002	0.363	0.001	0.271	7.83	0.09	2.27	3.45	52.4	0.6	0.001	0.002	
3.50	8.065	0.004	0.024	0.045	0.002	0.371	0.001	0.422	7.9	0.15	1.62	2.57	52.8	1	0.002	0.002	
4.00	7.971	0.004	0.024	0.036	0.001	0.446	0.001	0.308	7.85	0.09	1.35	3.94	52.5	0.6	0.000	0.002	
5.00	7.946	0.003	0.024	0.032	0.001	0.507	0.001	0.217	7.8	0.05	1.92	10.00	52.2	0.4	0.001	0.002	
6.00	7.91	0.004	0.024	0.031	0.001	0.396	0.001	0.222	7.81	0.04	1.37	11.44	52.3	0.3	0.002	0.002	
7.00	8.086	0.003	0.024	0.034	0.001	0.51	0.001	0.114	7.76	0.05	4.18	14.87	51.9	0.3	0.002	0.002	
8.00	7.865	0.003	0.024	0.033	0.001	0.317	0	0.394	7.81	0.05	0.94	20.26	52.2	0.3	0.005	0.002	
DC395	Biotite	HP	J= 0.003703±0.000016														
0.50	45.373	0.048	0.178	0.18	0.107	0.326	0.158	0.142	4.44	6.42	89.68	0.10	29.4	42.2	0.024	0.030	
1.00	19.969	0.014	0.194	0.043	0.008	0.333	0.044	0.054	7.79	0.69	60.72	1.46	51.3	4.5	0.002	0.039	
1.25	9.662	0.006	0.199	0.016	0.002	0.355	0.007	0.062	7.76	0.14	19.52	7.16	51.1	0.9	0.000	0.042	
1.50	8.026	0.005	0.197	0.015	0.001	0.41	0.001	0.145	7.73	0.07	3.77	16.12	50.9	0.4	0.000	0.042	
1.75	7.865	0.005	0.201	0.016	0.001	0.422	0.001	0.143	7.64	0.06	2.85	14.59	50.3	0.4	0.001	0.043	
2.00	7.905	0.006	0.19	0.021	0.001	0.366	0.001	0.242	7.72	0.09	2.12	7.64	50.9	0.6	0.000	0.040	

Watts	40Ar/39Ar	±	38Ar/39Ar	±	37Ar/39Ar	±	36Ar/39Ar	±	40Ar*/39ArK	±	%40Ar atm	% 39Ar	Age	±	Ca/K	Cl/K
2.50	7.983	0.006	0.195	0.018	0.002	0.289	0.001	0.265	7.76	0.11	2.45	6.29	51.1	0.7	0.000	0.041
3.00	8.04	0.004	0.196	0.014	0.001	0.436	0.001	0.139	7.75	0.06	3.69	17.47	51	0.4	0.000	0.041
3.50	8.018	0.008	0.198	0.023	0.003	0.289	0.001	0.299	7.79	0.14	2.19	3.97	51.3	0.9	0.000	0.042
4.00	7.983	0.007	0.2	0.023	0.002	0.281	0.001	0.317	7.73	0.14	2.62	4.44	50.9	0.9	0.000	0.042
4.50	7.902	0.007	0.2	0.018	0.002	0.367	0.001	0.294	7.74	0.12	1.51	4.55	51	0.8	0.000	0.043
5.00	7.97	0.008	0.197	0.029	0.003	0.384	0.001	0.437	7.84	0.17	0.80	3.38	51.6	1.1	0.001	0.042
5.50	7.858	0.008	0.202	0.018	0.002	0.407	0.001	0.398	7.73	0.13	1.17	5.14	50.9	0.8	0.000	0.043
6.00	7.989	0.01	0.197	0.031	0.004	0.318	0.002	0.321	7.82	0.17	1.04	2.65	51.5	1.1	0.001	0.042
7.00	7.934	0.008	0.195	0.021	0.002	0.38	0.001	0.305	7.74	0.12	2.05	5.06	50.9	0.8	0.000	0.041
DC398-1 Biotite 1x3mm J= 0.003771±0.000024																
0.50	120.508	0.036	0.21	0.16	0.102	0.316	0.411	0.065	4.81	6.86	96.03	0.07	32.4	45.9	0.000	0.026
1.00	35.001	0.008	0.174	0.029	0.005	0.438	0.1	0.021	6.48	0.6	81.47	1.43	43.6	4	0.000	0.032
1.50	9.585	0.004	0.164	0.011	0.001	0.314	0.008	0.033	7.44	0.08	22.42	8.48	49.9	0.6	0.000	0.034
1.75	7.895	0.003	0.165	0.014	0.001	0.443	0.002	0.119	7.5	0.06	5.12	9.72	50.3	0.4	0.001	0.034
2.00	7.749	0.004	0.164	0.01	0.001	0.442	0.001	0.136	7.5	0.05	3.30	9.74	50.3	0.3	0.000	0.034
2.25	7.7	0.004	0.165	0.011	0.001	0.324	0.001	0.197	7.52	0.06	2.40	8.10	50.4	0.4	0.000	0.034
2.50	7.69	0.004	0.164	0.012	0.001	0.295	0.001	0.309	7.52	0.08	2.23	6.53	50.4	0.5	0.000	0.034
2.75	7.711	0.004	0.165	0.013	0.001	0.255	0.001	0.384	7.58	0.09	1.62	5.23	50.8	0.6	0.000	0.034
3.25	7.761	0.004	0.166	0.014	0.002	0.316	0.001	0.303	7.61	0.09	1.71	4.62	51.1	0.6	0.000	0.035
4.00	7.736	0.004	0.163	0.012	0.001	0.226	0.001	0.282	7.56	0.08	2.19	5.74	50.7	0.5	0.000	0.034
5.00	7.672	0.004	0.165	0.012	0.001	0.415	0.001	0.29	7.57	0.06	1.37	7.98	50.8	0.4	0.000	0.034
6.00	7.637	0.004	0.164	0.013	0.001	0.421	0	0.256	7.54	0.05	1.37	14.02	50.6	0.3	0.000	0.034
7.00	7.652	0.004	0.165	0.011	0.001	0.41	0.001	0.297	7.56	0.05	1.24	8.44	50.7	0.3	0.000	0.034
8.00	7.665	0.004	0.165	0.013	0.001	0.389	0.001	0.254	7.57	0.05	1.25	9.90	50.8	0.3	0.000	0.034
DC398-2 Biotite spots 2x2mm J= 0.003774±0.000026																
5.00	14.42	0.004	0.181	0.014	0.001	0.274	0.025	0.024	7.27	0.18	49.60	9.00	48.8	1.2	0.000	0.037
5.00	11.689	0.006	0.179	0.014	0.002	0.291	0.016	0.031	7.27	0.15	37.82	8.59	48.8	1	0.000	0.037
5.00	11.714	0.005	0.179	0.019	0.002	0.245	0.015	0.034	7.41	0.16	36.68	6.17	49.7	1.1	0.000	0.037
5.00	8.901	0.004	0.182	0.009	0.001	0.646	0.005	0.038	7.48	0.07	16.03	25.93	50.3	0.4	0.001	0.038
5.00	8.737	0.004	0.179	0.012	0.001	0.419	0.005	0.054	7.45	0.08	14.82	20.20	50	0.5	0.000	0.038
5.00	7.946	0.004	0.181	0.012	0.001	0.554	0.002	0.122	7.49	0.07	5.91	30.10	50.3	0.5	0.001	0.038
DC418 Biotite HP J= 0.003704±0.000016																
0.50	100.718	0.035	0.103	0.211	0.064	0.378	0.341	0.067	6.82	5.81	93.14	0.20	45	37.9	0.000	0.006
1.00	18.028	0.006	0.044	0.047	0.002	0.324	0.037	0.035	7.46	0.39	58.61	6.82	49.2	2.5	0.000	0.005
1.25	9.923	0.006	0.038	0.04	0.002	0.281	0.008	0.05	7.69	0.13	22.40	9.92	50.7	0.9	0.001	0.005
1.50	8.885	0.007	0.038	0.084	0.003	0.36	0.004	0.116	7.77	0.16	12.15	5.56	51.2	1.1	0.002	0.005
1.75	8.576	0.006	0.036	0.045	0.002	0.369	0.003	0.115	7.76	0.12	9.33	8.66	51.1	0.8	0.000	0.005
2.00	8.39	0.005	0.035	0.032	0.001	0.358	0.003	0.097	7.7	0.09	8.16	13.87	50.7	0.6	0.001	0.005
2.25	8.279	0.008	0.035	0.063	0.002	0.326	0.002	0.222	7.84	0.15	4.84	5.57	51.6	1	0.000	0.005

Watts	40Ar/39Ar	±	38Ar/39Ar	±	37Ar/39Ar	±	36Ar/39Ar	±	40Ar*/39ArK	±	%40Ar atm	% 39Ar	Age	±	Ca/K	Cl/K
2.50	8.807	0.01	0.037	0.061	0.004	0.295	0.004	0.17	7.83	0.22	10.25	3.77	51.6	1.4	0.000	0.005
3.00	8.486	0.009	0.036	0.067	0.003	0.309	0.003	0.158	7.8	0.16	7.43	4.95	51.4	1	0.000	0.005
3.50	8.389	0.008	0.036	0.053	0.003	0.309	0.003	0.169	7.78	0.14	6.63	5.37	51.3	0.9	0.000	0.005
4.00	8.422	0.007	0.036	0.047	0.002	0.286	0.003	0.145	7.8	0.13	7.06	7.16	51.4	0.8	0.001	0.005
4.50	8.411	0.007	0.037	0.068	0.003	0.337	0.003	0.172	7.79	0.15	6.85	5.31	51.3	1	0.000	0.005
5.00	8.484	0.008	0.035	0.054	0.002	0.472	0.003	0.154	7.75	0.15	8.25	5.97	51	1	0.000	0.005
5.50	8.586	0.012	0.035	0.104	0.006	0.26	0.004	0.293	7.91	0.32	6.40	2.46	52.1	2.1	0.000	0.005
6.00	8.596	0.009	0.035	0.09	0.004	0.365	0.004	0.218	7.74	0.24	9.11	3.70	51	1.6	0.002	0.005
7.00	8.181	0.006	0.034	0.045	0.001	0.381	0.002	0.141	7.72	0.09	5.45	10.72	50.9	0.6	0.000	0.004
DC439 Biotite >250um J= 0.003784±0.000026																
0.50	78.584	0.024	0.085	0.254	0.055	0.238	0.263	0.069	4.71	5.06	93.87	0.17	31.9	34	0.120	0.005
1.00	10.966	0.005	0.035	0.044	0.003	0.356	0.012	0.063	7.78	0.22	28.68	3.14	52.4	1.5	0.005	0.004
1.50	8.418	0.003	0.034	0.025	0.001	0.586	0.003	0.09	7.74	0.07	8.10	14.05	52.1	0.5	0.000	0.004
1.75	8.037	0.004	0.033	0.041	0.001	0.285	0.001	0.235	7.81	0.08	2.68	7.34	52.5	0.6	0.002	0.004
2.00	7.909	0.004	0.033	0.025	0.001	0.296	0.001	0.307	7.77	0.08	1.70	8.52	52.3	0.5	0.003	0.004
2.25	7.931	0.003	0.033	0.027	0.001	0.269	0.001	0.233	7.74	0.07	2.39	9.47	52.1	0.4	0.001	0.004
2.50	8.006	0.005	0.033	0.048	0.003	0.205	0.001	0.657	7.79	0.2	2.15	3.50	52.4	1.3	0.006	0.004
3.00	7.868	0.003	0.033	0.03	0.001	0.237	0.001	0.481	7.76	0.09	1.22	7.45	52.2	0.6	0.003	0.004
3.50	7.758	0.013	0.033	0.139	0.002	1.878	0	0.913	7.71	0.14	0.40	6.72	51.9	1	0.006	0.004
4.00	7.849	0.004	0.033	0.026	0.001	0.229	0.001	0.528	7.76	0.09	0.98	7.92	52.2	0.6	0.003	0.004
4.50	7.86	0.004	0.033	0.03	0.001	0.342	0.001	0.479	7.79	0.09	0.75	7.34	52.4	0.6	0.001	0.004
5.00	7.9	0.004	0.033	0.029	0.002	0.282	0.001	0.457	7.75	0.1	1.64	6.28	52.2	0.7	0.005	0.004
6.00	7.871	0.005	0.034	0.027	0.002	0.176	0.001	0.466	7.77	0.09	1.13	8.22	52.3	0.6	0.009	0.004
7.00	7.92	0.004	0.033	0.036	0.006	0.116	0.001	0.578	7.75	0.13	1.78	5.11	52.1	0.9	0.035	0.004
8.00	8.017	0.005	0.033	0.041	0.019	0.049	0.001	0.473	7.84	0.13	1.84	4.77	52.7	0.9	0.140	0.004
DC450 Biotite 4x3mm J= 0.003789±0.000026																
0.50	216.397	0.027	0.186	0.115	0.061	0.369	0.743	0.037	6.2	5.8	97.13	0.57	41.9	38.7	0.079	0.009
1.00	12.402	0.006	0.048	0.041	0.003	0.438	0.016	0.044	7.98	0.22	35.41	11.32	53.7	1.5	0.000	0.007
1.50	9.326	0.005	0.046	0.037	0.002	0.404	0.005	0.079	7.98	0.13	14.13	17.35	53.7	0.9	0.002	0.007
1.75	9.779	0.006	0.046	0.06	0.004	0.447	0.007	0.135	8.22	0.27	15.15	8.23	55.3	1.8	0.006	0.007
2.00	9.229	0.008	0.046	0.071	0.005	0.487	0.005	0.225	8.24	0.35	9.20	5.61	55.5	2.3	0.000	0.007
2.50	8.876	0.007	0.046	0.047	0.004	0.402	0.003	0.207	8.14	0.22	7.46	9.63	54.8	1.5	0.000	0.007
3.00	8.845	0.006	0.045	0.056	0.004	0.38	0.003	0.213	8.23	0.23	6.02	9.00	55.4	1.5	0.000	0.007
3.50	8.756	0.007	0.046	0.048	0.004	0.471	0.003	0.301	8.19	0.29	5.24	7.18	55.1	1.9	0.000	0.007
4.00	10.201	0.008	0.046	0.067	0.006	0.426	0.009	0.141	8.14	0.37	18.98	5.59	54.8	2.4	0.001	0.007
5.00	8.962	0.007	0.047	0.053	0.005	0.357	0.004	0.215	8.16	0.27	7.93	7.85	54.9	1.8	0.002	0.007
6.00	8.873	0.007	0.046	0.06	0.005	0.357	0.004	0.278	8.23	0.3	5.85	6.42	55.4	2	0.001	0.007
7.00	8.93	0.009	0.045	0.081	0.009	0.354	0.005	0.333	7.99	0.47	8.33	4.33	53.8	3.1	0.006	0.007
8.00	8.671	0.007	0.043	0.057	0.005	0.398	0.003	0.295	8.12	0.28	4.95	6.92	54.7	1.8	0.003	0.007
DC468 Biotite 200-250um J= 0.003795±0.000024																

Watts	40Ar/39Ar	±	38Ar/39Ar	±	37Ar/39Ar	±	36Ar/39Ar	±	40Ar*/39ArK	±	%40Ar atm	% 39Ar	Age	±	Ca/K	Cl/K
0.50	50.768	0.038	0.073	0.397	0.113	0.31	0.18	0.11	5.43	5.77	88.91	0.12	36.8	38.7	0.254	0.001
1.00	14.094	0.013	0.032	0.167	0.032	0.249	0.029	0.111	6.97	0.97	48.79	0.74	47.1	6.5	0.126	0.002
1.50	9.298	0.005	0.026	0.054	0.007	0.153	0.007	0.066	7.51	0.14	18.71	4.84	50.7	1	0.037	0.002
2.00	10.539	0.003	0.026	0.03	0.003	0.168	0.011	0.031	7.58	0.1	28.03	10.70	51.2	0.7	0.021	0.002
2.25	7.906	0.004	0.024	0.036	0.004	0.156	0.001	0.214	7.69	0.08	2.37	7.22	51.9	0.5	0.018	0.002
2.50	7.895	0.005	0.024	0.047	0.003	0.189	0.001	0.308	7.74	0.09	1.56	6.98	52.2	0.6	0.015	0.002
2.75	7.976	0.005	0.024	0.059	0.004	0.226	0.001	0.387	7.85	0.15	0.88	5.00	53	1	0.016	0.002
3.25	7.907	0.004	0.024	0.056	0.003	0.217	0.001	0.311	7.76	0.09	1.44	6.96	52.4	0.6	0.012	0.002
4.00	7.814	0.004	0.024	0.037	0.002	0.217	0.001	0.241	7.69	0.06	1.32	10.76	51.9	0.4	0.010	0.002
5.00	7.796	0.004	0.024	0.038	0.002	0.22	0.001	0.248	7.69	0.06	1.20	11.47	51.9	0.4	0.010	0.002
6.00	7.766	0.003	0.024	0.039	0.003	0.203	0.001	0.256	7.67	0.06	1.13	12.09	51.7	0.4	0.016	0.002
7.00	7.794	0.004	0.024	0.032	0.002	0.166	0.001	0.253	7.68	0.06	1.32	10.50	51.8	0.4	0.010	0.002
8.00	7.806	0.004	0.024	0.035	0.006	0.076	0.001	0.208	7.67	0.06	1.57	12.61	51.8	0.4	0.044	0.002
DC532	Biotite	>250um	J= 0.002707±0.000012													
2.00	222.072	0.088	0.221	0.298	0.459	0.364	0.81	0.117	3.04	21.63	98.56	0.04	14.8	104.8	0.293	0.001
2.20	129.466	0.098	0.148	0.373	0.367	0.287	0.468	0.149	8.46	17.65	92.34	0.05	40.8	84.3	0.000	0.006
2.40	36.711	0.027	0.042	0.204	0.037	0.253	0.092	0.075	11.17	1.97	67.46	0.56	53.7	9.3	0.067	0.002
2.50	27.435	0.019	0.035	0.155	0.025	0.291	0.056	0.083	12.06	1.39	52.92	0.76	58	6.6	0.022	0.002
2.60	18.173	0.017	0.027	0.151	0.016	0.224	0.023	0.095	12.09	0.69	29.25	1.31	58.1	3.3	0.000	0.002
2.70	15.423	0.011	0.025	0.106	0.011	0.25	0.013	0.106	12.07	0.43	17.67	1.88	58	2	0.010	0.002
2.80	15.611	0.014	0.026	0.108	0.012	0.261	0.015	0.123	11.73	0.58	20.33	1.64	56.4	2.7	0.002	0.002
2.90	14.986	0.016	0.025	0.138	0.014	0.257	0.013	0.136	11.81	0.55	15.45	1.47	56.8	2.6	0.000	0.002
3.10	14.583	0.013	0.025	0.099	0.011	0.279	0.011	0.14	11.93	0.47	13.44	1.84	57.4	2.2	0.018	0.002
3.30	15.981	0.018	0.027	0.153	0.016	0.219	0.016	0.108	11.75	0.57	21.16	1.35	56.5	2.7	0.017	0.002
3.60	14.233	0.191	0.021	0.265	0.013	0.293	0.016	0.21	10.07	2.16	24.38	1.61	48.5	10.3	0.029	0.001
3.90	21.179	0.014	0.03	0.135	0.015	0.265	0.036	0.068	11.49	0.73	43.00	1.37	55.2	3.5	0.015	0.002
4.10	21.798	0.018	0.032	0.162	0.022	0.313	0.039	0.091	11.64	1.05	42.24	0.87	56	5	0.000	0.002
4.40	19.403	0.007	0.026	0.057	0.003	0.238	0.027	0.03	11.66	0.25	39.29	7.56	56.1	1.2	0.009	0.002
4.70	15.216	0.008	0.023	0.058	0.003	0.218	0.012	0.052	11.83	0.21	21.05	6.27	56.9	1	0.000	0.002
5.10	13.927	0.005	0.023	0.06	0.001	0.422	0.007	0.059	11.87	0.14	14.34	23.74	57.1	0.7	0.003	0.002
5.50	12.827	0.006	0.021	0.046	0.001	0.601	0.003	0.079	11.93	0.11	6.71	44.26	57.3	0.5	0.008	0.002
6.00	13.75	0.009	0.023	0.101	0.008	0.281	0.006	0.157	12.31	0.3	6.85	2.76	59.2	1.4	0.027	0.002
7.00	23.037	0.021	0.03	0.188	0.03	0.292	0.032	0.126	15.07	1.26	28.15	0.67	72.1	5.9	0.000	0.002

TABLE C3: Muscovite thermochronology data

Watts	40Ar/39Ar	±	38Ar/39Ar	±	37Ar/39Ar	±	36Ar/39Ar	±	40Ar*/39ArK	±	%40Ar atm	% 39Ar	Age	±	Ca/K	Cl/K
DC058-1 Muscovite		HP		J= 0.003664±0.000016												
0.50	77.348	0.041	0.068	0.356	0.081	0.347	0.253	0.1	9.57	6.95	87.36	0.11	62.2	44.4	0.000	0.001
1.00	15.151	0.021	0.018	0.282	0.02	0.327	0.027	0.124	8.55	1	41.85	0.45	55.7	6.4	0.000	-0.000
1.50	20.275	0.02	0.022	0.188	0.012	0.342	0.045	0.078	8.02	1.03	59.96	0.75	52.3	6.6	0.000	-0.000
2.00	12.357	0.006	0.016	0.062	0.002	0.353	0.016	0.04	7.74	0.2	37.30	4.82	50.4	1.3	0.000	-0.000
2.50	9.744	0.005	0.015	0.065	0.001	0.438	0.007	0.05	7.74	0.11	20.59	10.29	50.5	0.7	0.000	-0.000
2.75	8.175	0.005	0.014	0.058	0	0.69	0.002	0.112	7.77	0.06	5.09	23.27	50.6	0.4	0.000	-0.000
3.00	8.158	0.005	0.014	0.062	0.001	0.426	0.002	0.105	7.79	0.06	4.56	10.02	50.7	0.4	0.000	-0.000
3.25	8.129	0.006	0.013	0.064	0.001	0.479	0.001	0.115	7.76	0.07	4.57	14.02	50.6	0.4	0.000	-0.000
3.50	8.002	0.006	0.014	0.06	0.001	0.43	0.001	0.178	7.78	0.07	2.62	7.50	50.7	0.5	0.000	-0.000
4.00	8.007	0.005	0.013	0.076	0.001	0.391	0.001	0.188	7.78	0.07	2.74	7.63	50.7	0.4	0.000	-0.000
4.50	8.208	0.008	0.014	0.097	0.003	0.373	0.002	0.206	7.84	0.14	3.91	3.04	51.1	0.9	0.002	-0.000
5.00	8.35	0.01	0.014	0.116	0.004	0.429	0.002	0.251	7.84	0.2	5.29	2.31	51.1	1.3	0.000	-0.000
6.00	8.163	0.007	0.013	0.092	0.003	0.336	0.002	0.258	7.87	0.14	3.03	3.14	51.3	0.9	0.001	-0.000
7.00	7.859	0.005	0.013	0.057	0.001	0.433	0	0.274	7.8	0.05	0.80	12.66	50.8	0.3	0.001	-0.000
DC295P Muscovite		HP		J= 0.003681±0.000018												
0.50	61.264	0.041	0.063	0.385	0.087	0.386	0.208	0.091	4.9	5.06	91.73	0.11	32.3	33	0.000	0.002
1.00	19.209	0.019	0.023	0.231	0.015	0.434	0.043	0.087	7.75	1.11	58.82	0.54	50.8	7.2	0.000	0.000
1.50	28.956	0.012	0.027	0.148	0.007	0.359	0.075	0.038	7.75	0.82	73.13	1.24	50.8	5.3	0.000	-0.000
2.00	9.862	0.006	0.015	0.069	0.001	0.461	0.007	0.055	7.85	0.13	20.35	7.22	51.4	0.8	0.000	-0.000
2.50	8.092	0.005	0.013	0.049	0	0.92	0.001	0.101	7.75	0.06	4.33	25.20	50.8	0.4	0.000	-0.000
2.75	8.351	0.005	0.014	0.055	0.001	0.387	0.002	0.093	7.82	0.07	6.33	11.37	51.2	0.5	0.001	-0.000
3.00	8.055	0.005	0.014	0.044	0.001	0.603	0.001	0.106	7.75	0.06	3.86	14.11	50.7	0.4	0.000	-0.000
3.25	7.893	0.006	0.013	0.082	0.001	0.549	0.001	0.239	7.75	0.07	1.74	9.30	50.7	0.5	0.000	-0.000
3.50	7.987	0.007	0.013	0.079	0.002	0.415	0.001	0.246	7.76	0.1	2.51	5.35	50.8	0.7	0.000	-0.000
4.00	7.987	0.006	0.014	0.087	0.002	0.35	0.001	0.215	7.79	0.09	2.22	5.54	51	0.6	0.000	-0.000
4.50	8.202	0.007	0.013	0.096	0.003	0.387	0.002	0.232	7.83	0.15	3.85	2.90	51.2	1	0.000	-0.000
5.50	8.012	0.007	0.014	0.073	0.002	0.419	0.001	0.27	7.8	0.11	2.21	4.16	51.1	0.7	0.000	-0.000
6.50	8.198	0.011	0.014	0.122	0.005	0.423	0.002	0.341	7.89	0.24	2.49	1.83	51.6	1.5	0.005	0.000
7.00	7.813	0.005	0.014	0.053	0.001	0.433	0	0.361	7.78	0.06	0.48	11.14	50.9	0.4	0.000	-0.000

Watts	40Ar/39Ar	±	38Ar/39Ar	±	37Ar/39Ar	±	36Ar/39Ar	±	40Ar*/39ArK	±	%40Ar atm	% 39Ar	Age	±	Ca/K	Cl/K
DC502	Muscovite	>250um	J= 0.002716±0.000014													
2.00	13.714	0.008	0.015	0.091	0.004	0.207	0.011	0.072	10.6	0.26	21.59	11.35	51.2	1.2	0.004	-0.000
2.30	12.07	0.01	0.015	0.099	0.005	0.27	0.006	0.11	10.64	0.22	10.23	10.31	51.4	1	0.000	-0.000
2.50	12.249	0.008	0.015	0.099	0.004	0.281	0.006	0.098	10.57	0.21	12.34	11.11	51	1	0.000	-0.000
2.60	12.099	0.009	0.014	0.086	0.006	0.232	0.006	0.117	10.63	0.23	10.23	8.30	51.3	1.1	0.000	-0.000
2.70	11.546	0.011	0.014	0.133	0.006	0.289	0.004	0.204	10.64	0.28	5.56	7.61	51.4	1.3	0.000	-0.000
2.90	11.553	0.009	0.014	0.106	0.006	0.226	0.004	0.149	10.56	0.21	6.71	9.16	51	1	0.003	-0.000
3.10	11.479	0.009	0.014	0.119	0.006	0.21	0.004	0.174	10.59	0.22	5.79	9.24	51.2	1.1	0.005	-0.000
3.40	11.657	0.012	0.014	0.175	0.007	0.247	0.005	0.167	10.68	0.26	5.89	6.94	51.6	1.2	0.000	-0.000
3.70	11.551	0.008	0.014	0.101	0.004	0.243	0.004	0.123	10.57	0.17	7.08	12.65	51.1	0.8	0.005	-0.000
4.10	11.506	0.01	0.014	0.109	0.006	0.306	0.004	0.175	10.65	0.23	5.19	8.01	51.5	1.1	0.000	-0.000
4.60	12.214	0.018	0.016	0.209	0.018	0.2	0.008	0.237	10.83	0.59	5.65	2.86	52.3	2.8	0.016	-0.000
5.00	12.485	0.019	0.017	0.248	0.018	0.269	0.009	0.214	10.76	0.64	7.58	2.48	52	3.1	0.000	-0.000
DC510	Muscovite	>250um	J= 0.002714±0.000014													
2.00	34.877	0.008	0.028	0.065	0.005	0.287	0.054	0.034	19.33	0.55	44.28	3.54	92.3	2.6	0.014	0.001
2.30	12.228	0.005	0.015	0.057	0.001	0.607	0.006	0.067	10.5	0.13	13.88	28.65	50.7	0.6	0.004	-0.000
2.50	10.696	0.005	0.014	0.07	0.001	0.448	0.001	0.152	10.43	0.07	2.15	24.81	50.3	0.3	0.001	-0.000
2.60	10.768	0.005	0.014	0.041	0.002	0.252	0.001	0.134	10.41	0.08	2.53	9.57	50.3	0.4	0.004	-0.000
2.70	11.198	0.009	0.014	0.085	0.005	0.236	0.003	0.172	10.49	0.19	4.03	3.12	50.7	0.9	0.002	-0.000
2.90	11.202	0.008	0.014	0.105	0.004	0.256	0.003	0.165	10.48	0.17	4.49	3.73	50.6	0.8	0.008	-0.000
2.90	11.031	0.006	0.014	0.072	0.003	0.267	0.002	0.152	10.52	0.12	3.26	5.45	50.8	0.5	0.000	-0.000
3.40	11.138	0.006	0.014	0.077	0.002	0.299	0.002	0.139	10.68	0.1	2.97	6.40	51.5	0.5	0.002	-0.000
3.70	11.69	0.006	0.014	0.076	0.003	0.237	0.003	0.12	10.99	0.12	4.83	5.97	53	0.6	0.005	-0.000
4.10	12.888	0.007	0.015	0.112	0.004	0.197	0.005	0.088	11.52	0.16	9.04	3.70	55.5	0.8	0.009	-0.000
4.60	13.076	0.01	0.016	0.132	0.007	0.192	0.007	0.146	11.36	0.32	10.60	2.21	54.8	1.5	0.006	0.000
5.50	12.266	0.012	0.015	0.106	0.005	0.282	0.004	0.118	11.16	0.21	6.86	2.86	53.8	1	0.000	-0.000
DC511	Muscovite	>250um	J= 0.002713±0.000014													
2.00	16.535	0.006	0.019	0.067	0.002	0.282	0.021	0.033	10.47	0.21	36.18	9.95	50.5	1	0.005	0.000
2.20	14.017	0.005	0.017	0.058	0.002	0.29	0.012	0.044	10.54	0.17	24.15	11.46	50.9	0.8	0.000	0.000
2.40	12.647	0.008	0.016	0.072	0.002	0.27	0.008	0.053	10.52	0.14	15.98	11.40	50.8	0.7	0.007	0.000
2.60	12.021	0.005	0.016	0.073	0.002	0.262	0.005	0.073	10.51	0.13	11.71	11.34	50.7	0.6	0.004	0.000
2.80	11.295	0.005	0.016	0.039	0.002	0.319	0.003	0.105	10.55	0.1	5.85	14.62	50.9	0.5	0.004	0.000

Watts	40Ar/39Ar	±	38Ar/39Ar	±	37Ar/39Ar	±	36Ar/39Ar	±	40Ar*/39ArK	±	%40Ar atm	% 39Ar	Age	±	Ca/K	Cl/K
3.00	11.475	0.007	0.016	0.076	0.002	0.263	0.004	0.09	10.53	0.12	7.21	10.16	50.8	0.6	0.000	0.000
3.20	11.36	0.008	0.016	0.08	0.003	0.258	0.003	0.112	10.54	0.13	5.89	8.06	50.9	0.6	0.006	0.000
3.40	11.586	0.008	0.017	0.083	0.004	0.252	0.004	0.11	10.61	0.15	6.49	5.49	51.2	0.7	0.002	0.000
3.70	11.728	0.009	0.016	0.093	0.004	0.327	0.004	0.103	10.6	0.17	7.87	5.80	51.1	0.8	0.003	0.000
4.10	11.857	0.007	0.017	0.093	0.004	0.253	0.005	0.112	10.58	0.18	8.90	5.23	51	0.9	0.003	0.000
4.60	11.975	0.008	0.016	0.106	0.004	0.275	0.005	0.114	10.54	0.21	9.94	4.75	50.9	1	0.006	0.000
5.50	13.094	0.012	0.018	0.201	0.012	0.269	0.01	0.143	10.57	0.46	14.44	1.75	51	2.2	0.010	0.000

DC512 Muscovite >250um J = 0.002712±0.000012

2.00	14.694	0.009	0.017	0.114	0.004	0.282	0.015	0.063	10.62	0.29	25.58	6.77	51.2	1.4	0.000	-0.000
2.30	11.065	0.006	0.014	0.061	0.002	0.245	0.002	0.113	10.50	0.10	3.25	13.97	50.7	0.5	0.001	-0.000
2.50	13.606	0.011	0.016	0.129	0.008	0.251	0.011	0.089	10.62	0.33	16.88	3.48	51.2	1.5	0.000	-0.000
2.60	13.224	0.013	0.016	0.196	0.012	0.274	0.01	0.16	10.66	0.52	10.49	2.21	51.4	2.5	0.000	-0.000
2.70	11.828	0.009	0.014	0.088	0.005	0.211	0.005	0.134	10.48	0.24	7.20	5.40	50.6	1.1	0.000	-0.000
2.90	10.958	0.006	0.014	0.069	0.002	0.191	0.002	0.14	10.47	0.11	2.45	12.99	50.5	0.5	0.001	-0.000
3.10	11.019	0.005	0.014	0.062	0.002	0.197	0.002	0.134	10.44	0.11	3.27	12.96	50.4	0.5	0.001	-0.000
3.40	10.886	0.006	0.014	0.059	0.002	0.202	0.002	0.129	10.42	0.10	2.60	15.76	50.3	0.5	0.001	-0.000
3.70	10.919	0.006	0.014	0.058	0.002	0.226	0.002	0.145	10.43	0.11	2.59	14.06	50.3	0.5	0.000	-0.000
4.10	11.579	0.008	0.014	0.108	0.004	0.214	0.005	0.12	10.40	0.19	6.37	6.26	50.2	0.9	0.000	-0.000
4.60	12.111	0.009	0.016	0.126	0.007	0.276	0.007	0.136	10.49	0.28	8.08	4.19	50.6	1.3	0.008	-0.000
5.00	13.711	0.016	0.019	0.213	0.014	0.237	0.013	0.135	10.43	0.56	14.68	1.95	50.3	2.7	0.011	0.000

DC515 Muscovite >250um J = 0.002711±0.000012

2.00	15.826	0.007	0.016	0.076	0.002	0.235	0.019	0.037	10.29	0.22	34.43	5.06	49.6	1.1	0.002	-0.000
2.20	13.046	0.008	0.014	0.088	0.003	0.268	0.009	0.058	10.51	0.18	18.20	3.48	50.7	0.8	0.000	-0.000
2.40	12.679	0.006	0.014	0.065	0.003	0.209	0.008	0.066	10.58	0.17	15.28	3.42	51	0.8	0.000	-0.000
2.60	12.205	0.006	0.014	0.065	0.002	0.226	0.006	0.064	10.49	0.13	13.17	5.37	50.6	0.6	0.002	-0.000
2.80	11.37	0.006	0.013	0.066	0.002	0.188	0.003	0.101	10.55	0.12	6.08	4.87	50.9	0.6	0.005	-0.000
3.00	11.855	0.007	0.014	0.095	0.003	0.233	0.005	0.088	10.53	0.15	9.83	3.80	50.8	0.7	0.002	-0.000
3.20	11.749	0.005	0.014	0.065	0.002	0.289	0.005	0.067	10.5	0.1	9.69	5.85	50.7	0.5	0.005	-0.000
3.40	11.875	0.006	0.014	0.069	0.002	0.268	0.005	0.067	10.5	0.12	10.60	5.21	50.6	0.6	0.000	-0.000
3.70	11.473	0.005	0.014	0.064	0.001	0.379	0.004	0.08	10.49	0.1	8.09	11.47	50.6	0.5	0.006	-0.000
4.10	11.27	0.005	0.013	0.072	0.001	0.286	0.003	0.082	10.51	0.09	6.06	8.25	50.7	0.4	0.004	-0.000
4.60	11.064	0.005	0.013	0.052	0.001	0.391	0.002	0.088	10.51	0.08	4.60	15.08	50.7	0.4	0.000	-0.000

Watts	40Ar/39Ar	±	38Ar/39Ar	±	37Ar/39Ar	±	36Ar/39Ar	±	40Ar*/39ArK	±	%40Ar atm	% 39Ar	Age	±	Ca/K	Cl/K
5.50	10.793	0.006	0.013	0.063	0	0.606	0.001	0.121	10.47	0.07	2.74	28.15	50.5	0.4	0.003	-0.000
DC519	Muscovite	>250um	J= 0.002710±0.000012													
2.00	31.1	0.014	0.03	0.135	0.015	0.279	0.073	0.045	10.51	0.95	65.11	1.55	50.6	4.5	0.006	0.000
2.30	11.48	0.006	0.015	0.073	0.001	0.367	0.003	0.078	10.54	0.1	7.58	22.07	50.8	0.5	0.001	0.000
2.60	10.908	0.005	0.015	0.053	0.001	0.307	0.002	0.137	10.48	0.08	3.19	21.22	50.5	0.4	0.002	0.000
2.70	11.424	0.008	0.015	0.112	0.005	0.285	0.004	0.169	10.55	0.2	4.98	5.25	50.9	1	0.002	-0.000
2.90	11.191	0.007	0.015	0.079	0.003	0.267	0.003	0.154	10.51	0.14	4.30	8.00	50.7	0.7	0.002	0.000
3.10	10.991	0.007	0.015	0.082	0.003	0.253	0.002	0.147	10.51	0.11	2.76	9.48	50.7	0.5	0.003	0.000
3.40	10.864	0.007	0.015	0.066	0.002	0.296	0.002	0.163	10.46	0.11	2.45	11.61	50.4	0.5	0.000	0.000
3.70	11.097	0.007	0.015	0.103	0.003	0.287	0.003	0.145	10.46	0.14	3.78	7.45	50.4	0.7	0.005	0.000
4.10	11.279	0.008	0.015	0.08	0.004	0.265	0.003	0.163	10.53	0.17	4.47	6.61	50.8	0.8	0.004	0.000
4.60	11.291	0.009	0.016	0.09	0.004	0.299	0.003	0.159	10.5	0.19	4.48	5.69	50.6	0.9	0.000	0.000
5.00	13.989	0.015	0.019	0.206	0.024	0.274	0.015	0.173	10.63	0.81	14.67	1.07	51.2	3.8	0.004	-0.000
DC528	Muscovite	>250um	J= 0.002708±0.000012													
2.00	16.755	0.01	0.022	0.11	0.007	0.225	0.023	0.059	10.22	0.42	37.98	3.36	49.2	2	0.002	0.001
2.30	21.83	0.011	0.026	0.112	0.009	0.196	0.041	0.053	10.21	0.64	52.56	2.85	49.2	3.1	0.024	0.001
2.50	13.783	0.008	0.019	0.099	0.006	0.278	0.012	0.078	10.54	0.29	22.24	4.11	50.8	1.4	0.000	0.001
2.60	14.418	0.01	0.02	0.126	0.008	0.287	0.015	0.095	10.49	0.43	25.74	3.13	50.5	2	0.006	0.001
2.70	12.928	0.011	0.019	0.138	0.008	0.253	0.009	0.123	10.73	0.35	15.02	3.11	51.7	1.6	0.006	0.001
2.90	14.377	0.008	0.021	0.073	0.004	0.255	0.014	0.064	10.5	0.28	26.29	6.81	50.6	1.3	0.006	0.001
3.10	14.829	0.007	0.02	0.078	0.003	0.236	0.015	0.047	10.45	0.23	28.95	7.98	50.3	1.1	0.004	0.001
3.40	11.614	0.005	0.017	0.049	0.001	0.313	0.004	0.064	10.49	0.09	9.28	22.46	50.6	0.4	0.002	0.000
3.70	11.525	0.005	0.017	0.058	0.001	0.258	0.004	0.083	10.49	0.11	8.59	20.52	50.5	0.5	0.004	0.001
4.10	11.009	0.005	0.017	0.045	0.001	0.3	0.002	0.123	10.54	0.09	3.75	18.87	50.8	0.4	0.002	0.001
4.60	11.082	0.008	0.019	0.082	0.005	0.224	0.002	0.22	10.57	0.18	3.12	5.76	50.9	0.8	0.005	0.001
5.00	13.521	0.022	0.023	0.172	0.025	0.21	0.014	0.184	10.54	0.81	16.51	1.03	50.8	3.8	0.021	0.001
DC536	Muscovite	>250um	J= 0.002705±0.000012													
2.00	29.743	0.016	0.034	0.147	0.019	0.198	0.069	0.054	10.35	1.08	63.70	0.75	49.8	5.1	0.009	0.001
2.20	24.736	0.014	0.032	0.11	0.012	0.221	0.049	0.054	10.97	0.78	54.24	1.20	52.7	3.7	0.027	0.002
2.40	16.503	0.014	0.026	0.156	0.013	0.228	0.021	0.097	10.94	0.62	29.94	1.08	52.6	2.9	0.019	0.002

Watts	40Ar/39Ar	±	38Ar/39Ar	±	37Ar/39Ar	±	36Ar/39Ar	±	40Ar*/39ArK	±	%40Ar atm	% 39Ar	Age	±	Ca/K	Cl/K
2.50	16.094	0.016	0.029	0.131	0.015	0.236	0.02	0.11	10.79	0.68	28.13	0.87	51.9	3.2	0.000	0.002
2.60	15.998	0.016	0.029	0.137	0.018	0.243	0.02	0.12	10.75	0.75	26.69	0.72	51.7	3.5	0.000	0.002
2.70	14.509	0.016	0.026	0.154	0.016	0.301	0.014	0.131	10.99	0.57	17.86	0.85	52.9	2.7	0.026	0.002
2.80	28.207	0.018	0.035	0.129	0.016	0.28	0.064	0.058	10.23	1.07	62.36	0.90	49.3	5.1	0.031	0.002
2.90	30.726	0.014	0.037	0.113	0.012	0.234	0.071	0.04	10.51	0.8	64.90	1.15	50.6	3.8	0.000	0.002
3.10	18.602	0.009	0.028	0.113	0.008	0.206	0.027	0.053	10.88	0.44	39.93	1.95	52.3	2.1	0.014	0.002
3.30	15.236	0.009	0.027	0.083	0.005	0.229	0.015	0.065	10.9	0.31	26.85	2.91	52.4	1.5	0.002	0.002
3.50	12.727	0.008	0.024	0.074	0.003	0.289	0.006	0.092	10.96	0.2	12.29	4.21	52.7	0.9	0.004	0.002
3.80	11.943	0.005	0.023	0.05	0.002	0.314	0.003	0.08	11	0.1	7.11	10.71	52.9	0.5	0.007	0.002
4.40	11.377	0.005	0.023	0.046	0.001	0.357	0.001	0.124	11.05	0.08	2.46	20.35	53.1	0.4	0.004	0.002
7.00	11.212	0.005	0.023	0.044	0	0.676	0.001	0.247	11.04	0.07	1.35	52.34	53.1	0.3	0.006	0.002

DC538 Muscovite >250um J = 0.002704±0.000012

2.00	52.354	0.019	0.046	0.116	0.03	0.226	0.146	0.052	11.31	2.15	77.30	0.68	54.4	10.2	0.003	0.000
2.30	119.364	0.022	0.092	0.132	0.04	0.228	0.374	0.035	11.57	3.18	90.15	0.67	55.6	15	0.094	0.001
2.50	162.302	0.023	0.121	0.113	0.05	0.212	0.521	0.041	12.24	5.22	92.39	0.53	58.7	24.7	0.103	0.001
2.60	100.937	0.02	0.077	0.123	0.04	0.263	0.311	0.043	11.81	3.61	88.05	0.64	56.7	17	0.011	0.001
2.70	74.263	0.025	0.057	0.156	0.04	0.245	0.214	0.049	13.23	2.74	81.60	0.63	63.4	12.9	0.011	-0.001
2.90	26.007	0.012	0.025	0.102	0.01	0.286	0.047	0.061	12.7	0.86	49.66	2.42	60.9	4	0.025	0.000
3.10	24.133	0.014	0.023	0.112	0.01	0.231	0.041	0.051	12.81	0.63	44.74	1.94	61.4	3	0.014	-0.000
3.40	17.984	0.011	0.019	0.098	0.01	0.206	0.02	0.072	12.46	0.45	28.33	3.16	59.8	2.1	0.029	0.000
3.70	14.044	0.008	0.016	0.096	0.01	0.174	0.011	0.069	11.11	0.24	18.94	5.73	53.4	1.1	0.038	-0.000
4.10	12.363	0.007	0.015	0.068	0.01	0.101	0.007	0.065	10.48	0.15	13.91	10.46	50.4	0.7	0.058	-0.000
4.60	11.582	0.005	0.014	0.078	0.00	0.138	0.004	0.12	10.54	0.14	8.38	28.32	50.7	0.7	0.039	-0.000
5.00	11.679	0.007	0.014	0.065	0.00	0.166	0.003	0.088	10.84	0.11	6.78	44.82	52.1	0.5	0.036	-0.000

DC543 Muscovite >250um J= 0.002702±0.000012

2.00	17.143	0.01	0.018	0.12	0.006	0.254	0.023	0.055	10.61	0.39	35.20	4.52	51	1.9	0.013	-0.000
2.30	11.575	0.006	0.014	0.068	0.002	0.194	0.004	0.075	10.45	0.11	7.50	13.14	50.3	0.5	0.006	-0.000
2.50	11.706	0.007	0.014	0.085	0.003	0.287	0.005	0.092	10.52	0.14	7.05	9.07	50.6	0.7	0.000	-0.000
2.60	12.076	0.009	0.014	0.123	0.005	0.235	0.006	0.127	10.62	0.25	7.13	5.50	51	1.2	0.009	-0.000
2.70	12.718	0.01	0.015	0.112	0.005	0.224	0.008	0.101	10.57	0.27	12.34	5.33	50.8	1.3	0.009	-0.000
2.90	11.652	0.007	0.014	0.078	0.003	0.242	0.004	0.099	10.56	0.14	6.50	9.91	50.8	0.7	0.007	-0.000
3.10	11.329	0.007	0.014	0.08	0.002	0.206	0.003	0.092	10.51	0.11	4.91	13.11	50.5	0.5	0.003	-0.000
3.40	11.221	0.007	0.014	0.072	0.002	0.203	0.003	0.106	10.48	0.12	4.04	11.91	50.4	0.6	0.002	-0.000

Watts	40Ar/39Ar	±	38Ar/39Ar	±	37Ar/39Ar	±	36Ar/39Ar	±	40Ar*/39ArK	±	%40Ar atm	% 39Ar	Age	±	Ca/K	Cl/K
3.70	11.379	0.007	0.014	0.074	0.003	0.24	0.003	0.105	10.47	0.13	5.14	10.78	50.4	0.6	0.007	-0.000
4.10	11.495	0.008	0.014	0.084	0.003	0.239	0.004	0.111	10.51	0.15	5.20	8.88	50.5	0.7	0.004	-0.000
4.60	12.119	0.008	0.014	0.11	0.004	0.24	0.006	0.09	10.65	0.18	7.89	6.43	51.2	0.8	0.007	-0.000
5.00	15.711	0.017	0.019	0.206	0.019	0.192	0.021	0.129	10.64	0.82	19.77	1.42	51.1	3.9	0.032	-0.001

TABLE C4: All thermochronology data arranged by sample number

Watts	40Ar/39Ar	±	38Ar/39Ar	±	37Ar/39Ar	±	36Ar/39Ar	±	40Ar*/39ArK	±	%40Ar atm	% 39Ar	Age	±	Ca/K	Cl/K
AH-02-003B	Biotite	HP	J= 0.003690±0.000018													
0.50	52.599	0.086	0.131	0.475	0.29	0.392	0.203	0.253	9.66	14.96	78.93	0.17	63.2	96.2	0.000	0.019
1.00	12.407	0.01	0.086	0.063	0.006	0.312	0.011	0.117	9.69	0.39	21.20	9.23	63.4	2.5	0.011	0.016
1.50	10.641	0.01	0.085	0.06	0.004	0.409	0.004	0.169	9.87	0.2	6.58	12.66	64.6	1.3	0.000	0.016
2.00	10.332	0.008	0.085	0.038	0.004	0.332	0.002	0.291	10.03	0.18	2.46	15.60	65.6	1.2	0.000	0.016
2.50	10.334	0.01	0.086	0.038	0.006	0.283	0.002	0.311	10.1	0.2	1.53	12.29	66	1.3	0.022	0.016
3.00	10.391	0.012	0.088	0.055	0.009	0.261	0.002	0.366	10.14	0.27	1.30	8.92	66.3	1.7	0.050	0.017
4.00	10.249	0.01	0.085	0.046	0.006	0.334	0.002	0.368	10.05	0.21	1.16	11.83	65.7	1.4	0.026	0.016
5.00	10.155	0.009	0.086	0.038	0.006	0.195	0.001	0.4	10.05	0.16	0.57	16.49	65.7	1.1	0.039	0.016
6.00	10.469	0.017	0.088	0.072	0.015	0.309	0.003	0.544	10.22	0.51	-0.06	4.72	66.8	3.3	0.047	0.017
7.00	10.439	0.01	0.089	0.049	0.011	0.3	0.002	0.363	10.12	0.29	1.83	8.09	66.2	1.8	0.054	0.017
AH-02-004B	Biotite	HP	J= 0.003694±0.000018													
0.50	45.27	0.028	0.135	0.121	0.045	0.266	0.158	0.078	1.95	3.48	95.56	0.81	12.9	23	0.000	0.021
0.75	24.658	0.019	0.108	0.065	0.015	0.235	0.074	0.06	3.95	1.27	83.71	2.73	26.1	8.3	0.000	0.018
1.00	14.201	0.015	0.093	0.083	0.009	0.294	0.024	0.097	7.71	0.71	44.87	3.99	50.7	4.6	0.000	0.017
1.50	9.551	0.005	0.09	0.028	0.002	0.237	0.003	0.113	8.86	0.1	7.19	27.53	58.1	0.7	0.004	0.017
1.75	9.493	0.007	0.089	0.031	0.002	0.327	0.002	0.185	9.08	0.12	4.13	19.90	59.5	0.8	0.007	0.017
2.00	9.864	0.011	0.091	0.055	0.006	0.253	0.003	0.316	9.26	0.29	5.17	7.60	60.7	1.9	0.009	0.017
2.50	9.87	0.01	0.091	0.049	0.005	0.293	0.003	0.273	9.24	0.27	5.45	8.13	60.6	1.7	0.012	0.017
3.00	9.461	0.009	0.09	0.046	0.004	0.233	0.002	0.282	9.02	0.19	3.99	10.65	59.1	1.3	0.012	0.017
3.50	9.626	0.012	0.09	0.06	0.009	0.241	0.003	0.535	9.18	0.49	2.59	4.22	60.1	3.2	0.001	0.017
4.25	9.733	0.017	0.091	0.079	0.011	0.284	0.003	0.507	9.27	0.49	2.51	4.07	60.7	3.1	0.030	0.017
5.00	10.227	0.018	0.094	0.08	0.018	0.216	0.005	0.469	9.23	0.78	6.27	2.48	60.5	5	0.070	0.018
7.00	9.686	0.01	0.088	0.043	0.014	0.146	0.002	0.416	9.34	0.27	2.47	7.90	61.2	1.8	0.122	0.017
AH-02-004H	Hornblende	HP	J= 0.003695±0.000018													
2.00	15.275	0.004	0.483	0.009	0.022	0.004	0.008	0.067	14.974	0.171	2.78	22.81	97.15±	1.08	12.733	0.107
2.50	28.836	0.038	0.456	0.087	0.192	0.037	0.289	0.112	13.003	13.48	59.67	0.27	84.66	85.74	12.733	0.094
3.00	9.424	0.004	0.481	0.007	0.02	0.004	0.006	0.051	9.121	0.092	3.75	45.66	59.8	0.59	12.733	0.106
3.25	9.228	0.008	0.48	0.014	0.03	0.007	0.017	0.101	8.969	0.539	0.88	6.13	58.82	3.48	12.733	0.106
3.50	9.434	0.009	0.481	0.017	0.033	0.008	0.023	0.097	8.714	0.676	4.96	4.76	57.18	4.37	12.733	0.106
4.00	9.498	0.008	0.479	0.016	0.03	0.007	0.018	0.093	9.019	0.529	3.11	5.91	59.14	3.41	12.733	0.106
4.50	9.619	0.009	0.476	0.016	0.035	0.008	0.023	0.092	9.353	0.649	0.02	4.51	61.29	4.18	12.733	0.105

Watts	40Ar/39Ar	±	38Ar/39Ar	±	37Ar/39Ar	±	36Ar/39Ar	±	40Ar*/39ArK	±	%40Ar atm	% 39Ar	Age	±	Ca/K	Cl/K
6.00	9.269	0.007	0.481	0.012	0.026	0.006	0.011	0.093	9.369	0.327	-1.90	9.96	61.4	2.11	12.733	0.107
AH-02-003H	Hornblende	HP	J= 0.003692±0.000018													
2.00	55.063	0.014	0.4	0.03	0.056	0.014	0.066	0.091	53.31	2.06	7.80	6.58	324.1	11.5	12.892	0.085
2.50	13.209	0.007	0.389	0.015	0.027	0.006	0.014	0.078	12.75	0.35	3.51	31.20	83	2.2	12.892	0.085
2.75	12.537	0.007	0.388	0.015	0.03	0.007	0.02	0.076	11.82	0.46	5.25	22.12	77	3	12.892	0.085
3.00	12.448	0.011	0.382	0.019	0.035	0.01	0.026	0.083	11.6	0.68	5.56	15.18	75.6	4.4	12.892	0.083
3.50	14.241	0.017	0.388	0.034	0.064	0.016	0.067	0.092	11.53	2.01	16.05	5.44	75.2	12.8	12.892	0.083
4.00	17.612	0.018	0.405	0.045	0.083	0.016	0.093	0.092	13.62	2.86	21.05	3.71	88.5	18.1	12.892	0.086
6.00	13.475	0.008	0.408	0.018	0.035	0.008	0.026	0.111	12.54	0.88	6.14	15.78	81.7	5.6	12.892	0.089
AH-02-013	Biotite	HP	J= 0.003697±0.000018													
0.50	34.32	0.062	0.113	0.346	0.144	0.277	0.129	0.22	3.57	8.32	88.35	0.40	23.6	54.8	0.000	0.016
1.00	9.825	0.012	0.068	0.065	0.006	0.282	0.007	0.176	8.07	0.4	16.46	8.75	53	2.6	0.000	0.012
1.25	8.798	0.008	0.069	0.049	0.004	0.274	0.002	0.296	8.37	0.21	4.01	17.09	55	1.3	0.000	0.012
1.50	8.497	0.009	0.071	0.038	0.005	0.356	0.001	0.643	8.34	0.27	0.49	12.68	54.8	1.8	0.000	0.013
1.75	8.545	0.013	0.072	0.059	0.005	0.316	0.002	0.638	8.38	0.32	0.28	10.27	55	2	0.000	0.013
2.00	8.66	0.014	0.073	0.07	0.008	0.316	0.002	0.648	8.35	0.48	1.04	7.12	54.9	3.1	0.000	0.013
2.50	8.537	0.011	0.071	0.052	0.006	0.411	0.002	0.526	8.33	0.28	0.80	10.40	54.7	1.8	0.001	0.013
3.00	8.5	0.01	0.072	0.056	0.005	0.41	0.001	0.792	8.38	0.29	-0.04	12.05	55.1	1.9	0.000	0.013
4.00	8.508	0.012	0.071	0.043	0.005	0.32	0.001	0.659	8.39	0.27	-0.04	11.30	55.1	1.7	0.000	0.013
5.00	8.654	0.014	0.069	0.078	0.01	0.399	0.003	0.596	8.39	0.5	-0.04	5.87	55.1	3.2	0.000	0.012
6.00	9.212	0.027	0.068	0.125	0.025	0.247	0.005	0.778	8.5	1.24	-0.04	2.33	55.8	8	0.000	0.012
7.00	9.51	0.032	0.07	0.172	0.033	0.296	0.007	0.845	8.56	1.89	-0.05	1.75	56.2	12.2	0.015	0.012
AH-03-021	Biotite	HP	J= 0.003700±0.000018													
0.50	93.868	0.093	0.179	0.433	0.335	0.446	0.368	0.214	4.49	22.55	94.97	0.04	29.8	148.1	0.259	0.018
0.75	31.062	0.03	0.091	0.16	0.042	0.372	0.089	0.131	6.97	3.42	76.63	0.30	45.9	22.3	0.000	0.013
1.00	10.902	0.02	0.08	0.097	0.016	0.302	0.014	0.216	7.82	0.89	25.26	0.82	51.4	5.8	0.000	0.015
1.25	8.952	0.011	0.077	0.045	0.004	0.349	0.004	0.185	7.91	0.25	10.78	3.56	52	1.6	0.002	0.014
1.50	8.234	0.011	0.076	0.059	0.004	0.302	0.002	0.38	7.96	0.21	2.25	3.39	52.4	1.4	0.000	0.014
1.75	8.363	0.009	0.076	0.036	0.003	0.314	0.002	0.24	7.9	0.17	4.94	4.80	51.9	1.1	0.001	0.014
2.00	8.243	0.006	0.073	0.032	0.002	0.379	0.001	0.283	8.02	0.11	2.48	8.62	52.7	0.7	0.004	0.013
2.25	8.104	0.006	0.073	0.034	0.001	0.299	0.001	0.407	8.01	0.09	0.99	11.23	52.7	0.6	0.001	0.014
2.50	8.119	0.007	0.075	0.038	0.003	0.244	0.001	0.509	8	0.13	0.98	6.57	52.7	0.9	0.005	0.014
3.00	8.059	0.007	0.075	0.035	0.002	0.206	0.001	0.385	7.96	0.1	0.97	8.70	52.4	0.6	0.006	0.014
3.50	8.001	0.005	0.075	0.026	0.002	0.201	0	0.419	7.96	0.07	0.35	12.43	52.4	0.4	0.010	0.014

Watts	40Ar/39Ar	±	38Ar/39Ar	±	37Ar/39Ar	±	36Ar/39Ar	±	40Ar*/39ArK	±	%40Ar atm	% 39Ar	Age	±	Ca/K	Cl/K
4.00	7.956	0.006	0.075	0.024	0.002	0.219	0	0.43	7.91	0.08	0.40	11.64	52.1	0.5	0.011	0.014
4.50	8.012	0.006	0.075	0.032	0.003	0.179	0	0.65	7.97	0.11	0.17	8.52	52.5	0.7	0.025	0.014
5.00	8.054	0.007	0.075	0.038	0.009	0.097	0.001	0.502	7.95	0.13	0.78	5.83	52.3	0.9	0.085	0.014
6.00	8.117	0.009	0.077	0.061	0.027	0.087	0.001	0.563	7.97	0.19	1.04	4.52	52.4	1.2	0.330	0.014
7.00	7.988	0.009	0.077	0.029	0.018	0.056	0.001	0.396	7.91	0.1	0.78	9.03	52	0.7	0.236	0.014
AH-02-022	Biotite	HP	J= 0.003698±0.000018													
0.50	44.435	0.089	0.071	1.327	0.316	0.39	0.181	0.328	9.92	17.8	72.07	0.10	65	114.5	0.000	0.005
0.75	16.276	0.022	0.041	0.208	0.021	0.285	0.033	0.161	8.07	1.56	48.58	1.59	53	10.1	0.000	0.004
1.00	8.264	0.005	0.024	0.035	0.001	0.318	0.002	0.143	7.73	0.1	6.46	39.46	50.8	0.6	0.002	0.002
1.25	7.986	0.015	0.019	0.118	0.007	0.399	0.002	0.666	7.8	0.43	-0.00	4.95	51.3	2.8	0.000	0.001
1.50	7.882	0.009	0.02	0.122	0.004	0.244	0.001	0.572	7.7	0.24	1.06	8.49	50.6	1.5	0.000	0.001
1.75	8.215	0.017	0.025	0.147	0.01	0.259	0.003	0.664	7.87	0.59	0.87	3.47	51.7	3.8	0.000	0.002
2.00	8.259	0.014	0.024	0.169	0.011	0.288	0.003	0.609	7.89	0.62	0.92	3.25	51.9	4	0.009	0.002
3.00	7.913	0.005	0.025	0.042	0.002	0.243	0.001	0.37	7.81	0.08	1.08	30.11	51.4	0.5	0.006	0.003
4.00	8.886	0.03	0.025	0.302	0.031	0.272	0.008	0.765	7.99	1.78	-0.01	1.15	52.6	11.6	0.000	0.002
7.00	8.139	0.01	0.026	0.099	0.005	0.244	0.002	0.493	7.84	0.27	2.23	7.42	51.6	1.8	0.002	0.003
AH-03-024-1	Hornblende	100-250um	J= 0.003729±0.000040													
1.00	1745.887	0.15	0.992	0.245	3.424	0.169	2.575	0.161	1172.413	208.673	37.98	0.04	3033.01	261.33	14.218	0.116
2.00	571.809	0.081	0.456	0.232	2.649	0.099	0.71	0.136	419.798	45.079	27.82	0.09	1699.68	118.21	12.578	0.069
3.00	35.098	0.007	0.25	0.018	2.006	0.01	0.065	0.024	17.478	0.473	50.36	8.37	113.91	2.99	11.139	0.051
3.50	21.82	0.005	0.236	0.016	1.983	0.008	0.037	0.024	12.093	0.268	44.74	15.19	79.57	1.72	11.027	0.049
3.75	19.559	0.008	0.235	0.02	2.014	0.01	0.025	0.053	13.534	0.403	30.46	6.76	88.83	2.58	11.185	0.050
4.00	13.652	0.009	0.233	0.018	2.005	0.011	0.008	0.092	12.139	0.251	10.58	9.66	79.87	1.61	11.151	0.050
4.25	14.39	0.012	0.235	0.033	2.006	0.015	0.015	0.148	11.429	0.694	17.55	2.90	75.3	4.48	11.096	0.050
5.00	15.511	0.004	0.234	0.01	1.992	0.007	0.017	0.025	11.274	0.138	27.68	35.21	74.29	0.89	11.099	0.050
5.50	12.937	0.006	0.228	0.018	1.961	0.009	0.009	0.094	11.227	0.264	12.47	8.68	73.99	1.71	10.909	0.048
6.00	12.158	0.005	0.245	0.017	2.07	0.008	0.006	0.099	11.315	0.182	6.54	13.10	74.56	1.18	11.534	0.053
AH-03-024-2	Hornblende	HP	J= 0.003601±0.000024													
1.00	778.147	0.114	0.69	0.17	0.399	0.123	1.569	0.122	1042.158	281.973	39.86	0.04	2812.1	385.42	11.100	0.079
2.00	299.841	0.05	0.386	0.125	0.244	0.156	0.573	0.073	328.775	29.673	26.44	0.11	1409.21	88.27	11.100	0.039
3.00	24.182	0.007	0.302	0.016	0.025	0.068	0.022	0.055	21.592	0.396	11.53	5.13	135.09	2.39	11.100	0.064
3.50	19.06	0.005	0.243	0.011	0.019	0.036	0.021	0.024	14.641	0.17	23.86	16.94	92.69	1.05	11.100	0.051
3.75	14.54	0.006	0.239	0.015	0.023	0.051	0.016	0.051	12.891	0.255	11.61	6.66	81.86	1.58	11.100	0.050
4.00	16.413	0.004	0.24	0.011	0.019	0.032	0.018	0.027	13.001	0.155	21.42	16.46	82.54	0.96	11.100	0.051

Watts	40Ar/39Ar	±	38Ar/39Ar	±	37Ar/39Ar	±	36Ar/39Ar	±	40Ar*/39ArK	±	%40Ar atm	% 39Ar	Age	±	Ca/K	Cl/K
4.25	13.056	0.007	0.243	0.022	0.026	0.061	0.017	0.058	12.212	0.305	6.17	4.58	77.64	1.9	11.100	0.051
4.50	13.453	0.007	0.242	0.017	0.023	0.061	0.016	0.063	12.221	0.307	9.11	5.62	77.7	1.91	11.100	0.051
5.00	13.085	0.007	0.243	0.02	0.027	0.065	0.02	0.063	11.778	0.389	9.46	3.85	74.94	2.42	11.100	0.051
5.50	13.739	0.009	0.247	0.026	0.032	0.106	0.027	0.079	12.242	0.655	10.08	2.76	77.83	4.07	11.100	0.051
6.50	12.609	0.004	0.245	0.011	0.018	0.03	0.005	0.05	12.302	0.09	3.25	37.85	78.2	0.56	11.100	0.052
AH-03-029-1 Hornblende 100-250um J= 0.003732±0.000038																
2.00	830.626	0.081	0.345	0.196	2.449	0.101	1.143	0.104	546.07	53.36	36.17	0.27	2004.7	118.3	11.181	0.034
3.00	32.569	0.011	0.128	0.042	2.916	0.014	0.019	0.134	28.95	0.81	10.96	9.74	185.1	5	16.513	0.026
3.50	14.626	0.01	0.123	0.038	2.911	0.012	0.009	0.168	13.66	0.46	5.04	11.69	89.7	3	16.490	0.025
4.00	18.47	0.009	0.124	0.03	2.926	0.011	0.01	0.115	16.8	0.39	8.72	17.38	109.7	2.5	16.585	0.025
4.25	13.831	0.008	0.122	0.035	2.934	0.011	0.009	0.144	12.72	0.4	6.45	12.28	83.7	2.6	16.620	0.024
4.75	13.411	0.008	0.124	0.03	2.891	0.01	0.008	0.117	12.25	0.31	7.96	19.98	80.7	2	16.406	0.025
5.25	17.034	0.014	0.127	0.062	2.973	0.016	0.018	0.186	13.78	1.01	15.43	5.07	90.5	6.5	16.788	0.025
5.75	16.15	0.013	0.125	0.051	2.922	0.015	0.014	0.185	13.8	0.79	12.25	8.09	90.6	5.1	16.531	0.025
6.00	14.022	0.009	0.124	0.027	2.946	0.011	0.01	0.117	12.55	0.36	9.49	15.50	82.6	2.3	16.732	0.025
AH-03-029-2 Hornblende HP J= 0.003607±0.000022																
2.00	83.366	0.011	0.104	0.056	0.041	0.011	0.09	0.038	67.18	1.3	22.36	3.57	391.4	6.8	16.550	0.015
3.00	27.872	0.007	0.114	0.024	0.032	0.007	0.019	0.057	26.9	0.38	5.12	7.46	167.1	2.3	16.550	0.021
3.50	19.538	0.007	0.129	0.022	0.033	0.007	0.018	0.07	18.69	0.4	5.41	7.56	117.7	2.4	16.550	0.025
4.00	15.356	0.004	0.127	0.016	0.028	0.004	0.011	0.048	14.47	0.17	6.66	19.11	91.8	1	16.550	0.025
4.50	18.369	0.005	0.13	0.021	0.029	0.005	0.012	0.059	17.47	0.24	5.96	14.75	110.3	1.4	16.550	0.026
4.75	15.726	0.005	0.131	0.019	0.03	0.005	0.014	0.062	14.91	0.27	5.93	11.27	94.5	1.6	16.550	0.025
5.00	13.692	0.004	0.129	0.015	0.029	0.004	0.012	0.047	12.83	0.18	6.99	14.63	81.6	1.1	16.550	0.025
5.50	13.831	0.005	0.127	0.018	0.029	0.005	0.013	0.057	12.76	0.24	8.36	13.16	81.2	1.5	16.550	0.025
6.50	15.338	0.005	0.135	0.022	0.032	0.005	0.019	0.066	13.65	0.39	11.58	8.49	86.7	2.4	16.550	0.026
AH-03-032 Hornblende HP J= 0.003701±0.000018																
0.50	43.622	0.067	0.2	0.261	0.125	0.346	0.154	0.152	5.22	6.43	87.00	0.18	34.5	42.1	0.000	0.036
1.00	10.426	0.01	0.214	0.029	0.003	0.332	0.01	0.091	7.76	0.28	25.08	7.73	51.1	1.8	0.000	0.045
1.25	14.78	0.015	0.214	0.047	0.008	0.344	0.026	0.078	7.72	0.61	47.08	2.96	50.8	4	0.000	0.045
1.50	8.112	0.005	0.212	0.016	0.001	0.46	0.002	0.157	7.77	0.08	3.98	18.71	51.2	0.5	0.000	0.045
1.75	7.866	0.005	0.211	0.017	0.001	0.306	0	0.51	7.8	0.08	0.64	20.27	51.3	0.5	0.001	0.045
2.00	8.034	0.011	0.211	0.028	0.004	0.361	0.001	0.458	7.92	0.18	0.39	6.72	52.1	1.2	0.002	0.045
2.50	8.074	0.011	0.211	0.032	0.005	0.319	0.001	0.555	7.93	0.25	0.33	5.12	52.2	1.6	0.001	0.045
3.00	8.072	0.009	0.209	0.035	0.004	0.267	0.001	0.44	7.91	0.18	1.01	6.98	52.1	1.2	0.004	0.045

Watts	40Ar/39Ar	±	38Ar/39Ar	±	37Ar/39Ar	±	36Ar/39Ar	±	40Ar*/39ArK	±	%40Ar atm	% 39Ar	Age	±	Ca/K	Cl/K
3.50	8.048	0.011	0.207	0.036	0.004	0.464	0.001	0.41	7.9	0.19	0.67	6.21	52	1.2	0.000	0.044
4.00	8.076	0.01	0.211	0.03	0.005	0.308	0.001	0.441	7.98	0.2	-0.14	5.54	52.5	1.3	0.000	0.045
4.50	8.111	0.014	0.209	0.041	0.006	0.323	0.002	0.516	7.98	0.27	-0.15	4.32	52.5	1.8	0.002	0.044
5.00	8.259	0.016	0.211	0.042	0.009	0.386	0.003	0.453	7.97	0.4	0.58	2.73	52.5	2.6	0.000	0.045
6.00	8.134	0.015	0.21	0.045	0.007	0.412	0.002	0.512	7.95	0.33	-0.15	3.37	52.3	2.1	0.000	0.045
7.00	7.95	0.008	0.212	0.02	0.003	0.306	0.001	0.527	7.9	0.14	-0.10	9.17	52	0.9	0.001	0.045
DC004-1	Hornblende	100-250um	J= 0.003741±0.000030													
2.00	176.023	0.018	0.225	0.042	1.301	0.023	0.279	0.03	98.36	2.69	44.42	1.41	565.2	13.3	7.260	0.037
3.00	12.791	0.004	0.205	0.012	1.461	0.007	0.01	0.036	10.34	0.12	19.39	19.86	68.4	0.8	8.310	0.043
3.25	10.037	0.005	0.199	0.014	1.385	0.008	0.004	0.081	9.28	0.12	7.43	14.44	61.5	0.8	7.873	0.042
3.50	10.143	0.005	0.195	0.014	1.37	0.008	0.004	0.098	9.45	0.13	6.71	14.31	62.7	0.9	7.789	0.041
3.75	10.331	0.007	0.194	0.019	1.368	0.009	0.006	0.114	9.35	0.2	8.76	7.93	62	1.3	7.768	0.041
4.00	10.658	0.007	0.197	0.019	1.383	0.01	0.007	0.113	9.49	0.23	9.96	6.37	62.9	1.5	7.850	0.042
4.50	10.563	0.009	0.203	0.026	1.408	0.013	0.008	0.166	9.17	0.4	11.14	3.89	60.9	2.6	7.972	0.043
5.00	11.072	0.006	0.201	0.016	1.377	0.009	0.007	0.092	9.72	0.2	11.69	8.25	64.4	1.3	7.823	0.043
5.50	10.687	0.009	0.201	0.02	1.388	0.013	0.007	0.127	9.22	0.28	12.38	5.26	61.2	1.9	7.881	0.043
6.00	9.659	0.005	0.202	0.013	1.378	0.008	0.004	0.095	9.11	0.11	5.59	18.28	60.5	0.7	7.852	0.043
DC004-2	Hornblende	HP	J= 0.003624±0.000018													
2.00	63.036	0.011	0.147	0.046	0.035	0.011	0.123	0.034	37.54	1.33	42.43	2.24	230.1	7.7	7.950	0.022
3.00	11.225	0.004	0.195	0.01	0.014	0.004	0.009	0.035	9.72	0.11	13.60	25.62	62.5	0.7	7.950	0.041
3.50	9.844	0.004	0.193	0.01	0.014	0.004	0.007	0.053	9.08	0.12	7.79	23.23	58.4	0.7	7.950	0.040
3.75	10.237	0.006	0.184	0.017	0.018	0.006	0.013	0.066	9.06	0.27	10.53	8.81	58.3	1.7	7.950	0.038
4.00	11.764	0.008	0.192	0.022	0.021	0.007	0.021	0.069	9.44	0.44	18.56	5.57	60.7	2.8	7.950	0.039
4.50	12.106	0.008	0.194	0.024	0.024	0.007	0.026	0.072	9.52	0.58	19.73	4.20	61.2	3.7	7.949	0.039
5.00	11.313	0.006	0.187	0.019	0.019	0.005	0.018	0.067	9.49	0.37	14.97	6.37	61	2.3	7.949	0.038
6.00	9.909	0.004	0.192	0.01	0.014	0.004	0.007	0.05	9.27	0.11	6.58	23.96	59.6	0.7	7.951	0.040
DC028	Biotite	200-250um	J= 0.003806±0.000022													
0.50	29.337	0.024	0.043	0.303	0.057	0.242	0.089	0.153	6.13	4	77.94	0.25	41.6	26.9	0.045	0.004
1.00	10.265	0.006	0.015	0.109	0.005	0.271	0.01	0.124	7.71	0.35	24.11	3.11	52.2	2.4	0.012	-0.000
1.50	8.187	0.004	0.013	0.066	0.001	0.284	0.002	0.189	7.63	0.13	6.58	10.08	51.6	0.8	0.001	-0.000
2.00	7.926	0.004	0.013	0.06	0.001	0.294	0.001	0.289	7.67	0.1	3.01	11.05	51.9	0.7	0.000	-0.000
2.25	7.944	0.006	0.013	0.084	0.002	0.324	0.001	0.46	7.72	0.17	2.30	5.93	52.2	1.2	0.001	-0.000
2.75	7.861	0.005	0.013	0.087	0.002	0.431	0.001	0.564	7.79	0.14	0.55	7.67	52.7	0.9	0.000	-0.000
3.25	7.84	0.004	0.013	0.068	0.002	0.33	0.001	0.428	7.72	0.11	1.21	9.21	52.2	0.7	0.002	-0.000

Watts	40Ar/39Ar	±	38Ar/39Ar	±	37Ar/39Ar	±	36Ar/39Ar	±	40Ar*/39ArK	±	%40Ar atm	% 39Ar	Age	±	Ca/K	Cl/K
4.00	7.788	0.004	0.013	0.05	0.001	0.326	0.001	0.462	7.65	0.09	1.65	11.41	51.7	0.6	0.000	-0.000
5.00	7.768	0.004	0.013	0.04	0.001	0.318	0.001	0.388	7.68	0.07	1.02	16.31	52	0.5	0.000	-0.000
6.00	7.82	0.004	0.013	0.06	0.002	0.312	0.001	0.467	7.72	0.1	1.11	10.12	52.2	0.6	0.000	-0.000
7.00	7.908	0.006	0.013	0.081	0.003	0.324	0.001	0.64	7.8	0.18	0.75	5.53	52.8	1.2	0.004	-0.000
8.00	7.843	0.004	0.013	0.062	0.002	0.256	0.001	0.481	7.7	0.12	1.59	9.33	52.1	0.8	0.001	-0.000
DC048-1	Hornblende	100-250um	J= 0.003734±0.000036													
2.00	28.945	0.025	0.047	0.204	3.811	0.029	0.078	0.105	10.27	2.45	62.38	3.62	67.9	15.9	21.474	0.004
3.00	10.37	0.006	0.023	0.056	4.215	0.008	0.009	0.076	9.1	0.22	12.07	52.01	60.3	1.4	24.059	0.002
3.25	13.204	0.018	0.025	0.16	4.067	0.02	0.022	0.178	9.27	1.18	24.79	7.64	61.4	7.7	23.098	0.001
3.75	10.7	0.011	0.022	0.12	4.101	0.013	0.011	0.156	9.23	0.54	11.23	18.08	61.1	3.5	23.381	0.001
4.25	14.069	0.023	0.03	0.279	4.245	0.024	0.031	0.197	8.13	1.83	35.58	4.84	54	11.9	24.052	0.002
5.00	12.027	0.018	0.027	0.165	4.334	0.019	0.02	0.2	8.65	1.23	22.11	7.32	57.4	8	24.662	0.002
5.50	21.287	0.04	0.038	0.541	4.446	0.042	0.072	0.243	8.08	5.25	52.66	1.73	53.6	34.3	24.810	0.003
6.00	14.072	0.025	0.028	0.294	4.327	0.026	0.028	0.224	9.72	1.87	22.22	4.74	64.3	12.2	24.539	0.003
DC048-2	Hornblende	HP	J= 0.003613±0.000022													
2.00	49.393	0.039	0.218	0.193	0.223	0.038	0.387	0.088	10.28	14.19	82.90	0.34	65.8	89.2	24.498	0.003
3.00	11.177	0.011	0.034	0.106	0.049	0.01	0.029	0.079	9.12	0.71	15.95	7.36	58.5	4.5	24.500	0.001
3.50	10.772	0.007	0.03	0.077	0.045	0.006	0.021	0.078	9.26	0.49	12.83	12.07	59.4	3.1	24.500	0.001
4.00	10.003	0.006	0.027	0.051	0.041	0.006	0.014	0.064	9.09	0.29	8.55	18.97	58.3	1.8	24.500	0.001
4.50	10.566	0.006	0.029	0.059	0.042	0.006	0.018	0.058	9.06	0.33	13.54	15.54	58.1	2.1	24.500	0.001
5.00	11.769	0.008	0.033	0.075	0.046	0.007	0.028	0.071	8.96	0.62	22.44	9.24	57.5	3.9	24.500	0.001
5.50	12.577	0.01	0.038	0.088	0.05	0.01	0.036	0.076	9.21	0.85	24.80	6.53	59.1	5.3	24.500	0.001
6.50	9.793	0.005	0.026	0.043	0.039	0.005	0.012	0.047	8.96	0.17	8.64	29.96	57.4	1.1	24.500	0.001
DC058-1	Muscovite	HP	J= 0.003664±0.000016													
0.50	77.348	0.041	0.068	0.356	0.081	0.347	0.253	0.1	9.57	6.95	87.36	0.11	62.2	44.4	0.000	0.001
1.00	15.151	0.021	0.018	0.282	0.02	0.327	0.027	0.124	8.55	1	41.85	0.45	55.7	6.4	0.000	-0.000
1.50	20.275	0.02	0.022	0.188	0.012	0.342	0.045	0.078	8.02	1.03	59.96	0.75	52.3	6.6	0.000	-0.000
2.00	12.357	0.006	0.016	0.062	0.002	0.353	0.016	0.04	7.74	0.2	37.30	4.82	50.4	1.3	0.000	-0.000
2.50	9.744	0.005	0.015	0.065	0.001	0.438	0.007	0.05	7.74	0.11	20.59	10.29	50.5	0.7	0.000	-0.000
2.75	8.175	0.005	0.014	0.058	0	0.69	0.002	0.112	7.77	0.06	5.09	23.27	50.6	0.4	0.000	-0.000
3.00	8.158	0.005	0.014	0.062	0.001	0.426	0.002	0.105	7.79	0.06	4.56	10.02	50.7	0.4	0.000	-0.000
3.25	8.129	0.006	0.013	0.064	0.001	0.479	0.001	0.115	7.76	0.07	4.57	14.02	50.6	0.4	0.000	-0.000
3.50	8.002	0.006	0.014	0.06	0.001	0.43	0.001	0.178	7.78	0.07	2.62	7.50	50.7	0.5	0.000	-0.000
4.00	8.007	0.005	0.013	0.076	0.001	0.391	0.001	0.188	7.78	0.07	2.74	7.63	50.7	0.4	0.000	-0.000

Watts	40Ar/39Ar	±	38Ar/39Ar	±	37Ar/39Ar	±	36Ar/39Ar	±	40Ar*/39ArK	±	%40Ar atm	% 39Ar	Age	±	Ca/K	Cl/K
4.50	8.208	0.008	0.014	0.097	0.003	0.373	0.002	0.206	7.84	0.14	3.91	3.04	51.1	0.9	0.002	-0.000
5.00	8.35	0.01	0.014	0.116	0.004	0.429	0.002	0.251	7.84	0.2	5.29	2.31	51.1	1.3	0.000	-0.000
6.00	8.163	0.007	0.013	0.092	0.003	0.336	0.002	0.258	7.87	0.14	3.03	3.14	51.3	0.9	0.001	-0.000
7.00	7.859	0.005	0.013	0.057	0.001	0.433	0	0.274	7.8	0.05	0.80	12.66	50.8	0.3	0.001	-0.000
DC080-H	Hornblende	100-250um	J= 0.003744±0.000028													
2.00	56.087	0.012	0.053	0.081	0.9	0.02	0.142	0.03	16.51	1.19	70.54	3.27	108.2	7.6	5.101	0.003
2.75	11.963	0.006	0.035	0.056	1.905	0.009	0.012	0.074	9.35	0.27	21.40	10.44	62.1	1.8	10.993	0.004
3.25	10.21	0.004	0.035	0.029	1.887	0.007	0.005	0.07	9.43	0.11	7.87	29.96	62.6	0.7	10.903	0.005
3.50	10.046	0.006	0.035	0.036	1.803	0.009	0.005	0.114	9.44	0.17	5.74	16.20	62.7	1.1	10.411	0.005
3.75	10.231	0.008	0.035	0.051	1.873	0.01	0.005	0.138	9.62	0.23	5.20	10.48	63.8	1.5	10.816	0.005
4.00	10.481	0.008	0.035	0.066	1.831	0.01	0.007	0.173	9.47	0.36	8.42	7.60	62.8	2.3	10.564	0.005
4.50	11.986	0.011	0.036	0.074	1.829	0.014	0.013	0.127	9.43	0.51	19.61	4.84	62.6	3.3	10.530	0.004
5.00	11.562	0.01	0.036	0.095	1.885	0.013	0.011	0.18	9.56	0.61	14.86	3.91	63.5	4	10.865	0.004
5.50	10.996	0.011	0.036	0.087	1.85	0.014	0.01	0.188	9.66	0.56	9.53	4.17	64.1	3.6	10.673	0.005
6.50	10.364	0.007	0.033	0.057	1.653	0.011	0.007	0.133	9.32	0.28	9.11	9.13	61.9	1.8	9.546	0.004
DC080-B1	Biotite	HP	J= 0.003630±0.000018													
0.25	53.092	0.086	0.084	1.02	0.308	0.427	0.208	0.222	2.78	13.2	94.06	0.04	18.1	85.6	0.000	0.002
0.50	23.302	0.055	0.041	1.199	0.143	0.469	0.081	0.263	5.74	6.31	71.13	0.08	37.2	40.5	0.000	0.000
0.75	11.116	0.014	0.021	0.148	0.007	0.405	0.01	0.099	7.35	0.42	33.10	2.11	47.5	2.7	0.008	0.001
1.00	8.911	0.008	0.018	0.102	0.005	0.303	0.004	0.15	7.86	0.19	11.17	3.84	50.8	1.2	0.014	0.001
1.25	8.666	0.006	0.019	0.058	0.003	0.238	0.003	0.096	7.9	0.1	8.74	8.57	51	0.6	0.016	0.001
1.50	8.526	0.006	0.018	0.073	0.003	0.219	0.002	0.106	7.92	0.09	6.97	8.93	51.1	0.6	0.017	0.001
1.75	8.398	0.006	0.018	0.059	0.003	0.295	0.002	0.17	7.99	0.1	4.69	8.03	51.6	0.6	0.011	0.001
2.00	8.185	0.007	0.018	0.062	0.003	0.246	0.001	0.198	7.96	0.08	2.64	9.02	51.4	0.5	0.018	0.001
2.50	8.083	0.006	0.018	0.044	0.005	0.146	0.001	0.319	7.96	0.09	1.34	9.40	51.4	0.5	0.040	0.001
3.00	8.103	0.006	0.018	0.054	0.009	0.098	0.001	0.266	7.95	0.08	1.74	9.20	51.3	0.5	0.099	0.001
3.50	8.068	0.007	0.018	0.066	0.004	0.223	0.001	0.335	7.94	0.1	1.33	6.83	51.3	0.6	0.025	0.001
4.00	8.053	0.005	0.018	0.062	0.009	0.098	0.001	0.29	7.94	0.08	1.20	8.84	51.3	0.5	0.095	0.001
4.50	8.058	0.008	0.018	0.074	0.014	0.087	0.001	0.328	7.94	0.1	1.20	7.24	51.3	0.6	0.160	0.001
5.00	8.138	0.009	0.018	0.103	0.006	0.272	0.001	0.445	8.03	0.15	0.66	4.39	51.9	0.9	0.026	0.001
5.50	8.173	0.01	0.018	0.104	0.005	0.33	0.001	0.435	8	0.18	1.24	3.26	51.6	1.1	0.008	0.001
6.00	8.263	0.012	0.018	0.149	0.008	0.439	0.002	0.516	8.03	0.29	1.18	1.95	51.8	1.8	0.006	0.001
7.00	8.03	0.006	0.018	0.064	0.005	0.173	0.001	0.374	7.96	0.08	0.71	8.28	51.4	0.5	0.040	0.001
DC080-B2	Biotite	HP	J= 0.003733±0.000018													
7.00	8.877	0.007	0.02	0.067	0.003	0.006	0.006	0.085	7.79	0.17	10.33	100.00	51.7	1.1	0.001	0.001

Watts	40Ar/39Ar	±	38Ar/39Ar	±	37Ar/39Ar	±	36Ar/39Ar	±	40Ar*/39ArK	±	%40Ar atm	% 39Ar	Age	±	Ca/K	Cl/K
DC169-1	Hornblende	HP	J= 0.003639±0.000016													
2.00	129.029	0.028	0.175	0.111	0.115	0.028	0.415	0.047	52.43	6.16	65.61	1.54	315	34	17.850	0.005
3.00	14.466	0.007	0.044	0.068	0.037	0.007	0.033	0.056	10.33	0.56	28.03	14.75	66.6	3.5	17.850	0.004
3.50	10.31	0.006	0.039	0.049	0.034	0.005	0.018	0.064	8.7	0.36	14.68	23.23	56.2	2.3	17.850	0.004
4.00	10.826	0.007	0.044	0.06	0.038	0.007	0.027	0.072	8.21	0.6	22.30	14.29	53.1	3.8	17.850	0.004
4.50	10.359	0.007	0.042	0.066	0.035	0.006	0.023	0.062	8.18	0.44	19.53	17.49	52.9	2.8	17.850	0.004
5.00	11.043	0.008	0.047	0.059	0.039	0.007	0.03	0.062	8	0.57	25.65	12.87	51.7	3.7	17.850	0.004
6.00	11.405	0.008	0.046	0.063	0.037	0.007	0.027	0.058	8.41	0.48	24.97	15.83	54.4	3.1	17.850	0.004
DC169-2	Hornblende	>250um	J= 0.003747±0.000028													
2.00	269.91	0.02	0.181	0.069	2.05	0.025	0.753	0.027	58.46	4.62	78.59	1.42	357.3	25.6	11.704	0.006
3.00	33.749	0.019	0.035	0.223	1.844	0.025	0.061	0.116	20.07	2.13	38.79	1.50	130.8	13.4	10.484	0.003
3.50	11.045	0.008	0.032	0.075	2.794	0.011	0.011	0.143	9.25	0.48	14.79	6.92	61.5	3.1	16.207	0.004
4.00	9.454	0.006	0.03	0.039	2.88	0.008	0.006	0.105	8.71	0.2	7.69	18.38	57.9	1.3	16.735	0.003
4.25	9.216	0.007	0.031	0.053	3.05	0.009	0.007	0.102	8.53	0.21	6.92	14.91	56.8	1.4	17.730	0.004
4.50	9.183	0.007	0.031	0.047	2.962	0.009	0.006	0.12	8.48	0.24	6.93	12.54	56.4	1.6	17.225	0.004
4.75	12.77	0.015	0.034	0.168	2.973	0.018	0.022	0.216	9.37	1.41	21.61	2.08	62.2	9.2	17.234	0.004
5.25	9.387	0.007	0.031	0.052	2.998	0.009	0.006	0.115	8.72	0.22	6.59	14.45	58	1.5	17.450	0.004
5.50	9.591	0.008	0.031	0.066	3.053	0.01	0.008	0.141	8.58	0.36	9.22	8.65	57.1	2.4	17.768	0.004
6.00	9.029	0.008	0.031	0.062	3.026	0.01	0.007	0.14	8.4	0.28	5.73	9.93	55.9	1.9	17.604	0.003
6.25	11.871	0.016	0.036	0.269	3.041	0.019	0.021	0.233	8.87	1.5	19.16	1.99	59	9.8	17.598	0.004
7.00	9.765	0.01	0.04	0.061	3.672	0.013	0.009	0.165	8.91	0.46	7.13	7.22	59.2	3	21.416	0.006
DC176-1	Hornblende	200-250um	J= 0.003807±0.000022													
2.00	157.06	0.052	0.171	0.258	0.654	0.091	0.422	0.088	43.07	9.38	72.22	0.11	273.9	55.4	3.282	0.017
3.00	14.211	0.008	0.156	0.029	0.843	0.014	0.021	0.075	8.92	0.48	36.66	2.27	60.2	3.2	5.659	0.032
3.50	8.304	0.005	0.15	0.013	0.834	0.008	0.002	0.119	8.01	0.09	3.53	10.25	54.2	0.6	5.646	0.031
4.00	8.015	0.003	0.162	0.009	0.822	0.007	0.002	0.087	7.89	0.05	1.91	34.78	53.4	0.3	5.568	0.034
4.25	7.987	0.004	0.156	0.012	0.806	0.007	0.002	0.143	7.87	0.08	1.52	12.46	53.2	0.6	5.454	0.032
4.50	8.242	0.005	0.149	0.016	0.797	0.009	0.003	0.18	7.92	0.15	3.56	6.52	53.6	1	5.391	0.031
5.00	8.162	0.005	0.158	0.015	0.804	0.008	0.002	0.176	7.94	0.12	2.52	8.17	53.7	0.8	5.441	0.033
5.50	8.778	0.007	0.149	0.026	0.821	0.01	0.005	0.165	8	0.24	8.02	3.90	54.1	1.6	5.542	0.031
6.00	8.606	0.007	0.163	0.024	0.832	0.011	0.004	0.224	7.94	0.28	6.51	3.16	53.7	1.9	5.612	0.034
7.50	8.131	0.004	0.152	0.009	0.785	0.007	0.002	0.107	7.97	0.06	2.18	18.37	53.9	0.4	5.325	0.032

Watts	40Ar/39Ar	±	38Ar/39Ar	±	37Ar/39Ar	±	36Ar/39Ar	±	40Ar*/39ArK	±	%40Ar atm	% 39Ar	Age	±	Ca/K	Cl/K	
DC176-2	Biotite	>250um	J= 0.003809±0.000024														
0.50	82.448	0.036	0.108	0.288	0.098	0.312	0.287	0.067	6.55	5	92.00	0.13	44.4	33.5	0.187	0.006	
1.00	14.228	0.011	0.051	0.076	0.011	0.284	0.026	0.068	7.3	0.53	47.66	1.16	49.5	3.5	0.033	0.007	
1.50	9.086	0.008	0.047	0.05	0.005	0.219	0.006	0.134	7.39	0.26	17.80	3.07	50.1	1.8	0.012	0.007	
1.75	8.028	0.005	0.046	0.029	0.003	0.25	0.002	0.158	7.52	0.11	5.82	5.47	50.9	0.8	0.009	0.007	
2.00	7.89	0.004	0.046	0.022	0.002	0.221	0.002	0.122	7.5	0.07	4.67	8.78	50.8	0.5	0.007	0.007	
2.25	7.808	0.006	0.046	0.058	0.005	0.211	0.002	0.37	7.6	0.18	1.37	3.14	51.5	1.2	0.018	0.007	
2.50	7.732	0.006	0.046	0.045	0.004	0.279	0.001	0.333	7.6	0.14	0.73	3.84	51.5	1	0.014	0.007	
3.00	7.711	0.004	0.046	0.04	0.003	0.224	0.001	0.255	7.55	0.08	1.55	6.26	51.2	0.6	0.012	0.007	
3.50	7.681	0.004	0.046	0.033	0.003	0.207	0.001	0.307	7.53	0.09	1.52	7.34	51	0.6	0.012	0.007	
4.00	7.719	0.005	0.045	0.031	0.004	0.2	0.001	0.255	7.5	0.1	2.31	5.76	50.8	0.7	0.018	0.007	
4.50	7.711	0.005	0.046	0.027	0.003	0.213	0.001	0.249	7.5	0.09	2.30	6.43	50.8	0.6	0.012	0.007	
5.00	7.707	0.005	0.045	0.031	0.003	0.269	0.001	0.323	7.57	0.1	1.24	6.17	51.3	0.6	0.013	0.007	
6.00	7.564	0.004	0.045	0.02	0.002	0.246	0.001	0.293	7.49	0.06	0.83	11.37	50.7	0.4	0.006	0.007	
7.00	7.55	0.004	0.045	0.021	0.002	0.194	0	0.352	7.48	0.06	0.80	13.07	50.7	0.4	0.006	0.007	
8.00	7.586	0.004	0.046	0.021	0.002	0.182	0	0.276	7.51	0.05	0.97	18.01	50.9	0.3	0.009	0.007	
DC178	Biotite	200-250um	J= 0.003810±0.000024														
0.50	48.825	0.029	0.05	0.634	0.062	0.43	0.162	0.098	5.39	4.55	88.86	0.19	36.7	30.6	0.003	-0.000	
1.00	12.71	0.006	0.018	0.141	0.006	0.343	0.02	0.059	7.22	0.35	43.08	2.46	49	2.4	0.002	0.000	
1.50	8.392	0.004	0.015	0.063	0.002	0.348	0.004	0.088	7.43	0.1	11.53	9.07	50.4	0.7	0.000	0.000	
1.75	7.796	0.004	0.015	0.053	0.002	0.374	0.001	0.211	7.53	0.09	3.49	9.21	51	0.6	0.000	0.000	
2.00	7.705	0.004	0.015	0.062	0.002	0.443	0.001	0.331	7.52	0.09	2.43	8.90	51	0.6	0.001	0.000	
2.25	7.695	0.004	0.015	0.056	0.002	0.282	0.001	0.369	7.56	0.1	1.85	9.62	51.2	0.7	0.004	0.000	
2.75	7.922	0.006	0.015	0.155	0.004	0.448	0.002	0.491	7.68	0.25	2.80	3.15	52.1	1.7	0.002	0.000	
3.25	7.739	0.005	0.015	0.065	0.002	0.387	0.001	0.394	7.57	0.12	2.26	7.23	51.3	0.8	0.000	0.000	
3.75	7.726	0.005	0.015	0.069	0.002	0.36	0.001	0.465	7.55	0.15	2.38	6.70	51.1	1	0.002	0.000	
4.25	7.694	0.005	0.015	0.064	0.002	0.39	0.001	0.444	7.59	0.11	1.41	8.23	51.5	0.8	0.000	0.000	
4.75	7.736	0.005	0.015	0.082	0.002	0.393	0.001	0.386	7.53	0.13	2.61	5.94	51.1	0.9	0.000	0.000	
5.50	7.718	0.005	0.015	0.067	0.002	0.426	0.001	0.437	7.55	0.12	2.26	6.53	51.1	0.8	0.002	0.000	
6.50	7.728	0.004	0.015	0.072	0.002	0.312	0.001	0.422	7.62	0.11	1.46	7.06	51.6	0.8	0.002	0.000	
7.50	7.644	0.003	0.015	0.04	0.006	0.077	0.001	0.322	7.54	0.06	1.54	15.72	51.1	0.4	0.035	0.000	
DC186-1B	Biotite	100-250um	J= 0.003748±0.000022														
0.50	40.956	0.027	0.074	0.253	0.079	0.225	0.134	0.089	2.69	3.43	93.22	0.23	18.1	22.9	0.170	0.007	
1.00	12.879	0.01	0.046	0.072	0.012	0.191	0.021	0.082	7.11	0.51	44.07	1.66	47.5	3.3	0.009	0.006	
1.50	9.117	0.005	0.046	0.031	0.003	0.222	0.006	0.108	7.58	0.18	16.63	6.36	50.5	1.2	0.008	0.007	

Watts	40Ar/39Ar	±	38Ar/39Ar	±	37Ar/39Ar	±	36Ar/39Ar	±	40Ar*/39ArK	±	%40Ar atm	% 39Ar	Age	±	Ca/K	Cl/K
1.75	8.593	0.006	0.046	0.032	0.003	0.174	0.004	0.116	7.58	0.14	11.52	6.41	50.5	0.9	0.004	0.007
2.00	8.85	0.005	0.046	0.042	0.004	0.208	0.004	0.141	7.71	0.19	12.50	4.88	51.4	1.2	0.010	0.007
2.25	8.445	0.006	0.045	0.041	0.004	0.199	0.003	0.208	7.69	0.19	8.41	4.58	51.3	1.2	0.006	0.007
2.50	8.212	0.006	0.047	0.036	0.004	0.194	0.002	0.223	7.71	0.14	5.76	5.72	51.4	0.9	0.012	0.007
3.00	8.209	0.005	0.047	0.038	0.004	0.178	0.002	0.295	7.8	0.16	4.50	4.90	52	1.1	0.007	0.007
3.50	8.011	0.004	0.047	0.024	0.003	0.156	0.001	0.203	7.73	0.08	3.32	9.13	51.5	0.5	0.011	0.008
4.00	8.17	0.006	0.047	0.039	0.004	0.199	0.002	0.357	7.77	0.19	4.39	5.01	51.8	1.3	0.013	0.007
5.00	7.977	0.005	0.046	0.034	0.005	0.133	0.001	0.262	7.65	0.1	3.84	7.82	51	0.7	0.025	0.007
6.00	7.851	0.004	0.046	0.029	0.004	0.125	0.001	0.31	7.68	0.08	2.05	9.91	51.2	0.5	0.020	0.007
7.00	7.907	0.005	0.046	0.032	0.006	0.141	0.001	0.424	7.69	0.13	2.40	6.59	51.3	0.8	0.029	0.007
8.00	7.762	0.004	0.047	0.024	0.002	0.223	0	0.255	7.67	0.05	1.33	26.79	51.1	0.3	0.012	0.007

DC186-2B Biotite HP J= 0.003643±0.000016

0.50	160.471	0.036	0.193	0.13	0.098	0.245	0.556	0.052	2.07	6.28	98.70	0.10	13.6	41	0.533	0.016
1.00	19.502	0.01	0.056	0.061	0.014	0.184	0.042	0.046	7.56	0.58	61.15	1.16	49	3.7	0.119	0.008
1.25	9.892	0.007	0.049	0.035	0.005	0.194	0.008	0.055	7.71	0.14	21.99	2.96	49.9	0.9	0.036	0.008
1.50	8.523	0.006	0.049	0.037	0.002	0.226	0.003	0.096	7.79	0.09	8.60	4.34	50.5	0.6	0.015	0.008
1.75	8.716	0.006	0.049	0.029	0.002	0.268	0.003	0.065	7.79	0.08	10.71	5.68	50.5	0.5	0.011	0.008
2.00	8.238	0.006	0.05	0.03	0.002	0.239	0.002	0.114	7.8	0.08	5.28	4.85	50.6	0.5	0.010	0.008
2.25	8.13	0.005	0.049	0.024	0.002	0.263	0.001	0.135	7.81	0.07	3.91	4.77	50.6	0.4	0.012	0.008
2.50	8.12	0.005	0.051	0.026	0.002	0.264	0.001	0.151	7.83	0.07	3.57	5.27	50.7	0.4	0.011	0.008
2.75	8.112	0.005	0.05	0.048	0.002	0.273	0.001	0.216	7.86	0.09	3.01	3.40	50.9	0.6	0.011	0.008
3.00	8.149	0.006	0.051	0.042	0.003	0.279	0.001	0.191	7.88	0.08	3.12	3.60	51.1	0.5	0.014	0.008
3.50	8.075	0.005	0.05	0.036	0.002	0.238	0.001	0.175	7.83	0.07	2.98	5.05	50.8	0.4	0.014	0.008
4.00	7.985	0.005	0.049	0.036	0.002	0.23	0.001	0.249	7.85	0.07	1.64	4.53	50.9	0.4	0.014	0.008
4.50	8.069	0.005	0.049	0.033	0.003	0.232	0.001	0.237	7.87	0.08	2.29	3.81	51	0.5	0.014	0.008
5.00	7.978	0.005	0.049	0.031	0.002	0.249	0.001	0.249	7.84	0.07	1.65	4.63	50.8	0.4	0.017	0.008
5.50	7.958	0.006	0.049	0.035	0.002	0.292	0.001	0.239	7.85	0.06	1.35	5.89	50.9	0.4	0.008	0.008
6.00	7.909	0.006	0.049	0.03	0.001	0.371	0.001	0.287	7.81	0.07	1.30	7.44	50.6	0.4	0.003	0.008
6.50	7.922	0.005	0.049	0.03	0.001	0.348	0.001	0.307	7.83	0.06	1.14	5.51	50.7	0.4	0.002	0.008
7.00	7.904	0.004	0.051	0.026	0.001	0.382	0	0.264	7.82	0.05	1.21	27.01	50.7	0.3	0.006	0.008

DC186-1H Hornblende 100-250um J= 0.003756±0.000024

2.00	92.975	0.014	0.134	0.056	0.86	0.02	0.178	0.034	43.79	1.79	53.14	2.48	274.7	10.4	4.914	0.020
2.50	26.881	0.012	0.191	0.037	2.298	0.015	0.046	0.075	15.33	1.03	42.89	3.28	101	6.6	13.476	0.038
2.75	12.298	0.009	0.172	0.034	1.861	0.012	0.014	0.126	9.3	0.53	23.68	5.27	61.9	3.5	10.912	0.036
3.00	11.63	0.006	0.184	0.018	1.914	0.009	0.011	0.076	9.22	0.27	20.80	12.03	61.4	1.8	11.274	0.038
3.25	10.025	0.006	0.165	0.024	1.603	0.009	0.008	0.15	8.66	0.35	13.28	9.95	57.7	2.3	9.420	0.034
3.50	10.294	0.008	0.161	0.022	1.609	0.01	0.008	0.112	8.87	0.27	13.63	11.12	59.1	1.8	9.467	0.033

Watts	40Ar/39Ar	±	38Ar/39Ar	±	37Ar/39Ar	±	36Ar/39Ar	±	40Ar*/39ArK	±	%40Ar atm	% 39Ar	Age	±	Ca/K	Cl/K
5.25	9.897	0.009	0.024	0.104	2.843	0.012	0.01	0.162	8.43	0.51	12.72	8.10	56.1	3.3	16.603	0.002
6.00	9.224	0.007	0.023	0.076	2.974	0.01	0.008	0.143	8.17	0.34	10.56	15.40	54.4	2.2	17.388	0.002
DC191-1	Biotite	HP	J= 0.003670±0.000016													
0.50	56.482	0.018	0.052	0.178	0.019	0.472	0.175	0.047	7.07	2.26	87.41	0.85	46.2	14.6	0.000	0.001
1.00	11.933	0.006	0.018	0.049	0.001	0.408	0.015	0.04	7.84	0.18	34.30	12.58	51.2	1.2	0.001	0.000
1.25	8.765	0.005	0.016	0.05	0.001	0.455	0.003	0.077	7.83	0.09	10.61	17.94	51.1	0.6	0.000	0.000
1.50	8.465	0.006	0.016	0.096	0.001	0.397	0.002	0.104	7.9	0.09	6.49	11.72	51.6	0.6	0.000	0.000
1.75	8.639	0.007	0.016	0.095	0.003	0.398	0.003	0.153	7.96	0.15	7.29	5.94	51.9	0.9	0.000	0.000
2.00	8.951	0.009	0.016	0.093	0.003	0.402	0.004	0.148	7.97	0.19	10.29	5.11	52	1.2	0.000	0.000
2.50	9.027	0.009	0.017	0.12	0.004	0.371	0.004	0.139	8.11	0.18	9.42	4.36	52.9	1.2	0.000	0.000
3.00	8.693	0.008	0.016	0.111	0.003	0.376	0.003	0.156	7.99	0.16	7.48	5.69	52.2	1	0.000	0.000
3.50	8.649	0.01	0.016	0.117	0.004	0.402	0.003	0.237	8.02	0.23	6.34	4.04	52.3	1.5	0.000	0.000
4.00	8.487	0.01	0.017	0.081	0.004	0.402	0.003	0.235	8.01	0.2	4.77	4.51	52.3	1.3	0.000	0.000
4.50	8.307	0.01	0.016	0.113	0.004	0.357	0.002	0.275	7.93	0.18	3.72	4.84	51.8	1.1	0.000	0.000
5.00	8.333	0.01	0.016	0.102	0.004	0.35	0.002	0.385	8	0.24	2.91	3.79	52.2	1.5	0.000	0.000
6.00	8.107	0.009	0.016	0.098	0.002	0.432	0.001	0.33	7.91	0.14	1.94	6.71	51.6	0.9	0.000	0.000
7.00	8.011	0.005	0.016	0.05	0.001	0.47	0.001	0.234	7.82	0.08	2.19	11.93	51	0.5	0.000	0.000
DC191-1	Biotite	HP	J= 0.003775±0.000018													
0.50	9.994	0.008	0.019	0.077	0.003	0.016	0.01	0.079	7.94	0.24	18.91	1.62	53.3	1.6	0.001	0.000
1.00	9.015	0.006	0.017	0.056	0	0.006	0.005	0.06	7.76	0.1	13.42	11.61	52.1	0.6	0.001	0.000
1.25	9.501	0.005	0.018	0.042	0.001	0.008	0.007	0.059	7.7	0.12	18.42	7.50	51.7	0.8	0.001	0.000
1.50	10.09	0.005	0.018	0.04	0	0.006	0.009	0.053	7.65	0.14	23.84	13.13	51.3	0.9	0.001	0.000
1.75	9.919	0.006	0.018	0.049	0.001	0.007	0.008	0.054	7.7	0.14	21.95	10.37	51.7	0.9	0.001	0.000
2.00	10.762	0.005	0.018	0.051	0.001	0.006	0.012	0.05	7.63	0.18	28.59	5.84	51.2	1.2	0.001	0.000
2.50	22.14	0.014	0.033	0.113	0.013	0.014	0.062	0.059	7.66	1.09	64.50	0.40	51.4	7.2	0.001	0.000
3.00	9.533	0.007	0.019	0.073	0.003	0.013	0.009	0.081	7.79	0.22	16.56	1.68	52.3	1.5	0.001	0.000
3.50	8.628	0.005	0.018	0.041	0.001	0.005	0.004	0.074	7.71	0.11	9.47	3.52	51.8	0.7	0.001	0.000
4.00	71.407	0.018	0.073	0.128	0.02	0.018	0.246	0.034	4.95	2.21	93.09	0.26	33.4	14.8	0.001	0.001
4.50	15.196	0.007	0.022	0.056	0.002	0.007	0.028	0.032	7.49	0.27	50.28	3.06	50.3	1.8	0.001	0.000
5.00	9.634	0.006	0.017	0.059	0.001	0.007	0.007	0.054	7.65	0.13	20.13	11.10	51.4	0.8	0.001	0.000
6.00	8.612	0.005	0.017	0.055	0.001	0.005	0.004	0.088	7.75	0.1	9.34	7.04	52	0.7	0.001	0.000
7.00	8.254	0.005	0.017	0.045	0	0.007	0.002	0.09	7.68	0.07	6.48	22.85	51.6	0.5	0.001	0.001
DC193	Biotite	HP	J= 0.003702±0.000018													
0.50	45.421	0.075	0.063	0.706	0.201	0.356	0.155	0.252	11.47	11.49	72.27	0.33	75	73.6	0.525	0.002

Watts	40Ar/39Ar	±	38Ar/39Ar	±	37Ar/39Ar	±	36Ar/39Ar	±	40Ar*/39ArK	±	%40Ar atm	% 39Ar	Age	±	Ca/K	Cl/K
1.00	10.699	0.013	0.016	0.129	0.007	0.336	0.011	0.129	7.89	0.44	24.92	8.30	52	2.9	0.000	-0.000
1.50	7.973	0.008	0.015	0.085	0.003	0.34	0.001	0.312	7.82	0.13	1.16	22.34	51.5	0.8	0.000	0.000
1.75	8.013	0.011	0.015	0.154	0.005	0.332	0.002	0.442	7.86	0.24	0.39	12.11	51.7	1.6	0.000	-0.000
2.00	8.163	0.015	0.015	0.189	0.009	0.299	0.003	0.443	7.94	0.36	0.09	7.30	52.3	2.3	0.006	0.000
2.50	8.479	0.021	0.016	0.308	0.018	0.375	0.005	0.467	7.92	0.72	0.72	3.27	52.1	4.7	0.000	-0.000
3.00	8.222	0.014	0.015	0.214	0.011	0.312	0.003	0.515	7.74	0.54	2.47	5.62	51	3.5	0.000	0.000
4.00	8.035	0.012	0.015	0.165	0.005	0.317	0.002	0.447	7.87	0.24	0.58	12.19	51.8	1.6	0.000	0.000
5.00	7.969	0.012	0.015	0.104	0.005	0.414	0.001	0.504	7.81	0.23	0.66	13.71	51.4	1.5	0.000	-0.000
7.00	7.982	0.01	0.014	0.129	0.004	0.302	0.001	0.502	7.88	0.2	0.16	14.83	51.9	1.3	0.000	-0.000
DC195	Hornblende	>250um	J= 0.003811±0.000026													
2.00	266.714	0.029	0.178	0.125	0.681	0.05	0.8	0.039	42.38	6.45	84.25	0.68	270.1	38.2	4.113	0.004
3.00	37.067	0.03	0.042	0.492	1.464	0.041	0.105	0.122	10.06	3.77	71.74	0.74	67.8	25	9.530	0.001
3.50	27.147	0.02	0.035	0.332	2.136	0.025	0.062	0.15	12.1	2.75	53.71	1.20	81.3	18.1	14.223	0.001
4.00	10.936	0.005	0.021	0.049	2.199	0.008	0.011	0.049	8.67	0.16	20.97	21.61	58.6	1.1	14.999	0.001
4.50	8.936	0.004	0.02	0.038	2.222	0.007	0.006	0.071	8.19	0.12	8.71	32.30	55.5	0.8	15.174	0.001
5.00	8.519	0.005	0.02	0.056	2.227	0.008	0.005	0.11	8.06	0.16	5.53	22.72	54.6	1.1	15.207	0.001
5.50	8.956	0.009	0.021	0.116	2.289	0.01	0.007	0.216	8.06	0.49	8.78	6.91	54.6	3.2	15.606	0.001
6.00	8.851	0.008	0.021	0.16	2.264	0.01	0.006	0.245	8.11	0.46	7.21	7.77	54.9	3.1	15.448	0.001
7.50	9.488	0.011	0.025	0.12	2.793	0.012	0.009	0.251	8.48	0.68	9.35	6.07	57.3	4.5	19.110	0.002
DC209	Hornblende	200-250um	J= 0.003812±0.000026													
2.00	338.6	0.087	0.299	0.268	3.132	0.092	1.094	0.099	39.48	17.04	88.60	0.51	253	101.8	20.400	0.016
3.00	17.289	0.015	0.15	0.054	3.481	0.017	0.038	0.114	8.7	1.3	48.59	6.26	58.9	8.7	23.731	0.029
3.50	8.929	0.006	0.147	0.023	3.405	0.008	0.008	0.117	8.09	0.27	9.18	27.21	54.8	1.8	23.372	0.030
4.00	8.87	0.007	0.148	0.026	3.401	0.009	0.007	0.125	8.16	0.29	7.80	26.57	55.2	1.9	23.348	0.031
4.50	9.596	0.01	0.15	0.031	3.429	0.011	0.011	0.161	7.97	0.54	15.87	14.80	54	3.6	23.518	0.031
5.00	12.902	0.018	0.157	0.07	3.497	0.02	0.026	0.224	8.17	1.79	33.22	4.08	55.3	11.9	23.914	0.032
5.50	11.989	0.017	0.146	0.099	3.493	0.018	0.023	0.186	8.28	1.29	28.03	5.22	56.1	8.6	23.934	0.029
6.00	11.356	0.013	0.154	0.046	3.466	0.015	0.018	0.212	8.58	1.15	21.71	6.38	58.1	7.7	23.773	0.031
7.50	12.528	0.011	0.258	0.029	4.038	0.013	0.022	0.122	8.77	0.8	28.77	8.96	59.3	5.3	27.731	0.055
DC219-1	Hornblende	100-250um	J= 0.003737±0.000032													
2.00	65.288	0.031	0.094	0.188	1.777	0.038	0.2	0.081	13.72	4.56	78.08	1.08	90.2	29.3	9.505	0.009
3.00	9.79	0.006	0.07	0.031	2.398	0.009	0.009	0.079	8.2	0.21	15.79	29.69	54.4	1.4	13.395	0.013
3.25	9.231	0.008	0.055	0.043	2.528	0.01	0.007	0.121	8.27	0.25	9.16	20.14	54.9	1.7	14.122	0.009
3.50	9.369	0.009	0.057	0.049	2.447	0.012	0.008	0.168	8.38	0.39	7.90	11.45	55.6	2.6	13.648	0.009

Watts	40Ar/39Ar	±	38Ar/39Ar	±	37Ar/39Ar	±	36Ar/39Ar	±	40Ar*/39ArK	±	%40Ar atm	% 39Ar	Age	±	Ca/K	Cl/K
4.00	9.952	0.01	0.059	0.048	2.48	0.012	0.01	0.137	8.32	0.4	14.01	12.49	55.2	2.6	13.849	0.010
4.50	10.275	0.014	0.064	0.094	2.511	0.017	0.012	0.216	8.73	0.77	8.95	5.62	57.9	5.1	13.992	0.011
5.00	11.238	0.016	0.079	0.091	2.51	0.019	0.018	0.23	8.17	1.24	20.27	3.75	54.3	8.1	13.947	0.014
6.00	9.276	0.009	0.057	0.046	2.514	0.011	0.007	0.156	8.24	0.35	8.83	15.77	54.7	2.3	14.065	0.009
DC219-2	Hornblende	HP	J= 0.003618±0.000020													
2.00	233.532	0.031	0.268	0.093	0.123	0.031	0.874	0.039	24.73	7.6	91.27	0.68	154.6	45.5	13.950	0.009
3.00	52.871	0.032	0.193	0.164	0.159	0.031	0.332	0.073	7.85	9	87.41	0.44	50.5	57.1	13.950	0.009
3.50	31.778	0.021	0.172	0.105	0.093	0.021	0.174	0.081	8.26	4.7	74.67	1.02	53.1	29.8	13.950	0.021
4.00	12.192	0.006	0.132	0.023	0.028	0.006	0.025	0.045	8.44	0.35	30.19	11.05	54.2	2.2	13.950	0.025
4.50	8.944	0.004	0.129	0.014	0.024	0.004	0.009	0.06	8.27	0.17	7.29	27.09	53.2	1	13.950	0.026
4.75	9.149	0.005	0.112	0.019	0.025	0.005	0.012	0.072	8.17	0.26	9.94	17.78	52.6	1.7	13.950	0.021
5.00	9.002	0.005	0.103	0.015	0.024	0.004	0.011	0.055	8.1	0.18	9.57	22.69	52.1	1.1	13.950	0.019
5.50	9.101	0.005	0.078	0.02	0.025	0.005	0.012	0.067	7.95	0.25	11.91	19.25	51.2	1.6	13.950	0.013
DC239	Hornblende	>250um	J= 0.003813±0.000028													
2.00	1151.288	0.091	0.529	0.399	3.037	0.108	1.008	0.126	912.55	90.1	22.62	0.19	2705.3	138.4	18.472	0.073
3.00	141.63	0.045	0.172	0.344	1.193	0.071	0.103	0.264	119.6	9.81	16.03	0.54	677.8	46.3	7.291	0.028
3.50	10.031	0.007	0.107	0.035	1.255	0.011	0.004	0.284	9.44	0.36	5.99	13.95	63.8	2.4	8.633	0.021
4.00	8.6	0.006	0.111	0.024	1.256	0.009	0.003	0.227	8.29	0.22	3.74	20.50	56.2	1.5	8.650	0.022
4.50	8.64	0.008	0.102	0.035	1.235	0.011	0.003	0.424	8.25	0.4	4.47	13.24	55.9	2.7	8.493	0.020
5.00	9.012	0.006	0.126	0.029	1.225	0.01	0.004	0.247	8.57	0.29	4.97	15.53	58	1.9	8.433	0.026
5.50	8.808	0.007	0.188	0.022	1.191	0.01	0.004	0.304	8.35	0.36	5.19	13.94	56.5	2.4	8.189	0.040
6.00	8.752	0.008	0.175	0.029	1.235	0.012	0.005	0.333	8.04	0.51	8.02	10.85	54.5	3.4	8.495	0.037
6.50	9.208	0.015	0.166	0.068	1.235	0.019	0.009	0.487	7.94	1.37	12.19	3.52	53.8	9.1	8.416	0.035
7.50	9.042	0.01	0.157	0.039	1.216	0.013	0.006	0.441	8.33	0.76	7.46	7.75	56.4	5.1	8.357	0.032
DC295P	Muscovite	HP	J= 0.003681±0.000018													
0.50	61.264	0.041	0.063	0.385	0.087	0.386	0.208	0.091	4.9	5.06	91.73	0.11	32.3	33	0.000	0.002
1.00	19.209	0.019	0.023	0.231	0.015	0.434	0.043	0.087	7.75	1.11	58.82	0.54	50.8	7.2	0.000	0.000
1.50	28.956	0.012	0.027	0.148	0.007	0.359	0.075	0.038	7.75	0.82	73.13	1.24	50.8	5.3	0.000	-0.000
2.00	9.862	0.006	0.015	0.069	0.001	0.461	0.007	0.055	7.85	0.13	20.35	7.22	51.4	0.8	0.000	-0.000
2.50	8.092	0.005	0.013	0.049	0	0.92	0.001	0.101	7.75	0.06	4.33	25.20	50.8	0.4	0.000	-0.000
2.75	8.351	0.005	0.014	0.055	0.001	0.387	0.002	0.093	7.82	0.07	6.33	11.37	51.2	0.5	0.001	-0.000
3.00	8.055	0.005	0.014	0.044	0.001	0.603	0.001	0.106	7.75	0.06	3.86	14.11	50.7	0.4	0.000	-0.000
3.25	7.893	0.006	0.013	0.082	0.001	0.549	0.001	0.239	7.75	0.07	1.74	9.30	50.7	0.5	0.000	-0.000
3.50	7.987	0.007	0.013	0.079	0.002	0.415	0.001	0.246	7.76	0.1	2.51	5.35	50.8	0.7	0.000	-0.000

Watts	40Ar/39Ar	±	38Ar/39Ar	±	37Ar/39Ar	±	36Ar/39Ar	±	40Ar*/39ArK	±	%40Ar atm	% 39Ar	Age	±	Ca/K	Cl/K
4.00	7.987	0.006	0.014	0.087	0.002	0.35	0.001	0.215	7.79	0.09	2.22	5.54	51	0.6	0.000	-0.000
4.50	8.202	0.007	0.013	0.096	0.003	0.387	0.002	0.232	7.83	0.15	3.85	2.90	51.2	1	0.000	-0.000
5.50	8.012	0.007	0.014	0.073	0.002	0.419	0.001	0.27	7.8	0.11	2.21	4.16	51.1	0.7	0.000	-0.000
6.50	8.198	0.011	0.014	0.122	0.005	0.423	0.002	0.341	7.89	0.24	2.49	1.83	51.6	1.5	0.005	0.000
7.00	7.813	0.005	0.014	0.053	0.001	0.433	0	0.361	7.78	0.06	0.48	11.14	50.9	0.4	0.000	-0.000

DC299	Biotite	>250um	J= 0.003814±0.000030													
0.50	158.86	0.027	0.126	0.175	0.07	0.231	0.559	0.042	-0.18	5.45	100.09	0.17	-1.2	37.5	0.000	-0.002
1.00	35.977	0.015	0.038	0.174	0.028	0.217	0.111	0.05	4.97	1.59	86.04	0.56	33.9	10.8	0.051	0.001
1.50	12.976	0.007	0.019	0.092	0.008	0.164	0.021	0.055	7.09	0.35	44.99	2.33	48.1	2.4	0.022	0.000
1.75	10.169	0.006	0.016	0.071	0.005	0.362	0.01	0.079	7.53	0.23	25.59	3.53	51.1	1.6	0.008	0.000
2.00	8.966	0.005	0.016	0.081	0.004	0.25	0.005	0.086	7.67	0.13	14.22	4.92	52	0.9	0.014	0.000
2.25	8.795	0.005	0.016	0.07	0.004	0.204	0.004	0.121	7.72	0.15	11.88	4.71	52.4	1	0.011	0.000
2.50	8.575	0.005	0.015	0.087	0.003	0.208	0.003	0.121	7.77	0.12	9.17	5.97	52.7	0.8	0.010	0.000
3.00	8.327	0.004	0.015	0.039	0.002	0.183	0.002	0.107	7.7	0.08	7.48	10.12	52.2	0.5	0.009	0.000
3.50	8.239	0.004	0.015	0.049	0.002	0.18	0.002	0.136	7.77	0.09	5.56	8.24	52.7	0.6	0.006	0.000
4.00	8.191	0.004	0.015	0.061	0.002	0.157	0.002	0.138	7.74	0.08	5.40	9.30	52.5	0.5	0.005	0.000
4.50	8.223	0.004	0.015	0.074	0.002	0.257	0.002	0.166	7.71	0.1	6.01	6.86	52.3	0.7	0.004	0.000
5.00	8.127	0.004	0.015	0.05	0.002	0.223	0.001	0.191	7.76	0.09	4.40	8.52	52.6	0.6	0.004	0.000
6.00	8.002	0.004	0.015	0.044	0.002	0.176	0.001	0.165	7.74	0.06	3.25	12.34	52.5	0.4	0.006	0.000
7.00	7.971	0.004	0.015	0.051	0.002	0.214	0.001	0.261	7.75	0.08	2.63	7.66	52.6	0.6	0.004	0.000
8.00	7.851	0.003	0.015	0.047	0.003	0.162	0.001	0.24	7.69	0.05	2.07	14.77	52.2	0.3	0.018	0.000

DC320	Hornblende	>250um	J= 0.003759±0.000024													
2.00	286.871	0.039	0.184	0.165	1.024	0.08	0.672	0.059	103.56	9.87	64.20	0.23	593.1	48.2	5.325	0.009
3.00	26.78	0.021	0.14	0.078	1.392	0.028	0.058	0.126	12.32	2.19	53.17	0.80	81.7	14.2	8.002	0.025
3.50	12.865	0.009	0.149	0.03	1.446	0.014	0.012	0.11	10.39	0.4	18.96	3.86	69.1	2.6	8.513	0.030
4.00	10.304	0.005	0.143	0.015	1.41	0.008	0.004	0.088	9.58	0.13	7.29	13.17	63.8	0.8	8.330	0.029
4.25	9.473	0.005	0.15	0.015	1.386	0.008	0.003	0.128	9.26	0.11	2.54	15.01	61.7	0.7	8.189	0.031
4.50	9.631	0.007	0.145	0.026	1.39	0.01	0.004	0.193	9.12	0.26	4.85	5.52	60.8	1.7	8.197	0.030
4.75	9.713	0.008	0.143	0.025	1.404	0.011	0.005	0.237	9.2	0.34	4.89	5.20	61.3	2.2	8.281	0.029
5.00	9.246	0.005	0.139	0.013	1.386	0.007	0.002	0.151	9.07	0.12	2.19	16.19	60.5	0.8	8.199	0.028
5.25	9.757	0.006	0.14	0.018	1.364	0.008	0.004	0.138	9.04	0.19	7.47	10.55	60.3	1.2	8.067	0.029
5.50	10.487	0.008	0.135	0.027	1.404	0.011	0.007	0.14	9.09	0.32	12.95	4.86	60.6	2.1	8.290	0.027
6.00	11.679	0.007	0.135	0.023	1.414	0.01	0.01	0.091	9.56	0.27	18.10	6.85	63.7	1.8	8.361	0.027
6.50	10.795	0.011	0.147	0.038	1.499	0.014	0.008	0.216	9.49	0.56	11.08	2.69	63.2	3.6	8.846	0.030
7.00	9.724	0.005	0.145	0.013	1.475	0.008	0.004	0.098	9.2	0.12	5.71	15.09	61.3	0.8	8.744	0.030

Watts	40Ar/39Ar	±	38Ar/39Ar	±	37Ar/39Ar	±	36Ar/39Ar	±	40Ar*/39ArK	±	%40Ar atm	% 39Ar	Age	±	Ca/K	Cl/K	
DC326	Biotite	>250um	J= 0.003759±0.000022														
0.50	87.188	0.026	0.08	0.228	0.063	0.431	0.305	0.045	3.21	3.45	96.30	0.10	21.6	23.1	0.135	-0.000	
1.00	27.085	0.011	0.03	0.132	0.011	0.385	0.072	0.038	7.28	0.79	72.89	0.52	48.7	5.2	0.023	0.000	
1.50	10.207	0.005	0.017	0.057	0.002	0.339	0.009	0.045	7.79	0.12	23.48	3.37	52.1	0.8	0.004	0.000	
2.00	8.667	0.004	0.016	0.044	0.001	0.373	0.003	0.072	7.81	0.07	9.85	7.28	52.2	0.5	0.000	0.000	
2.25	8.293	0.004	0.016	0.039	0.001	0.356	0.002	0.084	7.82	0.06	5.61	6.73	52.3	0.4	0.002	0.000	
2.50	8.072	0.004	0.016	0.04	0.001	0.417	0.001	0.189	7.85	0.07	2.70	6.68	52.5	0.4	0.000	0.000	
2.75	7.982	0.004	0.015	0.05	0.001	0.365	0.001	0.273	7.87	0.07	1.34	5.62	52.6	0.5	0.001	0.000	
3.00	7.995	0.004	0.015	0.046	0.001	0.437	0.001	0.294	7.9	0.07	0.94	4.84	52.8	0.4	0.002	0.000	
3.25	8.014	0.004	0.015	0.055	0.001	0.468	0.001	0.33	7.94	0.08	0.67	3.97	53	0.5	0.002	0.000	
3.50	8.112	0.004	0.015	0.068	0.002	0.275	0.001	0.365	7.93	0.12	1.84	3.04	53	0.8	0.003	0.000	
4.00	8.094	0.005	0.015	0.075	0.002	0.42	0.001	0.365	7.95	0.11	1.31	3.17	53.2	0.7	0.001	0.000	
5.00	8.063	0.004	0.016	0.056	0.001	0.278	0.001	0.204	7.87	0.07	2.27	5.11	52.6	0.4	0.003	0.000	
6.00	8.047	0.003	0.015	0.038	0.001	0.435	0.001	0.187	7.9	0.05	1.81	7.20	52.8	0.3	0.002	0.000	
7.00	7.986	0.004	0.015	0.036	0	0.495	0.001	0.352	7.85	0.07	1.79	12.58	52.5	0.5	0.000	0.000	
8.00	7.966	0.004	0.015	0.041	0	1.62	0	0.321	7.87	0.05	1.43	29.81	52.6	0.3	0.000	0.000	
DC330	Biotite	>250um	J= 0.003763±0.000024														
0.50	76.804	0.025	0.08	0.173	0.045	0.416	0.26	0.054	4.82	3.73	93.66	0.12	32.5	24.9	0.044	0.005	
1.00	11.662	0.148	0.025	0.159	0.003	0.432	0.017	0.157	6.85	1.08	40.91	1.71	45.9	7.1	0.004	0.002	
1.25	9.319	0.006	0.024	0.055	0.003	0.42	0.006	0.103	7.81	0.19	15.78	2.11	52.2	1.2	0.005	0.002	
1.50	8.765	0.004	0.025	0.04	0.002	0.257	0.004	0.072	7.74	0.09	11.51	4.18	51.8	0.6	0.006	0.002	
1.75	8.792	0.004	0.025	0.027	0.002	0.292	0.004	0.062	7.74	0.08	11.87	5.30	51.8	0.5	0.005	0.002	
2.00	8.283	0.004	0.024	0.036	0.001	0.331	0.002	0.126	7.75	0.08	6.29	4.88	51.9	0.6	0.003	0.002	
2.25	8.891	0.004	0.024	0.045	0.002	0.346	0.004	0.085	7.8	0.11	12.16	3.75	52.2	0.8	0.002	0.002	
2.50	8.289	0.004	0.024	0.047	0.002	0.442	0.002	0.137	7.79	0.09	5.74	3.71	52.2	0.6	0.001	0.002	
2.75	8.252	0.004	0.025	0.042	0.001	0.595	0.002	0.148	7.81	0.09	5.19	3.91	52.3	0.6	0.002	0.002	
3.00	8.038	0.004	0.024	0.04	0.002	0.399	0.001	0.324	7.86	0.11	2.03	3.77	52.6	0.7	0.002	0.002	
3.25	8.032	0.004	0.024	0.041	0.002	0.363	0.001	0.271	7.83	0.09	2.27	3.45	52.4	0.6	0.001	0.002	
3.50	8.065	0.004	0.024	0.045	0.002	0.371	0.001	0.422	7.9	0.15	1.62	2.57	52.8	1	0.002	0.002	
4.00	7.971	0.004	0.024	0.036	0.001	0.446	0.001	0.308	7.85	0.09	1.35	3.94	52.5	0.6	0.000	0.002	
5.00	7.946	0.003	0.024	0.032	0.001	0.507	0.001	0.217	7.8	0.05	1.92	10.00	52.2	0.4	0.001	0.002	
6.00	7.91	0.004	0.024	0.031	0.001	0.396	0.001	0.222	7.81	0.04	1.37	11.44	52.3	0.3	0.002	0.002	
7.00	8.086	0.003	0.024	0.034	0.001	0.51	0.001	0.114	7.76	0.05	4.18	14.87	51.9	0.3	0.002	0.002	
8.00	7.865	0.003	0.024	0.033	0.001	0.317	0	0.394	7.81	0.05	0.94	20.26	52.2	0.3	0.005	0.002	
DC342	Hornblende	>250um	J= 0.003768±0.000026														
2.00	211.681	0.025	0.161	0.101	0.525	0.049	0.479	0.04	78.69	4.87	63.04	0.41	468.5	25.5	2.738	0.012	

Watts	40Ar/39Ar	±	38Ar/39Ar	±	37Ar/39Ar	±	36Ar/39Ar	±	40Ar*/39ArK	±	%40Ar atm	% 39Ar	Age	±	Ca/K	Cl/K
3.00	35.628	0.021	0.134	0.11	0.986	0.033	0.072	0.129	17.79	2.78	49.08	0.42	117	17.7	5.532	0.025
4.00	10.583	0.005	0.164	0.014	1.391	0.007	0.006	0.057	9.38	0.11	11.73	13.03	62.6	0.7	8.254	0.034
4.25	8.724	0.003	0.169	0.011	1.367	0.006	0.002	0.096	8.59	0.07	1.98	22.70	57.5	0.5	8.117	0.035
4.50	8.523	0.004	0.171	0.01	1.374	0.007	0.002	0.113	8.44	0.07	1.29	19.07	56.5	0.5	8.160	0.036
4.75	8.775	0.005	0.165	0.013	1.365	0.008	0.003	0.139	8.5	0.13	3.32	10.40	56.8	0.8	8.101	0.035
5.00	9.888	0.006	0.174	0.016	1.372	0.009	0.005	0.132	9.1	0.2	7.97	6.54	60.8	1.3	8.141	0.036
5.25	8.757	0.006	0.157	0.015	1.371	0.009	0.003	0.176	8.44	0.17	3.54	7.51	56.5	1.1	8.137	0.032
5.50	8.964	0.007	0.159	0.021	1.366	0.01	0.004	0.196	8.54	0.23	4.50	5.22	57.1	1.5	8.107	0.033
5.75	9.49	0.01	0.153	0.028	1.381	0.013	0.006	0.216	8.57	0.4	8.92	2.91	57.3	2.6	8.180	0.032
6.00	9.295	0.008	0.154	0.028	1.376	0.012	0.005	0.258	8.71	0.42	5.36	2.80	58.2	2.8	8.151	0.032
6.50	9.013	0.007	0.153	0.023	1.373	0.01	0.004	0.224	8.54	0.3	4.69	4.04	57.1	1.9	8.142	0.031
7.50	9.1	0.006	0.182	0.017	1.422	0.009	0.004	0.185	8.62	0.24	5.06	4.94	57.6	1.6	8.451	0.038

DC370	Hornblende	200-250um	J= 0.003815±0.000032													
2.00	192.82	0.044	0.224	0.335	2.967	0.054	0.511	0.085	55.35	11.61	71.64	0.73	345.6	66	19.513	0.024
3.00	12.355	0.009	0.134	0.039	1.666	0.011	0.014	0.138	9.35	0.59	24.38	14.12	63.2	3.9	11.510	0.027
3.50	8.92	0.006	0.152	0.022	1.66	0.009	0.005	0.165	8.27	0.25	7.54	31.01	56	1.7	11.483	0.031
4.00	9.13	0.008	0.169	0.028	1.732	0.011	0.007	0.278	8.24	0.55	9.80	17.24	55.8	3.7	11.972	0.035
4.50	8.756	0.01	0.164	0.04	1.67	0.014	0.007	0.355	7.9	0.73	9.31	12.37	53.6	4.8	11.526	0.034
5.00	10.893	0.019	0.145	0.149	1.681	0.024	0.019	0.53	8.02	3.08	23.99	2.99	54.4	20.6	11.373	0.029
5.50	9.957	0.016	0.135	0.09	1.64	0.02	0.013	0.436	8.61	1.65	11.83	5.04	58.3	11	11.193	0.028
6.00	11.986	0.031	0.135	0.224	1.725	0.038	0.027	0.471	9.75	3.86	14.46	1.82	65.9	25.6	11.527	0.026
7.50	9.127	0.014	0.14	0.052	1.685	0.02	0.007	0.299	8.03	0.61	11.85	14.67	54.4	4.1	11.654	0.028

DC395	Biotite	HP	J= 0.003703±0.000016													
0.50	45.373	0.048	0.178	0.18	0.107	0.326	0.158	0.142	4.44	6.42	89.68	0.10	29.4	42.2	0.024	0.030
1.00	19.969	0.014	0.194	0.043	0.008	0.333	0.044	0.054	7.79	0.69	60.72	1.46	51.3	4.5	0.002	0.039
1.25	9.662	0.006	0.199	0.016	0.002	0.355	0.007	0.062	7.76	0.14	19.52	7.16	51.1	0.9	0.000	0.042
1.50	8.026	0.005	0.197	0.015	0.001	0.41	0.001	0.145	7.73	0.07	3.77	16.12	50.9	0.4	0.000	0.042
1.75	7.865	0.005	0.201	0.016	0.001	0.422	0.001	0.143	7.64	0.06	2.85	14.59	50.3	0.4	0.001	0.043
2.00	7.905	0.006	0.19	0.021	0.001	0.366	0.001	0.242	7.72	0.09	2.12	7.64	50.9	0.6	0.000	0.040
2.50	7.983	0.006	0.195	0.018	0.002	0.289	0.001	0.265	7.76	0.11	2.45	6.29	51.1	0.7	0.000	0.041
3.00	8.04	0.004	0.196	0.014	0.001	0.436	0.001	0.139	7.75	0.06	3.69	17.47	51	0.4	0.000	0.041
3.50	8.018	0.008	0.198	0.023	0.003	0.289	0.001	0.299	7.79	0.14	2.19	3.97	51.3	0.9	0.000	0.042
4.00	7.983	0.007	0.2	0.023	0.002	0.281	0.001	0.317	7.73	0.14	2.62	4.44	50.9	0.9	0.000	0.042
4.50	7.902	0.007	0.2	0.018	0.002	0.367	0.001	0.294	7.74	0.12	1.51	4.55	51	0.8	0.000	0.043
5.00	7.97	0.008	0.197	0.029	0.003	0.384	0.001	0.437	7.84	0.17	0.80	3.38	51.6	1.1	0.001	0.042
5.50	7.858	0.008	0.202	0.018	0.002	0.407	0.001	0.398	7.73	0.13	1.17	5.14	50.9	0.8	0.000	0.043
6.00	7.989	0.01	0.197	0.031	0.004	0.318	0.002	0.321	7.82	0.17	1.04	2.65	51.5	1.1	0.001	0.042

Watts	40Ar/39Ar	±	38Ar/39Ar	±	37Ar/39Ar	±	36Ar/39Ar	±	40Ar*/39ArK	±	%40Ar atm	% 39Ar	Age	±	Ca/K	Cl/K
7.00	7.934	0.008	0.195	0.021	0.002	0.38	0.001	0.305	7.74	0.12	2.05	5.06	50.9	0.8	0.000	0.041
DC397	Hornblende	>250um	J= 0.003771±0.000026													
2.00	718.498	0.13	0.347	0.423	1.523	0.236	1.055	0.16	483.98	78.73	36.88	0.16	1873.6	189.6	5.586	0.029
3.00	9.048	0.008	0.058	0.053	1.444	0.012	0.006	0.225	8.07	0.39	8.49	10.75	54.1	2.6	8.621	0.010
3.50	58.686	0.009	0.042	0.073	3.214	0.012	0.091	0.028	34.56	0.79	41.71	11.14	221	4.7	19.387	0.003
4.00	19.046	0.007	0.024	0.064	3.245	0.009	0.02	0.043	14.42	0.28	24.61	19.75	95.6	1.8	19.592	0.001
4.50	11.897	0.007	0.022	0.087	3.513	0.009	0.01	0.091	10.3	0.28	13.25	18.18	68.7	1.9	21.222	0.001
5.00	10.694	0.009	0.022	0.123	3.439	0.011	0.01	0.126	9.35	0.37	11.48	12.16	62.5	2.5	20.766	0.001
5.50	10.38	0.012	0.022	0.15	3.539	0.013	0.011	0.154	8.5	0.53	16.04	8.14	56.9	3.5	21.385	0.001
6.00	14.29	0.012	0.024	0.217	3.387	0.014	0.02	0.138	10.17	0.85	26.71	5.45	67.9	5.6	20.396	0.001
7.50	12.252	0.007	0.026	0.089	3.614	0.01	0.011	0.103	10.52	0.35	13.63	14.27	70.2	2.3	21.868	0.002
DC397-2	Hornblende	HP	J= 0.003703±0.000016													
2.00	289.472	0.107	0.168	0.493	1.373	0.15	0.548	0.149	158.23	26.34	47.04	0.55	832	110.9	15.839	0.008
3.00	13.541	0.01	0.023	0.115	1.304	0.021	0.012	0.107	11.47	0.39	15.34	36.14	75	2.5	18.543	0.001
3.50	11.806	0.024	0.024	0.272	1.308	0.037	0.012	0.242	9.69	0.89	17.10	21.18	63.6	5.7	18.556	0.002
4.00	10.632	0.017	0.023	0.247	1.405	0.026	0.01	0.225	9.38	0.68	9.58	13.37	61.6	4.4	19.895	0.001
4.50	10.803	0.02	0.029	0.196	1.386	0.029	0.011	0.261	9.69	0.92	6.86	9.87	63.6	5.9	19.599	0.003
5.50	10.92	0.024	0.022	0.258	1.349	0.033	0.014	0.239	9.16	1.03	11.37	7.02	60.2	6.6	18.933	0.001
7.00	49.55	0.015	0.049	0.125	1.4	0.029	0.148	0.044	8.91	1.84	82.07	11.87	58.6	11.9	19.829	0.001
DC398-1	Biotite	1x3mm	J= 0.003771±0.000024													
0.50	120.508	0.036	0.21	0.16	0.102	0.316	0.411	0.065	4.81	6.86	96.03	0.07	32.4	45.9	0.000	0.026
1.00	35.001	0.008	0.174	0.029	0.005	0.438	0.1	0.021	6.48	0.6	81.47	1.43	43.6	4	0.000	0.032
1.50	9.585	0.004	0.164	0.011	0.001	0.314	0.008	0.033	7.44	0.08	22.42	8.48	49.9	0.6	0.000	0.034
1.75	7.895	0.003	0.165	0.014	0.001	0.443	0.002	0.119	7.5	0.06	5.12	9.72	50.3	0.4	0.001	0.034
2.00	7.749	0.004	0.164	0.01	0.001	0.442	0.001	0.136	7.5	0.05	3.30	9.74	50.3	0.3	0.000	0.034
2.25	7.7	0.004	0.165	0.011	0.001	0.324	0.001	0.197	7.52	0.06	2.40	8.10	50.4	0.4	0.000	0.034
2.50	7.69	0.004	0.164	0.012	0.001	0.295	0.001	0.309	7.52	0.08	2.23	6.53	50.4	0.5	0.000	0.034
2.75	7.711	0.004	0.165	0.013	0.001	0.255	0.001	0.384	7.58	0.09	1.62	5.23	50.8	0.6	0.000	0.034
3.25	7.761	0.004	0.166	0.014	0.002	0.316	0.001	0.303	7.61	0.09	1.71	4.62	51.1	0.6	0.000	0.035
4.00	7.736	0.004	0.163	0.012	0.001	0.226	0.001	0.282	7.56	0.08	2.19	5.74	50.7	0.5	0.000	0.034
5.00	7.672	0.004	0.165	0.012	0.001	0.415	0.001	0.29	7.57	0.06	1.37	7.98	50.8	0.4	0.000	0.034
6.00	7.637	0.004	0.164	0.013	0.001	0.421	0	0.256	7.54	0.05	1.37	14.02	50.6	0.3	0.000	0.034
7.00	7.652	0.004	0.165	0.011	0.001	0.41	0.001	0.297	7.56	0.05	1.24	8.44	50.7	0.3	0.000	0.034
8.00	7.665	0.004	0.165	0.013	0.001	0.389	0.001	0.254	7.57	0.05	1.25	9.90	50.8	0.3	0.000	0.034

Watts	40Ar/39Ar	±	38Ar/39Ar	±	37Ar/39Ar	±	36Ar/39Ar	±	40Ar*/39ArK	±	%40Ar atm	% 39Ar	Age	±	Ca/K	Cl/K
DC398-2	Biotite spots	2x2mm	J= 0.003774±0.000026													
5.00	14.42	0.004	0.181	0.014	0.001	0.274	0.025	0.024	7.27	0.18	49.60	9.00	48.8	1.2	0.000	0.037
5.00	11.689	0.006	0.179	0.014	0.002	0.291	0.016	0.031	7.27	0.15	37.82	8.59	48.8	1	0.000	0.037
5.00	11.714	0.005	0.179	0.019	0.002	0.245	0.015	0.034	7.41	0.16	36.68	6.17	49.7	1.1	0.000	0.037
5.00	8.901	0.004	0.182	0.009	0.001	0.646	0.005	0.038	7.48	0.07	16.03	25.93	50.3	0.4	0.001	0.038
5.00	8.737	0.004	0.179	0.012	0.001	0.419	0.005	0.054	7.45	0.08	14.82	20.20	50	0.5	0.000	0.038
5.00	7.946	0.004	0.181	0.012	0.001	0.554	0.002	0.122	7.49	0.07	5.91	30.10	50.3	0.5	0.001	0.038
DC400	Hornblende	>250um	J= 0.003776±0.000026													
2.00	130.213	0.309	0.204	1.87	2.541	0.399	0.554	0.613	17.85	94.97	80.29	0.04	117.7	606.1	7.760	0.056
2.50	34.098	0.045	0.085	0.531	1.53	0.061	0.088	0.307	15.01	8.11	50.63	0.42	99.5	52.3	9.004	0.013
3.00	12.083	0.009	0.066	0.05	1.456	0.012	0.012	0.135	9.33	0.5	21.90	7.50	62.4	3.3	9.286	0.011
3.50	8.215	0.004	0.061	0.02	1.43	0.007	0.003	0.099	7.84	0.1	4.65	39.36	52.6	0.7	9.157	0.011
3.75	8.016	0.005	0.059	0.027	1.4	0.008	0.003	0.185	7.78	0.16	2.71	24.89	52.2	1.1	8.963	0.010
4.00	8.527	0.008	0.058	0.059	1.415	0.012	0.005	0.345	7.71	0.57	7.63	7.48	51.7	3.8	9.027	0.010
5.00	8.678	0.008	0.064	0.042	1.435	0.012	0.006	0.24	7.57	0.43	11.28	9.22	50.9	2.9	9.173	0.011
7.00	8.496	0.008	0.062	0.042	1.48	0.011	0.005	0.233	7.77	0.32	7.47	11.09	52.1	2.1	9.467	0.011
DC414	Hornblende	200-250um	J= 0.003779±0.000026													
2.00	81.116	0.029	0.066	0.216	3.484	0.032	0.23	0.062	18.19	3.85	77.43	2.31	119.9	24.6	22.101	0.004
2.50	54.772	0.071	0.045	1.444	3.463	0.079	0.207	0.26	14.05	16.17	71.41	0.47	93.3	104.7	21.002	0.002
3.00	12.45	0.013	0.019	0.215	3.727	0.016	0.019	0.164	8.82	0.95	27.72	9.06	59.1	6.2	24.034	0.001
3.50	9.691	0.009	0.018	0.117	3.343	0.01	0.009	0.148	8.21	0.42	14.55	19.28	55.1	2.8	21.562	0.000
4.00	9.158	0.006	0.016	0.07	3.48	0.008	0.008	0.098	8.21	0.23	10.49	39.62	55.1	1.5	22.476	0.000
4.50	11.142	0.015	0.02	0.258	3.676	0.017	0.017	0.269	8.3	1.37	22.47	6.57	55.7	9	23.674	0.001
5.00	11.625	0.015	0.019	0.426	3.827	0.018	0.021	0.223	7.99	1.39	27.81	5.32	53.6	9.2	24.628	0.001
5.50	11.791	0.019	0.02	0.386	3.671	0.02	0.021	0.244	8.04	1.52	28.10	4.91	54	10	23.654	0.000
7.50	9.786	0.01	0.017	0.179	3.814	0.012	0.011	0.169	8.23	0.57	14.29	12.45	55.3	3.8	24.644	0.000
DC418	Biotite	HP	J= 0.003704±0.000016													
0.50	100.718	0.035	0.103	0.211	0.064	0.378	0.341	0.067	6.82	5.81	93.14	0.20	45	37.9	0.000	0.006
1.00	18.028	0.006	0.044	0.047	0.002	0.324	0.037	0.035	7.46	0.39	58.61	6.82	49.2	2.5	0.000	0.005
1.25	9.923	0.006	0.038	0.04	0.002	0.281	0.008	0.05	7.69	0.13	22.40	9.92	50.7	0.9	0.001	0.005
1.50	8.885	0.007	0.038	0.084	0.003	0.36	0.004	0.116	7.77	0.16	12.15	5.56	51.2	1.1	0.002	0.005

Watts	40Ar/39Ar	±	38Ar/39Ar	±	37Ar/39Ar	±	36Ar/39Ar	±	40Ar*/39ArK	±	%40Ar atm	% 39Ar	Age	±	Ca/K	Cl/K
1.75	8.576	0.006	0.036	0.045	0.002	0.369	0.003	0.115	7.76	0.12	9.33	8.66	51.1	0.8	0.000	0.005
2.00	8.39	0.005	0.035	0.032	0.001	0.358	0.003	0.097	7.7	0.09	8.16	13.87	50.7	0.6	0.001	0.005
2.25	8.279	0.008	0.035	0.063	0.002	0.326	0.002	0.222	7.84	0.15	4.84	5.57	51.6	1	0.000	0.005
2.50	8.807	0.01	0.037	0.061	0.004	0.295	0.004	0.17	7.83	0.22	10.25	3.77	51.6	1.4	0.000	0.005
3.00	8.486	0.009	0.036	0.067	0.003	0.309	0.003	0.158	7.8	0.16	7.43	4.95	51.4	1	0.000	0.005
3.50	8.389	0.008	0.036	0.053	0.003	0.309	0.003	0.169	7.78	0.14	6.63	5.37	51.3	0.9	0.000	0.005
4.00	8.422	0.007	0.036	0.047	0.002	0.286	0.003	0.145	7.8	0.13	7.06	7.16	51.4	0.8	0.001	0.005
4.50	8.411	0.007	0.037	0.068	0.003	0.337	0.003	0.172	7.79	0.15	6.85	5.31	51.3	1	0.000	0.005
5.00	8.484	0.008	0.035	0.054	0.002	0.472	0.003	0.154	7.75	0.15	8.25	5.97	51	1	0.000	0.005
5.50	8.586	0.012	0.035	0.104	0.006	0.26	0.004	0.293	7.91	0.32	6.40	2.46	52.1	2.1	0.000	0.005
6.00	8.596	0.009	0.035	0.09	0.004	0.365	0.004	0.218	7.74	0.24	9.11	3.70	51	1.6	0.002	0.005
7.00	8.181	0.006	0.034	0.045	0.001	0.381	0.002	0.141	7.72	0.09	5.45	10.72	50.9	0.6	0.000	0.004

DC423	Hornblende	>250um	J= 0.003782±0.000026													
2.00	180.778	0.037	0.105	0.314	0.582	0.093	0.259	0.09	115.69	7.73	35.65	0.45	654.7	36.7	2.676	0.008
3.00	22.095	0.018	0.142	0.078	1.106	0.027	0.021	0.257	18.07	1.64	15.83	1.68	119.2	10.5	6.905	0.027
3.50	9.148	0.005	0.145	0.018	1.228	0.008	0.003	0.131	8.96	0.11	2.07	24.32	60.1	0.7	7.969	0.030
4.00	8.698	0.004	0.15	0.012	1.244	0.007	0.002	0.162	8.55	0.12	1.92	38.70	57.4	0.8	8.078	0.031
4.25	8.742	0.008	0.151	0.027	1.247	0.011	0.004	0.227	8.46	0.26	2.23	10.13	56.8	1.7	8.076	0.031
4.50	8.933	0.009	0.16	0.026	1.268	0.013	0.005	0.243	8.36	0.36	4.81	6.96	56.1	2.4	8.191	0.033
5.00	10.113	0.021	0.164	0.076	1.339	0.026	0.013	0.499	8.79	1.9	4.32	1.52	59	12.5	8.421	0.034
7.00	9.019	0.006	0.177	0.018	1.401	0.009	0.003	0.173	8.79	0.17	2.26	16.24	59	1.1	9.107	0.037

DC439	Biotite	>250um	J= 0.003784±0.000026													
0.50	78.584	0.024	0.085	0.254	0.055	0.238	0.263	0.069	4.71	5.06	93.87	0.17	31.9	34	0.120	0.005
1.00	10.966	0.005	0.035	0.044	0.003	0.356	0.012	0.063	7.78	0.22	28.68	3.14	52.4	1.5	0.005	0.004
1.50	8.418	0.003	0.034	0.025	0.001	0.586	0.003	0.09	7.74	0.07	8.10	14.05	52.1	0.5	0.000	0.004
1.75	8.037	0.004	0.033	0.041	0.001	0.285	0.001	0.235	7.81	0.08	2.68	7.34	52.5	0.6	0.002	0.004
2.00	7.909	0.004	0.033	0.025	0.001	0.296	0.001	0.307	7.77	0.08	1.70	8.52	52.3	0.5	0.003	0.004
2.25	7.931	0.003	0.033	0.027	0.001	0.269	0.001	0.233	7.74	0.07	2.39	9.47	52.1	0.4	0.001	0.004
2.50	8.006	0.005	0.033	0.048	0.003	0.205	0.001	0.657	7.79	0.2	2.15	3.50	52.4	1.3	0.006	0.004
3.00	7.868	0.003	0.033	0.03	0.001	0.237	0.001	0.481	7.76	0.09	1.22	7.45	52.2	0.6	0.003	0.004
3.50	7.758	0.013	0.033	0.139	0.002	1.878	0	0.913	7.71	0.14	0.40	6.72	51.9	1	0.006	0.004
4.00	7.849	0.004	0.033	0.026	0.001	0.229	0.001	0.528	7.76	0.09	0.98	7.92	52.2	0.6	0.003	0.004
4.50	7.86	0.004	0.033	0.03	0.001	0.342	0.001	0.479	7.79	0.09	0.75	7.34	52.4	0.6	0.001	0.004
5.00	7.9	0.004	0.033	0.029	0.002	0.282	0.001	0.457	7.75	0.1	1.64	6.28	52.2	0.7	0.005	0.004
6.00	7.871	0.005	0.034	0.027	0.002	0.176	0.001	0.466	7.77	0.09	1.13	8.22	52.3	0.6	0.009	0.004
7.00	7.92	0.004	0.033	0.036	0.006	0.116	0.001	0.578	7.75	0.13	1.78	5.11	52.1	0.9	0.035	0.004
8.00	8.017	0.005	0.033	0.041	0.019	0.049	0.001	0.473	7.84	0.13	1.84	4.77	52.7	0.9	0.140	0.004

Watts	40Ar/39Ar	±	38Ar/39Ar	±	37Ar/39Ar	±	36Ar/39Ar	±	40Ar*/39ArK	±	%40Ar atm	% 39Ar	Age	±	Ca/K	Cl/K
DC446	Hornblende	>250um	J= 0.003786±0.000026													
2.00	232.75	0.024	0.164	0.119	0.543	0.048	0.478	0.038	99.6	4.91	57.37	0.76	577.2	24.4	3.094	0.013
3.00	42.236	0.019	0.236	0.061	1.298	0.027	0.048	0.161	31.69	2.41	24.20	1.01	204.4	14.7	8.185	0.048
3.50	12.377	0.009	0.309	0.022	1.889	0.012	0.007	0.181	11.36	0.42	7.28	4.64	76	2.7	12.273	0.067
4.00	10.163	0.004	0.303	0.011	1.862	0.007	0.004	0.119	9.87	0.13	3.30	21.83	66.2	0.9	12.150	0.066
4.50	10.101	0.005	0.305	0.009	1.823	0.007	0.004	0.095	9.81	0.11	3.31	23.30	65.8	0.7	11.896	0.067
5.00	9.562	0.005	0.3	0.012	1.651	0.008	0.004	0.145	9.23	0.16	3.50	15.75	62	1.1	10.766	0.065
5.50	9.635	0.006	0.305	0.014	1.856	0.009	0.004	0.178	9.4	0.2	2.55	14.34	63.1	1.3	12.119	0.067
6.00	10.007	0.008	0.31	0.021	1.836	0.011	0.006	0.208	9.5	0.36	4.01	5.57	63.7	2.4	11.952	0.067
7.50	9.697	0.006	0.366	0.016	1.85	0.008	0.004	0.12	9.43	0.15	2.77	12.80	63.3	1	12.079	0.081
DC450	Biotite	4x3mm	J= 0.003789±0.000026													
0.50	216.397	0.027	0.186	0.115	0.061	0.369	0.743	0.037	6.2	5.8	97.13	0.57	41.9	38.7	0.079	0.009
1.00	12.402	0.006	0.048	0.041	0.003	0.438	0.016	0.044	7.98	0.22	35.41	11.32	53.7	1.5	0.000	0.007
1.50	9.326	0.005	0.046	0.037	0.002	0.404	0.005	0.079	7.98	0.13	14.13	17.35	53.7	0.9	0.002	0.007
1.75	9.779	0.006	0.046	0.06	0.004	0.447	0.007	0.135	8.22	0.27	15.15	8.23	55.3	1.8	0.006	0.007
2.00	9.229	0.008	0.046	0.071	0.005	0.487	0.005	0.225	8.24	0.35	9.20	5.61	55.5	2.3	0.000	0.007
2.50	8.876	0.007	0.046	0.047	0.004	0.402	0.003	0.207	8.14	0.22	7.46	9.63	54.8	1.5	0.000	0.007
3.00	8.845	0.006	0.045	0.056	0.004	0.38	0.003	0.213	8.23	0.23	6.02	9.00	55.4	1.5	0.000	0.007
3.50	8.756	0.007	0.046	0.048	0.004	0.471	0.003	0.301	8.19	0.29	5.24	7.18	55.1	1.9	0.000	0.007
4.00	10.201	0.008	0.046	0.067	0.006	0.426	0.009	0.141	8.14	0.37	18.98	5.59	54.8	2.4	0.001	0.007
5.00	8.962	0.007	0.047	0.053	0.005	0.357	0.004	0.215	8.16	0.27	7.93	7.85	54.9	1.8	0.002	0.007
6.00	8.873	0.007	0.046	0.06	0.005	0.357	0.004	0.278	8.23	0.3	5.85	6.42	55.4	2	0.001	0.007
7.00	8.93	0.009	0.045	0.081	0.009	0.354	0.005	0.333	7.99	0.47	8.33	4.33	53.8	3.1	0.006	0.007
8.00	8.671	0.007	0.043	0.057	0.005	0.398	0.003	0.295	8.12	0.28	4.95	6.92	54.7	1.8	0.003	0.007
DC457	Hornblende	200-250um	J= 0.003791±0.000026													
2.00	1275.17	0.094	0.602	0.211	1.516	0.113	1.345	0.102	907.63	87.75	28.56	0.17	2689.6	135.1	7.362	0.071
3.00	29.113	0.024	0.72	0.04	2.062	0.029	0.055	0.117	17.15	1.95	39.78	1.30	113.6	12.5	13.234	0.160
3.50	11.22	0.008	0.643	0.015	1.954	0.011	0.009	0.15	9.69	0.43	12.88	6.76	65.1	2.8	12.749	0.144
4.00	9.352	0.005	0.654	0.009	1.956	0.007	0.005	0.071	8.68	0.11	7.44	23.79	58.4	0.8	12.803	0.147
4.50	8.759	0.004	0.639	0.007	1.956	0.007	0.004	0.077	8.48	0.09	3.52	35.12	57.1	0.6	12.811	0.143
5.00	8.761	0.006	0.635	0.01	1.958	0.008	0.004	0.116	8.44	0.15	3.62	17.17	56.8	1	12.812	0.142
5.50	9.362	0.009	0.607	0.016	1.899	0.011	0.007	0.179	8.6	0.38	6.68	5.96	57.9	2.5	12.385	0.136
6.00	10.537	0.018	0.587	0.03	1.911	0.021	0.014	0.33	9.08	1.36	8.69	1.85	61.1	9	12.348	0.130
6.50	9.602	0.014	0.508	0.024	1.801	0.017	0.009	0.328	8.75	0.85	5.60	3.01	58.9	5.6	11.727	0.113

Watts	40Ar/39Ar	±	38Ar/39Ar	±	37Ar/39Ar	±	36Ar/39Ar	±	40Ar*/39ArK	±	%40Ar atm	% 39Ar	Age	±	Ca/K	Cl/K
7.50	9.167	0.011	0.627	0.017	1.981	0.014	0.007	0.226	8.46	0.46	5.83	4.86	56.9	3	12.927	0.140
DC464	Hornblende	200-250um	J= 0.003793±0.000026													
2.00	16.825	0.009	0.173	0.028	1.181	0.013	0.026	0.061	10.3	0.48	38.52	6.48	69.2	3.2	7.677	0.035
2.50	16.576	0.026	0.176	0.125	1.223	0.036	0.033	0.257	10.27	2.52	32.28	0.82	69	16.6	7.586	0.036
3.00	10.02	0.007	0.173	0.022	1.183	0.01	0.006	0.174	9.08	0.3	8.99	10.78	61.1	2	7.723	0.036
3.50	9.001	0.006	0.174	0.017	1.187	0.008	0.003	0.157	8.61	0.17	4.08	14.69	58	1.1	7.767	0.037
4.00	8.511	0.005	0.171	0.014	1.158	0.008	0.003	0.127	8.31	0.11	2.37	23.79	56	0.7	7.581	0.036
4.50	8.592	0.005	0.168	0.014	1.145	0.008	0.003	0.182	8.36	0.14	2.73	22.64	56.3	1	7.495	0.035
5.00	9.14	0.008	0.17	0.023	1.14	0.011	0.005	0.206	8.37	0.31	7.58	8.62	56.4	2	7.449	0.035
5.50	9.627	0.014	0.174	0.054	1.184	0.019	0.008	0.262	8.5	0.66	8.38	3.09	57.3	4.4	7.653	0.036
7.50	8.84	0.007	0.173	0.022	1.192	0.01	0.004	0.194	8.4	0.23	4.05	9.10	56.6	1.5	7.794	0.036
DC468	Biotite	200-250um	J= 0.003795±0.000024													
0.50	50.768	0.038	0.073	0.397	0.113	0.31	0.18	0.11	5.43	5.77	88.91	0.12	36.8	38.7	0.254	0.001
1.00	14.094	0.013	0.032	0.167	0.032	0.249	0.029	0.111	6.97	0.97	48.79	0.74	47.1	6.5	0.126	0.002
1.50	9.298	0.005	0.026	0.054	0.007	0.153	0.007	0.066	7.51	0.14	18.71	4.84	50.7	1	0.037	0.002
2.00	10.539	0.003	0.026	0.03	0.003	0.168	0.011	0.031	7.58	0.1	28.03	10.70	51.2	0.7	0.021	0.002
2.25	7.906	0.004	0.024	0.036	0.004	0.156	0.001	0.214	7.69	0.08	2.37	7.22	51.9	0.5	0.018	0.002
2.50	7.895	0.005	0.024	0.047	0.003	0.189	0.001	0.308	7.74	0.09	1.56	6.98	52.2	0.6	0.015	0.002
2.75	7.976	0.005	0.024	0.059	0.004	0.226	0.001	0.387	7.85	0.15	0.88	5.00	53	1	0.016	0.002
3.25	7.907	0.004	0.024	0.056	0.003	0.217	0.001	0.311	7.76	0.09	1.44	6.96	52.4	0.6	0.012	0.002
4.00	7.814	0.004	0.024	0.037	0.002	0.217	0.001	0.241	7.69	0.06	1.32	10.76	51.9	0.4	0.010	0.002
5.00	7.796	0.004	0.024	0.038	0.002	0.22	0.001	0.248	7.69	0.06	1.20	11.47	51.9	0.4	0.010	0.002
6.00	7.766	0.003	0.024	0.039	0.003	0.203	0.001	0.256	7.67	0.06	1.13	12.09	51.7	0.4	0.016	0.002
7.00	7.794	0.004	0.024	0.032	0.002	0.166	0.001	0.253	7.68	0.06	1.32	10.50	51.8	0.4	0.010	0.002
8.00	7.806	0.004	0.024	0.035	0.006	0.076	0.001	0.208	7.67	0.06	1.57	12.61	51.8	0.4	0.044	0.002
DC469-1	Hornblende	100-250um	J= 0.003797±0.000026													
2.00	363.579	0.06	0.315	0.186	1.454	0.1	1.168	0.079	46.36	18.64	87.37	0.31	292.5	108.6	6.174	0.022
3.00	12.841	0.012	0.079	0.059	2.035	0.015	0.018	0.137	8.96	0.76	27.56	6.04	60.3	5.1	11.527	0.014
3.75	8.452	0.004	0.074	0.019	1.961	0.007	0.003	0.098	8.23	0.1	2.67	60.52	55.5	0.6	11.203	0.014
4.25	8.873	0.008	0.076	0.033	1.947	0.01	0.005	0.158	8.18	0.25	6.58	18.61	55.2	1.7	11.107	0.014
4.75	9.962	0.012	0.079	0.059	1.941	0.015	0.011	0.181	7.9	0.61	16.72	6.41	53.3	4	11.007	0.015
5.50	11.262	0.017	0.084	0.077	1.982	0.019	0.018	0.258	8.18	1.36	21.49	3.78	55.2	9.1	11.197	0.015
6.50	10.656	0.014	0.08	0.071	1.984	0.017	0.014	0.232	8.19	0.97	17.49	4.34	55.3	6.4	11.220	0.015

Watts	40Ar/39Ar	±	38Ar/39Ar	±	37Ar/39Ar	±	36Ar/39Ar	±	40Ar*/39ArK	±	%40Ar atm	% 39Ar	Age	±	Ca/K	Cl/K
DC469-2	Hornblende	>250um	J= 0.003799±0.000024													
2.00	425.177	0.053	0.292	0.241	1.121	0.097	1.1	0.075	120.04	18.3	70.74	0.24	677.8	86.1	5.443	0.023
3.00	32.968	0.042	0.092	0.451	1.59	0.056	0.084	0.363	22.09	8.96	22.82	0.41	145.4	56.6	9.143	0.022
3.50	13.557	0.02	0.089	0.132	1.767	0.024	0.02	0.333	10.52	1.95	17.58	1.80	70.7	12.9	11.491	0.017
4.00	8.714	0.004	0.081	0.022	1.686	0.007	0.004	0.133	8.36	0.15	4.19	28.53	56.4	1	11.183	0.015
4.50	8.454	0.005	0.081	0.025	1.699	0.008	0.003	0.222	8.32	0.21	1.25	19.21	56.2	1.4	11.259	0.015
5.00	8.338	0.005	0.078	0.02	1.691	0.008	0.003	0.189	8.21	0.16	1.44	24.96	55.4	1.1	11.218	0.015
5.25	8.98	0.01	0.08	0.075	1.691	0.013	0.007	0.363	8.12	0.81	6.88	5.17	54.8	5.4	11.136	0.015
5.50	8.924	0.013	0.079	0.071	1.686	0.015	0.007	0.355	8.24	0.74	4.74	4.87	55.6	4.9	11.097	0.015
6.00	8.514	0.009	0.078	0.043	1.665	0.011	0.005	0.328	8.11	0.49	3.17	8.59	54.7	3.2	11.011	0.014
7.50	8.856	0.01	0.088	0.052	1.923	0.012	0.007	0.32	8.05	0.63	7.02	6.22	54.3	4.2	12.721	0.017
DC473-1	Hornblende	200-250um	J= 0.003800±0.000024													
2.00	188.585	0.045	0.235	0.204	1.008	0.076	0.411	0.099	78.32	11.24	56.90	0.23	470	59.4	5.261	0.037
2.50	44.935	0.054	0.395	0.213	0.932	0.096	0.112	0.439	31.51	14.28	16.56	0.16	204.1	87.4	4.267	0.090
3.00	17.75	0.031	0.402	0.081	0.948	0.047	0.038	0.468	13	5.32	15.21	0.41	87	34.8	5.580	0.089
3.50	10.339	0.011	0.248	0.035	0.813	0.017	0.01	0.386	8.59	1.11	13.49	2.25	58	7.3	5.271	0.053
4.00	8.937	0.007	0.192	0.02	0.783	0.011	0.003	0.275	8.53	0.28	3.61	8.05	57.6	1.9	5.170	0.041
4.50	8.335	0.004	0.144	0.014	0.755	0.007	0.002	0.238	8.17	0.13	1.79	19.45	55.2	0.9	5.007	0.030
5.00	8.295	0.004	0.126	0.014	0.749	0.008	0.002	0.295	8.23	0.15	0.60	17.91	55.5	1	4.966	0.026
5.50	8.306	0.004	0.131	0.015	0.728	0.007	0.002	0.213	8.17	0.11	1.53	22.05	55.2	0.7	4.835	0.027
6.00	8.55	0.008	0.126	0.026	0.729	0.012	0.003	0.446	8.32	0.42	1.17	5.93	56.1	2.8	4.798	0.026
7.50	8.351	0.004	0.128	0.014	0.747	0.007	0.002	0.22	8.21	0.12	1.72	23.55	55.4	0.8	4.964	0.026
DC473-2	Hornblende	>250um	J= 0.003802±0.000022													
2.00	230.145	0.034	0.272	0.119	1.009	0.052	0.428	0.062	111.39	7.53	50.36	0.35	637.1	36.3	5.906	0.043
3.00	40.515	0.029	0.403	0.1	0.932	0.044	0.057	0.295	28.85	5.02	23.66	0.38	187.8	31	5.461	0.087
3.50	15.236	0.026	0.443	0.055	0.902	0.042	0.031	0.347	10.14	3.25	26.52	0.59	68.3	21.5	5.605	0.099
4.00	11.066	0.01	0.243	0.03	0.811	0.016	0.01	0.219	9.22	0.65	14.85	3.07	62.2	4.3	5.323	0.052
4.50	8.911	0.005	0.149	0.015	0.73	0.009	0.003	0.224	8.56	0.17	3.68	12.75	57.8	1.2	4.849	0.031
5.00	8.329	0.004	0.118	0.012	0.717	0.007	0.001	0.201	8.26	0.09	0.87	25.14	55.8	0.6	4.774	0.024
5.50	8.48	0.004	0.116	0.013	0.701	0.007	0.002	0.127	8.22	0.08	3.13	28.07	55.5	0.6	4.667	0.023
5.75	8.299	0.005	0.114	0.02	0.706	0.009	0.002	0.316	8.07	0.19	2.15	10.52	54.5	1.2	4.691	0.023
6.00	9.406	0.013	0.124	0.065	0.736	0.021	0.009	0.448	8.65	1.16	2.66	1.58	58.4	7.7	4.737	0.025
6.50	8.761	0.009	0.125	0.04	0.741	0.014	0.004	0.463	8.43	0.57	1.27	3.43	56.9	3.8	4.868	0.025
7.50	8.453	0.005	0.123	0.016	0.758	0.008	0.002	0.25	8.28	0.16	1.75	14.13	55.9	1	5.047	0.025

Watts	40Ar/39Ar	±	38Ar/39Ar	±	37Ar/39Ar	±	36Ar/39Ar	±	40Ar*/39ArK	±	%40Ar atm	% 39Ar	Age	±	Ca/K	Cl/K
DC476-1	Hornblende	200-250um	J= 0.003803±0.000022													
2.00	265.286	0.051	0.201	0.281	1.025	0.092	0.847	0.085	36.17	17.11	85.96	0.71	232.5	103.2	5.158	0.007
3.00	30.75	0.031	0.1	0.295	4.776	0.033	0.092	0.23	10.84	6.28	62.22	1.65	72.9	41.4	31.421	0.017
3.50	11.171	0.011	0.098	0.062	6.577	0.012	0.018	0.155	8.83	0.86	19.92	11.48	59.6	5.7	44.497	0.019
4.00	9.34	0.008	0.093	0.034	6.568	0.01	0.012	0.124	8.54	0.45	8.50	21.12	57.7	3	44.526	0.018
4.50	8.836	0.007	0.091	0.034	6.527	0.008	0.01	0.12	8.31	0.37	6.18	26.02	56.1	2.5	44.281	0.017
5.00	9.291	0.008	0.094	0.039	6.586	0.01	0.012	0.142	8.41	0.53	8.91	17.94	56.8	3.5	44.600	0.018
5.50	9.871	0.01	0.098	0.065	6.59	0.011	0.015	0.211	8.47	0.97	12.24	9.75	57.2	6.4	44.674	0.019
6.00	11.982	0.02	0.127	0.095	6.753	0.021	0.028	0.38	9.41	3.2	15.26	3.65	63.4	21.2	45.506	0.026
7.50	10.09	0.014	0.126	0.058	6.941	0.014	0.019	0.259	8.09	1.46	16.93	7.68	54.7	9.7	46.970	0.026
DC476-2	Hornblende	>250um	J= 0.003805±0.000022													
2.00	403.091	0.046	0.292	0.147	1.203	0.064	1.268	0.055	48.77	11.95	88.17	0.80	307.1	69.2	7.215	0.007
3.00	35.731	0.026	0.088	0.256	4.333	0.029	0.092	0.179	15	4.96	56.53	1.74	100.2	32.2	29.138	0.011
3.50	13.729	0.014	0.091	0.075	6.194	0.016	0.025	0.17	9.62	1.3	28.65	6.27	64.9	8.6	42.401	0.017
4.00	9.651	0.007	0.088	0.026	6.373	0.008	0.012	0.067	8.39	0.26	13.84	30.62	56.7	1.7	43.677	0.016
4.50	9.834	0.008	0.092	0.033	6.497	0.009	0.013	0.093	8.45	0.38	14.44	21.07	57.1	2.5	44.562	0.017
5.00	8.91	0.008	0.095	0.034	6.722	0.009	0.011	0.105	8.23	0.36	7.79	19.38	55.6	2.4	46.178	0.018
5.50	9.271	0.01	0.098	0.063	6.688	0.011	0.013	0.183	8.59	0.73	6.19	10.76	58	4.8	45.950	0.019
6.00	9.936	0.014	0.102	0.068	6.748	0.014	0.017	0.169	8.17	0.9	15.31	6.73	55.3	6	46.400	0.020
7.50	13.487	0.023	0.283	0.071	8.962	0.024	0.036	0.214	9.46	2.36	24.85	2.63	63.8	15.6	62.066	0.062
DC502	Muscovite	>250um	J= 0.002716±0.000014													
2.00	13.714	0.008	0.015	0.091	0.004	0.207	0.011	0.072	10.6	0.26	21.59	11.35	51.2	1.2	0.004	-0.000
2.30	12.07	0.01	0.015	0.099	0.005	0.27	0.006	0.11	10.64	0.22	10.23	10.31	51.4	1	0.000	-0.000
2.50	12.249	0.008	0.015	0.099	0.004	0.281	0.006	0.098	10.57	0.21	12.34	11.11	51	1	0.000	-0.000
2.60	12.099	0.009	0.014	0.086	0.006	0.232	0.006	0.117	10.63	0.23	10.23	8.30	51.3	1.1	0.000	-0.000
2.70	11.546	0.011	0.014	0.133	0.006	0.289	0.004	0.204	10.64	0.28	5.56	7.61	51.4	1.3	0.000	-0.000
2.90	11.553	0.009	0.014	0.106	0.006	0.226	0.004	0.149	10.56	0.21	6.71	9.16	51	1	0.003	-0.000
3.10	11.479	0.009	0.014	0.119	0.006	0.21	0.004	0.174	10.59	0.22	5.79	9.24	51.2	1.1	0.005	-0.000
3.40	11.657	0.012	0.014	0.175	0.007	0.247	0.005	0.167	10.68	0.26	5.89	6.94	51.6	1.2	0.000	-0.000
3.70	11.551	0.008	0.014	0.101	0.004	0.243	0.004	0.123	10.57	0.17	7.08	12.65	51.1	0.8	0.005	-0.000
4.10	11.506	0.01	0.014	0.109	0.006	0.306	0.004	0.175	10.65	0.23	5.19	8.01	51.5	1.1	0.000	-0.000
4.60	12.214	0.018	0.016	0.209	0.018	0.2	0.008	0.237	10.83	0.59	5.65	2.86	52.3	2.8	0.016	-0.000
5.00	12.485	0.019	0.017	0.248	0.018	0.269	0.009	0.214	10.76	0.64	7.58	2.48	52	3.1	0.000	-0.000

Watts	40Ar/39Ar	±	38Ar/39Ar	±	37Ar/39Ar	±	36Ar/39Ar	±	40Ar*/39ArK	±	%40Ar atm	% 39Ar	Age	±	Ca/K	Cl/K	
DC510	Muscovite	>250um	J= 0.002714±0.000014														
2.00	34.877	0.008	0.028	0.065	0.005	0.287	0.054	0.034	19.33	0.55	44.28	3.54	92.3	2.6	0.014	0.001	
2.30	12.228	0.005	0.015	0.057	0.001	0.607	0.006	0.067	10.5	0.13	13.88	28.65	50.7	0.6	0.004	-0.000	
2.50	10.696	0.005	0.014	0.07	0.001	0.448	0.001	0.152	10.43	0.07	2.15	24.81	50.3	0.3	0.001	-0.000	
2.60	10.768	0.005	0.014	0.041	0.002	0.252	0.001	0.134	10.41	0.08	2.53	9.57	50.3	0.4	0.004	-0.000	
2.70	11.198	0.009	0.014	0.085	0.005	0.236	0.003	0.172	10.49	0.19	4.03	3.12	50.7	0.9	0.002	-0.000	
2.90	11.202	0.008	0.014	0.105	0.004	0.256	0.003	0.165	10.48	0.17	4.49	3.73	50.6	0.8	0.008	-0.000	
2.90	11.031	0.006	0.014	0.072	0.003	0.267	0.002	0.152	10.52	0.12	3.26	5.45	50.8	0.5	0.000	-0.000	
3.40	11.138	0.006	0.014	0.077	0.002	0.299	0.002	0.139	10.68	0.1	2.97	6.40	51.5	0.5	0.002	-0.000	
3.70	11.69	0.006	0.014	0.076	0.003	0.237	0.003	0.12	10.99	0.12	4.83	5.97	53	0.6	0.005	-0.000	
4.10	12.888	0.007	0.015	0.112	0.004	0.197	0.005	0.088	11.52	0.16	9.04	3.70	55.5	0.8	0.009	-0.000	
4.60	13.076	0.01	0.016	0.132	0.007	0.192	0.007	0.146	11.36	0.32	10.60	2.21	54.8	1.5	0.006	0.000	
5.50	12.266	0.012	0.015	0.106	0.005	0.282	0.004	0.118	11.16	0.21	6.86	2.86	53.8	1	0.000	-0.000	
DC511	Muscovite	>250um	J= 0.002713±0.000014														
2.00	16.535	0.006	0.019	0.067	0.002	0.282	0.021	0.033	10.47	0.21	36.18	9.95	50.5	1	0.005	0.000	
2.20	14.017	0.005	0.017	0.058	0.002	0.29	0.012	0.044	10.54	0.17	24.15	11.46	50.9	0.8	0.000	0.000	
2.40	12.647	0.008	0.016	0.072	0.002	0.27	0.008	0.053	10.52	0.14	15.98	11.40	50.8	0.7	0.007	0.000	
2.60	12.021	0.005	0.016	0.073	0.002	0.262	0.005	0.073	10.51	0.13	11.71	11.34	50.7	0.6	0.004	0.000	
2.80	11.295	0.005	0.016	0.039	0.002	0.319	0.003	0.105	10.55	0.1	5.85	14.62	50.9	0.5	0.004	0.000	
3.00	11.475	0.007	0.016	0.076	0.002	0.263	0.004	0.09	10.53	0.12	7.21	10.16	50.8	0.6	0.000	0.000	
3.20	11.36	0.008	0.016	0.08	0.003	0.258	0.003	0.112	10.54	0.13	5.89	8.06	50.9	0.6	0.006	0.000	
3.40	11.586	0.008	0.017	0.083	0.004	0.252	0.004	0.11	10.61	0.15	6.49	5.49	51.2	0.7	0.002	0.000	
3.70	11.728	0.009	0.016	0.093	0.004	0.327	0.004	0.103	10.6	0.17	7.87	5.80	51.1	0.8	0.003	0.000	
4.10	11.857	0.007	0.017	0.093	0.004	0.253	0.005	0.112	10.58	0.18	8.90	5.23	51	0.9	0.003	0.000	
4.60	11.975	0.008	0.016	0.106	0.004	0.275	0.005	0.114	10.54	0.21	9.94	4.75	50.9	1	0.006	0.000	
5.50	13.094	0.012	0.018	0.201	0.012	0.269	0.01	0.143	10.57	0.46	14.44	1.75	51	2.2	0.010	0.000	
DC512	Muscovite	>250um	J = 0.002712±0.000012														
2.00	14.694	0.009	0.017	0.114	0.004	0.282	0.015	0.063	10.62	0.29	25.58	6.77	51.2	1.4	0.000	-0.000	
2.30	11.065	0.006	0.014	0.061	0.002	0.245	0.002	0.113	10.50	0.10	3.25	13.97	50.7	0.5	0.001	-0.000	
2.50	13.606	0.011	0.016	0.129	0.008	0.251	0.011	0.089	10.62	0.33	16.88	3.48	51.2	1.5	0.000	-0.000	
2.60	13.224	0.013	0.016	0.196	0.012	0.274	0.01	0.16	10.66	0.52	10.49	2.21	51.4	2.5	0.000	-0.000	
2.70	11.828	0.009	0.014	0.088	0.005	0.211	0.005	0.134	10.48	0.24	7.20	5.40	50.6	1.1	0.000	-0.000	
2.90	10.958	0.006	0.014	0.069	0.002	0.191	0.002	0.14	10.47	0.11	2.45	12.99	50.5	0.5	0.001	-0.000	
3.10	11.019	0.005	0.014	0.062	0.002	0.197	0.002	0.134	10.44	0.11	3.27	12.96	50.4	0.5	0.001	-0.000	
3.40	10.886	0.006	0.014	0.059	0.002	0.202	0.002	0.129	10.42	0.10	2.60	15.76	50.3	0.5	0.001	-0.000	
3.70	10.919	0.006	0.014	0.058	0.002	0.226	0.002	0.145	10.43	0.11	2.59	14.06	50.3	0.5	0.000	-0.000	

Watts	40Ar/39Ar	±	38Ar/39Ar	±	37Ar/39Ar	±	36Ar/39Ar	±	40Ar*/39ArK	±	%40Ar atm	% 39Ar	Age	±	Ca/K	Cl/K
4.10	11.579	0.008	0.014	0.108	0.004	0.214	0.005	0.12	10.40	0.19	6.37	6.26	50.2	0.9	0.000	-0.000
4.60	12.111	0.009	0.016	0.126	0.007	0.276	0.007	0.136	10.49	0.28	8.08	4.19	50.6	1.3	0.008	-0.000
5.00	13.711	0.016	0.019	0.213	0.014	0.237	0.013	0.135	10.43	0.56	14.68	1.95	50.3	2.7	0.011	0.000
DC515	Muscovite	>250um	J= 0.002711±0.000012													
2.00	15.826	0.007	0.016	0.076	0.002	0.235	0.019	0.037	10.29	0.22	34.43	5.06	49.6	1.1	0.002	-0.000
2.20	13.046	0.008	0.014	0.088	0.003	0.268	0.009	0.058	10.51	0.18	18.20	3.48	50.7	0.8	0.000	-0.000
2.40	12.679	0.006	0.014	0.065	0.003	0.209	0.008	0.066	10.58	0.17	15.28	3.42	51	0.8	0.000	-0.000
2.60	12.205	0.006	0.014	0.065	0.002	0.226	0.006	0.064	10.49	0.13	13.17	5.37	50.6	0.6	0.002	-0.000
2.80	11.37	0.006	0.013	0.066	0.002	0.188	0.003	0.101	10.55	0.12	6.08	4.87	50.9	0.6	0.005	-0.000
3.00	11.855	0.007	0.014	0.095	0.003	0.233	0.005	0.088	10.53	0.15	9.83	3.80	50.8	0.7	0.002	-0.000
3.20	11.749	0.005	0.014	0.065	0.002	0.289	0.005	0.067	10.5	0.1	9.69	5.85	50.7	0.5	0.005	-0.000
3.40	11.875	0.006	0.014	0.069	0.002	0.268	0.005	0.067	10.5	0.12	10.60	5.21	50.6	0.6	0.000	-0.000
3.70	11.473	0.005	0.014	0.064	0.001	0.379	0.004	0.08	10.49	0.1	8.09	11.47	50.6	0.5	0.006	-0.000
4.10	11.27	0.005	0.013	0.072	0.001	0.286	0.003	0.082	10.51	0.09	6.06	8.25	50.7	0.4	0.004	-0.000
4.60	11.064	0.005	0.013	0.052	0.001	0.391	0.002	0.088	10.51	0.08	4.60	15.08	50.7	0.4	0.000	-0.000
5.50	10.793	0.006	0.013	0.063	0	0.606	0.001	0.121	10.47	0.07	2.74	28.15	50.5	0.4	0.003	-0.000
DC519	Muscovite	>250um	J= 0.002710±0.000012													
2.00	31.1	0.014	0.03	0.135	0.015	0.279	0.073	0.045	10.51	0.95	65.11	1.55	50.6	4.5	0.006	0.000
2.30	11.48	0.006	0.015	0.073	0.001	0.367	0.003	0.078	10.54	0.1	7.58	22.07	50.8	0.5	0.001	0.000
2.60	10.908	0.005	0.015	0.053	0.001	0.307	0.002	0.137	10.48	0.08	3.19	21.22	50.5	0.4	0.002	0.000
2.70	11.424	0.008	0.015	0.112	0.005	0.285	0.004	0.169	10.55	0.2	4.98	5.25	50.9	1	0.002	-0.000
2.90	11.191	0.007	0.015	0.079	0.003	0.267	0.003	0.154	10.51	0.14	4.30	8.00	50.7	0.7	0.002	0.000
3.10	10.991	0.007	0.015	0.082	0.003	0.253	0.002	0.147	10.51	0.11	2.76	9.48	50.7	0.5	0.003	0.000
3.40	10.864	0.007	0.015	0.066	0.002	0.296	0.002	0.163	10.46	0.11	2.45	11.61	50.4	0.5	0.000	0.000
3.70	11.097	0.007	0.015	0.103	0.003	0.287	0.003	0.145	10.46	0.14	3.78	7.45	50.4	0.7	0.005	0.000
4.10	11.279	0.008	0.015	0.08	0.004	0.265	0.003	0.163	10.53	0.17	4.47	6.61	50.8	0.8	0.004	0.000
4.60	11.291	0.009	0.016	0.09	0.004	0.299	0.003	0.159	10.5	0.19	4.48	5.69	50.6	0.9	0.000	0.000
5.00	13.989	0.015	0.019	0.206	0.024	0.274	0.015	0.173	10.63	0.81	14.67	1.07	51.2	3.8	0.004	-0.000
DC528	Muscovite	>250um	J= 0.002708±0.000012													
2.00	16.755	0.01	0.022	0.11	0.007	0.225	0.023	0.059	10.22	0.42	37.98	3.36	49.2	2	0.002	0.001
2.30	21.83	0.011	0.026	0.112	0.009	0.196	0.041	0.053	10.21	0.64	52.56	2.85	49.2	3.1	0.024	0.001
2.50	13.783	0.008	0.019	0.099	0.006	0.278	0.012	0.078	10.54	0.29	22.24	4.11	50.8	1.4	0.000	0.001
2.60	14.418	0.01	0.02	0.126	0.008	0.287	0.015	0.095	10.49	0.43	25.74	3.13	50.5	2	0.006	0.001
2.70	12.928	0.011	0.019	0.138	0.008	0.253	0.009	0.123	10.73	0.35	15.02	3.11	51.7	1.6	0.006	0.001

Watts	40Ar/39Ar	±	38Ar/39Ar	±	37Ar/39Ar	±	36Ar/39Ar	±	40Ar*/39ArK	±	%40Ar atm	% 39Ar	Age	±	Ca/K	Cl/K
2.90	14.377	0.008	0.021	0.073	0.004	0.255	0.014	0.064	10.5	0.28	26.29	6.81	50.6	1.3	0.006	0.001
3.10	14.829	0.007	0.02	0.078	0.003	0.236	0.015	0.047	10.45	0.23	28.95	7.98	50.3	1.1	0.004	0.001
3.40	11.614	0.005	0.017	0.049	0.001	0.313	0.004	0.064	10.49	0.09	9.28	22.46	50.6	0.4	0.002	0.000
3.70	11.525	0.005	0.017	0.058	0.001	0.258	0.004	0.083	10.49	0.11	8.59	20.52	50.5	0.5	0.004	0.001
4.10	11.009	0.005	0.017	0.045	0.001	0.3	0.002	0.123	10.54	0.09	3.75	18.87	50.8	0.4	0.002	0.001
4.60	11.082	0.008	0.019	0.082	0.005	0.224	0.002	0.22	10.57	0.18	3.12	5.76	50.9	0.8	0.005	0.001
5.00	13.521	0.022	0.023	0.172	0.025	0.21	0.014	0.184	10.54	0.81	16.51	1.03	50.8	3.8	0.021	0.001
DC532	Biotite	>250um	J= 0.002707±0.000012													
2.00	222.072	0.088	0.221	0.298	0.459	0.364	0.81	0.117	3.04	21.63	98.56	0.04	14.8	104.8	0.293	0.001
2.20	129.466	0.098	0.148	0.373	0.367	0.287	0.468	0.149	8.46	17.65	92.34	0.05	40.8	84.3	0.000	0.006
2.40	36.711	0.027	0.042	0.204	0.037	0.253	0.092	0.075	11.17	1.97	67.46	0.56	53.7	9.3	0.067	0.002
2.50	27.435	0.019	0.035	0.155	0.025	0.291	0.056	0.083	12.06	1.39	52.92	0.76	58	6.6	0.022	0.002
2.60	18.173	0.017	0.027	0.151	0.016	0.224	0.023	0.095	12.09	0.69	29.25	1.31	58.1	3.3	0.000	0.002
2.70	15.423	0.011	0.025	0.106	0.011	0.25	0.013	0.106	12.07	0.43	17.67	1.88	58	2	0.010	0.002
2.80	15.611	0.014	0.026	0.108	0.012	0.261	0.015	0.123	11.73	0.58	20.33	1.64	56.4	2.7	0.002	0.002
2.90	14.986	0.016	0.025	0.138	0.014	0.257	0.013	0.136	11.81	0.55	15.45	1.47	56.8	2.6	0.000	0.002
3.10	14.583	0.013	0.025	0.099	0.011	0.279	0.011	0.14	11.93	0.47	13.44	1.84	57.4	2.2	0.018	0.002
3.30	15.981	0.018	0.027	0.153	0.016	0.219	0.016	0.108	11.75	0.57	21.16	1.35	56.5	2.7	0.017	0.002
3.60	14.233	0.191	0.021	0.265	0.013	0.293	0.016	0.21	10.07	2.16	24.38	1.61	48.5	10.3	0.029	0.001
3.90	21.179	0.014	0.03	0.135	0.015	0.265	0.036	0.068	11.49	0.73	43.00	1.37	55.2	3.5	0.015	0.002
4.10	21.798	0.018	0.032	0.162	0.022	0.313	0.039	0.091	11.64	1.05	42.24	0.87	56	5	0.000	0.002
4.40	19.403	0.007	0.026	0.057	0.003	0.238	0.027	0.03	11.66	0.25	39.29	7.56	56.1	1.2	0.009	0.002
4.70	15.216	0.008	0.023	0.058	0.003	0.218	0.012	0.052	11.83	0.21	21.05	6.27	56.9	1	0.000	0.002
5.10	13.927	0.005	0.023	0.06	0.001	0.422	0.007	0.059	11.87	0.14	14.34	23.74	57.1	0.7	0.003	0.002
5.50	12.827	0.006	0.021	0.046	0.001	0.601	0.003	0.079	11.93	0.11	6.71	44.26	57.3	0.5	0.008	0.002
6.00	13.75	0.009	0.023	0.101	0.008	0.281	0.006	0.157	12.31	0.3	6.85	2.76	59.2	1.4	0.027	0.002
7.00	23.037	0.021	0.03	0.188	0.03	0.292	0.032	0.126	15.07	1.26	28.15	0.67	72.1	5.9	0.000	0.002
DC536	Muscovite	>250um	J= 0.002705±0.000012													
2.00	29.743	0.016	0.034	0.147	0.019	0.198	0.069	0.054	10.35	1.08	63.70	0.75	49.8	5.1	0.009	0.001
2.20	24.736	0.014	0.032	0.11	0.012	0.221	0.049	0.054	10.97	0.78	54.24	1.20	52.7	3.7	0.027	0.002
2.40	16.503	0.014	0.026	0.156	0.013	0.228	0.021	0.097	10.94	0.62	29.94	1.08	52.6	2.9	0.019	0.002
2.50	16.094	0.016	0.029	0.131	0.015	0.236	0.02	0.11	10.79	0.68	28.13	0.87	51.9	3.2	0.000	0.002
2.60	15.998	0.016	0.029	0.137	0.018	0.243	0.02	0.12	10.75	0.75	26.69	0.72	51.7	3.5	0.000	0.002
2.70	14.509	0.016	0.026	0.154	0.016	0.301	0.014	0.131	10.99	0.57	17.86	0.85	52.9	2.7	0.026	0.002
2.80	28.207	0.018	0.035	0.129	0.016	0.28	0.064	0.058	10.23	1.07	62.36	0.90	49.3	5.1	0.031	0.002
2.90	30.726	0.014	0.037	0.113	0.012	0.234	0.071	0.04	10.51	0.8	64.90	1.15	50.6	3.8	0.000	0.002
3.10	18.602	0.009	0.028	0.113	0.008	0.206	0.027	0.053	10.88	0.44	39.93	1.95	52.3	2.1	0.014	0.002

Watts	40Ar/39Ar	±	38Ar/39Ar	±	37Ar/39Ar	±	36Ar/39Ar	±	40Ar*/39ArK	±	%40Ar atm	% 39Ar	Age	±	Ca/K	Cl/K
3.30	15.236	0.009	0.027	0.083	0.005	0.229	0.015	0.065	10.9	0.31	26.85	2.91	52.4	1.5	0.002	0.002
3.50	12.727	0.008	0.024	0.074	0.003	0.289	0.006	0.092	10.96	0.2	12.29	4.21	52.7	0.9	0.004	0.002
3.80	11.943	0.005	0.023	0.05	0.002	0.314	0.003	0.08	11	0.1	7.11	10.71	52.9	0.5	0.007	0.002
4.40	11.377	0.005	0.023	0.046	0.001	0.357	0.001	0.124	11.05	0.08	2.46	20.35	53.1	0.4	0.004	0.002
7.00	11.212	0.005	0.023	0.044	0	0.676	0.001	0.247	11.04	0.07	1.35	52.34	53.1	0.3	0.006	0.002

DC538 Muscovite >250um J = 0.002704±0.000012

2.00	52.354	0.019	0.046	0.116	0.03	0.226	0.146	0.052	11.31	2.15	77.30	0.68	54.4	10.2	0.003	0.000
2.30	119.364	0.022	0.092	0.132	0.04	0.228	0.374	0.035	11.57	3.18	90.15	0.67	55.6	15	0.094	0.001
2.50	162.302	0.023	0.121	0.113	0.05	0.212	0.521	0.041	12.24	5.22	92.39	0.53	58.7	24.7	0.103	0.001
2.60	100.937	0.02	0.077	0.123	0.04	0.263	0.311	0.043	11.81	3.61	88.05	0.64	56.7	17	0.011	0.001
2.70	74.263	0.025	0.057	0.156	0.04	0.245	0.214	0.049	13.23	2.74	81.60	0.63	63.4	12.9	0.011	-0.001
2.90	26.007	0.012	0.025	0.102	0.01	0.286	0.047	0.061	12.7	0.86	49.66	2.42	60.9	4	0.025	0.000
3.10	24.133	0.014	0.023	0.112	0.01	0.231	0.041	0.051	12.81	0.63	44.74	1.94	61.4	3	0.014	-0.000
3.40	17.984	0.011	0.019	0.098	0.01	0.206	0.02	0.072	12.46	0.45	28.33	3.16	59.8	2.1	0.029	0.000
3.70	14.044	0.008	0.016	0.096	0.01	0.174	0.011	0.069	11.11	0.24	18.94	5.73	53.4	1.1	0.038	-0.000
4.10	12.363	0.007	0.015	0.068	0.01	0.101	0.007	0.065	10.48	0.15	13.91	10.46	50.4	0.7	0.058	-0.000
4.60	11.582	0.005	0.014	0.078	0.00	0.138	0.004	0.12	10.54	0.14	8.38	28.32	50.7	0.7	0.039	-0.000
5.00	11.679	0.007	0.014	0.065	0.00	0.166	0.003	0.088	10.84	0.11	6.78	44.82	52.1	0.5	0.036	-0.000

DC543 Muscovite >250um J= 0.002702±0.000012

2.00	17.143	0.01	0.018	0.12	0.006	0.254	0.023	0.055	10.61	0.39	35.20	4.52	51	1.9	0.013	-0.000
2.30	11.575	0.006	0.014	0.068	0.002	0.194	0.004	0.075	10.45	0.11	7.50	13.14	50.3	0.5	0.006	-0.000
2.50	11.706	0.007	0.014	0.085	0.003	0.287	0.005	0.092	10.52	0.14	7.05	9.07	50.6	0.7	0.000	-0.000
2.60	12.076	0.009	0.014	0.123	0.005	0.235	0.006	0.127	10.62	0.25	7.13	5.50	51	1.2	0.009	-0.000
2.70	12.718	0.01	0.015	0.112	0.005	0.224	0.008	0.101	10.57	0.27	12.34	5.33	50.8	1.3	0.009	-0.000
2.90	11.652	0.007	0.014	0.078	0.003	0.242	0.004	0.099	10.56	0.14	6.50	9.91	50.8	0.7	0.007	-0.000
3.10	11.329	0.007	0.014	0.08	0.002	0.206	0.003	0.092	10.51	0.11	4.91	13.11	50.5	0.5	0.003	-0.000
3.40	11.221	0.007	0.014	0.072	0.002	0.203	0.003	0.106	10.48	0.12	4.04	11.91	50.4	0.6	0.002	-0.000
3.70	11.379	0.007	0.014	0.074	0.003	0.24	0.003	0.105	10.47	0.13	5.14	10.78	50.4	0.6	0.007	-0.000
4.10	11.495	0.008	0.014	0.084	0.003	0.239	0.004	0.111	10.51	0.15	5.20	8.88	50.5	0.7	0.004	-0.000
4.60	12.119	0.008	0.014	0.11	0.004	0.24	0.006	0.09	10.65	0.18	7.89	6.43	51.2	0.8	0.007	-0.000
5.00	15.711	0.017	0.019	0.206	0.019	0.192	0.021	0.129	10.64	0.82	19.77	1.42	51.1	3.9	0.032	-0.001

D1 Selected structural and lithological data used for the map and legend in Appendix D

Sample	Rock type	Structure	Defined	Strike	Dip	Ddir.	Plunge	Trend	Defined	Northing	Easting	Location
DC004	Plagioclase amphibolite	Foliation	Amphibole, plagioclase	230	16	N				5578185	421973	North Plant Rd
		Foliation	Amphibole, plagioclase	235	14	N						
DC025	Laybird pegmatite	Foliation	Biotite and quartz layers	255	31	N				5573818	413230	Plant Rd, Sp A, Br 30
		Dyke	Pegmatite	165	34	S						
		Foliation	Biotite and quartz layers	265	45	NW						
DC026	Biotite schist	Foliation	Biotite and quartz layers	250	57	N				5573777	413370	Plant Rd, Sp A, Br 30
DC045	Bitotie psammite	Foliation	Biotite and quartz layers	100	25	S				5573550	410692	Plant Rd, Sp A, Br 30
	Bitotie psammite	Foliation	Biotite and quartz layers	060	4	SE						
DC047	Laybird pegmatite	Contact		070	35	S				5573552	410416	Plant Rd, Sp A, Br 30
DC080	Calc-silicate amphibolite	Foliation	Amphibole, biotite	100	20	S				5571584	415929	South Cusson Rd
	Calc-silicate amphibolite	Foliation	Amphibole, biotite	095	15	S						
DC125	Plagioclase amphibolite	Foliation	Amphibole, biotite, plagioclase	065	32					5582842	413638	South Cusson Rd
DC130A	Metasandstone	Foliation	Bedding, mica	314	21	NE				5574446	419949	Plant Rd, Sp A, Br 30
	Metasandstone	Foliation	Bedding, mica	277	22	N						
	Metasandstone	Foliation	Bedding, mica	274	29	N						
DC133	Metasandstone	Foliation	Bedding, mica	172	85	W				5574310	420679	Plant Rd, Sp A, Br 30
DC135	Phyllite	Foliation	Phyllite	302	69	NE				5574175	420909	Plant Rd, Sp A, Br 30
DC136	Metasandstone	Foliation	Bedding, mica	260	69	N				5574072	420957	Plant Rd, Sp A, Br 30
DC139	Metasandstone	Foliation	Bedding, mica	255	65	N				5543221	418464	Plant Rd, Sp A, Br 30
DC140	Metasandstone	Foliation	Bedding, mica	285	54	N				5573216	418764	Plant Rd, Sp A, Br 30
DC163	Garnet–sillimanite–biotite paragneiss	Foliation	Biotite	116	40	SW				5598008	415715	Cariboo Alp
	Garnet–sillimanite–biotite paragneiss	Foliation	Biotite	110	39	SW						
DC199	Biotite–sillimanite–schist	Foliated	Biotite	080	29	S				5588446	416635	North Fosthall Creek
DC202	Marble	Foliated	Mica with graphite	105	34	SW				5588791	416669	North Fosthall Creek
DC203	Laybird pegmatite	Contact		103	73	SW				5587823	417589	North Fosthall Creek
	Laybird pegmatite	Fracture	LB	030	75	SE						
DC205	Amphibolite		Amphibole, biotite	270	25	N				5587928	417498	North Fosthall Creek
DC209	Plagioclase amphibolite		Amphibolte, plagioclase layers	114	36	SW				5588095	417457	North Fosthall Creek
DC211	Sillimanite–garnet–paragneiss		Sillimanite, biotite	117	37	SW				5588303	417287	North Fosthall Creek
DC215	Garnet–biotite–paragneiss	Foliation	Biotite, quartz layers	110	43					5588881	417206	North Fosthall Creek
DC216	Marble	Foliation	Mica with graphite	095	61	S				5588881	417206	North Fosthall Creek
DC219	Calc-silicate amphibolite	Foliation	Amphibole, quartz layers	095	66	S				5588920	417587	North Fosthall Creek
	Calc-silicate amphibolite		Amphibole, quartz layers	098	82	SW						
DC220	Calc-silicate amphibolite		Amphibole, quartz layers	102	44	SW				5588920	417587	North Fosthall Creek
DC221	Calc-silicate amphibolite		Amphibole, quartz layers	101	55	SW				5588797	417824	North Fosthall Creek
DC222	Calc-silicate gneiss		Amphibole, quartz layers	092	48	S				5588732	417852	North Fosthall Creek
DC225	Marble		Mica with graphite	102	57	SW				5588604	418856	North Fosthall Creek
DC242	Phyllite	Cleavage	Mica	270	36	N				5576600	426265	Cameron Lake Rd, Br 10
DC246	Phyllite	Parting	Mica	272	51	N				5576425	428245	Cameron Lake Rd, Br 10
DC261	Calc-silicate gneiss	Foliation	Calc-silicate	295	54	NE				5572106	431220	Cameron Lake Rd, Br 10
DC278	Calc-silicate gneiss		Psammite	247	16	NW				5573214	428238	Cameron Lake Rd, Br 10

Sample	Rock type	Structure	Defined	Strike	Dip	Ddir.	Plunge	Trend	Defined	Northing	Easting	Location
DC295B	Psammite	Foliation	Phyllite	217	18	NW				5573093	426253	Cameron Lake Rd, Br 5
DC295C	Phyllite	Foliation	Muscovite	195	31	NW				5572999	426291	Cameron Lake Rd, Br 5
	Phyllite	Foliation	Muscovite	198	35	NW						
DC295D	Psammite	Foliation	Bedding	195	32	NW				5572999	426291	Cameron Lake Rd, Br 5
DC295P	Ladybird pegmatite									5572965	426367	Cameron Lake Rd, Br 5
DC299	Calc-silicate gneiss	Foliation	Amphibole, biotite	150	30	SW				5572143	426826	Cameron Lake Rd, Br 5
DC300	Psammite	Foliation	Mica	152	25	SW				5572088	426711	Cameron Lake Rd, Br 5
DC303	Psammite	Foliation	Mica	150	28	SW				5570841	420879	S Cusson top
DC321	Garnet-sillimanite-biotite paragneiss	Foliation	Biotite Layers	129	44	SW				5595800	414320	Fawn Lakes
DC324	Garnet amphibolite	Foliation	Amphibole, biotite	123	21	SW				5596089	414723	Fawn Lakes
DC330	Biotite-quartzofeldspathic gneiss	Foliation	Biotite layers in grey gneiss	134	45					5596404	415431	Fawn Lakes
	Biotit-quartzofeldspathic gneiss	Foliation	Biotite layers in grey gneiss	134	39	SW						
DC331	Garnet biotite semipelite	Foliation	Biotite layers and flaggy layers	112	53					5596679	414521	Fawn Lakes
DC331	Garnet-sillimanite-biotite paragneiss	Foliation	Biotite and sillimanite layers	154	37	SW				5596684	415500	Fawn Lakes
DC332	Garnet-sillimanite-biotite paragneiss	Foliation	Biotite and sillimanite layers	171	29	SW				5596512	415405	Fawn Lakes
	Garnet-sillimanite-biotite paragneiss	Foliation	Biotite and sillimanite layers	105	39	SW	20	255 sillimanite		5596512	415405	Fawn Lakes
	Garnet-sillimanite-biotite paragneiss	Foliation	Biotite and sillimanite layers	109	51	W	20	248 sillimanite		5596512	415405	Fawn Lakes
	Garnet-sillimanite-biotite paragneiss	Foliation	Biotite and sillimanite layers	110	54	SW				5596512	415405	Fawn Lakes
DC333	Garnet-sillimanite-biotite paragneiss	Foliation	Biotite and sillimanite layers	127	44	SW				5596429	415406	Fawn Lakes
	Garnet-sillimanite-biotite paragneiss	Foliation	Biotite and sillimanite layers			SW				5596502	415444	Fawn Lakes
	Garnet-sillimanite-biotite paragneiss	Fracture		335	48	SW				5596445	415368	Fawn Lakes
	Garnet-sillimanite-biotite paragneiss	Fracture		345	44					5596445	415368	Fawn Lakes
	Garnet-sillimanite-biotite paragneiss	Fracture		340	70	NE				5596445	415368	Fawn Lakes
	Garnet-sillimanite-biotite paragneiss	Fracture		343	57	NE				5596445	415368	Fawn Lakes
	Garnet-sillimanite-biotite paragneiss	Fracture		341	55	NE				5596445	415368	Fawn Lakes
	Garnet-sillimanite-biotite paragneiss	Fracture		355	65	NE				5596445	415368	Fawn Lakes
DC334	Garnet-sillimanite-biotite paragneiss	Fracture		353	63	NE				5596445	415368	Fawn Lakes
	Garnet-sillimanite-biotite paragneiss	Fracture		333	63	NE				5596445	415368	Fawn Lakes
	Garnet-sillimanite-biotite paragneiss	Fracture		347	64	NE				5596445	415368	Fawn Lakes
DC335	Garnet-sillimanite-biotite paragneiss	Foliation	Biotite and sillimanite layers	215	43	NE	25	250 sillimanite		5596478	415324	Fawn Lakes
	Garnet-sillimanite-biotite paragneiss	Foliation	Biotite and sillimanite layers	215	43	NE	30	255 sillimanite		5596478	415324	Fawn Lakes
	Garnet-sillimanite-biotite paragneiss	Fracture		340	57	NW				5596478	415324	Fawn Lakes
	Garnet-sillimanite-biotite paragneiss	Fracture		358	58					5596478	415324	Fawn Lakes
	Garnet-sillimanite-biotite paragneiss	Fracture		340	50	NE				5596478	415324	Fawn Lakes
DC336	Garnet-biotite-psammite	Foliation	Biotite and sillimanite layers	123	58	NE				5596438	415216	Fawn Lakes
	Garnet-biotite-psammite	Foliation	Biotite and sillimanite layers	125	46	NE				5596438	415216	Fawn Lakes
	Garnet-biotite-psammite	Fracture		358	68	SW				5596438	415216	Fawn Lakes
	Garnet-biotite-psammite	Fracture		359	64	SW				5596438	415216	Fawn Lakes
DC337	Garnet-biotite-psammite	Foliation	Biotite	129	59	NE				5596390	415252	Fawn Lakes
	Garnet-biotite-psammite	Fracture		354	58	NE				5596390	415252	Fawn Lakes
	Garnet-biotite-psammite	Fracture		351	71	SW				5596390	415252	Fawn Lakes
	Garnet-biotite-psammite	Fracture		38	67	NE				5596390	415252	Fawn Lakes
	Garnet-biotite-psammite	Fracture		29	85	NE				5596390	415252	Fawn Lakes

Sample	Rock type	Structure	Defined	Strike	Dip	Ddir.	Plunge	Trend	Defined	Northing	Easting	Location	
DC340	Garnet–sillimanite–biotite paragneiss	Foliation	Biotite and sillimanite layers	73	46					5592998	420260	Mount Symonds	
	Garnet–sillimanite–biotite paragneiss	Foliation	Biotite	88	35					5592998	420260	Mount Symonds	
DC341	Garnet–biotite paragneiss	Foliation	Biotite	81	41	SE				5502980	420300	Mount Symonds	
DC342	Garnet amphibolite	Foliation	Hornblende	86	41	S				5592908	420255	Mount Symonds	
DC343	Garnet amphibolite	Foliation	Hornblende	93	48	SE				5592844	420223	Mount Symonds	
DC344	Garnet amphibolite	Foliation	Hornblende	110	63	S				5592820	420104	Mount Symonds	
DC345	Garnet amphibolite	Foliation	Hornblende	65	48	S				5592604	420220	Mount Symonds	
	Garnet amphibolite	Foliation	Hornblende	104	49	SW				5592604	420220	Mount Symonds	
	Garnet amphibolite	Foliation	Hornblende	108	54	SE				5592604	420220	Mount Symonds	
	Garnet amphibolite	Foliation	Hornblende	111	49	SW				5592604	420220	Mount Symonds	
	Garnet amphibolite	Foliation	Hornblende	111	48	SW				5592604	420220	Mount Symonds	
	Garnet amphibolite	Foliation	Hornblende	114	41	SW				5592604	420220	Mount Symonds	
	DC346	Quartzite	Parting	Muscovite	112	43	SW				5592559	420275	Mount Symonds
		Quartzite	Parting	Muscovite	106	41	SW				5592559	420275	Mount Symonds
Quartzite		Parting	Muscovite	110	33	SW				5592559	420275	Mount Symonds	
Quartzite		Parting	Muscovite	103	39	SW	15	280	sillimanite	5592559	420275	Mount Symonds	
Quartzite		Parting	Muscovite	114	38	SW				5592559	420275	Mount Symonds	
Quartzite		Fracture		208	73	SW				5592559	420275	Mount Symonds	
Quartzite		Fracture		205	67	SW				5592559	420275	Mount Symonds	
Quartzite		Fracture		211	69	NW				5592559	420275	Mount Symonds	
Quartzite		Fracture		203	78	NW				5592559	420275	Mount Symonds	
DC347		Quartzite	Parting	Muscovite	110	53	NW				5502561	720192	Mount Symonds
	Quartzite	Parting	Muscovite	98	49	NW				5502561	720192	Mount Symonds	
	Quartzite	Parting	Muscovite	95	46	SW				5502561	720192	Mount Symonds	
	Quartzite	Parting	Muscovite	96	55	SW				5502561	720192	Mount Symonds	
DC348	Quartzite	Parting	Muscovite	103	48	SW				5592561	419876	Mount Symonds	
	Quartzite	Parting	Muscovite	100	40	SW				5592561	419876	Mount Symonds	
DC349	Quartzite	Parting	Muscovite	108	44	SW				5592561	420386	Mount Symonds	
	Quartzite	Parting	Muscovite	103	49	SW				5592561	420386	Mount Symonds	
	Quartzite	Parting	Muscovite	100	42	SW				5592561	420386	Mount Symonds	
	Quartzite	Parting	Muscovite	110	43	SW				5592561	420386	Mount Symonds	
	Quartzite	Fracture		199	77	SW				5592561	420386	Mount Symonds	
	Quartzite	Fracture		209	74	SW				5592561	420386	Mount Symonds	
DC349b	Garnet–sillimanite–biotite paragneiss	Foliation	Biotite and sillimanite layers	101	49	NW				5592560	420370	Mount Symonds	
	Garnet–sillimanite–biotite paragneiss	Foliation	Biotite and sillimanite layers	116	56	NW				5592561	420386	Mount Symonds	
	Garnet–sillimanite–biotite paragneiss	Foliation	Biotite and sillimanite layers	103	56	SW				5592561	420386	Mount Symonds	
DC350	Quartzite	Parting	Muscovite	111	46	SW				5592455	420360	Mount Symonds	
	Quartzite	Parting	Muscovite	113	42	SW				5592455	420360	Mount Symonds	
	Quartzite	Parting	Muscovite	114	48	SW				5592455	420360	Mount Symonds	
DC350b	Garnet–sillimanite–biotite paragneiss	Foliation	Biotite and sillimanite layers	97	40	SW				5592455	420360	Mount Symonds	
	Garnet–sillimanite–biotite paragneiss	Foliation	Biotite and sillimanite layers	94	40	SW				5592455	420360	Mount Symonds	
	Garnet–sillimanite–biotite paragneiss	Foliation	Biotite and sillimanite layers	99	40	S				5592455	420360	Mount Symonds	
DC351	Garnet–plagioclase amphibolite	Fracture	Amphibole, biotite, plagioclase	205	77	NW				5587287	409899	Twin Peaks	

Sample	Rock type	Structure	Defined	Strike	Dip	Ddir.	Plunge	Trend	Defined	Northing	Easting	Location
	Garnet-plagioclase amphibolite	Fracture	Amphibole, biotite, plagioclase	290	36	NE						
	Garnet-plagioclase amphibolite	Fracture	Amphibole, biotite, plagioclase	203	74	NW						
	Garnet-plagioclase amphibolite	Partings	Qtz	090	46	S						
	Garnet-plagioclase amphibolite	Partings	Qtz	095	43	SW						
	Garnet-plagioclase amphibolite	Foliation	Amphibole, biotite	089	38	SE						
	Garnet-plagioclase amphibolite	Foliation	Amphibole, biotite	085	39	SE						
	Garnet-plagioclase amphibolite	Foliation	Amphibole, biotite, plagioclase	087	32	SE						
DC452	Garnet-plagioclase amphibolite	Foliation	Amphibole, biotite, plagioclase	237	58	NW				5587287	409899	Twin Peaks
	Garnet-plagioclase amphibolite	Foliation	Amphibole, biotite, plagioclase	243	53	NW						
	Garnet-plagioclase amphibolite	Foliation	Amphibole, biotite, plagioclase	241	56	NW						
	Garnet-plagioclase amphibolite	Foliation	Amphibole, biotite, plagioclase	238	61	NW						
	Garnet-plagioclase amphibolite	Foliation	Amphibole, biotite, plagioclase	245	54	NW						
	Garnet-plagioclase amphibolite	Foliation	Amphibole, biotite, plagioclase	244	56	NW						
DC453	Garnet-sillimanite-biotite paragneiss	Foliation	Biotite, sillimanite	160	30	SW	33	266	Paragneiss	5587143	409812	Twin Peaks
	Garnet-sillimanite-biotite paragneiss	Foliation	Biotite, sillimanite	282	72	NW	45	228	Paragneiss			
	Garnet-sillimanite-biotite paragneiss	Foliation	Biotite, sillimanite	216	50	NW						
	Garnet-sillimanite-biotite paragneiss	Foliation	Biotite, sillimanite	246	66	NW						
DC455	Garnet-sillimanite-biotite paragneiss						33	290	Qtz	5587094	409778	Twin Peaks
DC456A	Lamprophyre		Biotite, sillimanite							5586658	409887	Twin Peaks
DC456	Garnet-sillimanite-biotite paragneiss	Foliation	Biotite, sillimanite	100	43	SW				5586658	409887	Twin Peaks
	Garnet-sillimanite-biotite paragneiss	Foliation	Biotite, sillimanite	097	59	SW						
	Garnet-sillimanite-biotite paragneiss	Foliation		012	54	SE						
DC457	Calc-silicate amphibolite	Foliation	Amphibole, plagioclase	124	37	SW						Twin Peaks
	Calc-silicate amphibolite		Amphibole, plagioclase	128	40	SW						
DC462	Garnet-sillimanite-biotite paragneiss											Twin Peaks
DC463	Garnet-sillimanite-biotite paragneiss	Foliation	Pegmatite	290	54		20	300	Qtz	5587214	409919	Twin Peaks
	Garnet-sillimanite-biotite paragneiss						31	262				
DC464	Garnet amphibolite	Foliation	Amphibole, plagioclase	215	21	NW	15	293		5587098	411440	Twin Peaks
DC465	Garnet-sillimanite-biotite paragneiss	Foliation	Paragneiss	215	22	NW	15	232		5587098	411440	Twin Peaks
				211	34							
DC466	Laybird pegmatite			199	29	NW	20	271		5587098	411440	Twin Peaks
				266	61	N	23	285				
DC467A	Garnet amphibolite									5587098	411440	Twin Peaks
DC467	Garnet-sillimanite-biotite paragneiss	Foliation	Biotite, sillimanite	275	48	N	44	321		5587098	411440	Twin Peaks
		Foliation	Biotite, sillimanite	260	68	NW						
		Foliation	Biotite, sillimanite	254	53	NW						
		Foliation	Biotite, sillimanite	252	50	NW						
		Foliation	Biotite, sillimanite	033	72	SE						
DC468	Garnet calc-silicate amphibolite	Foliation	Biotite, sillimanite	265	54	NW	8	254		5587274	410993	Twin Peaks
		Foliation	Biotite, sillimanite	251	50	NW						
		Foliation	Biotite, sillimanite	250	51	NW						
DC469	Plagioclase amphibolite	Foliated	Amphibole, plagioclase	243	58	NW				5587283	410739	Twin Peaks
DC470	Garnet-sillimanite-biotite paragneiss	Foliation	Biotite, sillimanite	261	52	NW				5587487	409971	Twin Peaks

Sample	Rock type	Structure	Defined	Strike	Dip	Ddir.	Plunge	Trend	Defined	Northing	Easting	Location
DC471	Garnet–sillimanite–biotite paragneiss	Foliation	Biotite, sillimanite	235	56	NW						
		Foliation	Biotite, sillimanite	247	49	NW						
		Foliation	Biotite, sillimanite	282	49	NW						
		Fracture		005	72	E						
		Fracture		003	76							
		Fracture		002	66	E						
		Foliation	Biotite, sillimanite	248	43	NW	2	246	Qtz		5587499	409921
DC472	Garnet–sillimanite–biotite paragneiss	Foliation	Biotite, sillimanite	249	41	NW						
		Foliation	Biotite, sillimanite	248	41	NW						
DC473	Calc-silicate amphibolite	Fractured		007	70	E						
		Foliation	Biotite, sillimanite	151	28	SW	27	244		5587499	409921	Twin Peaks
DC474	Ladybird pegmatite	Foliation	Biotite, sillimanite	069	70	SW	8	241				
		Foliation		256	57	NW	54	22		5587415	409940	Twin Peaks
DC475	Lamprophyre	Foliation		258	54	NW						
		Foliation		254	53	NW						
		Fracture		344	83	NE						
DC476	Amphibolite	Foliation	Paragneiss and Psammite	218	22	NW				5587698	409972	Twin Peaks
		Foliation	Paragneiss and Psammite	216	18	NW						
		Foliation	Paragneiss and Psammite	212	21	NW						
DC477	Ultramafic	Foliation		345	67	NE				5587801	409994	Twin Peaks
		Foliation		005	66	E						
DC478	Ultramafic	Foliation	Migmatite	264	58	NW				5587944	410064	Twin Peaks
		Foliation		260	44	NW				5587380	409923	Twin Peaks
DC479	Garnet–sillimanite–biotite paragneiss	Foliation		5587393	409922	Twin Peaks						
		Foliation	Biotite, sillimanite	266	64	NW	11	280	5587266	409729	Twin Peaks	
		Foliation	Biotite, sillimanite	272	63	N						
DC480	Calc-siliate Amphibolite	Foliation	Biotite, sillimanite	259	57	NW						
		Fracture		002	63	E						
		Foliation		242	48	NW						
		Foliation		244	49	NW						
DC490	Quartzite	Foliation		267	63	N						
		Foliation		261	64	N						
		Foliation		262	59	N						
		Foliation	Bedding, mica	80	35	S						Plant Creek
DC500a	Garnet–sillimanite–biotite paragneiss	Foliation	Biotite, sillimanite, leucosome				45	303	Sillimanite	5597255	415370	Cariboo Alp
		Foliation	Biotite, sillimanite, leucosome	172	47		35	296	Sillimanite	5597255	415370	Cariboo Alp
		Foliation	Biotite, sillimanite, leucosome	128	59	W	37	245	Sillimanite	5597255	415370	Cariboo Alp
		Foliation	Biotite, sillimanite, leucosome	150	48	SW	53	262	Sillimanite	5597255	415370	Cariboo Alp
		Foliation	Biotite, sillimanite, leucosome	135	57	SW	47	286	Sillimanite	5597255	415370	Cariboo Alp
		Foliation	Biotite, sillimanite, leucosome	142	50	SW	61	274	Sillimanite	5597255	415370	Cariboo Alp
		Foliation	Biotite, sillimanite, leucosome	147	42	SW	50	255	Sillimanite	5597255	415370	Cariboo Alp

Sample	Rock type	Structure	Defined	Strike	Dip	Ddir.	Plunge	Trend	Defined	Northing	Easting	Location
	Garnet–sillimanite–biotite paragneiss	Foliation	Biotite, sillimanite, leucosome	123	52	SW	54	256	Sillimanite	5597255	415370	Cariboo Alp
	Garnet–sillimanite–biotite paragneiss	Foliation	Biotite, sillimanite, leucosome	110	53	SW	53	254	Sillimanite	5597255	415370	Cariboo Alp
	Garnet–sillimanite–biotite paragneiss	Foliation	Pegmatite	118	65	SW	56	249	Sillimanite	5597255	415370	Cariboo Alp
	Garnet–sillimanite–biotite paragneiss	Foliation	Pegmatite	145	63	SW	37	279	Sillimanite	5597255	415370	Cariboo Alp
	Garnet–sillimanite–biotite paragneiss	Foliation	Pegmatite	137	32	SW	40	281	Sillimanite	5597255	415370	Cariboo Alp
	Garnet–sillimanite–biotite paragneiss	Fold	Pegmatite	74	79	SW	30	276	Sillimanite	5597255	415370	Cariboo Alp
	Garnet–sillimanite–biotite paragneiss	Fold	Pegmatite	170	62	SE	45	253	Sillimanite	5597255	415370	Cariboo Alp
	Garnet–sillimanite–biotite paragneiss	Fold		125		W	43	257	Sillimanite	5597255	415370	Cariboo Alp
	Garnet–sillimanite–biotite paragneiss	Fold				SW	39	247	Sillimanite	5597255	415370	Cariboo Alp
DC500b	Biotite–quartzofeldspathic gneiss	Foliation	Biotite, sillimanite, leucosome	135	48	SW	29	247		5597250	415370	Cariboo Alp
	Biotite–quartzofeldspathic gneiss	Foliation	Biotite, sillimanite, leucosome	125	47	SW	31	248				
	Biotite–quartzofeldspathic gneiss	Foliation	Biotite, sillimanite, leucosome	138	36	SW	30	277				
	Biotite–quartzofeldspathic gneiss	Foliation	Biotite, sillimanite, leucosome	124	30	SW	48	265				
	Biotite–quartzofeldspathic gneiss	Foliation	Extension fractures	125	68	SW	46	242				
	Biotite–quartzofeldspathic gneiss	Foliation	Extension fractures	356	53	SW	42	267				
	Biotite–quartzofeldspathic gneiss	Foliation	Extension fractures	359	80	E	37	244				
	Biotite–quartzofeldspathic gneiss	Fracture	Extension fractures	45	85	E	34	241				
	Biotite–quartzofeldspathic gneiss	Fracture		47		SE	30	242				
	Biotite–quartzofeldspathic gneiss	Fracture				SE	40	230				
	Biotite–quartzofeldspathic gneiss	Fracture					36	275				